Pure

Bangor University

DOCTOR OF PHILOSOPHY

A study of electro-active properties of polymer/ceramic comosites

Abdullah, Mat Johar

Award date:
1990

Awarding institution:
Bangor University

Link to publication

General rights
Copyright and moral rights for the publications made accessible in the public portal are retained by the authors and/or other copyright owners and it is a condition of accessing publications that users recognise and abide by the legal requirements associated with these rights.

- Users may download and print one copy of any publication from the public portal for the purpose of private study or research.
- You may not further distribute the material or use it for any profit-making activity or commercial gain
- You may freely distribute the URL identifying the publication in the public portal ?

Take down policy
If you believe that this document breaches copyright please contact us providing details, and we will remove access to the work immediately and investigate your claim.

Download date: 19. Sept. 2024

A STUDY OF ELECTRO-ACTIVE PROPERTIES OF POLYMER/CERAMIC COMPOSITES

Mat Johar Abdullah

B.Sc.(Hons.)(Nat. Univ. Malaysia), M.Sc.(Durham, U.K.)

A thesis submitted to the University of Wales
in candidature for the degree of
Doctor of Philosophy

School of Electronic Engineering Science
University College of North Wales
Bangor
GWYNEDD
UNITED KINGDOM

November 1990

****

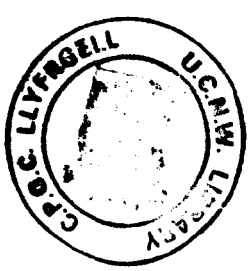

ACKNOWLEDGEMENTS

I should like to thank my supervisor, Dr.D.K.Das-Gupta, for his guidance and help in the preparation of this thesis and to Prof. J.J.O'Reilly for allowing me to use school's facilities. I am indebted to Dr.T.Yagi from Daikin Industries Ltd of Japan for a generous supply of PIEZEL samples.

My thanks also go to Mr.T.Welsh, Mr.S.Farrington, Mr.I.Wynne and Mr.J.Berry for their technical help during the course of the work.

I wish to express my appreciation to the Universiti Sains Malaysia for granting study leave and also the Public Services Department of Malaysia for providing a scholarship.

My particular gratitude goes to my parents for their endless advice and encouragement and to my wife for her moral support.

ABSTRACT

Ceramic-polymer composites with different compositions have been prepared and their electrical properties (absorption current, quasi-steady-state conduction current, dielectric and pyroelectric behaviour) have been studied. In addition, similar measurements have been made on a commercially available ceramic-polymer composite, PIEZEL™. The ceramics used include Lead Zirconate Titanate (PZT) and Barium Titanate ($BaTiO_3$) while the polymers were Polyvinylidene Fluoride (PVDF), copolymer of Vinylidene Fluoride-Trifluoroethylene (VDF-TrFE) and Polypropylene (PP). Analysis of data revealed that the process of charging and discharging currents of the composites involves charge carrier hopping through localised states (trapping sites) distributed throughout the bulk whereas the steady-state electrical conduction in these composites may originate from an ionic hopping mechanism.

Dielectric properties of the composites in the frequency range of 10Hz to 100KHz have been measured using an a.c. bridge technique. Results show that the dielectric loss process is dominated by the polymer phase whereas the ceramic phase may have a significant contribution at low frequencies and high temperatures. With the increase of ceramic content in the composite, dielectric permittivity and loss were observed to increase. Measured dielectric permittivities of the composites were generally in agreement with the calculated values.

The pyroelectric activity of the composites has been measured by the direct method. For samples with a high content of ceramic phase, calculated pyroelectric coefficient data appear to be comparable to those observed. The inherent high pyroelectric activity of the composites is essentially due to the ceramic phase while the high dielectric permittivity of the polymer is required to maintain a large dielectric displacement flux in the medium. Higher pyroelectric activity has been achieved in PZT5/VDF-TrFE (or PZT5/PVDF) composites in comparison with that of the other composites in the present work. The pyroelectric figure of merit in these particular composites was found to be about four times higher than that of the single phase ceramic.

CONTENTS

CHAPTER 4. ELECTRICAL CONDUCTION AND ASSOCIATED PROCESSES IN CERAMIC-POLYMER COMPOSITE

****

CHAPTER 1

INTRODUCTION

1.1. Background

There is a need of a better performance pyroelectric materials for diverse industrial, medical, public services and consumer products applications. Pyroelectric materials exhibit changes in the electrical polarization with changes in temperature and this effect tends to be largest in ferroelectric materials (subgroup of pyroelectric materials which posses a spontaneous electric polarization that can be reversed or reoriented by application of an electric field ; see chapter 2 for materials classification). Examples of these ferroelectric materials include lead niobate($PbNbO_3$), triglycine sulphate(TGS), titanate and niobate ceramics, single crystals lithium niobate($LiNbO_3$) and lithium tantalate($LiTaO_3$) and lead zirconate titanate(PZT) ceramics.

Since every pyroelectric material has its own advantages

as well as disadvantages, a wide range of pyroelectric materials is necessary not only for improving the pyroelectric detector performance but also to meet the demand for specific applications of detectors. The choice of the pyroelectric material is mainly determined by: (a) its figure of merit, (b) the detector size, (c) availability and durability of the pyroelectric material, (d) environment in which the material has to operate, (e) the radiation levels to be detected.

The performance of the pyroelectric detector is usually described by voltage responsivity (i.e. the pyroelectric voltage output per unit energy of incident radiation), current responsivity (i.e. the pyroelectric current generated per unit energy of incident radiation) and detectivity (i.e. the inverse of noise equivalent power (NEP) where NEP is defined as the incident energy required to produce a signal equal to that of detector noise). The voltage and current responsivities as well as the detectivity depend not only on the particular pyroelectric material but also on the characteristics of the amplifier employed for detecting the pyroelectric voltage [1,2]. In terms of material's parameters, the voltage responsivity is proportional to $p/(\varepsilon c)$, the current responsivity is proportional to p/c while the detectivity is proportional to $p/[c(\varepsilon \tan\delta)^{1/2}]$, where p is the pyroelectric coefficient, ε is the permittivity, $\tan\delta$ is the loss tangent and c is the volume specific heat. Hence $p/(\varepsilon c)$, p/c and $p/[c(\varepsilon \tan\delta)^{1/2}]$ could be considered as the figures of merit of pyroelectric materials. For many pyroelectric applications, it is convenient to define the

voltage pyroelectric figure of merit as given by p/ε .

Single crystals such as TGS and $LiTaO_3$ have high pyroelectric figure of merit and thus they are good materials for pyroelectric detection [2]. However TGS has rather low Curie point (T_C=322K) which is of disadvantage for some applications. Pyroelectric ceramics such as PZT and lead titanate ($PbTiO_3$) possess a number of attributes which make them more promising for diverse applications (see section 1.2). A significant pyroelectric effect can be induced in polyvinylidene fluoride (PVDF) polymers (see chapter 6). Although the polymer's figure of merit (for detectivity) is low as compared to ceramic and single crystal, the figure of merit for voltage responsivity is comparable to ceramic and not very much different as compared to single crystal [2]. The material is readily available in the form of thin films and has found use in the pyroelectric vidicon [3]. Recently, ceramic/polymer composites emerged which have been shown to have better piezoelectric properties (the change in electrical polarization with mechanical stress) as compared to the homogenously poled ferroelectric ceramics (see section 1.4). The interest in these composites stems from a need of piezoelectric materials which are flexible, large areas, complicated shapes or large improvement in the piezoelectric properties. It appears that there is not much work have been done on the pyroelectric properties of ceramic/polymer composites. Obviously, the pyroelectric properties of these composites would mainly depend on the properties of its single phase components (ceramics and polymers). The following

sections (sections 1.2 and 1.3) describe a brief account of the properties of the ferroelectric ceramics and pyroelectric polymers in general.

1.2. Ferroelectric Ceramics

A polar axis can be induced on ceramics by the application of sufficiently high electric field. This important consequence of the orientability of the polar axis is an advantage as compared to single crystals which have fix direction of polar axis. In addition, ceramics can readily be prepared in complex compositions and hence can be adapted for particular applications.

After poling treatment, the polarization of each crystallite in the ceramic is aligned to those directions allowed by the symmetry (the feature of atomic arrangement in the crystal) of the lattice and nearest to that of the electric field. The net polarization and hence the non-zero dipole moment is created which will respond to applied electric field or mechanical stress as those of single crystals as long as the field or stress is well below that needed to switch the polar axis. However, since the original crystallographic directions of the crystallite in the ceramic were oriented at random, the alignment of polar axes can not be as perfect as in a single crystal of the material. A measured value of polarization (charge per unit area) will give a good indication of this dipole alignment. There are

some other factors such as imperfections and grain boundaries effect which may result in preventing a maximum polarization to be achieved in ceramics. Well poled barium titanate($BaTiO_3$) ceramic for example has a polarization of $8x10^{-2}$ Coul/m^2 [4] while a value for single crystal is $26x10^{-2}$ Coul/m^2 [5].

It is common that the evidence of charge-field (or polarization-field) hysteresis is used as one of the criteria for the material to be accepted as ferroelectric. This is basically achieved by applying an alternating voltage to the test material and the voltage which corresponds to the stored charge on the test material is displayed against the applied voltage[6]. A typical of polarization(P)-field(E) hysteresis loop in ferroelectric is shown in Figure 1.1. The charge(Q) stored in the sample capacitor is proportional to the electric displacement(D). From the relation: $D = \varepsilon_o E + P$ (see chapter 4, Eq.(4.7)), it is obvious that since $\varepsilon_o E$ is usually negligible in comparison to P, the spontaneous polarization(P_s) is taken as the saturation value of the electric displacement extrapolated to zero field . The remanent polarization, denoted by P_r is taken to be the displacement at zero field, i.e. $P_r=D(E=0)$. The value of P_r is normally be used to asses the quality of ceramic compositions since generally the large piezoelectric effect results from high value of P_r. At the highest field where the polarization is saturated (corresponds to point A in Fig.1.1), most of the polar axes are aligned preferentially. As the field reduces to zero, and then becomes large in the reversed direction, the dipole moment reverses in the opposite direction and saturates

as the field increases further. The magnitude of field at which the dipole moment switches to opposite direction is designated as coercive field (E_c), i.e. E_c=E(P=0). It is worth noting that the shape of hysteresis depends on the material and the frequency of applied field[7]. Hence careful consideration has to be taken when examining the material with this kind of measurement, as the nonlinear lossy dielectric may also produce a kind of hysteresis loop, but with different shape of course[2,7].

Usually the ferroelectric crystal has regions in which the direction of spontaneous polarization in one region is different from the next region. This region is called domain and the boundary between the domains is called domain wall. The application of electric field (E) will cause the domain wall to be displaced so that the domain volume of width d, with the spontaneous polarization parallel to the electric field expands (refer to Figure 1.2). At sufficiently strong electric field, the whole crystal will have the spontaneous polarization parallel to the field when the optimum polarization is achieved. Likewise, if the field is reversed and increased adequately, the polarization will be saturated in the opposite direction. By this means, the reversal of spontaneous polarization follows the change of the electric field with some delay which yields the hysteresis loop as in Fig.1.1.

Most ferroelectrics have a transition temperature (T_c) called Curie point at which the spontaneous polarization has a finite value below it and vanishes if the temperature is

increased above that point. Usually a high dielectric permittivity is demonstrated in the vicinity of the Curie point. Above this point, the relative permittivity (ε') follows the Curie-Weiss law [5]:

$$\varepsilon' = C/(T-T_o) \quad , \quad T>T_c \tag{1.1}$$

where C is a Curie-Weiss constant, T temperature and T_o(Curie-Weiss temperature), which does not coincide with the Curie point, is defined as the temperature at which the extrapolated curve of the inverse of ε' meets the temperature axis.

A knowledge of piezoelectric and pyroelectric activity is always desirable as evidence for ferroelectricity, although their effects may not be the determinant factor for the confirmation. In any case, the poling process usually results in dielectric absorption with storage of charge much larger than those associated with the ferroelectric effect. These charges would be released by thermal change or by mechanical stress but the process is irreversible, hence it does not constitute a true effect. Further related characteristic of ferroelectric ceramic will be treated in the next chapter.

1.3. Pyroelectric Polymers

Pyroelectricity can be induced in polymers by suitable application of a large electric field. Among the pyroelectric polymers, PVDF and copolymers of vinylidene fluoride(VDF) with

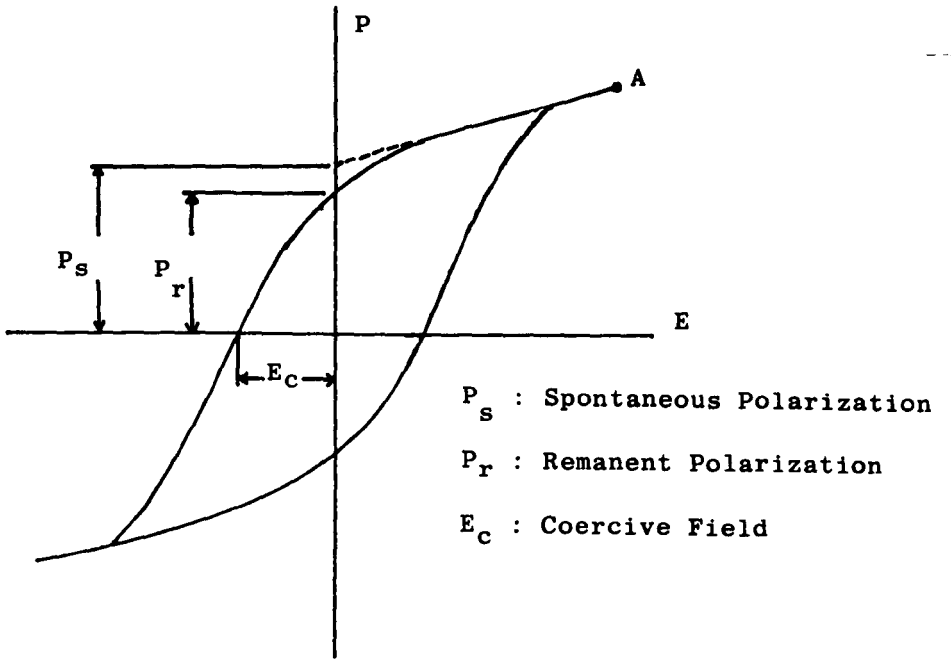

Fig.1.1. Typical ferroelectric hysteresis loop

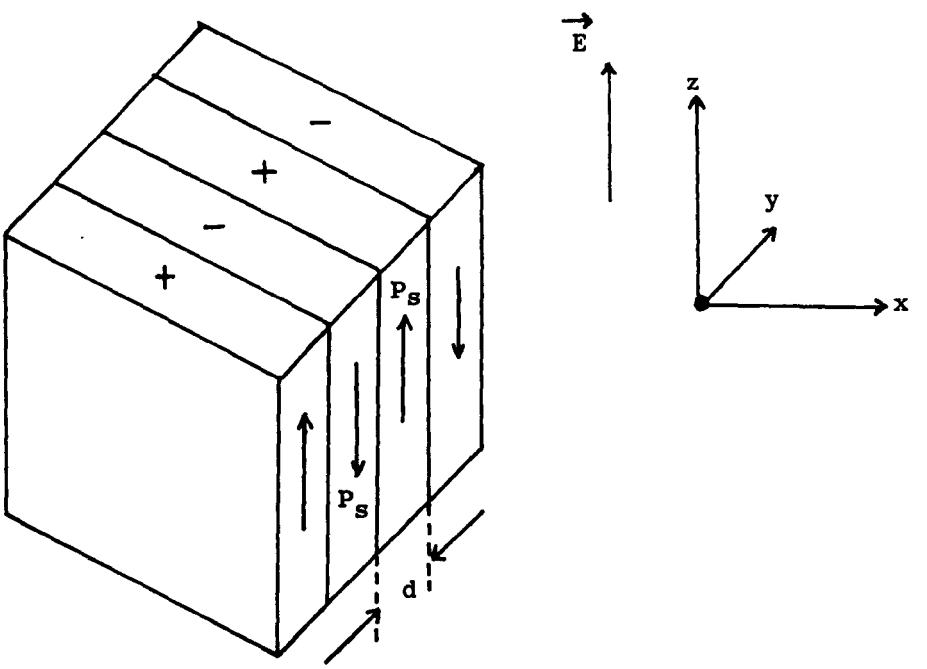

Fig.1.2. A model of domain structure showing the direction of spontaneous polarization

trifluoroethylene(TrFE) and tetrafluoroethylene(TFE) show relatively high pyroelectric activity (see chapter 6). These pyroelectric polymers have unique properties compared with other pyroelectric materials such as inorganic oxides, in that they are flexible and mechanically robust and also can be obtained as a thin film of very large size.

The detailed structure and related properties of PVDF are given in chapter 2. It should be noted that β-phase crystals (having all-trans conformation) of PVDF is the most polar because all its dipole vectors are aligned essentially normal to the chain direction. It is obtained by stretching or by electrical poling of the unpolar form (α-phase) of PVDF film (see chapter 2). The stretched film requires subsequent electrical poling so that the random orientation of crystallites within the polymer film become preferentially aligned to give a net dipole moment. Poling can be accomplished by the application of an electric field to the electroded polymer film at an elevated temperatures and subsequent cooling while the field is still applied. Alternatively, it could be achieved at room temperature in relatively shorter times by the technique of corona charging[8,9].

Mechanism related to pyroelectricity in PVDF is described in chapter 6. Basically, the improvement in the pyroelectric activity of the polymer may be made by increasing the dipolar alignment within the crystalline phase, which may be achived by the improvement in the fabrication process and in the technique of poling[10].

VDF-TrFE and VDF-TFE copolymers crystallize directly from the melt into the polar form crystals (β-phase) over a wide range of composition[11]. Although some early results show that the pyroelectric activity in these copolymers are not better than that of PVDF [12,13] (see chapter 6), the copolymers do not need to be stretched, which may be an advantage in some applications.

1.4. Ferroelectric Composite

Ferroelectric composites may be designed to combine the superior properties of the ferroelectric ceramics and polymers. It would be of great advantage to have such flexible composite with high pyroelectric activity and low thermal conductivity for pyroelectric detector arrays.

The composites may be produced by several methods such as : (a) ceramic particles dispersed in a polymer matrix, (b) ceramic rods embedded in a polymer matrix, (c) replamineform technique, which is based on the template of natural coral [14].

Some interesting results on piezoelectric properties of the composites appeared in the literature. Skinner et al[14] showed that the piezoelectric voltage coefficient g_{33} ($g_{33} = d_{33}/\varepsilon$, where d_{33} is the piezoelectric strain coefficient and ε is the permittivity) of the composite prepared by replamineform technique is about 15 times better than that of single phase ceramic. In another work, Runt and Galgoci[15]

reported that the hydrostatic piezoelectric figure of merit $d_h g_h$ (where $d_h = d_{33} + 2d_{31}$, $g_h = d_h/\varepsilon$) for composite produced by embedding PZT rods in polymers (e.g. nylon) is about 5 times that of PZT. This improvement in the piezoelectric figure of merit is very useful for hydrophones[14,15].

Ceramic/polymer composites exhibit pyroelectricity if they are suitably poled [16,17]. Newnham et al[16] suggested that the large thermal expansion mismatch between the two phases of the composite (e.g. composites where ferroelectric ceramic rods embedded in polymer) could contribute significantly to the total pyroelectricity. This means that a suitably chosen modes of phase interconnection can have composite property that improve the pyroelectric figure of merit beyond those possible with the single phase. Early results on the pyroelectric properties of ceramic/polymer composites obtained by several researchers are given in chapter 6. These works were primarily concern to maximize the pyroelectric figure of merit (p/ε). Obviously, more work is needed to produce and characterize the pyroelectric ceramic/polymer composites to meet the demand for better pyroelectric materials in diverse applications.

1.5. Aims of Present Work

In view of the need for pyroelectric materials with good pyroelectric figure of merit and of some encouraging results

on the pyroelectric properties of ceramic/polymer composites obtained by previous researchers [16,17,18], the present work is aimed at producing pyroelectric ceramic/polymer composites system and to characterize their electrical properties.

The first ceramic/polymer composite available for use in the present work was PIEZEL, a commercial product of Daikin Industries Limited of Japan. It is prepared by mixing PZT ceramic powder and VDF-TrFE copolymer and rolled into a flexible film. The received film was unpoled and unelectroded. As the work progressed, the hot roller machine became available in our laboratories at the final stage of the work and several ceramic/polymer composites were produced (the detailed fabrication process of the composites can be found in chapter 4). The ceramics powder used include PZT and $BaTiO_3$ while the polymers were PVDF, VDF-TrFE and polypropylene(PP). Although the ceramics used are far from ideal as pyroelectrics, they can be used as a model in the present composite system in which the ferroelectric ceramics have been dispersed in the polymer matrix. The use of different polymers serves to test the effect of the different properties of binding matrix on the overall electrical properties of composites.

The composites are characterized by measuring the transient (absorption and resorption) and conduction currents, the dielectric properties (permittivity and loss) as well as the pyroelectric current. Details of the transient and conduction currents in ceramic/polymer composites have not yet been reported in literatures. Thus, the present work is

carried out to study these currents at various fields and temperatures and to identify the responsible mechanism for them. Furthermore, the information obtained on the electrical conduction level and the mechanism involved will be discussed in relation with the measured pyroelectric properties of the composites.

The permittivity and loss in composites were determined by measuring the capacitance and the conductance of the sample in the frequency range of 10 Hz to 100 kHz, using an a.c. bridge technique. This measurement is accomplished at various temperatures to determine their temperature dependence characteristics. The information obtained from these data can be combined with data from the pyroelectric current measurements to evaluate the voltage pyroelectric figure of merit of the materials.

The direct method was used to investigate the pyroelectric activity of composites. In this method, the poled samples were heated at linear heating rate and generated pyroelectric currents were measured as a function of temperature. The effect of different poling parameters (electric field, temperature, time) on the pyroelectric activity were also investigated to determine the optimum poling condition.

The structure and related properties of polymers and ferroelectric ceramics are presented in chapter 2. This is followed by the principles of ferroelectricity and basic polarization process in chapter 3.

Chapter 4 provides the theory of electrical conduction

and associated processes (polarization mechanisms), experimental details (sample preparation, experimental system and measurement procedure), experimental results and the discussion of these results. For the sake of completeness, theories on various models of the electrical conduction have been included and used appropriately in the data analysis.

The relevant theory of the dielectric dispersion in solid single phase polymer and ceramic together with that of composite is presented in chapter 5. Further, the results of the dielectric properties of composites obtained in the present work along with the discussion are included.

Chapter 6 presents theories and evidence of pyroelectricity, results of the present pyroelectric studies on composites and the discussion.

Finally, chapter 7 includes the general discussion and conclusion of the electrical conduction, dielectric and pyroelectric properties of ceramic/polymer composites in the present work. Some suggestions to improve the present experimental technique and to enhance the pyroelectric properties of the composites have been included at the end of the chapter.

CHAPTER 2

STRUCTURE AND RELATED PROPERTIES OF POLYMERS AND FERROELECTRIC CERAMICS

2.1. Types of Ferroelectrics

Much of the behaviour of ferroelectric materials can be understood in terms of an information obtained from a study of their structural properties [1]. Generally, the study involves a determination of crystallographic configuration of atomic arrangement in relation to a polarization process that occurs in the materials. Hence, the ferroelectric materials may be classified according to certain basic features of their structure ; briefly as in the following.

(a) Compounds with corner sharing oxygen octahedra.

This group of materials includes perovskite type (e.g. $BaTiO_3$, PZT, etc), $(Bi_2O_2)^{2+}$ compounds (e.g. Bismuth titanate), Lithium niobate and tantalate, and tungsten bronze

type compounds (e.g. lead niobate, strontium barium niobate, sodium barium niobate). It contains corner sharing octahedra of O^{2-} ions with a cation B^{b+} (b= 3 to 6) near to its centre. The octahedra forms a continuous network by sharing corner O^{2-} with six neighbouring octahedra [2]. Between the octahedra are spaces occupied by A^{a+} ions where a varies from 1 to 3. In the prototype forms, the A^{a+} and B^{b+} ions have mean positions at the geometric centres of the surrounding O^{2-} ions giving a non-polar lattice. In the polar form, both A and B ions are displaced (which resulted in distortions of the octahedra and changes in the lattice dimensions) in the same direction relative to the geometric centres and so confer polarity on the lattice. However, the formation of dipoles through the displacement of ions does not necessarily lead to a polar phase, since in some cases a compensating pattern of dipoles is formed resulting in a zero overall moment.

(b) Compounds containing oxygen tetrahedra.

These oxides ferroelectrics contain BO_4 groups in which the B^{b+} (b= 4 to 6) ion lies near the centre of a tetrahedron with O^{2-} ions at each corner. Lead germanate ($Pb_5Ge_3O_{11}$) and Gadolinium Molybdate ($Gd_2(MoO_4)_3$) are examples of materials which belong to this group.

(c) Hydrogen bonded compounds.

This group generally contains hydrogen bonds coupled to the structural ions such as phosphate and glycine. The example of the materials that belong to this group include

potassium dideuterium phosphate (KD_2PO_4), Triglycine sulphate (TGS) and Rochelle salt (RS).

(d) Organic polymers.

This group of materials consists of long chain molecules that contain dipoles of covalently bonded atoms which can be oriented by a combination of mechanical and electrical treatments. A wide range of polymers are piezoelectric and some of them posses a reorientable polar axis [3,4]. Polyvinylidene fluoride (PVDF) and its copolymers have been shown to be ferroelectric [5-7] which successfully have been used in many device applications, for example in underwater devices as well as in medical sensors [8-10]. Due to its high compliances and the fact that they are readily formed into robust thin films, polymers with improved ferroelectric properties seem likely to emerge as attractive sensor materials in future.

In the following sections, the basic structure and related properties of ferroelectric perovskite ceramics and organic polymers will be given since these materials are used in the fabrication of ceramic-polymer composites in the present work.

2.2. Structural and Physical Properties of Ferroelectric Ceramics

The perovskite crystals have the general formula ABO_3 (derived from mineral perovskite calcium titanate ($CaTiO_3$)), where A (larger radius cation) situated at the apices of cubic cell, B (small radius cation) at the body centres and the oxygens (O^{2-}) at the face centres (se Fig. 2.1). The structure can also be regarded as a set of BO_6 octahedra arranged in a simple cubic pattern and linked together by shared oxygen atoms, with the A atoms occupying the spaces in between. Such a structure allows considerable variations of composition, by substitutions of A and(or) B ions by other ions of compatible ionic size. A large number of elements therefore have suitable radii(r) for the perovskite structure, e.g. Ba^{2+} (r= 160 pm), Pb^{2+} (r= 132 pm), K^{+} (r= 133 pm), Ti^{4+} (r= 60 pm), Zr^{4+} (r= 87 pm), Nb^{5+} (r= 69 pm), etc. Thus, a wide range of properties could be generated by these ions substitutions [11]. More complex compositions can easily be achieved in ceramic form than in single crystals [1], allowing the control of the characteristics of the material for different applications.

Barium titanate ($BaTiO_3$) was the first ferroelectric perovskite to be discovered [12] which has been used as piezoelectric material since then. Above its Curie point (T_C ~403 K), $BaTiO_3$ exhibits a cubic perovskite structure as shown in Fig.2.2 [13,14]. It consists of cubically close packed layers of composition BaO_3 in each of which the Ba^{2+} ions are

surrounded by six O^{2-} ions. The Ti^{4+} ions are located in those octahedra interstices in the BaO_3 lattice which are surrounded exclusively by O^{2-} ions.

During cooling, the cubic latice becomes unstable at around 403 K and the distortion occurs which transform the crystal into a tetragonal phase. Extreme dielectric anomalies (the peak in dielectric permittivity) accompany this transition which marks the onset of the replacement of the centro-symmetric cubic structure by a tetragonal phase [13]. In the tetragonal phase the Ti^{4+} and O^{2-} ions move relative to Ba^{2+} resulting in the formation of a polar lattice structure[1]. It has been verified that the Ti^{4+} ion in the tetragonal structure, does in fact move physically in phase with an applied electric field, as expected [15]. Upon further cooling, another transition occurs at about 273 K accompanied by a change to orthorhombic phase and at even lower temperature ($\sim$ 183 K), a third transformation occurs below which the symmetry is rhombohedral. In each phase, the polarization produced by the displaced ions would correspond to the polarization of the lattice, as it results from the vector addition of the polarization components of Ti-O chains[16]. As with the Curie transition, the ionic polarizability increases (giving a high spontaneous polarization) at the second and third transitions with resulting peaks in the permittivity-temperature relation. Such characteristics are well reflected in the dimensional change of the lattice in the respective phases. The exact transition temperatures are dependent on crystallite size, rate of

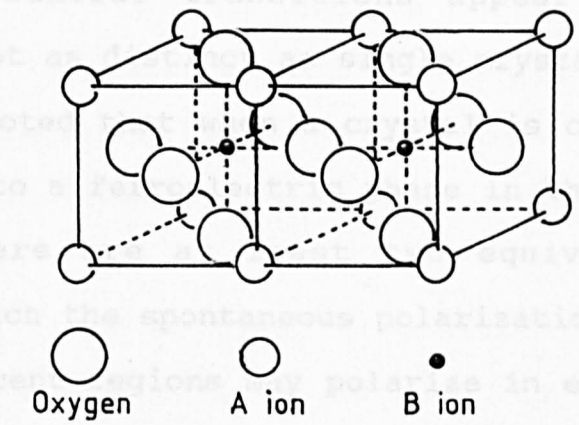

Fig. 2.1. Perovskite ABO_3 crystal structure.

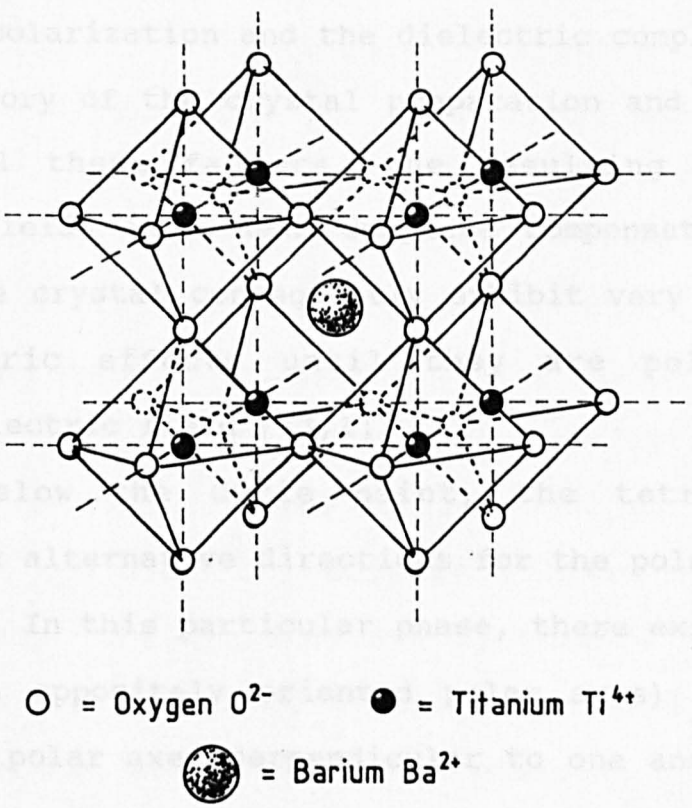

Fig. 2.2. Perovskite cubic structure of $BaTiO_3$.

temperature variation, condition of stress and precise purity of the material. Similar transitions appear in ceramic materials but are not as distinct as single crystals[13].

It is to be noted that when a crystal is cooled from a paraelectric phase to a ferroelectric phase in the absence of applied fields there are at least two equivalent polar directions along which the spontaneous polarization may occur. In a crystal, different regions may polarize in each of these directions mentioned above and form domains. A single domain configuration is rarely achieved in a virgin crystal in the absence of applied fields and the observed domain pattern depends on many factors including the crystal symmetry, the electrical conductivity, the defect structure, the magnitude of the spontaneous polarization and the dielectric compliance, as well as the history of the crystal preparation and sample geometry. With all these factors, the resulting domain structure usually yields in a near complete compensation of polarization and the crystal consequently exhibit very small, if any, pyroelectric effects until they are poled by application of an electric field [13,1].

In $BaTiO_3$ below the Curie point, the tetragonal structure allows six alternative directions for the polar axis of each domain [13]. In this particular phase, there exist 180° walls (regions with oppositely oriented polar axes) and 90° walls (regions with polar axes perpendicular to one another). The domain walls move in applied fields so that the volume of material with its polar axis parallel (or as near parallel as the lattice orientation allows) to the applied field is

increased. Movements of 180° domain walls are not accompanied by a dimensional change since it involves only a reversal (or partial reversal) of the polar axis. The movement of 90° walls, on the other hand, requires the conversion of a polar into a non-polar axis and is therefore accompanied by a dimensional change [13,14].

At sufficiently high dc field (typically : 0.5 - 5×10^6 V m^{-1}), 180° domains are aligned as near as the lattice orientation allows, to the applied field direction, whereas 90° walls are moved in a limited manner due to the stresses involved in the changes of axial direction. In ac fields the domain walls vibrate and the resulting fluctuations in dipole directions make a significant contribution to the polarizability. Such contribution is shown as a large increase in dielectric permittivity with electric field strength. Similar effect has also been observed in dielectric loss behaviour [14]. However, under static electric field bias, domain movement is inhibited, resulting in the fall of permittivity with increasing magnitude of static field [14].

In ceramic, both 90° and 180° walls are generally present and will be oriented according to the lattice structure of the crystal whose axes are randomly oriented throughout the material. Consequently, the observed P-E hysteresis loop in ceramic are much slanted than those of single crystals, which tend to be 'square' in shape [13]. The coercive field is greater than in single crystal and the saturation polarization is less because defects and internal strain (due to local stresses) inhibit wall movement. Domain walls are liable to

clamping by mechanisms such as local stresses (such as arise from changes of axial direction which inhibit 90° wall movement) and lattice defects (occuring in both types of wall which may immobilize the walls movement). The result of clamping is a lower permittivity and loss and a further departure from a usual P-E hysteresis loop [17].

At temperatures just below and up to the Curie point, the domain wall mobility increases while the clamping effects diminish. The ionic polarizability also increases, allowing a greater polarizability with respect to external fields. At the Curie point, the freedom of oscillation of ions reaches a maximum so that the dielectric permittivity reaches a maximum and the dissipation factor (tan δ) a minimum magnitude [14].

The ferroelectric behaviour of the ceramic depends greatly on the crystallite (grain) size, which in turn depends on exact composition and processing conditions of the material. Result of Heywang [18] showed that the effect of small grain size is to increase the small field dielectric permittivity in the region between the Curie point and the second transiton temperature in $BaTiO_3$ ceramics. However, Arlt et al [19] and Shaikh et al [20] showed that the dielectric permittivity increases sharply with increase in grain size, reaching maxima at about (0.5 - 1) μm and decreases with further increase in grain size. Arlt et al [19] attributed the high increase of dielectric permittivity in fine-grained $BaTiO_3$ as due to the increasing contribution of 90° domain walls (the total area of 90° domain walls per volume strongly increases in the fine-grained ceramic). At grain sizes (0.5 -

1) μm and lower, however, gradual ferroelectric structural changes occur (resulting in the formation of different domain structure) which causes the decrease of dielectric permittivity.

As regards the spontaneous polarization, it was found to decrease with the decrease in grain size [20]. This is to be expected since as the grain size decreases, the crystallinity also decreases and finally one reaches an amorphous state where ferroelectricity ceases. An alternative explanation is that in the smallest grains, the polarization may be completely clamped by local stresses preventing domain reversal in external fields [1]. At intermediate grain sizes, domain reversal becomes possible while at the largest grain sizes, bulk ferroelectric behaviour becomes dominant.

An enormous effort has been made to study the properties of compositionally modified $BaTiO_3$ ceramics. Accordingly, a large range of properties have been generated by such solid solution systems [13]. Obviously, composition is only one factor controlling dielectric properties. Other factors such as particle size, the mixing proces, the pressing and sintering all contributes to the characteristics of a dielectric.

Lead zirconate titanate ($Pb(Zr_{1-x}Ti_x)O_3$ or PZT) system constitute one of the most important series of ferroelectric materials used in ceramics for industrial piezoelectric transducers. It has continuously been improved by different compositional variations. The phase diagram of the system is shown in Fig.2.3 [13]. At high temperatures, the complete

mixed-crystal series exhibits a cubic perovskite structure. For a system of less than 50 mole% zirconate content, such a material changes to the tetragonal ferroelectric phase at the Curie point. No further phase transitions are found below this point. Between 50 and nearly 100% zirconate content, the transition leads directly from the cubic to the rhombohedral phase (Rh I). A second transition occurs with decreasing temperature to another rhombohedral phase (Rh II). Although both phases appear to be simple cell rhombohedral by X-ray diffraction, they are distinguishable by neutron diffraction studies, electrical measurements and thermal expansion studies [13,1]. The boundary between tetragonal and rhombohedral forms is nearly independent of temperature (morphotropic). In a composition of more than about 95% lead zirconate content, an antiferroelectric phase [13] with orthorhombic symmetry (A_O) is formed adjacent to rhombohedral ferroelectric phase (see Fig.2.3).

In tetragonal phase, both 180° reversal and 90° reorientation of domains can occur during poling. Experimental results showed that 180° reversals are virtually complete whereas only 53% of 90° reorientation can occur which drops to 44% after removing the field [13]. The polarization is attributed to the polarizability of the Ti-O chains (as in the case for $BaTiO_3$) with an additional contribution from lead oxide dipole (which arises because of the partially covalent bonds of the lead ions as evidenced from the chemistry of the lead-oxygen compounds). In the titanium-rich tetragonal region, a lead atom coordinates with four oxygen atoms, and

forms dipole as shown in Fig.2.4(a). This would directly contribute to an increase in the coupling of parallel Ti-O chains leading to a larger polarization. In the rhombohedral phase, the lead atom coordinates with three oxygen atoms (see Fig.2.4(b)), in which case, the (Zr,Ti)-O chains retain only minor significance for the ferroelectricity as a result of the reduced titanium content. Also, due to higher zirconium content ($0.1 < x < 0.45$), the polarizability of the (Zr,Ti)-O chains are low, resulting in relatively low permittivity. The polarization aligns with the {111} direction, in which alternating TiO_3 and PbO_3 dipoles are formed (see Fig.2.4(b)) [16]. For rhombohedral compositions near the phase boundary, 70° and 110° domain reorientation can occur in addition to the 180° reorientation, with the former two behaving much as 90° walls in the tetragonal materials[13].

Most of the piezoelectrically active PZT compositions have the value of x=0.47, which is close to the morphotropic boundary, shown in Fig.2.3. For a value of x in the range of 0.45 to 0.50, the rhombohedral and tetragonal forms may coexist and the ferroelectric properties are also enhanced. It is believed that the enhanced ferroelectric properties in this region is because of the increased ease of reorientation of domains during poling [13].

For technical applications, the lead zirconate titanate ceramic is modified by adding further oxides. A technically important group of additions is characterized by being incorporated as ions with higher positive charge into the lattice. Representative of this group are large trivalent ions

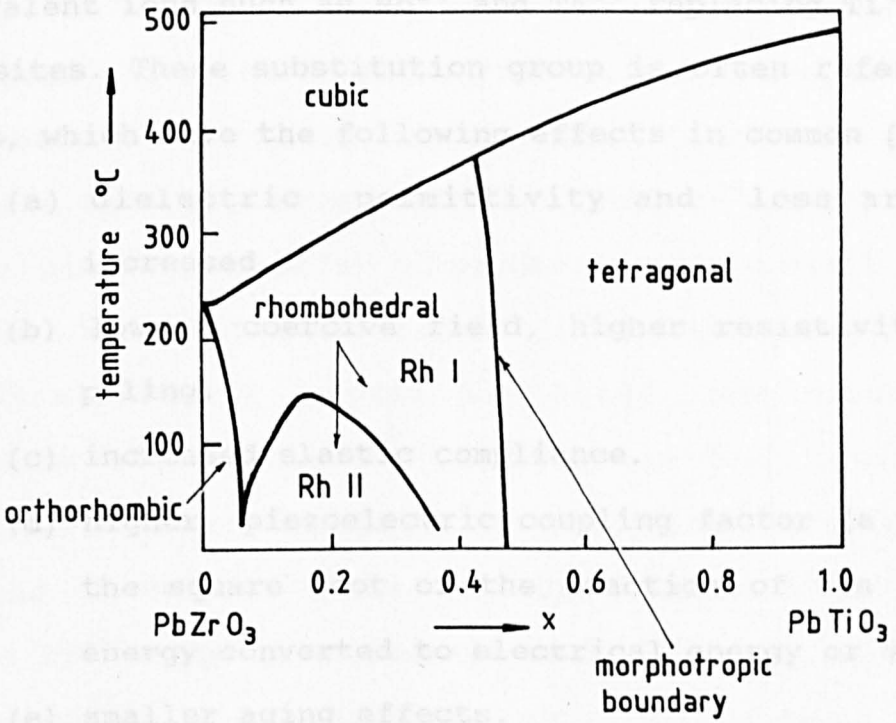

Fig. 2.3. Phase diagram of $Pb(Zr_{1-x}Ti_x)O_3$ ceramics.

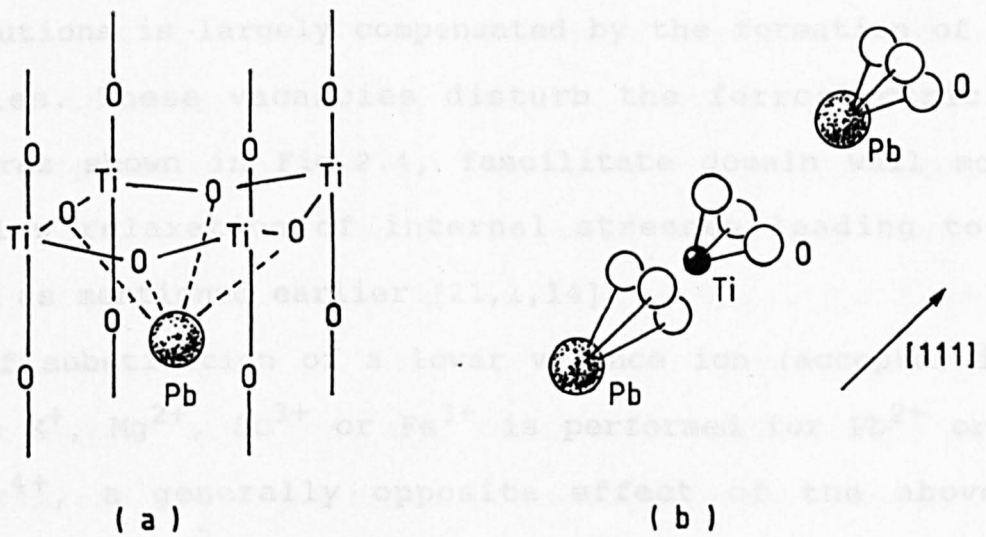

Fig. 2.4. Dipole formation in $Pb(Zr,Ti)O_3$.
(a) Parallel Ti-O chains in the tetragonal phase coupled by directional covalent bonds of the oxygen atoms in the transversal chains and covalent coupling by tetrangular Pb-O bonds.
(b) Covalently bonded TiO_3 and PbO_3 dipoles in rhombohedral phase.

replacing Pb^{2+} at A-sites, e.g. La^{3+} and Nd^{3+} and smaller pentavalent ions such as Nb^{5+} and Ta^{5+} replacing Ti^{4+} and Zr^{4+} at B sites. These substitution group is often referred to as donors, which have the following effects in common [13]:

(a) dielectric permittivity and loss are greatly increased.

(b) lower coercive field, higher resistivity, easier poling.

(c) increased elastic compliance.

(d) higher piezoelectric coupling factor (a measure of the square root of the fraction of the mechanical energy converted to electrical energy or vice versa)

(e) smaller aging effects.

Many of the properties of this family are explained on the basis of vacancies fascilitating domain boundary motion [21]. The excess positive charge introduced by the substitutions is largely compensated by the formation of Pb^{2+} vacancies. These vacancies disturb the ferroelectric PbO structures shown in Fig.2.4, fascilitate domain wall motion and allow relaxation of internal stresses leading to the effects as mentioned earlier [21,1,14].

If substitution of a lower valence ion (acceptor ions) such as K^{+}, Mg^{2+}, Sc^{3+} or Fe^{3+} is performed for Pb^{2+} or for $(Zr,Ti)^{4+}$, a generally opposite effect of the above is produced [13]. It is assumed from size considerations that K^{+} enters the Pb position while Sc^{3+}, Fe^{3+} and Mg^{2+} substitute for $(Zr,Ti)^{4+}$. Ceramic materials doped in this way display even more unfavourable properties than nonmodified PZT

ceramics ; it exhibits an even higher p-type conductivity [16]. It is suggested that these ions, diminish the number of A position vacancies normally present and cause the existence of oxygen vacancies in the lattice. Since the perovskite structure (and many other oxide structures) can be regarded as a three-dimensional array of oxygen ions in contact with metal ions that fill the interstices, it is clear that only small concentrations of oxygen vacancies can occur without appearance of new phases. Vacancies in the oxygen position will therefore tend to shrink the cell size, as evidenced from the case of $BaZrO_3$, where the substitution of Sc^{3+} for the smaller Zr^{4+} actually shrank the unit cell [13]. The shrinking and distortion of the cells by oxygen vacancies is thought to contribute to the high coercive field and the lowered dielectric permittivity.

Donors or acceptors are separately used only in doping concentrations of 2 atom.% at most. If elements of both groups are used together, forming complex ceramics, their main effects compensate one another partially or totally, depending on the ratio [16]. Examples of such a system are solid solutions of $Pb(Zr,Ti)O_3$ with $Pb(Mg_{1/3}Nb_{2/3})O_3$ [22] and $Pb(Nb_{1/2}Fe_{1/2})O_3$ [23].

It can be seen that the structural modification of the PZT system has proved to be an exceedingly versatile for range of properties that can be used for many applications.

2.3. General Structure of Polymers

Polymers are materials with a very large molecules comprising hundreds or thousands of atoms, formed by successive linking of one or two (ocassionally more) types of small molecules into a long molecular chain or network structures [24]. Thus, a single molecular chain commonly contains a thousand or more repeat units and reaches a total length in excess of 1 μm [25].

As in many other solid materials, the individual atoms or molecules are held together by stabilising forces acting between them. The amount of stabilization achieved is at its greatest when molecules adopt regular rather than random arrangements [24,25]. In the regular or crystalline arrangement (crystal structure), the molecules pack together in such a way to minimise the total intermolecular energy. A small group of atoms or molecules called unit cell may well be used to represent the crystal structure.

Although the molecules are held firmly in place in the crystal lattice, they still posses vibrational and possibly rotational energy [24]. As the temperature of the crystalline solid approaches its melting point, the vibrational motion becomes more active, finally causing the collapse of the crystal structure at the melting point itself. At this point, the regular packing of solid state is replaced with the disorder of the liquid state.

As the temperature falls below the melting point, the ordered solid state strives to emerge. However, the regular

arrangement of molecules cannot arise instantaneously, since the process takes time to occur. If a molten polymer is rapidly cooled (or quenched), there is insufficient time for any significant crystallization to occur which results in the formation of amorphous solid. Nevertheless, some polymers posses some degrees of crystallinity while many others are found to be completely amorphous. It should also be noted that crystalline bulk polymers contain a proportion of amorphous phase so that the classificaton of crystalline and amorphous polymers may not be used too rigidly [24].

The degree of crystallinity, most often in the range of 5-50% , depends on the molecular structure of the polymer (e.g. factors such as branching, crosslinking and other chemical variations can suppress crystallization) and on the thermo-mechanical history of the particular sample [24,25]. Crystalline regions start to grow at isolated points (or nuclei), which then develop throughout the material or until they encounter the boundary of another growing crystalline region. The crystallization of a large amount of material on a single nucleus results in the formation of a single crystal. Well-formed individual single crystals can be obtained only under carefully controlled conditions (often more easily from solution than from the melt). Normally, nucleation (a process of creating local order among small numbers of molecular units in neighbouring chains) occurs at a number of points in the liquid and a polycrystalline solid is then formed. The final size of the individual crystal grains or crystallites depends on the concentration of nucleating centres [24].

The structure of crystalline phase of a polymer may be determined from the study of X-rays diffraction patterns. Obviously, the long chain nature of polymer molecules leads to complex morphologies of the material. In general, the molecules of the crystalline phase adopt an extended zigzag or a helical conformation and lie parallel to each other. X-ray evidence show that at the molecular level, the polymer chains pack together side by side in the crystalline regions. As well exemplified by linear polyethylene (grown from dilute solution), the crystalline phase takes the form of very thin plates (called lamella), with lateral dimensions of the order of 10-20 μm and with a thickness of only about 10 nm (see Fig.2.5). Electron diffraction studies show that the chain axis of the polymer molecule lies approximately perpendicular to the plane of the lamella. Since the polymer molecular chain is known to be much longer than the thickness of the crystal, the chain must fold back upon itself at regular intervals along the chain in the manner shown in Fig.2.5 [25,26]. The fold length, which corresponds to the thickness of the lamella, is extremely consistent, although it varies with the crystallization conditions, such as temperature and solvent. Once formed the crystals may increase their fold length when they are subsequently heated to higher temperature [24]. The exact arrangement of the folds is difficult to characterize, but in some cases it is believed to be tight, with chains re-entering the crystal at adjacent sites. The nature of the crystal obtained from the melt is not the same as that grown from solution, however, a large number of subsequent

investigations have shown that chain folding in polymer crystals is a general phenomenon [25,27,28].

When crystallized from the melt, polymers usually exhibit spherulites structure which consists of a radiating array of crystal lamella as shown in Fig.2.6. It appears that spherulites grow radially from nucleation centres (e.g. small crystals, extraneous solid particles) with twisting and branching and the ultimate size of the spherulite will be determined by the original concentration of nuclei. Thus, the main structure of a spherulite is a radial array of twisted lamella-like blades called fibrils. It has been concluded that the polymer crystals in a spherulite are similar to those from solution but are highly elongated in the radial radiation [24]. Amorphous phase of several different kinds (e.g.portions of molecules which comprise 'loose folds', dangling ends of molecules, branch points, etc) exists between the fibrous crystals within the spherulites at the fold surface and between the spherulites themselves. The boundary between spherulites in these polymers somewhat resembles the grain boundary observed in the microstructures of other classes of materials [24].

If the polymer is deformed by an orientation process (such as stretching or rolling), the spherulites are first deformed to an elliptical shape [29] followed by disruption of the spherulite structure. For larger deformation, the morphology becomes fibrillar with the molecular chains becoming oriented preferentially parallel to the direction of deformation [24]. It is this orientation process, coupled with

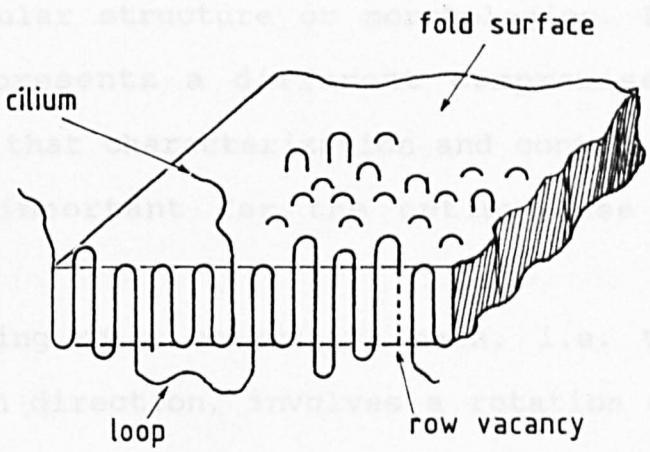

Fig. 2.5. Schematic model of a chain-folded lamella.

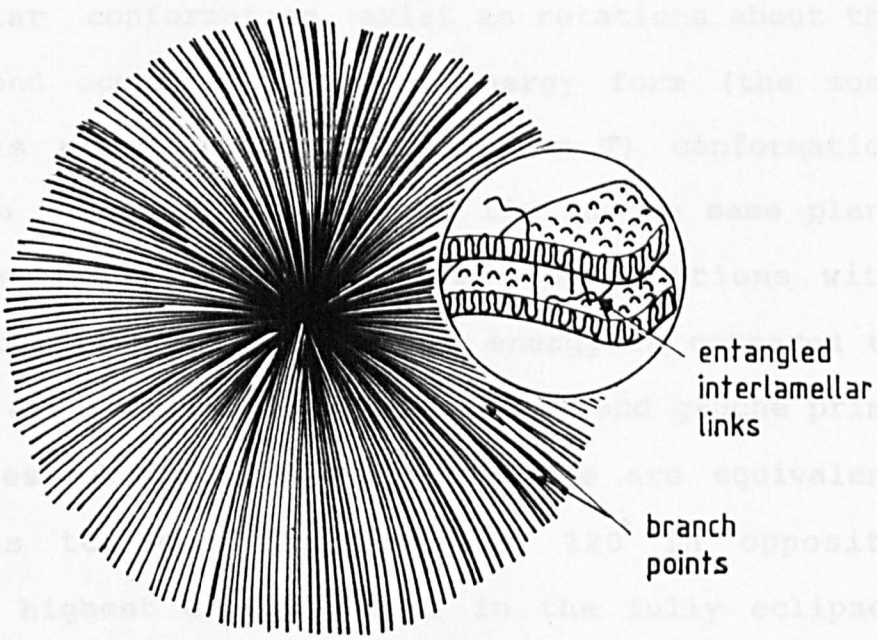

Fig. 2.6. Schematic diagram of spherulitic structure showing radial growth of lamellar crystals.

the aforementiond crystallization process which lead to a wide range of molecular structure or morphologies. Each different morphology represents a different compromise in physical properties, so that characterization and control of morphology becomes very important for the optimum use of polymeric materials.

The folding of a molecular chain, i.e. the periodical change of chain direction, involves a rotation about chemical bonds of the molecules. In all polymer chains, the direction taken by a bond is strongly dependent on the position of the preceding bond in the chain . This will give rise to the spatial arrangement of atoms or molecular conformation for any particular polymer [24]. In polyethylene ($[-CH_2-CH_2-]_n$), several molecular conformation exist as rotations about the C-C chemical bond occur. The lowest energy form (the most stable state) is referred to as trans (or T) conformation which occur when the four carbon atoms lie in the same plane (rotation angle = 0°). The other two conformations with minimum energy but with slightly higher energy as compared to T conformation, are referred to as gauche (G) and gauche prime (G'). The energies of these two conformations are equivalent but corresponds to bond rotations of 120° in opposite directions. The highest energy occurs in the fully eclipsed state (rotation angle = 180°), where the component of the molecule most strongly interact with each other [30].

Polypropylene ($[-CH_2-CH(CH_3)-]_n$) is formally derived from polyethylene by the substitution of one of the H atoms on alternate C atoms of the chain by a methyl ($-CH_3$) group.

Depending on the method of polymerization process, polypropylene may exist in three different molecular structures, i.e. isotactic, syndiotactic or atactic, each configuration has different arrangement of methyl group. These structures are distinct configurations, which can not be interconverted by simple rotation about bonds. This form of tacticity arises in all chain polymers in which atoms of the backbone carry two dissimilar atoms or groups. Obviously the configuration affects the way in which adjacent molecule can fit together in the dense packing of the solid and hence controls the strength of forces between molecules from which the mechanical properties of the material are determined [24,25].

In the following section, structure and related properties of polyvinylidene fluoride (PVDF) and its copolymer will be given, from which the importance of chain conformation and the relative position of neighbouring chains to dipole moment and polarization will become apparent for its relatively high piezo- and pyroelectricity activity as compared to other polymers.

2.4. Structure and Related Properties of Polyvinylidene Fluoride and its Copolymers

Polyvinylidene fluoride (PVDF) is a semicrystalline polymer whose monomer unit (or repeat unit) is $(-CH_2-CF_2-)$. Different phases of PVDF can be formed by various physical,

thermal and electrical treatments. Thus, the crystallization and morphology of PVDF is complicated because it can crystallize in at least four polymorphic forms [31].

There are three types of chain conformation involved in crystal formation, each of which posseses a component of a net dipole moment perpendicular to the polymer chain (see Fig.2.7). It may be observed that the polymer chains of PVDF pack in the crystal's unit cell in one of two ways. The resultant dipoles of polymers chains may be in parallel configuration which give a crystal with a net dipole moment or it may be aligned in an anti-parallel configuration and thus there is no net dipole moment in the crystal.

PVDF crystallizes (the degree of crystallinity is approximately 50%) from the melt below 423 K into spherulitic structures [32] consisting of Form II crystals (α-phase) [33], in which the chain adopts the TGTG conformation and the chains pack in an anti-parallel configuration such that there is no net dipole moment in the crystal (antipolar crystal). The molecular chain conformation is shown in Fig.2.7 while the crystal's unit cell as viewed along the chain axes is shown in Fig.2.8 [34]. The crystallographic data for the crystal along with those for the other crystal forms of PVDF is shown in Table 2.1 [34].

When subjected to deformation by stretching (to several times of the original length), or rolling at temperatures below about 373 K [35], polymer chains within the α-phase become extended to the all-trans (planar zigzag) conformation and the structure is transformed into the β-phase as shown in

Figs. 2.7 and 2.8. The new crystal form has a net dipole moment but the random orientation of crystallites within a polymer film results in zero polarization until the crystallites become preferentially oriented by the application of a suitable electric field (poling). The amount of conversion from Form II to Form I depends on the draw ratio and the draw temperature [35].

Table 2.1. Crystallographic Data for Crystal Forms of PVDF

Crystal Form	Cell constants	Molecular conformation
I (β)	a=8.58 Å, b=4.91 Å, c=2.56 Å (orthorhombic)	All trans (planar zigzag)
II (α)	a=4.96 Å, b=9.64 Å, c=4.62 Å (orthorhombic)	TGTG′
IV (δ)	equivalent to Form II	TGTG′
III (γ)	a=4.96 Å, b=9.58 Å, c=9.23 Å, β=92.9° (monoclinic)	TTTGTTTG′

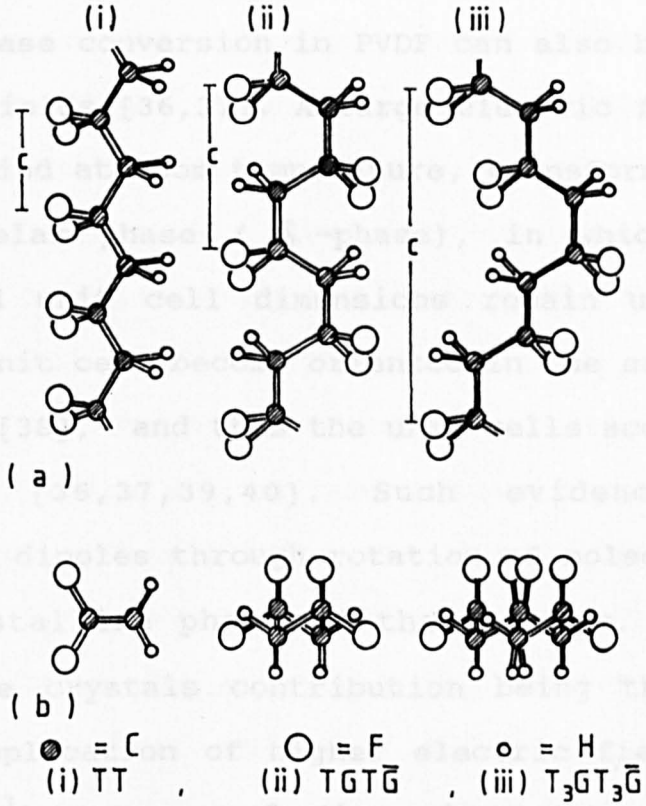

Fig. 2.7. Schematic models of the crystalline conformations of PVDF molecules: (a) viewed normal to the chain axes. (b) viewed parallel to the chain axes.

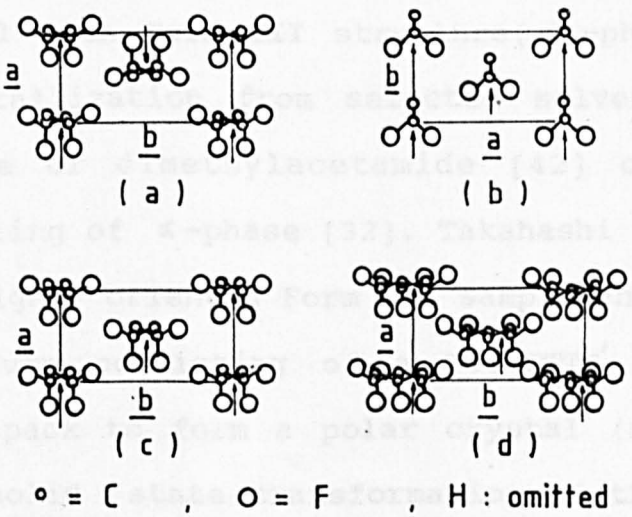

Fig. 2.8. Schematic models of the unit cells of four of the PVDF crystal forms viewed parallel to the chain axes. (Arrows indicate dipole moment ⊥ chain axis).
(a) Form II (α-phase) , (b) Form I (β-phase), (c) Form IV (δ-phase) and (d) Form III (γ-phase).

Crystal phase conversion in PVDF can also be induced by large electric fields [36,37]. A large electric field ($\sim 1 \times 10^8$ V m^{-1}) when applied at room temperature, transform the unpolar α-phase to a polar phase (δ -phase), in which the chain conformation and unit cell dimensions remain unaltered but dipoles in the unit cell become oriented in the same direction (see Fig.2.8) [38], and thus the unit cells acquire a net dipole moment [36,37,39,40]. Such evidence for the reorientation of dipoles through rotation of molecular segment within the crystalline phase of the polymer, support the argument for the crystals contribution being the source of polarization. Application of higher electric fields (greater than 3×10^8 V m^{-1}) causes a further phase transformation to that of the β -phase [36,39]. The crystal transformation depends upon temperature of application as well as magnitude of field [41].

PVDF crystal with Form III structure(γ -phase) can be obtained by crystallization from selected solvents such as dimethylsulfoxide or dimethylacetamide [42] or by high-temperature annealing of α-phase [32]. Takahashi and Tadokoro [43] produced a highly oriented Form III sample and proposed a monoclinic structure consisting of a TTTGTTTG' conformation where the chains pack to form a polar crystal (see Figs.2.7 and 2.8). The solid state transformation of the antipolar α-phase to the polar form γ-phase led to the suggestion that the polar δ-phase might transform to an antipolar analog of the γ-phase which would be called the ε-phase [44]. Lovinger [45] showed evidence for the existence of such a

phase but it was present in only a small amounts among the dominant $\mathcal{T}$-phase. The $\mathcal{T}$-phase can be readily transformed into Form I by mechanical deformation [31].

The melting point for PVDF depends on the method of preparation, the sample history and the crystalline content of the material [32,46]. For Form II phase, it is in the range 443-463 K [32,46] and for Forms I and III, it is approximately 463-493 K [47]. Studies of the temperature dependence of the dielectric permittivity and loss [48] showed that there is a loss peak at 343 K (110 Hz) associated with molecular motion in Form II crystalline regions (α_c) and another peak appears at about 383 K (110 Hz) which is attributed to molecular motion in Form I crystalline regions. Dielectric measurements on drawn and undrawn PVDF films [48-50] showed that the dielctric permittivity in drawn sample is higher than that for undrawn one, which may be attributed to the orientation of non-crystalline molecules in the plane parallel to the film surface. The loss peak which is attributed to the α_c process of Form II was observed to disappear in the drawn sample, which is predominantly contain Form I phase. Indeed the frequency spectra analysis provides a wealth of information about the relaxation characteristic which may be used to study the dielectric process in the polymer. Further treatment on the dielectric properties of PVDF will be given in chapter 5.

The repeat unit for PVDF (monomer : CH_2CF_2) has a large dipole moment ($m = 7.56 \times 10^{-30}$ C.m , or 2.27 D) [51,52]. In the all-trans conformation (the phase which received most attention), the component of this dipole moment normal to the

chain axis is about $7x10^{-30}$ C.m (= 2.1 D), and it is packed so that the crystal posseses a spontaneous polarization (see Fig.2.8(b)) [51]. A simple estimate of the spontaneous polarization (P_s) by summation of the dipole moments of the CH_2CF_2 groups over a crystal unit cell yields (assuming 100% alignment, 100% crystallinity of the films, dipole density(N) = $1.8x10^{28}$ dipoles. m^{-3} with each dipole having dipole moment(m) = 2.1 D) $P_s = \sum N\ m = 130\ mC.m^{-2}$ for a rigid dipole model [1]. Broadhurst et al [51,53] predicted the value of P_s = 220 $mC.m^{-2}$ by taking into account the contribution from reaction field due to surrounding medium (i.e. near the surface of crystals). A recent work by Al-Jishi and Taylor [54] however, found that the model which considers the effects of both the orthorhombic crystal structure and of the finite separation between the monopoles of the molecular dipole, gives the value of P_s = 127 $mC.m^{-2}$, which is in a good agreement with the value obtained from the rigid dipole model. In their model [54], the Lorentz field (the field which is due to the polarization charge on the surface of the surrounding crystals) is much smaller than the one adopted by Broadhurst et al [53]. The measured spontaneous polarization [55-57] from hysteresis measurement of PVDF (estimated to be about 50% crystallinity) is generally in the range 50-80 $mC.m^{-2}$, which may correspond well to the value predicted by the rigid dipole model [1].

In the drawn sample, the crystals are oriented in such a way that the main chain c-axis is aligned in the stretch direction while the b-axis is oriented randomly in the plane

normal to the stretch axis [35]. Such random orientation give no macroscopic polarization in the film. To confer polarization in the film, it is subjected to a strong poling field (beyond its coercive value) which preferentially aligns the polar axes of the crystal along the poling direction, that is, perpendicular to the film plane. X-ray [39,58,59] and infrared spectroscopy [60,61] reveal that dipoles within the crystalline phase of PVDF have become preferentially aligned in the direction of the applied field and remain aligned when the field is decreased. The surface charge density that remains is numerically equal to the polarization (net dipole moment per unit volume). This surface charge density is referred to as the remanent polarization (P_r). As the direction of the applied electric field is reversed, the charge on the electrode decreases smoothly until a critical field (coercive field) is reached at which point the charge decreases rapidly and changes sign. Such field-induced dipolar alignment of crystalline dipoles suggests that the crystal is ferroelectric.

Various experimental findings showing the behaviour of the hysteresis curve (indicative of the reversible direction of polarization) of P_s , e and infrared absorbance against bias field [60,62-67] have been reported for PVDF, which support that the material is ferroelectric. The presence of domain structure and Curie point (T_c) is another criteria of ferroelectric crystals, which is yet to be established for PVDF. Although a distinct Curie point has not been observed for the PVDF, piezoelectric and pyroelectric activities start

to decrease when the film is subjected to temperature above 353 K [68,69]. The loss in activity has been shown to be accompanied by a decrease in preferred alignment of dipoles within the polymer crystallites [70]. It has also been reported [70] that the largest portion of the thermal depolarization occurs through reorientation of dipoles in 60° increments. An empirical exrapolation of residual activity versus temperature of aging yields an expected complete loss of polarization (and hence the Curie point) near temperature 478 K [70], which is close to the melting point of β-phase PVDF. It appears that the domain structure has not been established. The finding of Bur et al [70] that depolarization appears to take place by rotation of dipoles in steps of 60° is consistent with the proposal made by Kepler and Anderson [58] that the rotation of molecular dipoles proceeds discretely in 60° increments as a result of field-induced polarization changes in the sample. It is believed that chains rotation proceeds in cooperative manner by formation and propagation of kinks (chain twisting) along their long axes [71].

The amorphous phase of PVDF has a glass transition temperature (T_g) between 223 and 233 K [72,73] and is thus in the rubbery state at room temperature. The reorientation of dipoles associated with the amorphous phase is observed as a peak in the thermally stimulated current at around T_g in samples which have been previously cooled to below T_g in an applied electric field [73]. Result of Tasaka et al [74] showed that the amorphous phase is partly oriented in oriented

PVDF films. Hence, it may be possible that dipolar orientation in the oriented amorphous phase contributes in part to the origin of P_s, as was suggested by several workers [75,76].

It has been well documented that piezo- and pyroelectric response from a PVDF polymer sample is directly related to remanent polarization [57,77,78], in which a linear relation between piezo- and pyroelectric coefficient and P_r has been observed. Thus, basically the improvement in the piezo- and pyroelectric activity of the polymer may be made by studying the process involved in the improvement of the value of P_r. Such improvement is partially achieved by the improvement in the fabrication process and in the technique of poling of the polymer, which results in an increase in the crystallinity and the degree of orientation of the crystals, as have been discussed by Broadhurst and Davis [51] and Wada [79]. A large volume of experimental results on piezoelectric properties of PVDF have been produced, some of which may be found in the references cited by Broadhurst and Davis [51], Kepler and Anderson [55] and Wada [79]. The mechanisms related to the piezoelectricity in PVDF or in polymers in general have also been discussed [51,55,79] and thus the treatment of its kind is beyond the scope of the present work.

The introduction of trifluroethylene ($CHFCF_2$ or TrFE) or tetrafluoroethylene (CF_2CF_2 or TFE) into PVDF through copolymerization process, yields polymers in which the comonomer units are distributed randomly in the chain [80]. Lando and Doll [81] first reported that the larger fluorine atoms replacing hydrogens on adjacent carbons in TrFE and TFE

interfered with the formation of the usual TGTG′ conformation of the polymer chain and forced the copolymers to crystallize from the melt into the all-trans conformation of the β - phase. A study of the effect of concentration of comonomer by Yagi et al [82] revealed that copolymers containing between 10 and 46 mole percent of TrFE exhibited a phase transition (observed as a peak in differential scanning calorimetry (DSC) result) below the melting point of the polymer. This transition was subsequently shown to involve a crystal-phase transformation from a ferroelectric to a paraelectric crystal, that is, a Curie transition [83-87], which is characterized by changes in lattice spacing as revealed by X-ray diffraction result [83,87], anomalous in the dielectric permittivity [83-85] and disappearance of remanent polarization and piezoelectricity [83-85]. In a recent X-ray study, Lovinger et al[88] found that copolymers with a large VDF content went from a well-ordered all-trans conformation to a paraelectric phase consisting of irregular conformational sequences packed in a disordered pseudohexagonal lattice. Results of Yamada and Kitayama [84] and Lovinger et al [89] showed that the Curie point of VDF/TrFE copolymers increases almost linearly with increasing VDF content in the range of ~ 50-80 mole% VDF. Extrapolation of the transition curve implies that the Curie point for PVDF is about 478 K. In the region where the VDF content less than 37 mole% and more than 80 mole%, the transition temperature was not observable from temperature characteristics of dielectric permittivity. In the case of the latter region , the melting of the polymer intervenes before

the copolymer can complete its ferroelectric transition process. This has been cited as the reason for the absence of a clearly identifiable T_c in PVDF. Another point worth noting is that the dielectric permittivity of the VDF/TrFE copolymers shows a highest value for 55 mole% VDF content, which can reach as high as 60 at the Curie point [83,85].

It has been observed that the remanent polarization (P_r) in VDF/TrFE copolymers is increased as the VDF content is increased, which can reach the value in the region 80-100 $mC.m^{-2}$ for 80 mole% VDF [84,90]. As in the case of homopolymer PVDF, the piezo- and pyroelectric responses in VDF/TrFE copolymers are related to the remanent polarization (P_r) [91,92]. However, unlike PVDF, the poled VDF/TrFE copolymers exhibit a nonlinear relationship between d_{31} and P_r. The relationship between apparent e_{31} and P_r for the latter material on the other hand, shows a linear behaviour and having the same gradient, regardless of VDF content for the undrawn samples [91,92]. Upon drawing, the gradient of the dependency increases by different amounts depending on the composition of the copolymer [90]. This means that other factor may give an additional contribution leading to the observed piezoelectric activity in drawn copolymer samples. Furukawa[90] attributes the piezoelectric activities of ferroelectric polymers to the electrostrictive coupling (as a result of polarization process), as has been accepted in general ferroelectrics [1]. The largest piezo- and pyroelectric activities were found in copolymer with 52 mole% VDF content for the same magnitude of P_r [90]. Indeed a

detailed quantitative treatment on the mechanism of piezoelectric activity in copolymers requires a large volume of data. At present, there still remains uncertainty in determining various contributions to the piezoelectric activity, often due to the complex structures of semicrystalline polymers [90].

From the above summary of polymer structure and morphology and its relation to basic polarization properties, it may be seen that the subject is much under discussion and it is likely that a new finding in this direction will certainly provide a better understanding.

CHAPTER 3

PRINCIPLES OF FERROELECTRICITY AND BASIC POLARIZATION PROCESS

3.1. Polarization Behaviour of Ferroelectrics

Ferroelectrics are materials which posses a spontaneous electric polarizaton (P_s) whose direction can be altered by an application of a suitable electric field [1-3]. The material may be classified from other dielectrics with respect to their electrical polarization, as shown in Table 3.1 [4]. It may be seen that ferroelectrics belong to the pyroelectric family which exhibit permanent value of polarizaton (known as spontaneous polarization), even in the absence of an applied electric field or stress. This spontaneous polarization results from inherent asymmetry within the basic crystal cell which gives rise to ionic and (or) electronic forces that create elemental dipole moments.

The primary property distinguishing ferroelectrics from other pyroelectrics is that the spontaneous polarization can

Table 3.1. Classification of Dielectrics

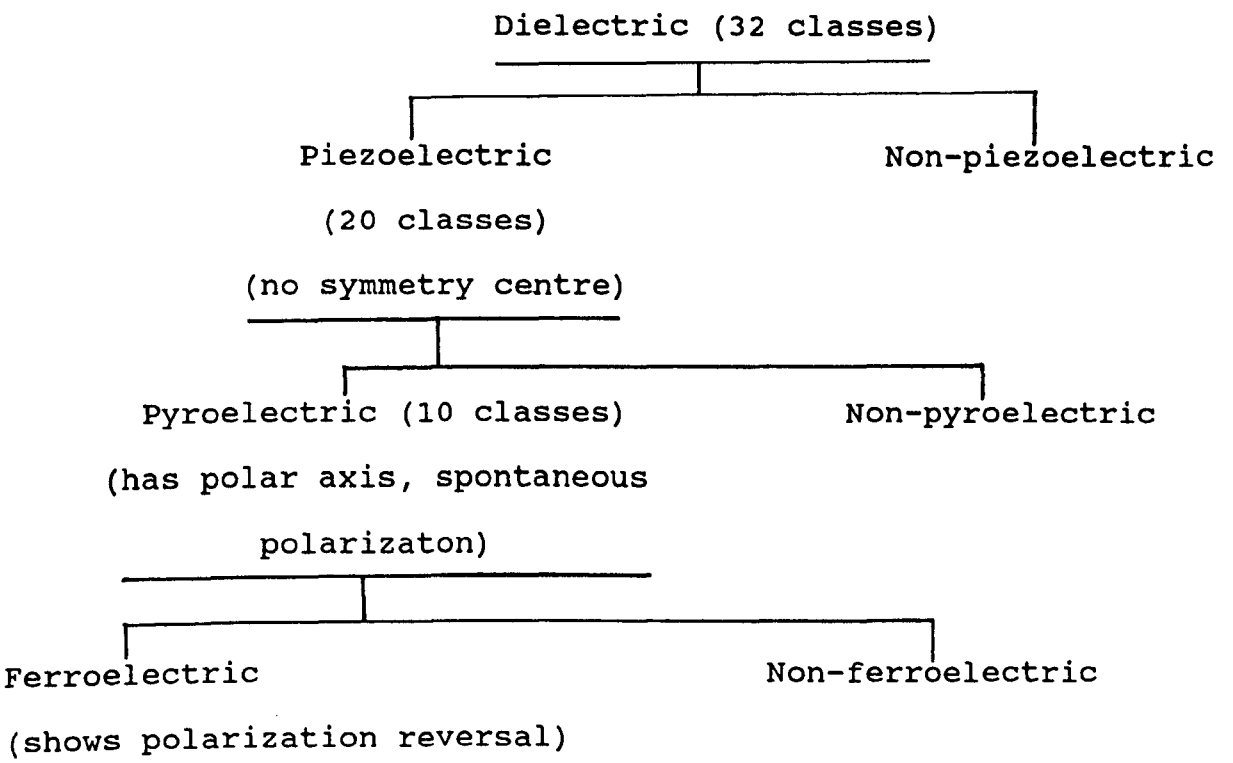

be reversed (at least partially) with an applied electric field. The application of a large alternating voltage to the ferroelectrics results in a non-linear polarizaton (P) change with the electric field (E), giving rise to a hysteresis loop (typically as shown in Fig.1.1), which is a characteristic feature of ferroelectrics. Thus, the term ferroelectric is derived from the analogy with ferromagnetic materials, which exhibits similar hysteresis behaviour for a plot of magnetization (B) against the applied magnetic field (H). Both types of materials also possess domains and show Curie-Weiss behaviour near their phase transition temperatures (as

mentioned in chapter 1).

The hysteresis loop parameters are usually defined by the coercive field (E_c), the remanent polarization (P_r) and the saturation or spontaneous polarization (P_s) (see Fig.1.1). The loop is normally symmetrical about the P and E axes so that $+E_c = -E_c$ and $+P_r = -P_r$. However, mechanical clamping, doping, impurities and radiaton effect (e.g. X-ray, γ-ray, neutron and electron bombardment) of the material can produce asymmetry and distortion in the loop [1,4,5]. The loop parameters depend not only on temperature but also on the measuring frequency. The values of P_r and P_s decrease as the frequency increases. This is primarily due to the basic limitation on the speed at which the domains can switch. The spontaneous polarizaton decreases with the increase of temperature and becomes zero at Curie point (T_c), where the transition to a paraelectric phase occur. The decrease in E_c with temperature is similar to that of P_s , and occurs at about the same rate. The rate at which the decrease of these parameters occur is indicative of the type of phase transition, either first order, second order or diffuse type [4,5]. The anomalous behaviour, in which the permittivity rises sharply to a very high peak, occur at T_c. Above T_c , the permittivity falls according to the Curie-Weiss relation (Eq.(1.1)).

It is of interest to characterize the behaviour of domain switching which give rise to the polarization reversal in ferroelectrics. The study of switching mechanisms normally employs a voltage that has a fast rise time (i.e.pulse) rather

than a slowly rising sine wave signal. A typical applied pulse train of electric field (± E) and the resultant current transients for a ferroelectric is shown in Fig.3.1. It may be observed that the transients caused by the first and third pulses are the full switching transients that occur during a complete reversal of the polarization from $+P_r$ to $-P_r$ or vice versa. There is no switching during the second and fourth pulses since the polarization direction is already in parallel with the applied field. The usual parameters defining the switching current transient are the peak current i_m , the time t_m at which i_m occurs and a switching time t_s , conveniently defined as the time at which i falls to $0.1i_m$. The shape of the switching current as shown in Fig.3.1 describes the full switching process which consists of an initial spike due to the charging of the linear dielectric component followed by a smooth humped curve due to the switching of the non-linear dielectric component [5]. For the switching which occurs with a small number of domains, the switching transient may have more than one peak and shows irregularity rather than smooth [10].

The applied pulse width (t_w) in Fig.3.1 is greater than the switching time (t_s) of ferroelectric. If, however, for a particular value of E, t_w is less than t_s at that value of E, then partial switching will occur. Such process can be schematically described as in Fig.3.2, where the switching is done with narrow pulses of the same polarity [5]. When the pulse width is decreased further, an unstable partial switching is observed [11] in which a certain amount of

polarization reversal occurs at each pulse followed by a relaxation to almost in its initial polarization state as the pulse is completed. Thus a large number of pulses is required to give a stable partial switching. The switching time (t_s) associated with the process has been observed to show either an exponential or power-law dependence of t_s on E. For $BaTiO_3$, the switching time followed an empirical exponential law [6]:

$$t_s \propto \exp(\alpha/E) \tag{3.1}$$

for fields (1-15) x 10^5 $V.m^{-1}$, while at higher fields up to 10^7 $V.m^{-1}$, it follows the power-law [7] :

$$t_s \propto E^{-n} \tag{3.2}$$

where $n \simeq 1.5$ for $BaTiO_3$ [7]. Eq.(3.1) has been experimentally verified for t_s ranging from 10^{-7} to 10^5 sec [5]. The constants α and n and the constant of proportionality are usually temperature dependent. The switching time usually decreases (becomes faster) as the temperature is increased closer to the Curie point [4,5].

The mechanism of polarization reversal may be very complex as there is no universal rule governing all ferroelectrics [4]. The complexity of the problem may be realised from the fact that the observed behaviour can be greatly affected by the nature of the electrodes [1], the nature of the crystal surface, electrical conductivity [8], the domain geometry [9] and the presence of defects [4].

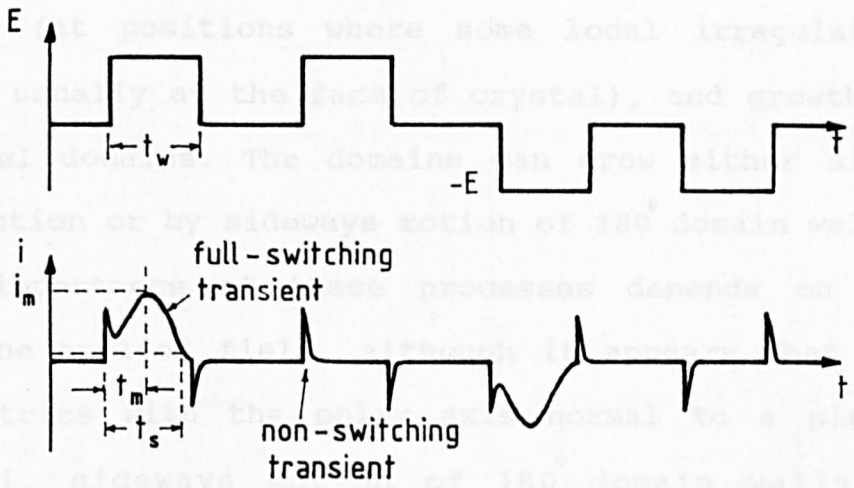

Fig. 3,1. Schematic of applied field pulses and resultant switching current transient observed in a ferroelectric.

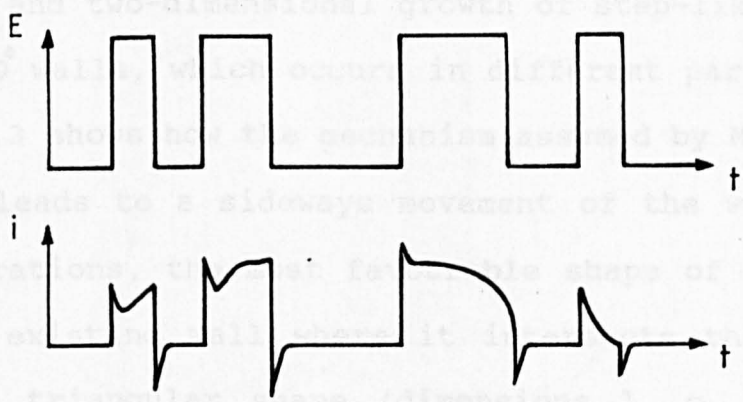

Fig. 3.2. Schematic of applied field pulses (narrow pulse width) and resultant partial switching transients in ferroelectric.

Polarization reversal can be accomplished either by the growth of existing domains antiparallel to the applied field, or by the nucleation (at positions where some local irregularity encourages it, usually at the face of crystal), and growth of new antiparallel domains. The domains can grow either along the polar direction or by sideways motion of 180° domain walls. The relative importance of these processes depends on the material and the applied field, although it appears that for most ferroelectrics with the polar axis normal to a plate-shaped crystal, sideways motion of 180° domain walls is preferred to forward motion [4] (see also chapter 1 for the effect of electric field on domain growth).

Miller[12] showed that complete polarization reversal in $BaTiO_3$ is accomplished by the nucleation of a single domain followed by sideways motion of the 180° domain wall across the entire crystal. Later, Miller and Weinreich [13] suggested a physical model that the observed sideways motion is caused by the nucleation and two-dimensional growth of step-like domains on existing 180° walls, which occurs in different parts of the crystal. Fig.3.3 shows how the mechanism assumed by Miller and Weireich [13] leads to a sideways movement of the wall. From energy considerations, the most favourable shape of a nucleus forming on an existing wall where it intersects the crystal surface is the triangular shape (dimensions 1, c, 2a) , as shown in Fig.3.4 [13,4]. Obviously, the speed of the process would depend on the temperature, impurity concentration of the material and applied field [1,4]. Through the calculation of the free energy involved in the process, the domain wall

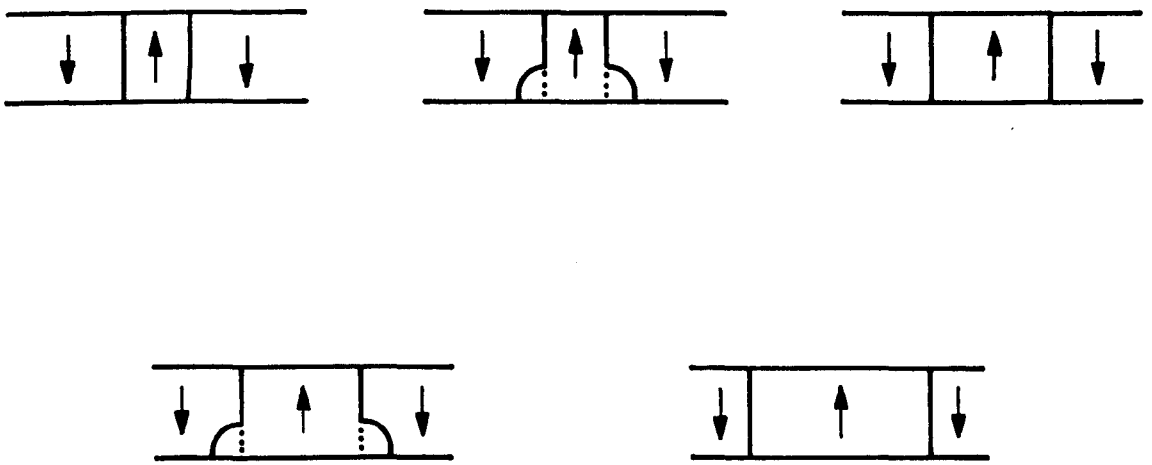

Fig. 3.3. Schematic process of nucleation and domain growth on existing 180° domain wall.

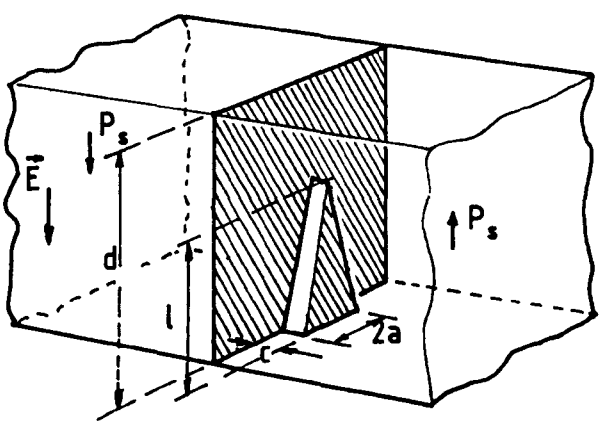

Fig. 3.4. Schematic drawing of a triangular step on a 180° domain wall.

velocity (which is proportional to the rate of nucleation) is given by [1,4]:

$$v = v_{\infty} \exp (- \delta /E) \qquad (3.3)$$

where v_{∞} is a constant and δ is a parameter which is temperature dependent and slightly dependent on E. If the nucleation rate is the rate-controlling process of polarization reversal, then Eq.(3.3) also describes the switching rate $(1/t_s)$, which is in agreement with the experimentally observed dependency of t_s on E (see Eq.(3.1)). The above derivation had been made under the assumption that the triangular step is one unit cell thick (in the low-field region). As the field is increased, however, it is possible that steps of two or more unit cells in thickness begin to form. This would modifies the velocity(v) in Eq.(3.3) through parameter δ , which is found to slightly increase with increasing field [1].

In general it is not obvious whether the wall velocity depends on the nucleation rate or the growth velocity of the steps [4]. Based on Hayashi's results [14,15] the behaviour of the wall velocity may be summarized as follows. At low fields an exponential law of the form as Eq.(3.3) describes the field dependence of the domain-wall velocity and is replaced by a power law at high fields. The value of δ in Eq.(3.3) changes with increasing field so that the transition to the high-field regime is smooth. Physically, this is due to the change of the relative importance of nucleation and sideways growth of

nuclei on the wall. The transition to a power law at high fields is due to the fact that two-dimensional triangular nuclei which are important at low fields cannot nucleate at high fields since the critical dimension in the a-direction (see Fig.3.4) becomes smaller than a lattice constant. Instead, one-dimensional nuclei are formed with their length along the polar axis and these grow in a two-dimensional manner. This explanation of the power-law dependence of domain-wall velocity appears to be more favourable than that suggested earlier (i.e. posibility of the appearance of steps with two or more unit cell in thickness at high field), since for $BaTiO_3$, according to Hayashi[14,15], triangular domains cannot nucleate at fields above 2.5×10^6 $V.m^{-1}$.

Barkhausen pulses are another characteristic feature of ferroelectric materials which appear during the reversal of spontaneous polarization, and consist of 'noise' (or transient current pulses) superimposed onto the displacement current, i.e. onto the switching pulse [1,4]. The term used is in analogy with that observed in ferromagnets by Barkhausen [16]. The pulses are resolved by monitoring the switching current as the polarization is slowly reversed by an electric field slowly increasing in either a smooth or step-like manner. Chynoweth [17] counted typically 10^5-10^6 Barkhausen pulses during complete polarization reversal in $BaTiO_3$. The total charge (i.e. $Q = \int i \, dt$) in the pulses corresponds to only a small fraction (10^{-3} - 10^{-2}) of the total charge switched. The switched charges associated with each pulse increases with crystal thickness and the pulse height increases with

increasing field. The pulse counting rate was found to vary approximately as the switching current so that the total count was field independent. From these observations, Chynoweth[17] concluded that the pulses were associated with the nucleation and forward growth of domains through the thickness of the crystal while the switching current was due to sideways motion of the domains. Miller [12] however, suggested that Barkhausen pulses occured when two growing domains came together giving rapid switching.

The shape of Barkhausen pulses in $BaTiO_3$ have been studied by Rudyak et al[18] who generally observed that the pulses associated with nucleation and forward motion of domains include a greater volume of repolarizing region and have a much sharper leading edge than the pulses associated with domain fusion. The large amount of data which has been collected for a number of materials showed that the number and shape of the pulses vary considerably from one material to another and with the defect content of the crystals [4]. It appears that although the subject of Barkhausen pulses may not be fully understood, it provides a way of studying polarization reversal in ferroelectric materials [1,4].

3.2. General Phenomenological Theories of Ferroelectrics

Phenomenological (or macroscopic) theories in ferroelectrics concern with the treatment of the material as a

continuum without regard to any molecular structure. It serves to describe the thermal, elastic and dielectric properties of the macroscopic system, and the laws of thermodynamics and classical mechanics are used to obtain the relationships between them [4].

It is usually assumed possible to describe a dielectric system by three independent variables, chosen one from the each conjugate pairs :

[temperature(T), entropy(S)]

[stress(X), strain(x)]

[electric field(E), polarization(P)]

where stress and strain are determined by six variables each (i.e. stress and strain tensor), and E and P by three variables each, giving a total of 20 thermodynamic coordinates to describe the system. For simplicity, the dielectric displacement variable (D) is chosen over P due to the fact that it is more accessible macroscopic variable, which can be obtained from : $D = \varepsilon_0 \varepsilon' E$ (chapter 4, Eq.(4.7)).

The most general and useful form for a macroscopic description of the system is an expression for a thermodynamic function consisting of the above variables. These thermodynamic functions are defined only for equilibrium states which apply to quasi-static or reversible processes and does not apply to non-equilibrium conditions which occur, for example, during the switching of a ferroelectric. To describe a thermodynamic function, let us take the first law of

thermodynamics which states that the change in internal energy per unit volume (dU) is given by :

$$dU = dQ + dW \tag{3.4}$$

where dQ is the quantity of heat given to a unit volume of dielectric and dW is the work done on this same volume by electrical (i.e. polarizing) and mechanical (i.e. stress) forces during the quasi-static transformation. Assuming reversibility of the process, the second law of thermodynamics relates dQ to the absolute temperature and entropy in the form: dQ = T dS. The total work done when the dielectric is subjected to an infinitesimal (small amount) change of strain and dielectric displacement in the presence of uniform stress and electric field is given by[4] :

$$dW = X_i \, dx_i + E_i \, dD_i \tag{3.5}$$

where subscript i refers to the components of the variables and the summation applies to the products of each component. Thus, dU can be written as :

$$dU = T \, dS + X_i \, dx_i + E_i \, dD_i \tag{3.6}$$

It may be seen from Eq.(3.6) that appropriate independent variables describing the internal energy U, are S, x_i and D_i , which are called the principle variables for internal energy. The other variables can be calculated by taking the first

derivatives of U :

$$T = (\partial U/\partial S)_{x,D} \quad , \quad X_i = (\partial U/\partial x_i)_{S,D} \quad , \quad E_i = (\partial U/\partial D_i)_{S,x} \tag{3.7}$$

which describe the calorimetric, elastic and dielectric equations of state respectively.

When the conditions of a specific problem or measurement suggest a different set of independent variables, it is convenient to define additional thermodynamic functions (or potentials). The equations of state can then be appropriately defined in a concise manner in accordance to those functions. Since three independent variables can be chosen in eight different ways from among the conjugate pairs (T,S), (X_i,x_i), and (E_i,D_i), this implies eight thermodynamic functions, as given in Table 3.2 [2-4].

The differential forms describing infinitesimal changes in these thermodynamic potentials are, using Eq.(3.6),

$$dA = -S\,dT + X_i\,dx_i + E_i\,dD_i \tag{3.8a}$$

$$dH = T\,dS - x_i\,dX_i - D_i\,dE_i \tag{3.8b}$$

$$dH_1 = T\,dS - x_i\,dX_i + E_i\,dD_i \tag{3.8c}$$

$$dH_2 = T\,dS + X_i\,dx_i - D_i\,dE_i \tag{3.8d}$$

$$dG = -S\,dT - x_i\,dX_i - D_i\,dE_i \tag{3.8e}$$

$$dG_1 = -S\,dT - x_i\,dX_i + E_i\,dD_i \tag{3.8f}$$

$$dG_2 = -S\,dT + X_i\,dx_i - D_i\,dE_i \tag{3.8g}$$

which explicitly indicate the three principle variables for

Table 3.2. Thermodynamic Functions

	Function	Principle Variables
Internal energy	U	S, x_i, D_i
Helmholtz free energy	$A = U-TS$	T, x_i, D_i
Enthalpy	$H = U-X_i x_i-E_i D_i$	S, X_i, E_i
Elastic enthalpy	$H_1 = U-X_i x_i$	S, X_i, D_i
Electric enthalpy	$H_2 = U-E_i D_i$	S, x_i, E_i
Gibbs free energy	$G = U-TS-X_i x_i-E_i D_i$	T, X_i, E_i
Elastic Gibbs energy	$G_1 = U-TS-X_i x_i$	T, X_i, D_i
Electric Gibbs energy	$G_2 = U-TS-E_i D_i$	T, x_i, E_i

each thermodynamic potential. For each thermodynamic potential, Maxwell relations can be generated. For example, from the internal energy equations of state (Eq.(3.7)), the Maxwell relations are :

at fixed D : $$(\partial T/\partial x_i)_{D,S} = (\partial X_i/\partial S)_{D,x} \qquad i=1,\ldots,6 \qquad (3.9)$$

at fixed x : $$(\partial T/\partial D_i)_{x,S} = (\partial E_i/\partial S)_{x,D} \qquad i=1,2,3 \qquad (3.10)$$

at fixed S : $$(\partial X_i/\partial D_j)_{S,x} = (\partial E_j/\partial x_i)_{S,D} \qquad i=1,\ldots,6 \; ; \; j=1,2,3 \qquad (3.11)$$

These types of relations are useful in practice either as a means of checking the internal consistency of two sets of measurements or in deducing the properties of a system subject to a set of constraints which may be difficult or inconvenient to produce experimentally. Some of the relations of this type are used in the related theory of macroscopic pyroelectricity which is given in chapter 6 of this thesis.

In macroscopic theories of ferroelectricity, it is often convenient to take the displacement (D_i), strain (x_i) and temperature (T) as independent variables [4]. The appropriate thermodynamic potential is then the Helmholtz free energy A (see Table 3.2) with the equations of state thus (from Eq.(3.8a)) :

$$-S = (\partial A/\partial T)_{x,D} \; , \quad X_i = (\partial A/\partial x_i)_{T,D} \; , \quad E_i = (\partial A/\partial D_i)_{T,x} \qquad (3.12)$$

From these equations of state, the linear differential form of these equations can be set up, thus :

$$dS = (\partial S/\partial T)_{D,x}\, dT + (\partial S/\partial x_j)_{D,T}\, dx_j + (\partial S/\partial D_j)_{x,T}\, dD_j \qquad (3.13)$$

$$dX_i=(\partial X_i/\partial T)_{D,x}\, dT + (\partial X_i/\partial x_j)_{D,T}\, dx_j + (\partial X_i/\partial D_j)_{x,T}\, dD_j \tag{3.14}$$

$$dE_i=(\partial E_i/\partial T)_{D,x}\, dT + (\partial E_i/\partial x_j)_{D,T}\, dx_j + (\partial E_i/\partial D_j)_{x,T}\, dD_j \tag{3.15}$$

where the coefficients in these equations provide a measure of the coupling between respective variables and are called compliances. Other compliances can be derived using the other thermodynamic potentials. Among the more important compliances are : elastic (stress to strain), permittivity (displacement to electric field), piezoelectric (stress or strain to displacement or electric field), pyroelectric (displacement to temperature) and thermal expansion (strain to temperature).

In the case of isothermal process, the linear equations of Eq. (3.14) and (3.15) can be written in conventional symbols as :

$$dX_i = c_{ij}^{D,T}\, dx_j - h_{ij}^{T*}\, dD_j \tag{3.16}$$

$$dE_i = -h_{ij}^{T}\, dx_j + \beta_{ij}^{x,T}\, dD_j \tag{3.17}$$

in which $h_{ij}^{*} \equiv h_{ji}$,

$$c_{ij}^{D,T} = (\partial X_i/\partial x_j)_{D,T} = (\partial^2 A/(\partial x_i\, \partial x_j))_{D,T} \tag{3.18}$$

is the isothermal elastic stiffness at fixed displacement,

$$\kappa_{ij}^{x,T} = (\partial E_i/\partial D_j)_{x,T} = (\partial^2 A/(\partial D_i \partial D_j))_{x,T} \qquad (3.19)$$

is the inverse isothermal permittivity at fixed strain and

$$h_{ij}^{T*} = -(\partial x_i/\partial D_j)_{x,T} = -(\partial E_j/\partial x_i)_{D,T}$$

$$= -(\partial^2 A/(\partial x_i \partial D_j))_T \qquad (3.20)$$

is an isothermal linear piezoelectric compliance. In a similar way, the other linear equations can be derived (either isothermally (dT=0) or adiabatically (dS=0)) by used of the other thermodynamic potentials. Some of these equations are (omitting T superscripts) :

$$dx_i = s_{ij}^{D}\, dX_j + g_{ij}^{*}\, dD_j \qquad (3.21)$$

$$dE_i = -g_{ij}\, dX_j + \kappa_{ij}^{X}\, dD_j \qquad (3.22)$$

$$dx_i = s_{ij}^{E}\, dX_j + d_{ij}^{*}\, dE_j \qquad (3.23)$$

$$dD_i = d_{ij}\, dX_j + \varepsilon_{ij}^{X}\, dE_j \qquad (3.24)$$

$$dX_i = c_{ij}^{E}\, dx_j - e_{ij}^{*}\, dE_j \qquad (3.25)$$

$$dD_i = e_{ij}\, dx_j + \varepsilon_{ij}^{x}\, dE_j \qquad (3.26)$$

where ε_{ij} : the dielectric permittivity

d_{ij} , e_{ij} , g_{ij} : the piezoelectric compliances

s_{ij} : elastic compliances

It may be observed that Eqs.(3.16),(3.17),(3.21)-(3.26) can be used to describe how the dielectric displacement (D) and the deformation (x) are induced by the application of electric field (E) and of external force (X) under isothermal condition. Therefore, the coefficients which appear in these equations are closely inter-related. For example by the substitution of Eq.(3.24) into Eq.(3.21), we get :

$$dx_i = s_{ij}^{D}\, dX_j + g_{ij}^{*}\, (d_{jk}\, dX_k + \varepsilon_{jk}^{X}\, dE_k)$$

$$=(s_{ij}^{D} + g_{ik}^{*}\, d_{kj})\, dX_j + g_{ik}\, \varepsilon_{kj}^{X}\, dE_j$$

and by comparing this equation with Eq.(3.23), we have :

$$s_{ij}^{E} = s_{ij}^{D} + g_{ik}^{*}\, d_{kj} \qquad (3.27)$$

and $$d_{ij}^{*} = g_{ik}\, \varepsilon_{kj}^{X} \qquad (3.28)$$

In a similar manner, the relations for the other coefficients can be obtained.

In ferroelectrics, the situation is more complex since

some of the most important characteristics of their properties (e.g. hysteresis loops) are non-linear and hence require an extension of the theory to higher orders. This means that the linear differential equations of the form such as Eqs.(3.13)-(3.15) need to be extended to higher orders in order to account for non-linear compliances. In practice, it is generally difficult to proceed in a fully consistent manner to higher orders, partly due to the complex nature of high rank tensors [4]. For example, an expansion of Helmholtz free energy (A) to third order may have the following terms [4] :

$$D_iD_jD_k\ (3),\ D_iD_jx_k\ (4),\ D_ix_jx_k\ (5),\ x_ix_jx_k\ (6) \qquad (3.29)$$

where the figures in bracket indicate that the coefficients of such terms in the Taylor expansion of free energy are tensors of rank 3, 4, 5 and 6 respectively. It is generally quite difficult to investigate the symmetry (lattice structure) restrictions imposed on tensors of high rank and simplification is often accomplished in non-linear theory by making use of a physical approximation (assumption) [4].

In describing the macroscopic anomalies of ferroelectric, Lines and Glass [4] assumed that the elastic Gibbs function (G_1) can be expressed in a very simple polynomial form, thus :

$$G_1 = (\alpha/2)\ D^2 + (\gamma/4)\ D^4 + (\delta/6)\ D^6 \qquad (3.30)$$

which can be used above and below the phase transition

anomaly. It is assumed that D is directed along one of the crystallographic axes only (i.e. spontaneous polarization occurs along this direction and the applied field is restricted to this direction also), that all stresses are zero and that the non-polar phase is centrosymmetric. The coefficients α, τ, δ are in general temperature dependent. The dielectric equation of state can be obtained by differentiating Eq.(3.30) with respect to D at constant temperature, thus :

$$E = \alpha D + \tau D^3 + \delta D^5 \qquad (3.31)$$

where E is parallel to D. By assuming that near the Curie point (T_c) , the parameter α depends on temperature in the linear fashion as :

$$\alpha = \beta (T - T_c) \qquad (3.32)$$

with β a positive constant ; it can be shown from Eq.(3.31) that (at E=0 , D=P_s) :

$$P_s^2 = \beta (T_c - T)/\tau \qquad (3.33)$$

also, the isothermal reciprocal permittivity ($\kappa = \partial E/\partial D$) below T_c :

$$\kappa^{X,T} = \beta (T - T_C) + 3 \gamma P_S^2$$

$$= 2 \beta (T_C - T) \quad , T < T_C \qquad (3.34)$$

Using Eqs.(3.33) and (3.34) , it can be sketched qualitatively that the P_S vs. T and $\kappa^{X,T}$ vs. T exhibit a second order ferroelectric transition near T_C .

In a similar manner , the nature of the transition for entropy and specific heat near T_C can be derived [4]. The continuous nature of the first derivatives of the free energy (e.g. P_S and S) and the discontinuous nature of second derivatives (e.g. specific heat : $c = T(\partial S/\partial T)$) conform with the normal definition of a second order phase transition. It is thus clear that the phenomenological picture is at least qualitatively able to describe transitions of this nature. The more elaborate theory concerning the so-called critical phenomena which occur very close to a second-order phase transition is given by Lines and Glass [4]. By taking an appropriate thermodynamic function and dielectric equation of state, phenomenological theories have also been found to qualitatively describe the nature of the first order transition [4].

In practice, the theory proves to be very useful for characterizing materials. The parameters β , γ and δ can be appropriately determined from dielectric and thermal measurements close to T_C [4] and hence P_S can be estimated. However, with increasing $|T-T_C|$, the need for a longer series expansion than that of the type of Eq.(3.30) and for

temperature-dependent parameters becomes increasingly apparent [4].

It appears that the basic strength of the thermodynamic theory of ferroelectricity is its mathematical simplicity and corresponding use in correlating the different macroscopic parameters of ferroelectrics. Its limitations are the purely macroscopic picture (which disregard any discussion on atomic or molecular basis or on the microscopic scale of the transition) and the restriction to equilibrium phenomena.

3.3. Polarizability and Basic Polarization Process

It is practicable to study a model of polarized dielectric in terms of units which may posses charge (q) and (or) electric moments (e.g. dipole moment). However, the properties of a unit can not be measured independently, and the environment of a unit is largely created by the other units. It is therefore difficult to select a suitable unit. A simple choice of unit might sometimes be the atoms or molecules.

In a strong ionic crystal, the binding between ions is by electrostatic forces (i.e. attraction force between charges of opposite sign) which provide the cohesion in the materials. It may be a sufficiently good approximation, in such a crystal, to use a carefully chosen point model (characterized by only charge and dipole moment). However in most

ferroelectrics, the crystals are partly covalent (i.e. the bond between atoms is by shared electron pair with the bonds are stronly directional, and each atom makes only a limited number of bonds), and only partly ionic [2]. As such the point model may not be exactly fit for this type of crystals. If a charge-density distribution in a material can be conveniently represented by fictional distributions of point charges, it is possible to divide the crystals into volume elements with each volume element represent by a point dipole charge. The dipole moment (m_i) of each volume element for a system of point dipole charges may be defined as :

$$m_i = q\, r_i \tag{3.35}$$

where r_i is a distance between charges +q and -q.

From Eq.(3.35), it may be inferred that a polarizable unit acquires an induced dipole moment (m_i) in a local field E_{Li} (note : the field differs from place to place), depending on the polarizability (α_i) of the unit. Thus, assuming a linear proportionality of m_i with respect to E_{Li} and m_i is parallel to E_{Li}, then :

$$\alpha_i = m_i/E_{Li} \tag{3.36}$$

It is difficult to calculate the effect of the surrounding units on the central unit (an atom or molecule). For simplification, the surrounding units are replaced by a continuum whose polarization is P. The effect of that

continuum on the unit under consideration can be represented by a contribution to the local field acting on the unit. Assuming that contribution is proportional to the polarization P, the local electric field can be written as :

$$E_L = E + \beta P \tag{3.37}$$

where E is the applied electric field and the β term represents electric interaction between the units. Following the model adopted by Lorentz and assuming a simple cubic lattices of the molecules with identical point dipoles, the value of β is determined to be $1/3\varepsilon_o$ [20,21]. By substituting this value of β and for P (chapter 4, Eq.(4.6)) into Eq.(3.37), thus :

$$E_L = (\varepsilon' + 2)E/3 \tag{3.38}$$

For a cubic lattice which has unidentical point dipoles such as that of $BaTiO_3$, the β factor varies from site to site in the lattice [2]. As mentioned in chapter 2, $BaTiO_3$ consists of strings of titanium and oxygen ions which lie in the direction of the polarization. Slater [19] showed that the β factor for the interaction between these ions is greater than any other ions which implied that the strings of titanium and oxygen in the direction of the polarization tend to become more polarized than the other ions in the lattice. Thus the local field varies strongly within the unit crystal cell.

In ferroelectric materials, units may posses both

permanent and induced dipole moments. Thus, polarization (P) in Eq.(3.37) may arise from both the polarizability of the material in the presence of a field (i.e.P_E) and from the spontaneous alignment of permanent dipoles. Assuming the dielectric medium is isotropic, we have from Eq.(3.36), the total P_E :

$$P_E = N_o \alpha E_L \tag{3.39}$$

where N_o: number of polarizable units per unit volume, $N_o = N_A \rho / M$, N_A : Avogadro's number, ρ the density, M the molecular weight of the material and α the polarizability of each polarizable unit . The principle sources of polarizability may be of the following types [20,21] :

α_e - electronic polarizability, due to the movement of the electron charge cloud relative to the nucleus of the atom.

α_a - atomic (ionic) polarizability, due to the displacement of the atomic nuclei relative to one another and the accompanying displacements of their electron clouds. In an ionic crystal, apart from the ions being polarized individually, the negative and positive ions will be displaced with respect to each other, leading to the effect of ionic polarization.

α_c - due to localized charge movements in ionic materials and to the rotation of dipoles in polar covalent solids.

α_b - due to interfacial polarization through the

presence of a second phase.

α_e gives rise to resonant frequencies at the 10^{15} Hz level, as evident in optical spectra, in which range all the other sources of polarizability are clamped. At low frequencies, this optical effect is constant and accounts for a part of the dielectric permittivity.

The ionic polarizability has a characteristic resonant frequency in the 10^{13} Hz region and are responsible for the absorption of infrared radiation. The value of α_a differs from atom to atom, typically in the range (0.04-5.31) x 10^{-40} $F.m^2$ [22]. As for electronic polarizability, there is only a small contribution to the loss from α_a below 10^{11} Hz. The electronic polarizability is insensitive to temperature and pressure (due to large binding force between electron and nucleus), whereas by contrast, ionic polarizability depends on the lattice bonds, which are very much affected by temperature changes. In the case of molecular solids, the force constants for bending or twisting of molecules (as inferred from vibrational spectroscopy), involving changes in angles between bonds, are generally much lower than those for bond stretching, so that bending modes are expected to make major contribution to atomic polarization [20,21].

Limited motion of charge carriers occurs by the mechanism known as 'hopping' by which a trapped electron may have a finite probability of moving from one site to another site without entering the conduction band. There is an energy barrier between these localized states (i.e. due to impurities or defects) which determines the rate at which transitions may

occur between them. An electric field applied across the sites, alters the energy of the charge residing in such trap sites and alters the transition rates in the two direction. The process is thermally activated, and its effect on the permittivity will depend on the concentration of defects and the local field. In some cases (where the applied electrical energy is small compared with thermal energy kT), the effect may be similar to dipolar rotation in solids containing rotatable dipoles [22]. For a high concentration of defects and (or) a high probability of hopping events, there will be a continuous flow of current rather than a limited oscillation between sites. The contribution of this process to the permittivity is generally small.

Some considerations on interfacial polarization and orientational (dipolar) polarization will be given in the next chapter.

Generally, materials which posses permanent dipoles are referred to as order-disorder type while those exhibit induced dipoles, as displacive type, in macroscopic terms. At T_c, the dipoles disappear in displacive type material (e.g. $PbTiO_3$); in the order-disorder type (which are only found when molecular groups appear in the structure, e.g. TGS), the dipoles continue to exist, but are now completely disordered in orientation, so that the overall polarization is zero. In actual situation, the distinction between order-disorder and displacive types can not be generallized and is more complicated, for which the distinction is perhaps better not made at all [4].

In the case of permanent molecular dipole orientation, an estimate of the magnitude of the average molecular moment ($\bar{m}$) in the direction of an applied electric field is given by [21] :

$$\bar{m} \simeq (m^2 E_L)/ 3kT \qquad (3.40)$$

where m is the permanent moment of each dipole and provided that $mE_L << kT$. Consequently, the polarization (P_D) due to dipolar orientation is thus :

$$P_D \simeq (N_o m^2 E_L)/3kT \qquad (3.41)$$

The quantity $m^2/3kT$ can be considered as an orientational polarizability, which adds to the normal deformational polarizability (α, consisting of α_e and α_a) to give a total effective polarizability (α_T) ; thus, neglecting the effect of α_b , we have :

$$\alpha_T = \alpha + m^2/3kT \qquad (3.42)$$

The Eq.(3.41) is only approximate and only valid for a system of free dipoles. Thus it may not be accurately applicable to a solid system, since the direction of orientation of dipole moments is related to crystal symmetry [21].

Thus, in approximation, for a dielectric system containing dipoles, the total polarization can be written as :

$$P \simeq N_o \alpha_T E_L \qquad (3.43)$$

or, assuming E_L is given by Eq.(3.38), thus :

$$P \simeq N_o \alpha_T (\varepsilon' + 2)E/3 \qquad (3.44)$$

From a well-known electrostatic relation (see chapter 4), the polarization may also be written as : $P = (\varepsilon' - 1)\ \varepsilon_o E$,where ε' is the relative permittivity of the medium and E the applied electric field. Hence, it can be derived that :

$$\varepsilon' - 1 = (N_o \alpha_T E_L)/(\varepsilon_o E) \qquad (3.45)$$

from which the macroscopic parameter (permittivity) may be related to the molecular quantities such as the polarizability (α_T) if the relationship between the microscopic local field (E_L) and the macroscopic field (E) could be appropriately determined.

Assuming the E_L-E relationship is given by Eq.(3.38), then Eq.(3.45) becomes :

$$\varepsilon' - 1 = [N_o \alpha_T (\varepsilon' + 2)]/3\ \varepsilon_o$$

(Clausius-Mosotti-Lorentz (CML) relation)

or after rearranging, we obtain :

$$\varepsilon' - 1 = (N_o \alpha_T / \varepsilon_o)/[1 - (N_o \alpha_T)/3\ \varepsilon_o] \qquad (3.46)$$

Eq.(3.46) predicts that as the dipole density of the material (N_o) approaches the value of $N_o = 3\ \varepsilon_o / \alpha_T$, then the permittivity becomes infinite. The implication is that at a finite density of the material, the polarization becomes infinite so that the molecular dipoles may spontaneously align themselves parallel to each other, even in a small applied field.

The other way of looking at Eq.(3.46) is that if lowering the temperature eventually allows the polarization to increase (through the increase of α_T) to such an extent, then at certain temperature by which $\alpha_T = 3\ \varepsilon_o/N_o$, the permittivity (and hence polarization) becomes infinite, giving the spontaneous polarization to appear in the crystal below that critical temperature. This is basically a ferroelectric effect which occurs in some crystalline materials, but the effect has not been observed in some other dielectric materials, which means that the CML relation may not be considered to be completely valid.

With the above restriction in mind, the CML relation can be used at low or high frequencies as follows. If a dielectric material exhibits a dispersion due to dipolar relaxation (see chapter 5), then the low frequency permittivity (ε_s) is given by (from CML relation) :

$$3(\varepsilon_s-1)/(\varepsilon_s+2) = N_o\ \alpha_T/\varepsilon_o \qquad (3.47)$$

At the high frequency side of the dipolar dispersion, the

corresponding permittivity (i.e. ε_∞) is given by (dipole orientation does not contribute) :

$$3(\varepsilon_\infty-1)/(\varepsilon_\infty+2) = N_o \alpha/\varepsilon_o \qquad (3.48)$$

where α_T and α are related by Eq.(3.42). By subtracting Eq.(3.48) from (3.47), we obtain :

$$\varepsilon_s - \varepsilon_\infty = \frac{(\varepsilon_s + 2)(\varepsilon_\infty + 2)N_o m^2}{27\ \varepsilon_o kT} \qquad (3.49)$$

which may be used to calculate the dipole moment for gases, dilute solutions of polar molecules in non-polar solvents and pure liquids of low polarity, from measurements of the dielectric dispersion [23,24].

Onsager provided an improved formula in the calculation of the local field at a molecule by taking a spherical cavity in the dielectric which is just large enough to accomodate one molecule [21]. The molecular dipole is supposed to be a point dipole, having a dipole moment m, located at the centre of the sphere. The local field (E_L) operating on the molecule could be resolved into two components (G and R) as : $E_L = G + R$, where G is the cavity field which is defined as that present at the centre if the molecule has its dipole moment removed in the presence of the applied field. The reaction field (R) is defined as the field at the centre of the cavity due to the polarization of the material external to the cavity caused by the molecule inside the cavity if the dipole moment is

restored to that molecule. This reaction field has no orienting effect on the molecule since it is always in parallel to the dipole moment (m) . It is this fact which has not been considered in the derivation of the local field which leads to the CML relation [21]. Using the local field from Onsager's model , it is shown that [23,24] :

$$\varepsilon_s - \varepsilon_\infty = \frac{\varepsilon_s(\varepsilon_\infty + 2)^2 N_o m^2}{(2\varepsilon_s + \varepsilon_\infty) 9\varepsilon_o kT} \qquad (3.50)$$

This relation is an improvement over that of Eq.(3.49) and successfully describes the behaviour of many fluids. However, it is still inadequate to interpret the dielectric properties of substances like water and many solids [21,23]. This drawback is related to the assumption used in the models that no correlations occur between the polar molecules.

Kirkwood and Frohlich improved the treatment to account for the effect of local ordering (such as directional interaction between the molecules) by introducing the correlation factor g (the value of g is determined by the number and orientation of the nearest polar neighbours to the group considered) so that m^2 is replaced by gm^2 in Eq.(3.50) [21]. It appears that the factor g for solid (e.g. solid bulk polymers) has not been determined whereas the values for many polymers in solid solution have been found to lie in the range 0.53-0.82 [25].

Further treatment on the polarization process will be given in chapters 4 and 5.

CHAPTER 4

ELECTRICAL CONDUCTION AND ASSOCIATED PROCESSES IN CERAMIC/POLYMER COMPOSITES

4.1. Introduction.

It is generally known that the electrical conductivity of the material depends on its physical nature, the purity and on the treatment they received. As such the level of conductivity might differ from sample to sample of the material which undergoes through different processing. However, the behaviour of its electrical conductivity could possibly be analysed in terms of a particular mechanism which is responsible for the observed characteristic. When a static electric field is applied to a sample of dielectric (a substance whose basic electrical property is polarization), the resulting current rises steeply then steadily decreases until a steady state value is reached. The resistivity of a dielectric is normally defined at the steady state level, and

its magnitude depends on the temperature. The decaying component of the flowing current which is sometime referred to as absorption current, is time, temperature and field dependent and involves many different processes. Removing the external field causes a time dependent current flow in the opposite direction (sometime called the resorption current). Generally, the absorption and resorption currents, I(t), have been observed to follow a relationship as:

$$I(t) = B(T)\ t^{-n} \qquad (4.1)$$

where B(T) is a temperature dependent factor, t is the time after application or removal of the field and n is a constant.

The origin of these dielectric absorption and resorption currents is still the subject of much controversy in the literature and a number of responsible mechanisms have been proposed. These include dipolar relaxation, charge injection leading to trapped space charge, hopping of charge carriers through localised sites, electrode polarization, interfacial polarization, bulk polarization and tunnelling process. It follows that a systematic study needs to be carried out by varying parameters (temperature, field strength, time, sample thickness, electrode material and thermal as well as electrical treatment) so that the origin of conduction processes in a particular material could be understood.

Das-Gupta and Joyner [1] in their study on the absorption currents in polyethylene terephthalate (PET) attributed the observed relaxation at low temperatures (80 -

273 K) as due to dipolar process while at high temperatures (above 273 K), it is assigned for either space charge accumulating at the crystalline-amorphous interfaces or to charge carrier hopping between localised states. Hanscomb and Kaahwa [2] also observed the dipolar relaxation in PET from the microsecond to millisecond range of transient current decay at temperatures < 413 K for fields strength up to $2x10^8$ V m^{-1}. As regard the steady state conduction, Sacher [3] concludes that the observed current after sample had been dried and annealed, may originate from ionic conduction while those conditioned in a dc field at elevated temperature showed electronic conduction. On the other hand, Taylor and Lewis [4] observed electronic conduction in unconditioned samples as well as conditioned ones which suggests that the trend proposed by Sacher[3] may not be always true.

Dipolar relaxation process has also been observed from current transient in PVDF at temperatures < 268 K [5]. In addition, another relaxation occurs at 10^{-5} Hz at 348 K which has been attributed to a space charge relaxation process [5]. On the other hand, Kaura and Nath [6] have observed the peak in the current transient curve and it had been attributed to the space charge injection with subsequent trapping in the bulk of PVDF (presumably at the crystalline-amorphous interface). Further analysis of steady state current at 303 K showed that its behaviour is governed by space charge limited conduction (obeying square law in current-voltage characteristics) [6]. Das-Gupta et al [5] however suggested that an ionic conduction is dominant at high fields and high

temperatures whereas space charge mechanism is probable at ambient temperatures. It seems clear that the understanding of the process involved is not satisfactorily resolved, and thus more systematic experimental work is needed in this respect.

As regard polycrystalline ceramic, the observed behaviour of its electrical conductivity is greatly governed by its chemical composition variation (including added impurities), which in most cases is quite complex. In addition, its microstructure (domain walls, crystallite size, grain boundaries) has also a great effect on the total conductivity of the material [7]. Most of the undoped PZT ceramics were reported to have p-type conductivity, which presumably is attributed to the holes in the oxygen valence band. With the addition of higher valence impurities than the host cations (e.g. Pb^{2+}), such as of Bi^{3+} or La^{3+}, the resistivity of the ceramic tends to increase by orders of magnitude. Furthermore, these doped PZT ceramics usually have sharp dielectric anomalies, lower coercive fields, smaller ageing effects and greater dielectric and acoustic loss. Some of these effects allow efficient poling to be achieved [7] and hence it is not surprising that marketed PZT ceramics would contain some added impurities. Similar situations are also found in $BaTiO_3$ ceramics [8]. Since these higher valence impurities occupy the lower valence site of substituted host ions, they therefore have donor properties, although the compensation of surplus charge is affected by vacant sites in the cation lattice [9]. Thus it appears that ionic impurities play a significant role in charge conduction of these

materials. However the interpretation of the ionic conduction in ceramics becomes further complicated in the complex ceramic (ceramic containing more than one additive type), which appears to be the latest trend of the ceramic products for ferroelectric applications [10].

Unlike the polymers, in which the decay of current after field application will take very long time to reach steady state, the absorption current in ceramic occur at relatively short duration of times which then give way to a steady state conduction. This is understandably related to its chemical and physical nature as have been mentioned previously. Ceramic/polymer composites constitute a new physical structure combining the two phases which is different in several respects from their single phases. It is therefore important to study its electrical conduction in order to know the contributing factors related to its use in device applications.

This chapter initially deals with the related theories of the electrical conduction mechanisms in solid dielectric which may be applied to the present study. Experimental details (apparatus, sample preparation and measurement procedure) are treated in separate section followed by the experimental results obtained and the discussion. Most of the results were obtained on 'PIEZEL', a piezoelectric ceramic/polymer composite, supplied by Daikin Industries Ltd of Japan. Results of the conductivity studies of the ceramic/polymer composites with different types of ceramic and polymer, prepared in the present work, are also given.

4.2. Related Theory

The degree to which a dielectric responds to an applied electric field could be most easily realised in the case of a parallel plate capacitor in which the dielectric is sandwitched between the two parallel metal electrodes. In a simple case (assuming negligible edge effects), the magnitude of electric field being produced between the electrodes is given by:

$$E = V / L \qquad (4.2)$$

where V is the applied voltage and L is the thickness of the dielectric. Following the application of electric field, the charges (electrons, ions and dipoles) in the dielectric will be redistributed under the action of electrostatic law, negative charges being attracted towards the positive electrode and vice versa; hence the material is polarized to some extent. This polarization would induce additional charge at the electrodes giving the total charge Q′ per unit area:

$$Q' = Q_o + P \qquad (4.3)$$

where Q_o is the charge per unit area for a vacuum dielectric and P is the polarization charge per unit area. It is always of interest to define the vacuum capacitance C_o as :

$$C_o = Q_o / V \qquad (4.4)$$

and the relative permittivity ε' as :

$$\varepsilon' = C' / C_o = (Q_o + P) / Q_o \qquad (4.5)$$

where C' is capacitance which is associated with the charge Q'. The value of ε' depends on the type of materials, and it is a measure of the amount of the polarization which occurs in the materials. By substituting $Q_o = \varepsilon_o E$ (from Coulomb's Law) in equation(4.5) the polarization can be expressed as :

$$P = (\varepsilon' - 1) \varepsilon_o E \qquad (4.6)$$

where ε_o is the permittivity of free space and the quantity $\varepsilon_o \varepsilon' E$ is called the dielectric displacement D in the material:

$$D = \varepsilon_o \varepsilon' E = \varepsilon_o E + P \qquad (4.7)$$

The above treatment is based on the simplified model, in which the dielectric medium is considered to be uniformly polarized in the applied field. Indeed many other effects (such as electrode polarization and interfacial polarization) would couple with the aforementioned mechanism which then may lead to the observed behaviour of the measured properties.

4.2.1. Electrode Polarization Effect

The existence of electrode polarization at electrode-dielectric interface could be realised by comparing it with well established p-n junction structure of semiconductor device. In both cases, there exist a charge distribution of some form near the interface, depending on the nature of its formation. In case of metal-dielectric interface formed by vacuum evaporation, it is normally thought to be a blocking contact at low and intermediate field strength, thus preventing the transfer of charge carriers from the electrode into the dielectric while it might accept carriers from the dielectric [12]. This type of interface could be distinguished from neutral contact and ohmic or injecting contact, which are usually present at the metal-dielectric interface, as presented in Fig.4.1 [13]. Blocking contact occurs when metal work function ψ_m is greater than dielectric work function ψ_d. In this case, in order to satisfy the thermal equilibrium requirement, charges may flow from the dielectric into the electrode, creating a space charge region W_o in the dielectric, adjacent to the interface. As a consequence, an equal number of charges but with opposite sign will reside on the metal electrode, thus establishing an internal field between the opposite charges at the interface.

When a dc electric field is applied to such metal-dielectric-metal with blocking contact, the charge carriers in the dielectric will be polarized and move towards the electrodes of opposite polarity and eventually a build up of

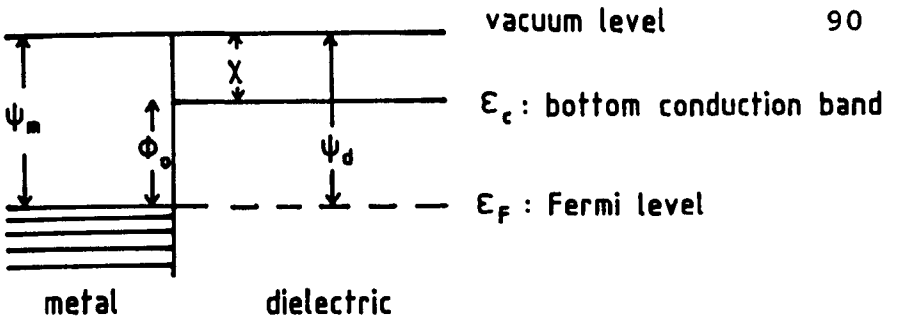

(a) neutral contact : $\psi_m = \psi_d$

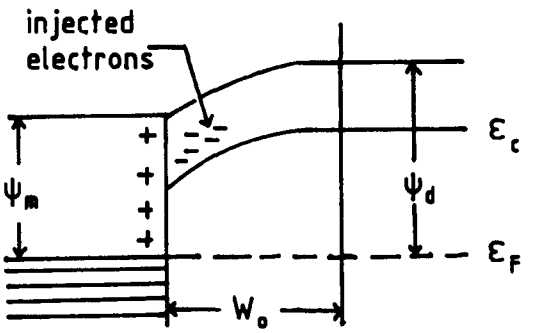

(b) ohmic or injecting contact : $\psi_m < \psi_d$

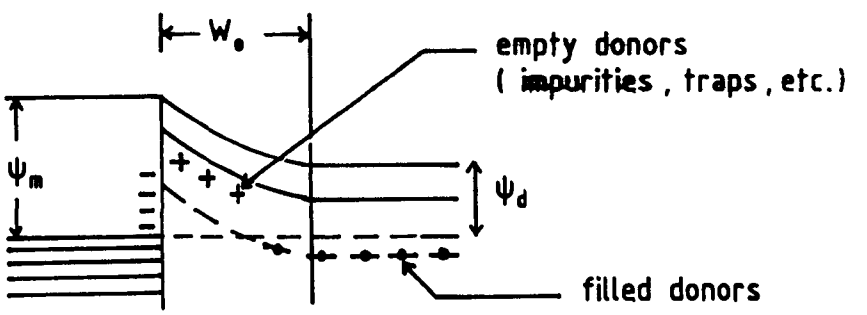

(c) blocking contact : $\psi_m > \psi_d$

W_o = space charge region ψ_m = metal work function
χ = electron affinity ψ_d = dielectric work function
Φ_o = interfacial barrier (= $\psi_m - \chi$)

Fig. 4.1. Energy diagrams of various metal-dielectric systems having different contacts.

charges will appear near the interfaces. It appears that the polarization field will be established across the dielectric in the opposite direction to that of the applied field, thus causing a distortion of potential which would effectively lead to a reduction of the field in the bulk of the dielectric. Such a mechanism is known as electrode polarization, which had been proposed to account for the observed absorption current in the dielectric [14,15].

Macdonald [16], in an attempt to account for the electrode polarization effect under the ac field, theoretically derived the admittance of the dielectric material having blocking contacts. The treatment applies for any degree of dissociation and recombination and with different mobilities of charge carrier. Although the derivation is generally applicable to any material which contains mobile carriers of any kind such as electrons, positive holes, positive ions (including donors), negative ions (including acceptors) or positive or negative ion vacancies, the final expression for capacitance and conductance are very complicated. Even the reduction of the expression for special cases still involves some assumptions and arbitrary parameters; thus it may not be worthwhile of further consideration in the present analysis.

Later, Macdonald [17] derived a normalized interface current in response to a step function of voltage of the system having blocking contacts, thus :

$$I_{iN} = \frac{\exp(-t/\tau_D)}{r-1}\left[\frac{M}{(t/\tau_D)^{1/2}}\left\{1+2\sum_{n=1}^{\infty}\exp\left(\frac{-n^2M^2}{t/\tau_D}\right)\right\}- 1\right] \qquad (4.8)$$

where τ_D is the dielectric relaxation time of the medium, the parameter r related to M as : $r = M \coth(M)$, $M = L / 2L_D$, L_D is the Debye length (i.e. the average distance an excess carrier must travel to establish space charge neutrality). From the plot of I vs. $(t/\tau_D)^{1/2}$ (see Fig.4.2) for $M=10^3$, the most part of the curve ($(t/\tau_D)^{1/2} < 0.1$) is found to be closely proportional to $t^{-1/2}$. The use of $M > 10^3$ does not give any significant difference from that of $M = 10^3$, thus this value of M is about the limit for a good $t^{-1/2}$ dependence of the current. The method of analysis had been extended for the system which has only one blocking contact whilst the other contact is free to discharge. The result obtained also showed similar dependence of current on time as in the previous case but its dependence may extend over longer period in practical situations. Such current behaviour which shows $t^{-1/2}$ dependence has also been found experimentally in several dielectric materials [18,19]. It should be mentioned, however, that it seems difficult to interpret the observed experimental result either in favour of the system with single blocking contact or in favour of dual blocking contacts system since the electrode polarization process also showed a very strong temperature dependence [16,17]. This is understandably due to the fact that the charge carriers concentration and its

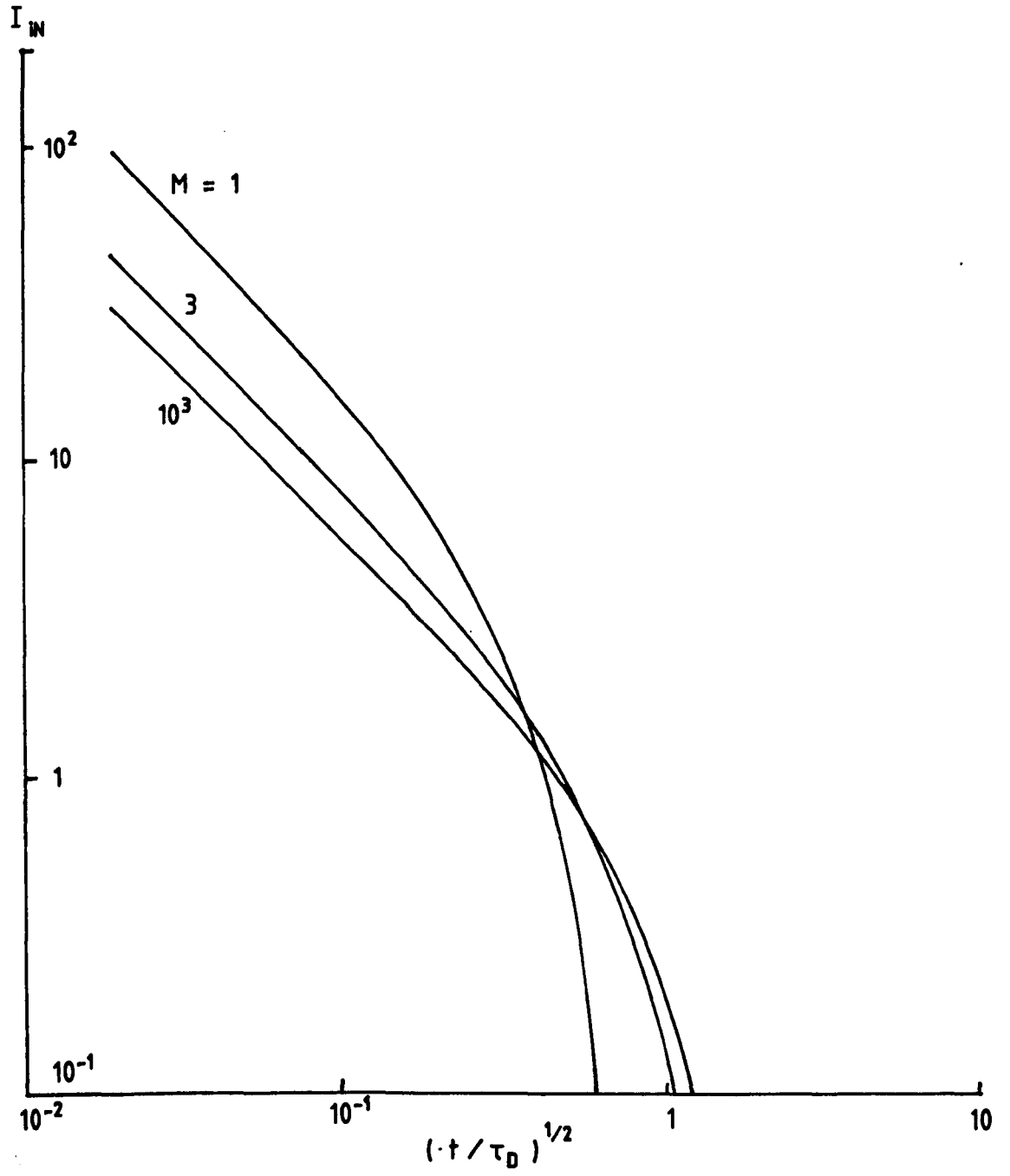

Fig. 4.2. The normalised interface charging current in response to a step function of applied potential vs. $(t/\tau_D)^{1/2}$ for dielectric systems having blocking contacts [17].

conductivity are dependent on the temperatures. The other point is that Macdonald [17] predicted a faster fall of current to occur, i.e. after $(t/\tau_D)^{1/2} > 0.3$ (see Fig.4.2) and this is probably in accordance with the experimental data obtained by Das-Gupta et al [5] on PVDF where there was a slow reduction in current after a broad peak had occured which they attributed as due to the space charges. Indeed the actual situation is quite complicated since the loss of charge carriers either by escape from the material or through neutralization by injected charge carriers (if the contact is not completely blocking) will slowly reduce the number of charge carriers present and results in the reduction of the current . Other factors affecting electrode polarization such as sample thickness is not yet known while the result of Macdonald [17] had indicated that the process is dependent on the electrode material.

4.2.2. Orientational Polarization Effect

Dipole moments which may permanently be present in the dielectric material would be consequently subjected to an orientational process by an application of an external field to give a net polarization in the applied field direction. The rate of orientational process would be highly dependent on molecule-molecule interaction and it is relatively slow process in comparison with electronic transitions or molecular vibrations. Hence its mechanism may be detected at relatively

low frequency region, which means that sufficient time has to be allowed after the application of an electric field for the orientation to attain equilibrium with the maximum polarization.

The behaviour of orientational polarization occuring in the dielectric may be further realised by considering its dielectric displacement D after subjected to an applied field. Consider at time t = 0 , a steady electric field E_o is applied across a dielectric. The dielectric displacement at subsequent time t is then given by [20,68]:

$$D(t) = \varepsilon_o \varepsilon_\infty E_o + \varepsilon_o(\varepsilon_s - \varepsilon_\infty)\psi(t)E_o \qquad (4.9)$$

where ε_∞ is the instantaneous dielectric permittivity at which the dipole has no contribution, ε_s is the static dielectric permittivity at which the maximum dipole polarization is attained and $\psi(t)$ is expressed as:

$$\psi(t) = 1 - \exp(-t/\tau) \qquad (4.10)$$

which describes the time development of the orientation process with τ is a characteristic time constant, usually called the dielectric relaxation time. The time derivative of $\psi(t)$ yields:

$$\dot{\psi}(t) = (1/\tau) \exp(-t/\tau) \qquad (4.11)$$

which is called the dielectric decay function describing the

decay of orientational polarization following removal of a previous electric field. The first term on the right hand side of Eq.(4.9) represents the instantaneous response of the material to the field while the second term represents the slower contribution from dipolar polarization.

For a continuous varying field, the expression for dielectric displacement D(t) from Eq.(4.9) becomes:

$$D(t) = \varepsilon_o \varepsilon_\infty E(t) + \varepsilon_o(\varepsilon_s - \varepsilon_\infty) \int_{-\infty}^{t} \psi(t-u) E(u)\, du \qquad (u < t < u + du) \qquad (4.12)$$

which gives the total value of the displacement at time t, i.e., a time (t-u) after application (between u to u+du) of an electric field E(u). Differentiating Eq.(4.12) with respect to t gives:

$$\frac{d}{dt} D(t) = \varepsilon_o \varepsilon_\infty \frac{d}{dt} E(t) + \varepsilon_o(\varepsilon_s - \varepsilon_\infty) \frac{d}{dt} \int_{-\infty}^{t} \dot{\psi}(t-u) E(u)\, du \qquad (4.13)$$

For convenience, let us introduce a variable x=t-u, and since D is proportional to the polarization charges per unit area of electrode (see Eq.4.7), $\frac{d\ D(t)}{dt}$ will be proportional to the current density $J_D(t)$ such that:

$$J_D(t) = \varepsilon_o \varepsilon_\infty \frac{d}{dt} E(t) + \varepsilon_o(\varepsilon_s - \varepsilon_\infty) \frac{d}{dt} \int_{0}^{\infty} \dot{\psi}(x) E(t-x)\, dx \qquad (4.14)$$

Eq.(4.14) may be applied to the case of step function field during charging and discharging of a dielectric as follows.

For charging, $E(t-x) = 0$ for $x > t$ and $E(t-x) = E_o$ for $x < t$. Hence for a single relaxation time, the charging current density is :

$$J_c(t) = \varepsilon_o (\varepsilon_s - \varepsilon_\infty) E_o \frac{d}{dt} \int_o^t \frac{\exp(-x/\tau)}{\tau} dx$$

or

$$= \varepsilon_o (\varepsilon_s - \varepsilon_\infty) E_o \frac{d}{dt} (1 - \exp(-t/\tau))$$

$$= \varepsilon_o (\varepsilon_s - \varepsilon_\infty) E_o \frac{\exp(-t/\tau)}{\tau} \qquad (4.15)$$

For discharging, $E(t-x) = E_o$ for $x>t$ and $E(t-x) = 0$ for $x<t$. Hence, the discharging current density is :

$$J_d(t) = \varepsilon_o (\varepsilon_s - \varepsilon_\infty) E_o \frac{d}{dt} \int_t^\infty \frac{\exp(-x/\tau)}{\tau} dx$$

$$= \varepsilon_o (\varepsilon_s - \varepsilon_\infty) E_o \frac{d}{dt} \exp(-t/\tau)$$

$$= -\varepsilon_o (\varepsilon_s - \varepsilon_\infty) E_o \frac{\exp(-t/\tau)}{\tau} \qquad (4.16)$$

Hence, the charging and discharging currents density associated with dipole orientation may be described as :

$$J_D(t) = \pm \varepsilon_o (\varepsilon_s - \varepsilon_\infty) E_o \dot{\psi}(t) \qquad (4.17)$$

where a negative sign corresponds to a discharging process. In both cases of charging and discharging, the current always decays with time although the direction of its flow is opposite to each other. It is therefore necessary to measure the decay function $\dot{\psi}(t)$ experimentally which may be used in the analysis of the component of the decaying currents. In view of this, the time constant of the measuring circuit must be kept as short as possible so that a sudden change of current during switching could be measured within a reasonable time scale.

A conduction current density J_{con} is always present in addition to the current $J_D(t)$ of Eq.(4.17), so that the total current density is :

$$J(t) = J_D(t) + J_{con} \qquad (4.18)$$

where J_{con} may have a contribution from electronic or ionic carriers. The presence of J_{con} component may further obscure the analysis of the transient currents as some of these carriers may pile up at the electrodes (in case of blocking contact as has been mentioned in section 4.2.1) and build up space charges which in turn oppose the flow of current. As a result, J_{con} decreases with time until a steady state value J_s is reached. Hence J(t) may be written as :

$$J(t) = J_D(t) + J_{sc}(t) + J_s \qquad (4.19)$$

where $J_{sc}(t)$ refers to the build up of space charges at the

vicinity of the electrode-dielectric interface. Further complications in the interpretation of the decaying current may arise if there is any interfacial polarization (see the next section) due to piling up of charge carriers at the boundaries of different regions in the bulk of the dielectric, or due to contribution from impurity phases. Apparently many experimental observations concerning the time dependence of absorption and resorption currents in polymer dielectrics are in favour of the decay form as t^{-n} (where n is a constant, often observed to be close to unity) at some regions of temperature and field and over certain period of time [1,5,21]. Obviously the t^{-n} dependence can not hold for infinite time since from Eq.(4.12) and (4.17),

$$D(t) = \int J_D(t)dt = \text{constant} \pm \varepsilon_o(\varepsilon_s - \varepsilon_\infty)E_o\int \dot{\psi}(t)dt \tag{4.20}$$

and for $\dot{\psi}(t) = Kt^{-n}$ (K is a constant, $n \leq 1$), as $t \to \infty$,

$$D(t) = \text{constant} \pm \varepsilon_o(\varepsilon_s - \varepsilon_\infty)E_o\int_0^\infty Kt^{-n}\,dt$$

would give infinite value, which is physically meaningless. Cole and Cole [22] showed that the decay funtion of the absorption current of the form t^{-n} could manifest a dipolar relaxation process if a sufficiently wide distribution of relaxation times exists in the dielectric. Thus as the t^{-n} dependence of absorption and resorption currents are observed in many cases of dielectrics, the transient current of the

form as described by Eq.(4.17) may be regarded as purely due to a dipolar process with a single relaxation time. Further treatment of Eq.(4.13) will lead to the Debye dispersion equation of the complex permittivity ε^* as [20] :

$$\varepsilon^* = \varepsilon_\infty + (\varepsilon_s - \varepsilon_\infty)/(1 + iw\tau) \qquad (4.21)$$

w : angular frequency of applied electric field.

which is found to be in good agreement with the experimental results for many polar liquids. Its theory, however, is less satisfactory in the case of the polymers and many solid dielectrics. Hence Eq.(4.17) may not give a full description of a dipolar process in a dielectric in general. This led Cole and Cole [23] to suggest a modification to Eq.(4.21), which yields the folowing expression :

$$\varepsilon^* = \varepsilon_\infty + (\varepsilon_s - \varepsilon_\infty)/[(1 + (iw\tau)^{1-a}] \qquad (4.22)$$

with the parameter a having values between 0 and 1. Following this, it is possible to express the transient current corresponding to Eq.(4.22), which is as follows.

The current which flows in the external circuit after application of an alternating voltage, given by the real part of $V = V_o \exp(iwt)$ is :

$$I(t) = \varepsilon^* C_o \frac{dV}{dt}$$

or $$I(t) = iw\varepsilon^* C_o V \tag{4.23}$$

Hence, the complex admittance Y(iw) of a dielectric described by Eq.(4.22) can be expressed as :

$$Y(iw) = iw\varepsilon^* C_o$$

$$= iwC_o\{ \varepsilon_\infty + (\varepsilon_s - \varepsilon_\infty)/[1 + (iw\tau)^{1-a}]\} \tag{4.24}$$

By applying a Fourier transform, a dc transient current $I_c(t)$ following application of a step voltage of magnitude V_o at time t=0 may be written as :

$$I_c(t) = \frac{C_o V_o}{\pi} \int_0^\infty \varepsilon^*(iw)\exp(iwt)\, dw \tag{4.25}$$

Rewriting Eq.(4.25) as a series in descending powers by using the Heaviside operational calculus, Cole and Cole [22] showed:

$$I_c(t) = C_o V_o(\varepsilon_s - \varepsilon_\infty)\frac{(1-a)}{\tau}(t/\tau)^{-a}$$

$$\cdot\sum_{n=1}^{\infty}\frac{(-1)^{n-1}n}{\Gamma[1+n(1-a)]}(t/\tau)^{(n-1)(1-a)} \tag{4.26}$$

where Γ: gamma function

from which for $t << \tau$, the current is given by :

$$I_c(t) = C_o V_o(\varepsilon_s - \varepsilon_\infty)\frac{1}{\Gamma(1-a)}(t/\tau)^{-a} \tag{4.27}$$

It is also possible to obtain an asymptotic expansion in negative powers of (t/τ), thus :

$$I_c(t) = C_o V_o(\varepsilon_s - \varepsilon_\infty)\frac{(1-a)}{\tau}(t/\tau)^{-(2-a)} \cdot \sum_{n=1}^{\infty} \frac{(-1)^{n-1}\, n}{\Gamma[1-n(1-a)]} \cdot (t/\tau)^{-(n-1)(1-a)} \qquad (4.28)$$

which for $t >> \tau$ yields the current as :

$$I_c(t) = \frac{C_o V_o(\varepsilon_s - \varepsilon_\infty)}{\tau}\frac{(1-a)}{\Gamma(a)}(t/\tau)^{-(2-a)} \qquad (4.29)$$

Hence from Eqs. (4.27) and (4.29) a double logarithmic plot of $I_c(t)$ vs. t would give a curve with limiting slopes -a for $t << \tau$ and -(2-a) for $t >> \tau$. Such a plot [22] is presented in Fig. 4.3 for various values of a and over certain period of times (t/τ). The dashed lines in the figure represent the limiting straight lines as obtained from Eqs. (4.26) and (4.28). It may be observed from the curves that the linearity at longer time span will hold for the values of 'a' closer to unity, whereas for a<<1 the curves are divided into two regions, each having different slopes with the transition of the gradient occuring at time comparable with the relaxation time. In the case of a=0, Eq. (4.26) reduces to the exponential form which is similar to the current derived from the Debye type dispersion as represented by Eq. (4.15).

As has been mentioned before, the t^{-n} dependence (Eq.(4.1) or its equivalent form of Eq.(4.27)) cannot hold for infinite time. The limitation of this dependence could also be

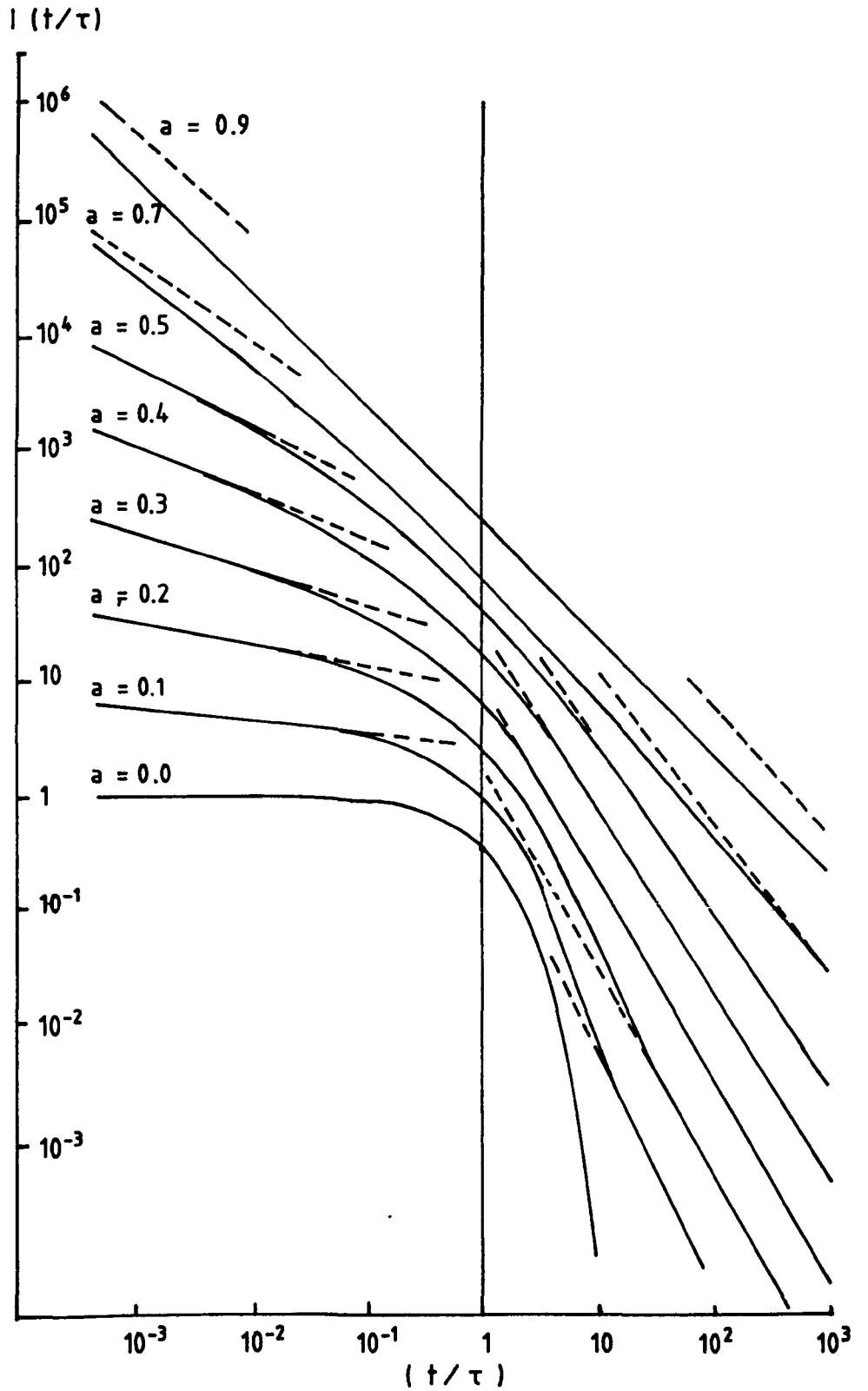

Fig. 4.3. Theoretical charging currents as a function of time. The curves for increasing value of (a) have been successively displaced vertically upward by half decade intervals for clarity [22].

seen at t=0 which predicts an infinite current and this contradicts the experimental observations. Furthermore the total charge as obtained by the integration of the current of the form of Eq.(4.1) tends to infinity for an infinite charging time t, which is unacceptable. This clearly demonstrates that Eq.(4.27) is valid only for short times ($t<<\tau$).

The presence of steady state current of finite amount may obscure the interpretation of experimental results in terms of Cole and Cole [22] treatment, as its value may be sufficiently large to mask the absorption current at longer times. In view of this, the discharging current could be used instead, provided the charging time is kept long in comparison with the relaxation time τ, so that relaxation characteristic may prevail during the discharging period of any dielectric exhibiting dispersion.

It is known that the dipolar relaxation process is strongly temperature dependent. As such, it may be possible to determine its thermal activation energy from current-time-temperature characteristics, assuming that the behaviour of the observed current has a significant contribution from a dipolar relaxation process. In this connection, the model of dipole as had been proposed by Frohlich [24] is adopted to describe the dipolar relaxation process under thermal treatment. The model essentially assumes that the dipole have equilibrium position 1 and 2, separated by a potential energy barrier of height ΔU as illustrated in Fig.4.4. In a microscopic scale, the dipoles of charge could be imagined as

being located in an equilibrium state 1 having finite potential energy, which after absorbing an amount of energy, is transferred to another equilibrium location of state 2, after climbing the potential barrier. The process of jumping from one state to another is governed by thermodynamical laws, which would give relaxation time τ associated to the frequency of jumping as:

$$\tau = \tau_o \exp(\Delta U/kT) \qquad (4.30)$$

where τ_o is the relaxation time at infinite temperatures, k is the Boltzman constant (= 1.3805 x 10^{-23} J/K) and T is the absolute temperature.

In the case of polymers, state 1 and state 2 may be considered to represent two orientations of a dipolar group about a valence bond linking the group to the other component of the molecule. The same expression as Eq.(4.30) may thus be applied, in which the molecule has to acquire an amount of energy ΔU to orientate themselves from state 1 to state 2. The change of relaxation times with temperature as described by Eq.(4.30) is in accordance with the Arrhenius law, in which the activation energy ΔU could be roughly estimated from a plot of log τ against 1/T. However, Eq.(4.30) is not accurate enough at temperatures near glass transition temperature T_g (i.e. the temperature where the occurence of sharp changes in temperature dependence of various properties are observed, which is attributed to a major change in the segmental mobility of the polymer chains). Based on the works

of Bueche [25] and Williams et al [26], the temperature dependence of relaxation time near T_g may be written as:

$$\tau(T) = \tau_g \exp\left[\frac{-C_1(T-T_g)}{C_2 + T - T_g}\right] \qquad (4.31)$$

where C_1 and C_2 are empirical constants and τ_g is the relaxation time at T_g. This expression has been found applicable to the dielectric relaxation associated with T_g, and occuring in the temperature region $T_g < T \leqslant T_g + 100^o$ for a large class of organic and inorganic materials which have an amorphous phase[26]. Since Eq.(4.31) was derived by considering the free volume for segmental motion of a molecule, it implied that the dielectric relaxation in polymers involved a cooperative movement mechanism of those molecules. Thus the glass transition temperature and hence the associated dielectric relaxation times are greatly influenced by the nature of molecular structure of the dielectric. This could be seen in the case of polyvinyl chloride where the addition of plasticiser causes a reduction in T_g as a result of the reduction in packing density of molecular chains [27]. In semicrystalline polymers where components of crystalline and amorphous phases may exist in different proportions, the relaxation spectrum becomes more complicated as different mechanisms occuring inside the crystalline regions and at the boundaries between the two phases may affect the relaxation processes taking place in the amorphous regions.

The fact remains that the dipolar relaxation process is

strongly temperature dependent and the activation energy of the process may be evaluated from the temperature dependence of the relaxation time. While an Arrhenius plot may be used to determine the activation energy at high temperature regions, the WLF(Williams, Landel and Ferry[26]) plot (as obtained from Eq.(4.31)) may have to be used to account for the process near T_g. The determination of T_g is normally carried out by measuring the volume contraction of a sample in a dilatometer and from the plot of volume against temperature, the value of T_g is obtained at the transition of the rate of volume change as illustrated in Fig.4.5.

As mentioned before, the discharging current may show a relaxation characteristic in a dielectric exhibiting dispersion in the time range of the measurement. Thus, it is possible to obtain the relaxation time as a function of temperature and hence the activation energy associated with such relaxation process. A typical transient current showing a relaxation characteristic may be seen from Fig.4.6, which is derived from Cole and Cole [22] and Wintle [28] by taking variable relaxation time τ to represent various temperatures. In principle, this time-dependent response can be transformed into its equivalent frequency-domain behaviour by a Fourier integral transformation. Thus, the complex dielectric permittivity of a dielectric following application of a step voltage V_o at time t=0 is given by:

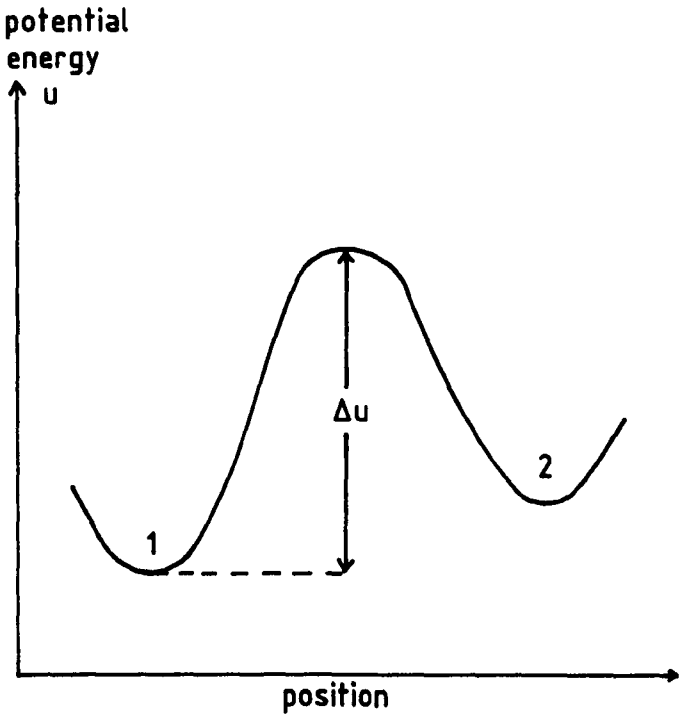

Fig. 4.4. Potential energy of dipolar model for a thermally activated process.

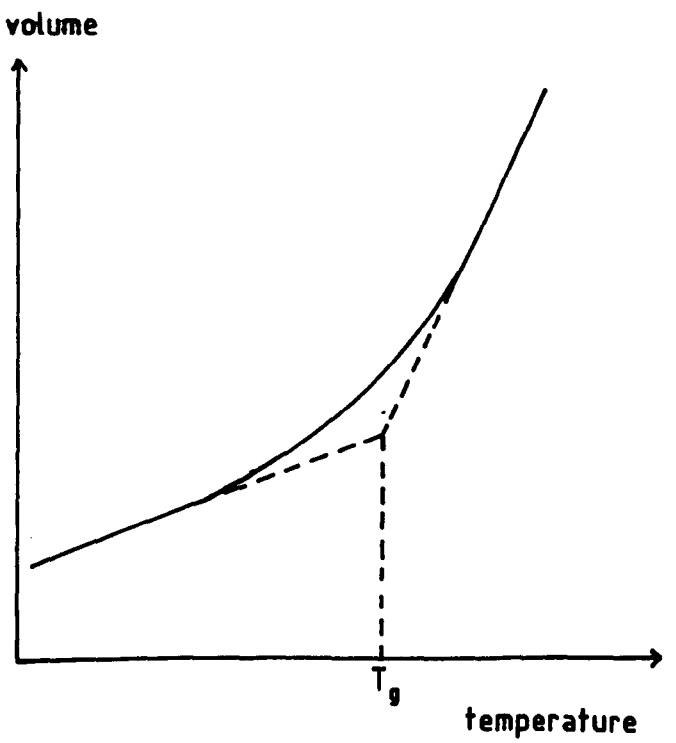

Fig. 4.5. Typical volumetic curve for the determination of the glass transition temperature.

$$\varepsilon^*(w) = \frac{1}{C_o V_o} \int_0^\infty I_c(t) \exp(-iwt)\, dt \qquad (4.32)$$

where $I_c(t)$ is the transient charging current at time t and other symbols are as previously defined. The above equation is only accounted for decaying component which may result from dipolar orientation process. Other components such as instantaneous value ε_∞ (due to atomic and electronic polarization) and the component due to conduction current may contribute to the total $\varepsilon^*(w)$, thus :

$$\varepsilon^*(w) = \varepsilon_\infty + \frac{1}{C_o V_o} \int_0^\infty I_c(t) \exp(-iwt)\, dt - i \frac{G}{wC_o} \qquad (4.33)$$

where G is the conductance.

The accurate Fourier transformation of transient current data involves very extensive numerical computation and thus an approximation due to Hamon [29] may be used to provide a simple transformation which gives the dielectric loss ε'' as:

$$\varepsilon''(f) = \frac{I(t)}{2\pi f C_o V_o} \qquad (4.34)$$

where I(t) is the transient current at time t and $f(=w/2\pi)$ is the frequency for which the dielectric loss is calculated, with $f= 0.1/t$. The Hamon approximation can be applied quite

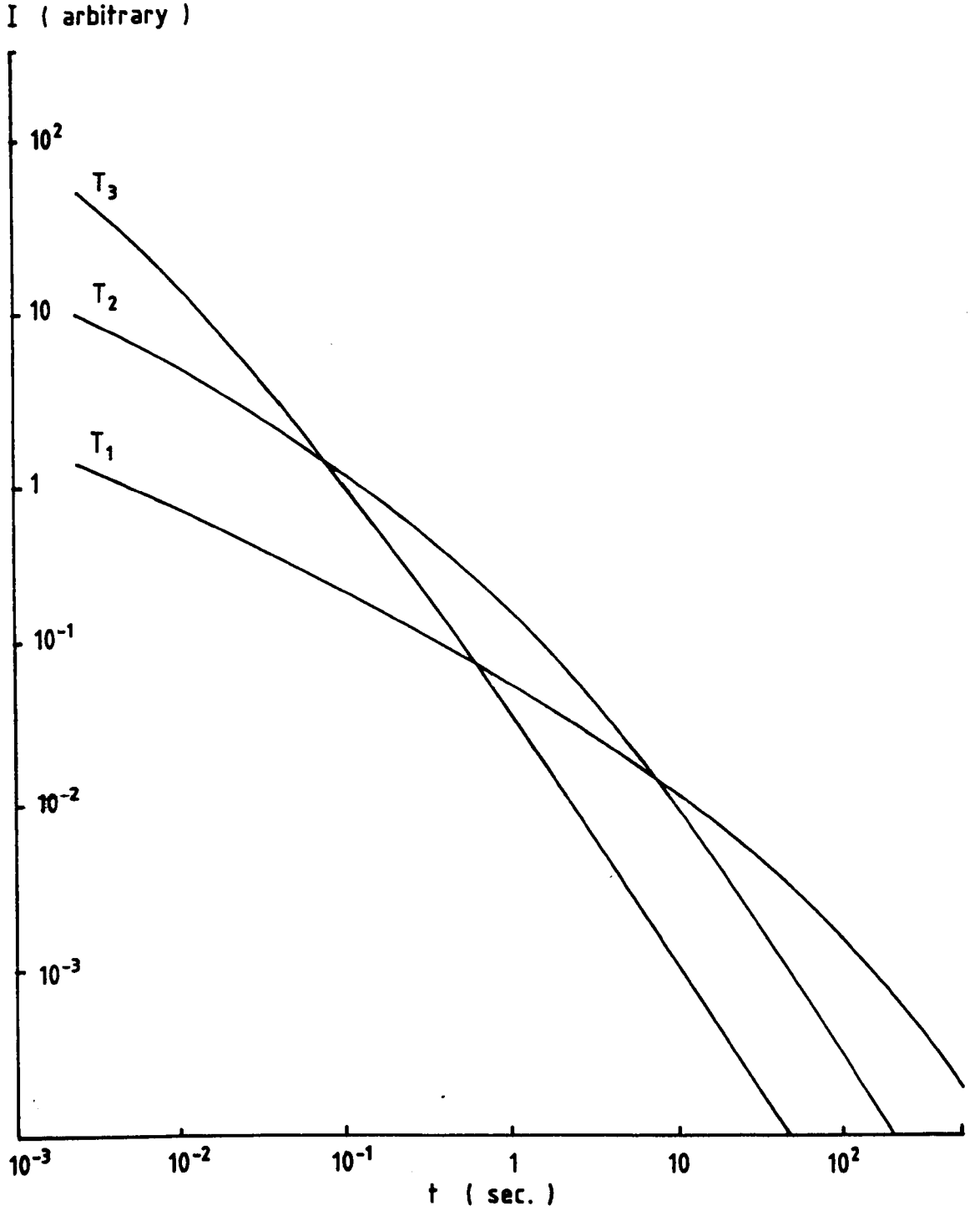

Fig. 4.6. Cole-Cole plots of transient current for a = 0.5 at various temperatures of T_1 , T_2 , T_3 ($T_3 > T_2 > T_1$) corresponding to τ = 100, 1, 0.01 [22, 28].

accurately for typical Debye-like relaxation processes in polymers. Therefore the transient current data provide a useful means in obtaining the information regarding the relaxation process in the low frequency region.

4.2.3. Interfacial Polarization.

Dielectric materials are bound to have some imperfections and regions of nonuniformity either originally existing in the material or arising during preparation and processing. The impurities which may have been introduced during processing may affects the conductivity of the dielectric as well as its dielectric behaviour. The presence of cracks or voids of some forms may create a discontinuity region which may also exert a great influence on the overall properties of the dielectric. Thus the knowledge concerning the mechanisms responsible for the dielectric behaviour in the presence of those effects are of great important in the understanding of the material properties for device applications.

In polycrystalline materials such as ceramics, the presence of grain boundaries may attract charges (ions, vacancies, injected electrons, etc.) to accumulate in the regions which could cause polarization of crystallites. These accumulated charges also induce image charges on electrodes and thus creating some dipole moments which would be superimposed on other polarization effects (electrode and

orientational polarizations) as have been mentioned in the previous sections. In single crystals, the charges accumulated at the defects (vacancies, dislocation, impurities) may cause such interfacial polarization [11]. It is obvious that the presence of defects in dielectrics may attract the formation of space charges which would induce image charges on nearby regions of different homogeneity and also on electrodes, giving rise to an interfacial polarization.

A composite of dielectric having components with different conductive properties may be one of the examples of heterogeneous system and a common example of this occurs in a dielectric which has been contaminated with conductive phase. Maxwell [30] and Wagner [31] were among the first who gave the treatment on the interfacial polarization by applying the model of a dielectric system having two different components of different permittivities and conductivities. The model, which is also known as a Maxwell-Wagner capacitor is shown in Fig.4.7(a) with its equivalent circuit as in Fig.4.7(b). The dielectric system is assumed to have two layers, each has thickness L_1 and L_2, permittivities ε_1 and ε_2, conductivities σ_1 and σ_2 and relaxation times τ_1 and τ_2 respectively. This is equivalent to an electric circuit network with one layer having a parallel combination of resistance R_1 and capacitance C_1 connected in series to the other layer with parallel combination of R_2 and C_2.

Following the application of a step electric field at time t=0, the electric field is developed across each layer in such a manner that the continuity of the normal component of

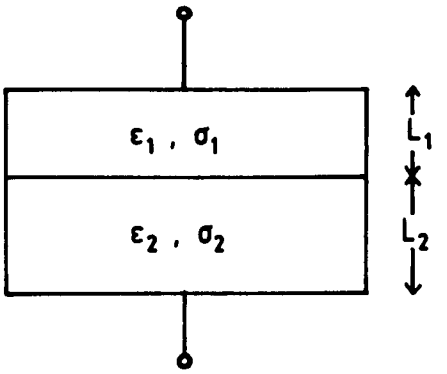

(a) physical structure of a double layer capacitor.

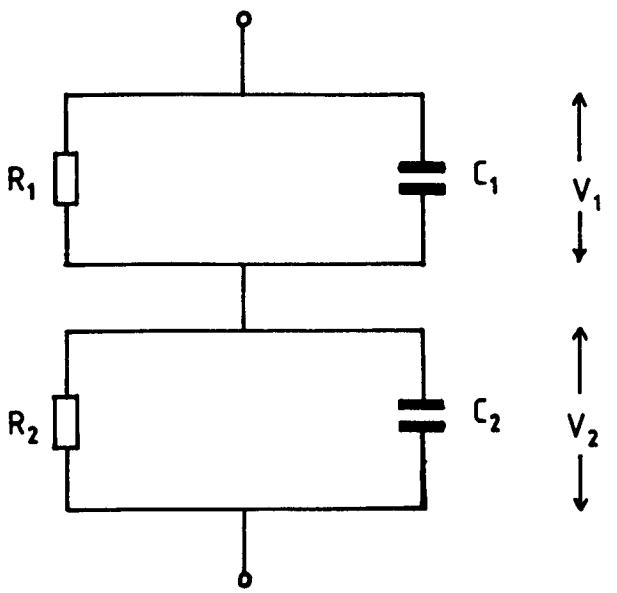

(b) equivalent circuit.

Fig. 4.7. Model of interfacial polerization in a double layer dielectric system.

the dielectric displacement is satisfied, thus:

$$\varepsilon_1 E_1 = \varepsilon_2 E_2 \tag{4.35}$$

where E_1 and E_2 are the fields across layers 1 and 2 respectively. After a finite time, the system reaches an equilibrium when a steady state current will be established across the dielectric giving:

$$\sigma_1 E_1 = \sigma_2 E_2 \tag{4.36}$$

Taking the total current I as satisfying the continuity condition, thus:

$$I = C_1 \frac{dV_1}{dt} + \frac{V_1}{R_1} = C_2 \frac{dV_2}{dt} + \frac{V_2}{R_2} \tag{4.37}$$

where V_1 and V_2 are the voltage drops across layer 1 and layer 2 and $V=V_1 + V_2$, which is the total voltage applied to the dielectric system.

The voltage V is shared by the two capacitors in a manner inversely proportional to their capacitance :

$$V_1 = V \frac{C_2}{C_1+C_2} \quad ; \quad V_2 = V \frac{C_1}{C_1+C_2} \quad ; \quad C_1 + C_2 = C \tag{4.38}$$

By substituting Eq. (4.38) into Eq. (4.37), we get :

$$\frac{t}{CR} = -\log\left(\frac{V}{R_2} - \frac{V_1}{R}\right) + \text{constant} \tag{4.39}$$

and

$$\frac{t}{CR} = -\log\left(\frac{V}{R_1} - \frac{V_2}{R}\right) + \text{constant} \tag{4.40}$$

where $R = R_1R_2/(R_1+R_2)$, or it can be further reduced to:

$$V_1 = V\,\frac{R_1}{R_1+R_2}\left(1-\left[1-\frac{\tau_2}{\tau}\right]\exp(-t/\tau)\right) \tag{4.41}$$

and

$$V_2 = V\,\frac{R_2}{R_1+R_2}\left(1-\left[1-\frac{\tau_1}{\tau}\right]\exp(-t/\tau)\right) \tag{4.42}$$

where

$$\tau = CR = (C_1 + C_2)\,R_1R_2/(R_1 + R_2) \tag{4.43}$$

which is the time constant of the complete circuit and it can also be written as:

$$\tau = (R_2\tau_1 + R_1\tau_2)/(R_1 + R_2) \tag{4.44}$$

and $\tau_1 = C_1R_1$, $\tau_2 = C_2R_2$.

Further analysis on the frequency response of the circuit would give the components of the complex dielectric permittivities ε' and ε'' as [11] :

$$\varepsilon' = \varepsilon_\infty + \frac{\varepsilon_s - \varepsilon_\infty}{1+w^2\tau^2} \tag{4.45}$$

$$\varepsilon'' = \frac{(\varepsilon_s - \varepsilon_\infty)w\tau}{1+w^2\tau^2} + \frac{1}{wC_o(R_1+R_2)} \tag{4.46}$$

where τ is given by Eq.(4.44) and other symbols are as previously defined.

It may be observed that the expression for ε' is exactly in the same form as that of the Debye dispersion equation(taking the real part of Eq.(4.21)), suggesting that the behaviour of the real part of complex permittivity is indistiguishable from that due to dipolar orientation mechanism. However the expression for ε'' contains a second term in addition to the usual formulation of Debye type characteristic. An inspection of Eq.(4.46) indicates that ε'' tends to infinity as the frequency of the applied electric fields approaches zero. Thus the contribution of the interfacial polarization lies in the low frequency region. This may analogously reflect that the interfacial polarization mechanism can be effectively seen at sufficiently longer times of absorption current measurements where the conductivity term plays a significant role as the time of the measurements increases.

The above treatment is based on the model that the dielectric is nicely divided into slabs stacked in series. If, however, the dielectric consists of particles of one material

embedded in a matrix of the other , the precise nature of the frequency dependence of the dielectric permittivity would depend on the shape and orientation of the particles although its magnitude would still depend upon the ratio of the quantities of the components of the material. Further treatment of this nature will be given in the next chapter.

4.2.4. Electron Tunnelling Model

The tunnelling of the electrons through an energy barrier in a dielectric medium could possibly be realised by considering the metal-dielectric-metal system having an energy diagrams as shown in Fig.4.8. At the metal-dielectric contact there is a potential energy barrier at which an electron in the metal electrode has to absorb a minimum energy ϕ_o to pass to the conduction band of the dielectric. The diagram has been simplified where the barrier shape has a rectangular form for identical metal electrodes used. If the metal used are not identical, the barier shape of Fig.4.8(a) would be in a trapezoidal form due to the different Fermi levels of the metals. For amorphous dielectrics, conduction and valence bands are not as well-defined as that shown in the figure, but due to the lack of long-range order in these type of dielectrics there is a smearing of the conduction and valence band edges resulting in a less defined forbidden energy gap [13]. This diffused band edge would create

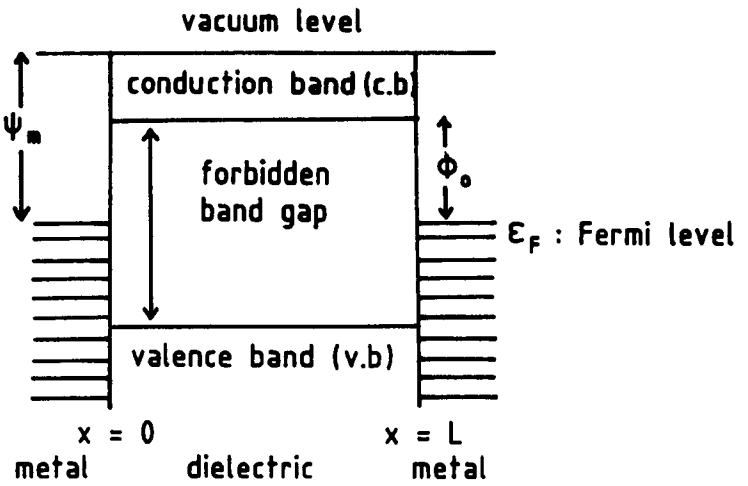

(a) Energy diagram of a metal-dielectric-metal system in the absence of an electric field.

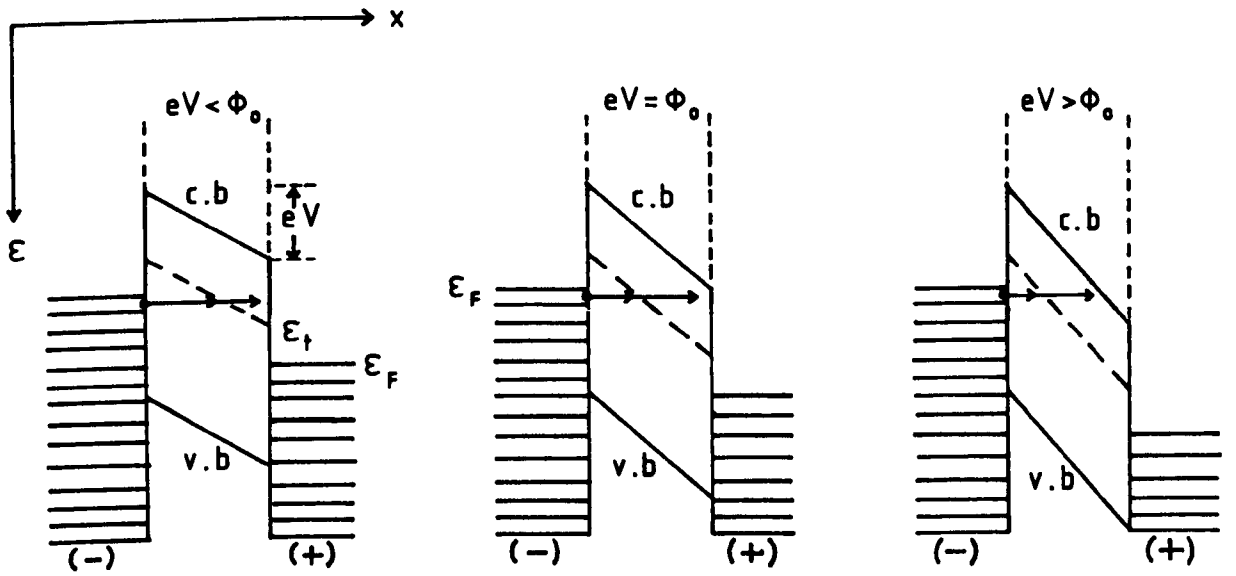

(+) , (−) : positive and negative voltage (V) polarity

(b) Modification of energy diagram of a metal-dielectric-metal system in the presence of an electric field E (= V / L) for the dielectric having empty traps at energy level ε_t.

Fig. 4.8. Energy diagrams of a metal-dielectric-metal system showing the tunnelling of electrons through the energy barrier.

localised states which act as trap sites for charge carriers. In polycrystalline dielectrics, traps may arise from grain boundaries, defects, from large stresses induced during processing and may also come from impurities. Since the tunnelling of electrons is not possible in an ideal thick dielectric, the model assumes the presence of a trap level or levels in the dielectric. In this regard, the most probable trap level would lie close to the Fermi level of the injecting electrode. There is much evidence from thermoluminesence studies on polymers which showed the existence of discrete shallow electronic traps which are empty at room temperature [32,33]. Thus the assumption of the presence of the trap level may be justified.

Application of a uniform electric field of finite magnitude modifies the energy barrier, by which the Fermi level of the positive electrode drops below the Fermi level of the negative electrode by eV, V being the applied voltage. Fig.4.8(b) shows the three cases where the energy diagram of a metal-dielectric-metal may be modified upon the application of the electric field. It may be obvious that a high electric field could aid in the process of tunnelling as long as the field does not reach the onset of breakdown.

Following Wilcox[34], the incremental current density dJ associated with the traps at a distance x from the interface may be written as :

$$dJ = -e \frac{d}{dt} n(x,\mathcal{E},t) \frac{x}{L} dx\, d\mathcal{E} \qquad (4.47)$$

where $n(x,\mathcal{E},t)$ is the concentration of trapped electrons per unit energy at a time t, which is given by :

$$n(x,\mathcal{E},t) = N(x,\mathcal{E}) \{f(0) + [f(E) - f(0)] \exp(-yt/\tau_o)\}$$

(this is for the charging case; for the discharging f(E) is replaced by f(-E))

(4.48)

where τ_o is a characteristic trapping time and $N(x,\mathcal{E})$ is the trapped density in the dielectric before field application. The tunnelling probability y for a standard rectangular barrier is given by :

$$y = \exp(-2Kx) \quad , \quad K = (2m^*\mathcal{E})^{1/2}/\hbar \tag{4.49}$$

where m^* is the electron effective mass and $\hbar = h/2\pi$ (h is plank's constant). The Fermi funtion f(E) is defined as :

$$f(E) = \{1 + \exp[\mathcal{E}_F - \mathcal{E} - eEx)/kT]\}^{-1} \tag{4.50}$$

where E is the applied electric field. This Fermi function refers to the distribution of electrons in the electrode adjacent to the traps being considered, since the rate of transfer of electrons is in effect controlled by the occupancy in the metal electrode [35].

Based on the work of Wilcox [34], the asymptotic limit at long times of the charging current density associated with a single trap energy level was derived by Wintle [35] in a

simplified form, thus :

$$J = J_o(t/\tau_o)^{-(1+\beta)} \Gamma(1+\beta) \ln^2(t/\tau_o) \qquad (4.51)$$

where J_o is the term dependent on the temperature, applied field and trap distribution, and

$$\beta = 1/(2Kx_o) \quad , \qquad (4.52)$$

x_o is a parameter characterizing the spatial distribution of the traps which allows for some change of trap concentration with depth. The trap concentration (or trap density) per unit energy can be represented by :

$$N(x,\mathcal{E}) = N_o \exp(-x/x_o)\ \delta(E) \qquad (4.53)$$

where N_o is a constant and $\delta(E)$ is a function which describes traps with a single energy level. The result of Eq.(4.51) can be readily seen by plotting the logarithm of the reduced absorption current against logarithm of reduced time as shown in Fig.4.9[35]. It may be seen that there is a considerable change in slopes of the curve upon changes in the parameter β, suggesting the great influence of trap distribution may have on the observed transient currents. Since most of the experimental observations showed that the time dependence of the absorption current is of the form t^{-n} (n being close to unity), the most probable values of β must be close to zero. Wintle[35] eventually concluded that it might be probable that

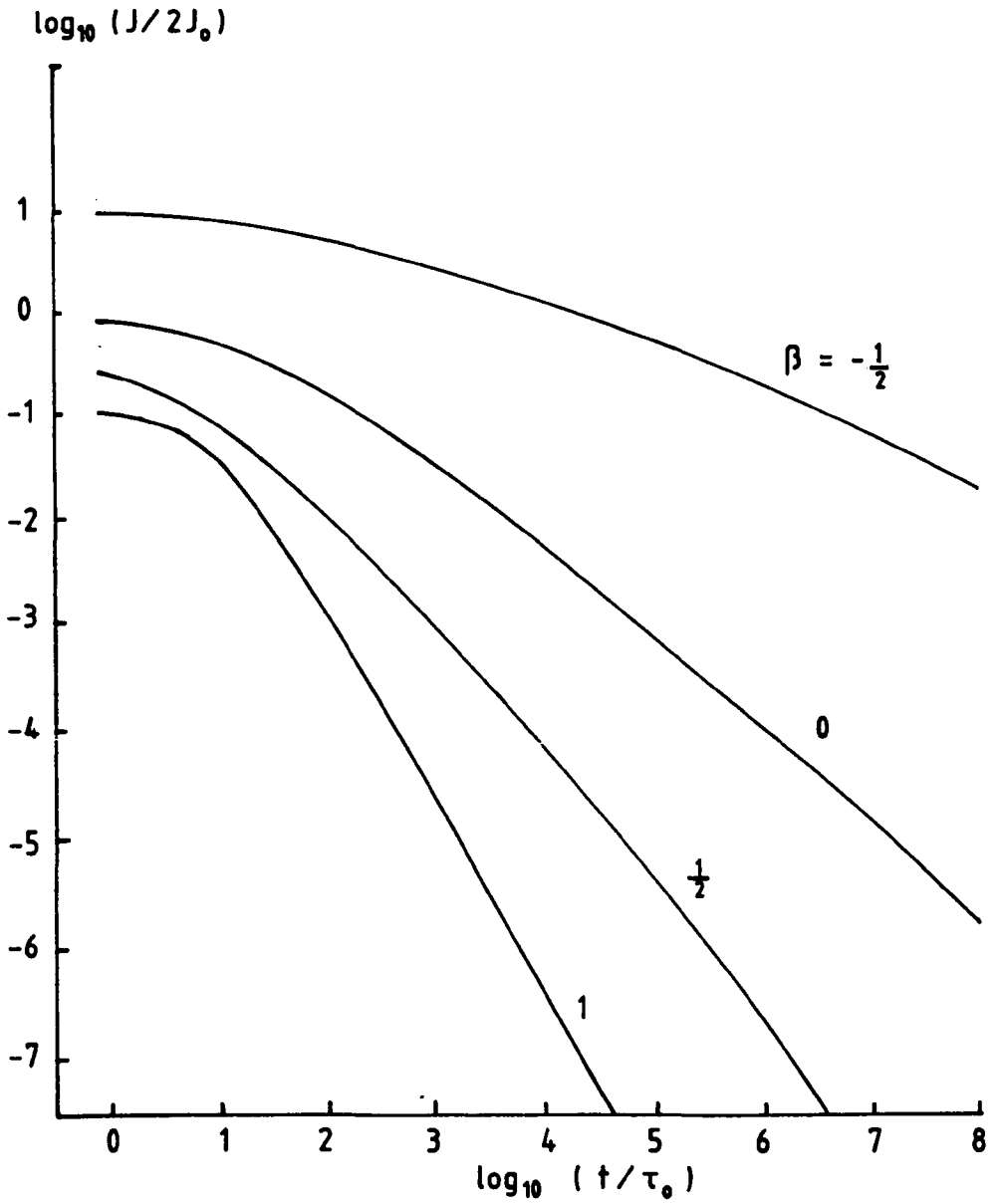

Fig. 4.9. Theoretical characteristics of absorption current density against time associated with electron tunnelling into traps. Values of the parameter β reflects the spatial distribution of the traps [35].

the tunnelling model accounts for the absorption current in polymer dielectrics for times up to $\sim 10^5$ sec although the detailed nature of trap distribution seemed very difficult to envisage. The theoretical consideration also predicts that the tunnelling current is proportional to field (up to 10^7 Vm^{-1}), varies inversely with thickness of the specimen and has a strong dependence on the electrode material [28,35]. Experimental evidences showed that the tunnel current is very weakly temperature dependent, as shown by the result of Pollack and Morris [36] on the Al-Al_2O_3-Al dielectric system, Esaki and Stiles [37] on the Al-Al_2O_3-SnTe system and Cherki et al[38] on the Ta-Ta_2O_5-metal system. While all these observations were made on inorganic oxides, the similar observation on polymers has not been reported. Nevertheless, the measurement of current level on various polymers have indicated that its isochronal current (current at constant time) behaviour involved an activation energy process [28]. Thus the possibility of a tunnelling mechanism responsible for the observed current behaviour in those polymers may be ruled out.

4.2.5. Schottky Emission Model

The Schottky emission model provides an alternative approach to account for the charge transport from metal electrode to the dielectric through a potential barrier, in addition to the tunnelling process which has been described in the previous section. The emission process basically involves the electrons from the metal electrode which upon receiving a

sufficient energy, will jump over the interfacial potential barrier ϕ_o (see Fig.4.8) into the dielectric conduction band. The process which is sometime known as Schottky injection, would produce the current whose magnitude is principally controlled by the rate at which electrons can be excited over that potential barrier.

By considering a neutral contact at metal electrode-dielectric interface, the process of Schottky injection can be schematically described with the help of Fig.4.10. In the ideal situation where the potential barrier ϕ_o is independent of the applied electric field E, the current density flowing in the system which is associated with the electron emission from the electrode into the dielectric is given by [13] :

$$J = A^* T^2 \exp(-\phi_o/kT) \qquad (4.54)$$

where A^* is the effective Richardson constant which is given by :

$$A^* = A = 4\pi ek^2 m/h^3 = 120 \text{ A/[cm}^2 \text{ (deg)}^2\text{]} \qquad (4.55)$$

(m : electron rest mass)

for thermionic emission into a vacuum. The value of A^* for thermionic emission into a semiconductor or a dielectric may be quite different from A (Richardson constant) , the difference being determined by various effects such as carrier effective mass, carrier mobility, electrode-dielectric contact, electron scattering effect and space charge effect in

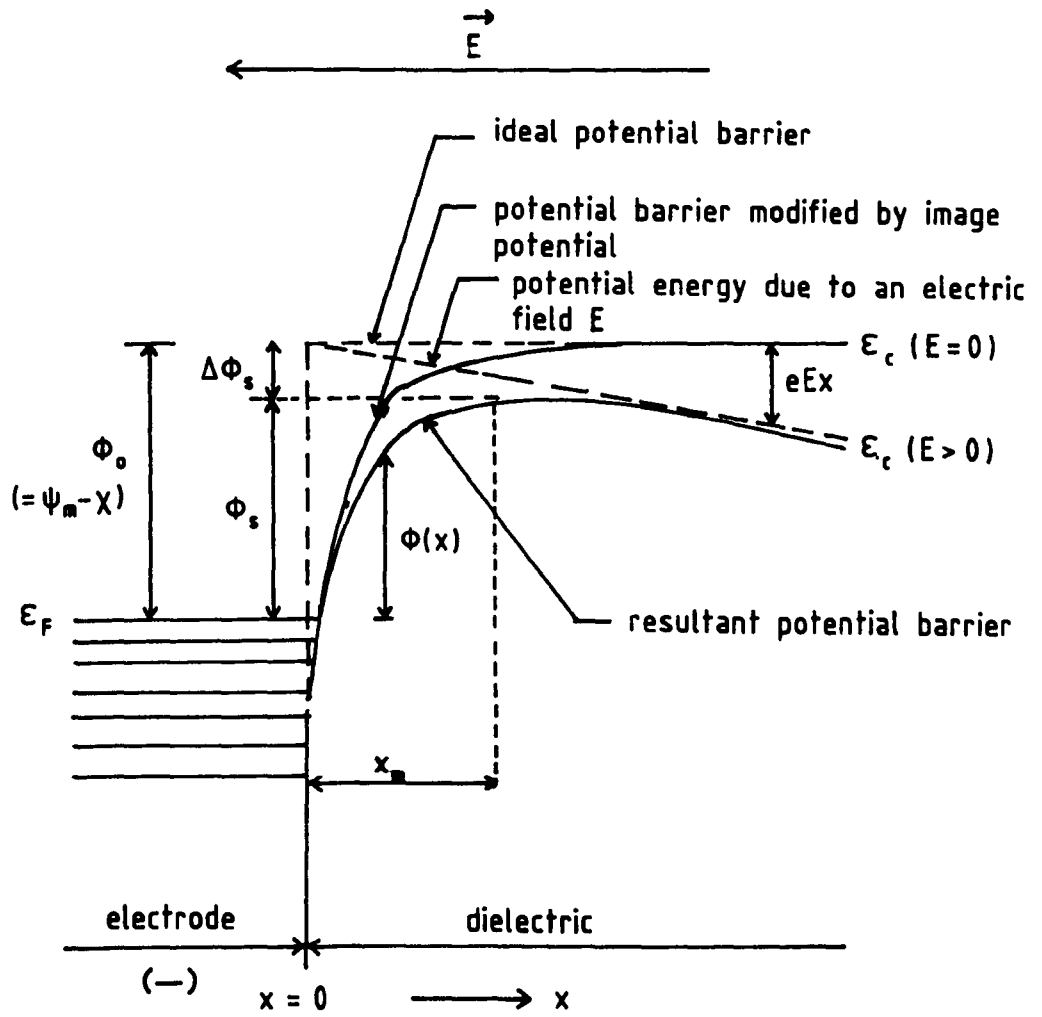

(—) : negative voltage polarity on metal electrode.

Fig. 4.10. Energy diagram showing the lowering of potential barrier due to the combination of the image force and the applied electric field for a neutral contact at the electrode-dielectric interface.

the vicinity of the interface[39].

In the actual situation, there is an image force due to electrons in the metal electrode near the elctrode-dielectric interface, having a potential energy ϕ_{im} :

$$\phi_{im} = - e^2/(16\pi\epsilon'\epsilon_o x) \quad ; x \neq 0 \qquad (4.56)$$

(ϵ' : high frequency relative permittivity of the dielectric [13])

which modifies the potential barrier ϕ_o, giving a new potential barrier as a funtion of distance x from the interface as :

$$\phi(x) = \phi_o + \phi_{im}$$

$$= \phi_o - e^2 /(16\pi\epsilon'\epsilon_o x) \qquad (4.57)$$

In the presence of a uniform electric field E across the metal-dielectric-metal system, the potential barrier is further modified and is given by :

$$\phi(x) = \phi_o - e^2 / (16\pi\epsilon'\epsilon_o x) - eEx \qquad (4.58)$$

The resultant potential barrier profile (see Fig. 4.10, represented by $\epsilon_c(E>0)$, ϵ_c being the bottom edge of conduction band of the dielectric) is obviously lower than the ideal step potential barrier. This lowering of the potential barrier due

to the combination of the image force and the applied electric field is called the 'Schottky effect', which is very well known phenomena in the field of semiconductors.

There is an optimum point by which the attenuation $\Delta\phi_s$ ($= \phi_o - \phi(x_m)$) of the barrier height due to the interaction of the applied field with the image potential, becomes a maximum and the potential barrier height becomes minimum. By setting $d\phi(x)/dx = 0$ from Eq.(4.58), the distance x_m from the interface corresponding to that situation, is given by :

$$x_m = \{ e/(16\pi\varepsilon'\varepsilon_o E) \}^{1/2} \qquad (4.59)$$

At this point, the potential barrier $\phi(x)$ is equal to ϕ_s, which is the effective potential barrier height. Thus by substituting x_m in Eq. (4.58),

$$\phi_s = \phi(x_m) = \phi_o - \left(\frac{e^3}{4\pi\varepsilon'\varepsilon_o} \right)^{1/2} E^{1/2} \qquad (4.60)$$

Hence the current density associated with the electron emission from the metal electrode into the dielectric by taking Schottky effect into account is given by (substituting ϕ_s for ϕ_o in Eq.(4.54)) :

$$J = A^* T^2 \exp(-\phi_o/kT) \exp(\beta_s E^{1/2}/kT) \qquad (4.61)$$

with $$\beta_s = \left(\frac{e^3}{4\pi\varepsilon'\varepsilon_o} \right)^{1/2}$$ = Schottky barrier lowering coefficient.

It is obvious from Eq.(4.60) that the effective barrier height is field dependent and thus one would expect the current flowing is also field dependent as in eq.(4.61). Thus by plotting log J vs. $E^{1/2}$ at a particular temperature, a straight line will be obtained with a slope determined by temperature and permittivity of the dielectric.

In the case of blocking contact between a metal electrode and a dielectric (see Fig.4.1 and Fig.4.11), the effective potential barrier will be different from that of neutral contact, due to the presence of depletion layer at the vicinity of the electrode-dielectric interface. The potential energy of the Schottky barrier as a function of distance x from the interface and measured from the bottom edge of the conduction band is given by [13,39] :

$$\phi_{sb}(x) = - \frac{e^2 N_d}{\varepsilon' \varepsilon_o} \left(Wx - \frac{x^2}{2} \right) \qquad (4.62)$$

where W is the width of depletion region or the width of the Schottky barrier which is given by [40] :

$$W = \left(\frac{2 \varepsilon' \varepsilon_o (\psi_m - \psi_d + eV)}{e^2 N_d} \right)^{1/2} \qquad (4.63)$$

where V is the applied voltage across the electrode-dielectric interface. It may be observed that W is field dependent and greater than W_o , the initial depletion width which

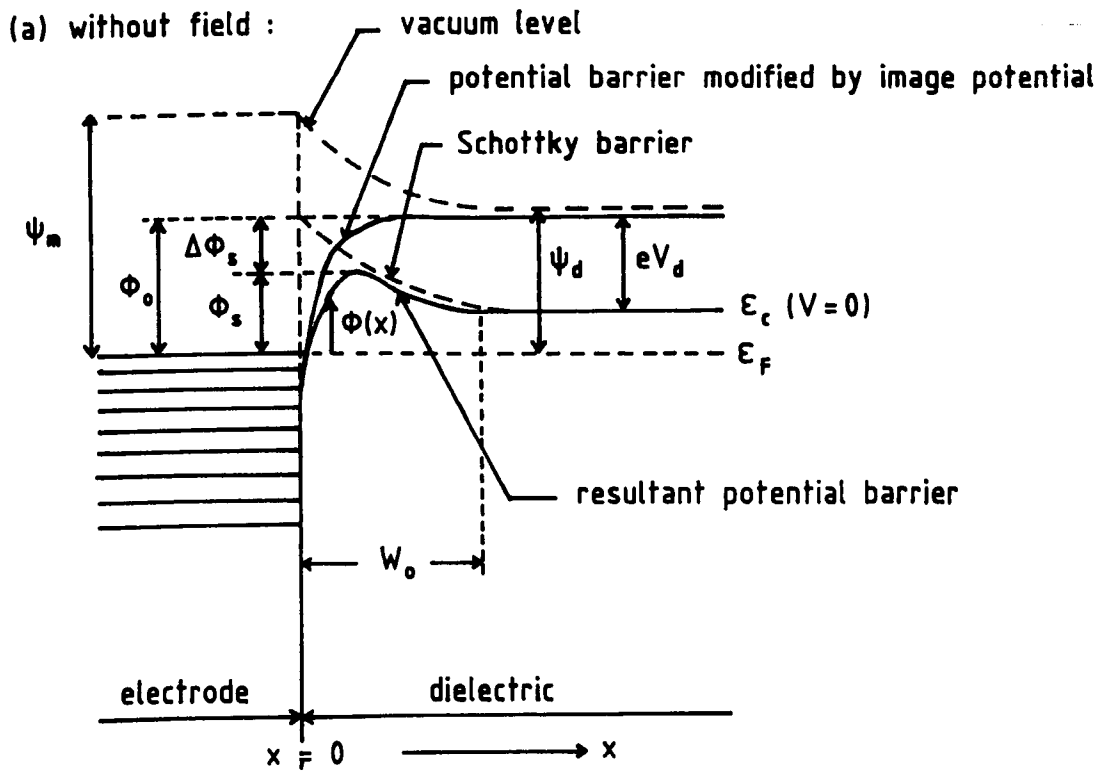

(b) with field :

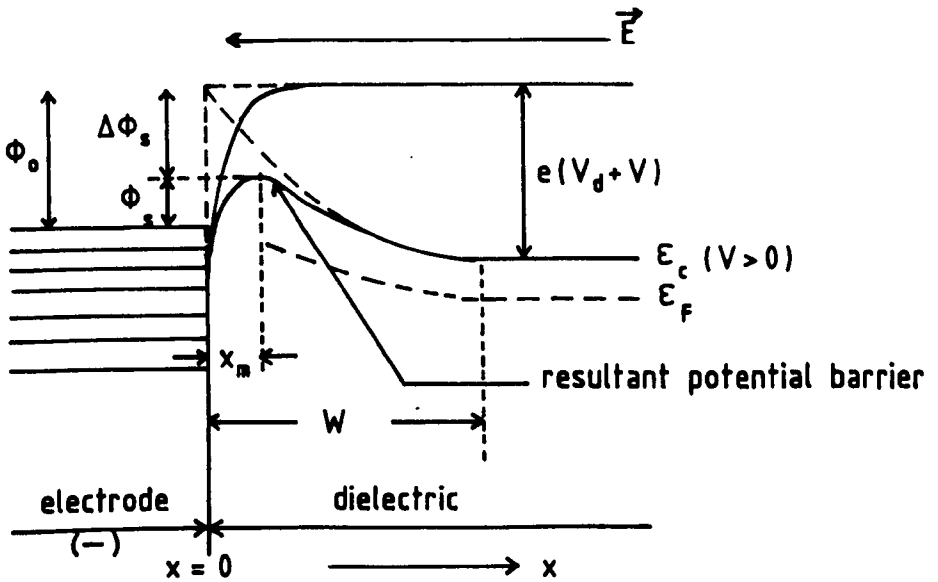

(−) : negative voltage (V) polarity on metal electrode.

Fig. 4.11. Energy diagram showing the lowering of potential barrier due to the combination of the image force and the depletion region effects for a blocking contact at the electrode-dielectric interface.

established the contact potential eV_d (V_d being the built-in voltage at the interface). N_d is the donor density in the dielectric, which may also arise from defects, vacancies or traps [13] .

As the applied field is increased, the depletion width W is increased and Schottky barrier is also increased. Thus the total potential barrier height measured from the Fermi level of the metal and taking the image potential (Eq.(4.56)) into account, is given by :

$$\phi(x) = \phi_o - \frac{e^2}{16\pi\epsilon'\epsilon_o x} - \frac{e^2 N_d}{\epsilon'\epsilon_o}\left(Wx - \frac{x^2}{2}\right) \qquad (4.64)$$

At an optimum point x_m, $\phi(x)$ will be equal to ϕ_s, which is the effective potential barrier at the interface. The value of x_m can be determined by setting $d\phi(x)/dx = 0$ and noting that for $W >> x_m$, term x^3 can be ignored, we get ,

$$x_m \simeq \frac{1}{4(\pi W N_d)^{1/2}} \qquad (4.65)$$

Substituting Eq.(4.65) into Eq.(4.64), the effective potential barrier ϕ_s is thus (assuming $W >> x_m$) :

$$\phi_s \simeq \phi_o - \left(\frac{e^6 N_d(\psi_m - \psi_d + eV)}{8\pi^2 (\epsilon'\epsilon_o)^3}\right)^{1/4} \qquad (4.66)$$

which is field dependent. Obviously field dependence of

current density can be obtained by substituting ϕ_s from Eq.(4.66) for ϕ_o in Eq.(4.54).

4.2.6. Hopping conduction mechanism

It is known that solid crystals are not free of imperfections. The degree of imperfections may vary from one to another depending on the nature of its occurence and subsequent treatment they received. In polycrystalline materials such as ceramics, the level of imperfections may be greater than single crystals since besides the presence of grain boundaries and domain walls, they are bound to have pores and impurity phases. Polymeric solid materials form another class of materials in which disorder and imperfections may exert a great influence on the nature of electrical conduction. Most of the polymeric solids are either amorphous or semicrystalline (consisting of a mixture of small crystalline regions or crystallites and amorphous phases). Thus some form of disordered phase (represented by amorphous phase) is always present in polymer which affects the overall distribution of electronic states and hence the electrical conduction process in the material.

For a random distribution of atoms in a disordered phase, the density of electronic energy states (both conduction and valence bands) tails into the forbidden energy gap and creates localised states. Such localised sites would allow the possibility of hopping processes to occur by which

electrons can jump over the potential barrier from one site to the next. There is also a possibility where the electron tunnelling mechanism may occur with the aid of such localised sites as has been described in previous section. However the dominant mechanism between the two depends on the shape of the barrier and the energy of the charge carriers.

The electron hopping model was originally proposed by Conwell[41] and Mott[42] and subsequently been refined by Kasuya[43] and Miller[44] who showed the agreement betwen the theories with the published experimental results. The model assumed that electrons move by hopping between states which are essentially localised around acceptor or donor impurities and which are initially empty. The Coulombic potential around the localised sites will be modified upon application of an electric field and a new equilibrium has to be established which facilitate the hops of electrons.

Pollak and Geballe [45] measured the ac conductivity in n-type silicon with various doping impurities at frequencies between 10^2 to 10^5 Hz and temperatures between 1 and 20 K and their results show that :

$$\sigma(w) = A(T)\ w^{n(T)} \qquad (4.67)$$

where A(T) and n(T) are weakly temperature dependent parameters with n having a value close to 0.8. They attributed the observed behaviour as due to polarization caused by a hopping process.

Jonscher [46] extends the treatment of the hopping

process by relating its characteristics to dc behaviour under high electric field as well as to small signal ac behaviour. He considered that the hopping process by charge carriers is not only due to electrons but it may also be due to ions which can make a discontinuous motion between localised sites. The difference between electronic and ionic hopping mechanisms may shows up in its characteristics in relation to the activation energy being observed. The field dependence of hopping conduction is thought to be due to enhancement of hopping probabilities by a high electric field. This is effectively seen as a lowering of the hopping barriers for charge carriers on localised sites or trap centres. For centres which are separated sufficiently far apart so as to avoid a significant overlapping of their Coulomb potentials, the mechanism gives a field dependence of current which follows the Poole-Frenkel type [47].

It can be further deduced that the corresponding behaviour to the Eq.(4.67) would give the imaginary part of dielectric susceptibility as :

$$\chi''(w) = \Lambda(T)\ w^{n(T)-1} \qquad (4.68)$$

where $\Lambda(T)=A(T)/\varepsilon_o$ is a weakly temperature dependent parameter, n is a value which lies in the range $0<n<1$ and $\chi''(w)$ is actually the frequency dependence of dielectric loss of the material, which is defined by the complex dielectric susceptibility $\chi^*(w)$:

$$\begin{aligned}\chi^*(w) &= \varepsilon^*(w) - 1 \\ &= \varepsilon'(w) - i\,\varepsilon''(w) - 1 \\ &= \chi'(w) - i\,\chi''(w)\end{aligned} \tag{4.69}$$

with $\chi(w) = \varepsilon'(w) - 1$ and $\varepsilon''(w) = \chi''(w)$. The value of ε'' in this case is taken in the form of:

$$\varepsilon''(w) = \frac{\sigma(w)}{w\,\varepsilon_o} \tag{4.70}$$

which is very easily derived from first principles (see section 5.3).

Eq. (4.68) would give the loss as nearly frequency independent if n is close to unity. This sort of behaviour is sometimes been interpreted in terms of Debye-type process in which the dipolar relaxation is characterized as having a wide distribution of relaxation times [48]. Jonscher[49], however, proposed that this type of frequency-independent loss behaviour is more suitably explained in terms of hopping conduction mechanism. It was further proposed that any dielectric system may be divided into the "matrix" and the "carriers" . The matrix is characterized by Debye-type processes due to dipolar relaxation or localized ionic charges which gives the dielectric loss of the form :

$$\chi''(w) = \frac{\varepsilon_s - \varepsilon_\infty}{1 + w^2\tau^2}\, w\tau \tag{4.71}$$

which can be derived from Eq. (4.21) and by noting that $\varepsilon^* = \varepsilon' - i\varepsilon''$ (see chapter 5). Obviously this behaviour will show a characteristic loss peaks which has a half-height width of 1.14 decades (see chapter 5) and this may readily be distinguished from the behaviour shown by Eq. (4.68) which it has been proposed as due to hopping carriers. Experimental evidence to support the proposed model is given by Jonscher [46], in which the loss ε'' ($\varepsilon'' = G/(wC_o)$; G being the conductance) is seen to consist of temperature-dependent peaks superimposed on an almost temperature-independent background of the silicon dioxide. From this result, the activation energy of the loss peak is evaluated to be 1.1 eV and the value of n from the plot of $\sigma'(w)$ against frequency is found to be approximately equal to unity, with very little temperature dependence.

The observations made on dielectric loss behaviour in many polymers and in a wide range of inorganic materials led to the suggestion that the dielectric loss in a very wide range of materials follows a "universal law of loss" over a wide range of frequencies as expressed by Eq. (4.68) [50]. Having said this, the dipolar solid materials may exhibit such frequency dependence of loss over certain range of frequencies, whereby the dipoles move by discontinuous hops or jumps between equilibrium position or orientational states. This behaviour may be readily distinguishable from the usual dipolar orientational process which led to the Debye-type dispersion equation (Eq. (4.21)) or Cole-Cole expression (Eq.(4.22)). However, in some materials, it is not certain

whether the observed behaviour of the type shown by Eq.(4.68) should be interpreted as due to dipolar or by charge hopping mechanism since both cases would give similar characteristics. By applying the Fourier transform to the Eq. (4.68), the corresponding dark relaxation current under step-funtion excitation would follow the widely observed behaviour as $I(t)=B(T)\ t^{-n}$ (Eq. (4.1)) where n has the same value as that of Eq. (4.68) [51]. In the light of this, Jonscher and Taiedy [51] showed that the time dependence of the dark current is the same as that of the current under photo-excitation (as measured in the multilayers system of stearic acid at a constant applied bias). This result would give a difficult task in the interpretation of the nature of the prevailing mechanism in the context of the above experimental observation since it apparently showed that the dipolar relaxation follows the same law as relaxation of polarization due to injected charge carriers. Another example of the universal behaviour has been observed in the case of the measured frequency dependence of the conductivity of an aluminium electrolytic capacitor [52]. The result showed that the conductivities follow the law as $\sigma'(w) \propto w^{0.80}$ over seven decades of frequencies (10^{-4} to 10^{3} Hz) at 275 K , while at 345 K it shows a weak loss peak superimposed upon a similar power law. These results led to the conclusion that the law of Eq. (4.68) represents a universal law of dielectric response which is found in a very wide range of dielectric materials regardless of their chemical composition, physical structure and the nature of the charge species responsible for polarization,

whether these are electrons, ions or dipoles [52]. The proposed model remains that the hopping conduction could show a frequency-dependence loss which give rise to characteristic loss peaks, however the nature of the peak may be difficult to be distinguished from that arising due to dipolar orientations. In the case of a relatively slow relaxation of polarization due to hopping carriers, the loss of energy suffered by carriers is almost frequency-independent over many decades of frequencies, which is often seen in low-loss materials. This model is in accordance with the universal power law of loss as represented by Eq. (4.68) with exponents in the range ± 1 and covers the common range of the observed types of dielectric response, from virtually frequency-independent flat losses, through various forms of assymmetric loss peaks to strongly dispersive behaviour. All these observed responses from different dielectric materials satisfy two extremely general criteria relating to the motions of the polarizing species [53] :

(1) The dipoles or charges responsible for the polarization execute sudden hopping or jumping transitions between preferred orientations or sites. The time scale of these transitions is very rapid in comparison with all other processes taking place in the material, in particular with the externally applied variable fields. The nature of these transitions is different from the dipole motions in a viscous medium due to Debye.

(11) Any sudden transition of an individual dipole or charge excites a much slower delayed response of the

neighbouring dipoles or charges through cooperative many-body interactions.

The empirical relation of the frequency dependence of the universal loss behaviour may be written as [52] :

$$1/\ \chi''(w) = (w/w_p)^{-m} + (w/w_p)^{1-n} \qquad (4.72)$$

where w_p is the loss peak frequency which is thermally activated parameters with the exponents m and (1-n) are such that :

$$0 < \begin{pmatrix} m \\ 1-n \end{pmatrix} < 1$$

The first term in Eq. (4.72) corresponds to the low frequency rising part of loss before the peak while the second term corresponds to the universal law (Eq.(4.68)), representing the decreasing function of loss with frequency which occur after the peak. Generally both m and (1-n) tend to decrease with decreasing temperature resulting in very broad peaks.

The corresponding time-domain behaviour of that shown by Eq.(4.72) may be described by two power law functions f(t) (where $I(t) \propto f(t)$) [53] :

$$f(t) \propto t^{-n} \quad , \quad t < 1/w_p \qquad (4.73)$$

and

$$f(t) \propto t^{-1-m} \quad , \quad t > 1/w_p \qquad (4.74)$$

which is distinguishable from the Debye-type behaviour

($f(t) \propto \exp(-w_p t)$), as shown in Fig.4.12. Obviously, the universal peak may require two separate sequential process, in contrast to the Debye loss peak which involve a single exponential process characterized by a relaxation time $\tau = 1/w_p$. However, the Debye-type response, may still provide a vital link between the two power law processes in the transition region. By inspecting Eq.(4.74), for negative exponent m, a strong low frequency dispersion may prevail, as shown in Fig.4.12 by the dashed curve. These cases have been treated by Dissado and Hill [54] , whose associated theory suggest that there is the existence of correlated states which arise from interactions between individual dipoles or charges in an interactive system. This means that the coupling between the local system (such as a system of double-minima potential or a system of two alternative configuration of states) necessitates reorientations at a particular site to cause further reorientations at other sites. The exponents m and n can be regarded as a consequence of interactions of dipoles or charges between preferred orientations or sites. Also, as a result of this interactions, the transition region between the two power laws (or near the loss peak frequency) follows the Debye-like behaviour which may be described by a function f(t), such that :

$$f(t) \propto \exp(-w_p t) \quad , \; t \approx 1/w_p \tag{4.75}$$

where the current I(t) associated with such process is $\propto f(t)$. These three types of transition processes are recognised as a

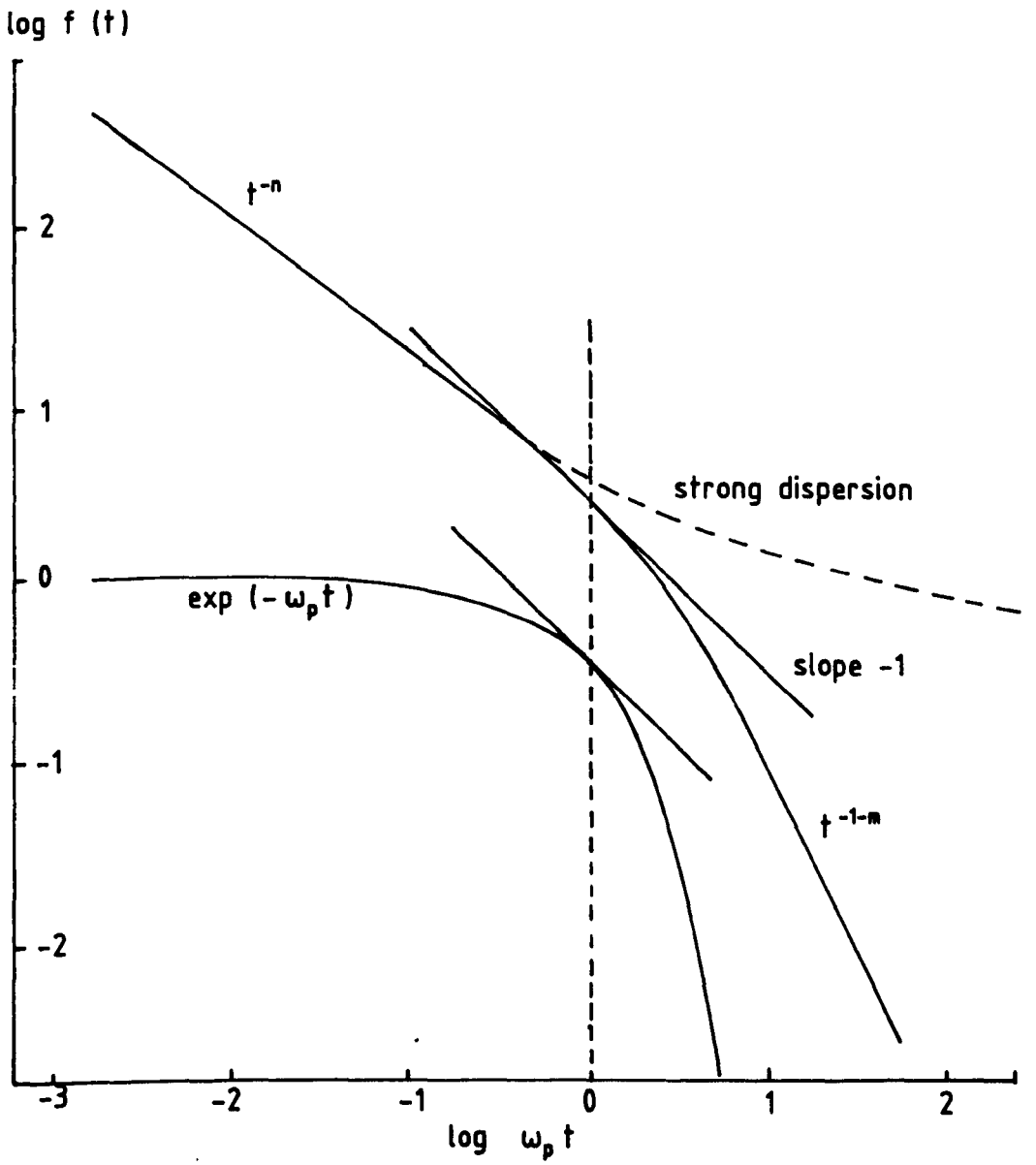

Fig. 4.12. The time-domain response function for the Debye process and for the 'universal' behaviour with the same loss peak frequency ω_p. The dashed curve corresponds to a strong low frequency dispersion.

result of many-body interactions which have been shown to give rise to the observed characteristics in the dielectric response [54,55]. The theory of the many-body model assumes that the system may be represented by the energy diagram in which the two potential wells correspond to the prefered orientation of the system and the total polarization is determined by the relative occupancies of the two wells. The nature of the transition between the two wells determines the characteristics of the observed behaviour of the power laws and the transition region between the power laws. The model suggests the power law behaviour as due to the mechanism of configuration tunnelling in which large numbers of interacting particles undergo a small adjustments which collectively give the result of large transition, while the transition region corresponds to the classical process of thermal excitation from one well to another (or from one preferred orientation to another) which might involve hoppimg of dipoles or charges. Thus, in view of the many-body model, the hopping process may dominate the transition region between the two power laws which are normally present in the dielectric response behaviour. The observed current in the region of this process is thermally activated. Further related theory concerning the dielectric response will be given in the next chapter.

4.2.7. Poole-Frenkel Effect

The Poole-Frenkel effect has been applied to describe a mechanism by which an electron is thermally excited from the traps to the conduction band over the lowering of the Coulombic potential barrier at a sufficiently high electric field, as schematically shown in Fig.4.13. Simmons [13] generalised the barriers to include donor sites, acceptor sites and traps which all tend to experience the Poole-Frenkel effect. The process is thus a bulk effect although the physical basis is similar to the situation for electrode-dielectric interface of the Schottky effect as has been described in section 4.2.5.

In this case, the potential energy of a trapped electron in a Coulombic field is given by [13] :

$$\phi_e = -e^2/(4\pi\varepsilon'\varepsilon_o x) \quad ; \quad x \neq 0 \qquad (4.76)$$

because the Coulombic attractive force to the electron is $e^2/(4\pi\varepsilon'\varepsilon_o x^2)$ for the Poole-Frenkel effect while for the Schottky effect it is $e^2/[4\pi\varepsilon'\varepsilon_o(2x)^2]$. Hence, in the presence of a uniform electric field across the dielectric in the direction shown in Fig.4.13, the modified potential barrier as a function of distance x from the trap site is given by :

$$\phi(x) = \phi_{ct} - e^2/(4\pi\varepsilon'\varepsilon_o x) - eEx \qquad (4.77)$$

where ϕ_{ct} is the ideal potential barrier due to the trap and E

is the applied electric field. Following the same argument as in the case for the Schottky effect, the Poole-Frenkel attenuation of a Coulombic barrier or the barrier lowering $\Delta\phi_{PF}$, is given by :

$$\Delta\phi_{PF} = \phi_{ct} - \phi(x_m) = \left(\frac{e^3}{\pi \varepsilon' \varepsilon_o}\right)^{1/2} E^{1/2} \tag{4.78}$$

where the distance x_m at which the modified potential barrier become maximum is :

$$x_m = \left(\frac{e}{4\pi \varepsilon' \varepsilon_o E}\right)^{1/2} \tag{4.79}$$

It may be observed that the barrier lowering due to the Poole-Frenkel effect is twice that due to the Schottky effect, i.e.,

$$\Delta\phi_{PF} = 2\,\Delta\phi_S \tag{4.80}$$

which is understandable due to different Coulombic forces experienced by electrons in those cases. In the Poole-Frenkel effect, the Coulombic interaction is between the escaping electron and the fixed positive charge while in the case of Schottky effect, it is between the electron and its mobile image in the electrode. Thus the Poole-Frenkel effect is effective only for the traps which are neutral when filled and positively charged when empty. Traps which are neutral when

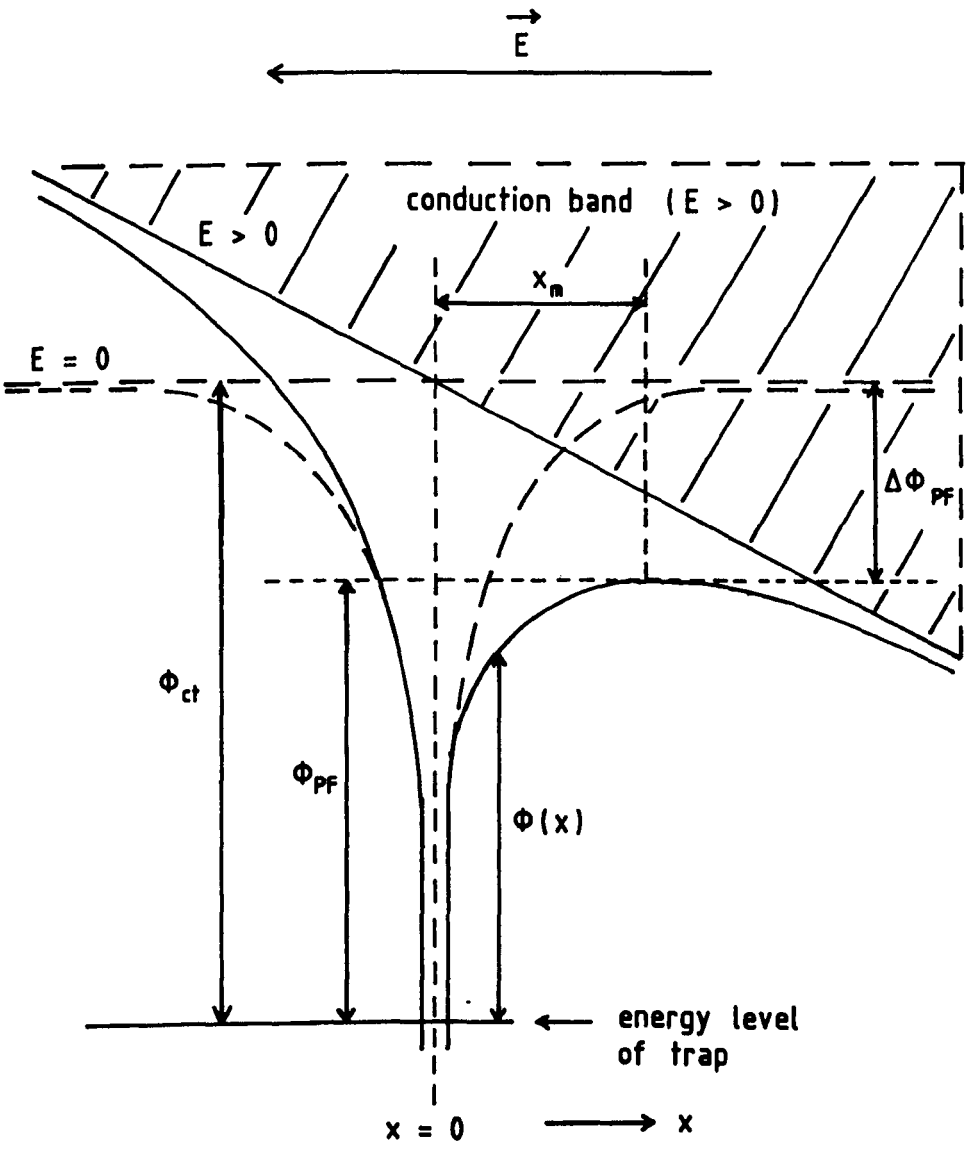

Fig. 4.13. Potential energy diagram illustrating the Poole-Frenkel effect for electron emission from a trap site.

empty and charged when filled will not exhibit the effect for lack of Coulombic interaction [39].

Based on a one-dimensional (planar) model, the field-dependent conductivity of the Poole-Frenkel effect may be written as :

$$\sigma = \sigma_o \exp (\beta_{PF} E^{1/2}/2kT) \tag{4.81}$$

where σ_o is the low field conductivity and

$$\beta_{PF} = \left(\frac{e^3}{\pi \varepsilon' \varepsilon_o} \right)^{1/2} \tag{4.82}$$

Many investigators have used the Poole-Frenkel model to interpret the high field conduction in the dielectrics [47,56-58]. Yeargan and Taylor [56] modified the conductivity expression given by Eq.(4.81), thus :

$$\begin{aligned} \sigma &= e\mu n_o \exp [-(\phi_{ct} - \Delta\phi_{PF})/rkT] \\ &= e\mu n_o \exp [(\beta_{PF} E^{1/2} - \phi_{ct})/rkT] \end{aligned} \tag{4.83}$$

where r is a parameter ranging from 1 to 2 depending on the position of the Fermi level, such that : r=1 for trap level above the Fermi level and r=2 for trap level position below the Fermi level. These conditions arise from the fact that the concentration of free carriers (n) is dependent on the

availability of electrons in the conduction band. For the case of the dielectric which has only donor sites with Fermi level approaching the donor level , the concentration of free carriers is :

$$n = n_o \exp(-\phi_{ct}/2kT) \tag{4.84}$$

where n_o is a parameter related to the effective density of states in the conduction band and the density of donor sites such that $n_o = (N_c N_d/2)^{1/2}$ while ϕ_{ct} is the energy difference between the emission site and the bottom of the conduction band which is the ideal potential barrier due to a trap. When traps are present and situated above the Fermi level which is well above the donor level , the number of electrons in the conduction band will be less since any emitted electrons will fill up the traps level first rather than the energy states in the conduction band. The concentration of free carriers in this case is :

$$n = n_o \exp(-\phi_{ct}/kT) \tag{4.85}$$

with parameter n_o related to the effective density of states in the conduction band; the density of donor sites and the density of traps are related thus $n_o = N_c(N_d - N_t)/2N_t$. Hence Eq.(4.83) can be rewritten for the two limiting cases :

(1) when the concentration of traps is small compared to the density of donor and free carriers :

$$\sigma = e\mu n_o \exp(-\phi_{ct}/2kT) \exp(\Delta\phi_{PF}/2kT)$$
$$= \sigma_o \exp(\Delta\phi_{PF}/2kT) \qquad (4.86)$$

and (11) when the concentration of excited electrons is small compared to the donor and trap (or acceptor) densities :

$$\sigma = e\mu n_o \exp(-\phi_{ct}/kT) \exp(\Delta\phi_{PF}/kT)$$
$$= \sigma_o \exp(\Delta\phi_{PF}/kT) \qquad (4.87)$$

where μ is the carrier mobility in the dielectric.

Obviously, the Poole-Frenkel model may be verified by plotting log σ vs $E^{1/2}$ which is expected to give a straight line with a slope depending on the cases as considered above. At some range of E, Schottky plot of log J vs $E^{1/2}$ may also produce a straight line with a similar slope. If this is the case, the two mechanism are difficult to be distinguished by only looking at those plots. One way to overcome this is by using metal electrodes with different work functions, which is expected to give different results for Schottky emission but not for Poole-Frenkel emission. However, other factors such as interface states at the electrode-dielectric interface and space charges in the bulk of the dielectric could modify the characteristic of the measured properties [13,59].

By comparing the measured slope to the limiting values (provided the high frequency value of ε' is known) , the barrier height ϕ_{ct} may be determined from the appropriate plot of log σ vs 1/T . The plot of log σ vs $E^{1/2}$ may also be used

to check the value of ε' from that obtained using conventional method of small signal ac measurement.

Ieda et al [57] extended Poole-Frenkel model to include the variation of the barrier height with the applied electric field in directions opposite and forward to the electric force experienced by an electron. The model seemed to give quite satisfactory results when compared with some experimental results. Many other modifications of the original Poole-Frenkel model have been made by various workers [47, 58, 60], which always involved some assumptions and new variables in the derivation of the conductivity expressions. It remains that while some models may fit very well to the experimental results of a specific materials, many other published results are not in full agreement with the numerical values of the parameter involved in the proposed model [58].

4.2.8. Space-Charge-Limited Conduction

Experimental observations have shown that space charges may be involved to some extent in the electrical conduction process of polymeric materials [1, 5, 28, 35]. These space charges may be injected from the metal electrodes into the polymer dielectrics which are subsequently kept in traps of different energetic levels. Obviously, the exact nature of the space charges contribution and the extent of its involvement in the conduction process are not very easy to be understood since the process may involve many different mechanisms (some

of which have been described in the previous sections).

The space-charge-limited (SCL) conduction theory in solids has been first proposed by Mott and Gurney [61] who have given a simplified analysis of space-charge injection into an ideal trap-free insulator. It is assumed that the free component of the space charges in the bulk of the insulator (which is different from the space charges formed at the vicinity of the electrode-dielectric interface) conducts the current to some extent, thus the term space-charge-limited current is used[13]. Simmons [13] suggests that the ohmic contact at the electrode-dielectric interface (see Fig.4.1) is necessary for SCL conduction process to occur since the charge carriers can be injected through such contact in which the cathode region can be considered as a charge reservoir that supplies charge to the anode region as demanded by the applied electric field bias conditions. The model of Mott and Gurney [61] which confined to the trap-free dielectric with a single species of charge carriers led to the steady state current density (J) expression as :

$$J_{SCL} = \frac{9}{8} \mu \varepsilon_o \varepsilon' V^2 / L^3 \qquad (4.88)$$

where μ is the mobility of the charge carriers, V is the applied voltage and other symbols are as previously defined. The above expression is normally referred to as the trap-free square law, the Child's law for solids or the Mott-Gurney square law. The proportionality of J to V^2 and to $1/L^3$ have been confirmed experimentally. However, it predicts much

higher currents than that observed in practice and also that the current does not predict any temperature dependence which is in contrary to observation [13]. As such the applicability of the model in practice is rather limited since most solid dielectrics contain some forms of traps which obviously modify the conduction current.

Rose [62] was the first who considered the SCL currents in the dielectrics which contain traps. In this case, a large fraction of the injected space charges may be localised in the traps and will not contribute to current flow. The ratio θ of free to trapped charge carriers in a dielectric containing shallow trap ($\mathcal{E}_t$ situated above $\mathcal{E}_F$) is [63] :

$$\theta = \frac{n}{n_t} = \frac{N_c}{gN_t} \exp\left(\frac{\mathcal{E}_t - \mathcal{E}_c}{kT}\right) \qquad (4.89)$$

where n is the free electron concentration, n_t the concentration of filled electron traps, N_c the effective density of states in the conduction band, N_t the concentration of traps, g the degeneracy factor (statistical weight) for the traps, $\mathcal{E}_t$ the trap energy level and $\mathcal{E}_c$ the bottom of conduction band energy level. The SCL current which incorporate the shallow traps can be shown to be given by [63]:

$$J_{SCL} = \frac{9}{8}\theta\mu\varepsilon_o\varepsilon' V^2 / L^3 \qquad (4.90)$$

It is clear that $J \propto V^2$ as in the case of trap-free and it is temperature dependent which justify the experimental observations.

The SCL current may only be observable if the injected free carrier density n_i exceeds the thermally generated free carrier density n_o . Hence for $n_o > n_i$, which may be true at relatively low voltages, the dielectric conductivity is expected to follow Ohm's law, the current density being given by :

$$J_{ohm} = en_o \mu V/L \qquad (4.91)$$

The transition from ohmic to SCL conduction occurs at voltage V_x , in which $J_{ohm} = J_{SCL}$, so that :

$$V_x = \frac{8\ en_o L^2}{9\ \theta\ \varepsilon'\varepsilon_o} \qquad (4.92)$$

Eq.(4.92) indicates that :

(1) The voltage for the transition V_x increases with increasing density of thermally generated carriers n_o .

(11) The smaller the value of θ , which means the higher the concentration of traps, then the value of V_x will be shifted to higher values.

The increase of applied voltage may increase the density of the carriers resulting from injection to such a level that the Fermi level moves up above the shallow traps level and the

traps are filled up or saturated. This condition is the limit of the trap filling process and is usually called the traps-filled limit (TFL) . Thus, any additional injected charges into the dielectric exist as free charges in the conduction band and contribute to the current , so that at the threshold voltage V_{TFL} , the current will rapidly jump from its trap-limited value to a trap-free SCL current. Beyond the TFL , the dielectric behaves as if it were trap-free with the current density J being given by Eq.(4.88) . On the assumption that the concentration of free carrier n at the onset of TFL is much less than the concentration of traps, i.e. $n << N_t$, then using the Poisson's equation, it gives :

$$\frac{dE_{TFL}}{dx} = \frac{eN_t}{\varepsilon' \varepsilon_o} \tag{4.93}$$

which gives the value of V_{TFL} as :

$$V_{TFL} = \int_0^L E_{TFL}\, dx = \frac{eN_t L^2}{2\, \varepsilon' \varepsilon_o} \tag{4.94}$$

Fig. 4.14 shows the schematic characteristics of log J - log V for a dielectric having a shallow discrete trapping level ($\varepsilon_t > \varepsilon_F$). At the lower voltages (region ab or ab') , the characteristic is ohmic ; in region bc or b'c', the SCL current predominates up to the point where TFL is satisfied (region cd or c'd'), beyond which the current increases rapidly and follows the trap-free square law (dd'e) . The

position of the onset of SCL current (i.e. V_x or V_x') is determined by the value of θ through Eq.(4.92) while the TFL condition (V_{TFL} or V_{TFL}') is dependent on the concentration of traps in the dielectric as can be inferred from Eq. (4.94).

For more complex cases, an account of trap distribution in the forbidden gap may have to be considered. This consideration is particularly important in dealing with amorphous dielectrics where a large amount of structural disorder can be found. In these materials, an electron trap which may originate from chemical impurity or structural defects, does not have a well defined energy level ; instead it may form a broad smearing out of the energy levels. Lampert and Mark [63] suggest a simple possible representation of such traps with the exponential distribution, such that :

$$N(\mathcal{E}) = N_o \exp [(\mathcal{E} - \mathcal{E}_c)/kT_t] \qquad (4.95)$$

where $N(\mathcal{E})$ is the concentration of traps per unit energy range at an energy $\mathcal{E}$ below the conduction band edge energy level $\mathcal{E}_c$, N_o is the value of $N(\mathcal{E})$ at the conduction band edge which is equal to $N_t/(kT_t)$ and T_t is a temperature parameter which characterises the exponential trap distribution. The physical significance of T_t is suggested to be the temperature in the final cooling-down stage of the preparation of the material at which annealing effectively ceases. The current-voltage response for the SCL current injection into a dielectric having such an exponential

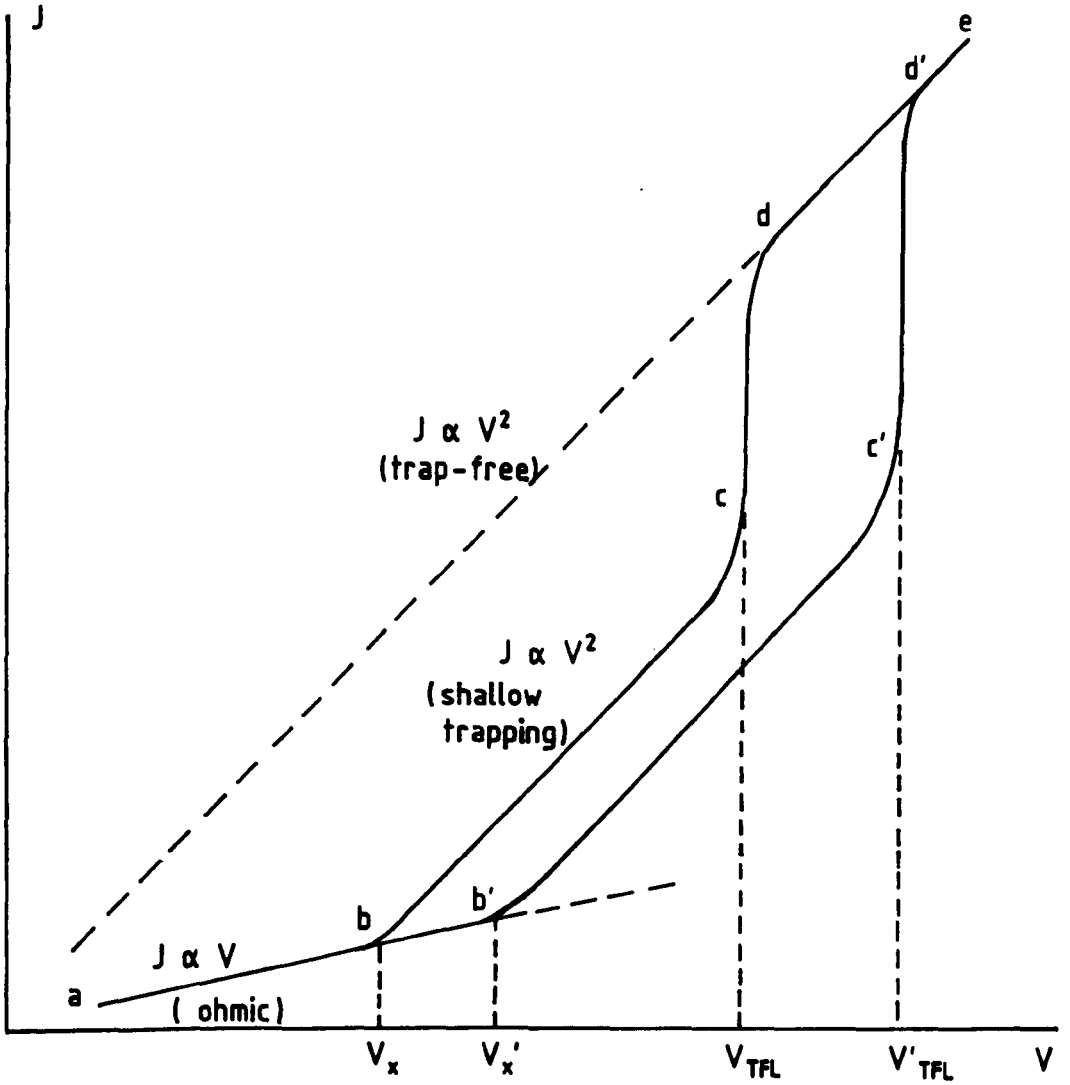

Fig. 4.14. Schematic SCL J-V characteristic for a dielectric containing a shallow discrete trapping level. The variation of V_x and V_{TFL} are related to the concentration of traps in the dielectric.

distribution of traps is given by :

$$J_{SCL} = N_c \mu e^{(1-s)} \left(\frac{\varepsilon_o \varepsilon' s}{N_t (s+1)} \right)^s \left(\frac{2s+1}{s+1} \right)^{(s+1)} \frac{V^{(s+1)}}{L^{(2s+1)}} \quad (4.96)$$

which was first derived by Mark and Helfrich [64]. A simplified version of this relation may be written as [63] :

$$J_{SCL} \simeq e \mu N_c \left(\frac{\varepsilon_o \varepsilon'}{e N_t} \right)^s \frac{V^{(s+1)}}{L^{(2s+1)}} \quad (4.97)$$

where $s = T_t/T$.

Further treatments on the SCL conduction involving deep traps, two-carrier injection with traps and recombination centres and different form of trap distribution may be referred to the work given by Kao and Hwang [39] and Lampert and Mark [63].

4.2.9. Ionic Conduction

It is well known that ionic conduction prevails in ionic crystals such as alkali halides (NaCl, KCl, etc) whose basic constituents are ions. Experimental observations have shown that the low field electrical conductivity σ in these materials can be expressed as [65] :

$$\sigma = \sigma_{oe} \exp\ (-\ \phi_e\ /kT\ ) + \sigma_{oi} \exp\ (-\ \phi_i\ /kT\ )$$

(4.98)

where σ_{oe} and σ_{oi} are constants. The first term is associated with the motion of extrinsically introduced defects with activation energy ϕ_e and is applicable in the lower temperature range. The other term is due to ionic movement (or creation of defect) within the originally perfect crystals which involves the activation energy ϕ_i and occur at relatively higher temperature region. Thus impurities may create chemical imperfections which would then give rise to ionic current (contribute to the first term of Eq.(4.98)), in addition to the currents originated from the defects in the crystals. The thermally generated lattice defects are normally associated with Frenkel and Schottky defects. In Frenkel defects, two types of imperfections are created as a result of an ion moving from a lattice site to an interstitial position within the lattice, i.e. vacant lattice site and interstitial ion. On the other hand, a Schottky defect is formed by the migration of an ion which was originally at a site of the perfect lattice to a surface position which effectively creates a vacant lattice site. Charge neutrality is preserved in the material by the fact that the vacancy of opposite charges may be produced in the volume of the crystals.

It can be inferred from the above observation that in non-ionic dielectric materials, chemical impurities which may have been introduced during preparation and processing , are responsible for the ionic current as a result of chemical

defects. In ceramic materials of perovskite structure such as $BaTiO_3$ and PZT , a trace of ions from various impurities are likely to be found, which are deliberately introduced during material preparation for phase stabilization and for several other reasons related to the improvement of the material properties [66]. In some cases, the added impurities can be regarded in a similar manner as a process of substitution doping in which a basic component (cation or anion) of the parent material is replaced with another element from the impurities. As a result, vacancies or interstitial ions are formed. These vacancies, in certain circumstances, may create a weak electrostatic field equal to that generated by a charge whose sign is opposite to that of the ion removed. The field eventually acts upon neighbouring ions and displaces them from equilibrium position, causing a local lattice distortion. Thus a kind of local polarization may be produced in a region of spherical symmetry about an isolated vacancy. However the polarization process may have to compete with the ionic conduction which occurs by means of cation and anion jumps to vacant sites, thus providing an ionic current.

An examination of natural polymeric materials shows that their structure is complex, consisting of crystalline and amorphous regions. In the polymer where the crystalline structure predominates, the material is relatively strong, rigid and more resistant to heat and dissociation, while for the mostly amorphous structure material, it is soft, elastic, absorptive and permeable to fluids [67]. In any case, the packing of polymer molecules is by weak van der Waals forces,

giving a weak electronic coupling between molecules and hence electronic conduction may be obstructed.

As in the case of perovskite ceramics, ionic impurities may be introduced during the preparation and processing of polymers. It is assumed that the ions are mainly derived from fragments of polymerization catalyst, degradation and dissociation products of the polymer and absorbed water. Thus a polymer like polyvinyl chloride (PVC) may most proably contain H_3O^+, Na^+, K^+ cations and OH^-, Cl^-, Br^- anions [68]. However the presence of ionic conduction may not be possible to detect by means of electrolysis method due to a very low conductivity of polymers. Hence, an indirect means of elucidating the nature of conduction has to be realised.

Mott and Gurney [61] provide a basic theoretical model by which an ionic conduction mechanism may be studied from the dependence of current on applied electric field. In this model, it is assumed that an ion may jump from one state to another over a potential energy barrier with an activation energy ΔU such that a low field current I is given by :

$$I = I_o \exp(-\Delta U/kT) \operatorname{Sinh}(edE/2kT) \qquad (4.99)$$

where $I_o = 2Aned\nu$, A is electrode area of the specimen, n density of mobile charge carriers (ionic concentration) , e the electronic charge, d the jump distance, E the electric field and ν can be regarded as the vibration frequency of ions in jumping from one state to the other. In high electric field region, $eEd >> 2kT$, Eq.(4.99) can be approximated thus:

$$I \simeq I_o \exp(-\Delta U/kT) \exp(edE/2kT) \qquad (4.100)$$

Hence a plot of ln I versus E at any particular temperature T should give a straight line at high fields with a slope of edE/2kT , from which the value of d may be evaluated. From the extrapolated values of currents at zero field plotted against reciprocal of temperature, a measure of activation energy associated with such mechanism may be obtained.

4.3. Experimental Details

Samples for measurements were placed in a stainless steel chamber under vacuum (less than 10^{-5} torr) so that the effect from atmospheric ions may be kept to a minimum. In addition, the good vacuum condition provides the following advantages :

(1) high field application to the samples can be made without a serious risk of electrical breakdown between the electrodes (breakdown field strength of air is 3.0×10^6 Vm^{-1})

(11) low temperature (below 273 K) measurements can be performed with no condensation on the samples and at the electrical connections.

(111) thermal degradation of the samples at high temperatures could be reduced to some extents.

Cable connections were kept as short as possible and were screened with copper jacket so as to minimise the effect of extraneous currents generated by electrostatics from the surrounding environment. This also ensures that the very low current may be measured, limited only by the specification of the electrometer used for current measurements.

Heating of the samples was accomplished by means of dc voltage heaters and a temperature controller which are capable of maintaining the temperatures to within ± 0.25 over a range of 73-403K. To obtain temperature below ambient, liquid nitrogen was fed into the double-walled dewar attached to the cold finger of the measurement chamber and the voltage to the heater was appropriately adjusted, thus allowing low

temperature measurements over a reasonable range.

4.3.1. Sample preparation

Most of the measurements of charging and discharging currents over a wide range of fields and certain range of temperatures were performed on ceramic/polymer composite of PIEZEL , since this was the only composite sample available in the initial stage of the present work. PIEZEL samples are reported to have been prepared by mixing fine PZT ceramic powder and fluoropolymer (copolymer of vinylidene fluoride (VDF) - Trifluoroethylene (TrFE)) at a temperature range of 443-493 K and then rolled at 373-443 K into approximately 250 μm sheet thickness. They are flexible and available in sizes as large as 20 cm x 20 cm [69, 70] . The samples were cut to an appropriate size of approximately 2.8 cm x 2.8 cm and their surfaces were cleaned with soft tissue moistened with iso-propyl alcohol (to remove dust and grease) and dried thoroughly before aluminium electrodes of dimension 2 cm x 2 cm (electrode thickness being approximately 600 Å) were evaporated on both sides of its surfaces in an evaporation chamber at $\sim 10^{-5}$ torr. Before any measurements were carried out, the samples were thermally conditioned at 373 K for at least 24 hours in an evacuated measurement chamber with its electrodes short circuited. This procedure of conditioning is adopted since it had been proven to give the repeatability of the measured current [1,5] , understandably due to the fact

that it may reduce the effect of any residual or remanent internal polarization.

At the latter stage of the present work, a hot roller machine became available in the laboratory which enabled some ceramic/polymer composites to be prepared. For this purpose, PVDF and VDF-TrFE were obtained from Laporte Trading of Luton, U.K. They were supplied in the form of pellets under the grades of Solef 11010 (copolymer VDF - TrFE) and Solef 1008 (homopolymer PVDF).

PZT ceramic powders were supplied by Unilator Technical Ceramics Ltd of Wrexham , U.K. They are of two types, i.e. PZT5 and PZT4. An examination under scanning electron microscope revealed that the grain sizes of PZT5 powder were in the range 0.2-0.4 μm diameter while that of PZT8 were in the range 1-2 μm diameter. PZT5 in the form of discs were also supplied by Unilator, having 2mm thickness and 2.5 cm diameter. These disc samples were already furnished with fired silver electrodes of 2 μm thickness. In order to compare with other samples, the silver electrodes were removed by polishing with a fine silicon carbide paper after which aluminium electrodes of 2 cm diameter were vacuum evaporated on both surfaces.

Taking the density of VDF-TrFE as 1.8 gm cm^{-3} and of PZT as 7.9 gm cm^{-3} (references [71-73]), composites of PZT5/VDF-TrFE with various volume compositions were prepared by the following method. The surface of rolling mill was first thoroughly cleaned with iso-propyl alcohol to remove any grease or dust. The temperature of the roller was then set at

443 K and the gap between the rollers was adjusted to an appropriate distance. As the temperature was stabilised, the polymer pellets were melted on the rollers which were kept rolling at low speed and hence a polymer film was formed, covering the surface of the rollers. While the rollers were kept on rolling, the ceramic powder was carefully dispersed into the polymer film and the two phases were allowed to mix properly under continuous rolling at a steady speed. After some time the composite flake was peeled off from the roller with a suitable tool. A second stage in the process was to press the composite into a film of a particular thickness. For this purpose, the composite was placed between the two chromium plated steel plates and the pressing was performed in a temperature-controlled hydraulic press at 438 K at a pressure of 100-300 kgf/cm^2. A good surface texture of the composite film has been achieved by the use of high quality chromium plates. The film may have to be pressed several times to achieve an approximately uniform thickness. A typical film thickness prepared in the present work falls in the range 100 to 350 μm with a thickness variations in a film in the range of 5-10% . Thus a considerable amount of time was spent in the preparation of the film. The film is allowed to cool to room temperature in the press to give a good surface texture and only a small size of film can be pressed at a time. Aluminium electrodes of dimension 2 cm x 2 cm were then vacuum evaporated on both sides of cleaned composite film of appropriate size (2.8 cm x 2.8 cm) followed by thermal treatment in an evacuated measurement chamber prior to any

measurement.

Composites of $BaTiO_3$ (density = 5.7 gm cm^{-3} , supplied by Cookson Group Plc of Middlesex, U.K.) and PVDF(density= 1.8 gm cm^{-3}) , PZT4/PVDF, PZT5/PVDF and PZT4/Polypropylene(PP) (PP: density = 0.9 gm cm^{-3} , in pellets form, obtained from Hercules Corporation, U.S.A.) were also prepared by the above method. In the case of PZT4/PP , the mixing was performed at 408 K and the pressing at 408-418 K . All the electrodes of these composite samples were vacuum deposited with aluminium of 2 cm x 2 cm dimension.

4.3.2. Measuring apparatus system

The electrical measuring circuit used in the present work is schematically shown in Fig.4.15. The vacuum system for the sample chamber is shown in Fig.4.16 and the sample holder attachment inside the chamber is shown in Fig.4.17.

Strips of mica were used to electrically isolate the brass block (containing heater element) and the copper block which served as a low tension electrode to the sample (see Fig.4.17). This unfortunately gave rise to an undesired thermal lag which reduced the transfer of thermal energy from the heaters or cold finger to the copper electrode. However, since the heater block was made from brass which has a large thermal capacity , it effectively served as a thermal reservoir. The heater block with its attachment was fixed to a

cold finger and linked to a double-walled stainless steel dewar which can be filled with liquid nitrogen to attain temperatures down to 73 K. The high tension copper electrode, in a form of a 1.8 cm hollow square, was incorporated inside a PTFE block which has a central aperture to allow thermal radiation of light to reach the sample. A Chromel-Alumel thermocouple was suitably incorporated in the low tension copper block using Araldite adhesive which provided electrical isolation and good thermal contact.

The sample vacuum chamber was made from stainless steel and its connections to the diffusion and rotary pumps are shown in Fig.4.16. The chamber is about 20 cm in depth and 23 cm in diameter, mounted vertically and sealed by a lid which incorporated the cold finger, sample holder and lead through units (an 'O' ring was used to ensure an air-tight seal). One of the lead through unit, has H.T. and L.T. leads and the other comprises heater lines and thermocouple connection. These units were housed in a screened aluminium box to prevent electrical noise. The breakdown strength of lead throughs used were about 10 kV .

The chamber was evacuated by means of an oil diffusion pump (Edwards Speedivac, model E04) , which was backed up by a rotary pump (Edwards Speedivac, model ES150). Pirani gauge was used to monitor the backing pressure whilst a Penning gauge recorded the high vacuum chamber pressure. A working pressure in the region of 10^{-6} torr was easily achieved and all the measurements were performed at this pressure. A solenoid valve was fitted to the rotary pump to prevent the passage of rotary

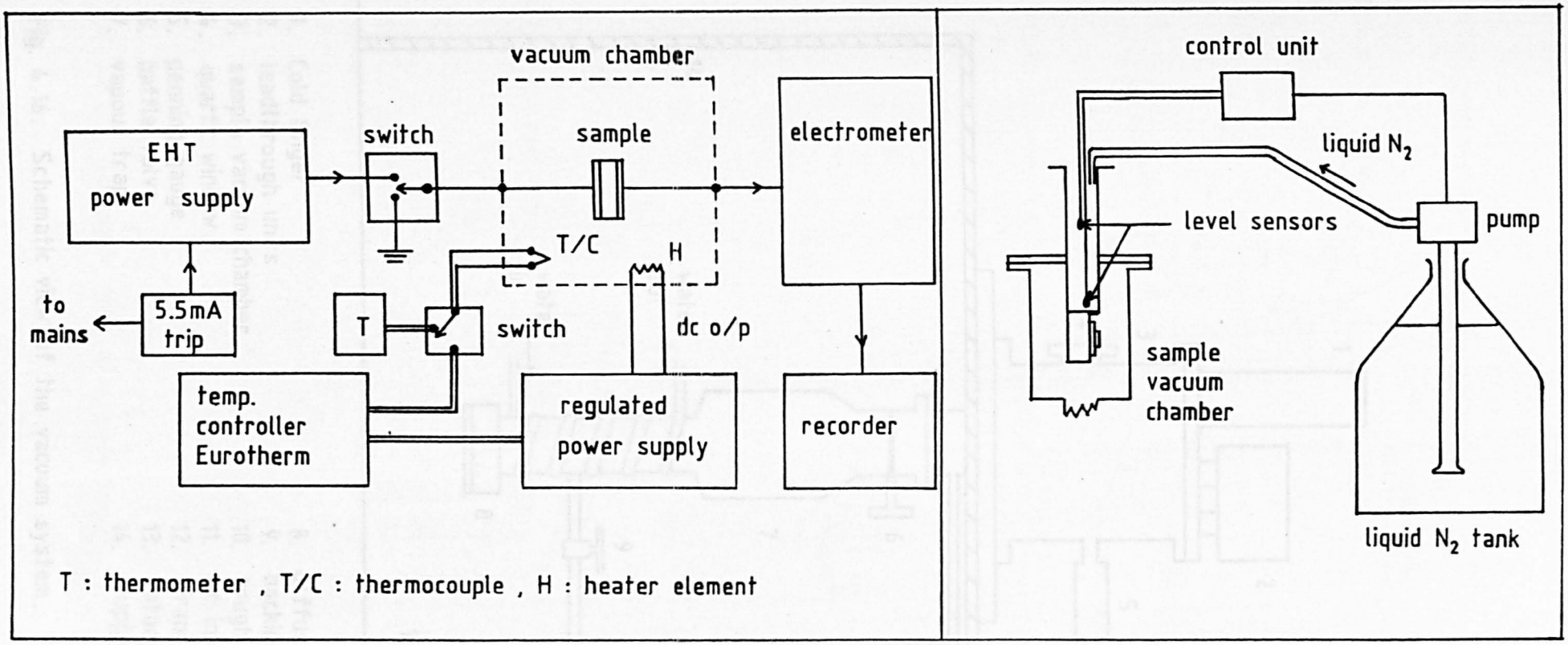

Fig. 4.15. Schematic diagram of apparatus system.
(a) measuring and temperature control circuitry
(b) low temperature feeding equipment.

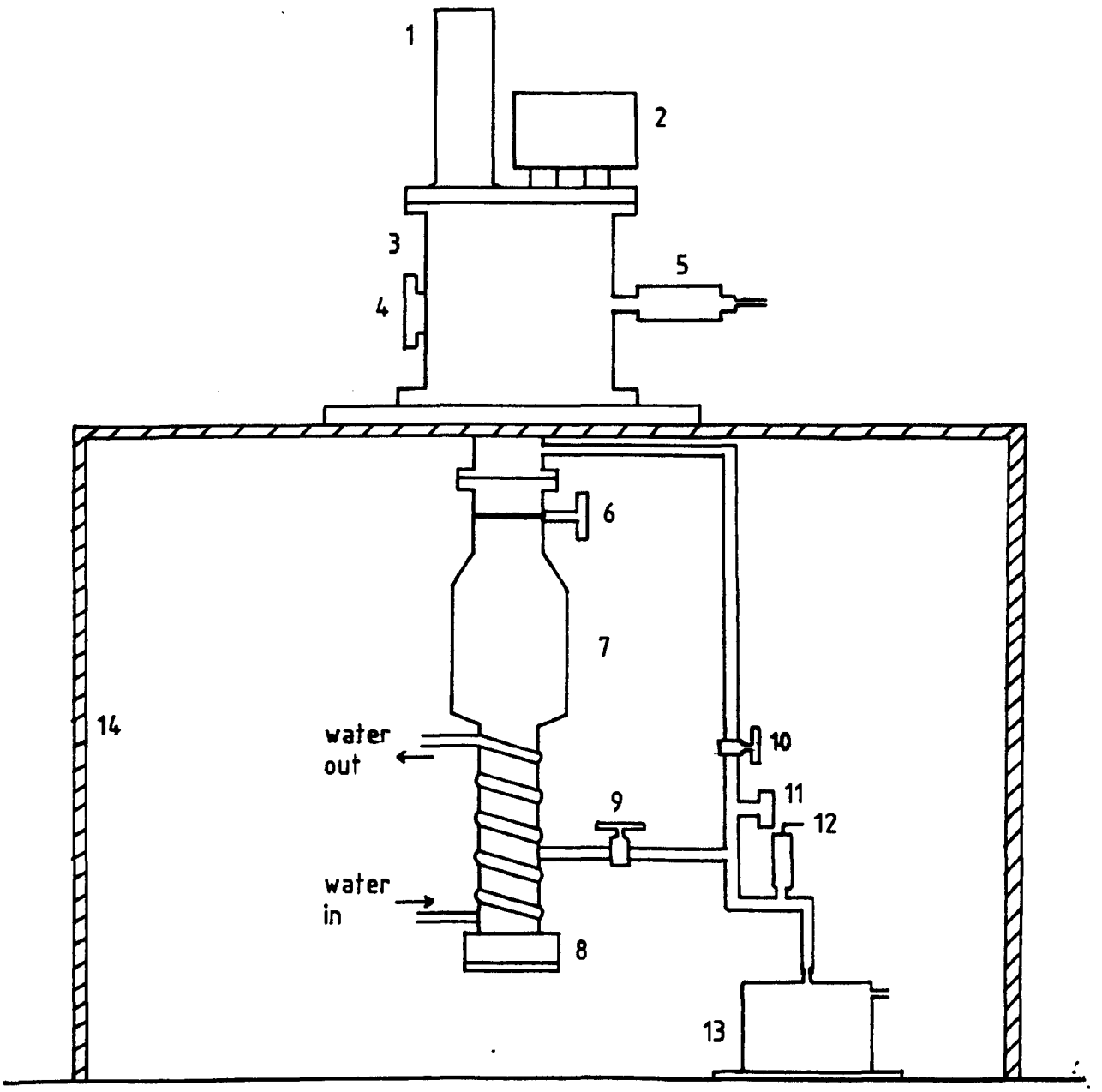

1. Cold finger
2. leadthrough units
3. sample vacuum chamber
4. quartz window
5. penning gauge
6. baffle valve
7. vapour trap
8. diffusion pump heater
9. backing valve
10. roughing valve
11. air inlet
12. pirani gauge
13. rotary pump
14. support stand

Fig. 4.16. Schematic view of the vacuum system.

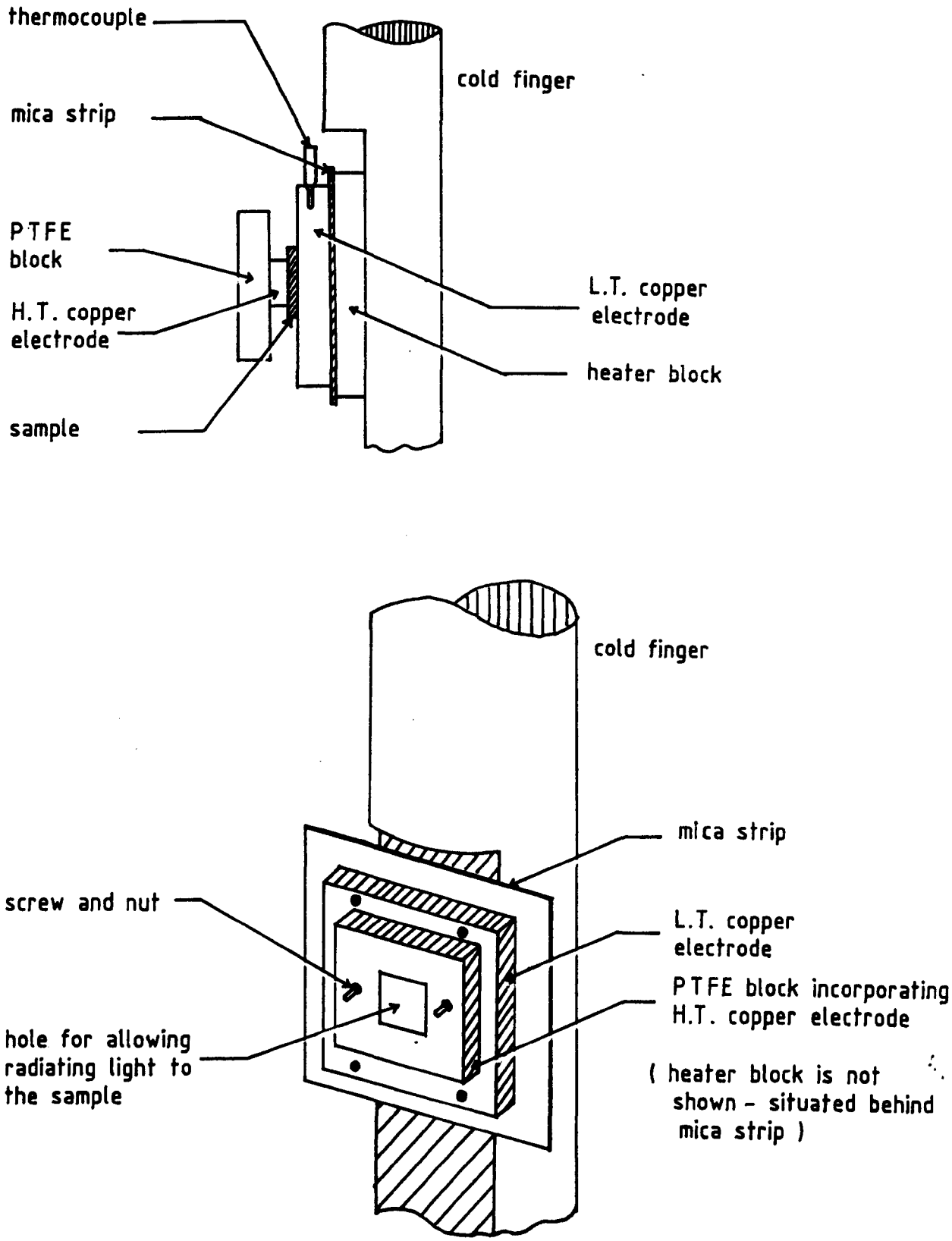

Fig. 4.17. Schematic view of sample holder.

pump's oil into the high vacuum system in the event of power failure whilst a thermal cut out prevented damage to the diffusion pump in the event of water supply failure.

A Brandenburg photomultiplier power supply (model 472R) was used as a voltage source to pole the sample in the range of 50 V to 2.1 kV . The supply had a good stability against a ± 7% mains change. Connection to the sample chamber was made using a screened coaxial cable. An over-current 5 mA trip was incorporated to the mains power suply to prevent any high voltage being fed to the input of the electrometer in the event of sample breakdown. The switch between the supply and the sample (shown in Fig.4.15(a)) was used either to short circuit the sample electrodes through the electrometer or to apply a step dc voltage to the sample. The current flowing through the sample was monitored by a Cary (model 401) or Keithley (model 602) electrometer which was chart recorded.

The main part of the temperature control system was a high stability Eurotherm temperature controller unit (type LP 96/DHS). This unit allows a satisfactory control of temperature within a range 73 K to 523 K. The sensing thermocouple was located at the L.T. copper electrode. A Farnell regulated power supply (type 30/55) was incorporated with the Eurotherm unit to give an appropriate voltage to the heater element. The ripple voltage of the temperature control system was less than 500 μV and hence it was possible to maintain an accurate temperature control to within ±0.25 K.

For low temperature settings (below ambient temperature), the cold finger was filled with liquid nitrogen.

This was achieved by incorporating Cryoproducts liquid level controller (logic unit) which sensed the level of liquid nitrogen in the cold finger and a pump which supplied a required amount of liquid nitrogen from a 25 litre dewar to the cold finger, as shown in Fig.4.15(b). The action allowed overnight measurements to be carried out efficiently at any particular setting temperature. By varying the amount of heat supplied to the sample, couple with the cold finger temperature, it is possible to obtain a low temperature range of 73 K-288 K, with an accuracy ±0.25 K.

4.3.3. Measurement and procedure

The measurements described in this chapter were performed to obtain information on the nature of the absorption and resorption currents as well as the electrical conduction mechanism in ceramic/polymer composites. The temperatures employed were in the range 293 K - 373 K while the fields were in the range $1.75 \times 10^5 - 1 \times 10^7$ V m^{-1} .

All the samples used were initially conditioned at 373 K for at least 24 hours , as previously described (see section 4.3.1), to reduce the effect of surface and space charges. The temperature was then lowered to the desired value where the electric field stress was applied, starting with a low field. After a series of fields (in increasing magnitude) have been applied and the absorption and resorption currents were measured, the temperature was raised to a higher level and the

experiments were repeated. In all cases, it was necessary to condition the sample thermally at a high temperature after each applied field to ensure that polarization effects were kept to a minimum. The above procedure was found to give good repeatability of the results.

Most of the results on the behaviour of charging and discharging currents were obtained on PIEZEL composite. For the purpose of comparison, some results on the charging and discharging currents were also obtained with single phase PZT ceramic at a limited range of temperatures. Results of charging and discharging currents in PZT/VDF-TrFE, PZT/PVDF, $BaTiO_3$/PVDF and PZT/PP composites were obtained at limited fields and temperatures.

4.4. Experimental Results

4.4.1. Charging and discharging currents in PIEZEL

Fig. 4.18 shows the behaviour of charging currents ($I_c(t)$) with time for different applied fields in the range of (0.175-5.6)x10^6 Vm^{-1} at room temperature (T=293K) in PIEZEL. The currents were measured for about 28 hours (=10^5 sec) (only up to 10^4 sec are shown in the figure), from which the steady-state current level was obtained at t=10^5 sec. The effect of various applied electric field at high temperature (T=363K) on $I_c(t)$ in this material is shown in Fig.4.19, from which it may be observed that the quasi-steady-state current tends to appear at earlier times as the field is increased. Similar effect on the behaviour of $I_c(t)$ at a fixed applied electric field with temperature variation has also been observed (see Figs.4.20 and 4.21).

The corresponding behaviour of discharging currents ($I_d(t)$) at room temperature and at T=363K is shown in Figs.4.22 and 4.23 respectively. The currents were obtained after the sample was pre-charged for ~28 hours and $I_d(t)$ was measured for 10^4 sec after the sample's electrodes been effectively shorted. Fig.4.24 shows the behaviour of $I_d(t)$ at high pre-applied field and at temperature in the range of 293-363K. From these results, it may be observed that the behaviour of $I_d(t)$ follows the familiar pattern, i.e. :

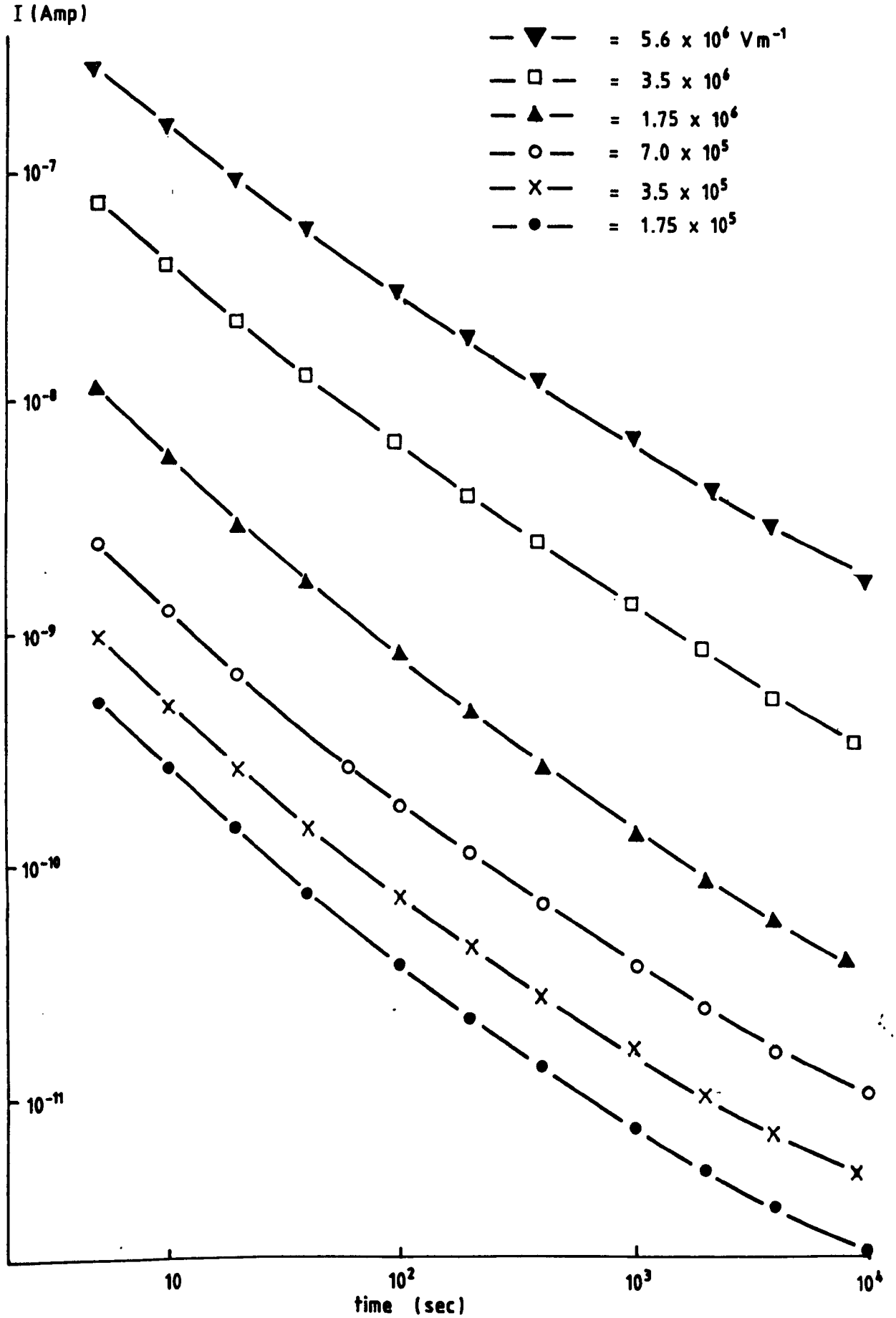

Fig. 4.18. Charging currents in PIEZEL for different fields at 293 K.

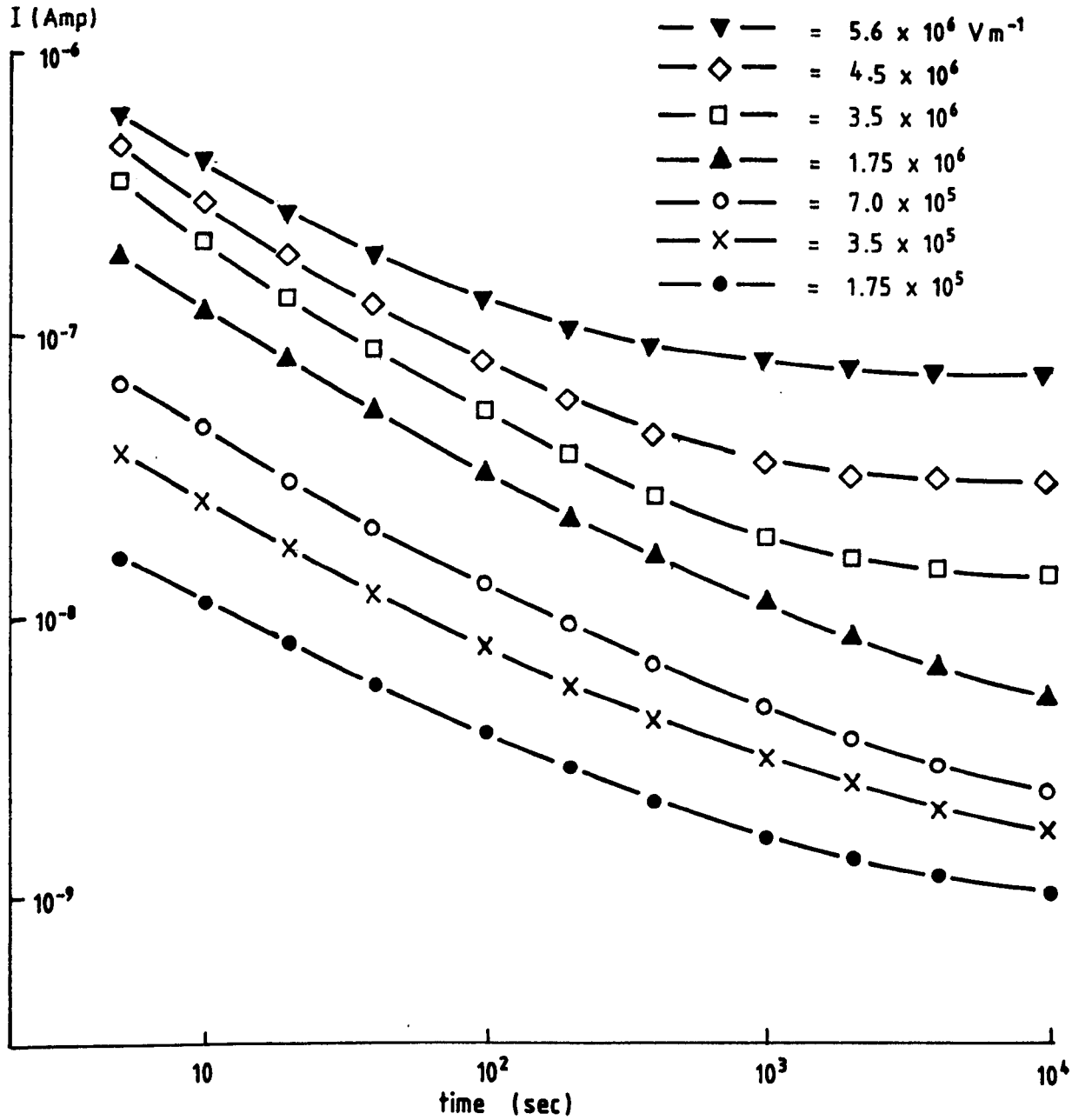

Fig. 4.19. Charging currents in PIEZEL for different fields at 363 K.

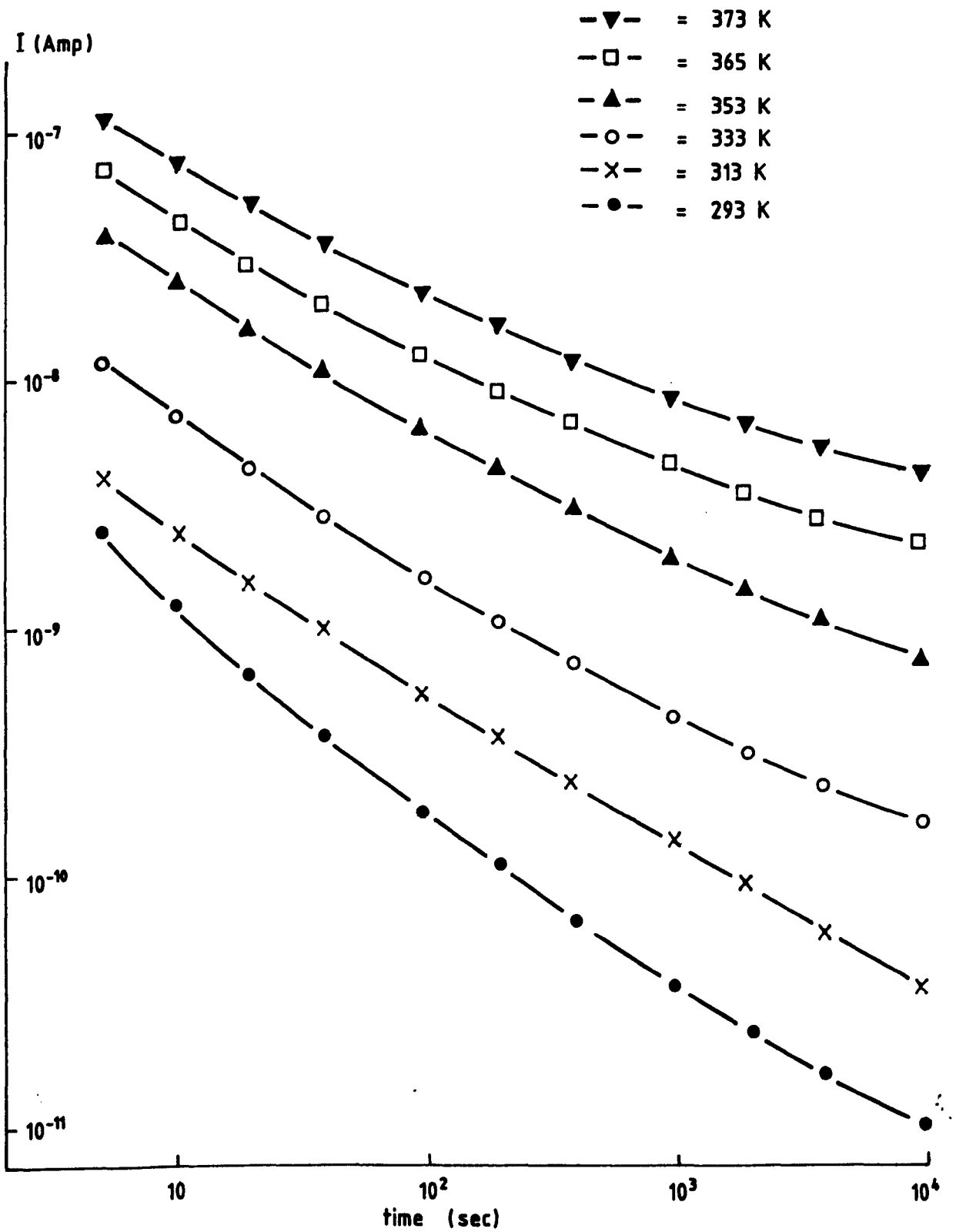

Fig. 4.20. Charging currents in PIEZEL for different temperatures at field 7×10^5 Vm^{-1}.

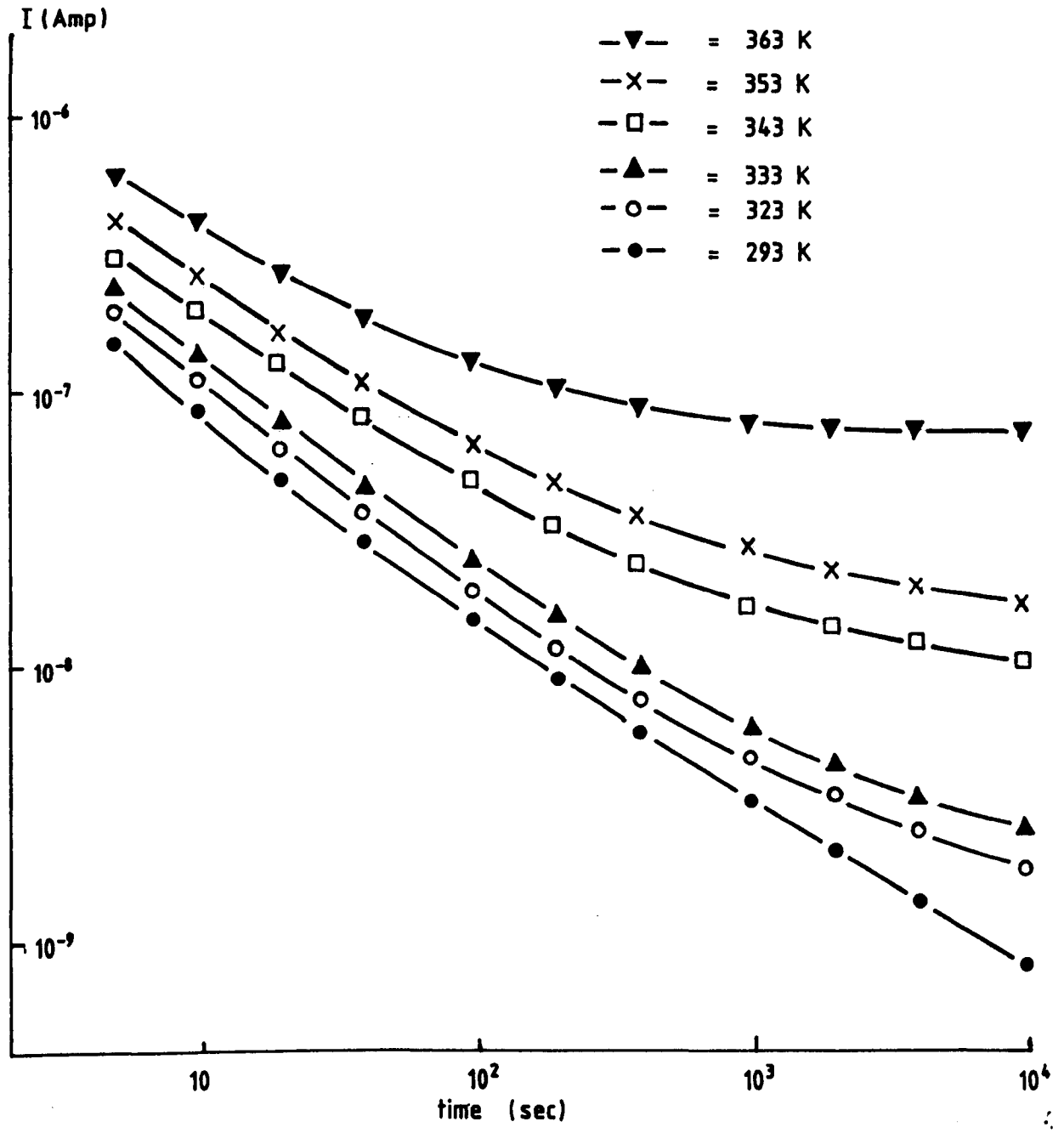

Fig. 4.21. Charging currents in PIEZEL for different temperatures at field 5.6×10^6 Vm^{-1}.

$$I_d(t) \propto t^{-n} \qquad (4.101)$$

with the value of n $\sim$ 0.6-1.04 (depends on the pre-applied field and temperature) in the range of fields (0.175-5.6)x10^6 Vm^{-1} and temperatures 293-363K.

Figs.4.25 and 4.26 show the behaviour of charging and discharging currents at specific temperature (variable field) and specific field (variable temperature) respectively. The polarity of $I_d(t)$ has been reversed for the purpose of clarity. It may be observed that the difference in magnitude between $I_c(t)$ and $I_d(t)$ at constant times increases with increasing charging fields (Fig.5.25) and with increasing temperature (Fig.4.26), demonstrating the influence of contributions of the steady-state conduction current at progressively shorter times. It should also be noted from Figs.4.25 and 4.26 that above a certain limit of field and temperature, the difference of $I_c(t)$- $I_d(t)$ decreases with time until a steady-state current I_s is reached.

Figs. 4.27 and 4.28 show the behaviour of isochronal (i.e. at constant times) charging currents for different fields at constant temperature of 293K and 363K respectively. It may be observed that the dependence of current on electric field is different for different regions of time, field and temperature. The dependence may be approximated to have the relationship as :

$$I_c(t) \propto E^p \qquad (4.102)$$

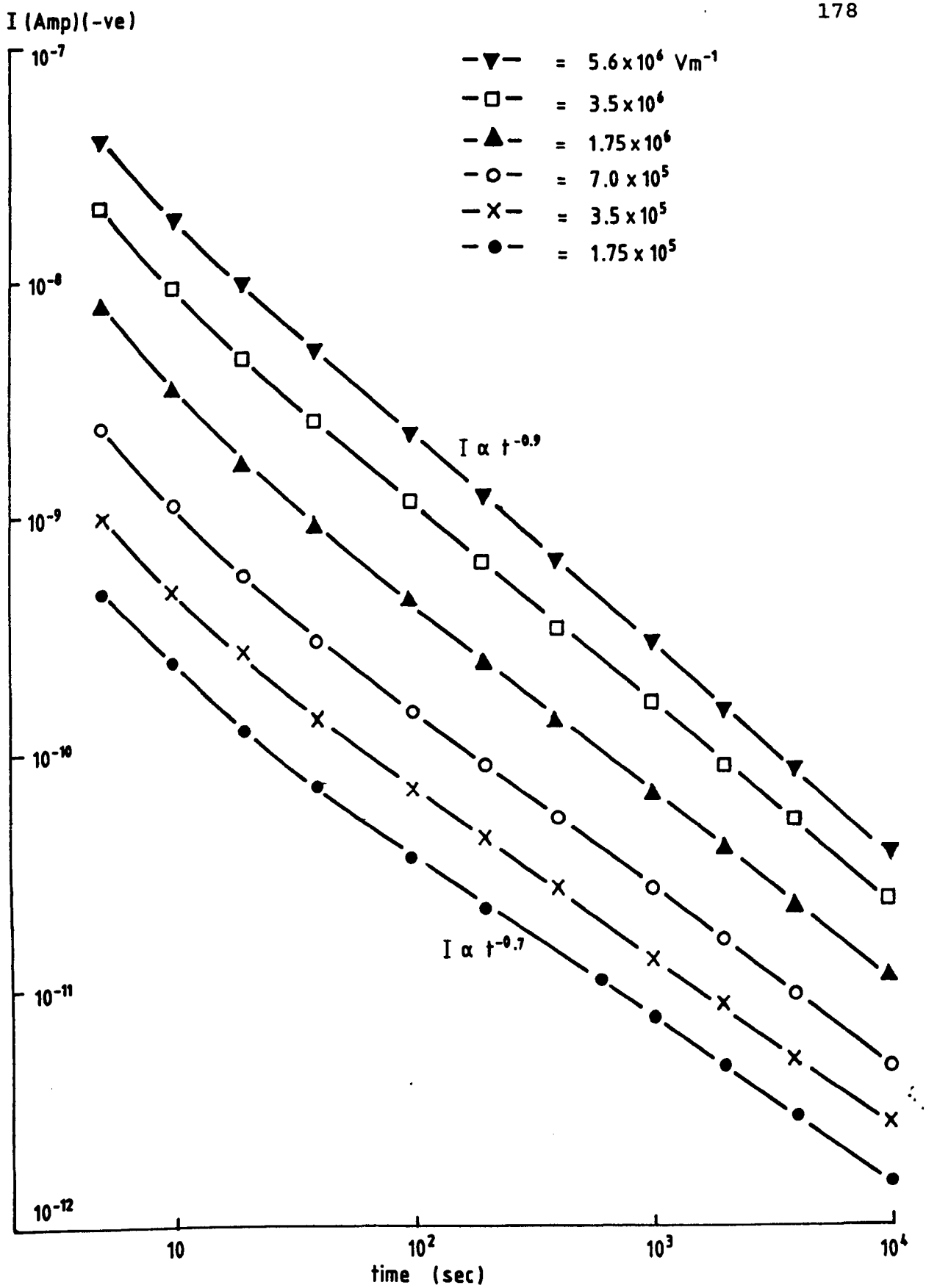

Fig. 4.22. Discharging currents in PIEZEL for different pre-applied fields at 293 K and charging time : 28 hours.

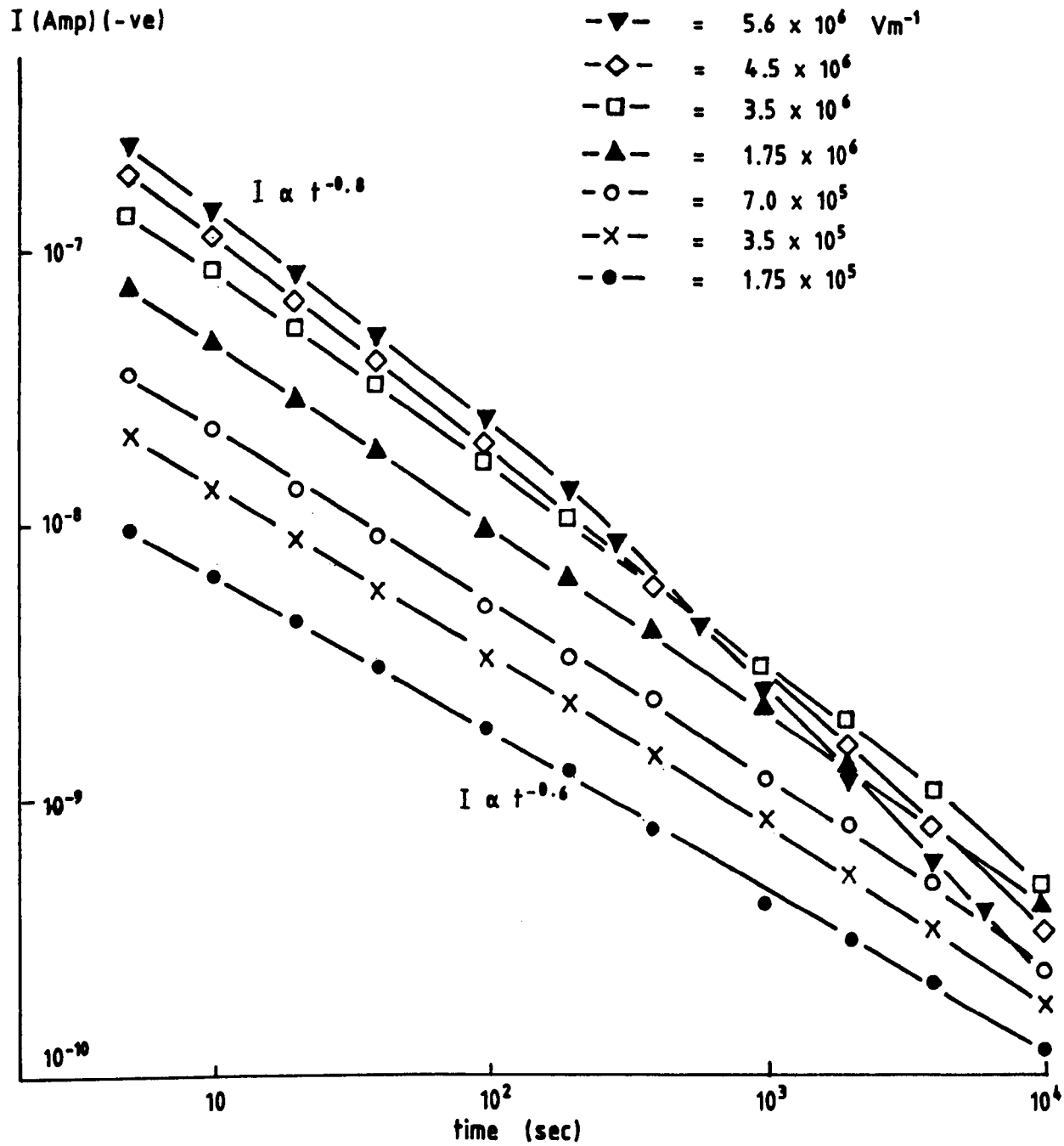

Fig. 4.23. Discharging currents in PIEZEL for different pre-applied fields at 363 K and charging time : 28 hours.

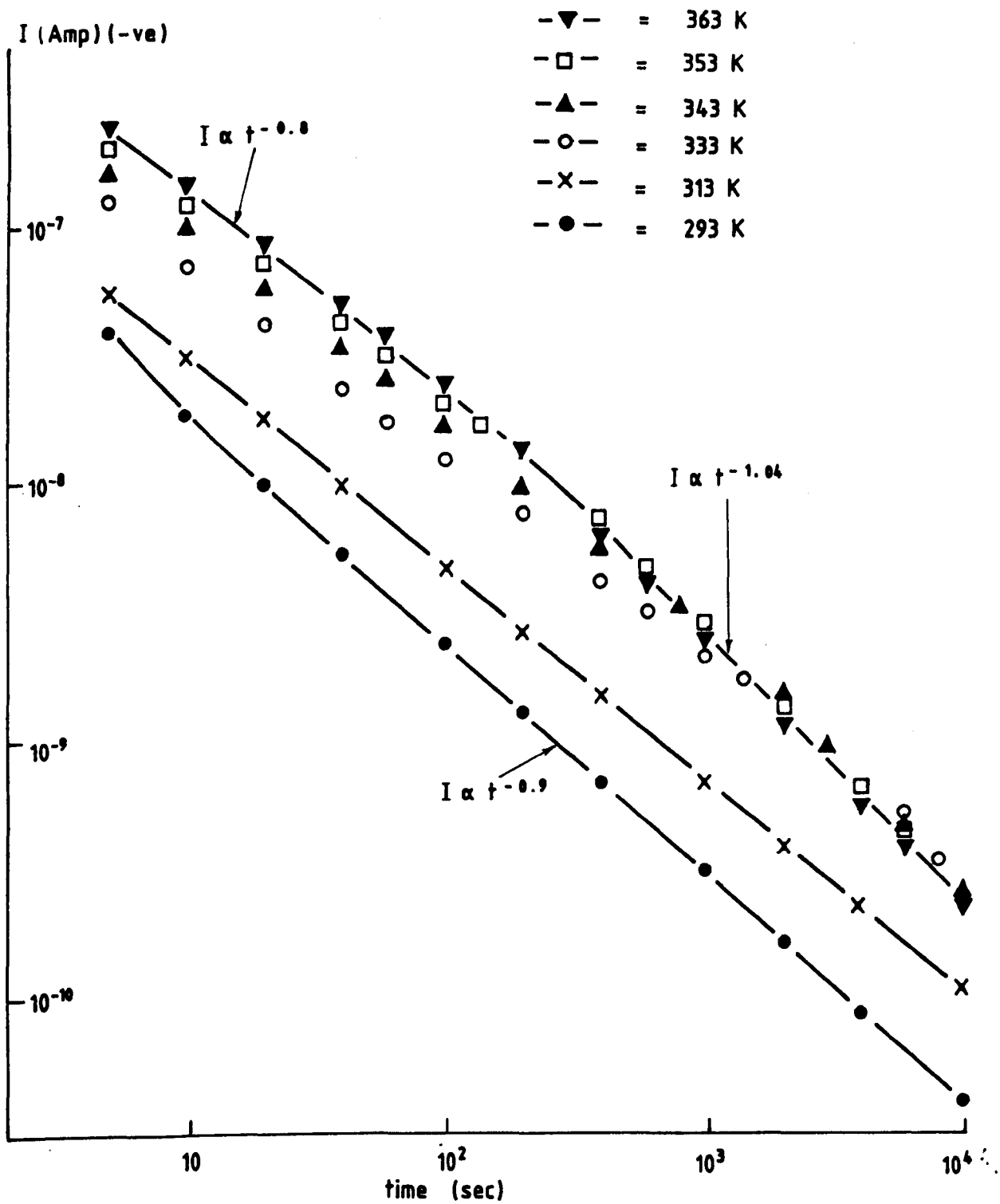

Fig. 4.24. Discharging currents in PIEZEL for different temperatures at pre applied field 5.6 x 10^6 Vm^{-1} and charging time : 28 hours.

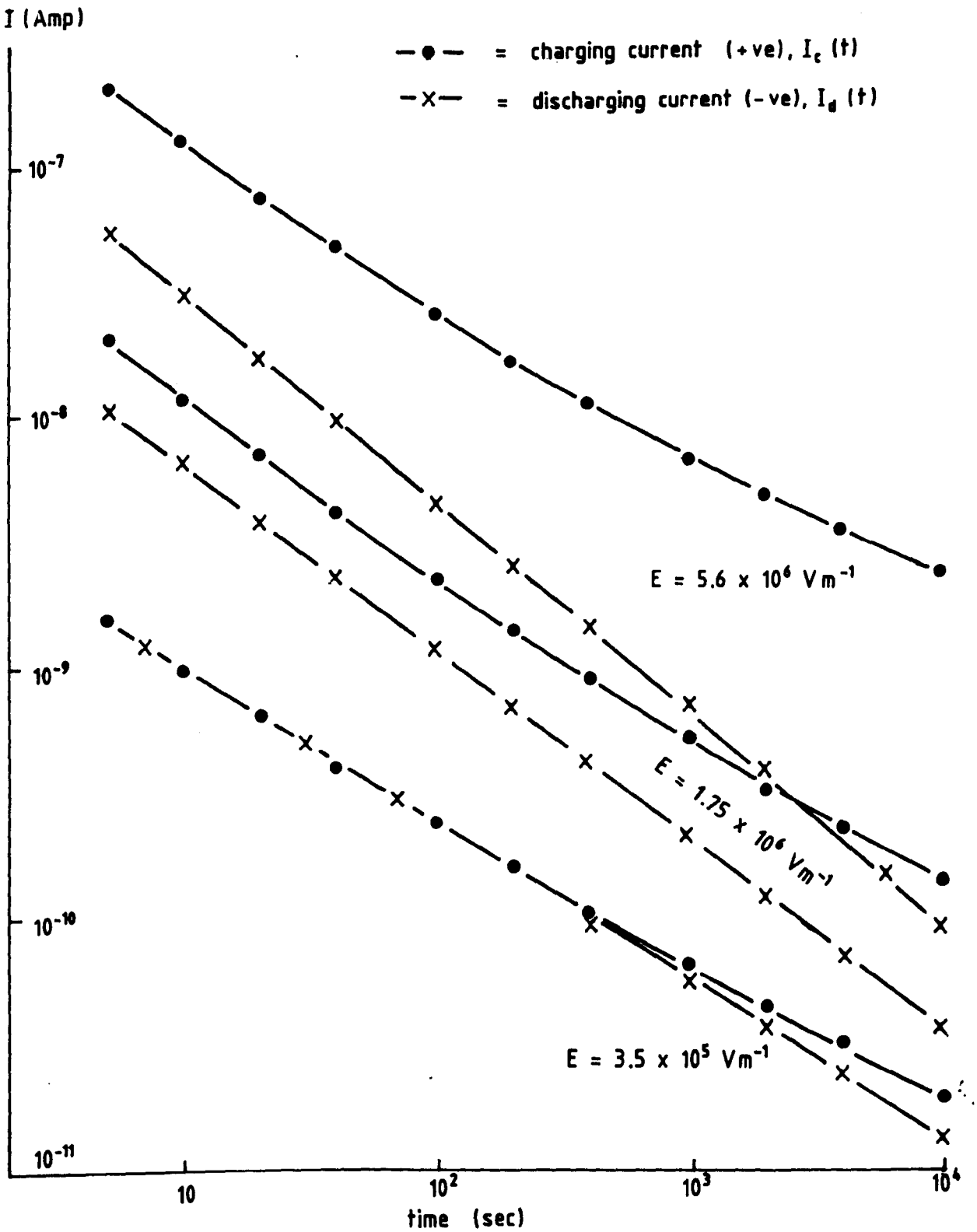

Fig. 4.25. Charging and discharging currents in PIEZEL at different fields and temperature 313 K. Charging time : 28 hours.

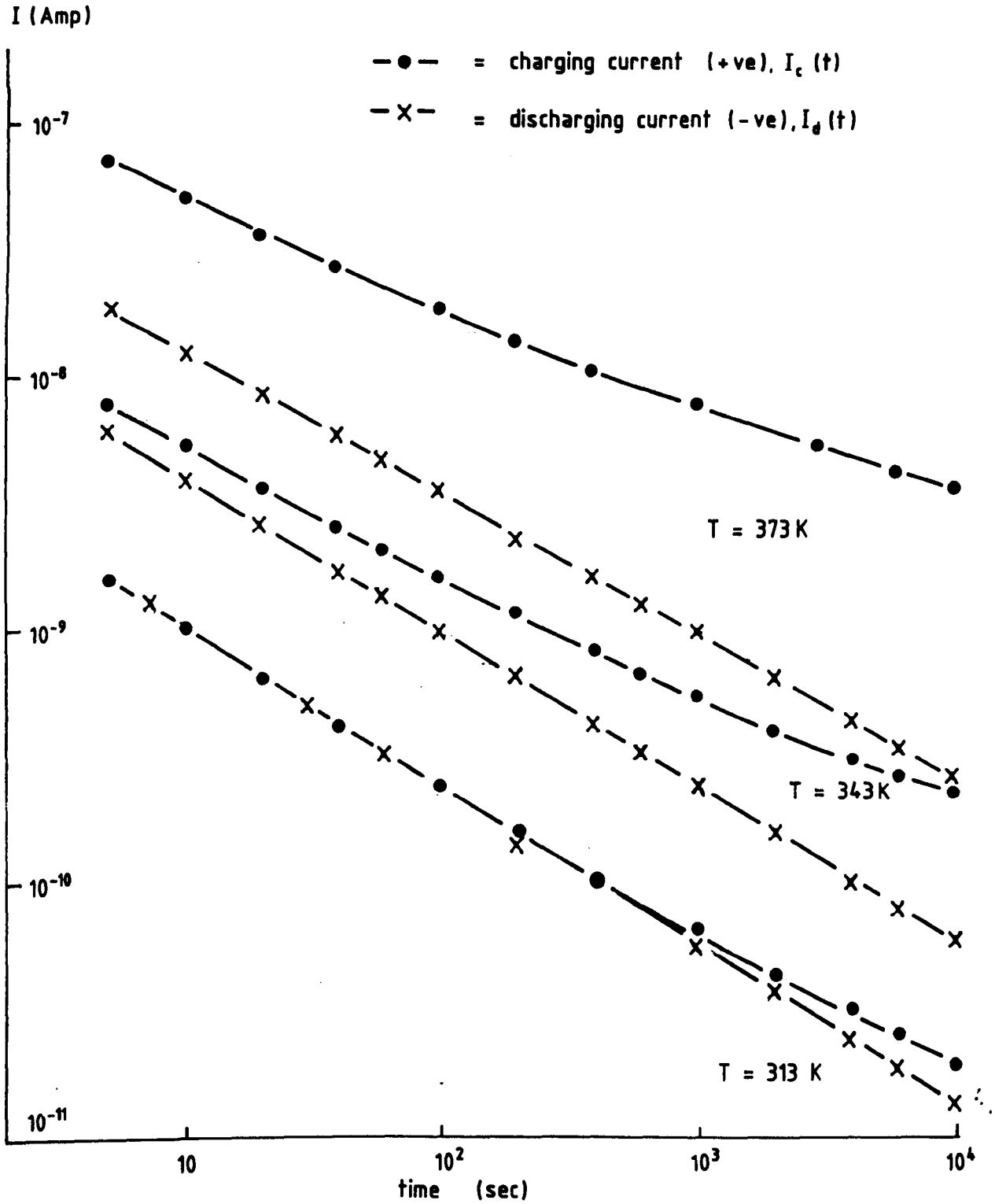

Fig. 4.26. Charging and discharging currents in PIEZEL at different temperatures and field 3.5×10^5 Vm^{-1}. Charging time : 28 hours.

with the values of p were found to be in the range of ~0.7-4.2 (depends on time, temperature and field) in the range of fields (0.175-5.6)x10^6 Vm^{-1}, temperatures 293-363K and times 10-10^4 sec. It was also observed that the p-values : (1) decreased for increasing temperature in the low-field region (~(0.175-1.8)x10^6 Vm^{-1}) and (11) decreased with time in the low-field region at high temperatures (T>293K).

The isochronal discharging currents against pre-applied field at room temperature is shown in Fig.4.29. It may be observed that their behaviour follows the relationship as :

$$I_d(t) \propto E^p \qquad (4.103)$$

At high temperature (T=363K), the range of pre-applied field in which the relationship of Eq.(4.103) holds, appear to confine to a smaller region at longer times ; beyond this range, the currents depart strongly from the corresponding charging currents (see Fig.4.30). The values of p (Eq.(4.103)) from the linear part of I_d-E plot lies in the range of ~0.54-1.23 for the time range of 10-10^4 sec and in the temperature range of 293-363K. It was also observed that the values of p : (1) decreased with time, and (11) decreased with an increase of temperature.

The activation energy associated with the charging and discharging processes may be evaluated by plotting the isochronal currents against the inverse temperatures. Fig.4.31 shows the plot of isochronal charging currents against the inverse temperature at applied field of 7x10^5 Vm^{-1}. The shape

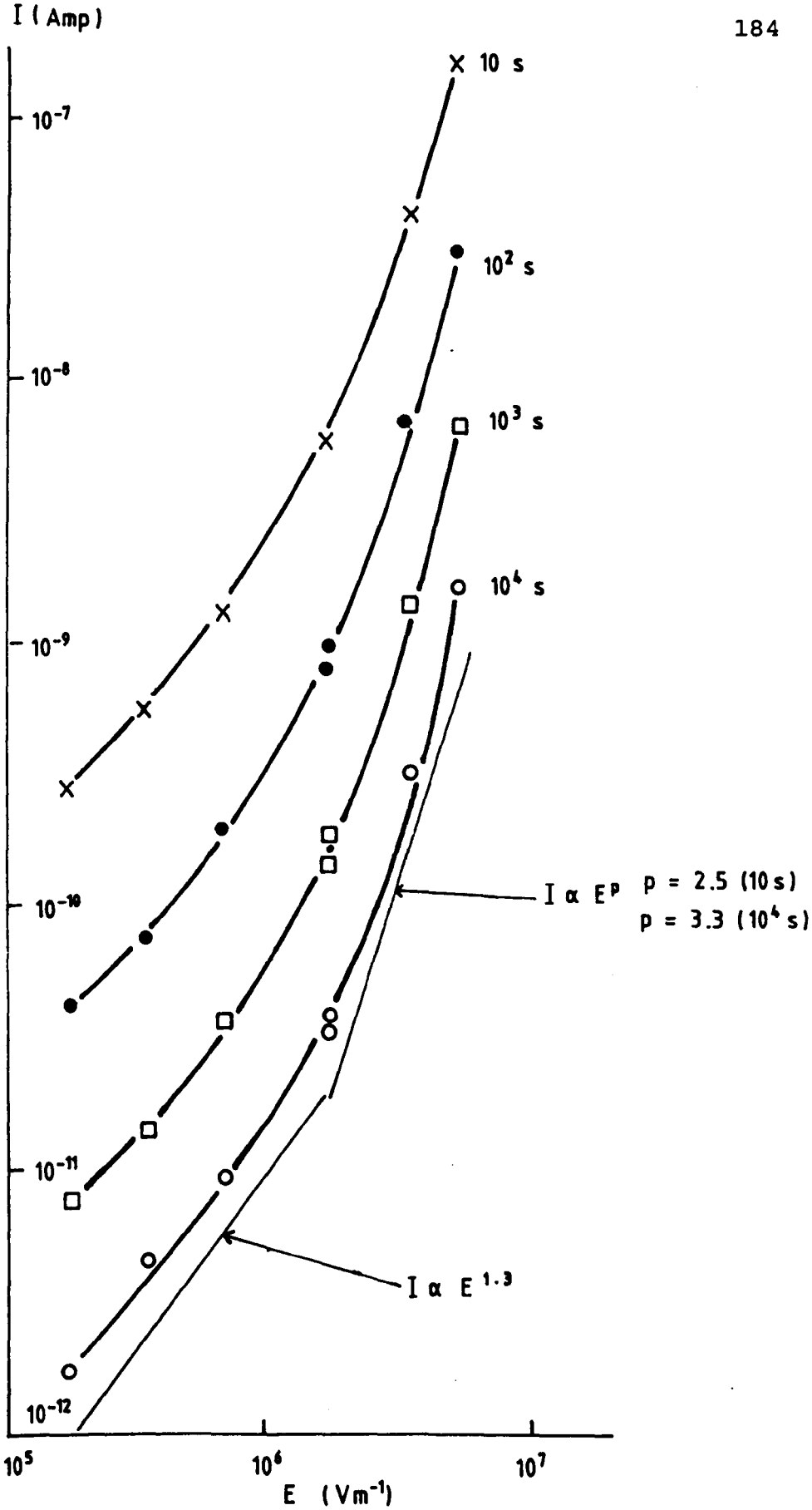

Fig. 4.27. Isochronal charging currents in PIEZEL at different fields and temperature 293 K.

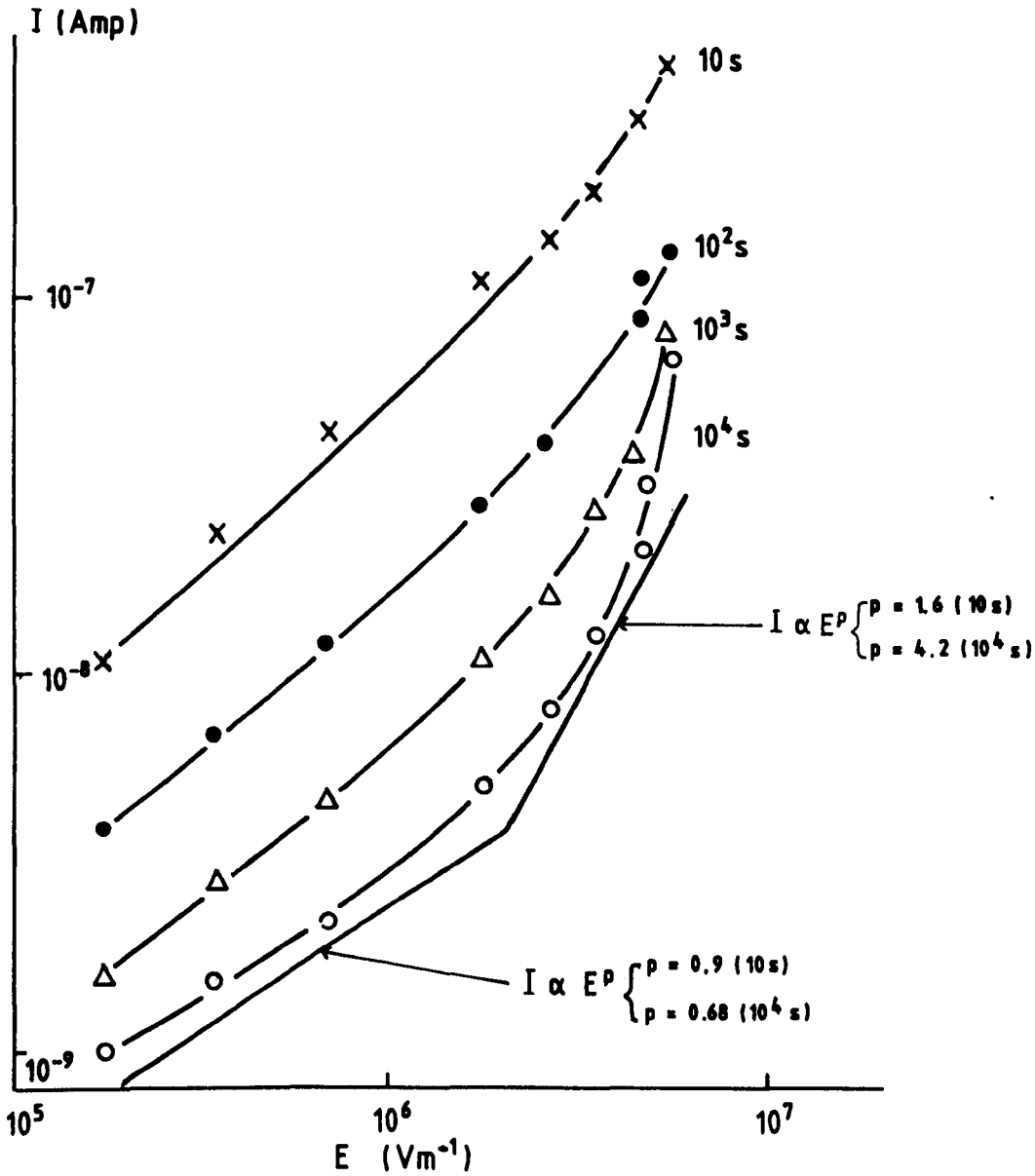

Fig. 4.28. Isochronal charging currents in PIEZEL at different fields and temperature 363K.

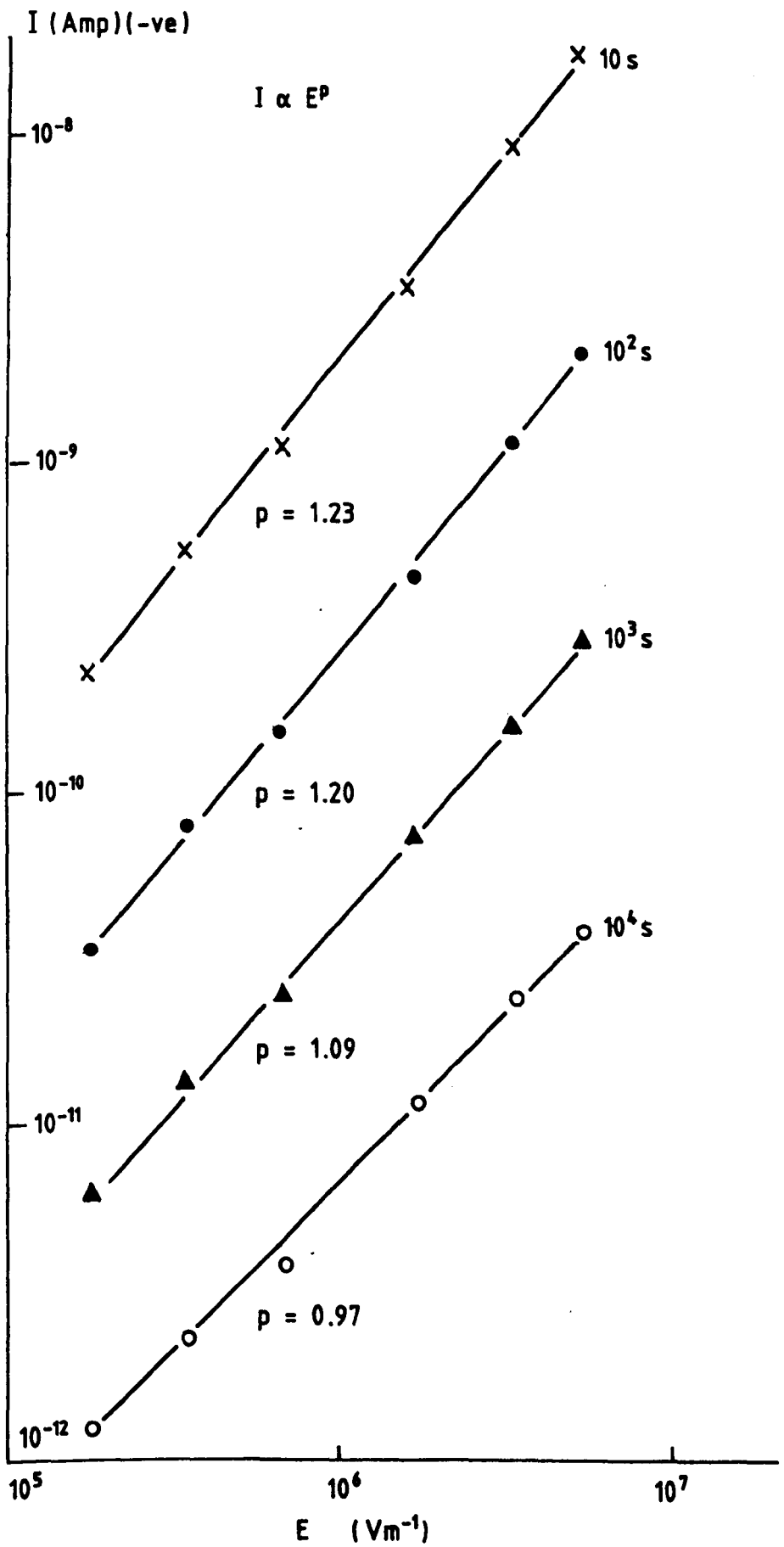

Fig. 4.29. Isochronal discharging currents in PIEZEL at different pre-applied fields and temperature 293K.

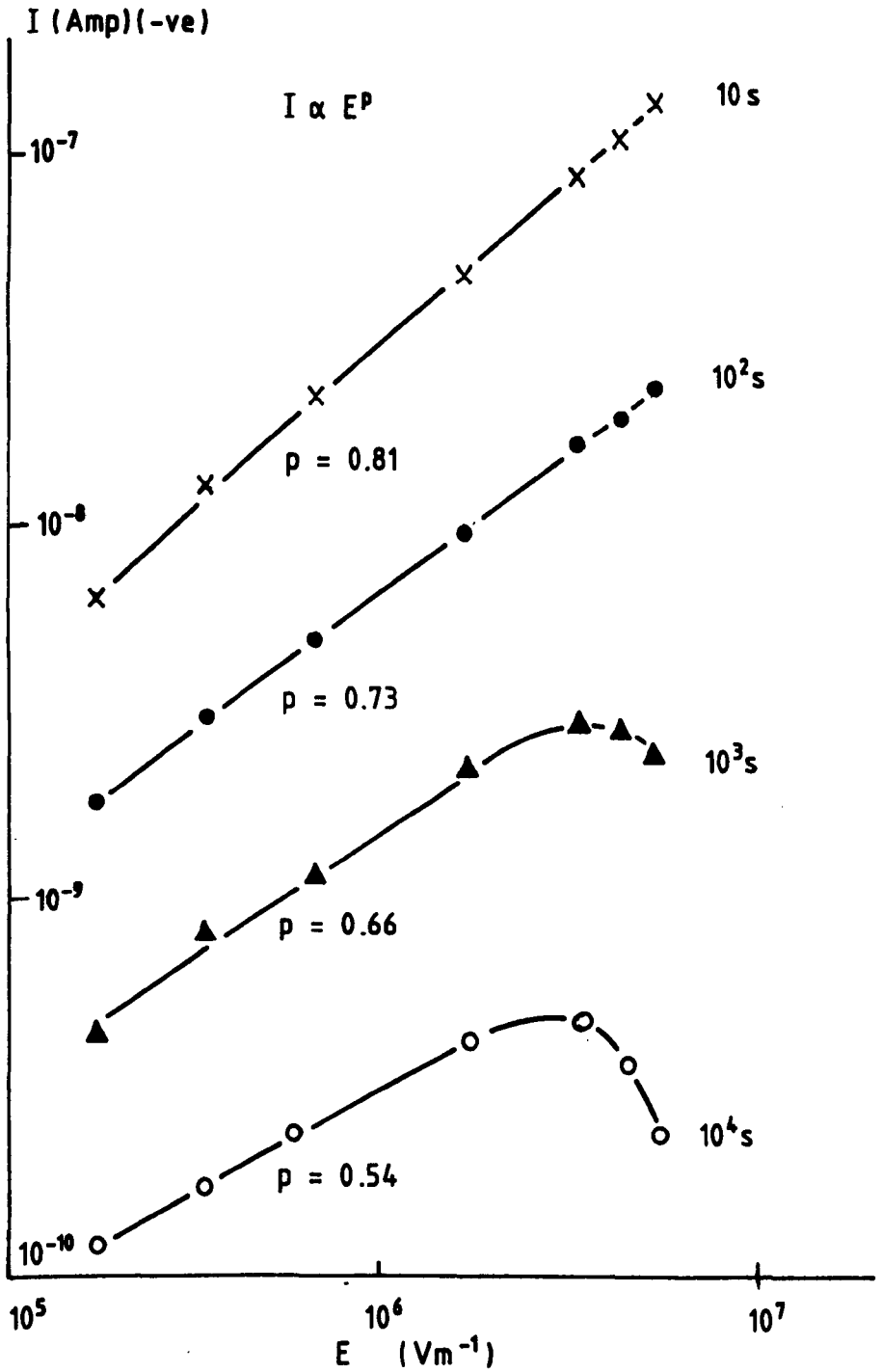

Fig. 4.30. Isochronal discharging currents in PIEZEL at different pre-applied fields and temperature 363 K.

of the curves may be approximated by two linear regions from which the values of activation energies may be evaluated from the slopes of the curves using the relation :

$$I = I_o \exp(-\Delta U/kT) \qquad (4.104)$$

where I_o is a characteristic constant, ΔU the activation energy, I the magnitude of the current , k the Boltzman constant and T the absolute temperature. It may be observed that at this low field (Fig.4.31), the activation energies at 10 sec after the field was applied, are 0.29 eV and 0.64 eV at low temperatures and high temperatures region respectively. These activation energies were observed to be increasing function of time in the present measurement. The microstructure of the material may create various heights of potential barrier against charge carriers movement which may lead to the appearance of the various levels of activation energies. It may also appear that after reaching a certain threshold temperature, a structural rearrangement occurs, thus modifying the potential barrier height and hence the activation energy.

It has also been observed that the activation energy associated with the charging process is field dependent. At shorter times (~10 sec) and high temperatures region (~338-373K), the activation energy is observed to decrease with the increase of applied field (the values being in the range 0.44-0.64 eV in the applied field range (0.7-5.6)x10^6 Vm^{-1}). At low -temperature region (~293-323K), the activation energies tend

to decrease as the electric field increases in the time region $5\text{-}10^4$ sec. Fig.4.32 shows the dependence of isochronal charging current on inverse temperature at $5.6\text{x}10^6$ Vm^{-1}. It may be observed that at low-temperature region ($\sim$293-323K), the currents at 10 sec are weakly dependent on temperature.

Fig.4.33 shows the behaviour of isochronal discharging current against inverse temperature at relatively low pre-applied field ($7\text{x}10^5$ Vm^{-1}). It may be observed that the currents increase with the increase of temperature in accordance with Eq.(4.104), from which the activation energy may be appropriately determined. As in the case of the charging currents, the discharging process executes an increasing amount of activation energy as the time increases.

It has also been observed that the activation energy is slightly decreased as the pre-applied field increases ; the values being typically in the range 0.29-0.36 eV for the pre-applied field in the range $(0.7\text{-}3.5)\text{x}10^6$ Vm^{-1} of 10 sec isochronal discharge current. At high pre-applied field (typically $5.6\text{x}10^6$ Vm^{-1}), the variation of current with temperature shows a relaxation behaviour which gives rise to a very broad peak (see Fig.4.34). The observed peak tends to shift to higher temperatures at shorter times, thus suggesting a presence of thermal activation process. The low-temperature region of the isochronal discharge currents (Fig.5.34) may be approximated by a linear dependence, from which the activation energy can be appropriately determined by the use of Eq.(4.104). The activation energy obtained from this region is slightly increased with time in the same manner as for the

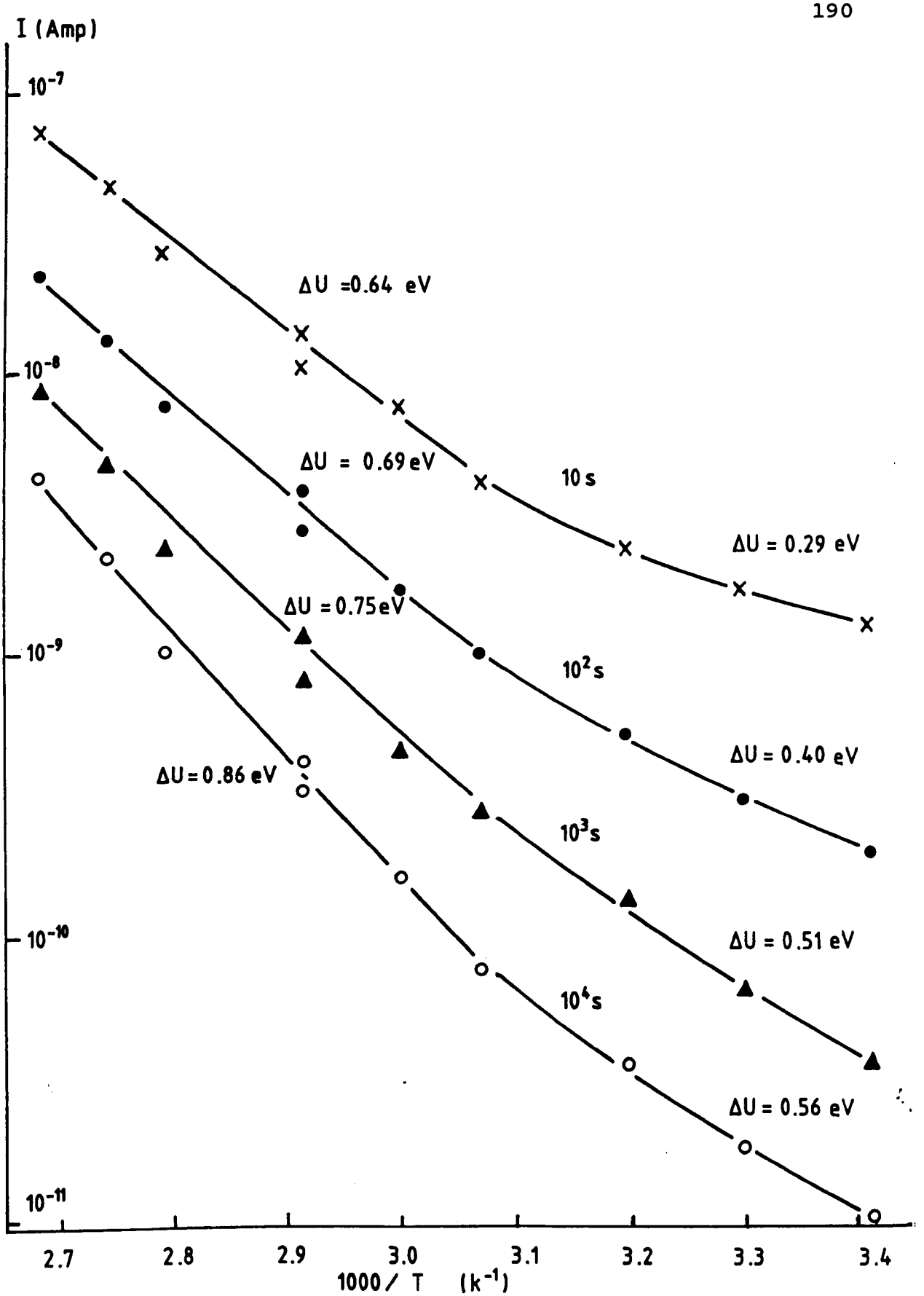

Fig. 4.31. Inverse temperature dependence of isochronal charging current in PIEZEL at field 7×10^5 V m^{-1}.

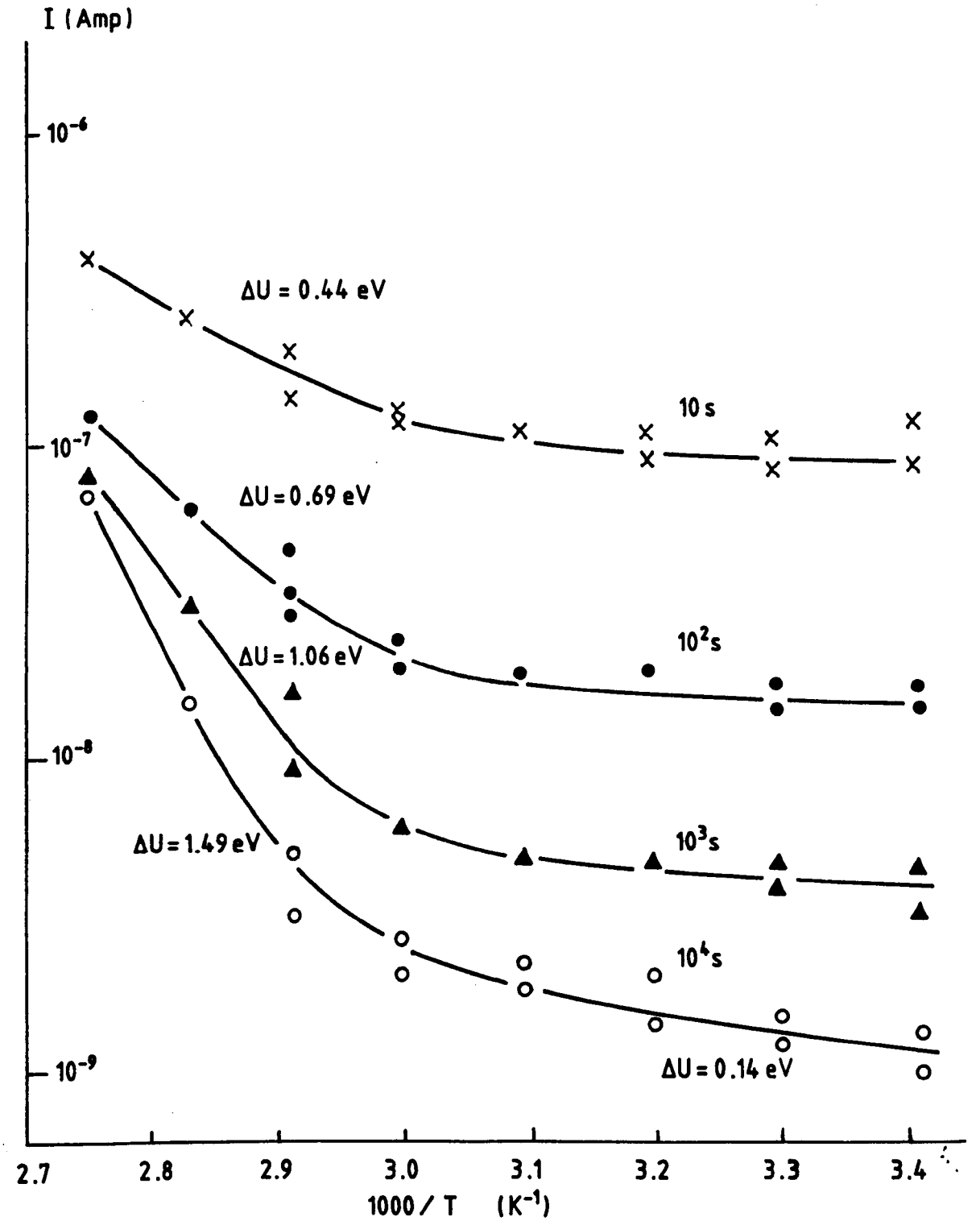

Fig. 4.32. Inverse temperature dependence of isochronal charging current in PIEZEL at field 5.6×10^6 Vm^{-1}.

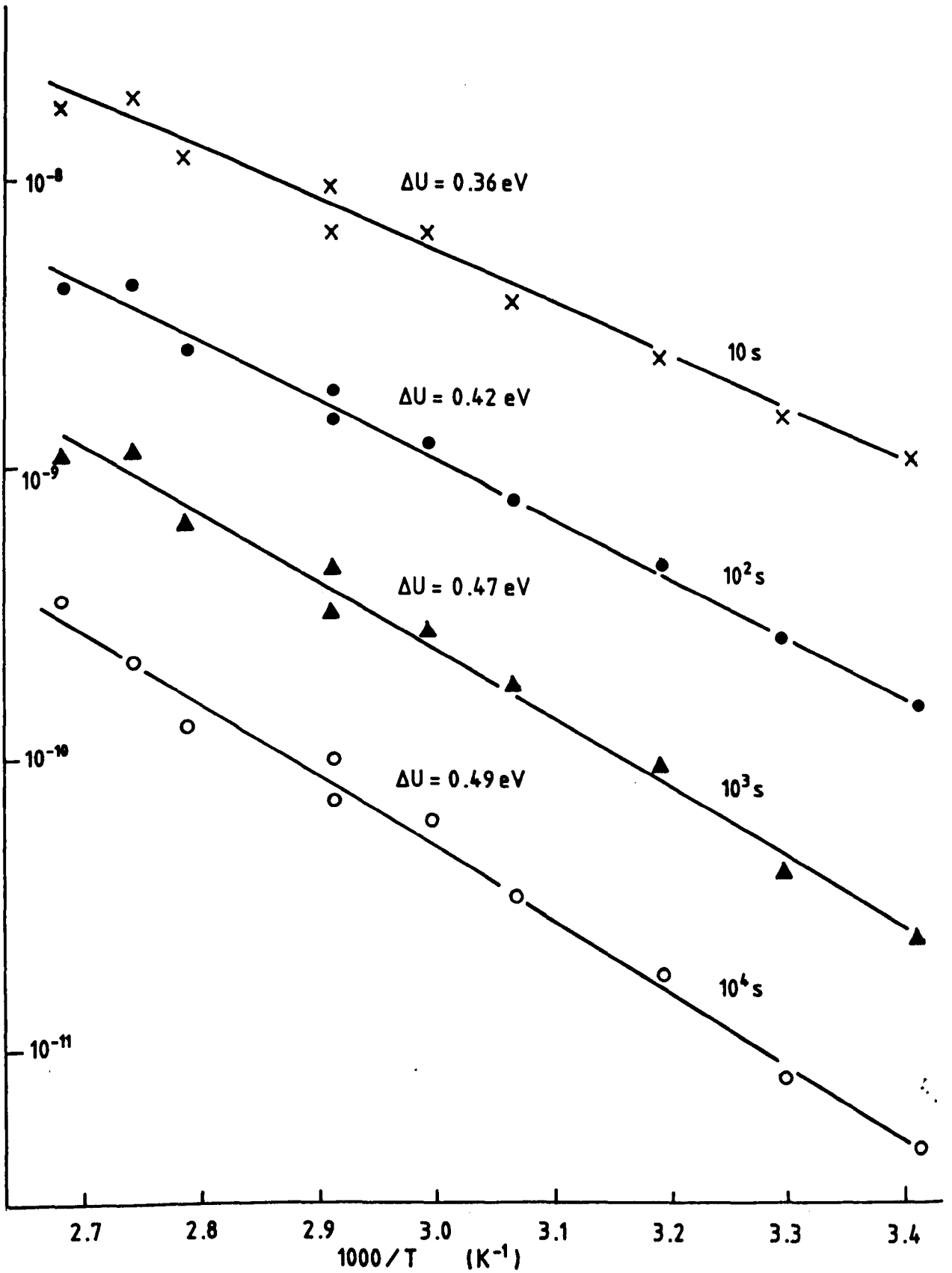

Fig. 4.33. Inverse temperature dependence of isochronal discharging current in PIEZEL. Pre-applied field : 7×10^5 Vm^{-1} and charging time : 28 hours.

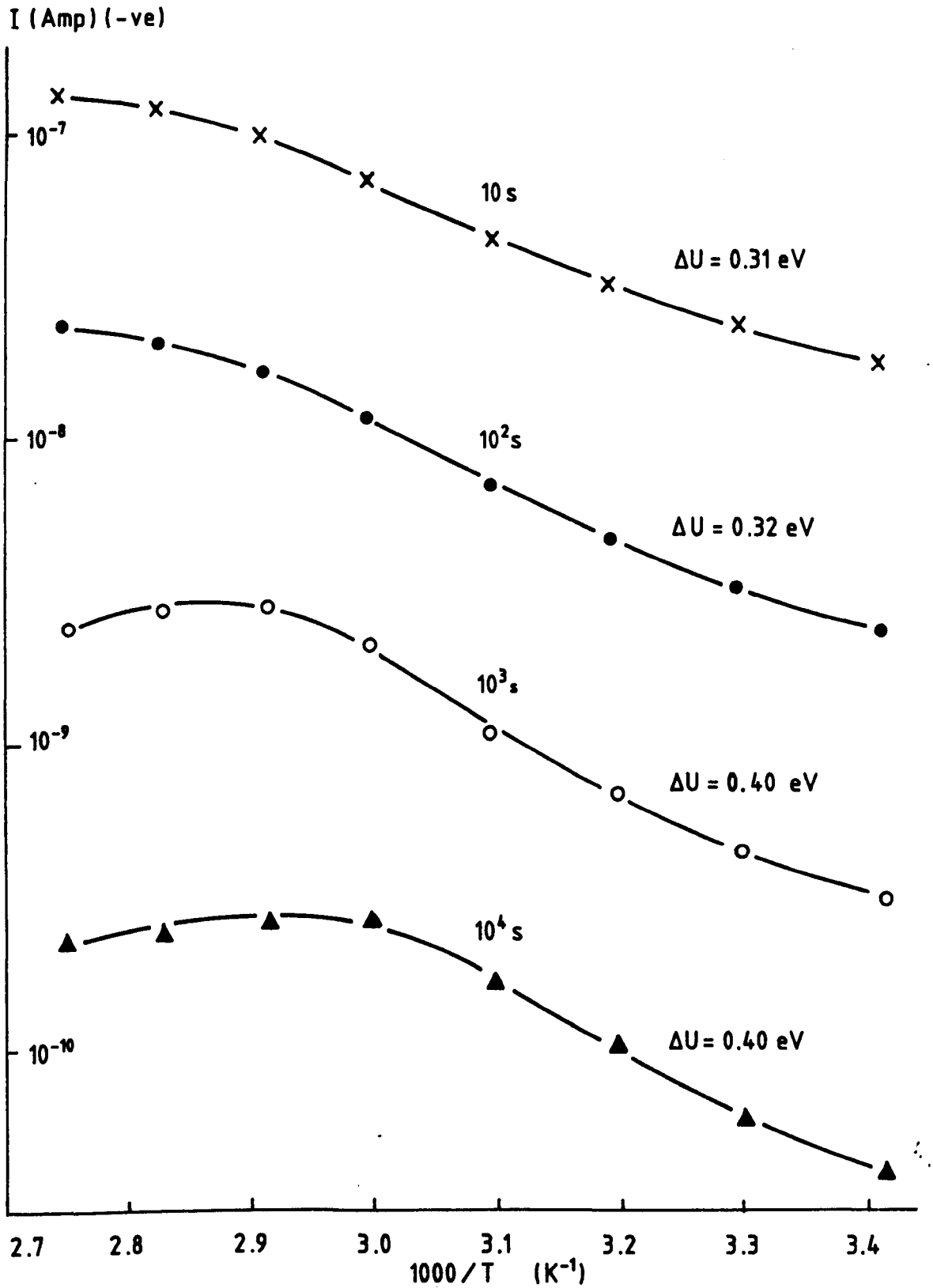

Fig. 4.34. Inverse temperature dependence of isochronal discharging current in PIEZEL . Pre-applied field : 5.6×10^6 Vm^{-1} and charging time : 28 hours.

lower pre-applied field case as mentioned before.

Following Hamon approximation [29] (see section 4.2.2), it is possible to transform the time-dependent discharging current data into its equivalent frequency-domain behaviour, from which the activation energy associated with the relaxation process such as of Fig.4.34 may be evaluated. Such transformation has been performed for the discharging current in Fig.4.24 and the results are shown in Fig.4.35. An activation energy of $\sim$1.0 eV was calculated from the peak shifts with temperature (Fig.4.36) by assuming that the process follows an Arrhenius type of equation (Eq.(4.30)).

4.4.2. Steady-state current in PIEZEL

Fig.4.37 shows the plot of steady-state current (current at 10^5 sec) against field in PIEZEL in the tempearure range 293-343K. The shape of the curves may approximately be divided into two regions. Taking the tangent to the curves in the low-field region ($E \gtrless 2\times10^6$) , the gradient of the tangent is found to decrease with an increase of temperature, i.e. from 1.3 to 0.6 in the temperature range of 293-343K. With these values of I-E dependence, it may be suggested that space charge is perhaps not the dominant conduction mechanism in the low-field region at these temperatures.

The gradient of I-E dependence in the high-field region is observed to be superlinear, i.e. fitting the relationship as $I_s \propto E^{3.43}$ in the temperature range 293-343K (see Fig.

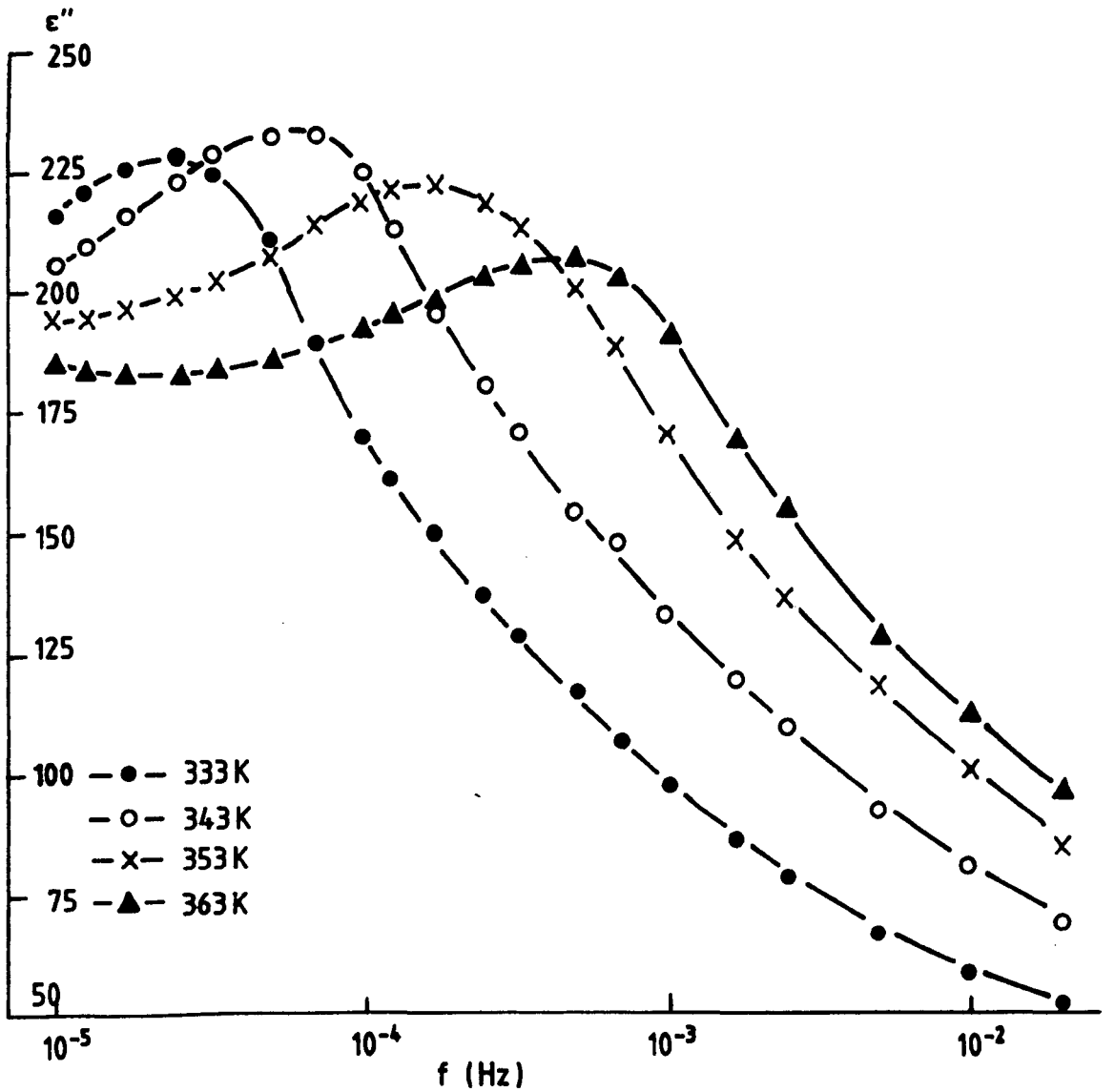

Fig. 4.35. Low frequency behaviour of dielectric loss in PIEZEL obtained using Hamon's approximation. Data were derived from Fig. 4.24.

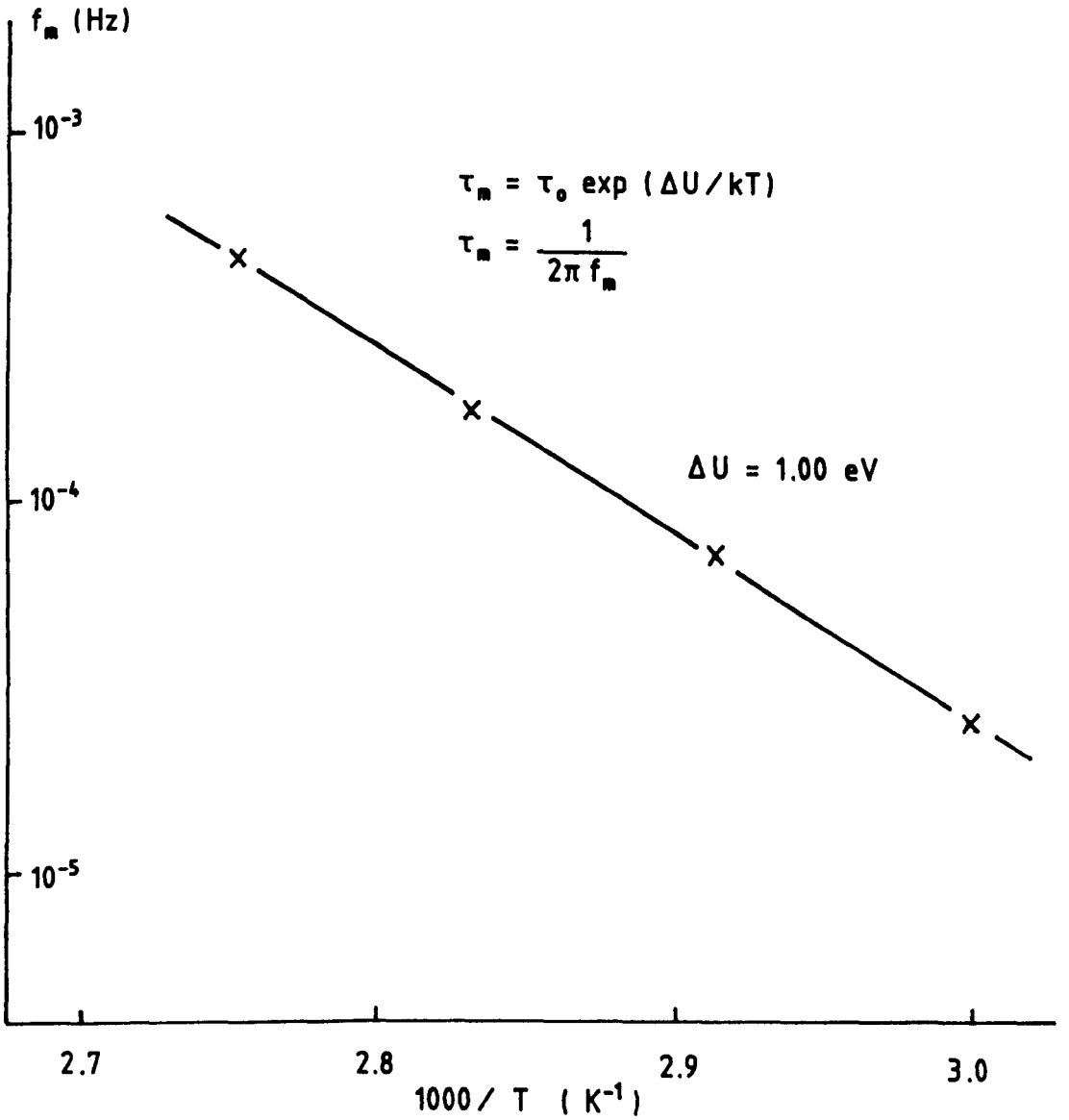

Fig. 4.36. Temperature dependence of low frequency dielectric loss peak in PIEZEL.

4.37). The results also show that the transition field at which that power law region begins, increases with increasing temperature. Such a behaviour may possibly suggest a presence of space charge conduction in presence of traps, which are exponentially distributed in energy in the band gap of the dielectric [40,64]. The high current in this region may be associated with the increase of charge carrier density or the increase of mobility due to the high electric field.

Fig.4.38 shows the field dependence of charging current at 10^5 sec in PIEZEL in the temperature range 358-373K. The low-field region of I-E dependence may still be approximated to show the relationship as $I_s \propto E^p$ (with $p \simeq 0.6$), but it only confines to a smaller range of fields. At high fields, the current increases substantially, possibly due to mutual enhancement between electrical conduction process and thermal effect that cause a rapid increase in the production of charge carriers.

The activation energy associated with steady-state current for fields $(0.7\text{-}5.6)\times10^6$ Vm^{-1} may be seen in Fig.4.39. It may be observed that the activation energy is field-dependent and it decreases with increasing field ; the value being in the range (0.46-0.78) eV. Also, higher activation energy may prevail beyond a certain limit of temperature. This temperature limit is observed to be shifted to lower temperature for a higher field. Such a behaviour suggests that the electrical conduction process in this material is field-assisted.

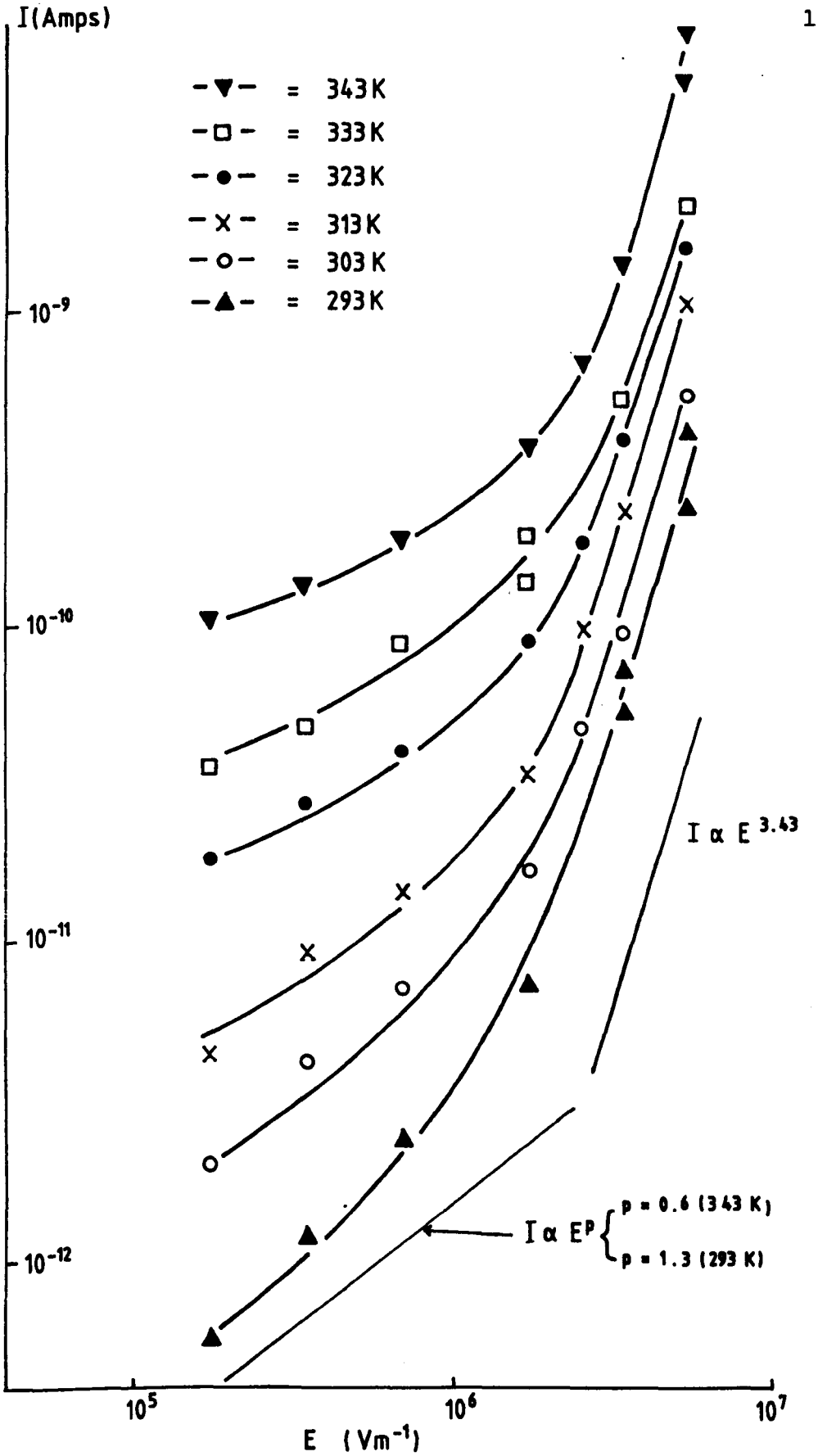

Fig. 4.37. Field dependence of steady state current (at 10^5 sec) in PIEZEL in the temperature range 293-343K.

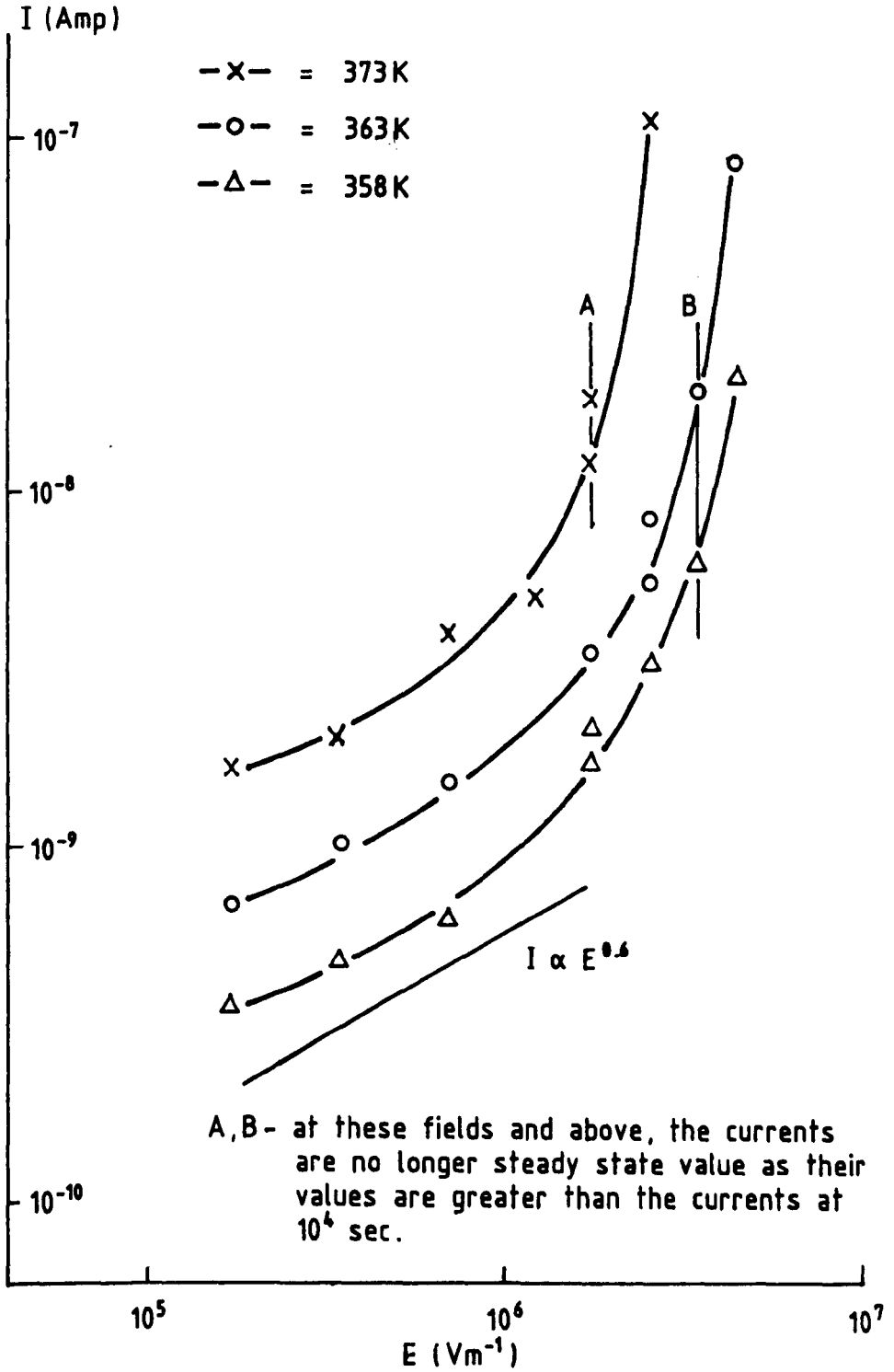

Fig. 4.38. Field dependence of charging currents at 10^5 sec in PIEZEL in the temperature range 358-373 K.

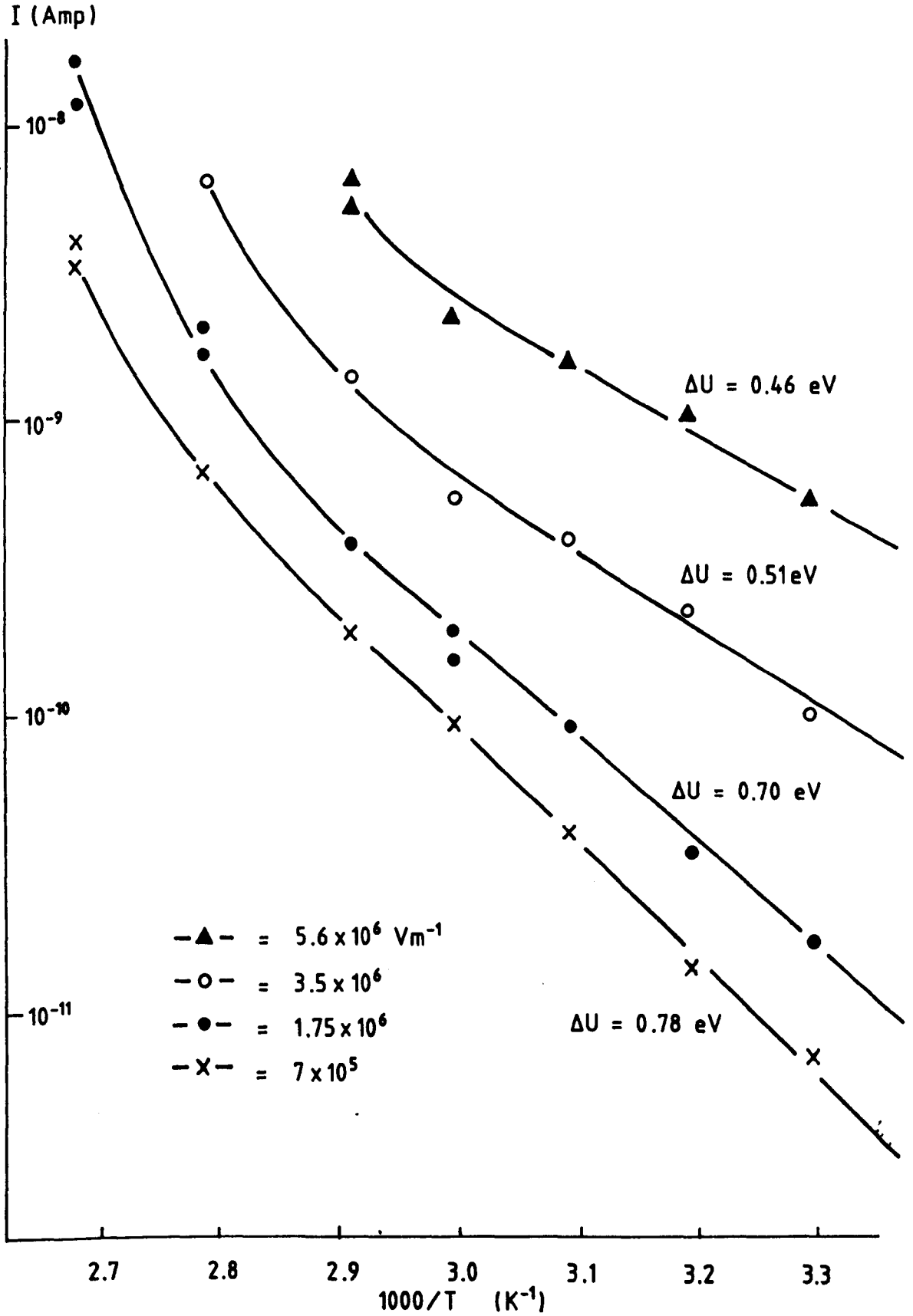

Fig. 4.39. Temperature dependence of isochronal charging current at 10^5 sec in PIEZEL for different charging fields.

4.4.3. Charging, discharging and steady-state currents in PZT

Fig. 4.40 shows the behaviour of charging currents $I_c(t)$ in PZT5 for fields in the range of $(0.75\text{-}10)\times10^5$ Vm^{-1} at temperature 343K. It may be observed that the charging current reaches a steady-state value at about 200 sec after field application. The conductivity, calculated from these results, appears to be approximately 9×10^{-10} ohm^{-1} m^{-1} at 343K. Indeed the magnitude of conductivity is higher at higher temperatures. The coresponding discharging currents $I_d(t)$ at 343K may be observed as in Fig.4.41, from which the rate of the current decay may approximately be divided into two regions, initially with the slope 0.5-0.6 followed by a faster decay with the slope 0.7-0.8.

The behaviour of $I_c(t)$ and $I_d(t)$ at fixed applied field of 1×10^6 Vm^{-1} for temperatures in the range of 303-343K may be observed from Fig.4.42. The difference of $I_c(t)$ and $I_d(t)$ becomes greater at higher temperature, indicating the dominance of steady-state current at higher temperature. The rate of decay of I_d may be described to follow Eq.(4.101) with the value of n depends on temperature (see Fig.4.42).

The plot of isochronal $I_c(t)$ against field at T=303K may be observed from Fig.4.43. The dependence may be described to fit Eq.(4.102) with the value of p=1, which is an ohmic behaviour. Similar dependency has also been observed at 323K and 343K, thus suggesting that the space charge is not the dominant contribution for the charging current in this

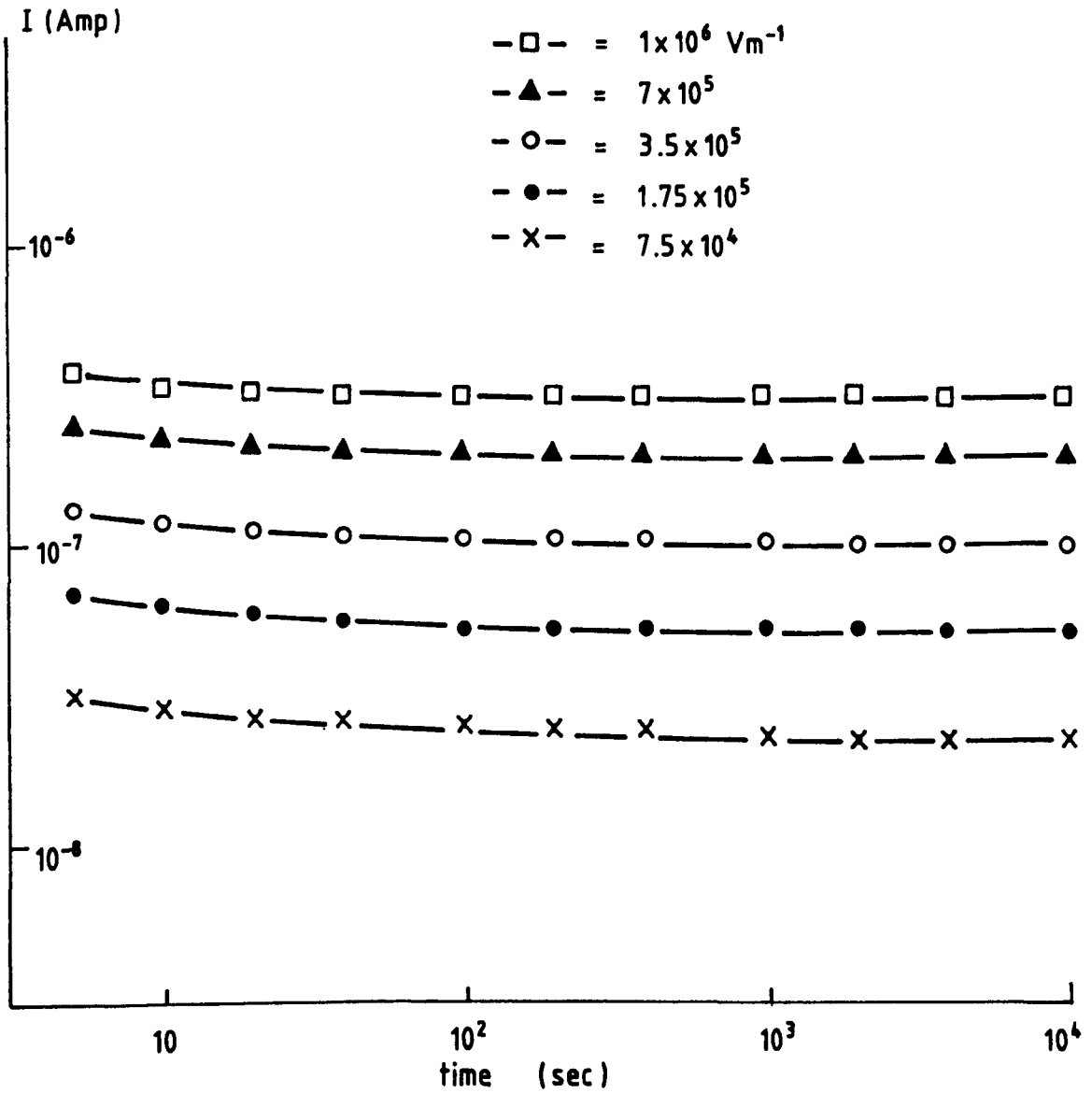

Fig. 4.40. Charging currents in PZT5for different fields at 343K.

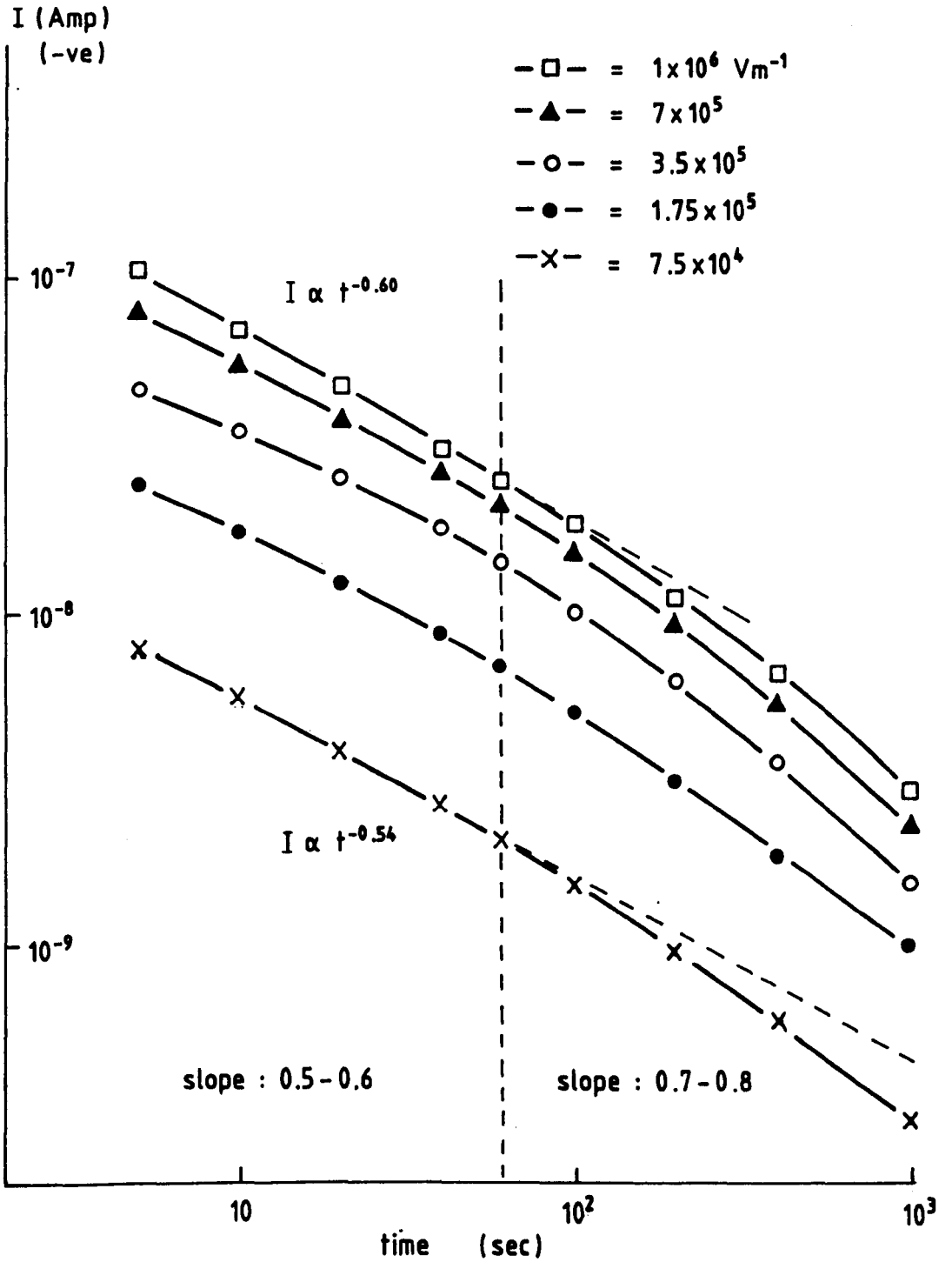

Fig. 4.41. Discharging currents in PZTs for different pre-applied fields at 343K and charging time : 2.8 hours.

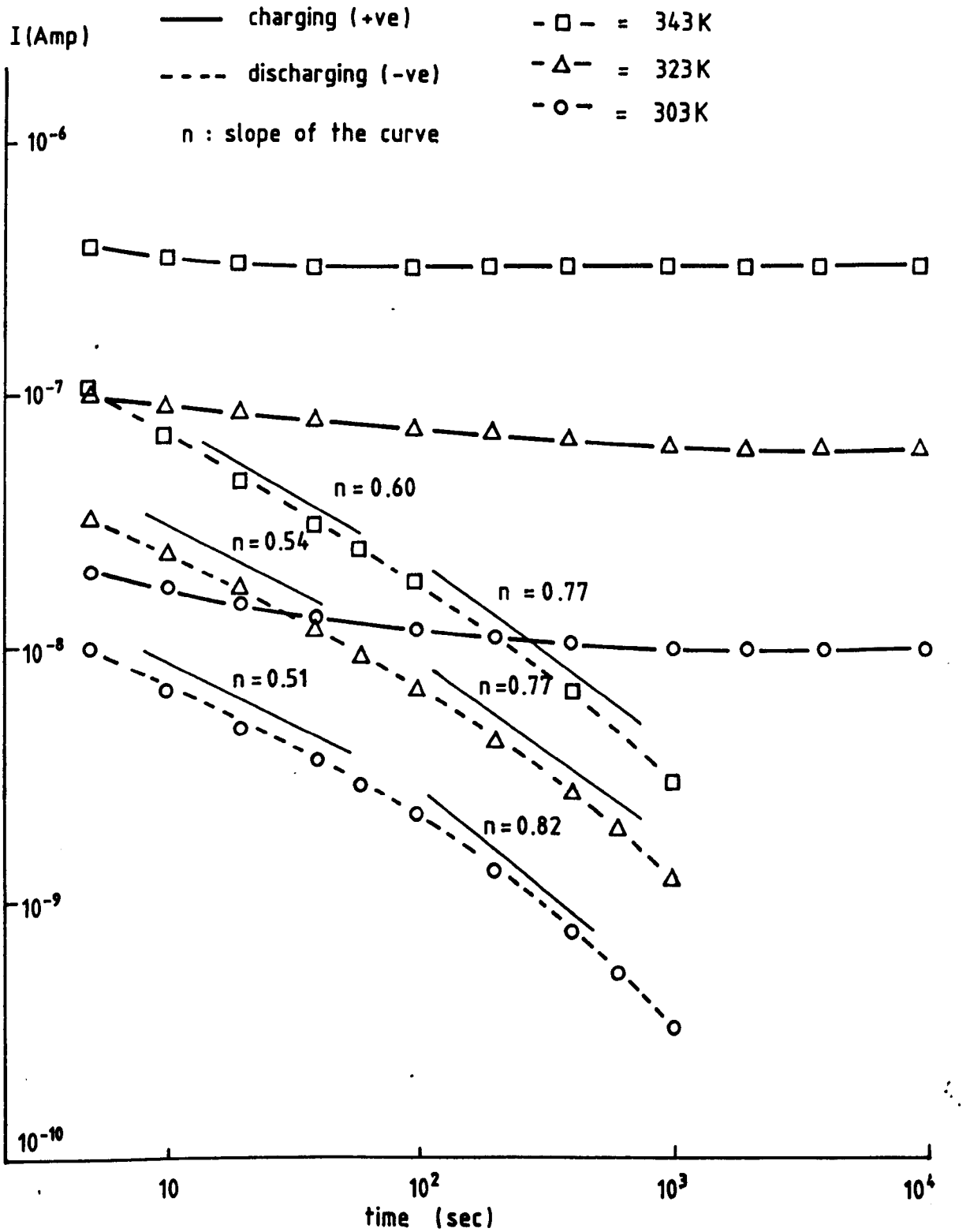

Fig. 4.42. Charging and discharging currents in PZT5 for different temperatures at field 1×10^6 Vm^{-1}.

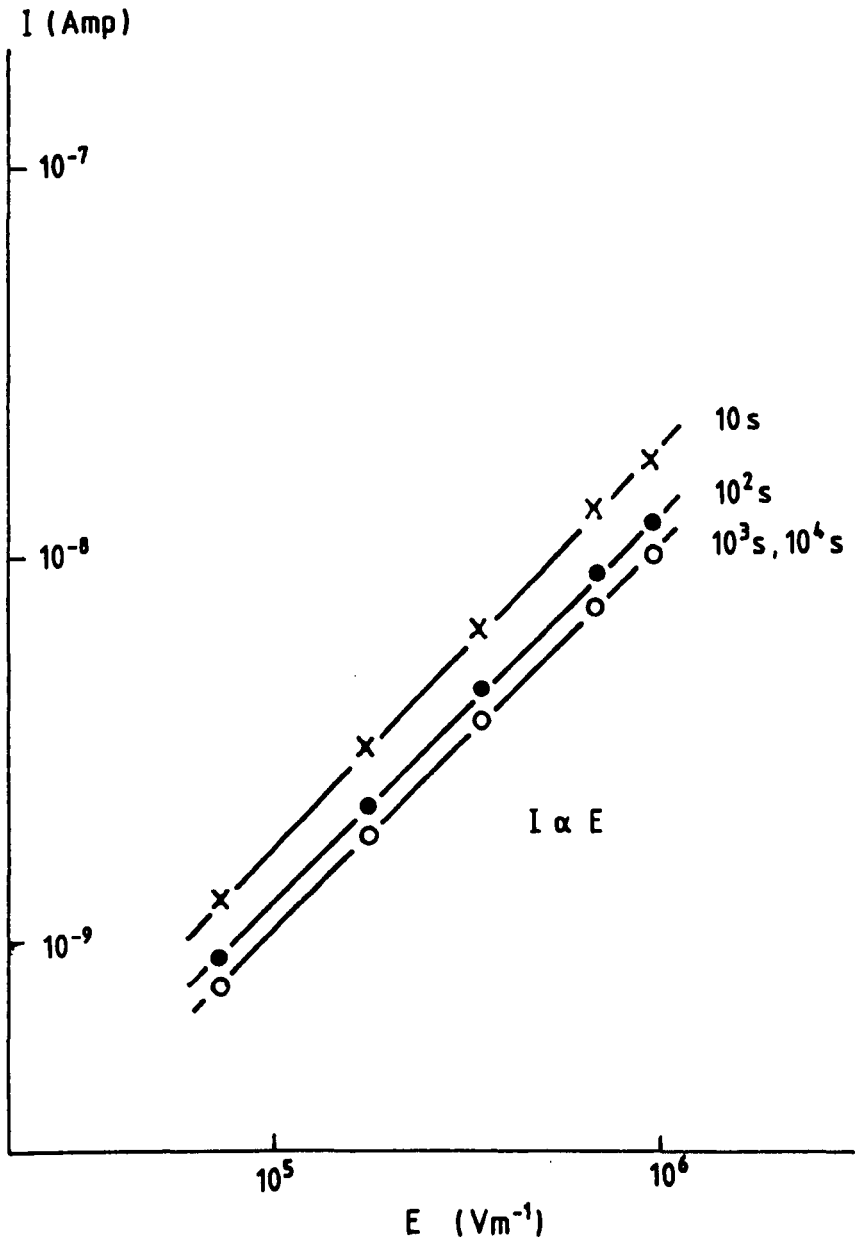

Fig. 4.43. Isochronal charging currents in PZTs at different fields and temperature 303 K.

material at these fields and temperatures.

Figs.4.44 and 4.45 show the behaviour of isochronal $I_d(t)$ against field at temperatures 303K and 343K respectively. At T=303K, the $I_d(t)$-E dependence follows the relationship as Eq.(4.103), with the value of p decreases from 0.95 (t=10 sec) to 0.75 ($t=10^3$ sec). The $I_d(t)$-E dependence at T=343K (Fig.4.45) shows a near saturation at high field, possibly due to field cleaning process during the charging of the sample.

The steady-state current dependence on electric field in PZT5 in the temperature range of 303-343K is shown in Fig.4.46, from which the behaviour may be described to be ohmic ($I \propto E$). This again may suggest, as in the case of the isochronal charging currents, the space charge conduction is not the dominant mechanism for the origin of the electrical conduction in this material for the ranges of fields and temperatures employed in the present work.

4.4.4. Charging and discharging currents in PZT5/VDF-TrFE composites

The behaviour of charging currents in PZT5/VDF-TrFE(50/50 Vol%) in the fields range $(0.175\text{-}7)\times10^6$ Vm^{-1} at temperature 363K may be observed from Fig.4.47. The current decreases progressively with time, and may reach a steady-state level at $\sim 10^5$ sec. The observed broad peak at low charging fields, which move to shorter times at higher fields,

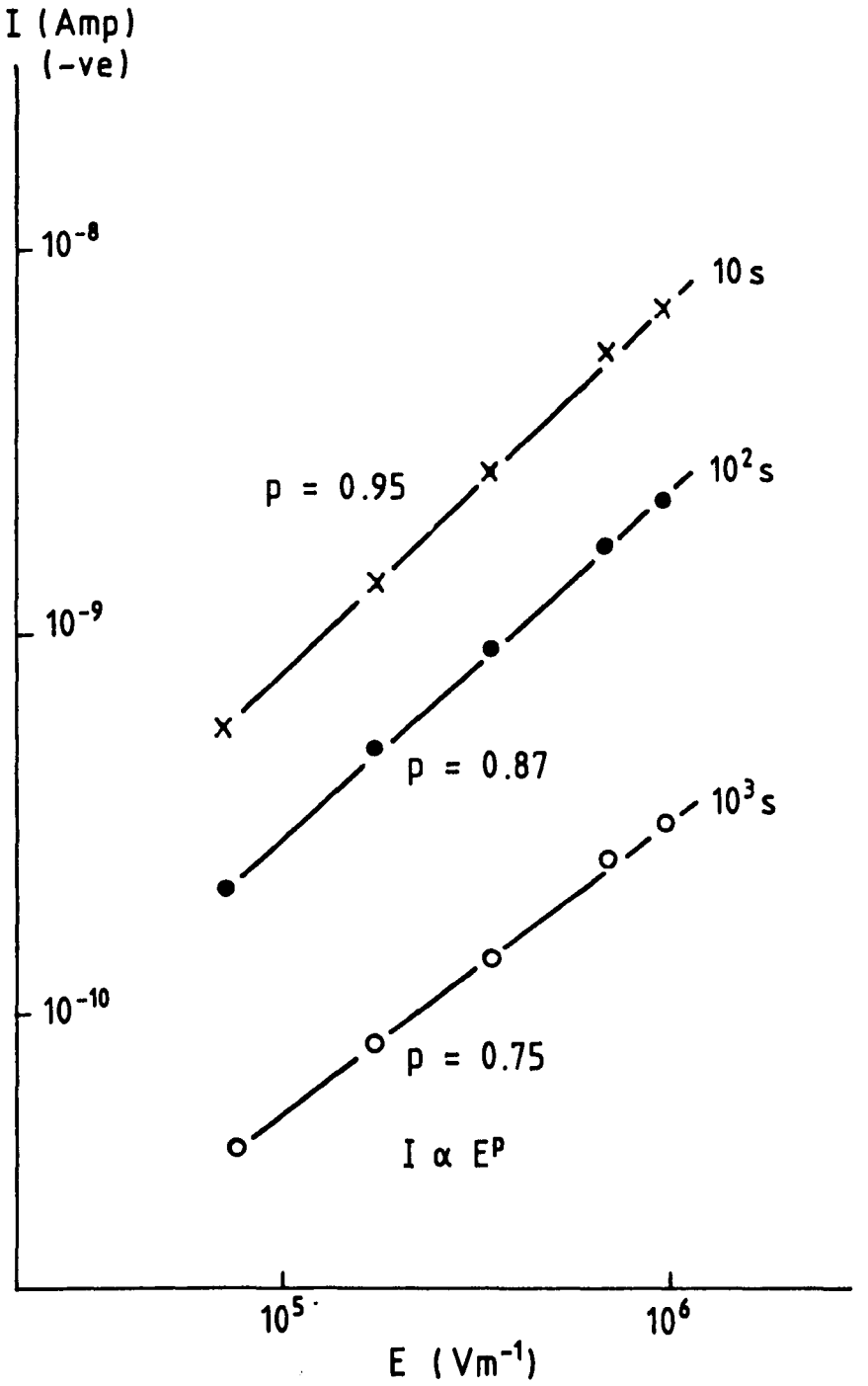

Fig. 4.44. Isochronal discharging currents in PZT5 at different pre-applied fields and temperature 303K.

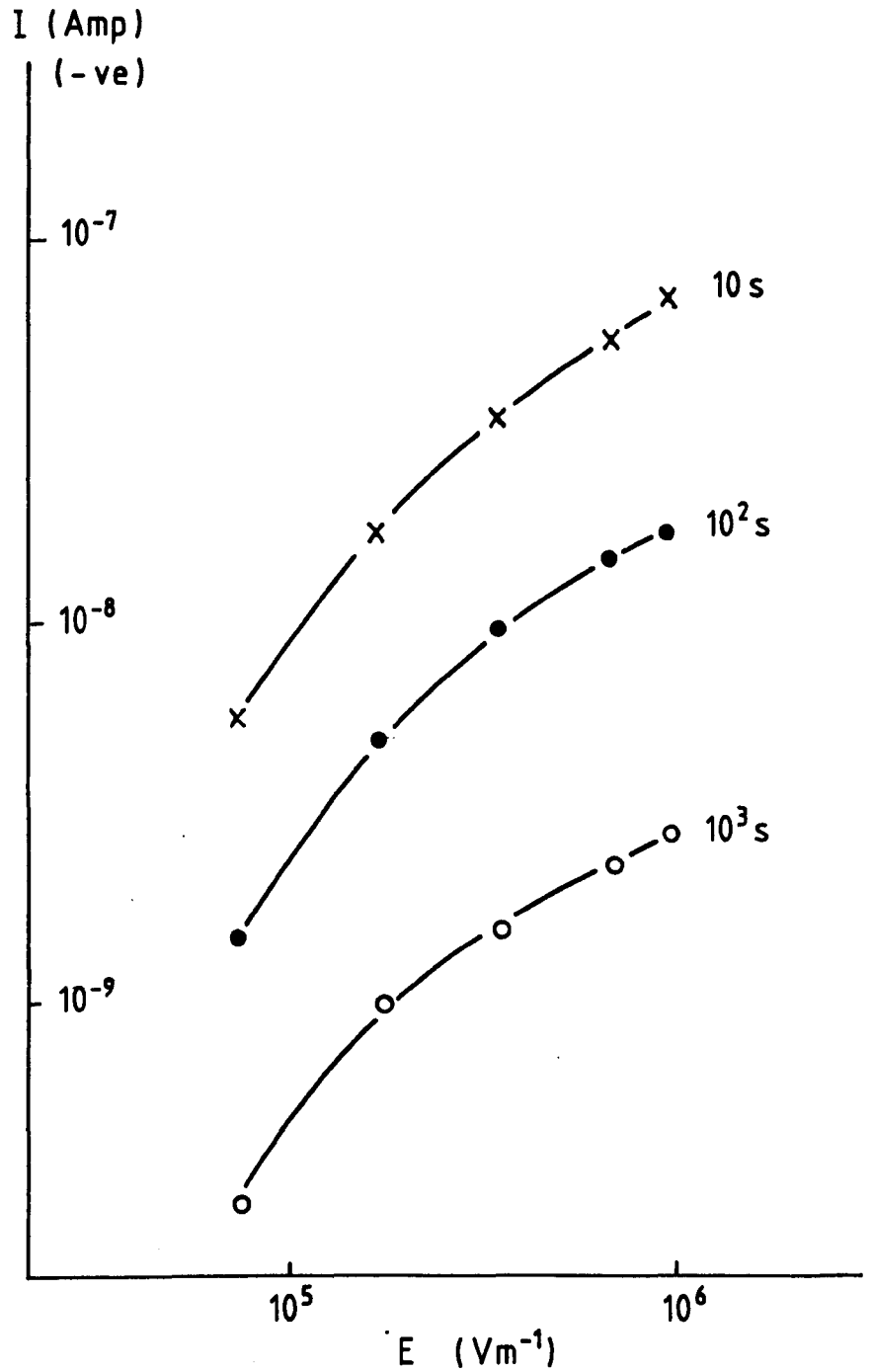

Fig. 4.45. Isochronal discharging currents in PZT5 at different pre-applied fields and temperature 343 K.

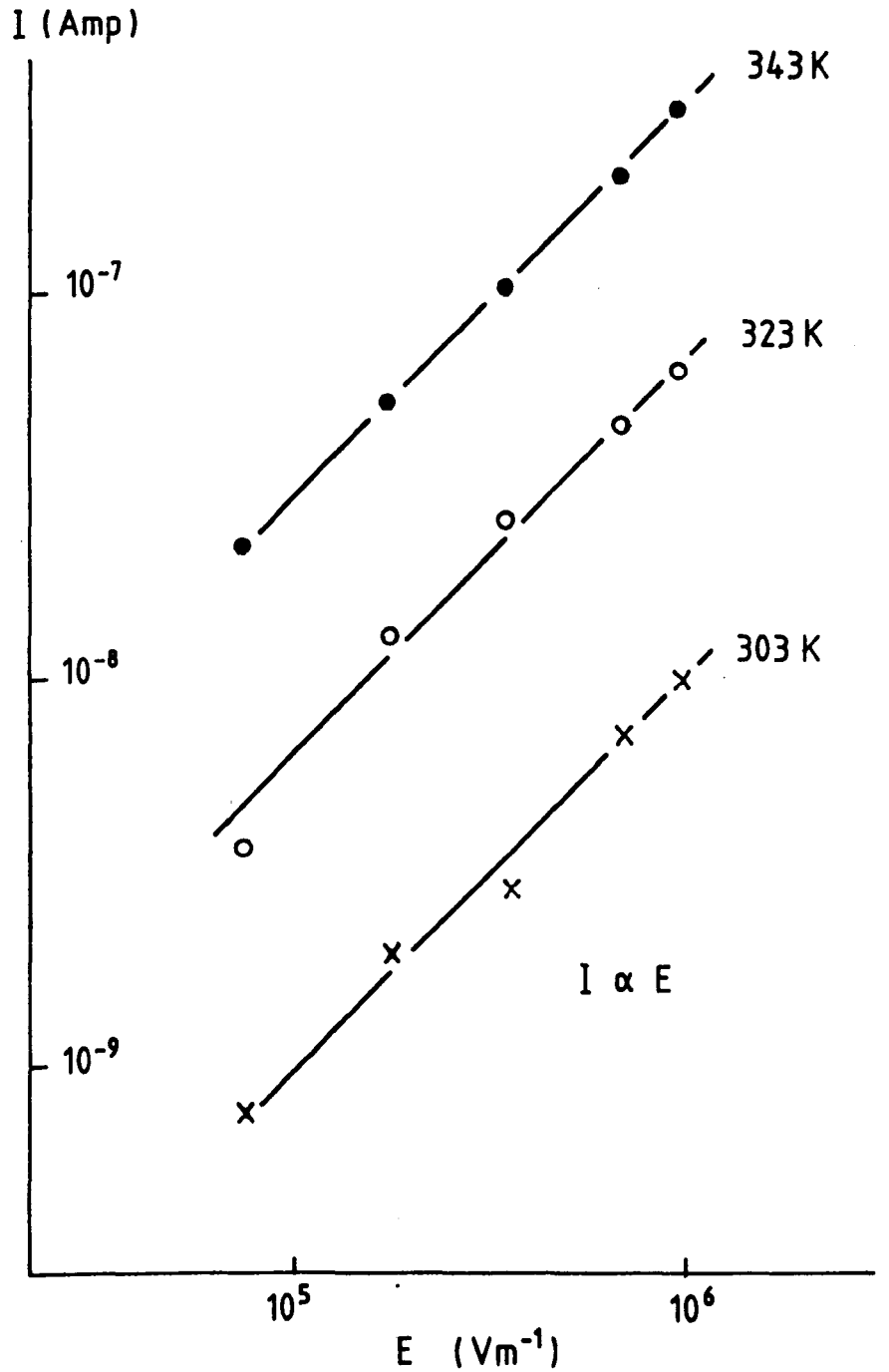

Fig. 4.46. Field dependence of steady state current (at 10^4 sec) in PZT5

may be due to space charges, as was the case observed in homopolymer PVDF by Das-Gupta et al [5]. The corresponding discharging currents ($I_d(t)$) is shown in Fig.4.48, from which the behaviour is observed to follow generally a relationship as Eq.(4.101), with the value of n increases with an increase of pre-applied field, i.e. in the range 0.51-0.87. The value of n was also observed to increase slightly with an increase of temperature, i.e. n=0.77-0.87 in the temperature range of 323-363K and at pre-applied field $7x10^6$ Vm^{-1} (see Fig.4.49).

The variation of $I_c(t)$ and $I_d(t)$ in different ceramic content of PZT5/VDF-TrFE composites at field $7x10^6$ Vm^{-1} and temperature 363K may be observed from Fig.4.50. It is expected that the magnitudes of $I_c(t)$ and $I_d(t)$ should be higher for composites with higher ceramic content. The slopes of $I_d(t)$ are observed to vary with the ceramic content of the composites but a systematic relationship may not be verified from these limited data.

Fig.4.51 shows the dependence of isochronal charging currents on electric field in PZT5/VDF-TrFE(50/50 Vol.%) at 363K. The dependence may be approximated to follow the relationship as Eq.(4.102) with the values of p were in the range of $\sim$0.6-0.84 (depends on time and field). The corresponding behaviour of $I_d(t)$ against pre-applied field may be observed as in Fig.4.52, from which the dependence of I_d on pre-E is found to decrease as the time increases, as normally is the case.

The variation of currents at 10^4 sec with temperature in three different compositions of PZT5/VDF-TrFE composites,

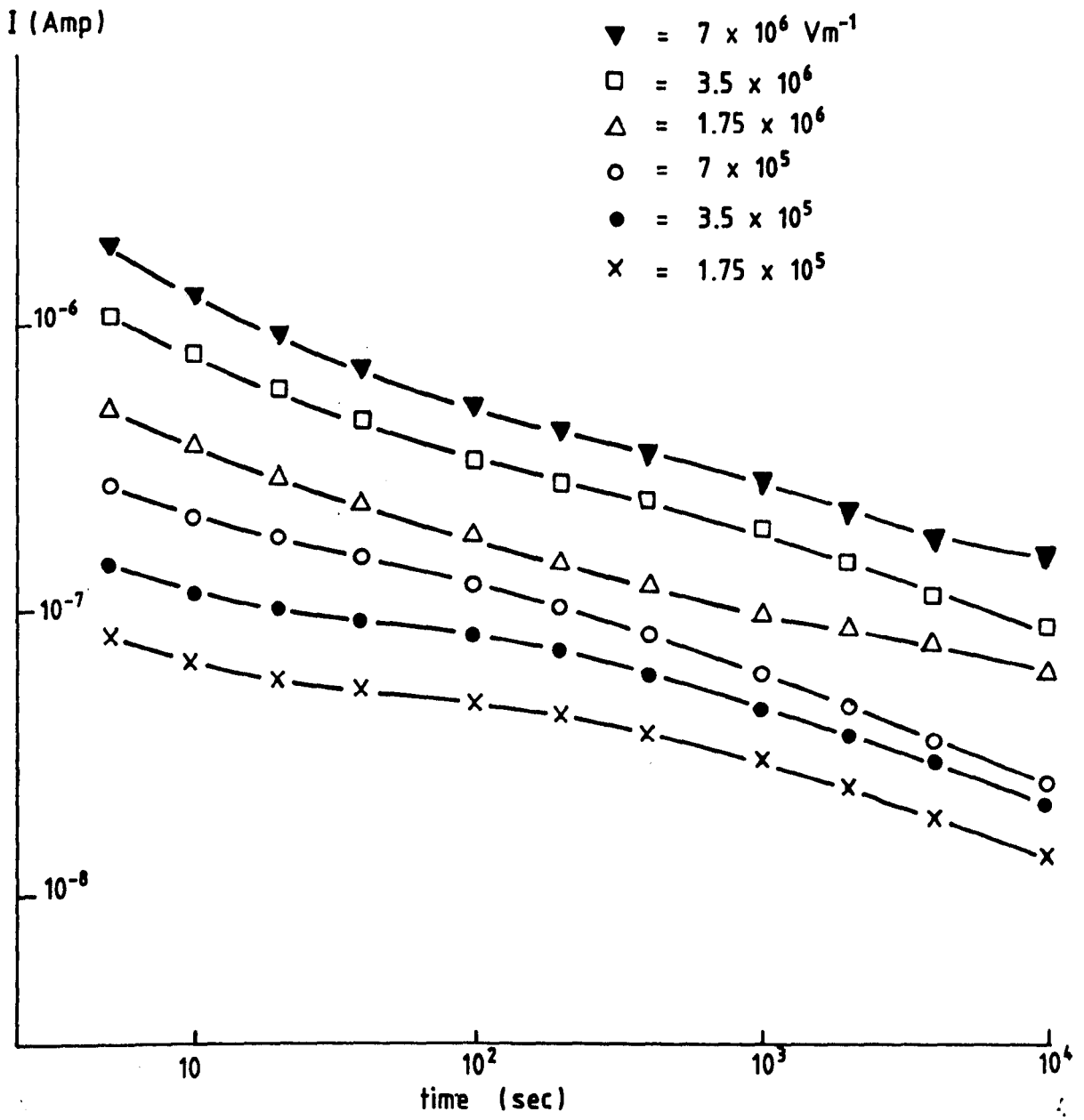

Fig. 4.47. Charging currents in PZT5/VDF-TrFE (50/50 Vol.%) for different fields at 363 K.

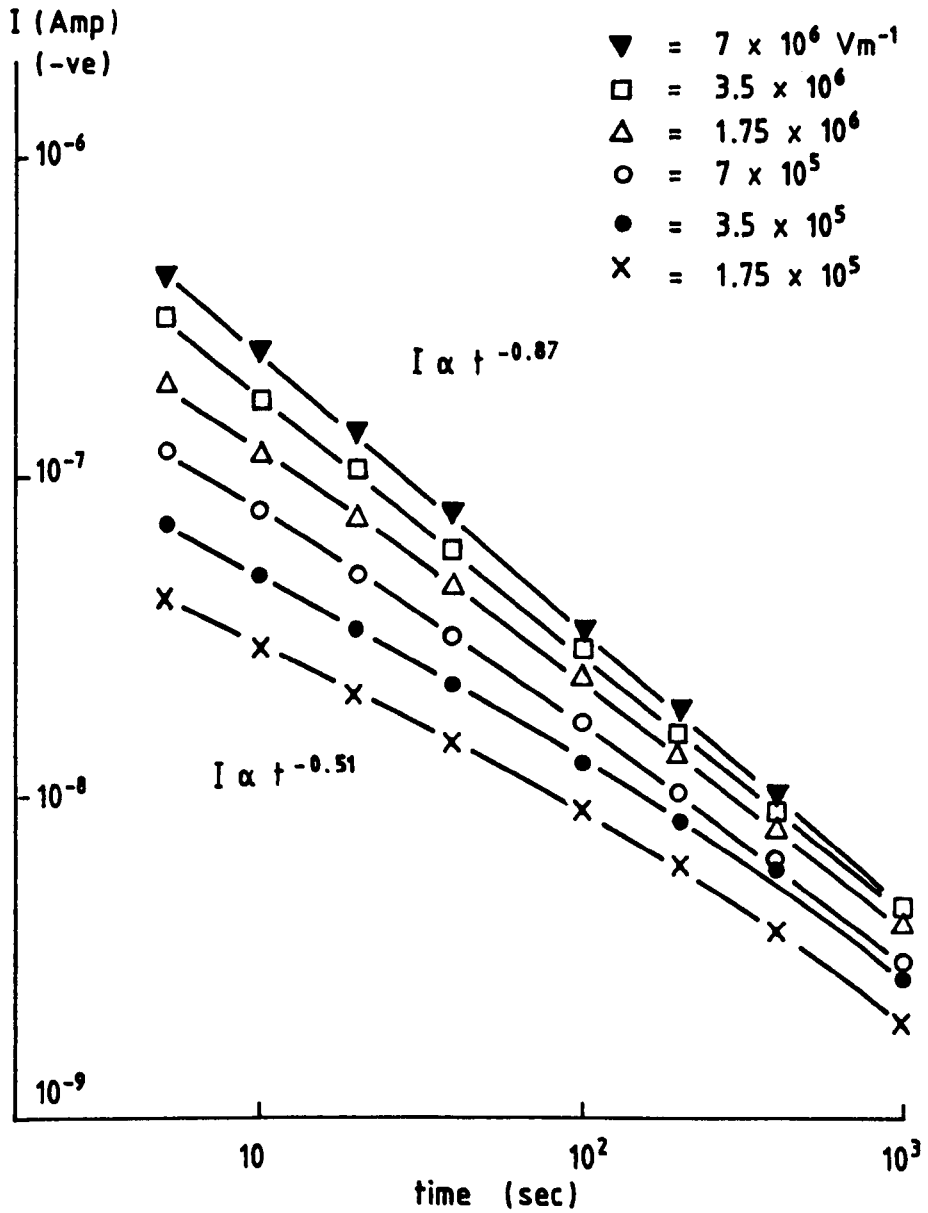

Fig. 4.48. Discharging currents in PZT5/VDF-TrFE (50/50 Vol.%) for different pre-applied fields at 363 K.

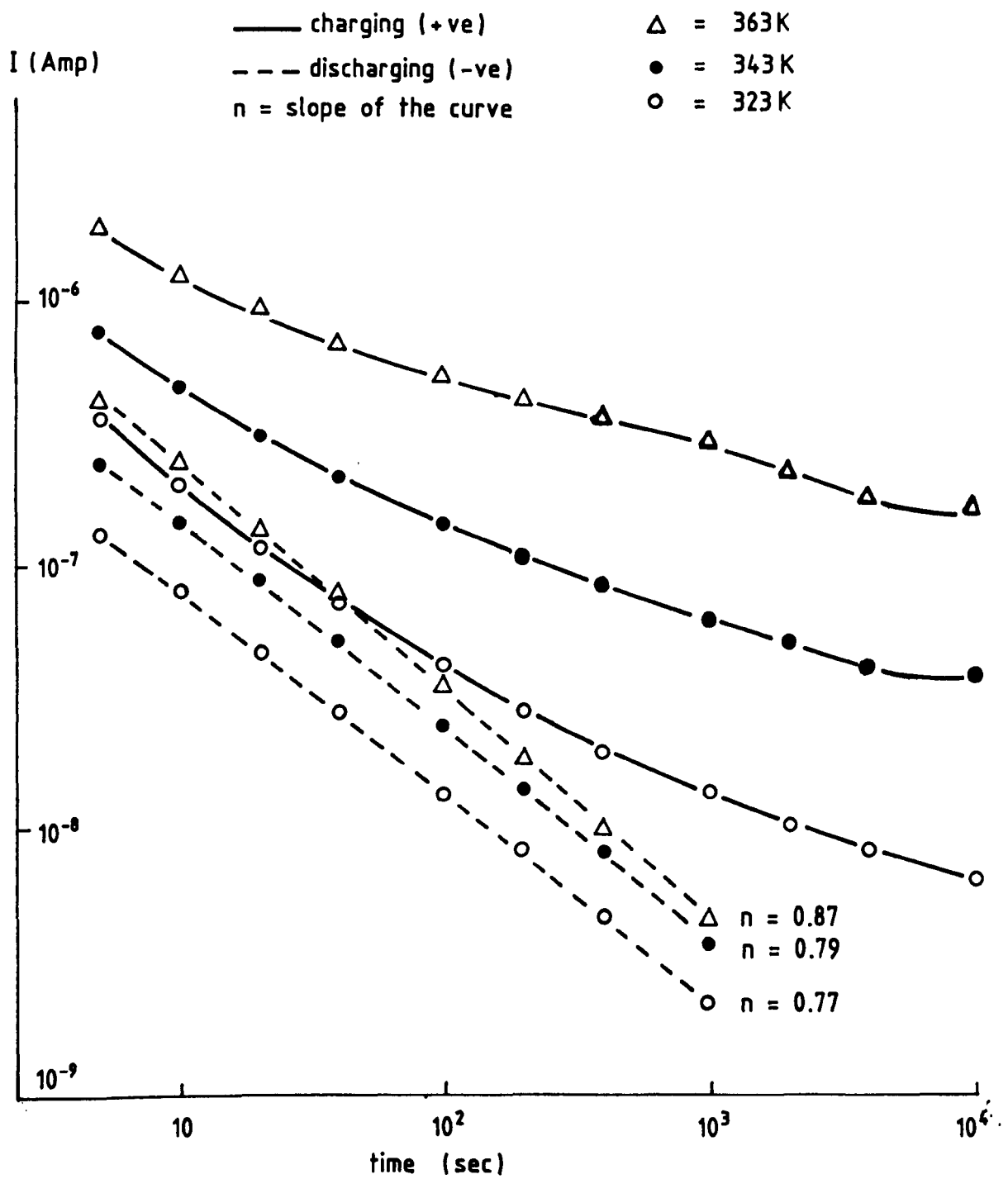

Fig. 4.49. Charging and discharging currents in PZT5/VDF-TrFE (50/50 Vol.%) for different temperatures at field 7×10^6 Vm^{-1}.

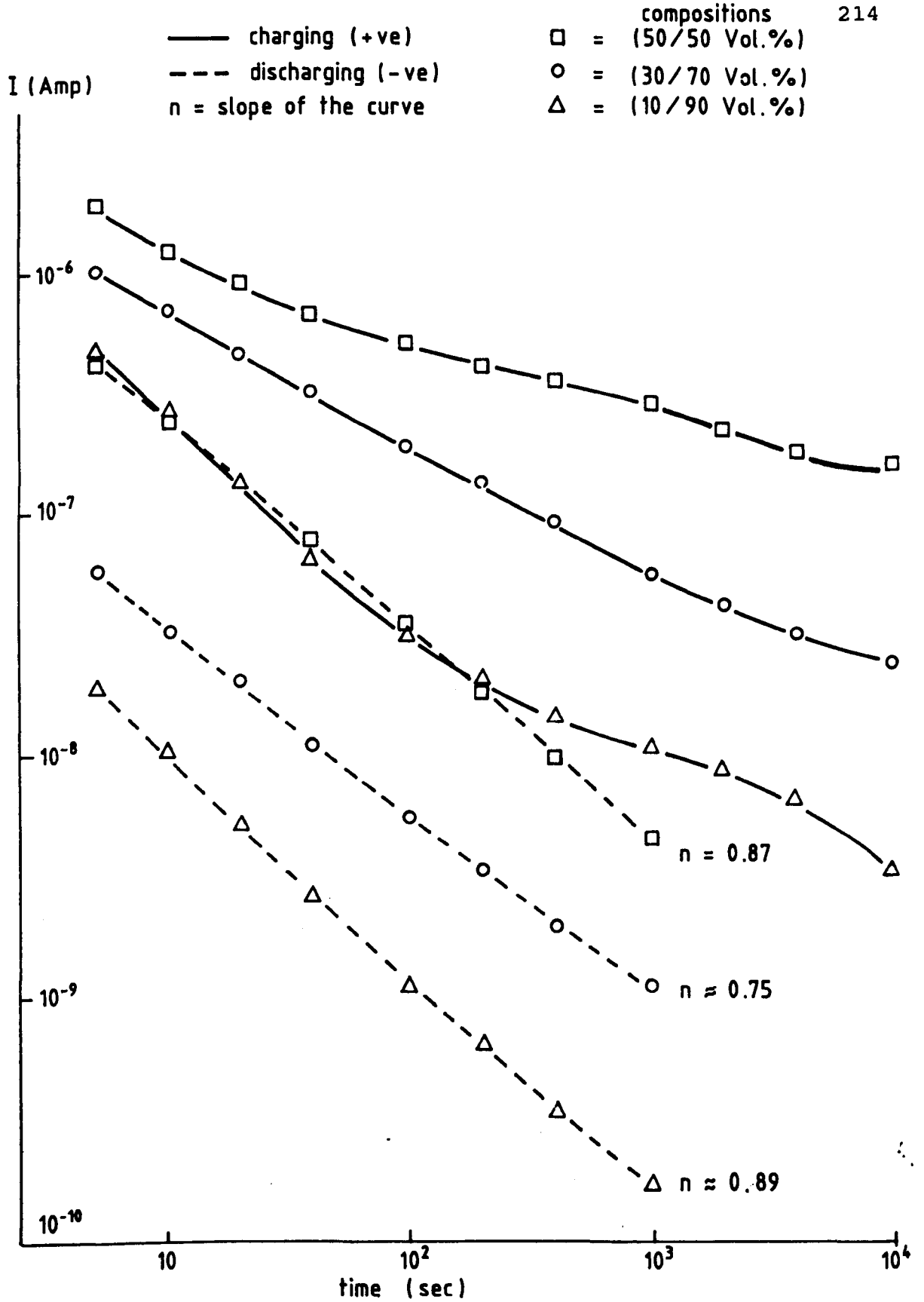

Fig. 4.50. Charging and discharging currents in different compositions of PZT5/VDF-TrFE at field 7 x 10^6 Vm^{-1} and temperature 363K.

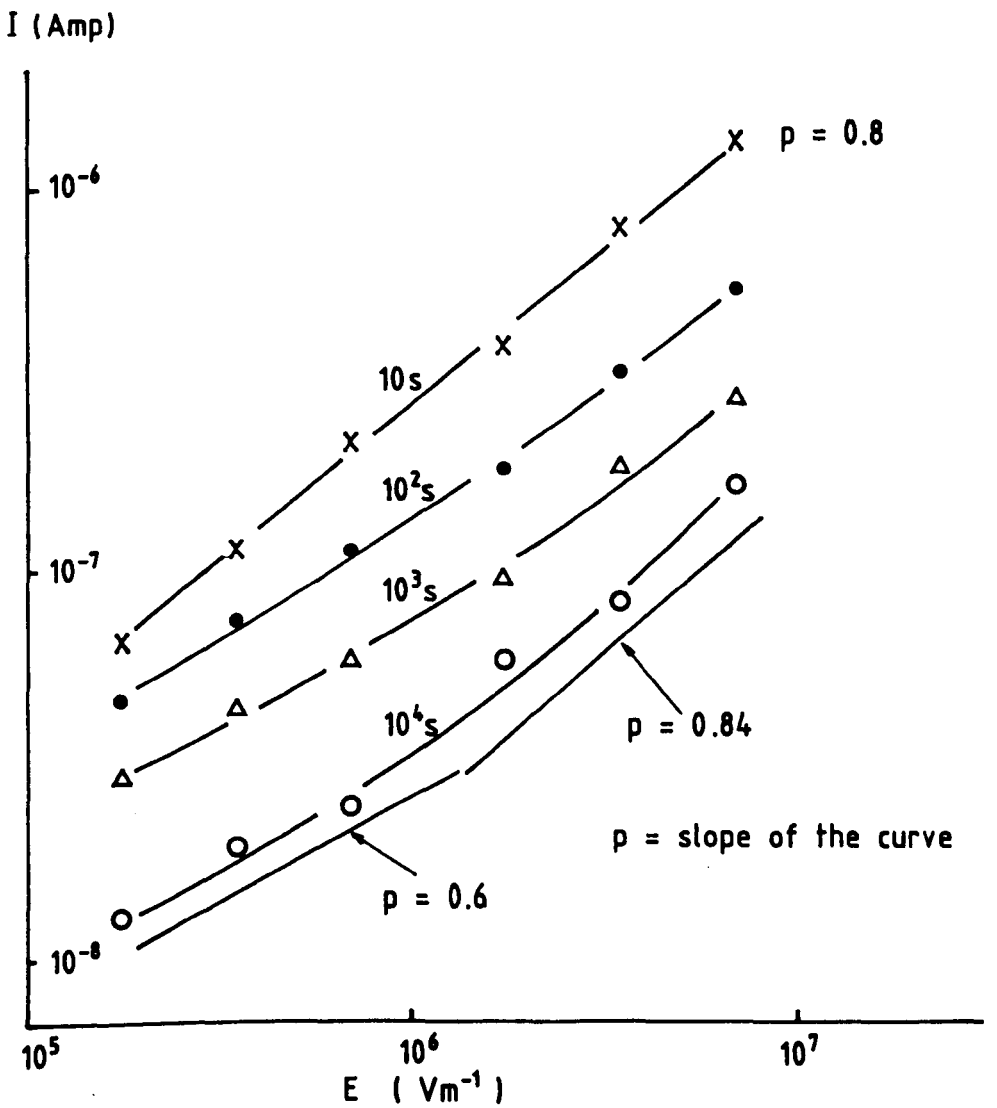

Fig. 4. 51. Isochronal charging currents in PZT5/VDF-TrFE (50/50 Vol.%) at different fields and temperature 363 K.

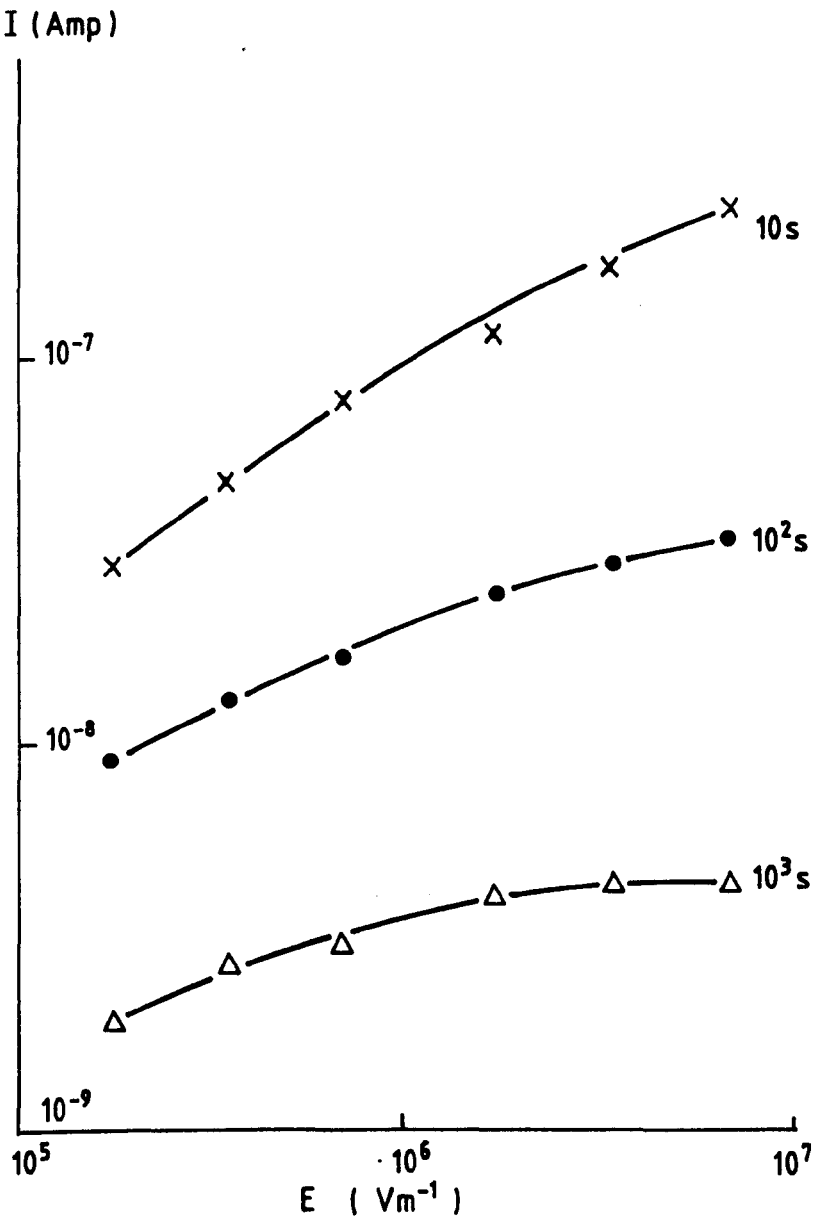

Fig. 4.52. Isochronal discharging currents in PZT5/VDF-TrFE (50/50 Vol.%) at different pre-applied fields and temperature 363 K.

measured at field 3.5×10^6 Vm^{-1} may be observed from Fig.4.53. Obviously, the difference in the magnitude of currents between these compositions is greater at high temperature, indicating possibly the increasing contribution of ceramic phase in the conduction process of the composites.

Fig.4.54 shows the behaviour of $I_c(10^4$ sec)-E dependence at three different temperatures in the range of 323-363K for PZT5/VDF-TrFE(50/50 Vol.%) composite. The dependence again may be approximated to follow the relationship as Eq.(4.102), with the slope of the curve depends on the range of fields and temperature, as in the case for PIEZEL composite. The slope of the curves, calculated for fields above $\sim 1 \times 10^6$ Vm^{-1}, appears to be 0.73, 0.73 and 0.84 at temperatures 323K, 343K and 363K respectively.

The dependence of $I_c(10^4$ sec) against field in PZT5/VDF-TrFE composites with different ceramic volume content at temperature 343K may be observed in Fig.4.55. A linear plot may be obtained through currents at high fields from which the slope was found to slightly increase with the increase of ceramic content in the composites. This would again indicate the increase contribution of ceramic phase in the conduction process of the composites.

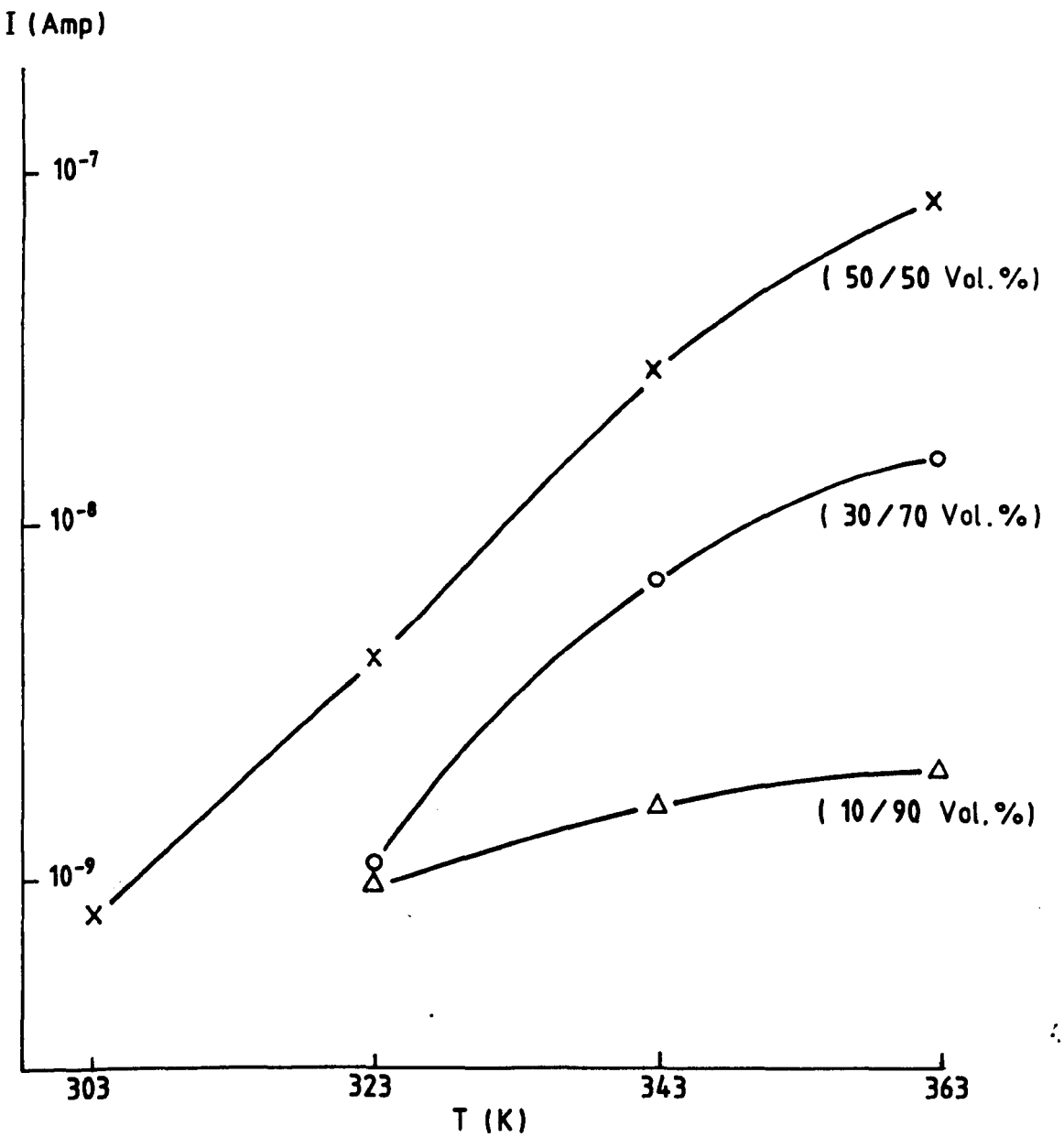

Fig. 4.53. Temperature dependence of charging current at 10^4 sec in different compositions of PZT5 / VDF - TrFE at field 3.5×10^6 Vm^{-1}.

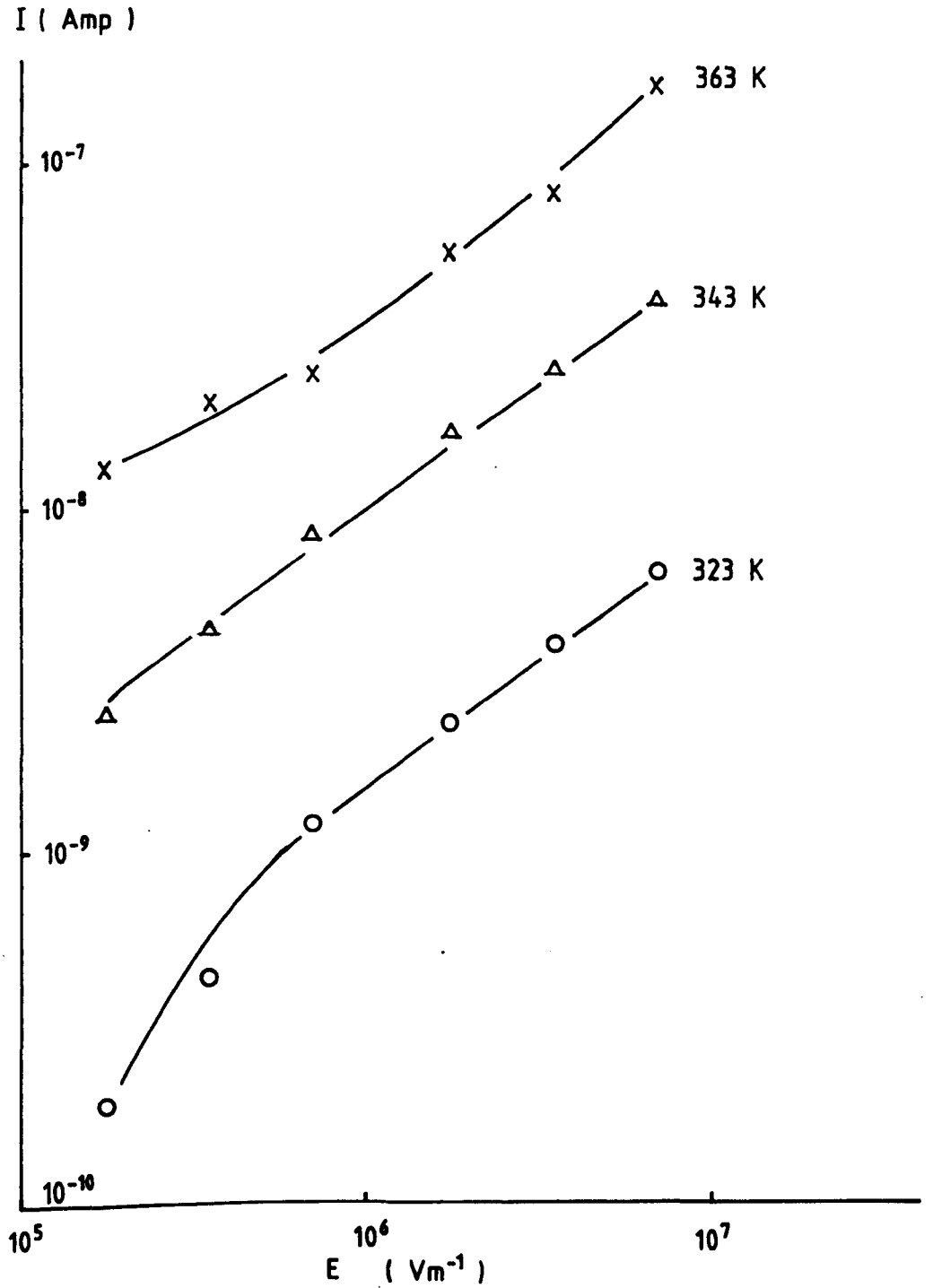

Fig. 4. 54. Field dependence of charging currents at 10^{4} sec in PZT5/VDF-TrFE (50/50 Vol.%) at different temperatures .

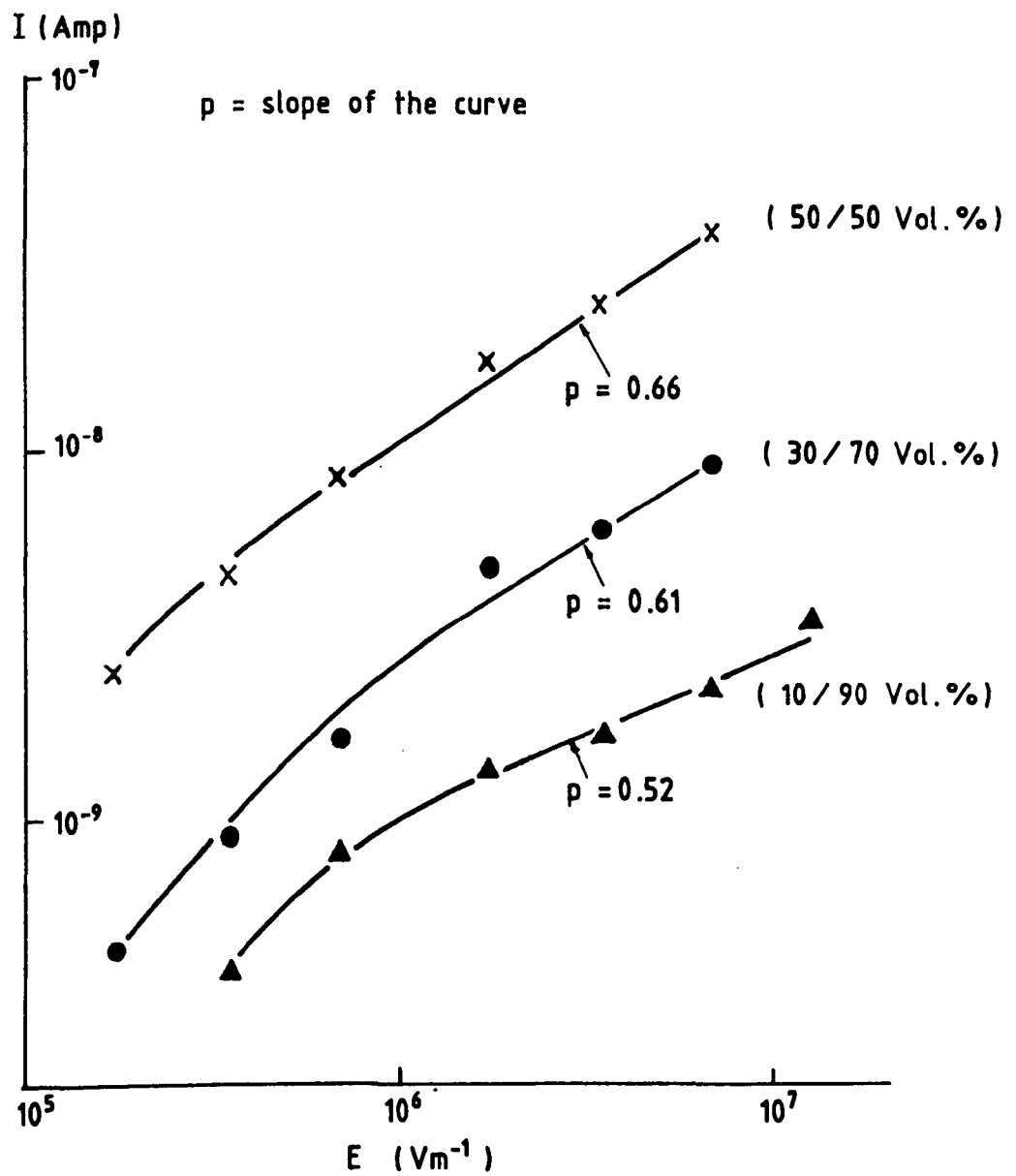

Fig. 4.55. Field dependence of charging currents at 10^4 sec in different compositions of PZT5/VDF-TrFE at 343 K.

4.4.5. Charging and discharging currents in PZT4/PVDF, PZT5/PVDF, $BaTiO_3$/PVDF and PZT4/PP composites

The behaviour of charging and discharging currents ($I_c(t)$ and $I_d(t)$) in PZT4/PVDF(50/50 Vol.%) in the field range of $(0.35\text{-}7)\times10^6$ Vm^{-1} at temperature 363K may be observed from Fig.4.56. At low fields, the $I_c(t)$ decays as usual, but as the field getting stronger, the current starts to level off before it rises slowly with time. The time at which the current begins to rise is shifted to shorter time at higher field. It may also be observed that the repeated measurement at field 7×10^6 Vm^{-1} produced approximately no difference in the magnitude of the current level. The repeated run was performed after the sample was short-circuited for 20 hours at the measuring temperature. It may be possible that a broad peak would appear at time longer than that observed in the present work or the I_c might continue to rise steadily with time. The rise of current over long period has also been observed in polymer such as high-density polyethylene [74,75] and in ceramic such as TiO_2 [76], in which it has been attributed to the space charges. The space charge contribution as a responsible mechanism for the rise in charging current with time, has also been proposed by Wintle [77]. In view of these, it may be possible that the observed behaviour of the rise of I_c with time in this composite is also associated with the space charges, which may be present in the bulk of the material or formed during the charging process [74-76], although more work need to be accomplished to fully explain

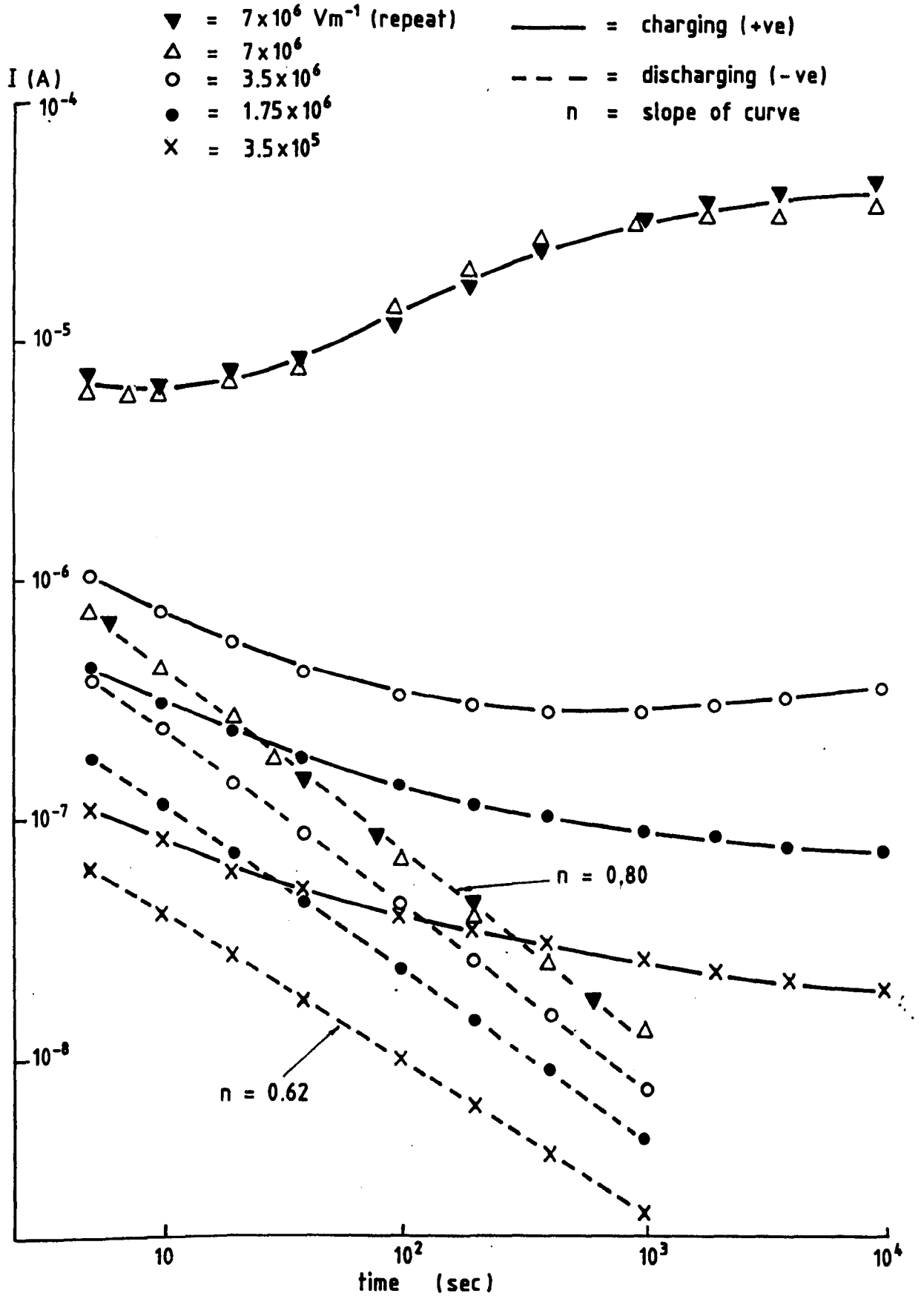

Fig. 4.56. Charging and discharging currents in PZT4/PVDF(50/50 Vol.%) for different fields at 363 K.

this behaviour.

Fig.4.57 shows the behaviour of $I_c(t)$ and $I_d(t)$ in PZT5/PVDF(50/50 Vol.%) composite in the field range (0.35-7)x10^6 Vm^{-1} at 363K. The $I_c(t)$ was observed to decay with time, without any obvious anomalous behaviour. At high pre-applied field (typically 7x10^6 Vm^{-1}), $I_d(t)$ decays initially with a slow rate then followed by a faster rate. Using Hamon approximation [29](see section 4.2.2), the $I_d(t)$ may be transformed into $\varepsilon''(f)$ for this particular pre-charging field at 363K. The $\varepsilon''(f)$ behaviour was found to show a relaxation peak at $\sim 10^{-3}$ Hz, which is quite similar to the one obtained for PVDF[5]. Thus, such a relaxation process may be associated with the interfacial charges in the bulk of the material.

The $I_c(t)$ and $I_d(t)$ behaviour in $BaTiO_3$/PVDF(40/60 Vol.%) in the field range of (0.35-7)x10^6 Vm^{-1} at 363K may be observed from Fig.4.58. Obviously, at low field, the steady-state current is seen to have reached at about 400 sec after the application of the field. As the field increases, the injection efficiency becomes appreciable. This is followed by increasing trapping of charge carriers, producing an enhanced reduction in current. It may also be observed that at high field, the I_c starts to rise after $\sim 10^3$ sec. This rise of current may be associated with the space charge, as in the case observed for PZT4/PVDF composite, mentioned earlier. There appears to be only a small change in magnitude of $I_d(t)$ for change in pre-applied fields at lower fields, suggesting possibly that only a small polarization charge have been involved in the charging process at those fields.

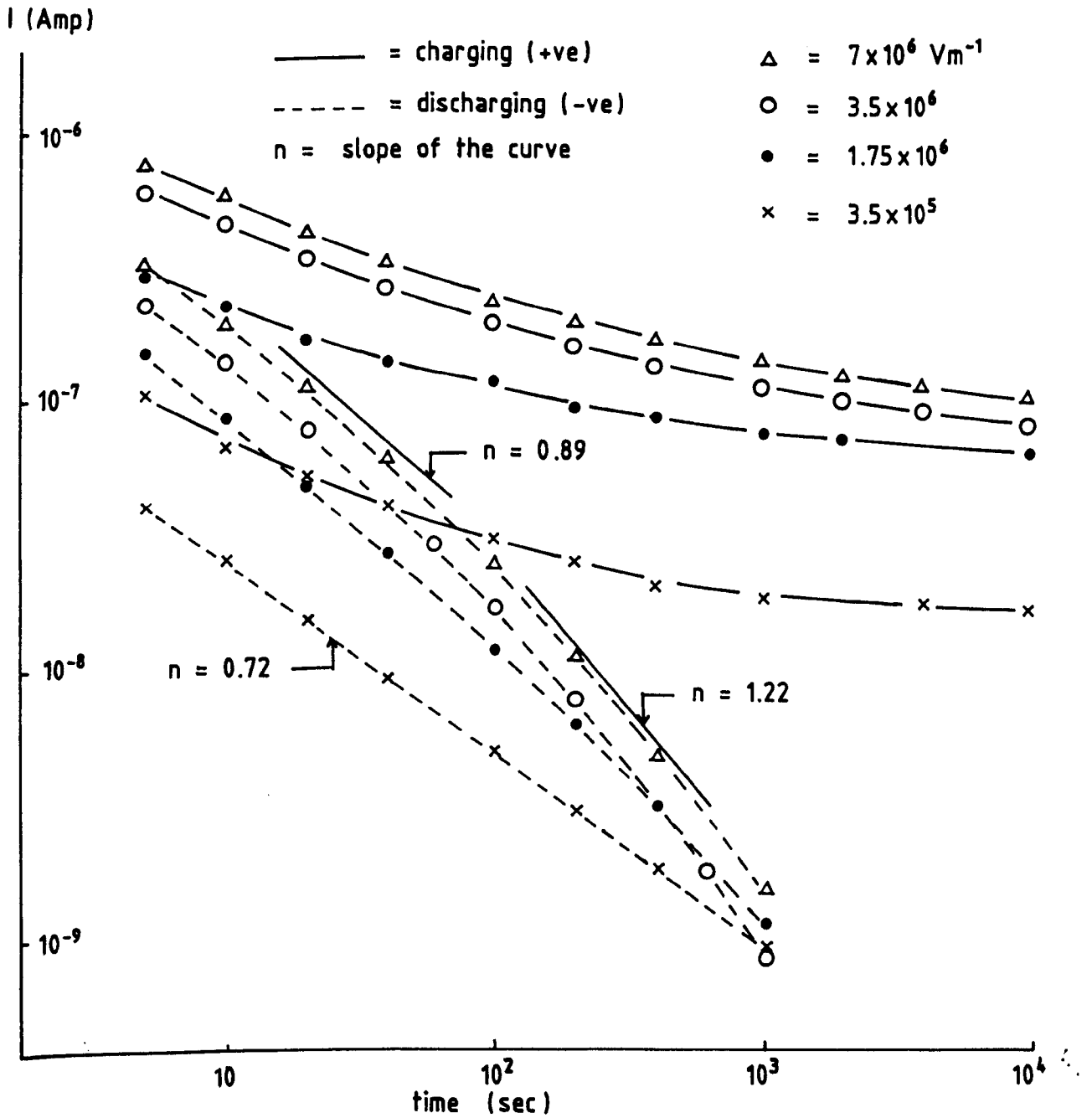

Fig. 4.57. Charging and discharging currents in PZT5/PVDF (50/50 Vol.%) for different fields at 363 K.

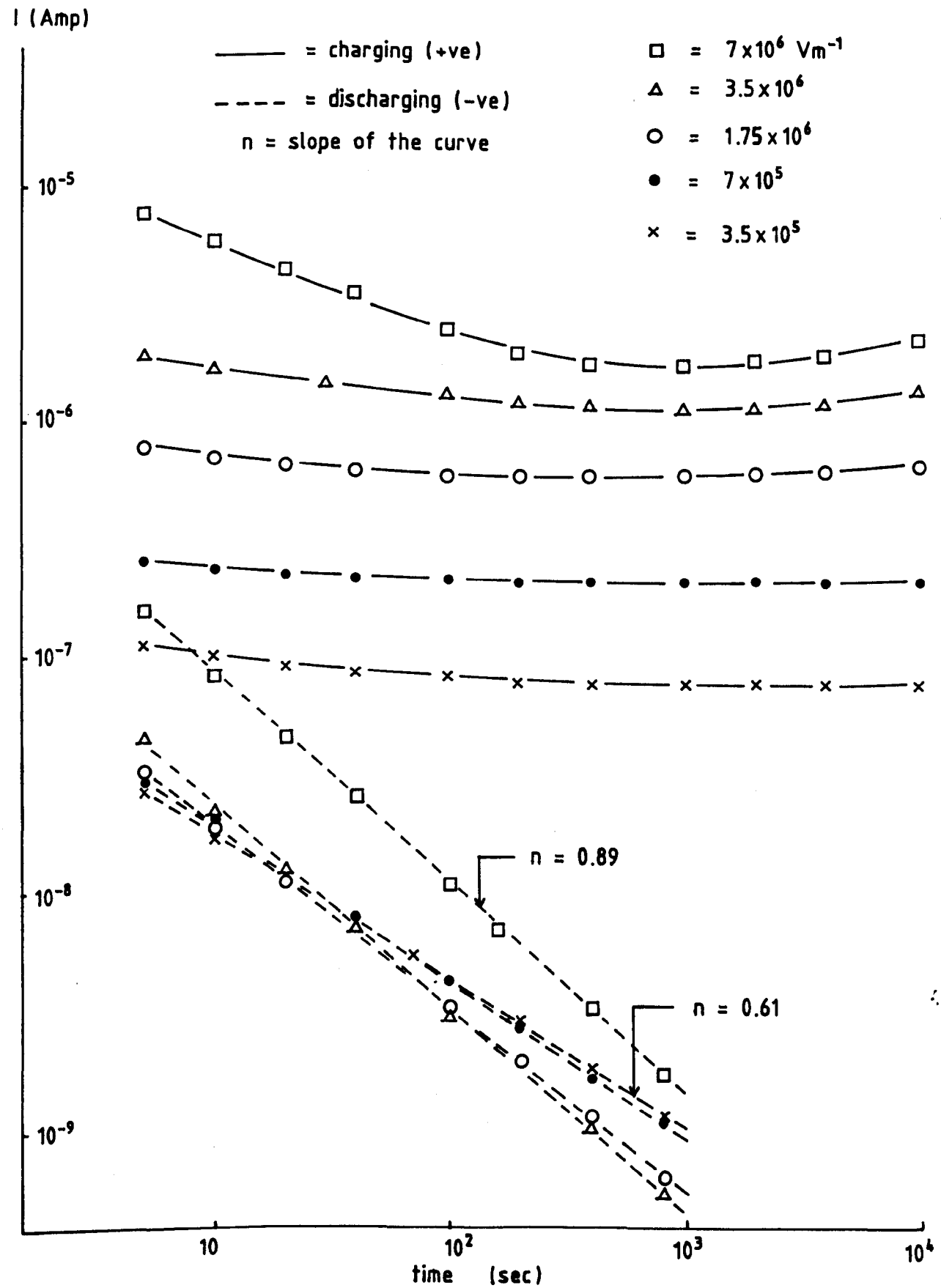

Fig. 4.58. Charging and discharging currents in $BaTiO_3$/PVDF (40/60 Vol.%) at 363 K.

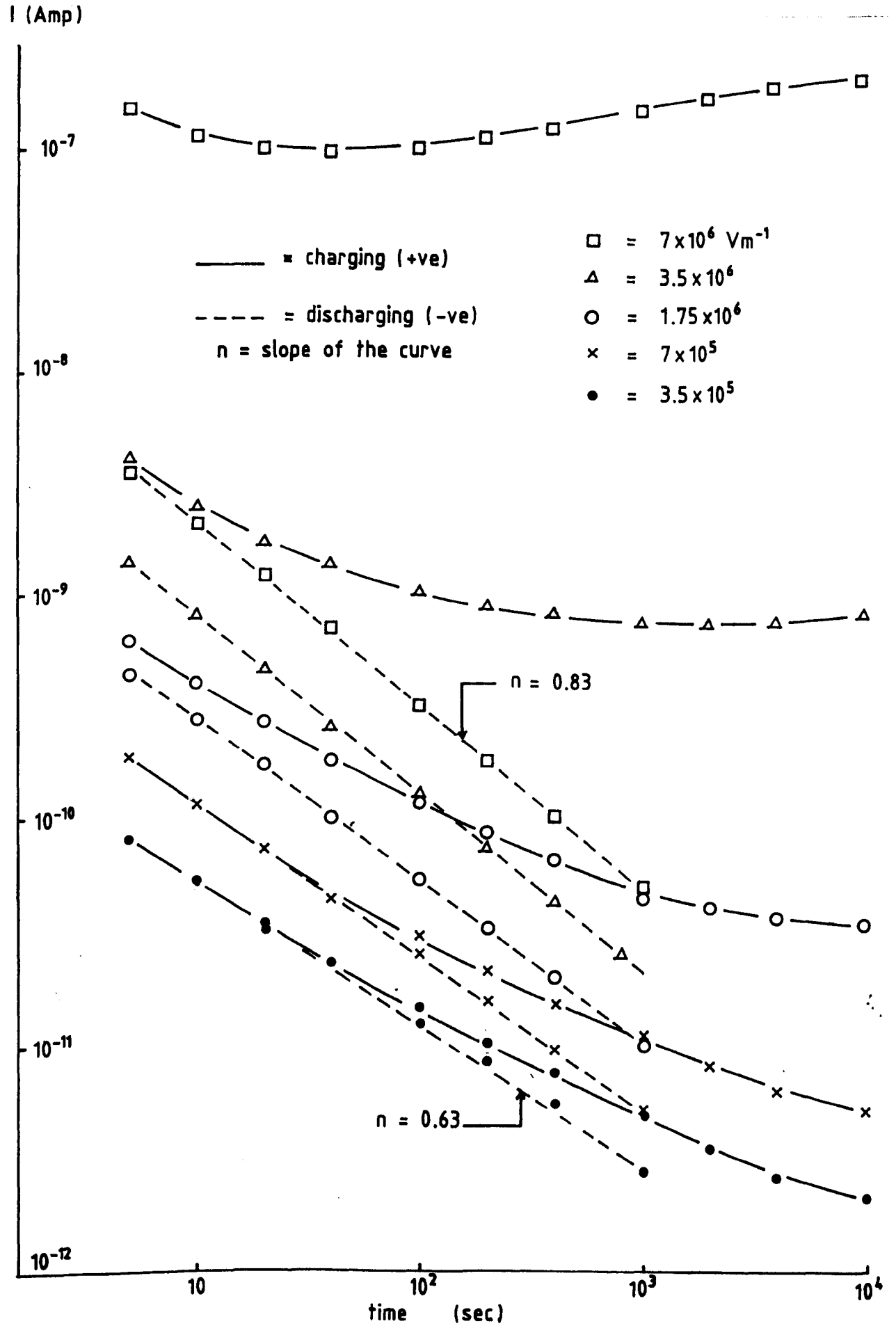

Fig. 4.59. Charging and discharging currents in PZT4/PP (50/50 Vol.%) at 363 K

Fig.4.59 shows the behaviour of $I_c(t)$ and $I_d(t)$ in PZT4/PP(50/50 Vol.%) composite in the field range of (0.35-7)x 10^6 Vm^{-1} at 363K. The $I_c(t)$ at low fields decay as usual, but at high field, the I_c begins to rise slowly after decaying for a certain period of time. It may be observed that the behaviour of $I_c(t)$ at $7x10^6$ Vm^{-1} is quite similar to that of $I_c(t)$ in PZT4/PVDF composite at the same field (see Fig.4.56) although the magnitudes are about 2 orders difference.

The behaviour of $I_d(t)$ for the above composites may generally be described to follow the relationship as Eq.(4.101), with the values of n are as in Table 4.1 at pre-applied fields (0.35-7)x10^6 Vm^{-1} and T=363K.

Table 4.1. Values of n in ceramic/polymer composites

composites	range of n
PZT5/PVDF(50/50 Vol.%)	0.72-1.22
PZT4/PVDF(50/50 Vol.%)	0.62-0.80
$BaTiO_3$/PVDF(40/60 Vol.%)	0.61-0.89
PZT4/PP(50/50 Vol.%)	0.63-0.83

4.5. Discussion

4.5.1. Transient (time-dependent) current in PIEZEL

From section 4.4.1, it may be observed that at low fields and temperatures (typically $\sim 10^5$ Vm^{-1} and 293K), the conduction current may not be so significant, thus the charging and discharging currents ($I_c(t)$ and $I_d(t)$) show approximately the same magnitude within the time range extended to $\sim 10^4$ sec, and decaying as t^{-n} with $n \simeq 0.7$. Such behaviour of current may be interpreted as due to dipolar and hopping carrier systems where carriers or dipoles move by discontinuous hops or jumps between stationary positional or orientational states, as suggested by Jonscher[46] and Jonscher and Taiedy[51].

As the temperature and field are increased, the differences in magnitudes of $I_c(t)$ and $I_d(t)$ were observed to depart strongly. This would naturally suggest that the conduction component of the currents becomes effective at those fields and temperatures which showed such currents departure. Adding to the complexity, this conduction current would possibly superimposed on one or several polarization and conduction processes (such as those given in section 4.2) which constitute the transient component of the current. The precise origin of this conduction current is yet to be determined. Due to the complexity of the process involved, only general suggestions had been made in describing the charge transport process in a single phase dielectric system.

For example, the space charge conduction mechanism has been suggested to occur in PVDF at ambient temperatures [5]. Kaura and Nath [6] suggested from the experimental result with PVDF that space charge injection into the bulk may ocur at ambient temperature (or slightly above) and charge carrier transport involving trapping is predominant. From the mobility measurement of charge carrier in polyethylene, Davies [78] proposed that the injected space charge from the metallic electrode may hop through trapping sites in the dielectric medium. Space charge conduction has also been observed in polyethylene and polyethylene terephthalate by Adamec and Calderwood [79] but they suggested that the space charges were derived from the bulk properties of the dielectric and did not originate from the injection process. The presence of space charge in PZT ceramics have always been associated with the incorporated impurities, which have been introduced for various purpose. Obviously, the kind and amount of impurities would determine the level of space charge contribution to the conductivity of the ceramics [66,80]. All these suggestions do indicate the importance of space charge in the conduction process although its origin is still under disputes. The present work also suggests that the space charges contribute in part to the conduction process, especially at high electric fields, as can be seen further in the following discussion.

The variation of currents with applied fields and temperatures has been measured in PIEZEL. From the dependence of I_c with E (Eq.(4.102)), it may be stated that at room temperature and low-field region (typically :$(0.175-1.8)\times10^6$

Vm^{-1}), the available space charge concentration may not be so much above the level of thermally generated free carrier density. This led to the almost ohmic behaviour of the I-E dependence. The insignificant contribution of space charge at low-field region and at room temperature may also lead to the observed dipolar (or hopping) carrier system from the current transient as mentioned earlier. In the high-field region, the space charge concentration may exceed the thermally generated free carrier density which possibly leads to the observed $p>>1$.

The sublinear dependence of I-E in the low-field region and at temperature above $\sim$293K may indicate the decreasing number of charge carriers available for conduction as a result of the trapping processes. It also appears that in this low-field region, the current tends to be less dependent on fields as the temperature increases. A possible reason for this behaviour may be due to more traps being created at high temperatures and thus reducing the number of charge carriers available for conduction. It is difficult to identify the kind of traps but it may be possible that the traps are related to structural defects (e.g. crystalline boundaries, grain boundaries, dislocations, interfacial boundaries), similar to that exist in some organic solids, which varies with temperature as [39] :

$$n_t \propto \exp(-\Delta U/kT) \qquad (4.105)$$

where n_t is the concentration of traps and ΔU is the energy

required to form a trap.

The observed increase of the activation energy values with time may possibly indicate that the charging current process involves the charge carrier trapping at the various levels of the trap distibution or it may also be explained in terms of dipolar orientation having a continuous spectrum of relaxation times. However, the latter process may not be readily observable in view of the presence of the conduction component at high fields and high temperatures but it is not totally improbable to occur at low-field and low-temperature regions.

The higher activation energy obtained at the high-temperature region as compared to that at the low-temperature region ($\sim$293-323K) of the I_C-1/T plot, may possibly indicate that at high temperatures, the charge carriers may have been trapped at deeper energy levels. The observed decrease in activation energies with applied electric fields at low-temperature region may possibly indicate an involvement of shallower traps at higher electric fields. At high charging field and in the high-temperature region, the involvement of traps with much deeper energy levels (> 1 eV) seems to appear together with a high production of charge carriers, which possibly indicate that the two processes may simultaneously occur.

The observed dependence of the transient current on temperature may suggest that the tunnelling process may not be a possible mechanism [28]. Electrode polarization may sometimes be used to described the transient current

behaviour. However many experimental results on polymeric system such as PET[1], PP[81] and PVDF[5] showed no detectable dependence of current on electrode materials, which may rule out the electrode polarization mechanism. In view of this, it would not be improbable that the electrode polarization is not the dominant mechanism for the observed current behaviour in the present ceramic/polymer composite system.

An analysis of data indicates that the discharging current process also involves different values of activation energy. Generally, if it is assumed that the charges which may have been trapped during the charging process, are not uniformly distributed through the thickness of the sample, then an internal field will arise. This internal field would effectively produce the short-circuit discharge current which is likely to be associated with trap delocalization of charges followed by subsequent retrapping. Obviously, the internal field would not be large enough to cause detrapping of charges with high activation energy (deep-trapped charges). Thus, the discharge currents would be associated with the process which involves relatively shallow-trapped charges, in which the charges would move by discontinuous hops between the states occupied by traps.

The observed relaxation behaviour from the discharge currents (Figs.4.34 and 4.35) is similar to the one obtained for PVDF in the same temperature and frequency range [5]. Thus, it is possible that such a relaxation process is associated with the interfacial charges accumulated at the boundaries between the crystalline and the amorphous regions

in the bulk of the material. The activation energy of ~1.0 eV as obtained for this relaxation appears to be higher than that associated with the assumed charge carrier hopping process mentioned earlier. Hence it is possible that these interfacial charges are trapped at deeper energy levels. Overlapping of the charge carrier hopping process and relaxation process due to interfacial charges would lead to the observed transient of the discharge current of the type shown in Fig.4.24 (for T=333-363K).

4.5.2. Transient current in ceramic/polymer composites prepared in the present work

In general, the observed transient current in ceramic/polymer composites prepared in the present work, shows similar behaviour as that for PIEZEL composite. The anomalous charging current which appears at high fields for PZT4/PVDF, $BaTiO_3$/PVDF and PZT4/PP composites may be related to the properties of ceramics and further work is needed to clarify this behaviour.

An estimate of the amount of charge carriers that involve in the discharging current may be calculated, thus :

$$Q_{disch} = \int B\, t^{-n} = \frac{B\, t^{1-n}}{1-n} \Bigg|_{t_1}^{t_2} \qquad (4.106)$$

where B is the discharge current at 1 sec value, which can be

obtained by extrapolating $I_d(t)$ curve. Table 4.2 shows the values of n and Q_{disch} (evaluated from t_1 = 5 sec to $t_2 = 10^3$ sec) for pre-E of $7x10^6$ Vm^{-1} and T=363K in the composites. Comments on this table can be found in section 7.1.

Table 4.2. Values of n and Q_{disch} in ceramic/polymer composites

composite	n	Q_{disch} (Coul.)
PZT5/VDF-TrFE(50/50 Vol.%)	0.87	$1.55x10^{-5}$
PZT5/PVDF(50/50 Vol.%)	0.89, then 1.22	$9.66x10^{-6}$
PZT4/PVDF(50/50 Vol.%)	0.80	$3.19x10^{-5}$
$BaTiO_3$/PVDF(40/60 Vol.%)	0.89	$5.66x10^{-6}$
PZT4/PP(50/50 Vol.%)	0.83	$0.16x10^{-6}$

4.5.3. Steady-state and quasi-steady-state conduction

The observed field-dependent activation energy for steady-state conduction in PIEZEL (Fig.4.39) suggest that the conduction process could be analysed in term of Schottky emission model, Poole-Frenkel effect or ionic conduction model. Fig.4.60 shows the Schottky conduction plot in PIEZEL at different temperatures in the range of 293-358K. It can be observed that for $E \lesssim 3.5x10^6$ Vm^{-1} the data fits quite well to a

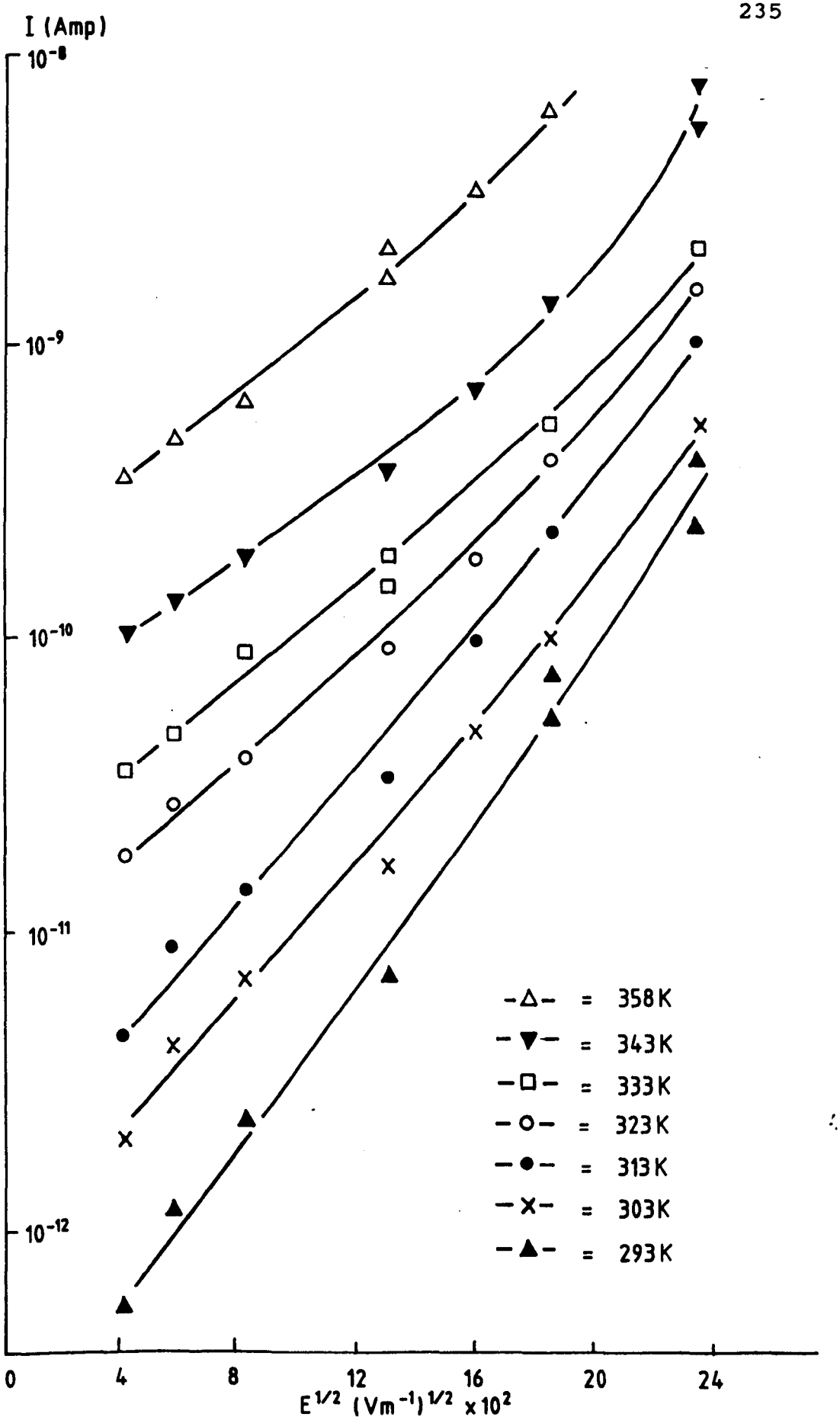

Fig. 4.60. Schottky conduction plot in PIEZEL at different temperatures.

linear dependence especially at low temperatures. From the slopes of the Schottky plots, the values of ε' were calculated to be in the range 0.22 to 0.55 in the temperature range 293-373K (see section 4.2.5. for the Schottky model, assuming neutral contact at the electrode-dielectric interface). The electrode-dielectric potential barrier in the absence of an electric field, ϕ_o , was found to be 0.94 eV as obtained from the plot of ($\ln J_o/T^2$) vs. 1000/T (see Eq.(4.61), J_o is the extrapolated value of J at E=0). It appears that the value of ε' from this model is unacceptable.

Fig.4.61 shows the Poole-Frenkel conduction plot in PIEZEL at temperatures 293-343K. The plots are reasonable straight lines at high fields region and deviates from the linear dependence at low fields. It may be observed that the lower limit of field at which the linear dependence begins, is shifted to higher values as the temperature increases. From the linear part of the plot, the calculated values of ε' (from Eq.(4.87)) were observed to be approximately 1.6 and independent of the temperature. This value is again unacceptable for PIEZEL. The magnitude of the potential barrier due to trap in the absence of applied electric field, ϕ_{ct} , obtained by extrapolation of ln σ(E=0) vs. 1000/T was found to be 0.71 eV.

Ionic conduction plot in PIEZEL in the temperature range 303-373K may be observed from Fig.4.62. Evaluation of the gradients of the linear part of the curves showed that the values tend to slightly increase with the increase of temperature in the high-temperature region. The values of the

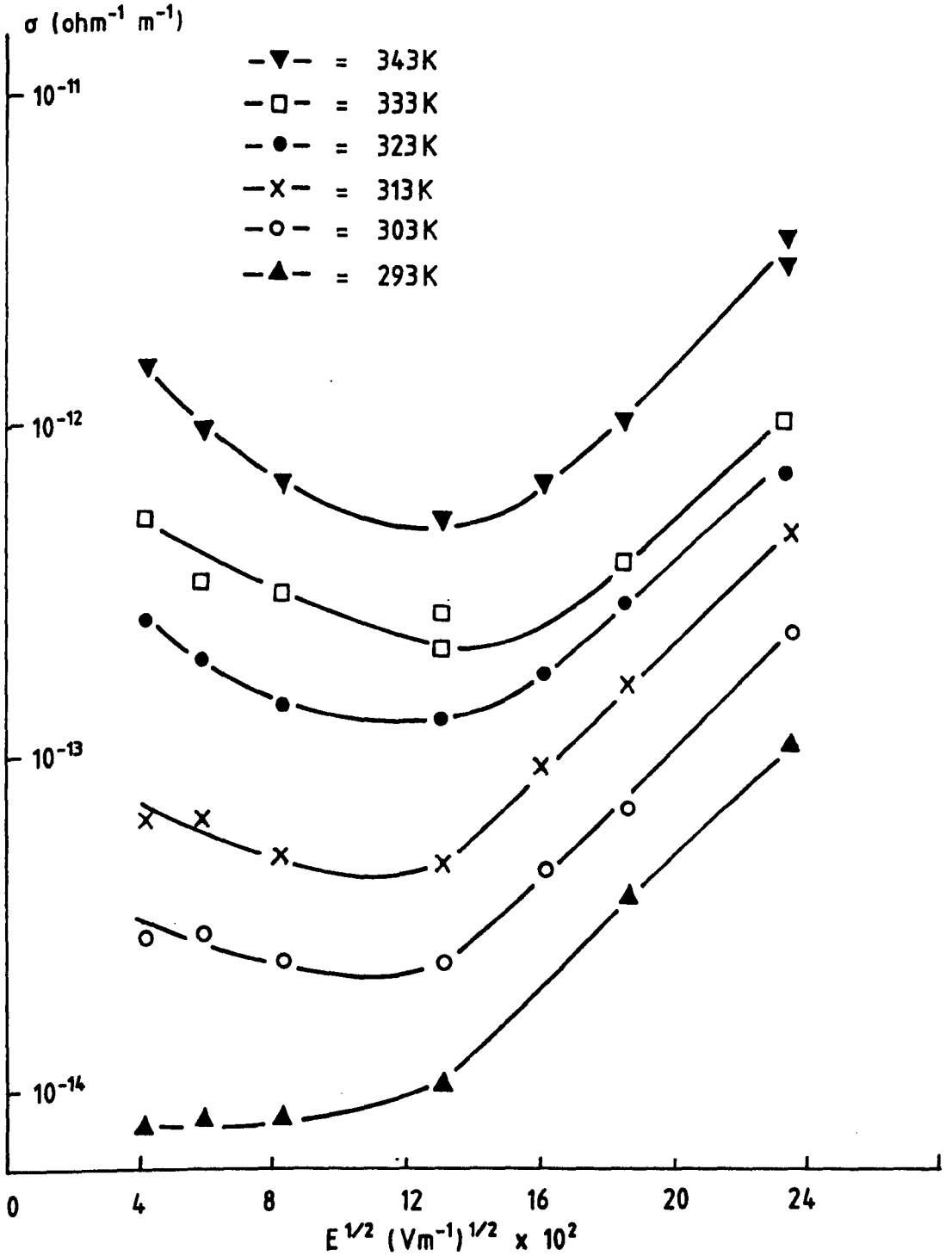

Fig. 4.61. Poole-Frenkel conduction plot in PIEZEL at different temperatures.

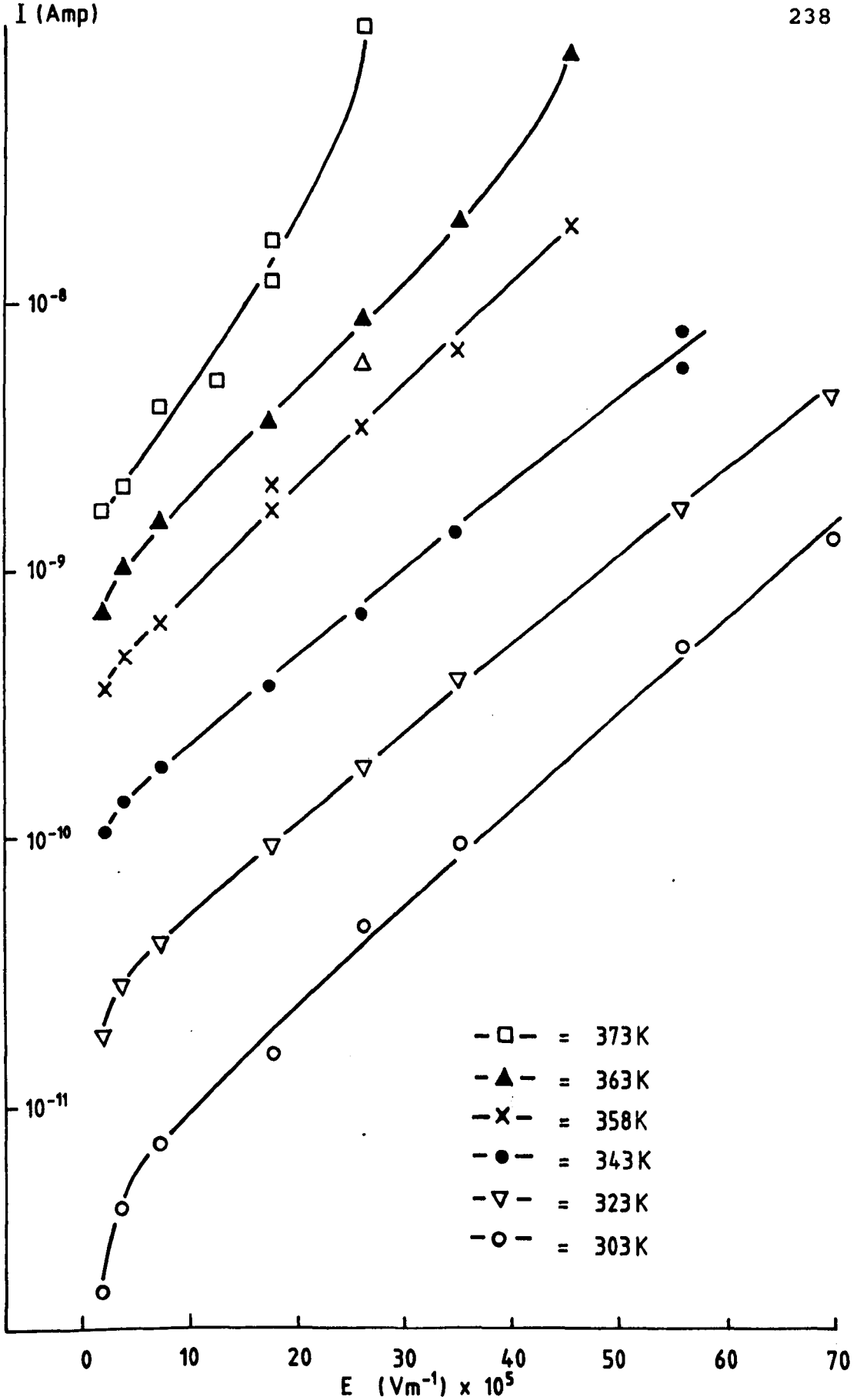

Fig. 4.62. Ionic conduction plot in PIEZEL at different temperatures.

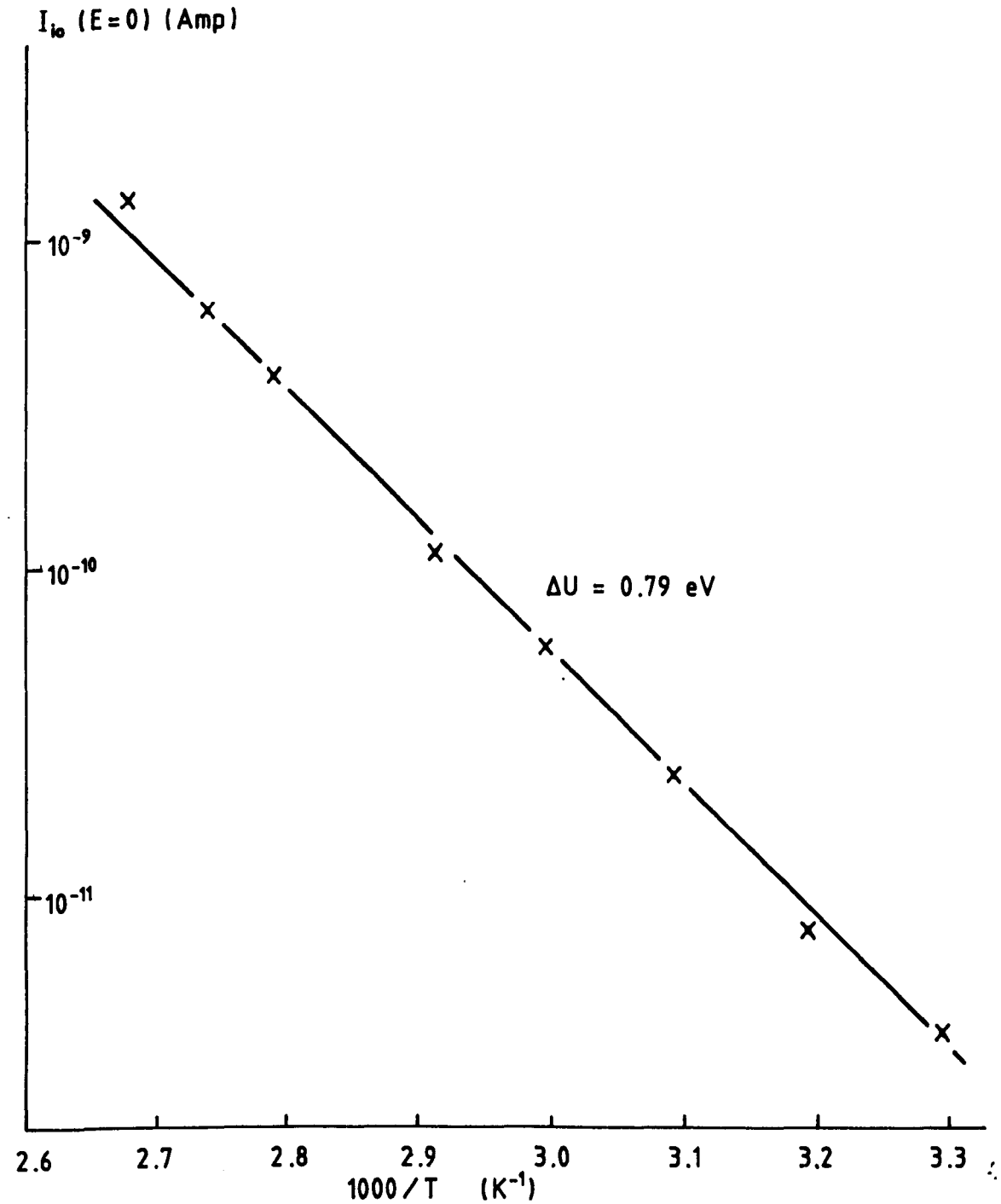

Fig. 4.63. Activation energy of ionic conduction in PIEZEL.

jump distance (d) , obtained from such plots appear to be in the range of 425-850 Å in the temperature range 293-373K (see Eq.(4.100) for the calculation of d). The activation energy associated with the ionic conduction mechanism, obtained by plotting ln I(E=0) vs. 1000/T was found to be 0.79 eV (see Fig. 4.63).

The steady-state electrical conduction in PZT may also be analysed in term of Schottky conduction. Fig.4.64 shows the plot of such conduction model in the temperature range of 303-343K. It may be observed that the data show a reasonably linear dependence at high-field region. From the linear part of the plot, the values of ε' were calculated to be in the range 0.25-0.35 in the temperature range 303-343K, which is again unacceptable. Thus the Schottky conduction is not the origin of steady-state conduction in this material.

The ionic conduction plot for PZT of the present work is shown in Fig.4.65 in the temperature range 303-343K. The calculated values of the jump distance (d) appear to increase with the increase of temperature, i.e. from 665 Å to 1020 Å. From the plot of extrapolated values of current at zero field (I(E=0)) vs. 1000/T , the activation energy is found to be 0.66 eV (see Fig.4.66). It may be possible that ionic conduction is achieved by means of cation and anion jumps to vacant sites. Such vacancies may have been formed in the material by the incorporated ionic impurities [66].

Ionic conduction has also been observed in many polymeric materials such as PVDF[5], Nylon[82], PVC[83] and PP[84,85,86]. The values of the jump distance obtained for

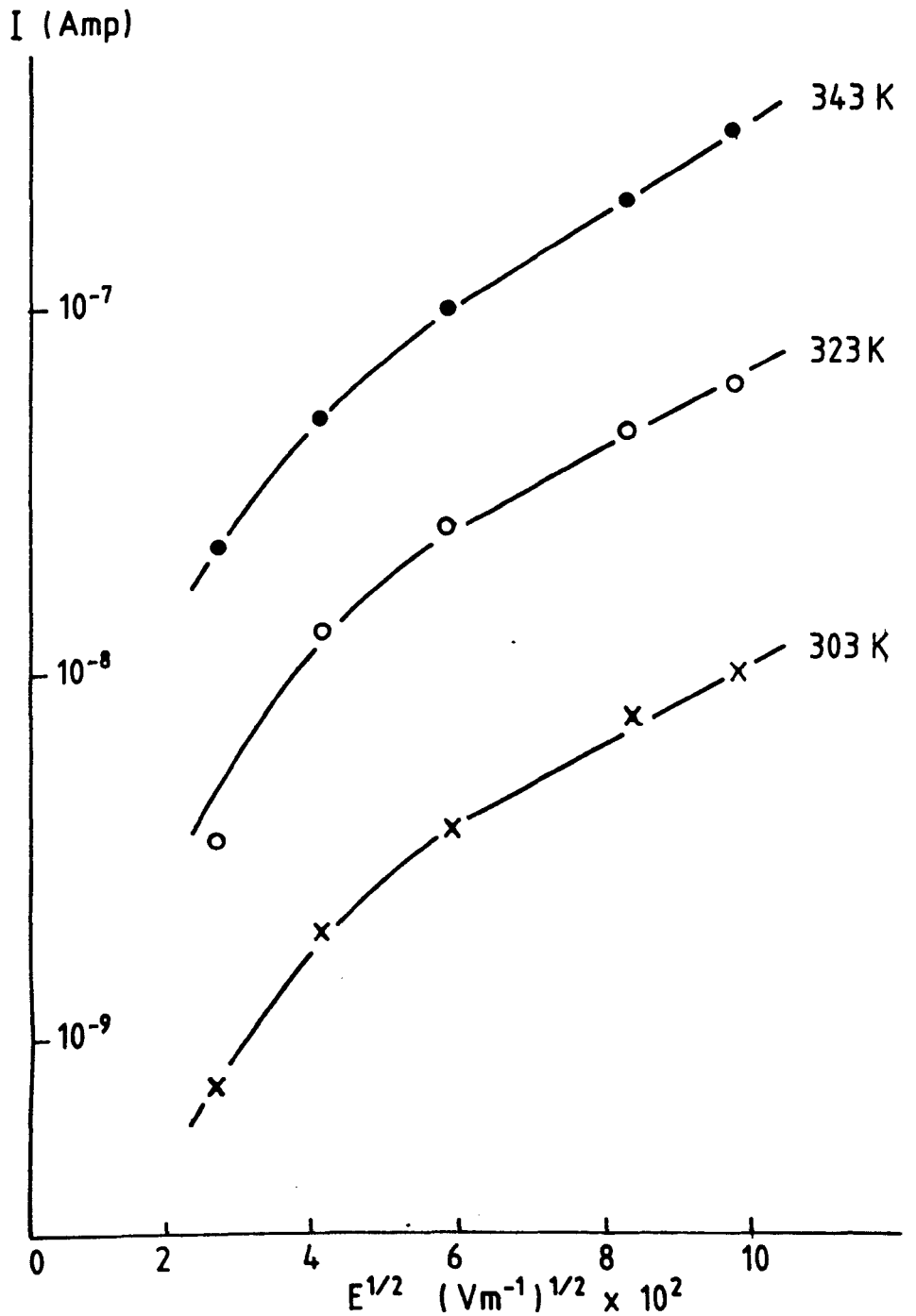

Fig. 4.64. Schottky conduction plot in PZT.

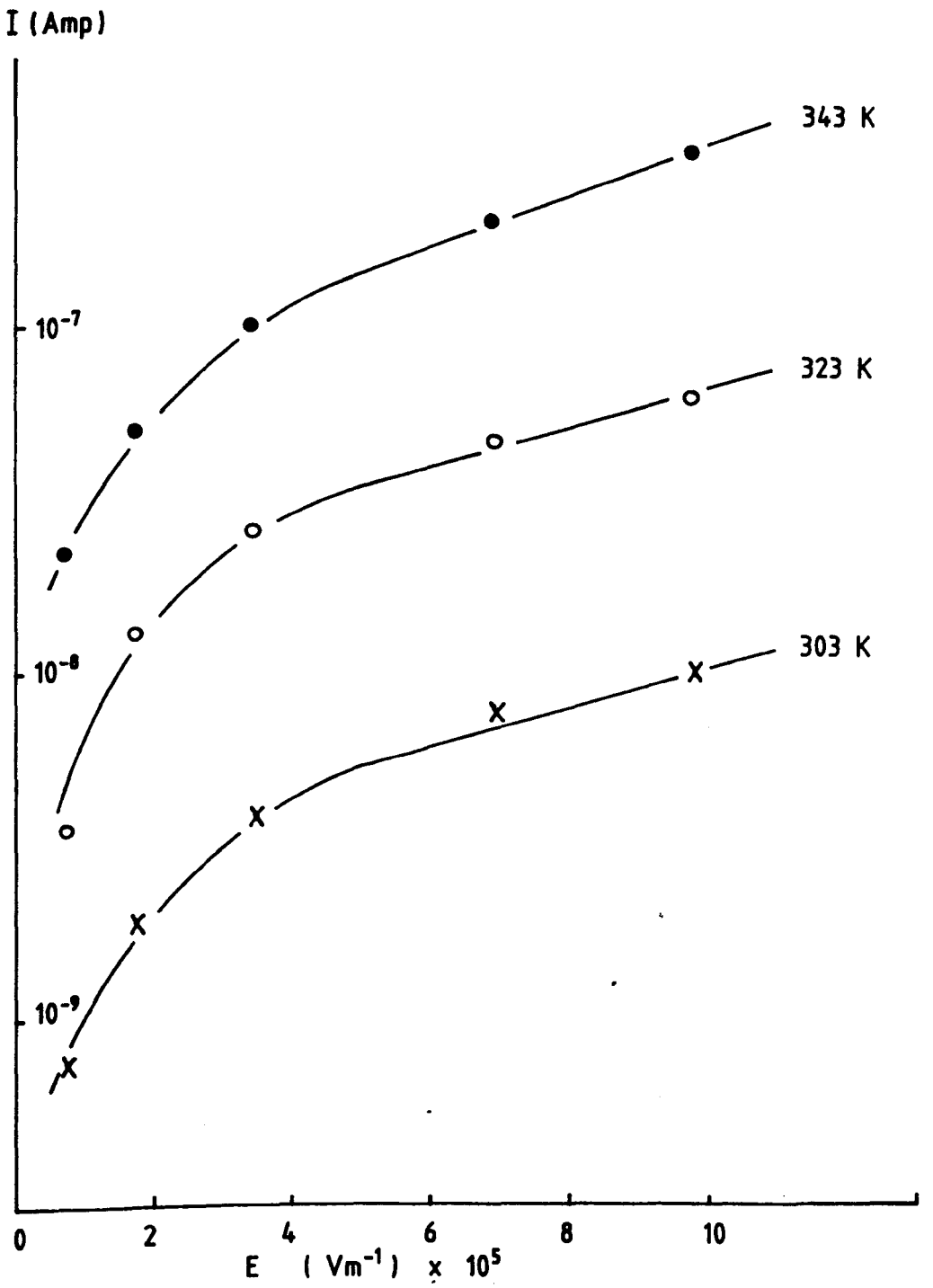

Fig. 4.65. Ionic conduction plot in PZT.

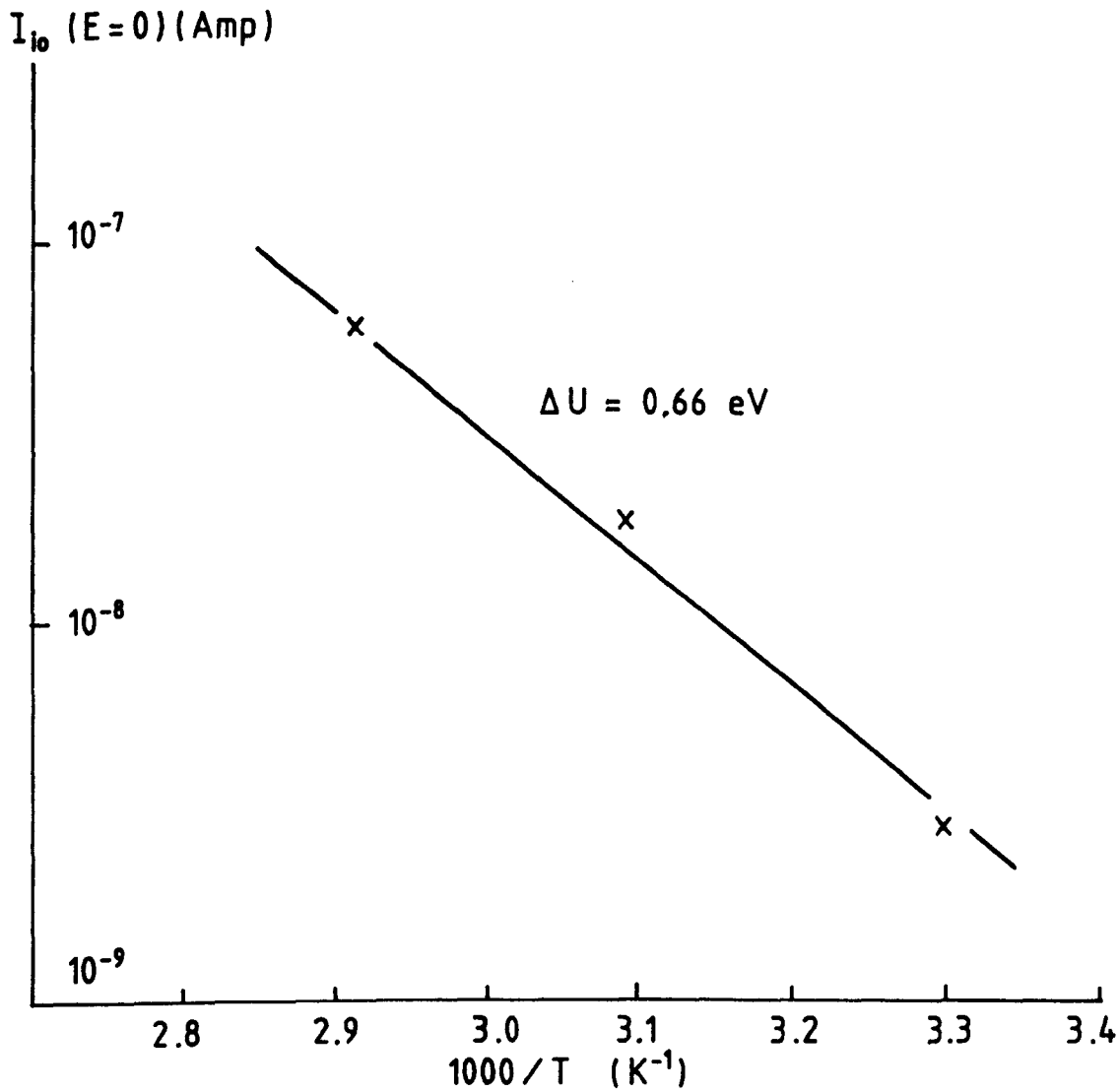

Fig. 4.66. Activation energy of ionic conduction in PZT.

PVDF in the temperature range 293-413K were (25±3)Å while the activation energy value was 0.89 eV [5].

The observed increase in the values of the jump distance in PIEZEL composite and PZT at high temperatures may possibly due to an increase of the mean free path of the ionic carriers. Such an increase in the values of the jump distance with temperature has also been reported for PVC in the glass transition region [83]. The variation of the jump distance with temperature was suggested to be related to the chain motion in the respective temperature region, in which ionic movement experience the change in the shape and height of potential barriers [83].

The steady-state current has not been observed in PZT5/VDF-TrFE composites in the range of temperature, field and time of the present work. As such only the quasi-steady-state current (current at 10^4 sec) may be used to analyse the conduction mechanism in this composite. Ionic conduction plot in PZT5/VDF-TrFE(50/50 Vol.%) composite is shown in Fig.4.67. It may be observed that the linear part of the curves extend to a lower field at higher temperature. The calculated values of the jump distance (d) from the linear part of the curves were 85 Å (323K), 105 Å (343K) and 150 Å (363K), while the activation energy associated with this ionic conduction process was evaluated to be 0.62 eV.

The ionic conduction plot in PZT5/VDF-TrFE composites with different ceramic volume fraction at temperature 343K is shown in Fig.4.68. The calculated values of the jump distance from the linear part of the curves were found to be 42 Å,

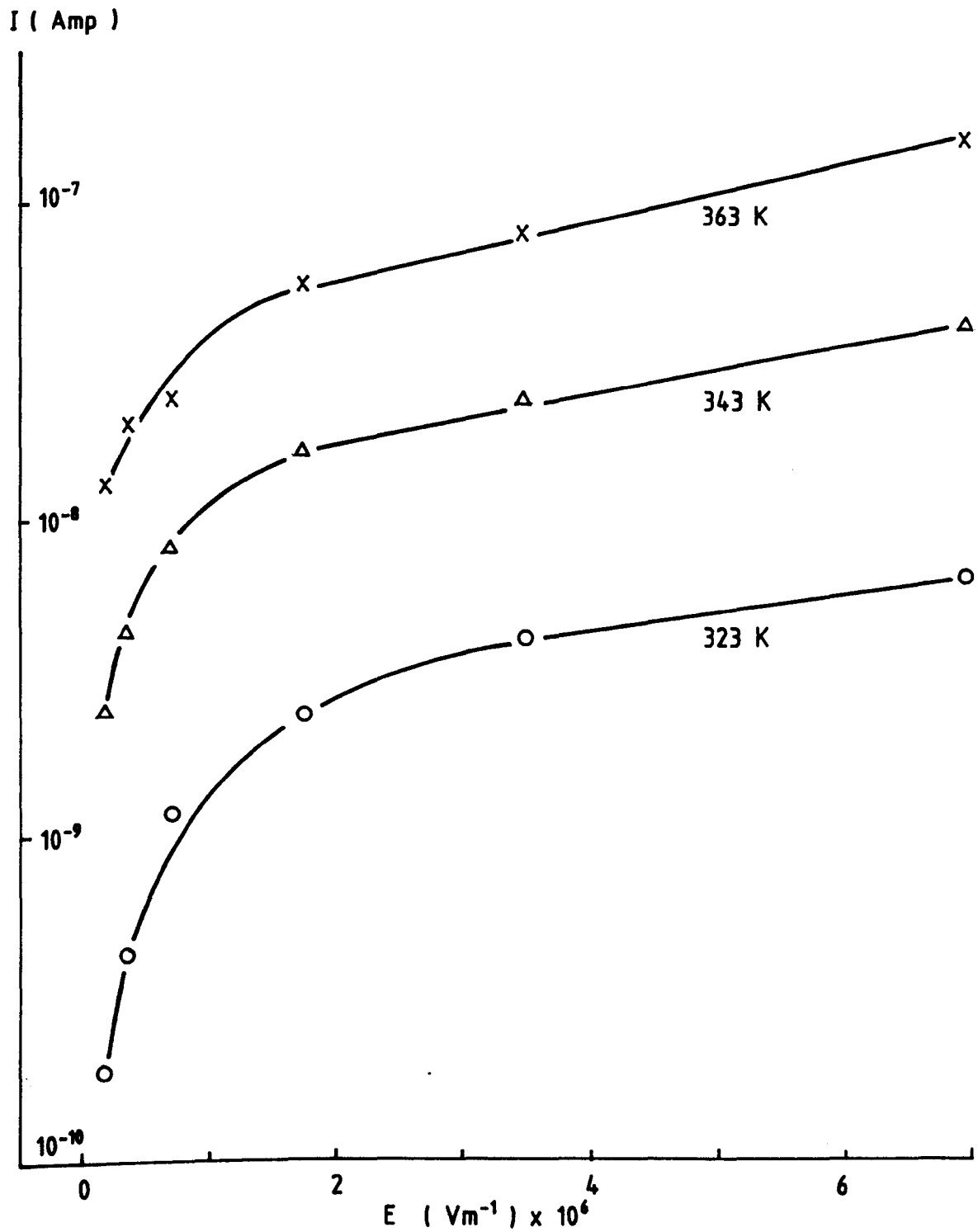

Fig. 4. 67. Ionic conduction plot in PZT5/VDF-TrFE (50/50 Vol.%)

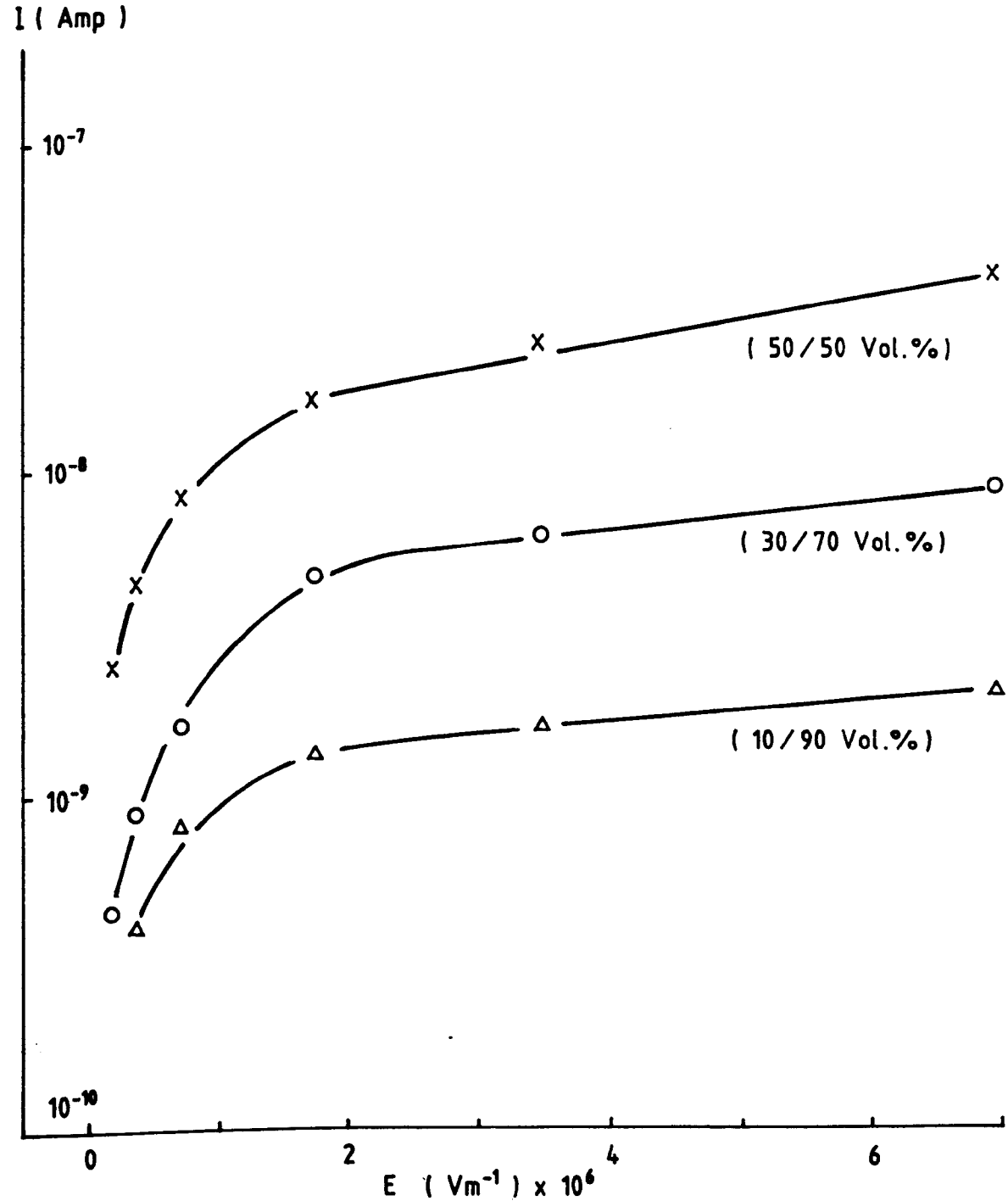

Fig. 4. 68. Ionic conduction plots in different compositions of PZT5/VDF-TrFE at 343 K.

70 Å and 105 Å for the (10/90 Vol.%), (30/70 Vol.%) and (50/50 Vol.%) compositions respectively. Although more data (particularly at high fields) is required for a detailed analysis, the present results may indicate that the addition of more PZT phase in the composite seems to increase the value of the jump distance.

The values of the jump distance obtained for PZT5/VDF-TrFE composites appear to be smaller than that for PIEZEL composite. It may be noted that the current at 10^4 sec used for ionic conduction plot in PZT5/VDF-TrFE composite is not a steady-state current and hence it may not be appropriate for the calculation of the d-values. For the purpose of comparison, the value of the jump distance, calculated for PIEZEL by using the current at 10^4 sec, was found to be 280 Å at 343K. This value is still higher than that of PZT5/VDF-TrFE(50/50 Vol.%) composite, i.e. 105 Å (at 343K). The difference may be due to the different bulk properties of the composites, which may arise from different phase components used in the fabrication or different procedures of sample preparation and further work is needed to clarify this. Ikezaki et al [86] suggested that the difference in the values of the jump distance obtained for polypropylene may be explained partly by the differences in the thermal history that the material received.

It appears from the present results that the increase of ceramic volume fraction would bring the properties of the composites closer to that of ceramic phase by the increase of the ionic conductivity of the material.

CHAPTER 5

DIELECTRIC PROPERTIES IN CERAMIC/POLYMER COMPOSITES

5.1. Introduction

The behaviour of a solid dielectric under a static electric field has been given in the previous chapter, from which some polarization mechanisms may be observed in its characteristics, depending upon the nature of the dielectric. In ionic solids, the electric field causes the displacement of ions from an equilibrium position which may effectively be seen as a fictitious dipole orientation. In molecular solids containing a permanent dipole moment, the dielectric polarizes in an external field by orientation of these dipole moment. The tendency to orientate in an electric field is influenced by thermal motion. It is a relatively slow process in comparison to electronic transitions or molecular vibrations. Furthermore, due to structural constraint, dipole orientation is not a continuous process; it is more in the nature of a

slight adjustment towards a maximum permissible orientation. Thus, sufficient time has to be allowed after the application of an electric field for the orientation to attain equilibrium with maximum polarization, and highest observable dielectric permittivity. On the other hand, if the polarization is measured immediately after field application, the dipole orientation may not have enough time to take place, resulting in a very low permittivity of the dielectric, due only to distortional effects (electronic or atomic displacement) . In the region between these time scale, a dispersion of dielectric permittivity may be shown in the dielectric spectral characteristics.

The above method of measuring the dielectric properties of a material (direct-current method) is perhaps the simplest way to study the polarization mechanism proces. Polarization or depolarization process with time (sometime referred to as dielectric relaxation) may thus be obtained over a wide range of frequencies (depending on the duration of the field application and the rise time of the step voltage). An alternative way of obtaining the information on the dielectric polarization is by the use of an alternating electric field method which forms the subject of the present chapter. This method is usually subdivided according to the frequency range used. The frequency range between 10^{-2} to 10^{6} Hz is the most convenient frequency range, where bridge methods may be used[1]. In this method the impedance of the sample capacitor is balanced against a known combination of discrete resistances, capacitances or inductances. The most versatile

form for these measurements is the use of Schering bridge with which it is possible to make very accurate measurements over the frequency range 10 to 10^5 Hz (the audio-frequency range). The present work reports the dielectric properties in ceramic/polymer composites in the region of this frequency range. In the beginning of the chapter, some theories related to the present work will be given. Some results on dielectric properties of single phase ceramic and polymer will also be given which may be used in analysing the dielectric properties of ceramic/polymer composites.

5.2. Related Theory and Some Dielectric Properties

The dielectric displacement D of a dielectric system subjected to a static electric field E is given by Eq.(4.7). For an alternating field $E=E_o \exp(iwt)$ (amplitude E_o, angular frequency w), the electric displacement will have a phase lag ($-\delta$), which can be mathematically expressed as :

$$D = D_o \exp [\, i(wt - \delta) \,] \qquad (5.1)$$

where the phase ($-\delta$) means that the electric field across the dielectric capacitor takes time to reach the equilibrium value, due to the polarization process. Eq.(5.1) can be written as :

$$D = D_o \text{ Cos } wt \text{ Cos } \delta + D_o \text{ Sin } wt \text{ Sin } \delta$$

$$- i(D_o \text{ Sin } \delta \text{ Cos } wt - D_o \text{ Sin } wt \text{ Cos } \delta) \qquad (5.2)$$

By defining the complex dielectric permittivity thus :

$$\varepsilon^* = \varepsilon' - i\varepsilon'' \quad , \qquad (5.3)$$

Eq.(4.7) can be written as :

$$D = \varepsilon_o(\varepsilon' - i\varepsilon'') E \qquad (5.4)$$

Substituting the expression for E and through usual mathematical manipulation, Eq.(5.4) becomes :

$$D = \varepsilon_o \varepsilon' E_o \text{ Cos } wt + \varepsilon_o \varepsilon'' E_o \text{ Sin } wt$$
$$- i(\varepsilon_o \varepsilon'' E_o \text{ Cos } wt - \varepsilon_o \varepsilon' E_o \text{ Sin } wt) \qquad (5.5)$$

Comparing Eq.(5.2) and (5.5),

$$\varepsilon' = \frac{D_o \text{ Cos } \delta}{\varepsilon_o E_o} \quad \text{and} \quad \varepsilon'' = \frac{D_o \text{ Sin } \delta}{\varepsilon_o E_o} \qquad (5.6)$$

giving the relation :

$$\tan \delta = \varepsilon''/\varepsilon' \qquad (5.7)$$

where tan δ is defined as dielectric loss tangent or dissipation factor, ε'' the dielectric loss and ε' the real part of complex permittivity. ε' and ε'' are experimentally observable quantities which may be used to characterize the dielectric dispersion over a range of frequencies.

Based on the basic theory of dielectric relaxation behaviour, Debye[2] derived the frequency dependence of the complex dielectric permittivity of dipolar system , which is given by Eq.(4.21). By equating the real and imaginary parts of both sides of Eqs.(4.21) and (5.3), thus :

$$\varepsilon' = \varepsilon_\infty + (\varepsilon_s - \varepsilon_\infty)/(1 + w^2 \tau^2) \qquad (5.8)$$

and

$$\varepsilon'' = (\varepsilon_s - \varepsilon_\infty) w\tau \ /(1 + w^2 \tau^2) \qquad (5.9)$$

where ε_s , ε_∞ and τ have been previously defined (section 4.2.2). The variation of ε' and ε'' against log frequency of the applied field for the Debye type dispersion behaviour is shown in Fig.5.1. From an inspection of Eq.(5.9), the maximum loss value occurs when $w\tau = 1$ which gives the maximum values of $\varepsilon''_{max} = (\varepsilon_s - \varepsilon_\infty)/2$. This value falls to half its maximum value when :

$$\frac{1}{2} \frac{(\varepsilon_s - \varepsilon_\infty)}{2} = \frac{(\varepsilon_s - \varepsilon_\infty) w\tau}{1 + w^2 \tau^2}$$

i.e. $w\tau =$ 0.27 or 3.73 , giving $\triangle \log (w\tau) = 1.14$ decades,

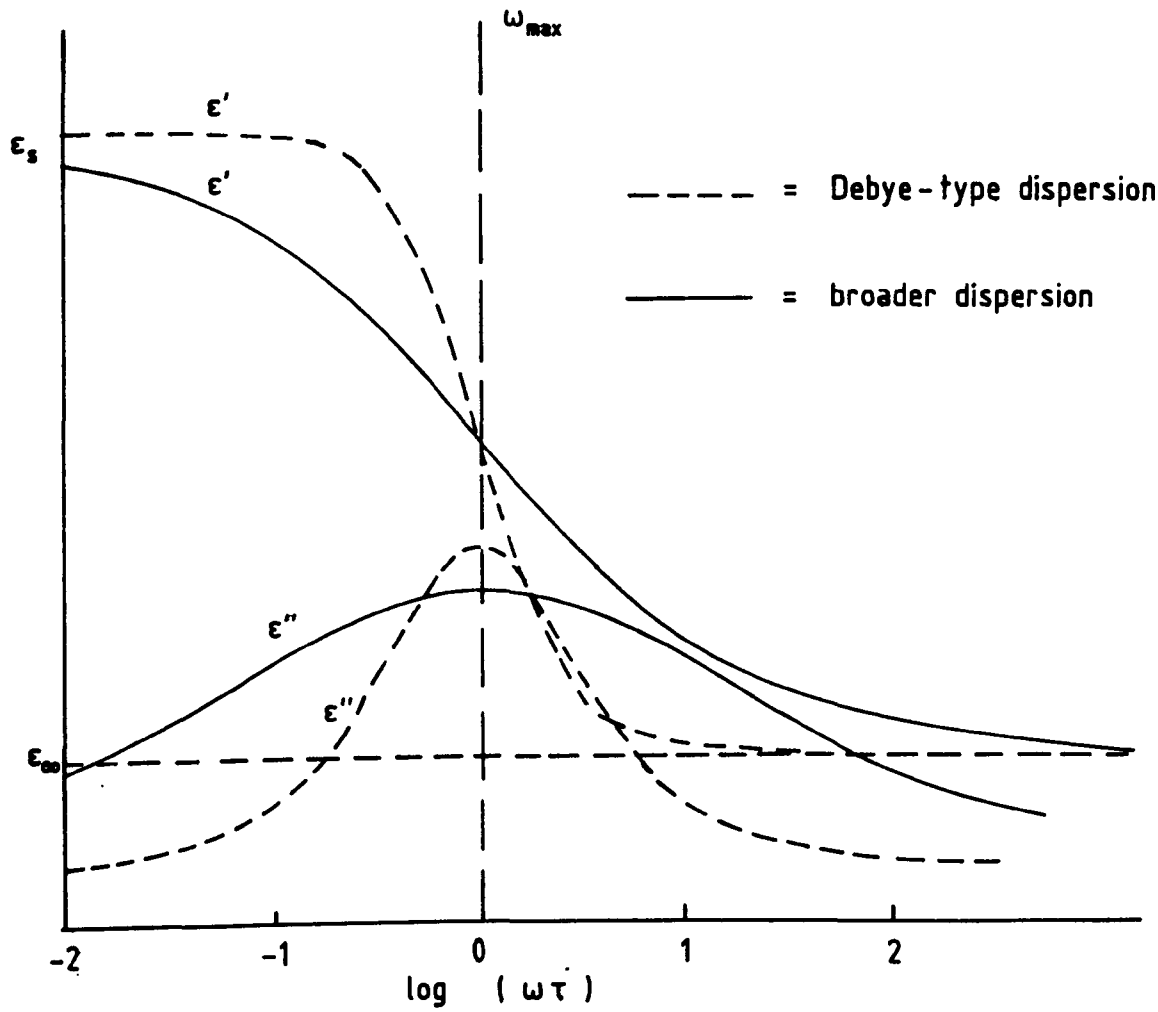

Fig. 5.1. Variation of ε' and ε'' against frequency for Debye-type dispersion behaviour and for broader dispersion behaviour.

which is the half-height width of the loss peak .

Debye's equations (Eq.(5.8) and (5.9)) were deduced for a process described by a single relaxation time. Relaxations observed in solid polymers, however, show broader dispersion curves and lower loss maxima than those predicted by the Debye model [1] (see Fig. 5.1), which means that the single relaxation time approximation is not valid. Several empirical corrections have been introduced in the single relaxation time equations in order to fit the experimentally observed dispersion curves. Such corrections have been introduced by Cole and Cole [3], Fuoss and Kirkwood [4] and Davidson and Cole [5]. The correction suggested by Cole and Cole [3] is given by Eq.(4.22). Davidson and Cole [5] improved the fit with experimental data by using a slightly different semi-empirical equation :

$$\varepsilon^* = \varepsilon_\infty + (\varepsilon_s - \varepsilon_\infty)/(1 + iw\tau)^b \qquad (5.10)$$

where b is a parameter, $0 < b < 1$.

The dependence of ε'' on ε' may be used to test the various modifications of Debye model in fitting the experimental data. By eliminating the parameter $w\tau$ in Eq.(5.8) and (5.9), an equation of a circle is obtained as :

$$\left(\varepsilon' - \frac{\varepsilon_s + \varepsilon_\infty}{2} \right)^2 + \varepsilon''^2 = \left(\frac{\varepsilon_s - \varepsilon_\infty}{2} \right)^2 \qquad (5.11)$$

which has a centre O $[(\varepsilon_s + \varepsilon_\infty)/2 , 0]$ and radius

$(\varepsilon_s - \varepsilon_\infty)/2$. It is usual to represent a plot of ε'' against ε' of Eq.(5.11) in a semicircle lying above the ε'-axis, as shown in Fig.5.2. Many experimental results on polar liquids[6] have shown an excellent agreement with this theoretical plot. However, as mentioned earlier, many other materials, particularly long-chain molecules and solid polymers show a broader dispersion curve, resulting in that the $\varepsilon'' - \varepsilon'$ curve falls inside the Debye semicircle (Fig.5.2). In this case, the centre of the semicircle is depressed below the ε'-axis (point 0′ in Fig.5.2)[3]. It may corresponds to a superposition of a group of Debye-like relaxation processes having a range of relaxation times that are symmetrically distributed about τ . Such a spread of relaxation times may be likely due to the effect of restraining forces along the molecular chain acting to influence the orientation of segmental dipoles attached to the polymer chain.

In some materials, the $\varepsilon'' - \varepsilon'$ curve is no longer symmetrical with respect to the vertical line through the centre. Davidson and Cole [5] have advanced a semi-empirical formula (Eq.5.10) to describe such a behaviour. Fig.5.3 shows a theoretical plot for this type of dispersion behaviour for different values of parameter b. It may be seen that for $b < 1$, Eq.(5.10) corresponds to a skewed distribution of relaxation times about τ , which is found to be very successful in representing the behaviour of materials at low temperatures [6]. Apart from better agreement with experimental data for certain materials, this behaviour

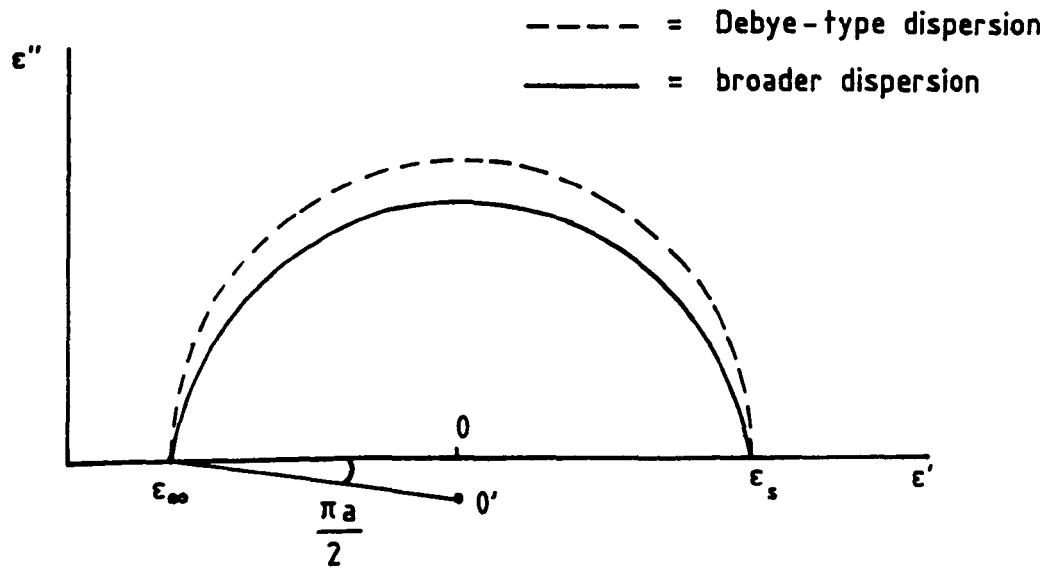

Fig. 5.2. Cole-Cole plot for a Debye-type dispersion and for a broader dispersion behaviours.

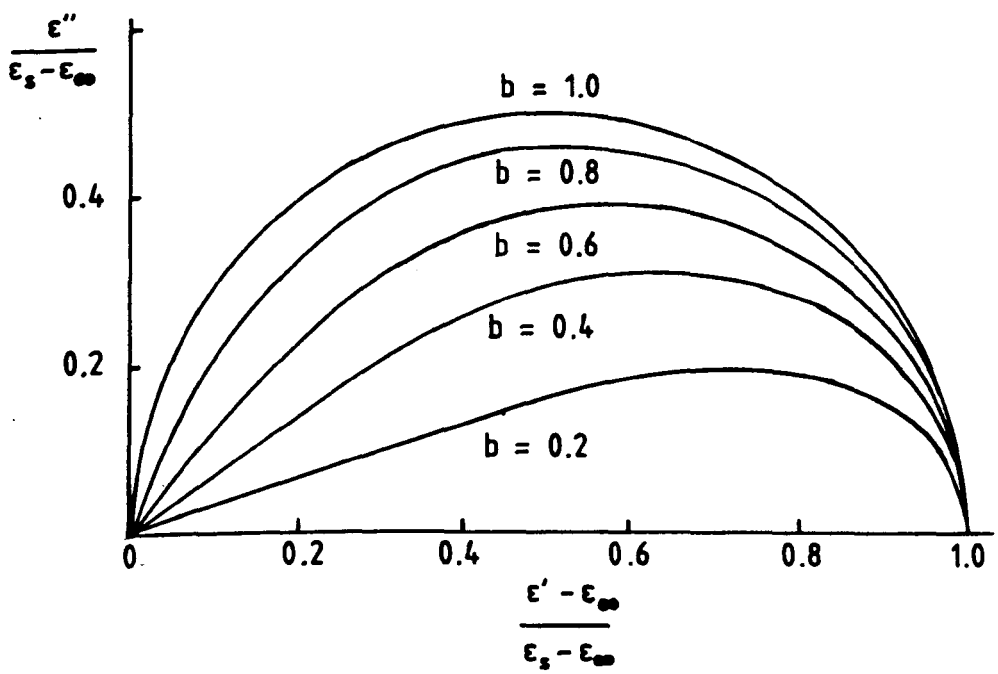

Fig. 5.3. A typical plot of Cole - Davidson dispersion behaviour.

however, may not be easy to interpret.

The plot of ε' vs log w is normally referred to as the dielectric dispersion - spectrum while that of ε'' vs log w is the absorption - spectrum. The most general statement that can be made about dielectric relaxation in linear systems[1] concerns the relationship between the real and imaginary part of the complex dielectric permittivity. The general result (which is one of the Kramers - Kronig relations) is given as [1] :

$$\Delta\varepsilon = \varepsilon_s - \varepsilon_\infty = \frac{2}{\pi} \int_{-\infty}^{+\infty} \varepsilon''(w)\, d(\ln w) \qquad (5.12)$$

where $\Delta\varepsilon$ is the dielectric relaxation strength or the dielectric increment and the RHS term referred to the area under the absorption curve. Eq.(5.12) implies that it is possible to establish the dielectric increment due to the dispersion process with which it is associated, by measuring the dielectric loss alone over a wide range of frequencies. This expression can be verified for dielectrics which show the Debye-type relaxation and those with approximate Debye behaviour (i.e. with peaks of dielectric loss which resemble Debye peaks but with a slightly wider or somewhat different shape) [7] .

5.2.1. Dielectric relaxation process in solid polymers

Polarization of a polymer in an electric field occurs

when units of the polymer chain tend to orient the dipolar groups and srongly polarizable bonds along the field. These redistribution of charges together with the effect of the thermal process determine the dielectric behaviour of polymers. Obviously, the physical structure of polymers (such as the packing of the molecule and the presence of defects) has a significant effect on its dielectric behaviour. These factors may give some understandings of the experimental fact that structural transitions in polymers are generally accompanied by changes in dielectric permittivity.

Dielectric relaxation processes do not involve large-scale structural rearrangement ; only those local motions of some parts of the molecule are changed. Thus it may readily be distinguished from structural transitions which involved a change in the specific volume of the material [8]. Several types of dielectric relaxation processes are usually present in a solid polymeric material, depending on the mobility of a dipole group. The nature and the extent of molecular mobility are controlled by the temperature. A typical characteristic of dielectric permittivity and loss as a function of temperature at a particular constant frequency is shown in Fig.5.4. At the very lowest temperature, close to absolute zero , the polymeric solid posseses very little thermal energy so that all atomic positions are stationary. As the temperature is raised, the thermal energy is acquired and various possible modes of molecular motions are subsequently energised. The different modes however require different amounts of energy to activate them and therefore there exist threshold temperatures

for each mode to be activated. Experimentally, these threshold temperatures can be detected as transitions in a wide variety of physical parameters (e.g. mechanical shear modulus, dielectric permittivity, heat capacity, refractive index). Dielectric relaxation processes are conventinally labelled as α, β, γ etc, beginning at the highest temperature.

In an amorphous polymer, the α- relaxation corresponds to the glass transition (i.e. the occurence of sharp change in temperature dependence of various properties, as defined in chapter 4), occuring at a temperature determined by the molecular structure of the polymer. Thus a bulky side group can decrease the glass transition temperature T_g by preventing the chains from packing together tightly and vice versa. T_g can also be effectively reduced by adding a plasticiser [9]. This relaxation is associated with the micro-Brownian motion of the whole chains and in addition there is at least one low-temperature (β, γ etc) subsidiary relaxation. The assignment of particular mechanisms to the β, γ etc relaxations depend on the nature of the polymer [1,8].

When a polymer posseses weak polar groups, dielectric relaxations may be scarcely observable, although the process of molecular rearrangement still occurs. By adding a few polar groups, the associated dielectric effect may be enhanced. In the presence of some small impurity molecules which may be polar or even ionic, various molecular processes in non-polar polymers may show up as a result of an interaction of the motion of the polymer chains with the displacement of the impurity molecules. For this reason, a

presence of even low concentration of a polar impurity may alter the dielectric characteristic of a non-polar polymer in a particular frequency region.

The interpretation of the relaxation behaviour in semicrystalline polymers can be difficult because of their complex two-phase structure. Various different mechanisms may take place in the amorphous regions, inside the crystals and at the crystalline-amorphous interface. As regards the dielectric loss peak, it may be possible to identify its origin, whether it is due to amorphous or crystalline phase by testing on different crystallinity of the material (note: the process of rapid quenching from the melt in the material preparation will reduce the crystallinity) [1].

The dielectric relaxation behaviour of polyethylene (PE) has probably been more widely studied than that of any other semi-crystalline polymer. Fig.5.5 shows the behaviour of dielectric loss tangent tan δ (as defined by Eq.5.7) in three types of PE at a frequency of 100 kHz [8]. PE is composed of hydrocarbon chains containing hundreds or thousands of carbon atoms ; the molecular formula is $(CH_2)_n$ where n is a large number but without a unique value (the chain length of the molecule depends on the methods of synthesis of the polymer). Low-density polyethylene (LDPE) has the side branches R which are mainly methyl group (CH_3-) or ethyl group ($-C_2H_5$), thus having chemical formula as :

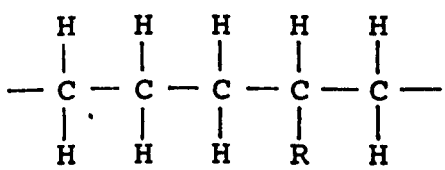

The other two forms of PE (high density polyethylene (HDPE) and linear polyethylene (LPE)) have the same basic chemical formula as above but with different number of R. The properties of these three forms of PE are shown as in Table 5.1 :

Table 5.1. Properties of PE in various forms

Types of polymer	LDPE	HDPE	LPE
No. of methyl group per 1000 carbon atom	21.5	3	< 1
No. of ethyl group per 1000 carbon atom	14.4	1	< 1
Density (gm cm^{-3})	0.91-0.92	0.93-0.94	0.96
Crystallinity (%)	60	87	93
Melting temperature(K)	378-393	393-413	413

It may be observed from Fig.5.5 that the α_c, α_a (or β) and τ peaks appear in the dielectric spectra of all forms of PE. The position and intensity of the α_c-peak is dependent on the crystallinity and crystallite size of the polymers; thus it is thought to be associated with the motion at the crystallite surfaces or the motion within the crystalline regions.

The lower temperature peak (α_a), which is often referred to as the β-peak is very pronounced in LDPE, is less intense in HDPE and hardly observable in LPE. The weak

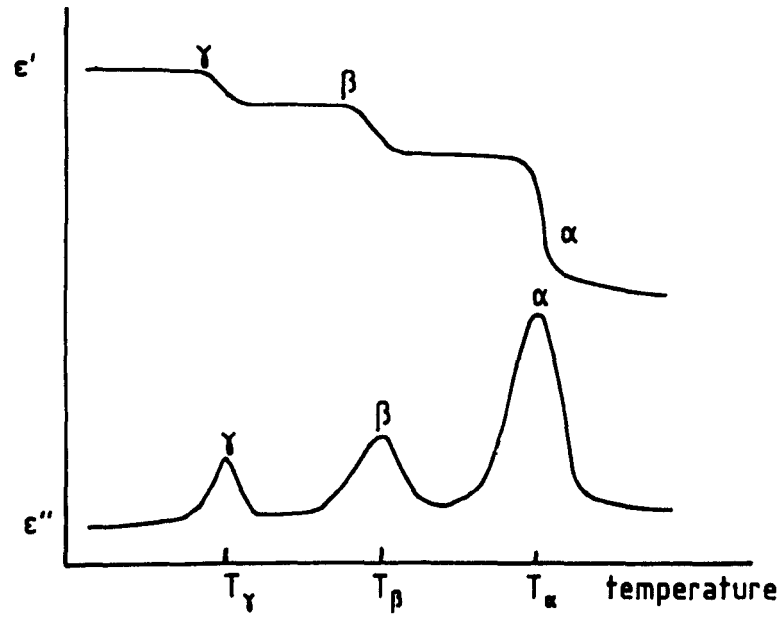

Fig. 5.4. A schematic typical behaviour of dielectric permittivity and dielectric loss in polymer.

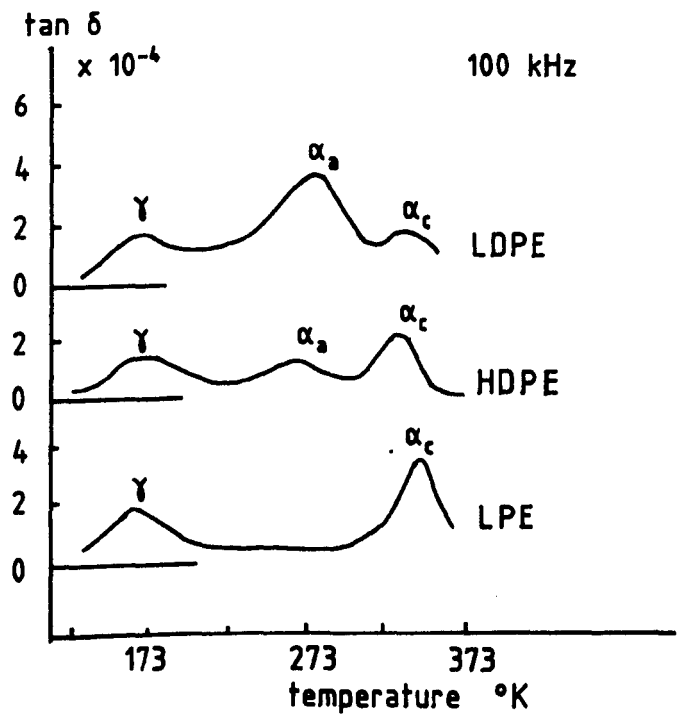

Fig. 5.5. Dielectric relaxations in low density (LDPE) , high density (HDPE) and linear (LPE) polyethylene.

appearance of the α_a-peak with the less number of branching group has been taken as an indication that it is associated with the motion of the side branches in the amorphous phase. The γ-peak at about 153 K is found in all three polymers. The assignment to this particular relaxation is quite uncertain. Hedvig[8] suggests that it is attributed to a crankshaft-type local motion in the main chain while Matsui et al [10] proposed that it is due to a dislocation-migration mechanism. On the other hand, Young [11] had attributed the relaxation to be associated with the amorphous phase and had been tentatively assigned to a glass transition in the amorphous region. Thus, in general, the assignment of the peaks in semi-crystalline polymers to a particular mechanism is rather difficult and often a matter for some debates.

It should also be noted that the dielectric loss peaks are found to be enhanced in an oxidized non-polar polymers such as polyethylene and polypropylene. The oxidation is thought to occur at the structural defects in which the oxidized regions may contain polar carbonyl (-CO) group [8]. By comparing the dielectric data with infrared spectroscopic measurements, it is concluded that the dielectric properties of polyethylene are mainly determined by the carbonyl groups (formed by oxidation) which are statistically distributed in the polymer chain and hence contribute to the three main relaxation peaks shown in the dielectric spectra [8]. The oxidation mechanism leading to the effective change in the dielectric properties of polymers is indeed a very complex process which is not all fully understood [8].

5.2.2. Dielectric relaxation in PVDF

Polyvinylidene fluoride(PVDF) is a polar semi-crystalline polymer with a monomer unit $-CH_2CF_2-$ in which polar side groups C-F are rigidly attached to the main chain. Thus C-F bond can not move independently but it rather moves along with the main chain. It is therefore to be expected that the dielectric properties of PVDF are sensitive to the structure of the molecular chain. It has been mentioned in chapter 2 that PVDF may exist in at least two stable crystal structures, i.e. the Form II (helix structure) and the Form I (planar zigzag structure). The Form II may be converted to the Form I following thermal and mechanical treatment. The dielectric relaxation behaviour of Form II PVDF have been studied extensively [12-14], from which mechanism related to the relaxation process may be investigated.

A typical α_c-relaxation occuring in Form II PVDF (prepared by compression molding, thickness 1 mm) is shown in Fig.5.6 [13]. It has also been observed[13] that the magnitude of ε''_{max} and the location of T_{max} are dependent on the method of polymerization process and the preparation of the material (see Table 5.2 and Fig.5.7). It is noted that sample S1 and sample S2 are from the same source while sample S3 is from different source. The preparation and the properties of these samples are listed as in Table 5.2. The results in Fig. 5.7 show that the magnitude of ε''_{max} is increased and T_{max} shifted to higher temperature with increasing density. A plot

Table 5.2. Properties of various Form II PVDF

Samples	Preparation	Film thickness (mm)	Melting point(K)	Density at 298 K (g/cc)
S1	compressed & molded	1	435	1.766
S2	casting & quenched to 77 K after heated at 428 K for 16 hours	0.4	434	1.778
S3		0.4	457	1.791

of $\Delta\varepsilon = \varepsilon_s - \varepsilon_\infty$ versus density is approximately linear with $\Delta\varepsilon = 0$ at density 1.74 g/cc (corresponding to amorphous PVDF) [13]. Other evidence shows that ε''_{max} is increased and T_{max} shifted to higher temperature with increasing crystallinity of the sample [12]. These results suggest that the α_c-relaxation is related to molecular motions in the crystalline regions. It is important to note that the magnitude of α_c-relaxation decreases upon uniaxial drawing. The result of Peterlin and Elwell [15] also showed that α_c-relaxation was markedly reduced by rolling. The decrease of α_c-relaxation in the drawn and rolled samples was thought to be related to the anisotropic structure in the crystalline regions as a result of drawing or rolling.

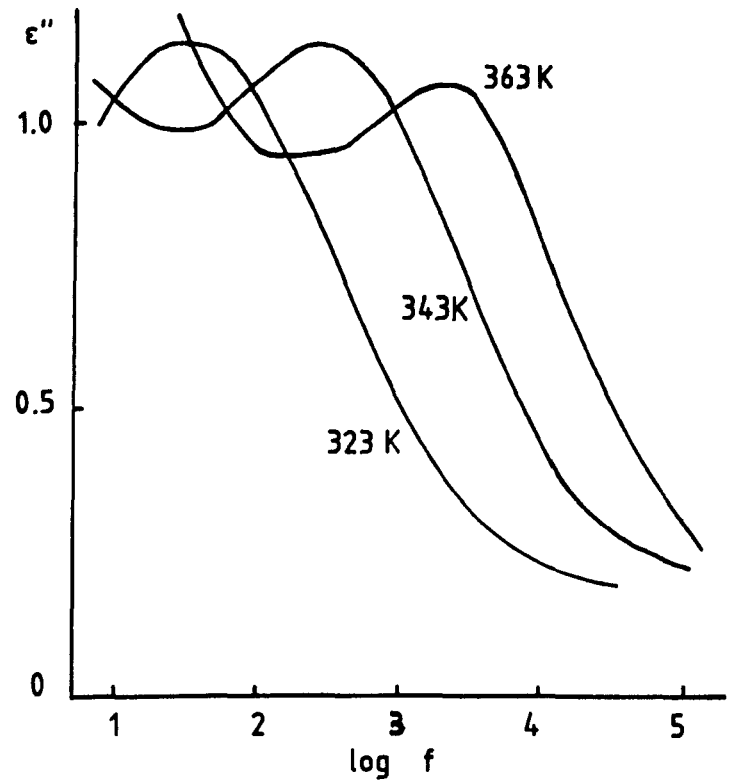

Fig. 5.6. Typical α_c - relaxation in Form II PVDF.

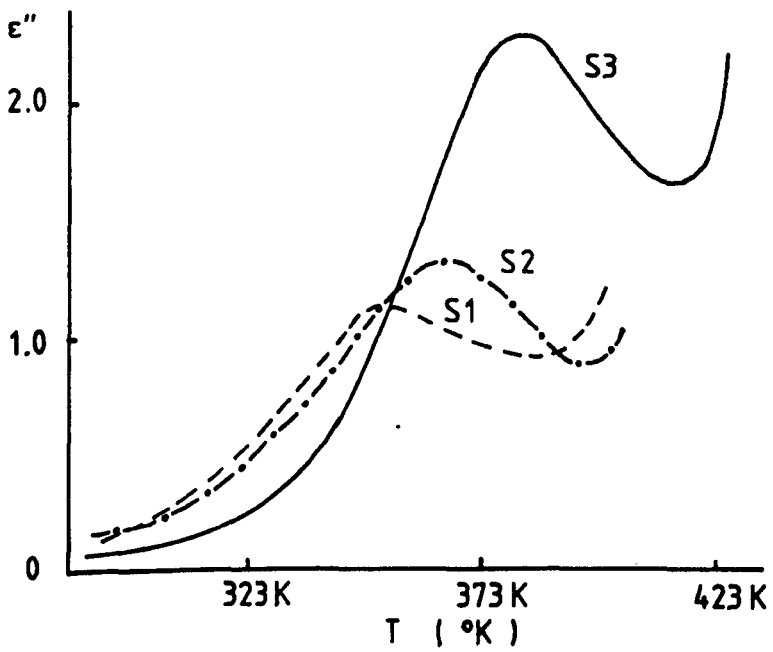

Fig. 5.7. α_c - relaxation in various samples of Form II PVDF at 1 kHz.

A lower temperature relaxation in Form II PVDF (the same sample as for α_c-relaxation) is shown in Fig.5.8 [13]. In this relaxation, it is noted that the temperature T_{max} at which the dielectric loss maximum occured is independent of the density. As regard the magnitude of ε''_{max}, in general, it is found to decrease with increasing density. Sasabe et al [12] have shown that ε''_{max} decreases with increase of crystallinity of the samples. These results have led to the conclusion that α_a-relaxation is attributable to micro-Brownian motion of molecular chain segments in the amorphous regions. In the uniaxial drawn samples, ε''_{max} of α_a-relaxation is observed to increse while T_{max} shifted slightly to higher temperature [13]. These characteristics presumably arise from molecular orientation along the direction of drawing. The increase of ε''_{max} may be due to the increase of the dipole polarization perpendicular to the direction of drawing and the shift of T_{max} may be interpreted as due to increase of internal friction in the molecular chains [13].

The third relaxation process (designated as β-relaxation) is located in the lowest temperature (Fig.5.9)[12], which was obtained on commercial grade Form II PVDF. This β-absorption is very small and as temperature increases, this absorption begins to overlap the α_a-absorption and hence becomes indistinguishable from it. The activation energy associated with this β-relaxation is relatively small as compared to α_c- and α_a-relaxations. It has also been observed [13] that the magnitude of the relaxation is inversely proportional to the degree of crystallinity. Based

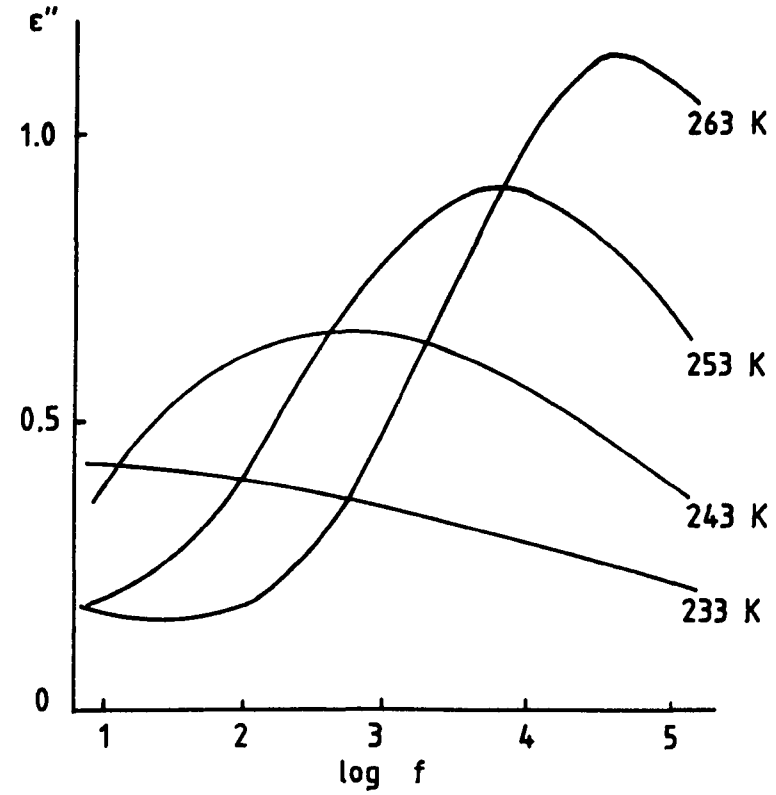

Fig. 5.8. α_a - relaxation in Form II PVDF.

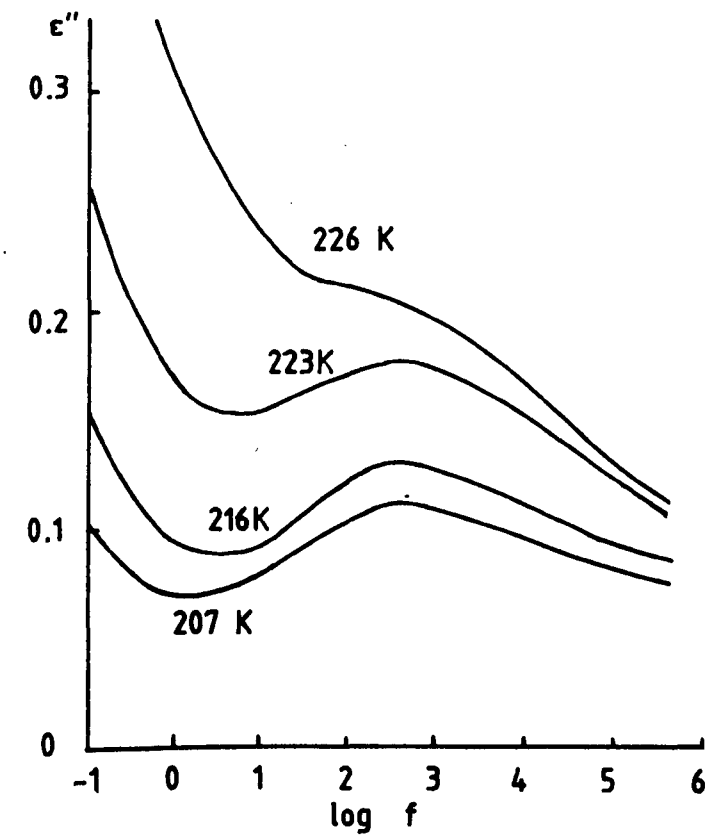

Fig. 5.9. β - relaxation in Form II PVDF.

on these results, β-relaxation has been attributed to local molecular motion in the amorphous regions.

The temperature dependence of dielectric loss ε'' in Form II PVDF [13] (sample prepared by casting from a diisobutyl ketone - dimethyl phthlate, thickness 0.4 mm) at different frequencies is shown in Fig.5.10 and 5.11. It may be observed that three dielectric relaxations, α_c, α_a and β occur at about 323 K, 238 K and 178 K respectively at 10 Hz. Such representation may be used to identify various relaxations in different temperature regimes at a particular frequency. Due to a weak β-relaxation, the peak associated with it is hardly observable at frequencies of 1 kHz and 100 kHz. A rapid increase of dielectric loss at high temperatures and low frequency is thought to be due to ionic conduction process [14,16].

Another relaxation in PVDF which occur in the frequency range 10^{-5} to 10^{-2} Hz at temperature from 333 K to 373 K has been observed by Das-Gupta and Doughty [17] and Das-Gupta et al [18]. This low frequency relaxation (α_i-relaxation) has been predicted by Sasabe et al [12] and it was assigned as due to interfacial polarization at crystalline-amorphous boundaries or to the rubbery flow of polymer chains. Similar low frequency dispersions have also been observed in polymethyl methacrylate [19] and PET [20], which have been attributed to interfacial or electrode polarization. However, since no electrode dependence of absorption currents has been observed in PVDF [21] and there is evidence of space charges effect [18,21], it has been suggested that the

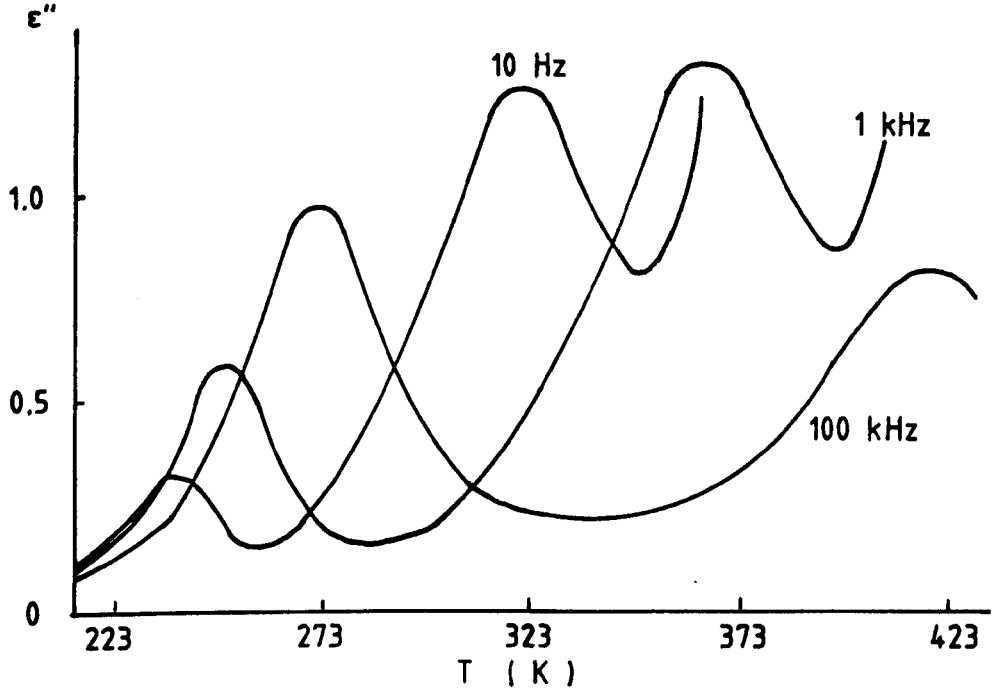

Fig. 5.10. The dependence of dielectric loss on temperature (223 to 423 K) in Form II PVDF at 3 different frequencies.

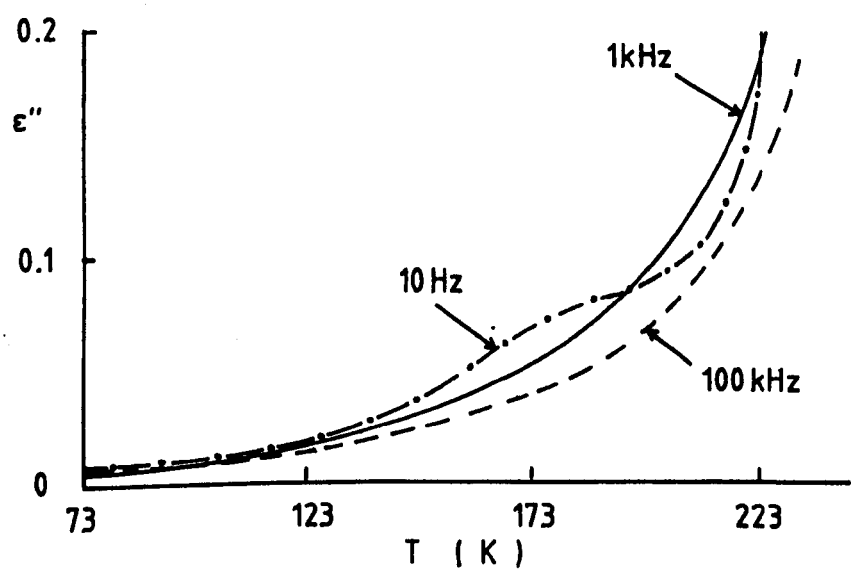

Fig. 5.11. The dependence of dielectric loss on temperature (73 to 223 K) in Form II PVDF at 3 different frequencies.

α_i-relaxation may be due to the motions of space charges trapped at the boundaries between the crystalline and amorphous regions.

5.2.3. Dielectric dispersion in ferroelectric ceramics

The behaviour of dielectric properties in ferroelectric ceramics may be very complex. This is due to the fact that it is polycrystalline in nature and that it can be prepared in different chemical compositions. In addition, the pre-treatment that the material received also affect the measured properties. Accordingly, it is to be expected that the material properties would be different from one to the other, prepared in different manners.

Ceramic $Pb(Zr_{1-x}Ti_x)O_3$ solid solutions have been shown to exhibit the striking dielectric and piezoelectric properties at concentrations near the morphotropic tetragonal-rhombohedral phase boundary, e.g. near x = 0.47 [22]. It is believed that the proximity to such a phase boundary not only fascilitates reorientation of domain walls during poling process but also increases the mobility of domain walls which enhances the dielectric permittivity and the piezoelectric effects. Fig.5.12 shows the temperature dependence of the real part of complex dielectric permittivity in a typical phase boundary composition of $Pb(Zr_{0.53}Ti_{0.47})O_3$ [22]. Kersten and Schmidt [23] have studied the frequency dependence of the dielectric properties in solid solutions of $Pb(Zr_{1-x}Ti_x)O_3$

with x=0.4, 0.48 and 0.6. Typical results of the frequency dependence of the dielectric loss at room temperature in those ceramics is shown in Fig.5.13. It may be observed that there is one relaxation peak at about 700 MHz, the position of which is independent of the Ti:Zr ratio. The relaxation strength, as expected, is greater for Ti concentration near the morphotropic phase. Results at different temperatures showed that the relaxation strength increases with inceasing temperature, whereas the relaxation peak frequency is nearly temperature independent [23]. The authors [23] attribute the observed properties as due to the many-body universal response as described by Jonscher, Dissado and Hill [24,25].

A great deal of results concerning the properties of various modified PZT have been accumulated [22] and thus there is a wide spectrum of compositional properties which might be used for different purposes. For example, with Strontium (Sr^{2+}) substitute for Pb^{2+}, the Curie point is lowered about 9.5 degree for every atom % added, which in turn raises the dielectric permittivity at room temperature [22]. Gerson et al [26] studied the dielectric properties in Strontium modified PZT, i.e. $Pb_{0.94}Sr_{0.53}Zr_{0.53}Ti_{0.47}O_3$ from which a very broad dielectric relaxation may be observed at around 2 GHz (see Fig.5.14). The relaxation was attributed to the domain and domain-wall motions, which are simultaneously present in any ferroelectric ceramics.

The low frequency dielectric properties in niobium modified PZT can be seen from Fig.5.15 [27]. It may be observed that there is little variation with frequency at

301 K and 373 K. At 413 K, however, the dissipation factor (tan δ) and permittivity both increase with decreasing frequency. These changes of dielectric permittivity and loss are less pronounced as compared to that of unmodified PZT (which has a lower resistivity) [27]. It thus seems more likely that the change in dielectric permittivity was due to interfacial polarization in the bulk with the aid of high electrical conductivity of the ceramic.

As in the case of PZT ceramics, the dielectric properties in $BaTiO_3$ ceramics are affected by its chemical composition as well as its physical structure [22]. Typical temperature dependence of dissipation factor (tan δ) in $BaTiO_3$ ceramic is shown in Fig.5.16 [28]. The high loses in region I have been associated with domain wall movements. The loss peaks at about 278 K and 393 K (for low field) appear to occur at the structural phase transition. Above the Curie temperature (T_C), the losses becomes independent of field. In region II and just above T_C the losses decrease steeply and do not depend on either the frequency or field. As the temperature is raised further, the losses increased again and becomes frequency-dependent but no field dependence is observed (region III).

The decrease of the losses just above T_C seems to be related with the diappearance of the ferroelectricity and experimental evidence seems to indicate that the disappearing domain walls are responsible for the observed effect. The residual losses in region II have been attributed to microstructural effects (grain boundaries, pores, second

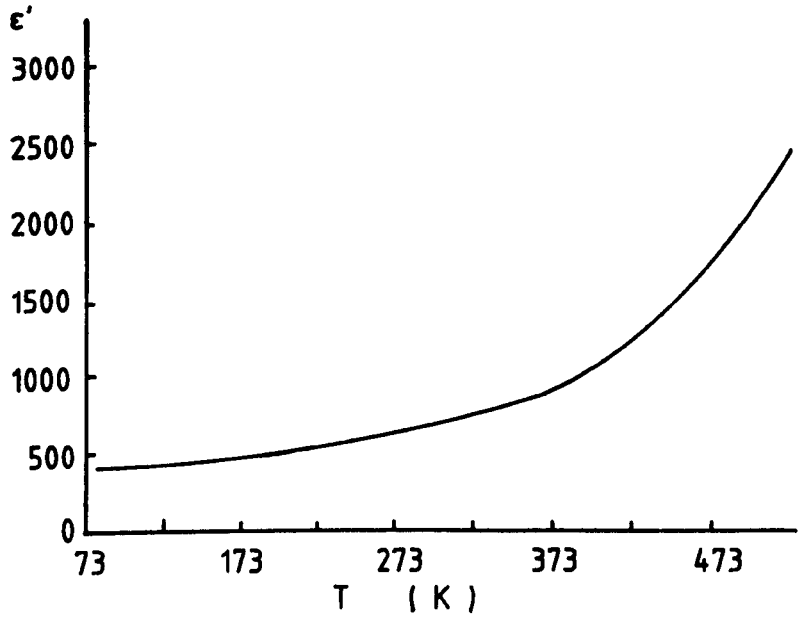

Fig. 5.12. Relative dielectric permittivity versus temperature in $Pb(Zr_{0.53}Ti_{0.47})O_3$.

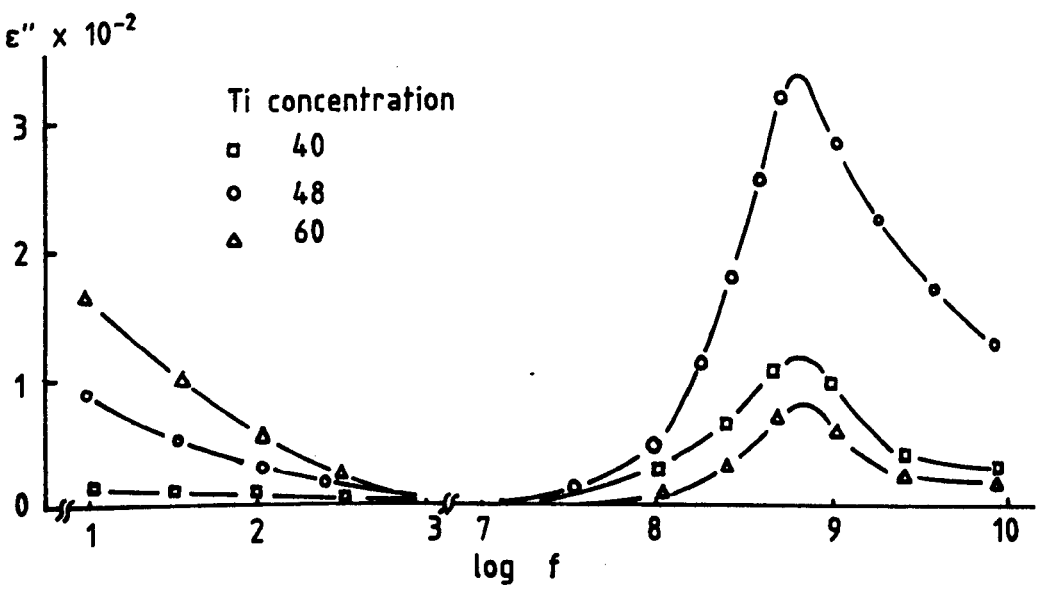

Fig. 5.13. Frequency dependence of dielectric loss in PZT ceramics with different Ti concentration at room temperature.

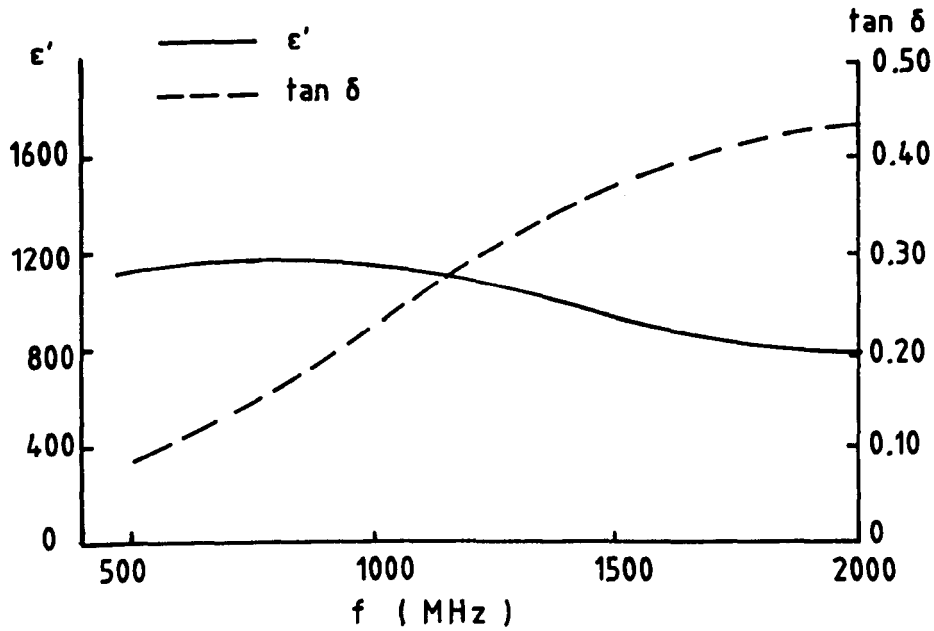

Fig. 5.14. The behaviour of dielectric properties in $Pb_{0.94}\ Sr_{0.06}\ Zr_{0.53}\ Ti_{0.47}\ O_3$ at room temperature.

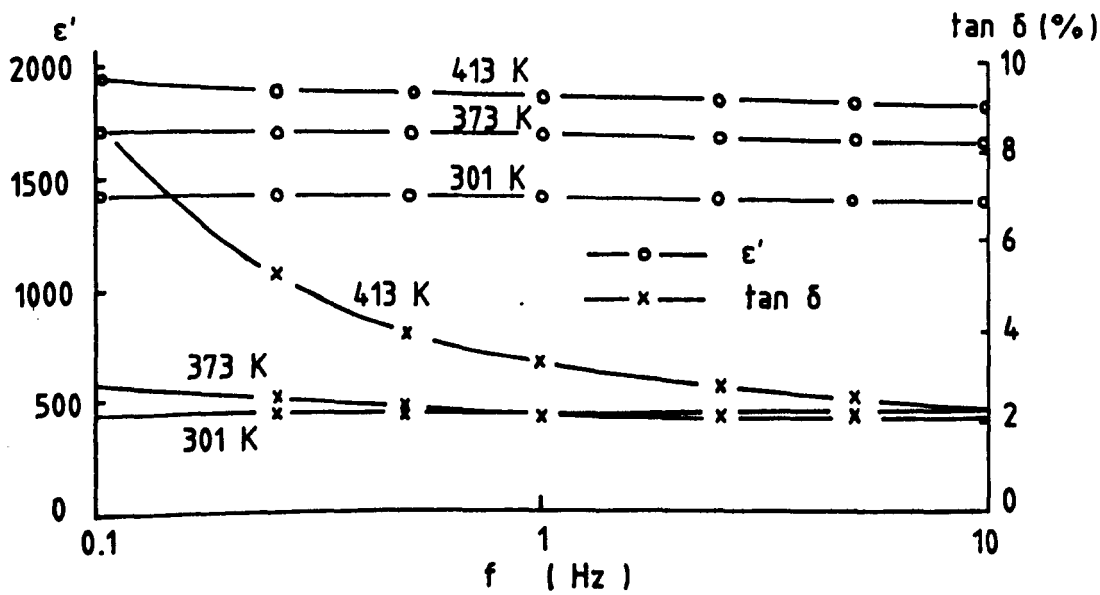

Fig. 5.15. The behaviour of dielectric properties in niobium modified PZT.

phases) and lattice effects [29]. The increase of the losses in region III is due to the free carrier conductivity initiated by temperature. For this reason, ferroelectric ceramics of higher resistivity (e.g. PZT) wil have region III shifted to higher temperature.

The practical ferroelectric ceramics have always been incorporated with dopant ions. The dopant ions that reduced the losses are characterized by a lower valence state than that of the substituted host lattice ions (e.g. A^{3+} at B^{4+} sites). These ions consequently act as an acceptor with the charge deficiency being compensated by vacancies in the oxygen lattice[29,30]. On the other hand, for dopant ions with a higher valence state as compared to the substituted ions (e.g. A^{3+} at B^{2+} sites, A^{5+} at B^{4+} sites, etc), the losses tend to increase. These ions therefore have donor properties, with the surplus charges being compensated by vacant sites in the cation lattice [29,31]. It appears from hysteresis measurements [32] that donor ions increase the domain wall mobility and thus the increase of losses may be related to that mobility. Conversely, the acceptor dopant ions fix the domain wall positions and thus reduce the domain wall losses. One possible explanation for the domain wall stabilization is that the acceptor dopant ions form a dipole-like with oxygen vacancies which orient themselves within each domain by the spontaneous polarization (P_s) and thus stabilize the existing direction of P_s and hence the entire domain wall configuration [29].

The dependence of dielectric permittivity on grain sizes

in $BaTiO_3$ ceramic may be seen from Fig.5.17[33]. It may be observed that the phase transition temperatures and permittivity are both vary with grain sizes. Taking the value of isothermal permittivity at 343 K, the dielectric permittivity is observed to reach maximum at about 0.4 μm and then decrease with further increase in grain size. A model has been proposed to account for this behaviour and a good agreement with the experimentally observed values has been obtained [33].

5.2.4. Related dielectric theory in ceramic/polymer composite

It is always of interest to determined the effective dielectric permittivity of heterogeneous material. Composites of ceramic/polymer in which the ceramic particles are dispersed in the polymer matrix, may be considered to be heterogenous. By assuming some special model of a heterogenous system, the effective dielectric permittivity may be derived in terms of the volume fraction and the dielectric permittivity of the constituent phases [34,35]. Brown [36] however has concluded that such information of volume fractions and dielctric permittivity of the constituent phases is not sufficient and that the knowledge of the statistics of the phase distribution is required.

The simplest heterogenous system is a system where two dielectrics are placed next to each other with a planar interface, either in series or in parallel arrangement. The series arrangement gives the lower bound while that of

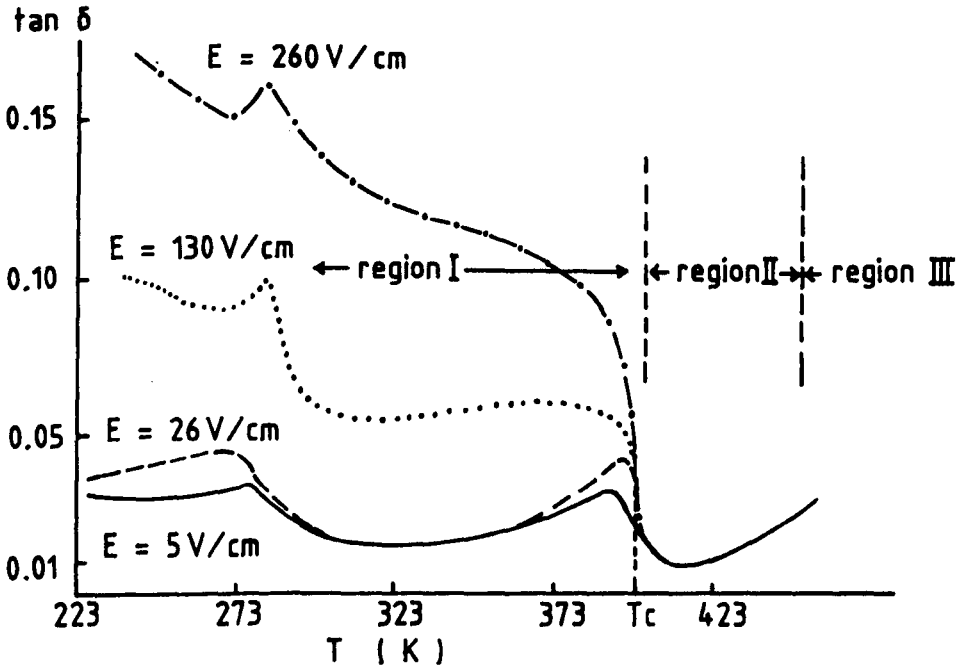

Fig. 5.16. Temperature dependence of dissipation factor (loss tangent) in $BaTiO_3$ for several ac fields at 1 kHz.

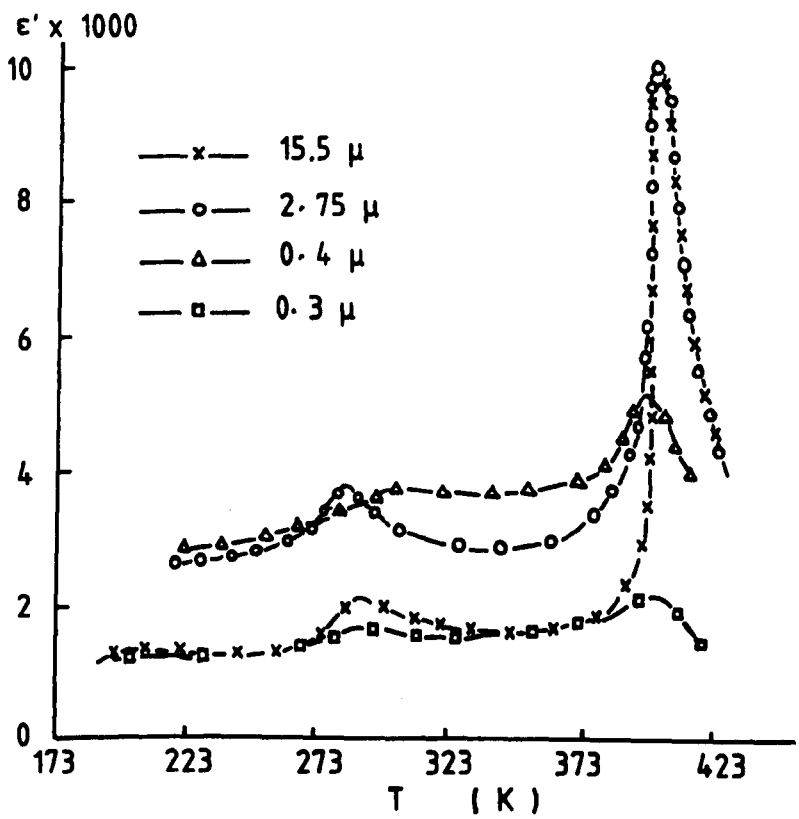

Fig. 5.17. Variation of dielectric permittivity with grain sizes in $BaTiO_3$ for different temperatures at 1 kHz and 1 V rms.

parallel gives the upper bound for the effective composite dielectric permittivity ε_c of the heterogenous material :

$$\left(\frac{v_{f1}}{\varepsilon_1} + \frac{v_{f2}}{\varepsilon_2} \right)^{-1} \leqslant \varepsilon_c \leqslant v_{f1}\,\varepsilon_1 + v_{f2}\,\varepsilon_2 \qquad (5.13)$$

where ε_1 and ε_2 are the permittivities of the dielectrics and v_{f1} and v_{f2} are their respective volume fractions. Banno and Saito [37] derived the dielectric permittivity for the "modified" cubes model which generalizes the parallel, series and cubes models of two-phase composite systems in which ceramic particles are dispersed in polymer matrix and is given by :

$$\varepsilon_c = \frac{a^2[a + (1-a)n]^2\,\varepsilon_1\,\varepsilon_2}{a\varepsilon_1 + (1-a)n\varepsilon_2} + \{1 - a^2[a + (1-a)n]\}\varepsilon_1 \qquad (5.14)$$

where $a^3/[a+(1-a)n]^3$ = volume fraction of phase 2 (ceramic particles) with dielectric permittivity ε_2, ε_1 is the permittivity of phase 1 (polymer matrix) and $n \geqslant 0$ (the value depends on volume fraction and the size of ceramic particles; for n=1, "modified" cubes model becomes cubes model). It has been observed [37] that the n value decreases with the decrease of the volume fraction of ceramics and that the n value for the smaller particle size is larger than that for the larger particle size. Such variation of n values is considered to be due to the difference in the surface

area[37].

Furukawa et al [38] have studied a composite system of epoxy resin (diglycidyl ether of bisphenol) and PZT ceramics. The magnitude of dielectric permittivities of the composite have been observed to lie within the bounds as expressed by Eq.(5.13). However these values are about 1.5-2.0 times greater than the theoretical values calculated using the expression of the permittivity of the composite system by assuming a spherical shape of the inclusions, which is [39]:

$$\varepsilon_c = \left(\frac{2\varepsilon_1 + \varepsilon_2 - 2v_f(\varepsilon_1 - \varepsilon_2)}{2\varepsilon_1 + \varepsilon_2 + v_f(\varepsilon_1 - \varepsilon_2)} \right) \varepsilon_1 \qquad (5.15)$$

where v_f is the volume fraction of the inclusions and ε_1 and ε_2 are the permittivities of the matrix and the inclusions. The discrepancy between the experimental results and theoretical values is suggested to be due to the distortional effect of the shape of PZT ceramics or due to their aggregation in the composite.

In deriving the dielectric permittivity of the composite in which ceramic particles are dispersed in the polymer matrix, Yamada et al [35] assumed that the shape of the particles to be ellipsoidal. In such a system, the dielectric permittivity of the composite is obtained as :

$$\varepsilon_c = \left(1 + \frac{s\, v_f\, (\varepsilon_2 - \varepsilon_1)}{s\varepsilon_1 + (\varepsilon_2 - \varepsilon_1)(1 - v_f)} \right) \varepsilon_1 \qquad (5.16)$$

where s is the parameter attributed to the shape of the ellipsoidal particles and other symbols are as previously defined in Eq.(5.15). It was found that the theoretical values of ε_c agreed well with observed values when the parameter s was 8.5. The specification demanded that the long ellipsoids of the particles are arranged perpendicular to the surface of the composite film which may be obtained as a result of the pressing of the film.

5.3. Measurement Technique

The measurement of dielectric properties (dielectric permittivity and dielectric loss) were carried out using the same measurement chamber as used for the current absorption studies, as illustrated in Figs.4.15, 4.16 and 4.17. For this purpose, the General Radio Bridge system model 1621 consisting of oscillator 1316, detector 1236 and variable capacitor/ resistor 1616 was used to measure the capacitance and resistance of the sample at different frequencies (10 Hz to 100 kHz). Alternatively, the data can be taken using an automated system comprising Solartron Frequency Response Analyser model 1250, a microcomputer and an ancillary unit containing selected resistors and capacitors, which has recently been developed in the laboratory. The system is capable of sweeping the frequency from 10^{-5} Hz to 65 kHz.

In considering the above measurement, a dielectric sample can be represented as a parallel combination of

resistance (R_p) and capacitance (C_p) as shown in Fig.5.18. This equivalent circuit may be used as a simple theoretical model of a dielectric, although in actual cases it may be rather complex (non-linear behaviour). The total impedance Z of the dielectric (refer to Fig.5.18) is given by :

$$1/Z = (1/R_p) + iwC_p \tag{5.17}$$

On application of the alternating voltage $V = V_o \exp(iwt)$, the capacitance simulates the quadrature or reactive out-of-phase loss while the resistance simulates the in-phase loss in the material. Thus the current I passing through the dielectric is composed of capacitive current I_C and resistive current I_R :

$$\begin{aligned} I &= I_C + I_R \\ &= iwC_pV + V/R_p \end{aligned} \tag{5.18}$$

From the relation $I = dQ/dt$, it can be shown that :

$$\begin{aligned} I &= \varepsilon^* C_o \, dV/dt \\ &= iw \, \varepsilon^* C_o V \\ &= wC_o(\varepsilon'' + i\varepsilon') V \end{aligned} \tag{5.19}$$

By comparing Eq.(5.18) and Eq.(5.19),

$$\varepsilon' = C_p/C_o \tag{5.20}$$

$$\varepsilon'' = 1/(R_pC_ow) \tag{5.21}$$

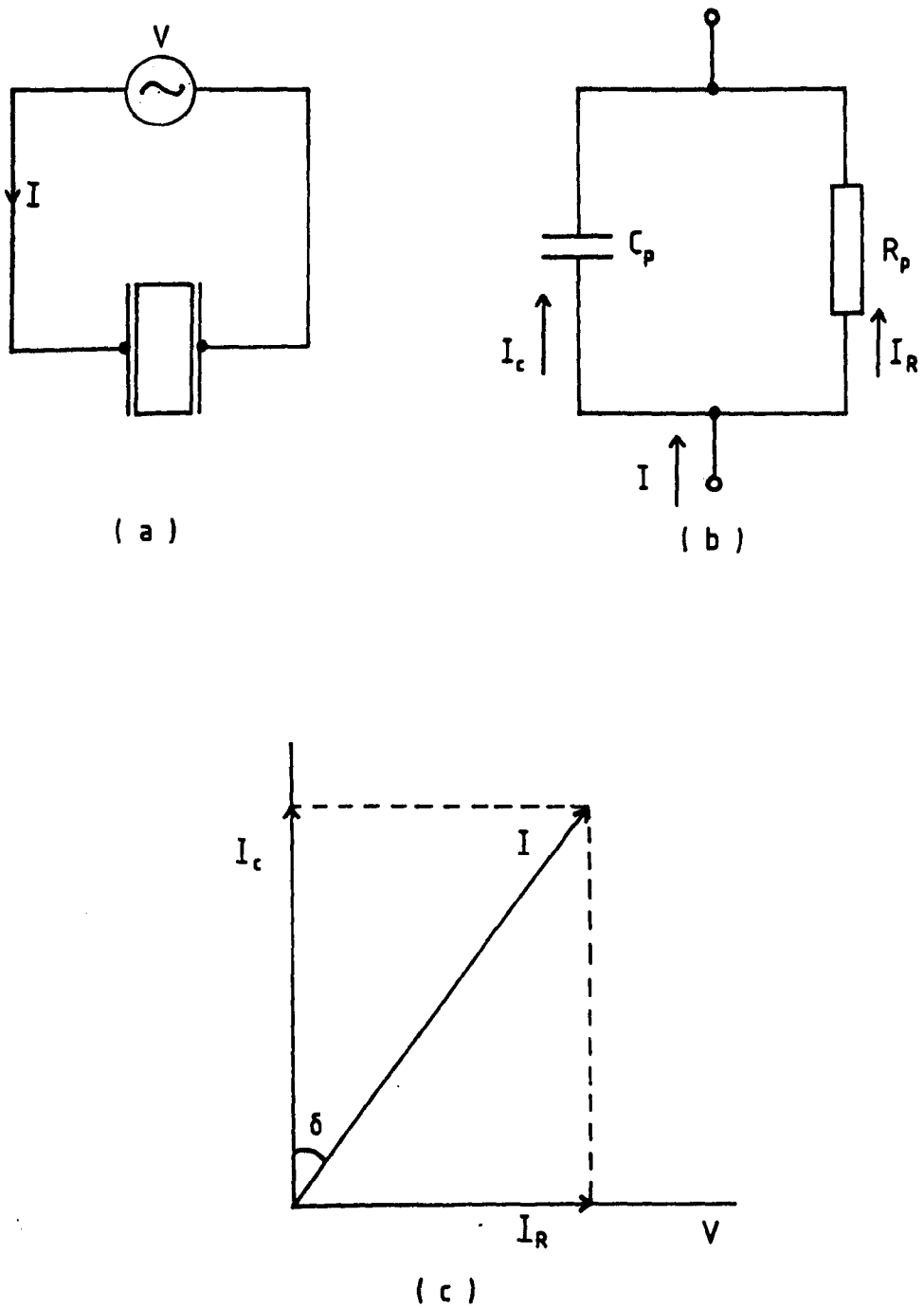

Fig. 5.18. AC losses in a dielectric : (a) Schematic circuit diagram, (b) parallel equivalent circuit of a dielectric with loss , (c) Argand diagram defining loss angle δ.

and $$\tan \delta = \varepsilon'' / \varepsilon' = 1/(R_p C_p w) \qquad (5.22)$$

The relative dielectric permittivity (ε'), dielectric loss (ε'') and the loss angle (δ) or dissipation factor ($\tan \delta$) can therefore be determined by measuring the equivalent circuit components of the specimen.

The ac conductance ($G_p = 1/R_p = \sigma A/L$) is a combination of dc conductance and the conductance arising from time-dependent polarization processes. For a dielectric with a geometric capacitance $C_o = \varepsilon_o A/L$, it can be shown from Eq.(5.21) that the dielectric loss associated with dc conductivity (σ_{dc}) can be written as :

$$\varepsilon'' = \sigma_{dc} / (\varepsilon_o w) \qquad (5.23)$$

from which a high value of σ_{dc} will give rise to high ε'' at low frequency.

5.4. Experimental Results and Discussion

5.4.1. Dielectric properties of PVDF, VDF-TrFE and PZT5

Fig. 5.19 shows the dielectric relaxation behaviour of homopolymer PVDF film (thickness $\sim$150 μm, obtained by rolling and hot-pressing the pellets form) at three temperatures in the frequency range of 10-10^5 Hz. The position of the dielectric loss peak is shifted to higher frequencies at higher temperatures. The relaxation may be attributed to the α_c-relaxation which is related to molecular motions in the crystalline regions [12,13]. The magnitudes of ε' and ε'' were observed to be comparable to that obtained by Kakutani[40] for the unstretched extruded PVDF film. Indeed, the values of ε' for the present PVDF film is slightly less than that of the stretched PVDF film [40]. This may be expected as the film stretching would result in the orientation of molecules in the amorphous phase in the direction of the drawing and consequently an increase in the values of ε' [40]. The value of ε' in the uniaxially stretched PVDF film is 15 [40], which is higher than that obtained in the present PVDF film (ε' = 9) at 110 Hz and temperature 343K. The values of dielectric loss in the present PVDF film (ε''=1.6) is comparable to that obtained for unstretched PVDF film (ε''=1.8) by Kakutani [40] at 110 Hz and temperature 343 K. Indeed, the value of dielectric loss obtained for uniaxially stretched PVDF film was much lower,

i.e. $\varepsilon'' = 0.3$ [40] at the same frequency and temperature. Since α_c-relaxation is assigned to be related to molecular motion in the α-form (Form II) crystals [40], the reduction in ε''-values may indicate a reduction of Form II crystals in the stretched film.

The variation of ε' and ε'' with frequency at three temperatures in VDF-TrFE copolymer film (thickness $\sim$160 μm, obtained by rolling and hot-pressing the pellets form) may be observed as in Fig.5.20. The relaxation in this copolymer may be associated with the crystalline phase as was suggested by Furukawa and Johnson [41] for VDF-TrFE (55/45 mol%) copolymer. The values of ε' obtained for the copolymer in the present work were found to be comparable to that of homopolymer PVDF. This will indicate that the composition of the copolymer is significantly different from that of the copolymer with composition $\sim$55/45 mol%, which exhibits the highest value of ε' ($\sim$50) at 343 K and 1 kHz [42].

Fig.5.21 shows the values of the complex permittivity of PVDF and VDF-TrFE in the temperature range of 293-373 K at 1 kHz. It may be observed that for PVDF, ε' increases with an increase of temperature whereas for VDF-TrFE, the values of ε' may show a peak at $\sim$368K.. The increase of ε' for PVDF in this temperature range had also been observed by Kakutani [40] and Yano [13]. At temperatures slightly over 373K, a kind of shoulder may be seen in its characteristics before it increases again up to the melting point ($\sim$428K) [13,40,43]. In the temperatures 428-473K, ε' was observed to decrease with an increase of temperature at 1 kHz, while at lower

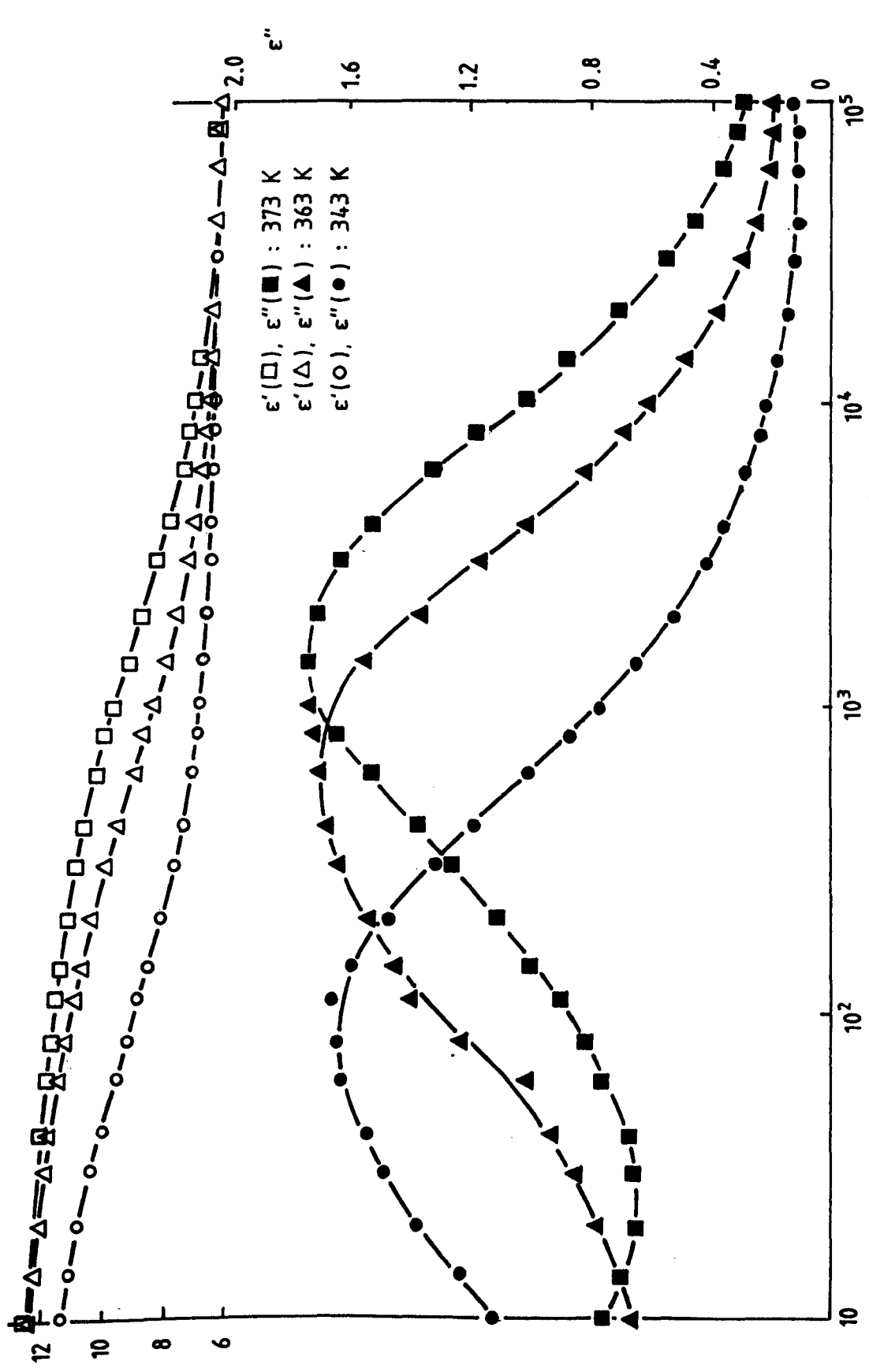

Fig. 5.19. Dielectric behaviour of homopolymer PVDF at different temperatures.

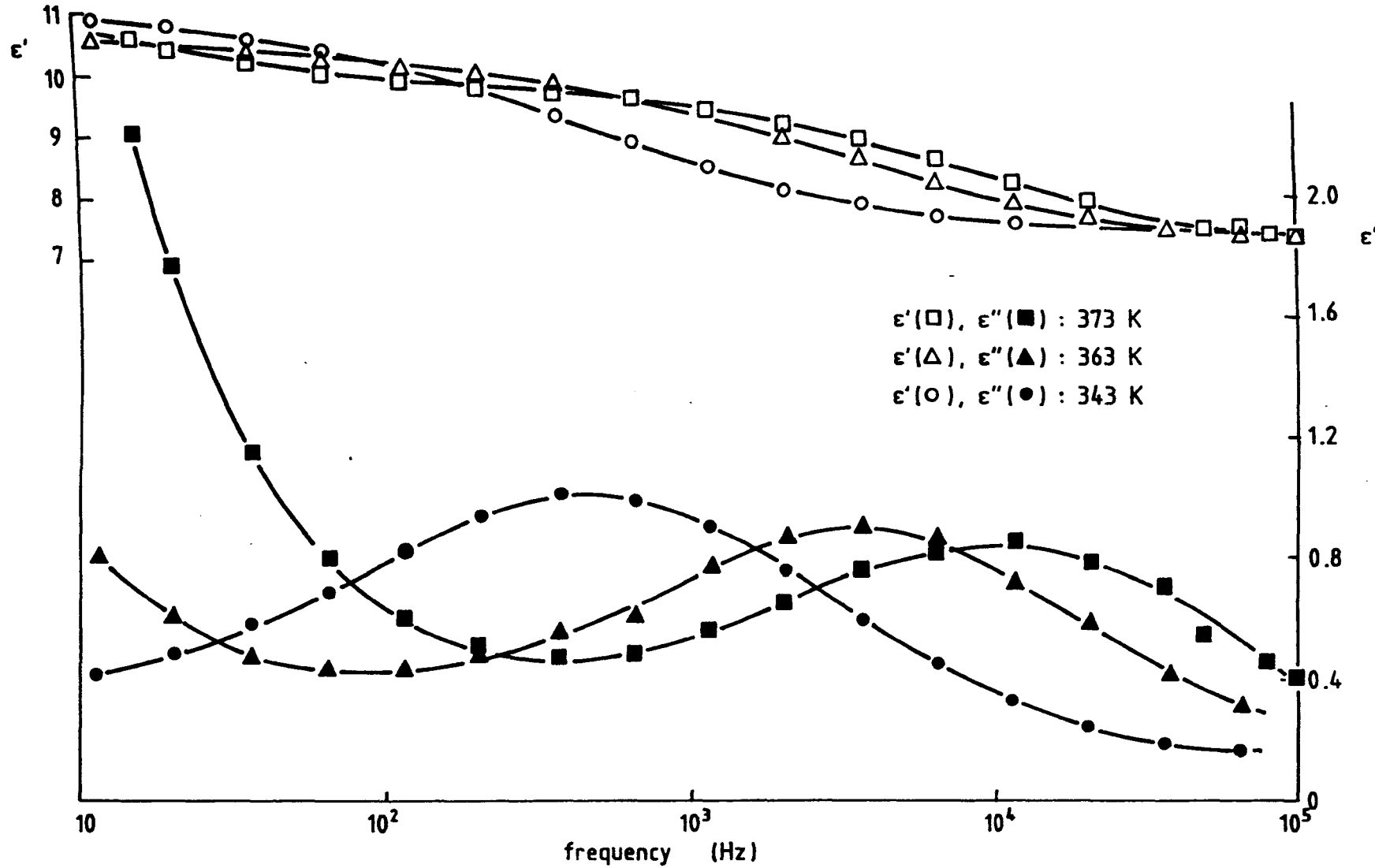

Fig. 5.20. Dielectric behaviour of copolymer VDF/TrFE at different temperatures.

frequencies ($\lesssim$ 1 kHz), ε' again increases with increasing temperature after showing an abrupt drop at about 428K [43]. The abrupt drop of ε' is presumably due to melting of PVDF [43].

The possible appearance of peak in ε' for VDF-TrFE (see Fig.5.21), again may be related to the molecular motion associated with the crystalline phase [41,44]. It follows that the peak of ε'' at $\sim$348K in VDF-TrFE (Fig.5.21) may be associated with the crystalline phase, designated as α-relaxation [41]. The ε'' peak at $\sim$368K and 1 kHz for PVDF appears to be associated with α_c-relaxation [40]. The magnitude and position of ε'' peak for PVDF in the present work were found to be similar to that obtained by Yano [13] in cast PVDF film. It should also be noted that the magnitude and position of ε'' peak depend on the density and the crystallinity of the sample, due to different preparation methods and the subsequent treatment that the samples may have received [12,13].

The behaviour of ε' and ε'' against temperature at 10 Hz for PVDF and VDF-TrFE may be observed from Fig.5.22. The increase in ε' with an increase of temperature for PVDF film follows the same behaviour as that obtained by Yano[13]. Again, the ε'' peak at $\sim$ 328K for PVDF may be associated with α_c-relaxation [13]. The relaxation peak which appears in VDF-TrFE (Fig.5.22) may be related to α-relaxation[41]. The rapid increase of ε'' above $\sim$363K in VDF-TrFE may be associated with ionic space charge conduction as had been observed in PVDF by Yano et al[43], Nakagawa and Ishida [14],

Osaki et al [16] and in VDF-TFE copolymer by Koizumi et al[45].

The activation energy (ΔU) associated with the α_c-relaxation process in PVDF, calculated by assuming that the process follows an Arrhenius type [12,13], was found to be 1.12 eV (see Fig.5.23), which is in good agreement with the result obtained by other workers[12-14,17,21]. It appears that the activation energy associated with the α-relaxation in VDF-TrFE copolymers has about the same magnitude as that of α_c-relaxation in PVDF (Fig.5.23). Furukawa and Johnson [41] also observed an increase of the dielectric loss peak frequency (f_m) with increasing temperature but with the shoulder appearing at ~343K for VDF-TrFE(55/45) copolymer. The activation energy calculation was modified so that the plot exhibits the usual linear behaviour of Arrhenius type dependence and the activation energy was found to be 0.53 eV[41]. In the present work, no shoulder was observed and the plot of f_m vs. 1/T showed a straight line (a typical of Arrhenius type temperature dependence) in the range of frequencies and temperatures employed. Thus the activation energy obtained for the copolymer in the present work may represent the actual potential barrier for molecular motion.

Fig.5.24 shows the behaviour of ε' and ε'' in PZT5 ceramic at three temperatures and in the frequency range of 10-10^5 Hz. It may be observed that there is no relaxation peak in ε'' in the present frequency range, which may indicate that there is no appreciable domain and domain-wall motions. The shape of the ε''-curve may possibly indicate that there will be

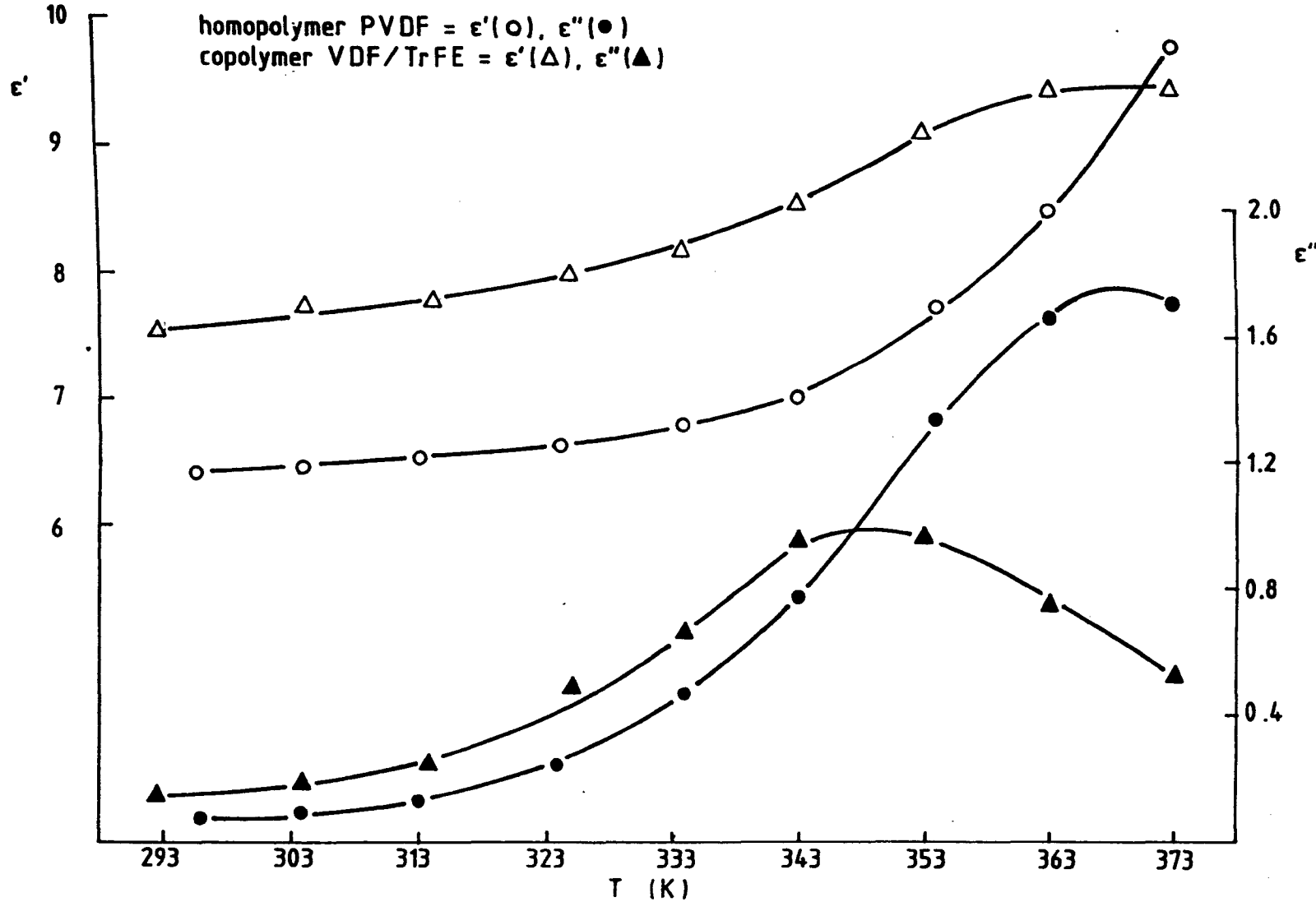

Fig. 5.21. Temperature dependence of dielectric properties in homopolymer PVDF and copolymer VDF / TrFE at 1 kHz.

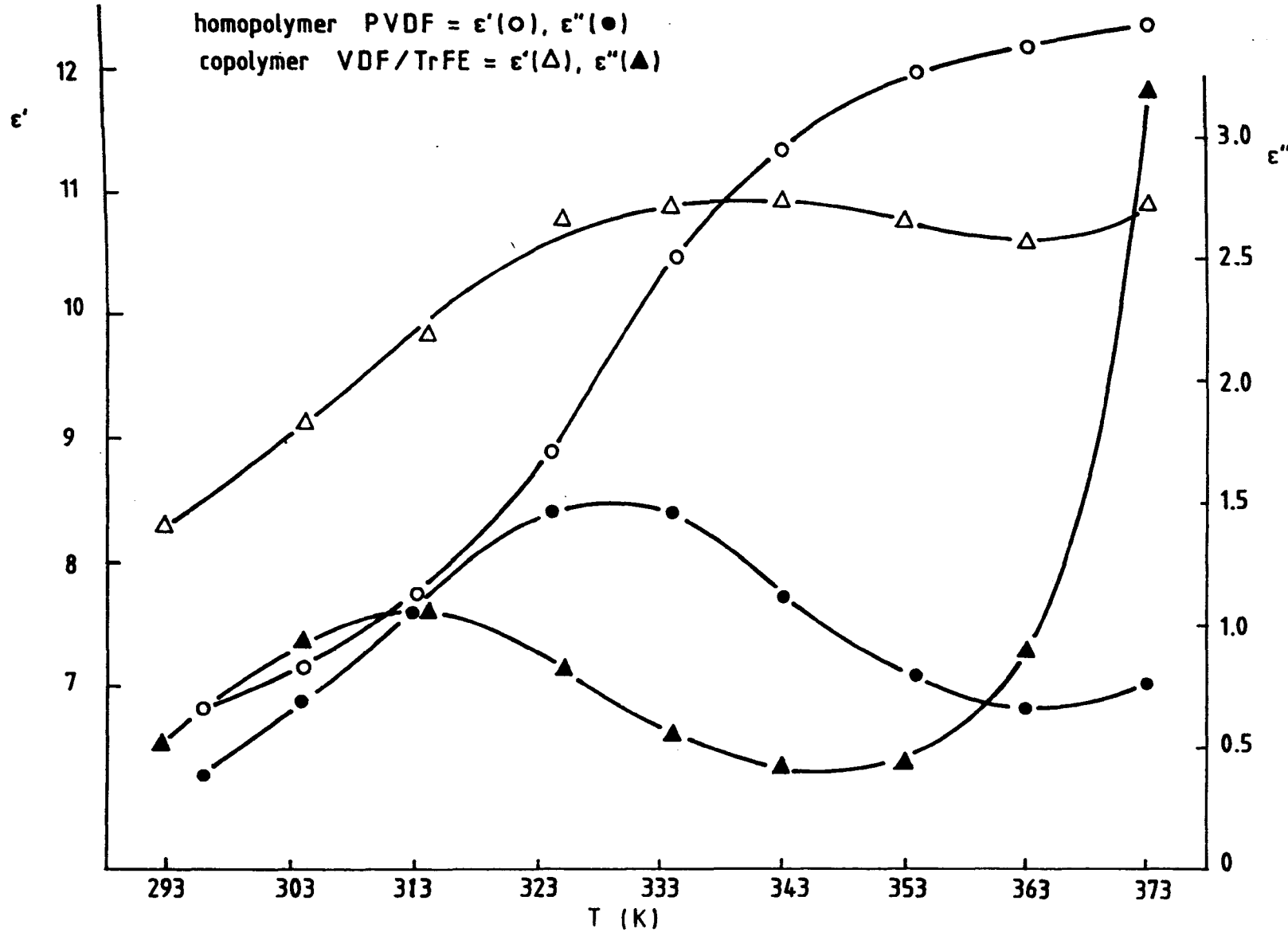

Fig. 5.22. Temperature dependence of dielectric properties in homopolymer PVDF and copolymer VDF / TrFE at 10 Hz.

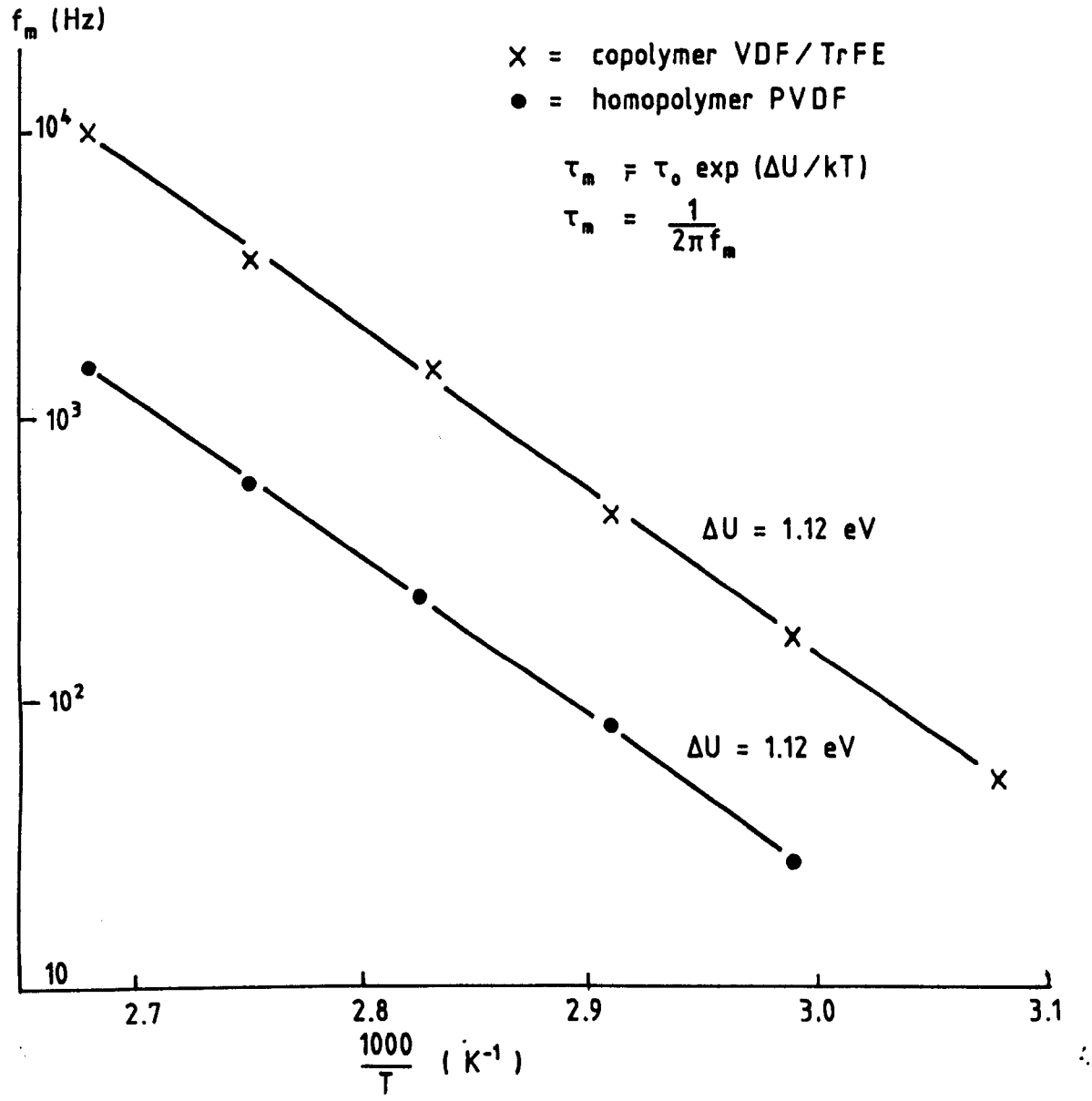

Fig. 5.23. Temperature dependence of peak frequency of dielectric loss in homopolymer PVDF and copolymer VDF / Tr FE.

a relaxation peak at higher frequencies, which will be in agreement with the result obtained by Gerson et al[26] and Kersten and Schmidt [23]. The variation of ε' and ε'' with temperatures at 10 Hz and 1 kHz in PZT5 ceramic may be observed as in Fig.5.25. The values of ε' are approximately constant below room temperature and increase with an increase of temperature above it. The increase of ε' with an increase of temperature had also been observed in unmodified PZT ceramic [22]. The values of ε'' at 10 Hz were found to increase drastically at high temperatures. Such an increase of ε'' may be attributed to conduction phenomena in the bulk as had been suggested by Gerson [27]. The fact that such an increase were found to be more pronounced in PZT ceramic with higher conductivity, may support the attribution of high ε'' suggested earlier[27]. Hardtl [29] attributed the high dielectric loss at high temperatures and low frequencies as due to the free carrier conductivity initiated by temperature. The observed increase of ε'' towards low temperatures may be associated with domain-wall movement as suggested by Hardtl[29] ; however more detailed investigations are necessary in this respect.

5.4.2. Dielectric properties in PIEZEL

Figs.5.26 and 5.27 show the behaviour of ε' and ε'' in the frequency range of $10\text{-}10^5$ Hz in PIEZEL at high temperatures and low temperatures respectively. The relaxation peak which occurs at high temperatures (Fig.5.26) may be

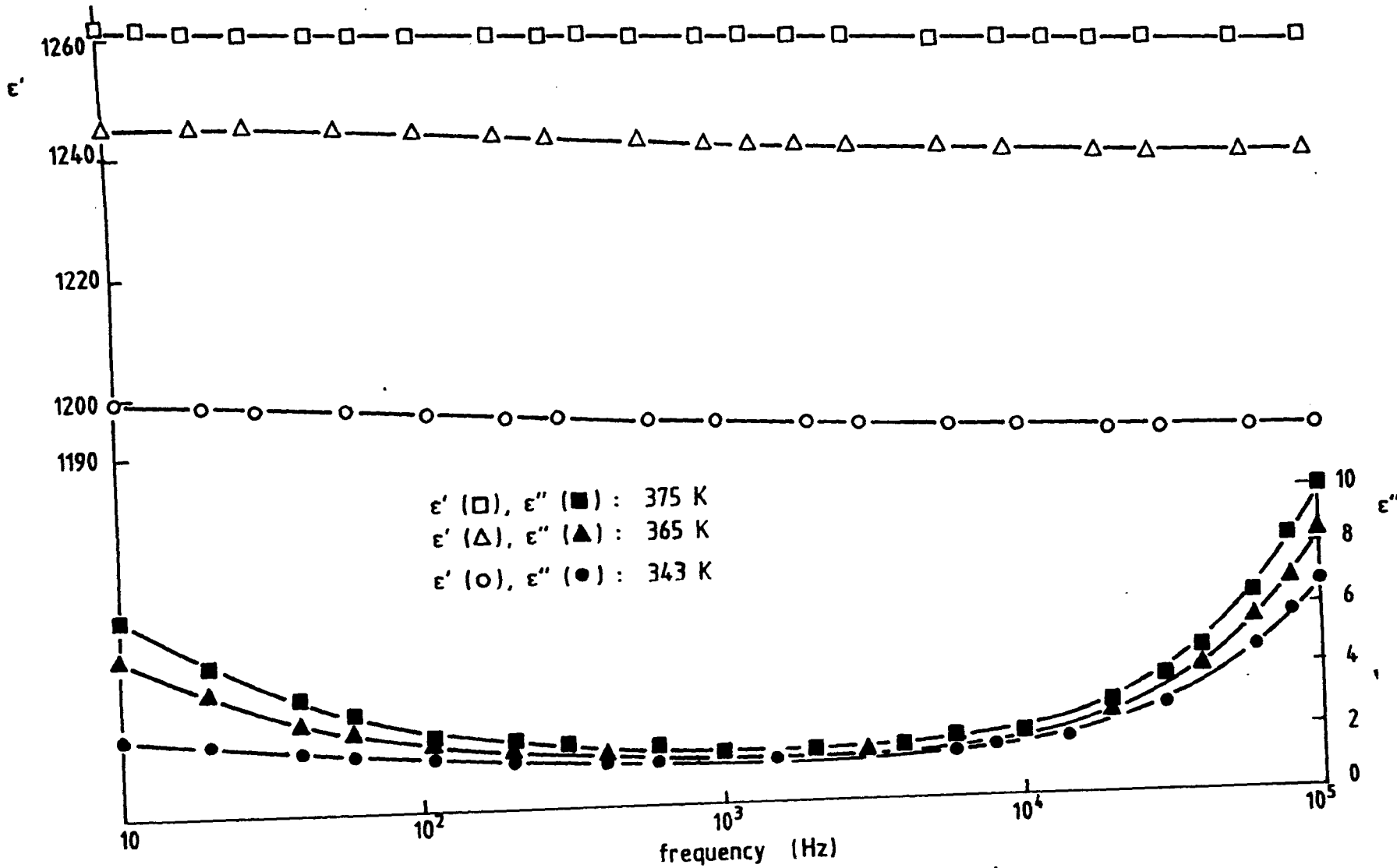

Fig. 5.24. Dielectric behaviour of PZT5 ceramics at different temperatures.

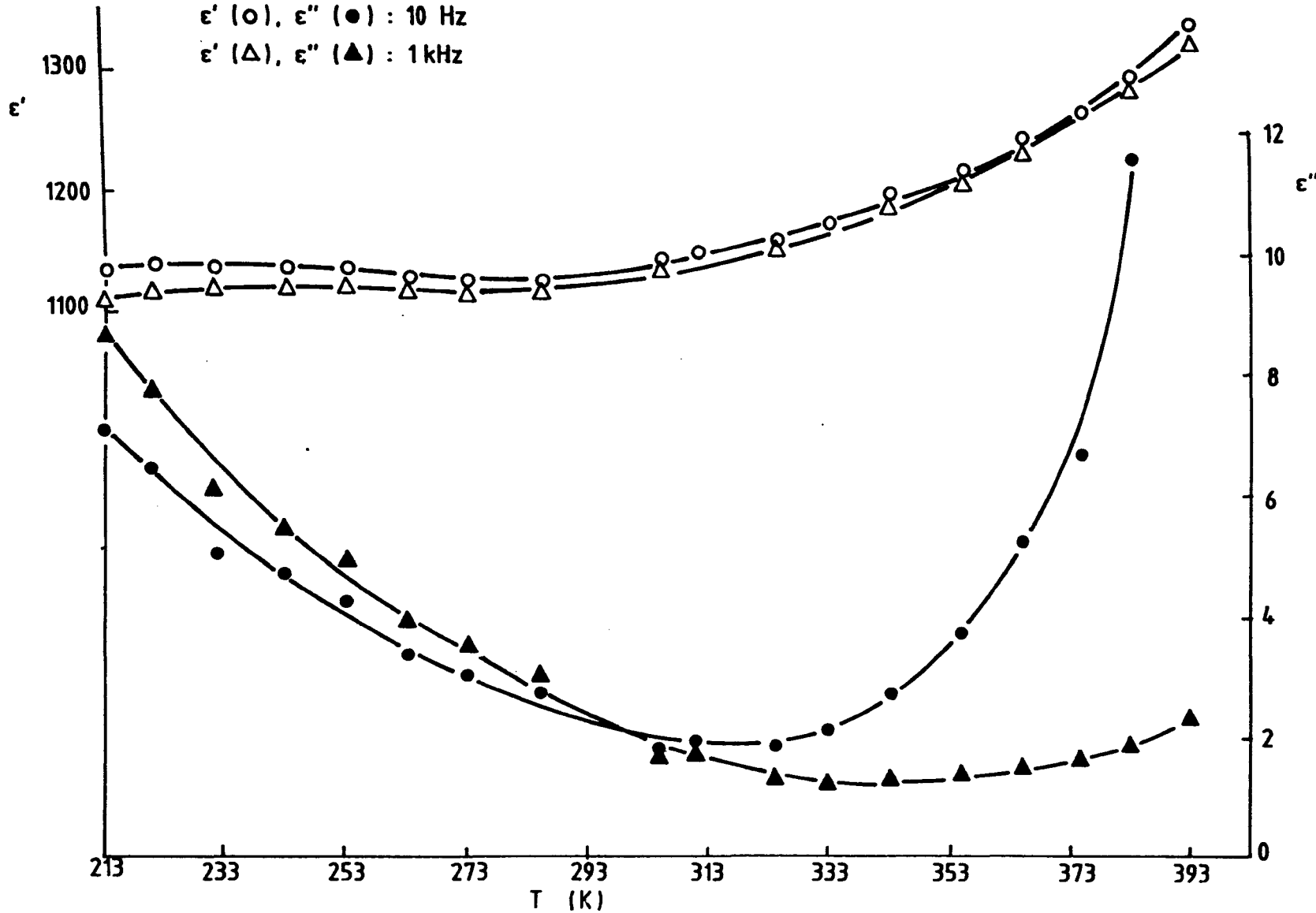

Fig. 5.25. Temperature dependence of dielectric properties in PZT5 at 10 Hz and 1 kHz.

associated with the molecular motion in the crystalline phase of the polymer(α-relaxation). The significant increase of ε'' at low frequencies and high temperatures may again be associated with the conduction mechanism which may possibly arise from both ceramic phase and polymer phase as mentioned in section 5.4.1. The broad relaxation at low temperatures (Fig.5.27) may be ascribed to the micro-Brownian motion of molecular chain segments in the amorphous regions of the polymer phase (β-relaxation), as has been suggested by Furukawa and Johnson[41] for VDF-TrFE(55/45 mol%) copolymer.

The variation of ε' and ε'' with temperatures at fixed frequencies (10 Hz and 1 kHz) in PIEZEL can be further observed as in Fig.5.28. The two relaxation peaks which appear at low temperatures and high temperatures may be designated as β-relaxation and α-relaxation respectively, in the polymer phase. Again, it may be observed that the value of ε'' increases drastically at low frequency and at higher temperatures, which may possibly be attributed to the conduction mechanism in the bulk of the composite. The loss peak at low temperature ($\sim$270K) appears to be in similar position as the β-relaxation obtained for VDF-TrFE(55/45) copolymer, which was at 268K [41] at 1 kHz. The position of high-temperature dielectric loss peak in PIEZEL ($\sim$348K) also appears to be quite similar to that obtained for α-relaxation in VDF-TrFE(55/45), i.e. 343K[41] at the same frequency of 1 kHz.

Although the nature of the dielectric loss process in PIEZEL appears to be similar to that of VDF-TrFE(55/45)

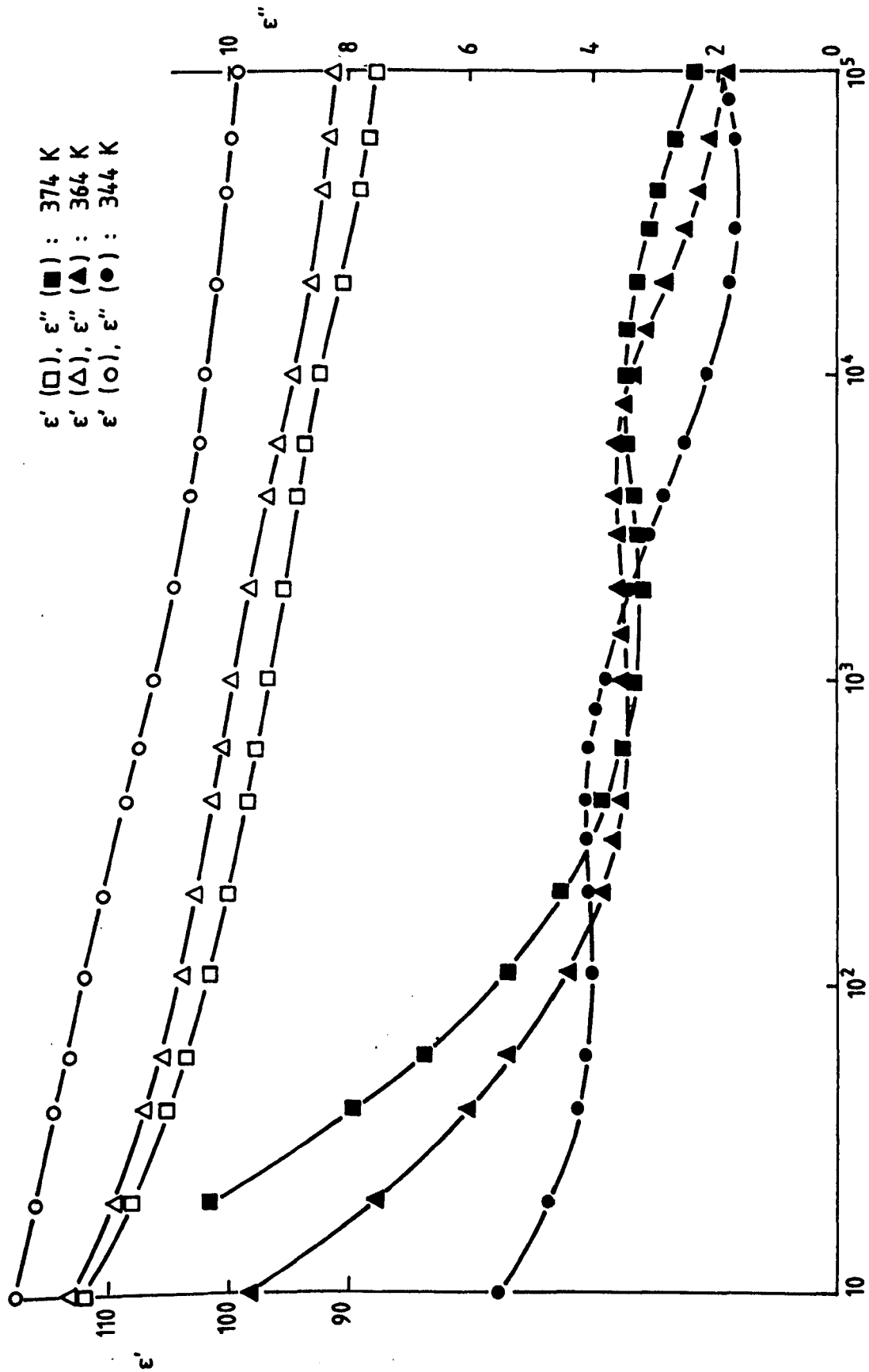

Fig. 5.26. Dielectric behaviour of PIEZEL at high temperatures.

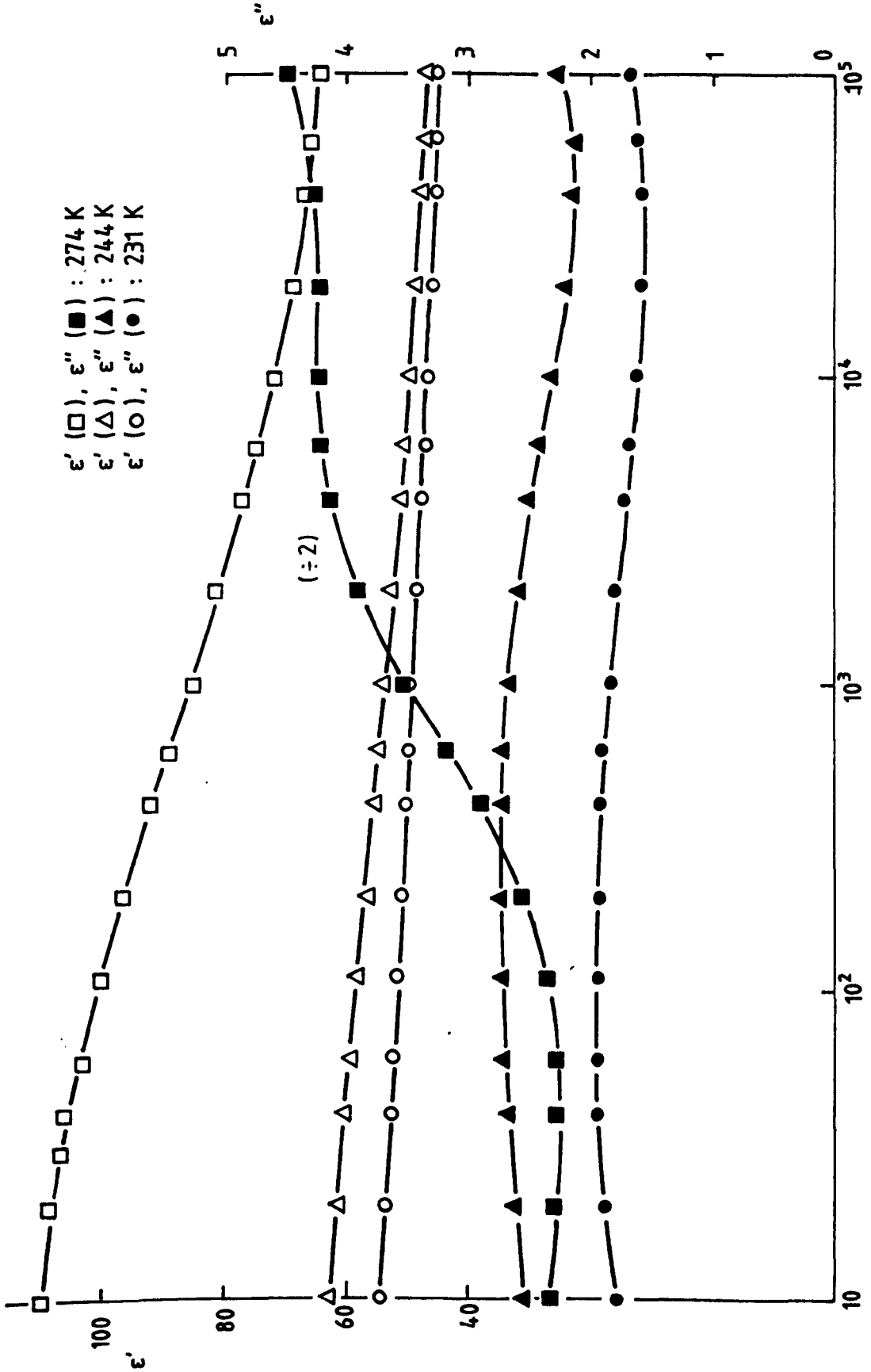

Fig. 5.27. Dielectric behaviour of PIEZEL at low temperatures.

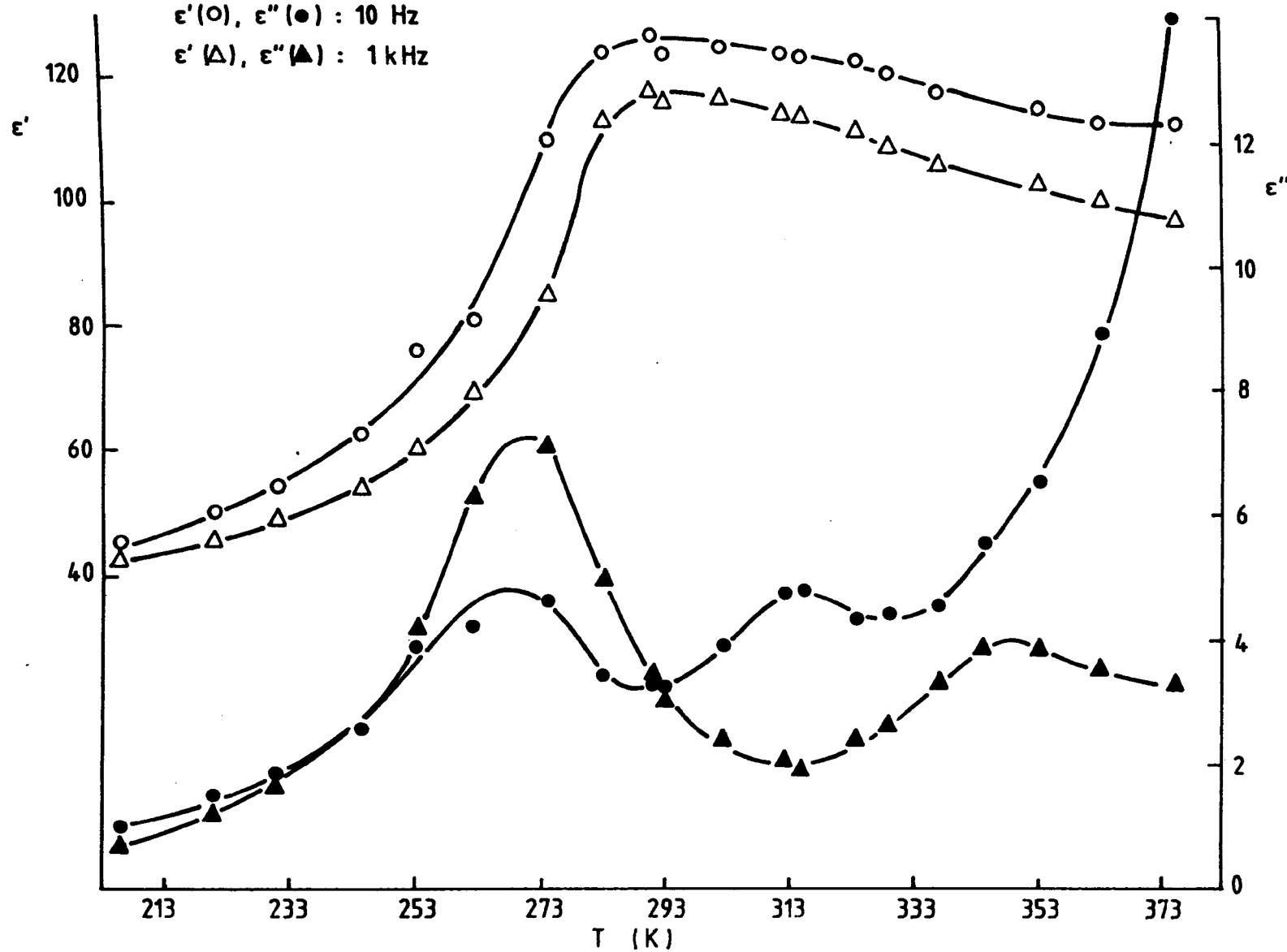

Fig. 5.28. Temperature dependence of dielectric properties in PIEZEL at 10 Hz and 1 kHz.

copolymer[41], the variation of ε' with temperature in these materials was quite different. It may be observed that the shoulder appears in ε'-T characteristics for PIEZEL at about 288K which may correspond well to that of VDF-TrFE copolymer[41] and it is due to β-relaxation. The peak due to α-relaxation in ε'-T characteristic appeared at $\sim$343K for VDF-TrFE [41], whereas no such peak appears in ε'-T characteristic of PIEZEL. Higashihata et al[46] also observed a peak in ε'-T characteristic for VDF-TrFE(52 mol% VDF) copolymer (at 343 K) and its composite with PZT (62 Vol%) (at 345K). The observed peak at 343 K appears to be located at the phase transition temperature(Curie temperature) of the copolymer [46]. PIEZEL is a commercial product of ceramic/polymer composite, in which the exact detail of the components and the fabrication process is not known. The absence of peak in ε'-T characteristic for PIEZEL may be due to compensation effect from impurities added during fabrication process and their thermal and mechanical history.

The variation of f_m (the frequency at which the dielectric loss peak of α-relaxation occurs) with the inverse of temperature (temperature range : 323-373K) shows a linear dependence of Arrhenius type with activation energy of 1.16 eV.

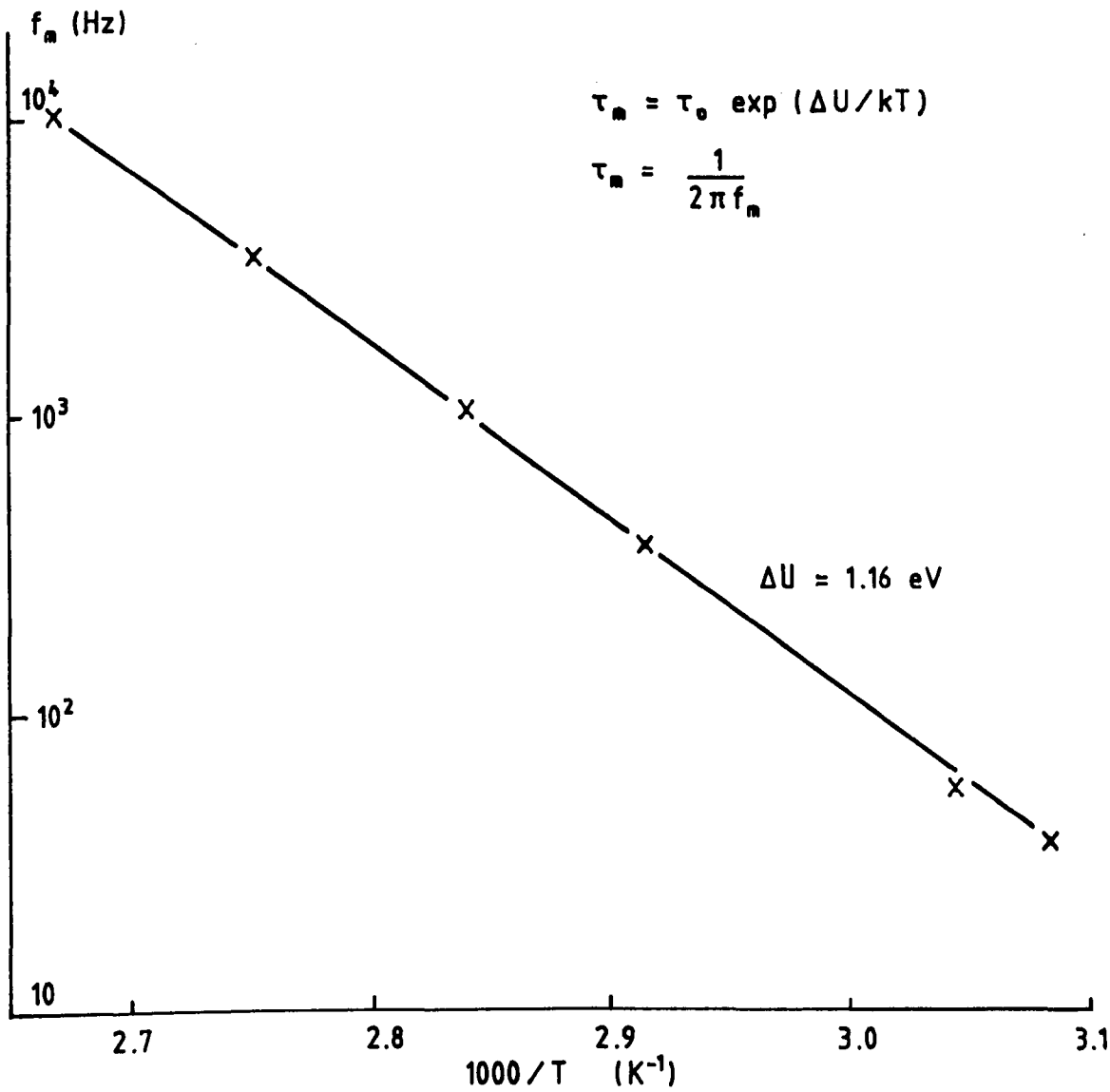

Fig. 5.29. Temperature dependence of peak frequency of dielectric loss in PIEZEL.

5.4.3. Dielectric properties in PZT5/VDF-TrFE composite

Fig.5.30 shows the behaviour of ε' and ε'' with frequency in PZT5/VDF-TrFE (50/50 Vol.%) at three different temperatures. The broad relaxation peak may be observed in ε''-f characteristic, which appears to be due to α-relaxation of the polymer phase. The rapid increase of ε'' at lower frequencies and high temperatures may possibly be attributed to the conduction mechanism in the bulk of the composite. This conduction may involve ionic impurities which may form space charge layers at the interface of inclusions (PZT particles) and the polymer matrix in the composite. The increase of ε' at low frequencies and high temperatures may also be attributed to the effect of interfacial charges. This process may resemble dipole polarization leading to the ε'-f characteristic which may be indistinguishable in form from that due to the conventional dipole orientation process [1,47]. It should also be noted that the composite may not be uniform (see further discussion in chapter 7) in which the ceramic particles concentration may be different from one region to another and the effect of this factor on the conduction process is not known.

The increase of ceramic volume fraction in the PZT5/VDF-TrFE composite results in an increase of the magnitude of the dielectric loss (Fig.5.31). It may also be observed that the behaviour of the dielectric loss is again similar to that of the polymer which shows α-relaxation process. The relaxation peak for (50/50 Vol.%) composition may not be readily seen,

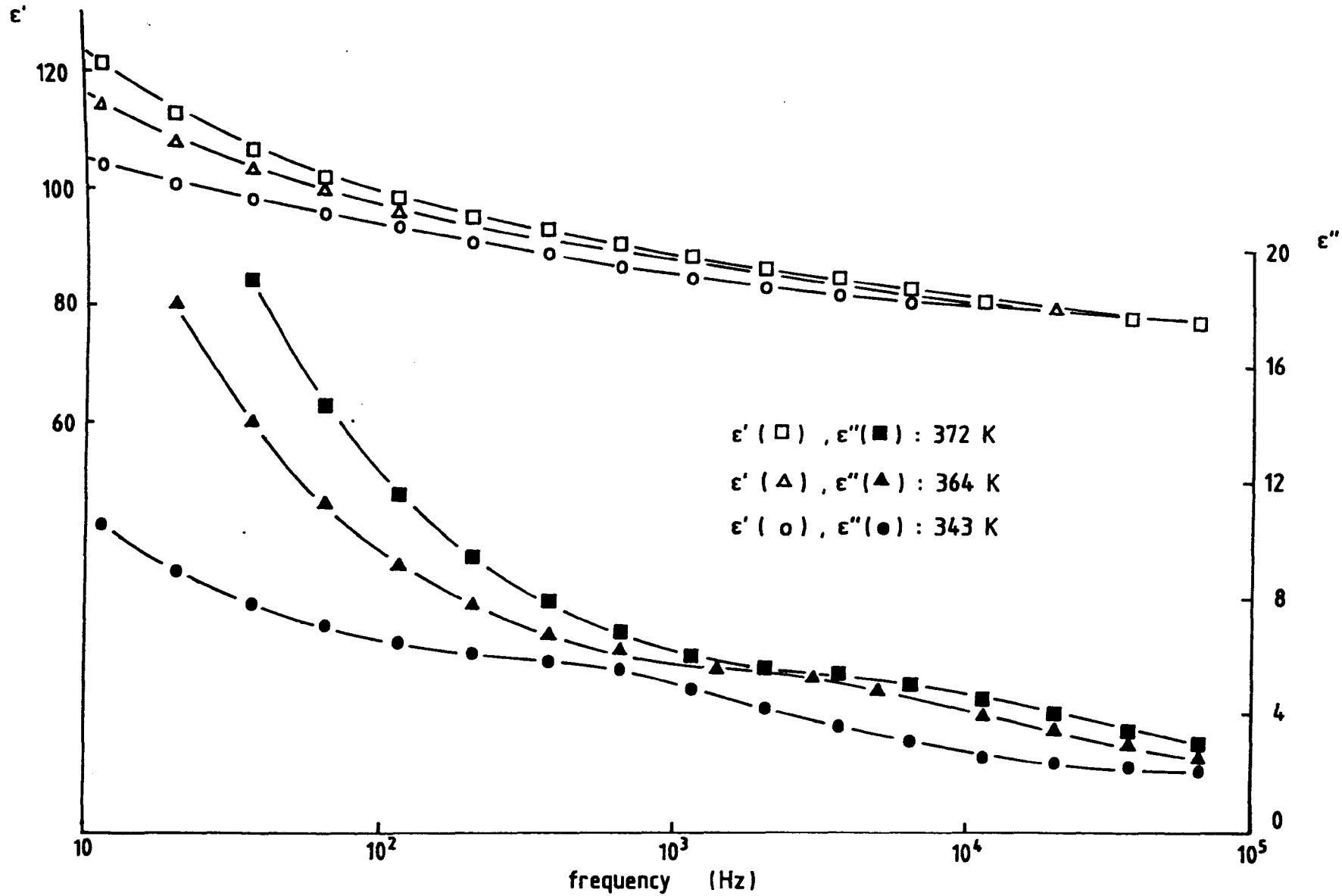

Fig. 5.30. Dielectric behaviour of PZT5 / copolymer VDF - TrFE (50/50 Vol.%) at different temperatures.

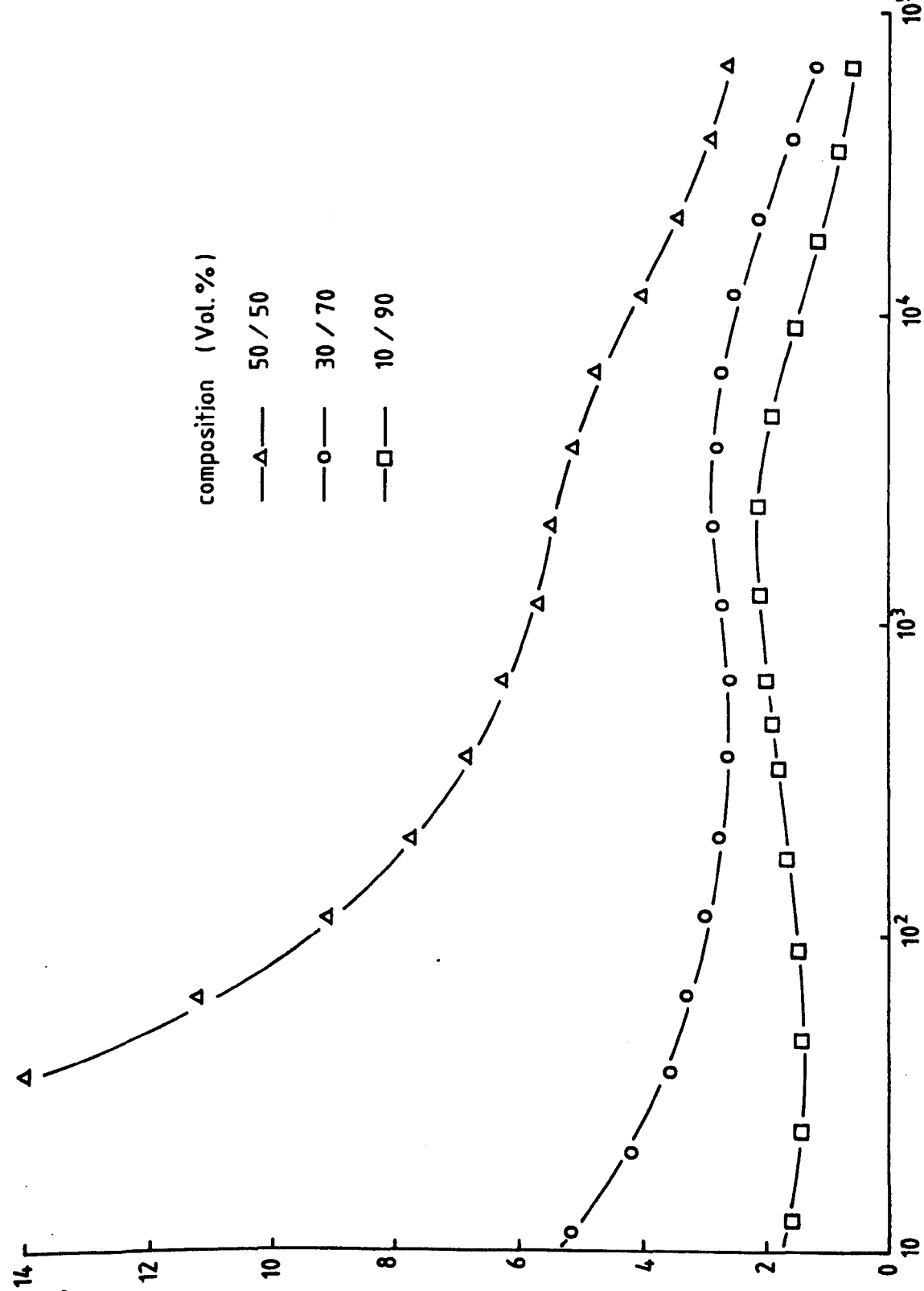

Fig. 5.31. Dielectric loss behaviour for different compositions of PZT 5 / copolymer VDF - TrFE at 363 K.

possibly due to the effect of the conduction mechanism which becomes more effective at low frequencies, as mentioned above. The slight decrease of the frequency of dielectric loss peak (f_m) in (10/90 Vol.%) composition as compared to that of copolymer, may be due to a slight change in the density and crystallinity of the copolymer as a result of minor variation in the treatment of the samples during fabrication. Sasabe et al[12] and Yano [13] reported such variation of peak position for PVDF samples, which have been attributed to the different density and crystallinity of the sample as a result of different fabrication process.

Fig.5.32 shows the variation of ε' and ε'' with temperature in the different compositions of PZT5/VDF-TrFE composites at 1 kHz. In all compositions the values of ε' were found to increase with an increase of temperature. The dielectric loss behaviour is again similar to that of copolymer, showing α-relaxation due to the polymer phase. Obviously, the magnitudes of ε'' were greater for the composition with high ceramic volume fraction. In the high-temperature region, the conduction term tends to be more effective, giving high values of ε'', which is particularly noticeable for the composition with high ceramic volume fraction. The dependence of peak frequency of dielectric loss with the inverse of temperature shows a straight line , indicating the Arrhenius type temperature dependence process (see Fig.5.33). The activation energies calculated from the slope of the curves were found to be 1.17 eV and 1.18 eV for (10/90 Vol.%) and (30/70 Vol.%) compositions respectively.

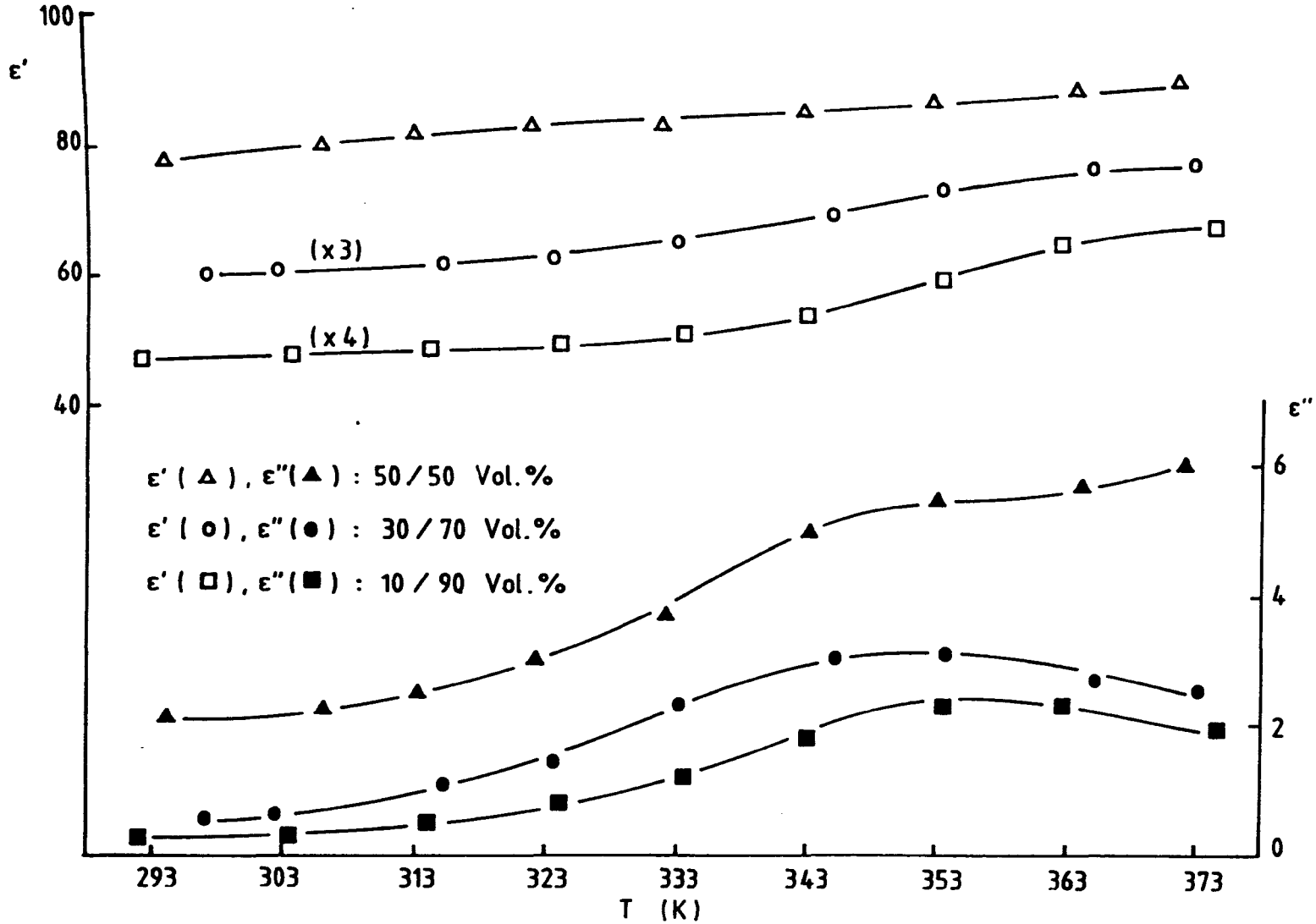

Fig. 5.32. Temperature dependence of dielectric properties in different compositions of PZT5 / copolymer VDF - TrFE at 1 kHz.

These values appear to be a little higher as compared to that obtained for the single phase copolymer (i.e. 1.12 eV) ; however, they are comparable to that obtained for PIEZEL composite (i.e. 1.16 eV). The higher activation energy obtained for the composites may possibly due to the effect of the ceramic particles being located in the polymer matrix.

The dependence of the dielectric permittivity of the composite on the ceramic volume fraction is shown in Fig.5.34. The value of ε' may be observed to increase with the increase of ceramic volume fraction which reaches a value of 85 for 50% volume ceramic composition. By using the value of ε'(VDF-TrFE) = 8.6 and ε'(PZT5) = 1190, the dielectric permittivity of the composite was calculated using the equation given by Wagner[39] (Eq.5.15), assuming a spherical shape of the inclusion. Solid curve in Fig.5.34 was generated using such an equation, from which it may be observed that the experimental data lie above the calculated values. This means that the inclusion may not be spherical in shape or it may form an aggregation with different shapes in the amorphous phase of the polymer.

The possibility of the ellipsoidal shape of the included particles may be considered. Based on the equation derived by Yamada et al [35] (Eq.(5.16)) for ellipsoidal shape of the inclusion, the values of the dielectric permittivity of the composites may be calculated by assuming a certain value of the shape factor (s). The calculated values of ε' were plotted in Fig.5.34 (dashed curve) for s= 7.5, 8.0 and 8.5. It may be observed that the curve with parameter s = 7.5-8.5 may

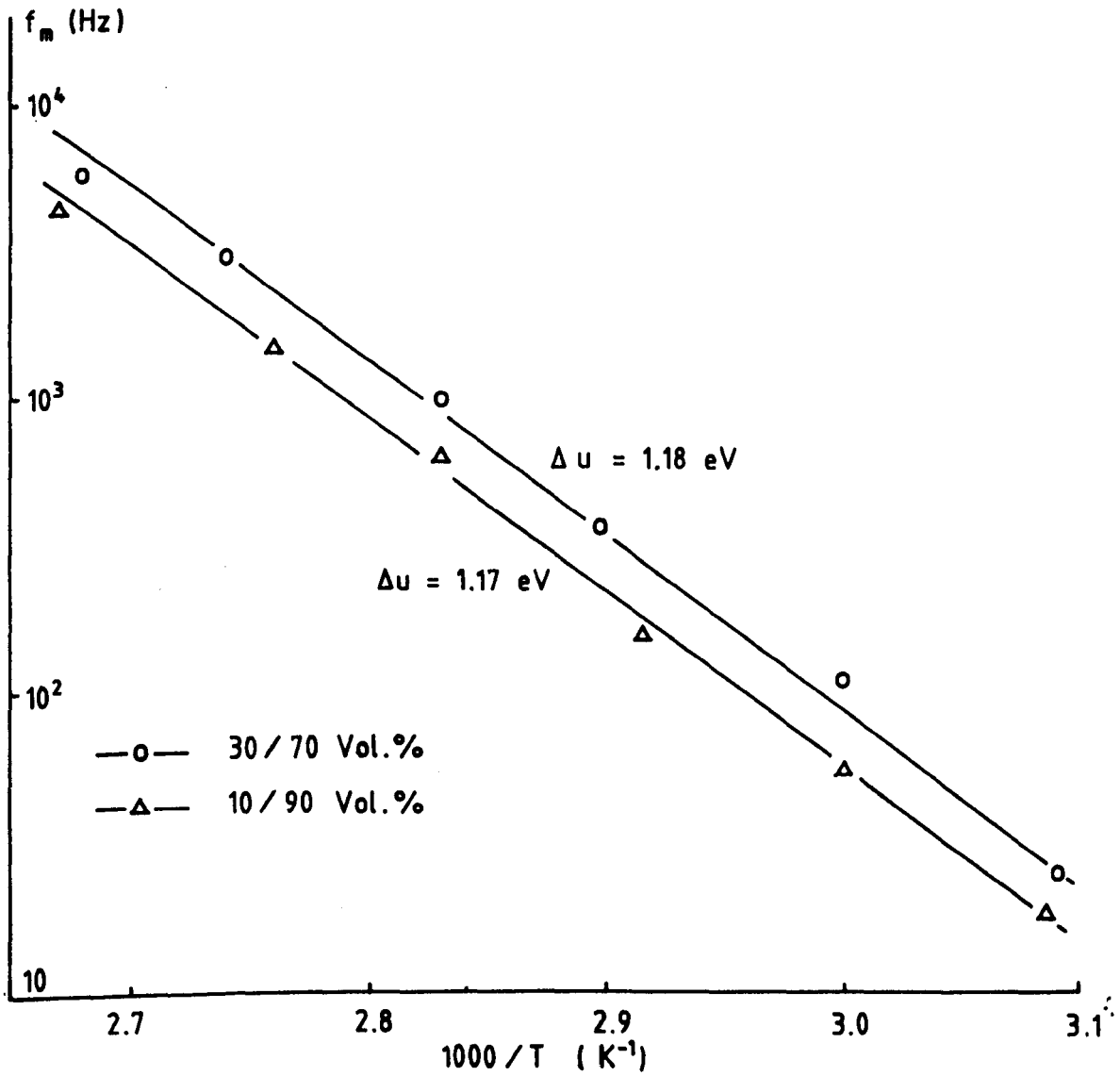

Fig. 5.33. Temperature dependence of peak frequency of dielectric loss in PZT5 / copolymer VDF - TrFE for 30/70 and 10/90 Vol.% compositions.

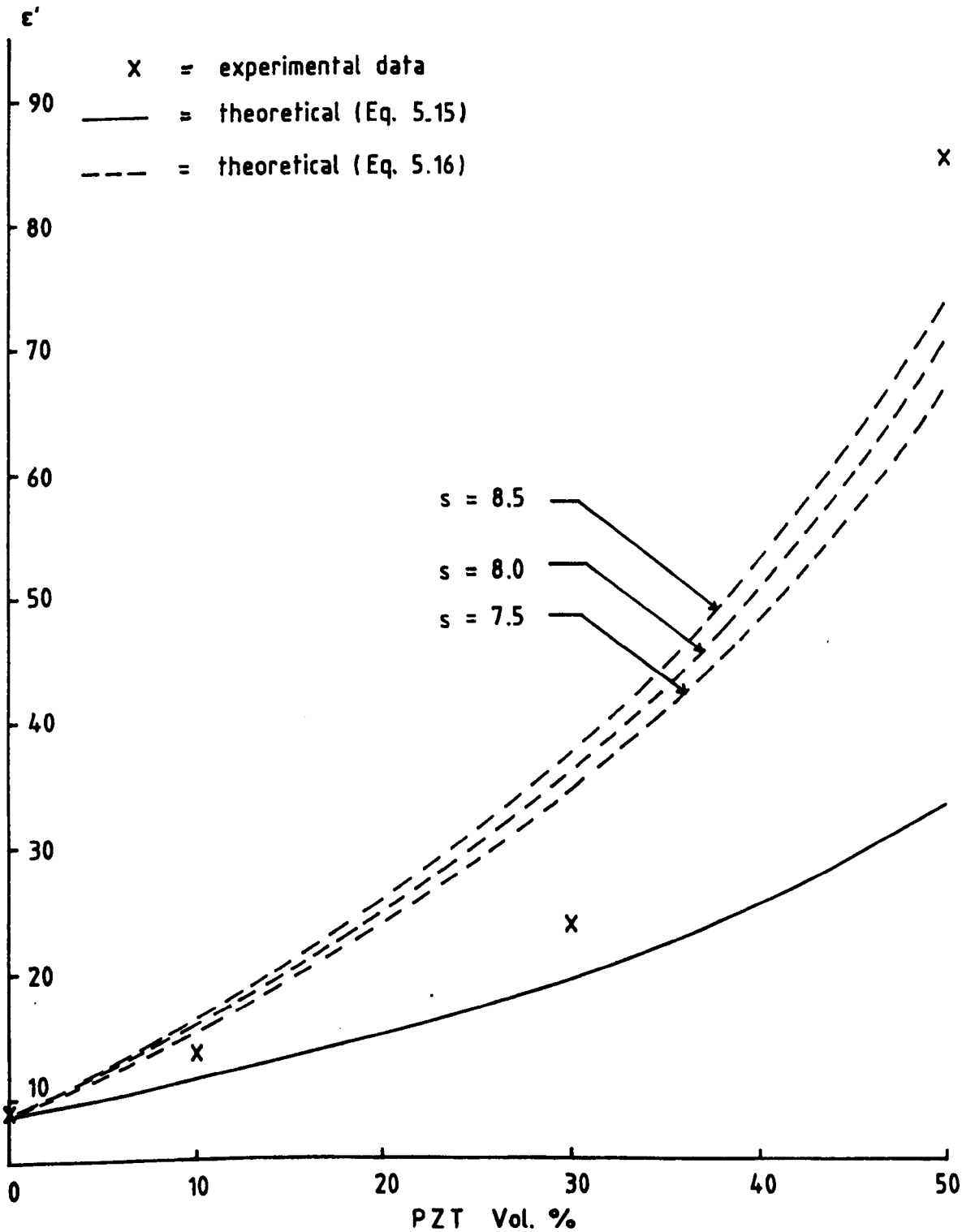

Fig.5.34. Theoretical and experimental dependence of permittivity on volume fractions of inclusion in PZT5/copolymer VDF - TrFE at 1 kHz and 343 K.

reasonably fit the experimental data. Yamada et al[35] found that the value of s = 8.5 gave a good agreement between the theoretical and experimental data in PZT/polymer composite (polymer : a mixture of PVDF and a fluorine elastomer, with the weight ratio of 3:2). This value of s demanded that the long ellipsoids of the PZT particles are arranged perpendicular to the surface of the composite film [35]. It may be difficult to accept this specification because it is most probable that the PZT powder was randomly distributed in the polymer matrix. However, it may be possible that the particles would be in a certain contact form, which resembles the above specification as a result of the film processing. The actual distribution of the particles remains to be investigated and this is the subject of further research.

5.4.4. Dielectric properties of PZT4/PVDF, PZT5/PVDF, $BaTiO_3$/PVDF and PZT4/PP composites

Figs.5.35, 5.36 and 5.37 show the behaviour of ε' and ε'' in PZT4/PVDF(50/50 Vol.%), PZT5/PVDF(50/50 Vol.%) and $BaTiO_3$/PVDF(40/60 Vol.%) composites as a function of frequency at three different temperatures. Using the value of ε'(PVDF) = 7, ε'(PZT) = 1200 and $\varepsilon'(BaTiO_3)$ = 1700, the calculated values of the permittivities (from Eq.(5.16), with s = 8) for PZT/PVDF and $BaTiO_3$/PVDF composites are about 60 and 42 respectively, which are rather low as compared to that of experimentally observed values (i.e. PZT4/PVDF : ε' = 94, PZT5/PVDF : ε' = 95

and $BaTiO_3$/PVDF : ε' = 71 at 343K ,1 kHz). From Eq.(5.16), the permittivity of the composite is predominantly determined by that of polymer and almost independent of ceramic. Assuming the value of ε'(PVDF) = 12, the calculted values of ε' for the composites appear to be in good agreement with the experimental values. Yamada et al[35] used the value of ε'(PVDF + fluorine elastomer) = 8.9 and obtained a good agreement between the calculated and experimental values of ε' in the PZT/polymer composite especially for composites with high ceramic volume fraction.

Now, assuming the value of s = 8 and the values of ε' for PVDF, PZT and $BaTiO_3$ equal to 7, 1200 and 1700 respectively, the source of uncertainty may lie in the actual volume fraction of the component phases present in the composite samples. Using Eq.(5.16), and the values of ε' for composites from the experimental data (i.e. ε'(PZT/PVDF)$\simeq$95), ε'($BaTiO_3$/PVDF) = 71), the calculated volume fraction of the ceramic phase (taking the above values of s and ε' for the single phase) appear to be 0.64 and 0.55 for PZT/PVDF and $BaTiO_3$/PVDF composites respectively. Indeed, these values of volume fraction are higher than the assumed values of 0.5 for PZT/PVDF and 0.4 for $BaTiO_3$/PVDF composites. However, in this calculation it has been assumed that the ceramic particles are ellipsoidal in shape. It may be possible that the shape factor(s) varies with the composition and the composites. Muralidhar and Pillai [48] found that the value of s = 7 gave a good fit between the calculated and the observed values of permittivities in various compositions of $BaTiO_3$/PVDF

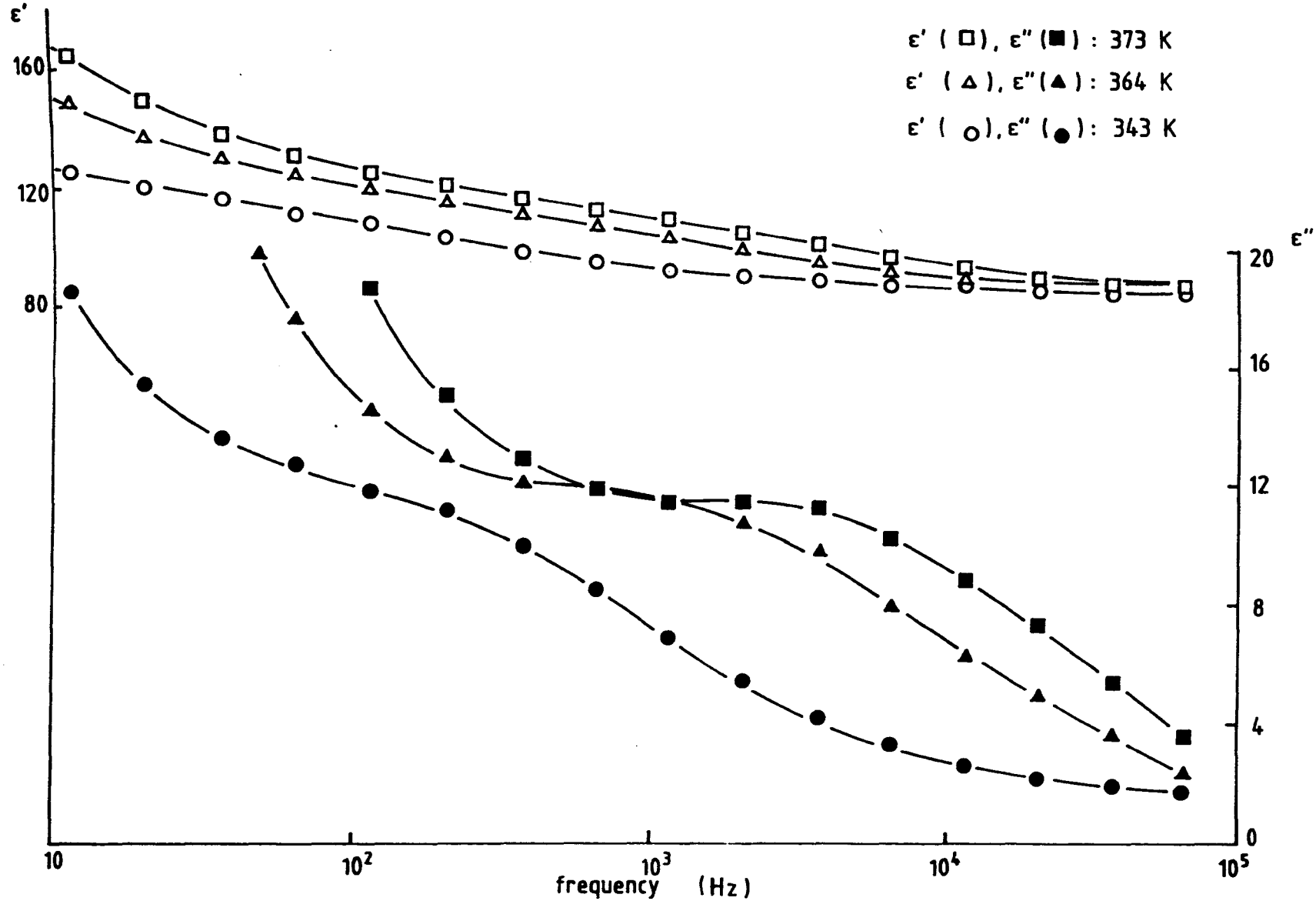

Fig. 5.35. Dielectric behaviour of PZT4 / PVDF(50/50 Vol.%) at different temperatures.

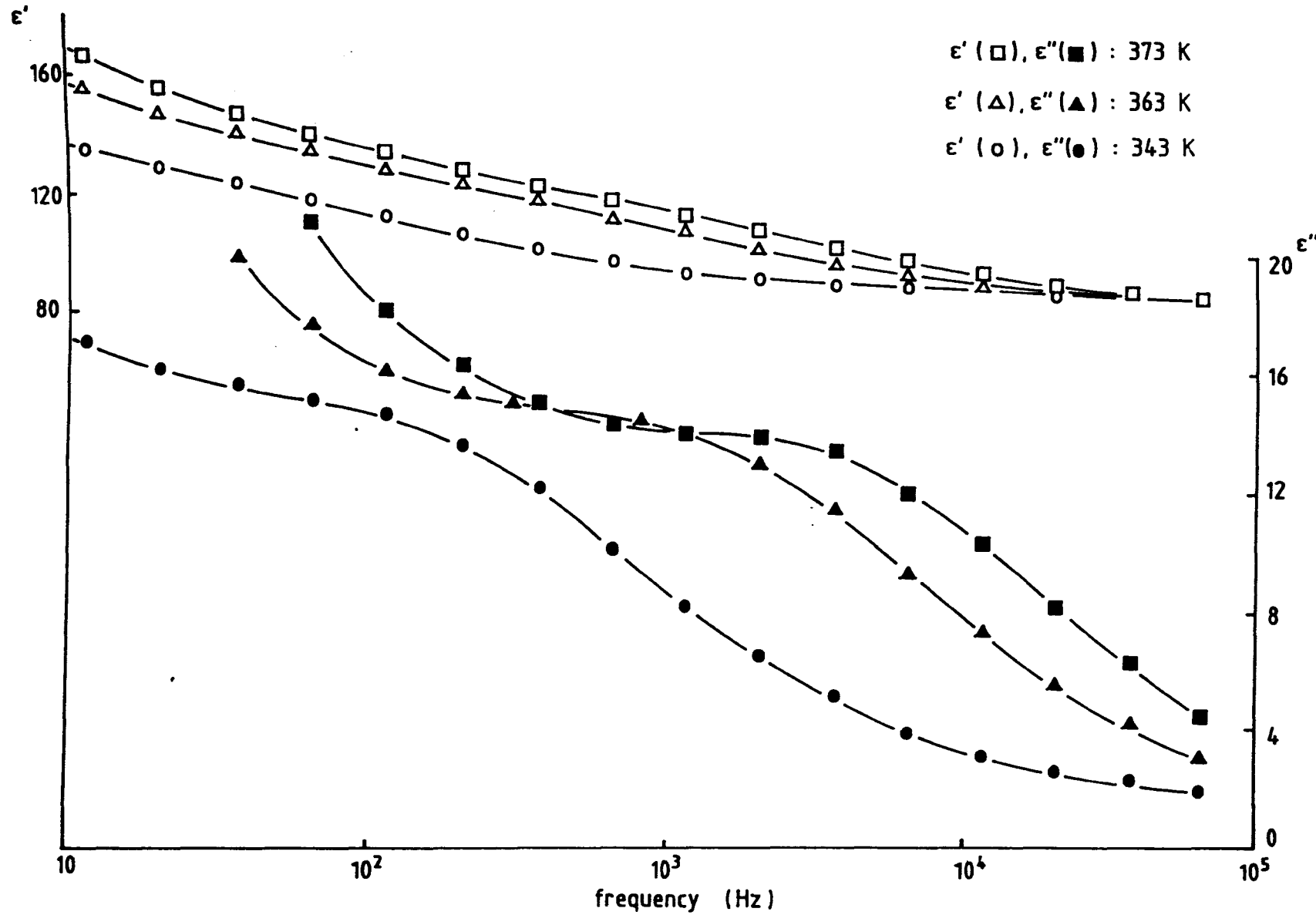

Fig. 5.36. Dielectric behaviour of PZT5/PVDF(50/50 Vol.%) at different temperatures.

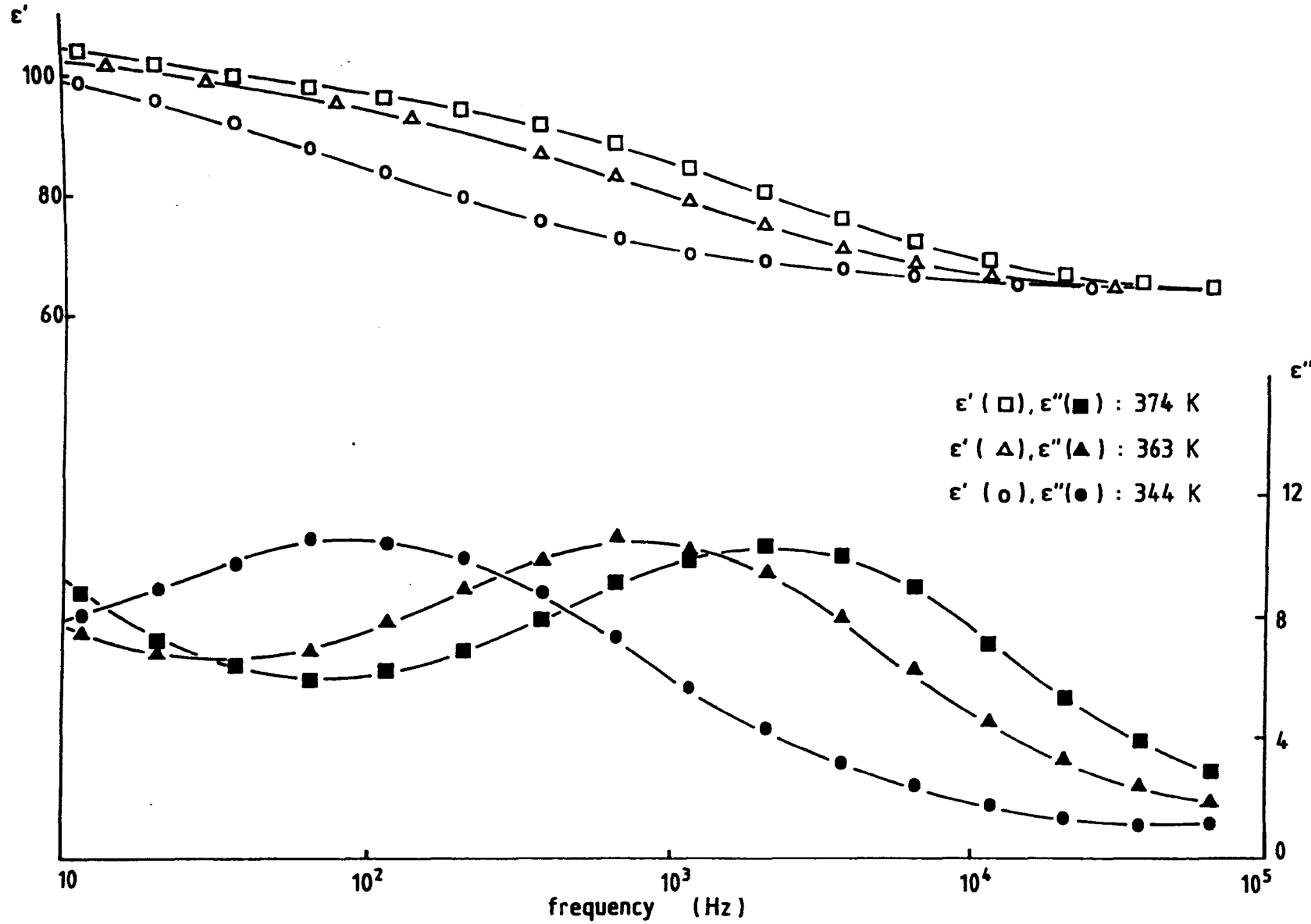

Fig. 5.37. Dielectric behaviour of $BaTiO_3$/PVDF (40/60 Vol.%) at different temperatures.

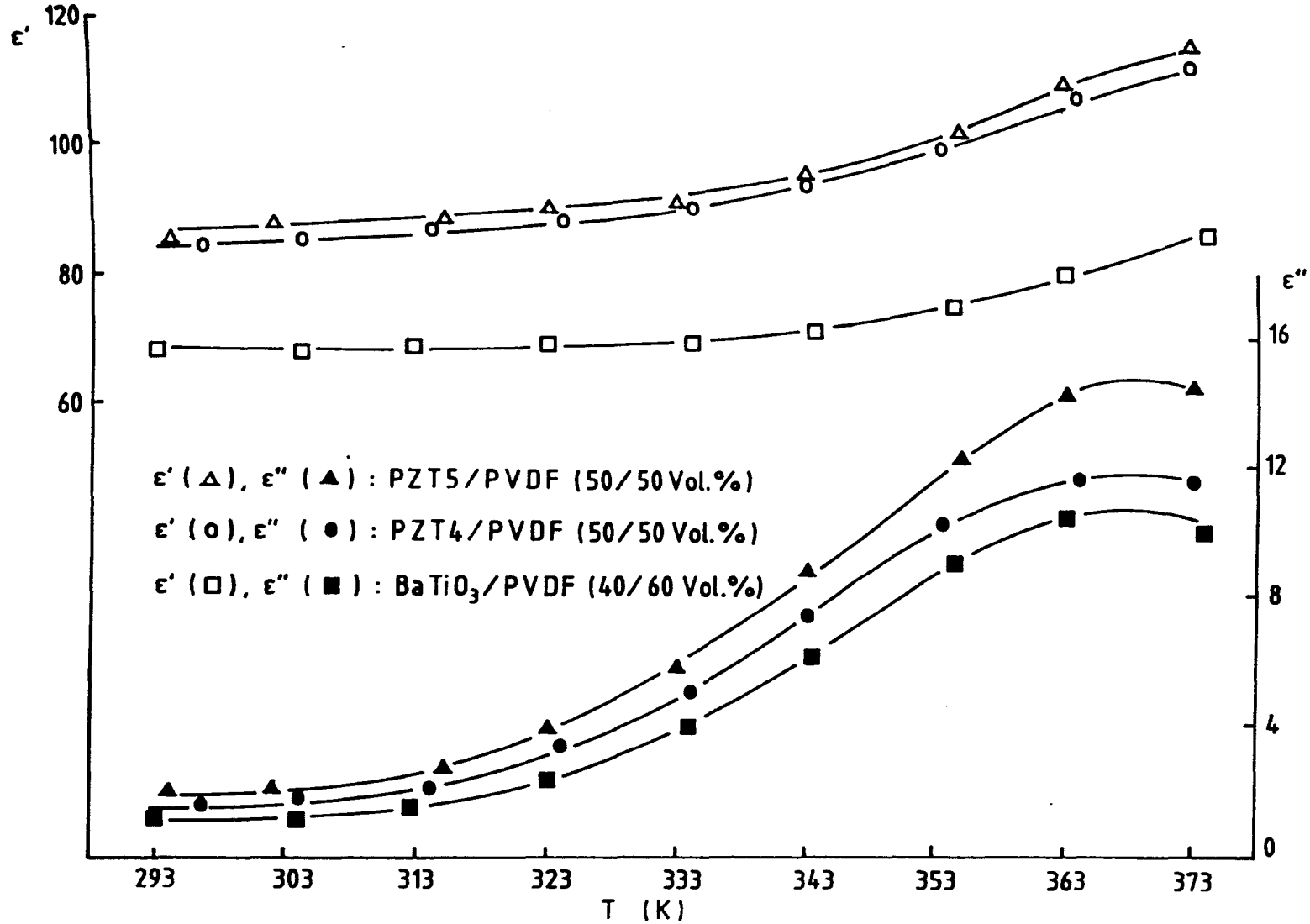

Fig. 5.38. Temperature dependence of dielectric properties in PZT4/PVDF, PZT5/PVDF and $BaTiO_3$/PVDF at 1 kHz.

composites. Obviously, more work may be required to clarify these observations.

All the above composites in the present work show high values of dielectric loss at high temperatures and low frequencies, which may again be attributed to the conduction mechanism in the bulk of the composite as mentioned in the previous section. The dielectric loss process in these composites appear to resemble to that of PVDF polymer, showing α_c-relaxation, and with a significant contribution of ceramic phase particularly at low frequencies and high temperatures (Figs. 5.35-5.38). The dielectric permittivities were found to increase with an increase of temperature in the same manner as that obtained for single phase polymer and ceramic.

Figs.5.39 and 5.40 show the dielectric properties in PZT4/PP(50/50 Vol.%) composite. Using the values of ε'(PP)=2.2, ε'(PZT)=1200, the calculated values of ε' for the composite from Eq.(5.16)(with s=8) is 19.3, which is higher as compared to the observed values (i.e. ε'=16.2 at 343K and 1 kHz). The dielectric loss peak which appear in the frequency range of 10-40 Hz at 373K and 383K may be related to the polymer phase. However, similar relaxation had not been reported for PP in the literature. Work et al[49] and Buckingham and Reddish[50] observed the dielectric loss peak in PP at $\sim 10^4$-10^5 Hz at room temperature. It is not clear whether the dielectric loss process were due to dipolar impurities and oxidation products or due to segmental motion of polymer chain [49,50]. Anderson and Mc Call[51] showed the presence of several loss peaks in PP in the frequency range 50-10^8 Hz at 298K. They have

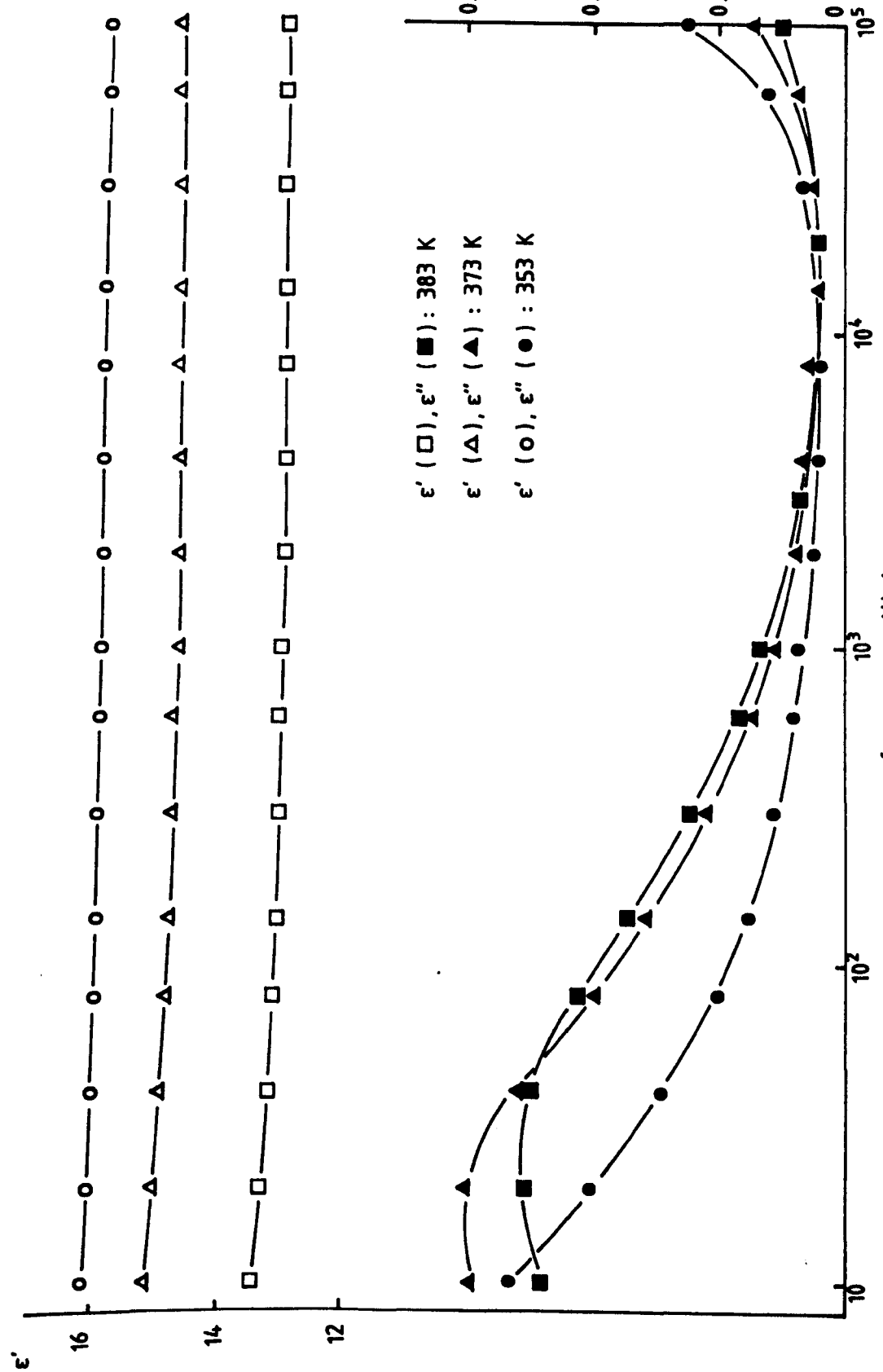

Fig. 5.39. Dielectric behaviour of PZT 4 / PP (50 / 50 Vol.%) at different temperatures.

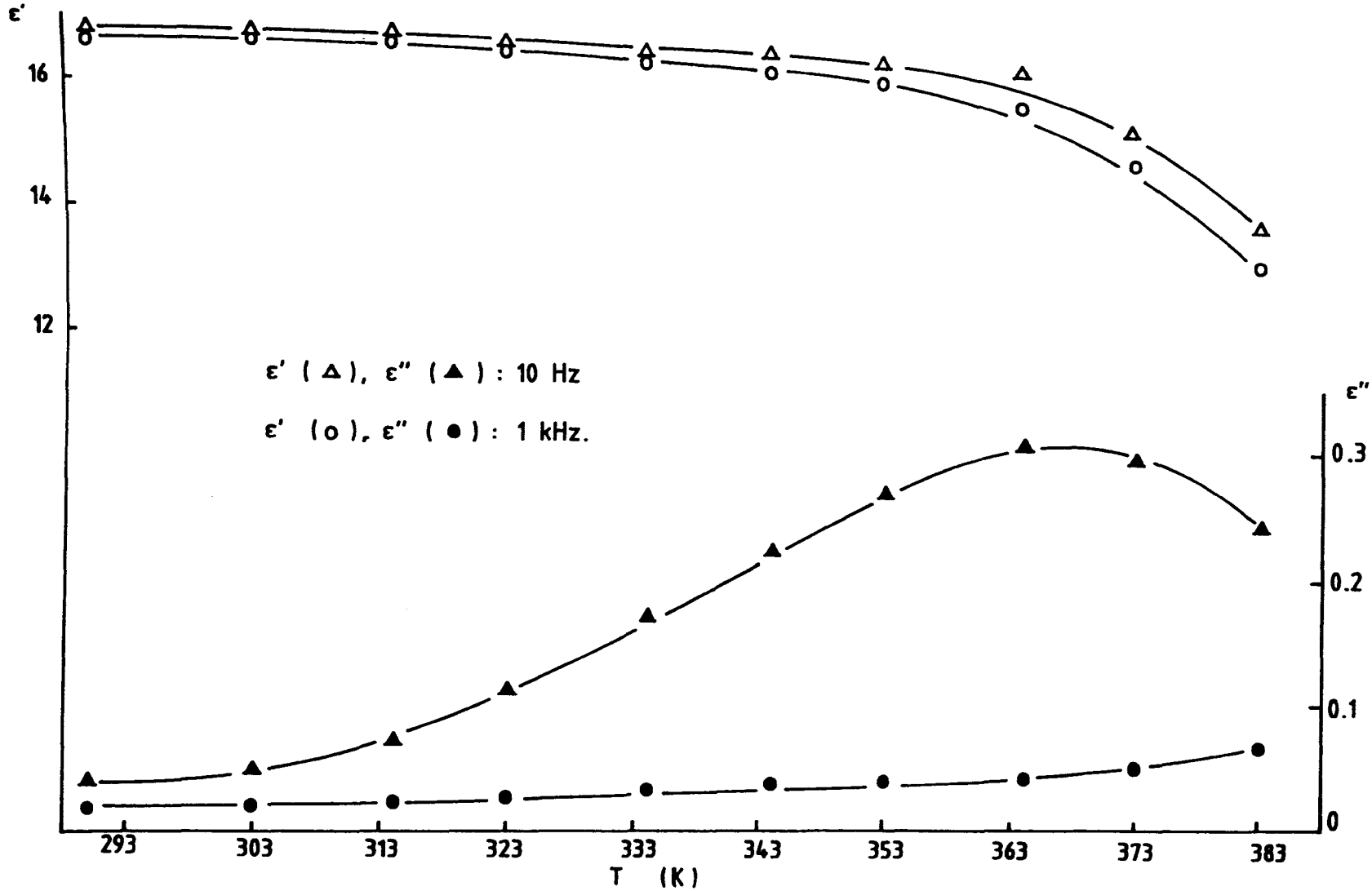

Fig. 5.40. Temperature dependence of dielectric properties in PZT4/PP (50/50 Vol.%)at 10Hz and 1kHz.

attributed the observed loss peaks as due to the presence of several polar species, each in low concentration. It remains that the loss peak at and around room temperature has not been observed in PZT4/PP composite in the present frequency range. Instead, the high temperature loss peak has been observed at around 10-40 Hz between 373K and 383K. The origin of this loss peak remains to be identified. The observed decrease of ε' with temperature in PZT4/PP composite (Fig.5.40) may be related to the polymer phase, which also shows the decrease in ε' with the increase of temperature [8].

CHAPTER 6

PYROELECTRIC PROPERTIES IN CERAMIC-POLYMER COMPOSITES

6.1. Introduction

Several single crystal and polycrystalline materials can develop a change in electric polarization (electric moment per unit volume) when they are subjected to a temperature change. This change in polarization may be detected by observing the flow of charge to and from the surfaces on change of temperature. Such phenomena is known as pyroelectric effect which can be found in 10 polar classes out of 32 crystal classes of materials in accordance to the symmetry system classification [1].

A continuous effort has been made in recent years to search for an improved pyroelectric materials which may be used for calorimetry and thermal detectors of radiation. The usefulness of such pyroelectric detectors may lie in its simplicity of construction and operation, its room temperature

operation (or any other convenient temperature) and the fact that they do not require an external bias field. Furthermore, pyroelectric detectors have another advantage over detectors such as photovoltaic and photoconductive devices, in that they can be operated over a wide spectral range, i.e. from the far infrared through visible radiation down to X-rays.

One of the routes towards optimizing the devices performance is by studying the materials properties and its characteristics in relation to its figures of merit requirement for various operations. Indeed, the usefulness of materials for specific applications does not necessarily depend on the figure of merit alone. Various considerations such as mechanical strength, chemical stability, aging behaviour, matching properties, power handling ability and ease of processing and fabrication may have to be taken into account. Triglycine sulphate (TGS) crystals have been the most extensively studied material for detector applications due to its high pyroelectric figure of merit. However, they are relatively fragile, water soluble and have a fairly low thermal conductivity so that they are unable to withstand high incident power densities. PZT ceramics also have high pyroelectric coefficient and comparable figure of merit with respect to TGS for high current responsivity; however its brittleness and the difficulty to be formed in a complex shape may restrict their use in some applications.

A considerable amount of research has been made into pyroelectric polymers particularly PVDF and its copolymers due to their ease of fabrication in any desired shape or size.

With the improvement in the manufacturing process of the polymer film (stretching and poling) [2], which improves the uniformity and pyroelectric properties, these new exciting materials have been exploited in various applications as thermal detector devices [2,3].

Pyroelectric PVDF also has a disadvantage when compared with ceramics. It is subjected to thermal depolarization when heated above 373 K for long periods, thus limiting its prolonged use above this temperature. However, in view of some useful properties (ease of fabrication, available in thin films, lightness, flexible etc), these polymers are of some considerable importance, and indeed PVDF may be a good choice for certain applications which can not be fulfilled with pyroelectric ceramics.

Ceramic/polymer composites have been found to exhibit piezoelectric properties superior to those exhibited by single phase piezoelectric materials [4,5]. A considerable amount of work have been produced concerning the piezoelectric properties of various ceramic/polymer composites [6-10] and their applications [10,11]. However, the pyroelectric properties of these composites have not been so much investigated. In this chapter, the results obtained on the pyroelectric properties of several ceramic/polymer composites will be presented.

6.2. Related Theory and Evidence of Pyroelectricity

The interpretation of the pyroelectric phenomenon in a material can not be made in isolation from its piezoelectric and other properties. In thermodynamic treatments of dielectric crystals and by choosing the elements of the stress tensor X_i , the components of the electric field E_i and the temperature T as the independent variables, the dependent variables are then the elements of the strain tensor x_i , the electric displacement D_i and the entropy S [1]. The appropriate thermodynamic potential is then the Gibbs free energy (G) (see chapter 3), which in its differential form, is given by Eq.(3.8e) :

$$dG = -S\ dT - x_i\ dX_i - D_i\ dE_i$$

which gives the equations of state as :

$$-S = (\partial G/\partial T)_{X,E} \quad , \quad -x_i = (\partial G/\partial X_i)_{E,T} \quad ,$$

$$\text{and} \qquad -D_i = (\partial G/\partial E_i)_{T,X} \tag{6.1}$$

The linear differential form of the variable D_i can be written as :

$$dD_i = (\partial D_i/\partial X_j)_{E,T}\ dX_j + (\partial D_i/\partial E_j)_{X,T}\ dE_j + (\partial D_i/\partial T)_{X,E}\ dT$$

(6.2)

from which it may be observed that the piezoelectric coefficient is defined by the first term and the permittivity by the second term. The third term in Eq.(6.2) defines the pyroelectric coefficient at constant stress and constant electric field.

From Eq.(6.1) and (6.2), the piezoelectric strain coefficient d may be written as :

$$d_{ij} = \left(\frac{\partial^2 G(T,X,E)}{\partial E_i \, \partial X_j} \right)_T$$

or $$d_{ij} = (\partial D_i/\partial X_j)_{E,T} = (\partial x_j/\partial E_i)_{X,T} \qquad (6.3)$$

and the pyroelectric coefficient p :

$$p_i = \left(\frac{\partial^2 G(T,X,E)}{\partial E_i \, \partial T} \right)_X$$

or $$p_i = (\partial D_i/\partial T)_{E,X} = (\partial S/\partial E_i)_{T,X} \qquad (6.4)$$

where i=1,2,3 and j=1,...,6 (the number of tensor components for strain and stress has been reduced to six terms, as defined by Lines and Glass [1]). The other piezoelectric coefficients (e_{ij}, h_{ij}, g_{ij}) can be derived in a similar way by choosing the appropriate independent variables from the conjugate pairs of (T,S), (X_i, x_i) and (E_i, D_i).

The displacement D_i can also be written as (from Eq.(4.7)) :

$$D_i = \varepsilon_o E_i + P_i \tag{6.5}$$

where P_i is the sum of the field-induced polarization and the spontaneous polarization. Under conditions of zero electric field (E=0) (i.e., with the sample is in short-circuited) and at constant stress, the displacement reduces to : $D_i = P_i$, giving the pyroelectric coefficient p (along the pyroelectric axis) :

$$\begin{aligned} p = (\partial P/\partial T)_X &= \left(\frac{\partial (Q/A)}{\partial T} \right)_X \\ &= \frac{1}{A}\left(\frac{\partial Q}{\partial T}\right)_X - \frac{Q}{A^2}\left(\frac{\partial A}{\partial T}\right)_X \end{aligned} \tag{6.6}$$

where P is the temperature-dependent polarization (or charge per unit area, P=Q/A) and A the electrode area. If it is assumed that there is a total dipole moment M in the sample between the electrodes, then : Q=AP=M/L (L is thickness of the sample), giving :

$$\begin{aligned} p &= \frac{1}{A}\frac{\partial \left(ML^{-1}\right)_X}{\partial T} \\ &= \frac{1}{AL}\left(\frac{\partial M}{\partial T}\right)_X - \frac{M}{AL^2}\left(\frac{\partial L}{\partial T}\right)_X \\ &= \frac{1}{AL}\left(\frac{\partial M}{\partial T}\right)_X - \frac{P}{L}\frac{\partial L}{\partial T} \end{aligned}$$

$$= \frac{1}{AL}\left(\frac{\partial M}{\partial T}\right)_X - P\theta \qquad (6.7)$$

where $\theta = (1/L)(\partial L/\partial T)$ is the thermal expansion coefficient in the thickness direction. It may be observed that Eq.(6.7) consists of contributions from dipolar (first term) and dimensional (second term).

It may noted that the stress-induced polarization contributes to the pyroelectricity (Eqs.(6.2),(6.4),(6.5)). Thus pyroelectricity may also be separated into two parts, primary and secondary. Primary pyroelectricity refers to the pyroelectricity which is observed when the sample dimensions are clamped while the temperature is changed. Secondary pyroelectricity is the additional contribution (due to the variation of piezoelectrically-induced polarization with temperature) observed when the sample is subsequently allowed to expand (or to relax to its equilibrium dimensions) freely. Hence the total pyroelectric coefficient p may be written in terms of primary and secondary components (p_P and p_S) as :

$$p = p_P + p_S \qquad (6.8)$$

Since all measurements are made under short-circuit conditions, the charges $\pm Q$ which appear on the electrodes as a result of polarization, may be treated as a function of strain x_j and temperature only. Thus :

$$dQ = (\partial Q/\partial T)_x \, dT + (\partial Q/\partial x_j)_T \, dx_j \qquad (6.9)$$

From Eq.(6.6) and (6.9), assuming $\partial A/\partial T = 0$,

$$p = \frac{1}{A}\left(\frac{\partial Q}{\partial T}\right)_X = \frac{1}{A}\left(\frac{\partial Q}{\partial T}\right)_x + \frac{1}{A}\left(\frac{\partial Q}{\partial x_j}\right)_T \left(\frac{\partial x_j}{\partial T}\right)_X \qquad (6.10)$$

which may be written as :

$$p = p_P + e_{ij}\,\theta_j = p_P + p_S \qquad (6.11)$$

where $e_{ij} = (1/A)(\partial Q/\partial x_j)_T$ is piezoelectric stress coefficient and $\theta_j = (\partial x_j/\partial T)_X$ is thermal expansion coefficient.

The value of p_P may be determined by measuring the pyroelectric coefficient of the sample under the constrained (clamped) condition to prevent any contribution from thermal expansion. However it is to be noted that the perfectly clamped condition can scarcely be achieved in practice. Under the constrained condition (e.g. in j-direction), the pyroelectric coefficient p_C may be written as:

$$p_C = p_P + e_{ij}\theta_{jC} \qquad (6.12)$$

where subscript C denotes the constrained condition and θ_{jC} the 'constrained' expansion coefficient in the j-direction. It may be seen that experimental determination of e_{ij}, θ_{jC} and p_C leads to a value for p_P $(=(1/A)(\partial Q/\partial T)_x)$ (from Eq.(6.12)) and p_S (from Eq.(6.8)). The value of p_S may also be estimated

directly from the thermal expansion and piezoelectric properties according to :

$$p_S = e_{ij}\,\theta_j = c_{jk}\,d_{ik}\,\theta_j \qquad (6.13)$$

where $$d_{ik} = (\partial D_i/\partial X_k)_T = (1/A)\,(\partial Q/\partial X_k)_T \qquad k= 1,2,...6$$

and $$e_{ij} = c_{jk}\,d_{ik} \qquad k= 1,2,....6$$

where c_{jk} is the elastic stiffness.

In principle, in order to understand pyroelectricity in any material, one has to consider the various mechanisms of the polarization (as due to space charges, dipoles or surface charges). The study of the pyroelectric behaviour as a function of temperature may help to understand the origins of pyroelectricity. In the following section, theoretical models describing the mechanisms by which pyroelectricity can occur will be given.

6.2.1. Theoretical models of pyroelectricity

Spontaneous polarization (P_s) in pyroelectric materials may originated from dipolar charges (oriented dipoles) or trapped (embedded) space charges. These polarization charges

may already present in the materials or induced by the application of strong electric fields (poling).

In ionic crystals (e.g. $BaTiO_3$, PZT), the displacement of ions (as the temperature is altered) relative to the geometric centre of unit cells would confer polarity on the lattice and thus give rise to an electrical dipole moment (or spontaneous polarization). In semicrystalline polymer such as PVDF , dipole moment can arise from the alignment of polarized covalent bonds (carbon-fluorine bond) which can be achieved by a combination of mechanical force and electric fields. This is referred to as a dipolar model. The electric dipole moment can also arise from embedded charges in inhomogenous material- referred as space charge model. The following will give further treatment on these two models.

Assuming the condition in which the dipoles are free to rotate (this is a much simplified model), the polarization induced by an application of an electric field (E_p) at temperature T is given by (see chapter 4, Eq.(4.6)):

$$P(T) = [\varepsilon'(T) - 1]\, \varepsilon_o E_p \qquad (6.14)$$

where $\varepsilon'(T)$ is the relative permittivity of the dielectric medium at temperature T. This polarization is maintained throughout the poling while the temperature is lowered to temperature T'(where the dipoles become immobile), after which the field is subsequently removed. The estimate of frozen-in polarization after removal of the poling field may be written as [1] :

$$P_o(T) = [\ \varepsilon'(T) - \varepsilon'(T')\ ]\ \varepsilon_o E_p \qquad (6.15)$$

where $\varepsilon'(T')$ is the relative permittivity at temperature T'. Eq.(6.15) provides a useful means in estimating the frozen dipole polarization in a dielectric. Obviously, the practical polarization value is different from $P_o(T)$ of Eq.(6.15) due to the fact that dipole rotation in solid dielectric is not free but subjected to interaction with the surrounding medium.

Mopsik and Broadhurst [12] used a more detailed model in calculating the frozen-in dipole polarization. The model (see Fig.6.1) was based on a dipole with a permanent moment m_o and polarizability α, situated at the centre of a spherical cavity (Onsager cavity). The cavity is embedded in a medium with a relative dielectric permittivity ε' and with a net electrical polarization P in the direction of applied field. It is assumed that any space charge that is trapped in the medium will be confined to the surface of the dielectric. Using the general expression of polarization (dipole moment per unit volume) as defined by :

$$P = N_o \langle m \rangle . \qquad (6.16)$$

where N_o is the number of dipoles per unit volume and $\langle m \rangle$ the mean effective dipole moment in the direction of P, the frozen-in dipole polarization present at zero applied field is calculated to be [12] :

$$P_o = (\varepsilon_\infty + 2) N_o m_o \langle \cos\theta \rangle / 3 \qquad (6.17)$$

where ε_∞ is the high frequency relative permittivity related to the polarizability (α) through the Clausius-Mossotti-Lorentz relationship (Eq.(3.48)). θ is the average angle of oriented dipole moment with respect to the direction of overall polarization P and $\langle \cos\theta \rangle$ is the average of unit component of dipole moment in the direction of P.

The differentiation of Eq.(6.17) and by the use of Eq.(6.6)(neglecting the change in electroded area) will lead to the pyroelectric coefficient p as [12,13] :

$$p = P_o \beta [\varepsilon_\infty/3 + \phi^2/(2\beta T) + \gamma \phi^2] \qquad (6.18)$$

where $\beta = (v)^{-1} dv/dT$ is the volume coefficient of thermal expansion, $\gamma = -v\, w^{-1} dw/dv$ is a Gruneisen constant for the dipole torsional frequency w, T is temperature and ϕ^2 is the mean squared torsional displacement of the dipole fluctuations. It can be seen from Eq.(6.18) that volume expansion (through parameter β) plays quite a significant role in this model. An additional contribution comes from the dipole fluctuation as a result of a temperature change. The magnitude of the effective dipole moment depends on the vibration amplitude of dipole, which in turn depends on temperature and strain. The parameter ϕ is difficult to be measured because of the large number of vibrational modes and molecular conformations contributing [13]. However the model seemed to give good agreement between theoretical and

experimental data on piezo- and pyroelectric properties of PVC by assuming the value of $\langle\phi^2\rangle^{1/2} = 14^o$ [12] and it may be noted that the X-Ray measurements on polyethylene molecules give the value of $\langle\phi^2\rangle^{1/2} = 10^o$ [14] which may justify the choice of ϕ value. Thus the model may account in a reasonable manner for the electret properties due to frozen-in dipolar orientation in a polar molecule materials.

Trapped spaced charge may be introduced in the process of forming an electret as a consequence of charge injection from the electrodes or due to bulk charge separation. An antisymmetrical distribution of such charges coupled with inhomogenous deformations, may contribute to the piezo- and pyroelectricity of the sample [15,16]. Wada and Hayakawa [16] considered a point charge q embedded in a bulk of electroded polymer film as shown in Fig.6.2. If the electrodes on both surfaces of the film are short-circuited, the induced charges q_1 and q_2 will appear on the electrodes, which may be written as :

$$q_1 = - q\, C_1 /(C_1 + C_2) \qquad (6.19)$$

$$q_2 = - q\, C_2 /(C_1 + C_2) \qquad (6.20)$$

where C_1 and C_2 are the respective capacitances between the electrodes and the plane passing q parallel to the electrodes. Eq.(6.19) and (6.20) indicate that if the ratio C_1/C_2 changes with applied strain and with a change of temperature, then q_1 and q_2 will change accordingly, resulting in a pyroelectric

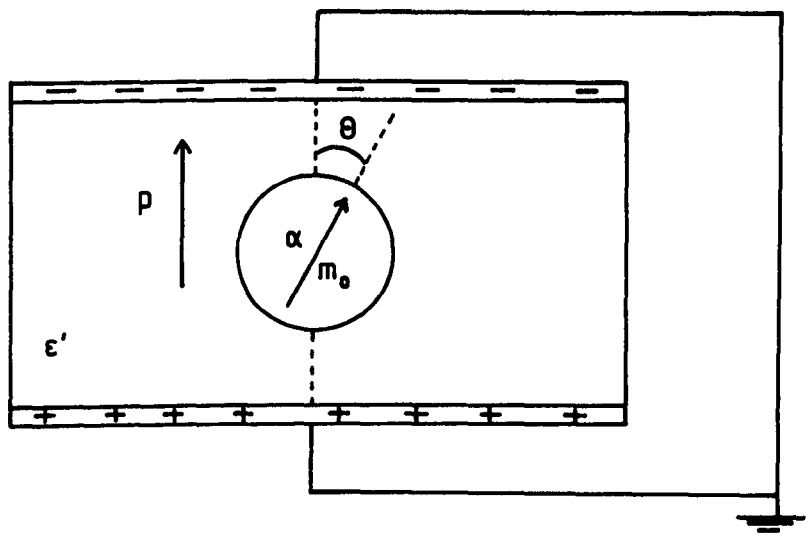

Fig. 6.1. A model of representative dipole inside a spherical cavity of a typical electret.

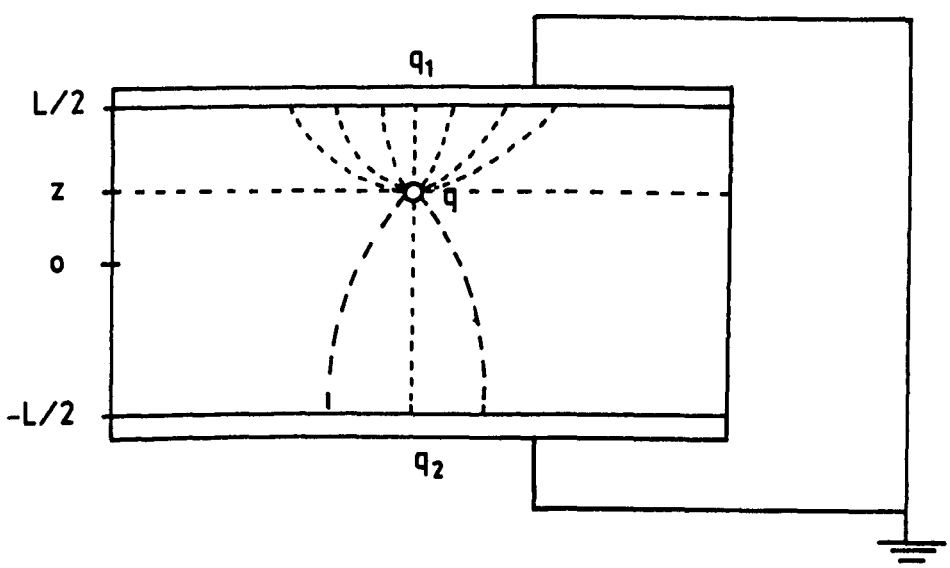

Fig. 6.2. Point charge q embedded in an electroded dielectric film of thickness L.

current in the external circuit. Such variation of C_1/C_2 with temperature is possible in heterogenous material where there is a gradient in various properties across the film. In particular, the heterogeneity may appear in the linear coeeficient of thermal expansion (η) and the temperature coefficient of permittivity ($\lambda = - d\,\varepsilon/dT$). By considering the electric displacement in the vertical direction (z-direction), the pyroelectric coefficient is deduced as[16,17]:

$$p = \langle p_i \rangle + \left\langle \left(\left(\frac{\lambda}{\varepsilon} - \eta \right) - \left\langle \frac{\lambda}{\varepsilon} - \eta \right\rangle \right) \left(\int_{-L/2}^{z} \rho \, dz \right) \right\rangle \qquad (6.21)$$

where $\eta(z) = - m\, \partial x/\partial T$ (m : Poisson's ratio, x applied strain, T temperature), ε is permittivity and ρ is the total charge density in the material (the sum of the real charge and the polarization charge). The angular brackets denote the average,

$$\text{e.g.} \quad \langle A(z) \rangle = \int_{-L/2}^{L/2} A \, \frac{dz}{\varepsilon} \Big/ \int_{-L/2}^{L/2} \frac{dz}{\varepsilon}$$

The first term in Eq.(6.21) provides a measure of intrinsic pyroelectricity which arise from internal strain in which the charges move out of the plane as a function of strain. This is different from the macroscopic displacement of the ion in the material. The second term in Eq.(6.21) within the braces however is caused by sample heterogeneity . Thus it may reasonably be concluded that pyroelectric properties may be induced, not only in the material with spontaneous

polarization but also in non-polar materials in which factors of heterogeneity of the material properties and the asymmetrical charge distribution are contributed. Salomon et al [18], however, have estimated that the contribution of space charge to the total pyroelectricity in PVDF polymer is relatively small (several orders of magnitude smaller than the measured value).

6.2.2. Pyroelectricity in polymers

Based on the model discussed above, it is possible to state that the requirements for large pyroelectricity in polymers are as follows :

(1) the presence of molecular dipoles with high electric moment and concentration.

(2) the dipoles have to be preferentially aligned by a suitable process.

(3) the need to stabilize dipole alignment (locking-in process).

Indeed, to evaluate this conditions for a particular polymer requires considerable data on the molecular and bulk structure and their properties.

Polyvinyl chloride (PVC) is an example of an amorphous polymer which shows relatively high piezo- and pyroelectricity when poled at a high temperature [12,19]. It has a polar repeat unit with an effective dipole moment of 3.6×10^{-30} C m (1.1 D) [20]. Mopsik and Broadhurst [12] showed that the

dipole polarization model provides a good agreement with the observed value of piezo- and pyroelectric properties of PVC. A study on pyroelectric behaviour of semicrystalline nylon 11 [21] reveals qualitatively that dipole orientation in the crystalline regions is responsible for the observed pyroelectric effect. It may be interesting to note that the reported value of pyroelectric coefficient for these polymers are comparable (4×10^{-6} C m^{-2} K^{-1} for PVC and 5×10^{-6} C m^{-2} K^{-1} for nylon 11 at room temperature [17]) even though their microscopic structures are different. Indeed the values quoted may be representative, as it is greatly dependent on the preparation conditions of the sample.

The process of space charge injection leading to a pyroelectric effect has been shown in an experiment carried out by Crosnier et al [22] on polypropylene (PP) film (typical value of pyroelectric coefficient : 2×10^{-8} C m^{-2} K^{-1} at room temperature). They have attributed the observed pyroelectric behaviour of corona-charged PP electret as due to : (1) the injected charges which are trapped in noncentrosymmetrical sites in the sample, and (11) the dipole orientation caused by the electric field created by the space charge. The dipoles can be either created during the injection process or are of intrinsic nature in the material [22]. However, since the material only posses a small dipole moment [23,24] and the fact that the nature of its absorption current at high fields and high temperatures may be described as due to hopping mechanism through localized states [25], it may be suggested that the pyroelectric effect is largely due to the trapped

space charges.

Polyvinyl fluoride (PVF) is another semicrystalline polymer which shows pyroelectric effect under a suitable treatments [26-28]. By measuring the responsivity of the material in response to a modulated black body radiation, Cohen et al [26] estimated the pyroelectric coefficient to be 2×10^{-5} C m^{-2} K^{-1} at room temperature, which is in good agreement with those reported by Phelan et al [27] who used the dynamic method [29] to estimate the coefficient. Cohen et al [26] attributed the observed pyroelectric behaviour as due to dipole orientation. Stephens et al [30], in an attempt to synthesize polymeric materials of high pyroelectric efficiency for use in pyroelectric vidicons, have found that laser-evaporated PVF film ($\simeq 5$ μm thickness) gives higher pyroelectric coefficient (1.8×10^{-5} C m^{-2} K^{-1}) as compared to PVDF film ($\simeq 5$ μm thickness, pyroelectric coefficient = 1.5×10^{-5} C m^{-2} K^{-1}), measured at room temperature and prepared in the same manner. They appear to suggest that laser evaporation modifies the original structure of the material and produces a polymer structure with a higher pyroelectric coefficient. Sirajuddin and Jayarama Reddy [31] measured the pyroelectric coefficient of laser-evaporated PVF with different electrode materials and different electrode polarity. The results show that the structure of Ag/PVF/Al with the silver electrode positively biased with respect to the aluminium, give a high pyroelectric coefficient, typically 1.44×10^{-5} C m^{-2} K^{-1} at 308 K. The variations in thermally stimulated discharge currents and pyroelectric

currents with different electrodes may suggest that there is a possibility of charge injection during the poling process which contributes to the polarization of the films and hence contributes in part to the pyroelectricity in PVF.

Among the pyroelectric polymers, polyvinylidene fluoride (PVDF) has attracted particular attention, due to the large piezoelectric and pyroelectric coefficients which can be induced in this material. Bergman et al [32], Glass et al [33] and Mc Fee et al [34] were the first to report a relatively large pyroelectric coefficient in PVDF. The reported values of pyroelectric coefficient at room temperature were 2.4×10^{-5} C m^{-2} K^{-1} for biaxially oriented films and about 7×10^{-6} C m^{-2} K^{-1} for uniaxially oriented films, which have been poled appropriately [32,34]. Kepler and Anderson[38] reported the values of $p=1.25\times10^{-5}$ $C.m^{-2}.K^{-1}$ and $p=2.7\times10^{-5}$ $C.m^{-2}.K^{-1}$ for biaxially and uniaxially oriented PVDF samples respectively at room temperature. Later, Kepler and Anderson[39] obtained the values of $p=2.8\times10^{-5}$ $C.m^{-2}.K^{-1}$ (biaxially) and $p=2.26\times10^{-5}$ $C.m^{-2}.K^{-1}$ (uniaxially) at room temperature. Das-Gupta and Doughty[56] showed that the induced piezoelectric activity in uniaxially stretched PVDF is enhanced with increasing of stretch ratio up to 7:1. Das-Gupta and Doughty[55,89] also showed that there exists a linear relationship between pyroelectric coefficient(p) and piezoelectric coefficient(d_{31}) of a biaxially stretched PVDF and thus one would expect that the magnitude of p is also subsequently enhanced with uniaxially stretching. In view of these data [55,56,89], it may be surprising to note the relatively high values of p in

biaxially oriented films as compared to that of uniaxially oriented PVDF, as reported by Bergman et al[32], Mc Fee et al[34] and Kepler and Anderson[39]. Indeed, the detail microstructure of these PVDF samples is very complex, and require further treatment for a detailed analysis. Nevertheless, it appears that the induced pyroelectric activity in PVDF may be attributed to the polar nature of the material as a result of stretching and poling by which molecular orientation (dipole orientation) may occur.

Pfister et al [35] studied the pyroelectric behaviour of extruded film of PVDF under various poling treatments. Experimental evidence shows that the reversible polarization (which give rise to pyroelectric effect) involves charge injection from the electrodes in addition to a field-induced structural change (probably the formation of oriented crystalline form I). The result also indicates that the reversible pyroelectric behaviour for short poling times ($\sim$seconds) appears to be predominantly trapping effect, which is associated with the charge injection process.

The temperature dependence of the pyroelectric coefficient in PVDF has been investigated by Burkard and Pfister [36] who found that the pyroelectric coefficient increases gradually from about 1×10^{-6} C m^{-2} K^{-1} at 170 K to about 1×10^{-5} C m^{-2} K^{-1} at 350 K with room temperature value being $\simeq 4 \times 10^{-6}$ C m^{-2} K^{-1}. Murayama and Hashizume [37] have shown that pyroelectricity in Form I PVDF is linearly related to piezoelectricity and suggested that the effect may originate from the same persistent polarization, due to

trapped charges (occuring at the surface or at defect regions of Form I crystallites).

From the above discussion the following observations on pyroelectricity of PVDF may be made :

(a) pyroelectric coefficient increases with increasing poling field and poling temperature (provided it is below the breakdown condition).

(b) pyroelectric coefficient increases with increasing poling time and levels off after approximately 2-3 hours.

(c) pyroelectric behaviour is reproducible for heating cycles below that of poling temperature, but the pyroelectricity decays with annealing at temperatures higher than poling temperature.

(d) pyroelectric effect is found to be dependent on the orientation of the sample.

(e) pyro- and piezoelectric coefficients are linearly correlated with each other.

The above facts suggest that the pyroelectricity in PVDF agrees qualitatively with either dipolar model or trapped charge mechanisms. It may be possible that different mechanisms may dominate for samples with different morphologies and also for different poling conditions.

Kepler and Anderson [38,39] have carried out some measurements in an attempt to determine the various contributions towards the magnitude of the total pyroelectricity in PVDF. Their results indicate that only about half of the total pyroelectricity could be accounted for on the basis of secondary pyroelectricity. The primary

pyroelectricity could not be detected, presumably due to its small contribution in this particular sample. In order to reconcile this problem, they suggested that reversible changes in crystallinity with temperature might account for a significant fraction of the total pyroelectric effect. Support for their hypothesis has been supplied by X-ray measurements of the electric field dependence of crystallinity [40] and by temperature dependent small-angle X-ray scattering [41]. Very recently, Nix et al [42] studied the various contributions of the origin of the pyroelectricity in low-draw ratio, high-draw ratio and voided low-draw Form I PVDF sheets. It was found that for high-draw ratio and voided low-draw sheets, the primary pyroelectricity contributes about 90% of the total pyroelectricity compared with 40% for the nonvoided sample with low-draw ratio (see Table 6.1). The reduction of secondary contribution for samples of high-draw ratio and voided low-draw is attributed to the reduction in transverse stiffness (c_{33}) of the sample. Alternatively, this is due to low thermal stress coefficient ($c_{jk}\,\theta_j$) in these samples as found experimentally [42] which led to small contribution of secondary pyroelectricity (see Eq.(6.13)). The molecular origins of the pyroelectricity are considered on the basis of estimates of the dipolar component of the pyroelectric response of an unclamped (mechanically free) sample. This component is shown to be larger for the nonvoided high-draw ratio sheet than for the other samples (Table 6.1). They suggested that this is associated with a significant difference in reversible changes in the crystallinity of these

Table 6.1. Typical Values of Primary, Secondary, Dipolar, Dimensional and Total Pyroelectricity for Well-poled Form I PVDF Samples.

Sample	Room Temp. Pyro Coeff. (x 10^{-6} C m^{-2} K^{-1})			
	macroscopic component		origin of response	
	primary (at const. strain)	secondary	dipolar (at const. stress)	dimensional
Low-draw ratio	-11.5	-18.0	-20.1	-9.4
	Total : -29.5		-29.5	
High-draw ratio	-28.6	-2.4	-24.9	-6.1
	Total : -31.0		-31.0	
Voided low-draw	-14.0	-4.3	-10.2	-8.1
	Total : -18.3		-18.3	

materials with temperature, in agreement with the observation made by Kepler and Anderson [39] and Kepler et al [40].

Broadhurst et al[43] proposed a dipolar model to account for pyroelectric activity of PVDF(in polar form). Their

results indicate that the largest contribution to the activity of this polymer arises from bulk dimensional changes rather than from changes in molecular dipole moments [note : a change in polarization (dipole moment per unit volume) can occur through changes in either the moment or the volume]. In their model, they assume that the polar crystalline form of PVDF has a permanent dipole moment, that they are polarizable and that they librate (oscillate) about the mean orientation. Employing this model, for negligible amounts of space charge at crystal-amorphous interfaces, they calculated that the dimensional change contributes about 50% of the experimentally observed pyroelectric effect, 27% may arise from the local field effect and 23% from dipole fluctuations. With the presence of space charge (which gives a contribution opposite that of the dipolar crystals), the model only accounts for about 75% of the observed pyroelectric activity in PVDF. It is however reported that the error in the calculated value of pyroelectric effect is probably no better than 20% due to uncertainty in experimental values of parameters being used. Thus, the magnitudes of each contribution are still uncertain in view of such a large error. Mc Kinney et al [44], however, verified quantitatively that pyroelectric activity in biaxially drawn PVDF (containing both Form I and Form II) is consistent with a model of aligned polar crystals, as proposed by Broadhurst et al [43], in which changes in polarization occurs under the influence of thermally induced stress.

Inoue et al[45] introduced a method of measuring the residual charge density on the electrodes sandwitching the

poled film, by which the mechanism of the pyroelectricity of poled Form I PVDF was studied. Their experimental results indicate that the pyroelectricity of Form I PVDF originates from heterocharges (due mainly to dipole orientation in the crystalline region), generated by poling. The mechanism of pyroelectricity is attributed to thermal reversibility of the density of these heterocharges. The result also showed that the use of different electrode materials (Aluminium, gold, copper) does not give any significant difference in the magnitude of the residual charge density and pyroelectric coefficient. This is in contrast with the result of Takahashi et al [46], who found that different electrode materials affect the pyroelectric activity of stretched PVDF film. This effect seems to involve charge injection process as was pointed out by Pfister et al [35].

Evidence of dipole orientation contribution towards the pyroelectric activity in PVDF, which is related to polar crystalline form, may be obtained from structural studies. Tamura et al [47] observed a reversible changes in the polarized infrared absorbance at wavelength 510 cm^{-1} upon repeating poling and depoling process, which they attributed to the dipole orientation in the Form I crystal. Such changes represent the degree of orientation of the polar axis along the electric field which gives rise to the remanent polarization (P_r) and hence the resultant pyroelectricity (temperature change of P_r) of the material. Results of Naegele and Yoon [48] and Furukawa et al [49] which show hysteresis behaviour of piezoelectric activity, also support of the

origin of remanent polarization as due to molecular dipole orientation in the electric field direction.

Kepler et al [50] reported that the alignment of dipoles in Form I PVDF could be established on the basis of X-ray diffraction. The degree of dipole orientation in the Form I PVDF crystal induced by poling was discussed by Kepler and Anderson [51] from their X-ray diffraction data. Das-Gupta and Doughty [52-56] have shown from the X-ray diffraction studies of suitably poled (both conventional and corona poling) film of PVDF that the poling does not only induce dipoles alignment but may also induce a structural change (from nonpolar phase to polar crystal phase) involving a rotation of polar unit cells which aligns the dipole moments towards the direction of the poling field. Their results [54-56] also indicate that the magnitude of pyroelectric coefficient is enhanced in uniaxially high-draw ratio film and also in a film which undergoes a structural conversion process. This suggests that pyroelectric activity may have a significant contribution from a dipolar effect, in which the dipole orientation in the Form I crystal is preferentially aligned. Results of Wang[57] and Wang and West[58] support the above finding but these authors have noted that the Form II to Form I conversion as inferred from X-ray data is only partially complete even at the highest field (1.1×10^9 V m^{-1}) used, indicating that further polarization may be achieved with still higher field strengths. All the above results provide strong evidence for the piezo- and pyroelectricity activity to be originating from the polar crystal phase of PVDF. It is still possible,

however, that not all of the activity is due to oriented dipoles in the polar crystal ; the possibility of space charge contribution may not be neglected, as suggested by several investigations [35,37,59].

Besides PVDF homopolymer, copolymers of vinylidene fluoride (VDF) with trifluoroethylene (TrFE) [60-62] and tetrafluoroethylene (TFE) [63-65] have been extensively studied in relation to their piezo- and pyroelectric properties. These copolymers have excited interest as they crystallize from melt or solution into a phase analogous to Form I of PVDF, removing the requirement for stretching and offering the potential for forming thin detector elements. Baise et al[63] measured the pyroelectric coefficient in a copolymer consisting of 95% VDF and 5% TFE and found values as high as 2.1×10^{-5} C m^{-2} K^{-1} at 303 K. Hicks et al[64] studied a copolymer containing 73% VDF and 27% TFE, in which ferroelectric hysteresis (as obtained using a Sawyer-Tower circuit) has been observed when a high sinusoidal field (8.25×10^{7} V m^{-1}, 60 Hz) was applied to the 25 μm copolymer sample at room temperature. Their results showed that the measured remanent polarization of the copolymer was in good agreement with a calculated value using a frozen dipole model [12] and measured piezoelectric coefficients. The origin of the ferroelectricity was concluded to arise from dipole moment of each monomer (CH_2=CF_2) unit of the polar phase.

Yamada [61] reported that VDF-TrFE (with 55 mole% of VDF) showed a large polarization under poling conditions where the electric field was 2×10^{7} Vm^{-1} , poling temperature 373 K

and poling time was 1 hour, giving one of the largest piezoelectric coefficient (d_{31}=42x10^{-12} C/N) that could be achieved in the polymers. Furukawa et al [62] investigated piezo- and pyroelectric properties in the 52/48, 65/35, and 73/27 mole% copolymers of VDF/TrFE. Their results showed that copolymer with molar composition 52/48 has the largest pyroelectric activity and as the VDF content increases, the pyroelectric activity seems to decrease, which is in good agreement with the result of Yamada [61] for the piezoelectric activity of various composition of VDF/TrFE. The result also indicates that the pyroelectricity is largely due to primary effect which may be due to reversible disordering of dipoles and this primary effect increases with increasing VDF content. Such disordering becomes more significant as the temperature approaches the transition temperature T_c (Curie point) of the respective copolymers. Result of Humphrey et al [66] supports the finding of Yamada [61] and Furukawa et al [62] and suggests that copolymer of VDF/TrFE (70/30) offers the optimal combination of piezoelectric activity and thermal stability. The pyroelectric coefficient for VDF/TrFE (56/44), as measured from the charge response to an infra-red source [67], poled at T_p = 348 K and E_p = 3 x 10^7 V. m^{-1} was 2 x 10^{-5} C m^{-2} K^{-1} at room temperature, which is very much lower than previously reported values for VDF/TrFE (51/49) [60], where p = 9 x 10^{-5} C m^{-2} K^{-1} (at room temperature), sample having been poled at T_p = 343K, E_p = 2 x 10^7 V m^{-1} and t_p = 1 hour. Such a large difference value of p may be due to different samples used and different poling conditions employed. Table 6.2 (obtained

from Humphrey et al [67]) provides a comparison of the dielectric, piezoelectric and pyroelectric properties of PVDF (uniaxially stretched) and the 56/44 and 70/30 VDF/TrFE copolymers. These results indicate that generally piezoelectric coefficients of VDF/TrFE are better than those of PVDF while its pyroelectric coefficient is marginally less interesting. Obviously, more effort is needed to produce a better pyroelectric properties of VDF/TrFE copolymer samples as compared to PVDF despite the fact that copolymer films do not need to be stretched which may be an advantage in some applications.

To summarize, both amorphous and semicrystalline polymers can be made piezo- and pyroelectric by suitable application of a large electric field. The net dipole polarization, which is temperature and pressure dependence, contributes to the significant effect of piezo- and pyroelectric activity of those polymers. Space charges embedded in the polymers may have small contribution towards piezo- and pyroelectric activity. The enhancement of the piezo- and pyroelectric effects is limited mainly by the available dipole moment per unit volume and breakdown strength of the polymers.

Table 6.2. A Comparison of the Properties of PVDF and the VDF/TrFE copolymers.

	PVDF (uniaxially stretched)	VDF/TrFE (56/44)	VDF/TrFE (70/30)
T_c(K)	> melting temp.	343	372
tan δ	0.02	0.021	0.025
ε'	11	11	10.7
d_{31}(pC N^{-1})	17.9	21.4	17.1
d_{32}(pC N^{-1})	0.9	21.4	17.1
d_h (pC N^{-1})	-8.3	-9.2	-6.4
d_{33}(pC N^{-1})	-27.1	-52	-40.6
p(μC $m^{-2}K^{-1}$)	27	20	-
Ageing at 343 K	-	65% loss in d_{31} after 1 hour	23% loss in d_{31} after 24 hours

6.2.3. Pyroelectricity in ferroelectric ceramics

Perls et al [68] were the first to report the pyroelectric behaviour of $BaTiO_3$ ceramic. They have established that the total pyroelectric effect observed in $BaTiO_3$ ceramics is in opposite direction to the secondary pyroelectric effect resulting from volumetric changes. The

primary pyroelectric effect was thus calculated to be twice the secondary pyroelectricity and in the opposite direction. The experiments unfortunately give little information concerning the basic mechanism underlying the observed phenomena. However, it may be stated that an increase in temperature may lead to the decrease of the total polarization by changing the direction or decreasing the magnitude of polarization within individual domains, and that this process is opposed by the increase in polarization (from piezoelectric contribution) as a result of the induced volumetric strain. The upper temperature limit of the pyroelectric sensitivity was observed to be closed to 393 K, which is designated as Curie point (T_C), above which the polarization decreases and hence the sensitivity is reduced. Indeed, the value of T_C depends on the chemical composition and physical perfection of the ceramic [69].

Cook et al [70] measured the pyroelectric coefficient in $BaTiO_3$ ceramic from 213 K to 333 K (on first heating) from which a peak in pyroelectric coefficient was observed at about 289 K. The peak appears to approximately coincide with the transition from orthorhombic to tetragonal symmetry as obtained from the variation of lattice parameters with temperature. The exact transition temperature is dependent on crystallite size, rate of temperature variation, condition of stress and precise purity of the material [69]. Their data [70] also indicate that secondary pyroelectricity in the region of room temperature is small and of opposite direction to the total effect. As a result, the primary pyroelectricity

in $BaTiO_3$ is larger than the total effect. The primary pyroelectricity is assigned to be due to aligned domains and switching of domains by 180° while secondary pyroelectricity originated from 90° domain switching and the secondary effect in aligned domains. Switching of some of the aligned domains by 180° during heating would also contribute to primary pyroelectricity. Due to appreciable energy barrier which must be overcome, it therefore appears likely that most of the 180° domain switching occurs only close to the Curie temperature.

Lead zirconate titanate (PZT) is another perovskite ferroelectric which has received a wide interest for pyroelectric applications. Cook et al [70] showed that the pyroelectric effect of $Pb(Zr_{0.52}Ti_{0.48})O_3$ + 1 wt% Nb_2O_5 is markedly lower upon second heating (see Fig.6.3). Such a large effect during the first heating was partly attributed to an irreversible disorientation by 90° switching of domains which presumably were oriented by 90° switching during poling and this contribution is largely absent on second heating. The calculated secondary pyroelectric effect and the total measured pyroelectric effect for this PZT is shown in Fig.6.4 [70], from which it may be observed that the primary pyroelectricity constitutes the main effect. The primary pyroelectric coefficient may be calculated using Eq.(6.11), which may be rewritten as :

$$p_i = (\partial P_i / \partial T)_x + \sum e_{ij} \theta_j \qquad (6.22)$$

where i and j represent the direction of charge and strain,

and other symbols are as previously defined. The first term is the primary pyroelectricity (p_p) while the second is the secondary pyroelectricity (p_s). For poled ferroelectric ceramics, Eq.(6.22) will be reduced to [70] :

$$p_3 = p_3' + (2\, e_{31}\, \theta_1 + e_{33}\, \theta_3) \qquad (6.23)$$

where p_3' is the primary pyroelectricity. The change in sign of secondary pyroelectricity (see Fig.6.4) is qualitatively assigned to the change in sign of the magnitude of θ_3 [70]. It remains that the pyroelectric effect in PZT is mainly due to primary pyroelectricity, attributed to the domain alignment.

A great deal of compositional modification has been undertaken to improve the properties of PZT for various types of application. Haertling and Land [71] have shown that the addition of lanthanum to the PZT system decreases the Curie temperature which suggests that these ceramics could have large room temperature pyroelectric coefficients. Result of Liu et al [72] showed that the pyroelectric coefficient of hot-pressed lanthanum doped PZT (or PLZT) with 8 at.% doping concentration is 1.7×10^{-3} C m^{-2} K^{-1} at room temperature, which is about 5 times higher than the undoped PZT. The magnitude of the pyroelectric coefficient has also been observed to increase with increasing lanthanum concentration due to the corresponding decrease in the Curie temperature. The high pyroelectric coefficient of modified PZT ceramics coupled with the fact that it can withstand a greater

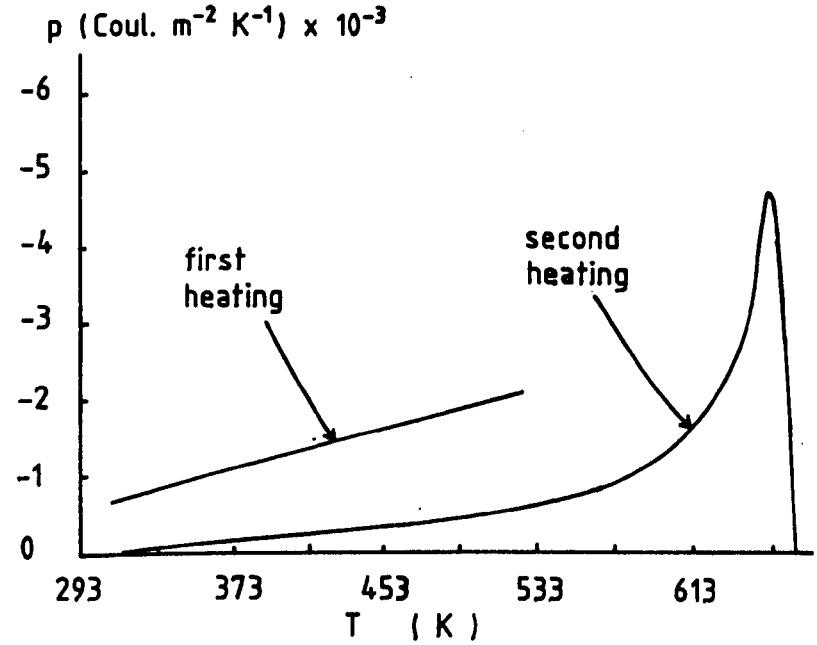

Fig. 6.3. Pyroelectric coefficiant in Pb ($Zr_{0.52}$ $Ti_{0.48}$) O_3 + 1 ωt % Nb_2O_5.

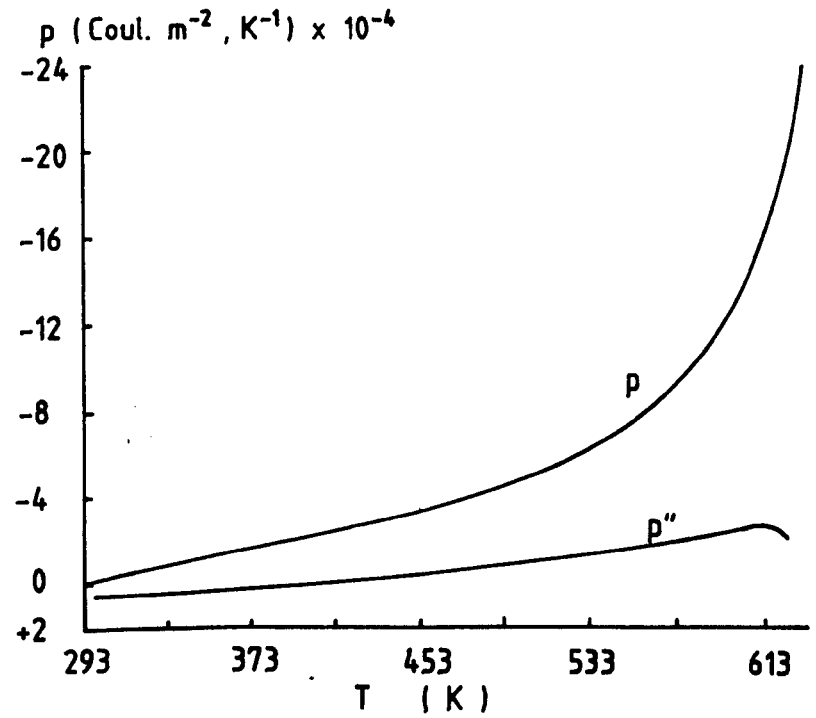

Fig. 6.4. Total and secondary pyroelectric effect in Pb ($Zr_{0.52}$ $Ti_{0.48}$) O_3 + 1 ωt % Nb_2O_5 after heating to 523 K.

radiation power densities, make them an ideal substitute for single crystal lithium tantalate ($LiTaO_3$) which normally operate at lower power densities of radiation [73].

A family of high performance pyroelectric ceramics based on the $PbZrO_3$-$PbTiO_3$-$PbFe_{1/2}Nb_{1/2}O_3$ system has been developed by Whatmore and Bell [74] and Whatmore and Ainger [75]. The dielectric permittivity, loss and dc resistivity of such system were observed to be reduced when doped with appropriate percentage of uranium (in the form of UO_3), allowing the dielectric properties and its resistivity to be controlled over a certain range. Typical pyroelectric coefficient reported for this ceramic system is 3.8×10^{-4} C m^{-2} K^{-1}, dielectric permittivity is 290 (at 1 kHz) and tan $\delta = 2.7 \times 10^{-3}$ at 298 K.

The other family of pyroelectruc ceramics is based on lead titanate ($PbTiO_3$). Pure lead titanate is very difficult to manufacture because of the high lattice strain at the ferroelectric phase transition, which make it mechanically unstable at room temperature [76]. For this reason, a wide range of dopants has been explored to stabilise its properties. The employed dopants include manganese, rare earth ions(e.g. La^{3+}, Nd^{3+}) [77], calcium and $Pb(Co_{1/2}W_{1/2})O_3$ [78]. Ichinose et al [79] studied the pyroelectric properties of $(Pb_{1-x}Ca_x)[(Co_{1/2}W_{1/2})_yTi_{1-y}]O_3$ (modified lead titanate ceramics). In the range of $x = 0.05$ to 0.28 , the pyroelectric coefficient is found to be hardly dependent on the temperature from room temperature to 373 K. As Ca concentration increases, the pyroelectric coefficient increases and reach a value of

4.43×10^{-4} C m^{-2} K^{-1} for x = 0.28. The change in relative permittivity for changes of Ca concentration is markedly small and the typical value of relative permittivity is approximately 200 (at 1 kHz) for x = 0.05 to 0.25 ; above x=0.25, the relative permittivity increases gradually. Such value of p and ε' provide a better pyroelectric properties as compared to PZT. The improvement in the pyroelectric properties is found to be due to the increase of spontaneous polarization (as measured from ferroelectric hysteresis by the Sawyer-Tower method) resulting from the decrease of Curie temperature with the increase in Ca concentration (for x = 0.05 to 0.30) [79].

6.2.4. Pyroelectricity in ceramic-polymer composite

A composite in which ferroelectric ceramic particles are dispersed in a polymer matrix exhibits pyroelectricity when poled [80,81]. The pyroelectric activity in such a system may arise from two possible mechanisms, i.e. (a) pyroelectricity of the ferroelectric, and (b) coupling of the heterogeneity of the composite (such as permittivity and thermal expansion) with polarization of ferroelectrics [17].

Harrison and Liu [80] reported the value of pyroelectric coefficient (measured by the direct method) in the range 0.6 to 2.0×10^{-4} C $m^{-2}K^{-1}$ at 300 K for composites made from a mixture of niobium doped PZT particles and silicone rubber. Although they are lower than that of PZT($p=4.9\times10^{-4}$ C $m^{-2}K^{-1}$),

their voltage pyroelectric figure of merit, p/ε' (see chapter 1 for definition) are 3.6 to 6.5 times higher.

Yamazaki and Kitayama [81] studied the pyroelectric properties of several ceramic-polymer composites, i.e. $PbTiO_3$/PVDF, PZT/PVDF and $PbTiO_3$/PE (with 62% volume of ceramic in each composite) by measuring the pyroelectric signal voltage in response to an incident radiation power from a sinusoidally modulated laser source. The pyroelectric signal voltage in each composite is observed to increase with the increasing radiation power and composite of $PbTiO_3$/PVDF shows about six times as high of the signal as compared to PZT/PVDF, whereas $PbTiO_3$/PE composite shows a much smaller signal. The pyroelectric coefficient of $PbTiO_3$/PVDF composite was calculated to be 1.3×10^{-4} C m^{-2} K^{-1} at room temperature, which is considerably larger than those of any other polymeric materials. It has also been observed that within the range of poling field $0.2\text{-}2 \times 10^{7}$ V m^{-1}, the pyroelectric coefficient is linearly dependent on poling field without any sign of saturation. A higher poling field is needed to properly polarize the composite and hence improve its pyroelectric properties.

Result of Bhalla et al [82] showed that the voltage pyroelectric figure of merit, p/ε' (p was measured by the direct method) in PZT/spurrs composite (spurrs is a complex polymer system, which has been developed primarily for casting and replication), fabricated by replamine technique [83], is about 2.2 times higher than that of PZT at temperature 343K and significantly enhanced at higher temperatures. On the

other hand, PZT/soft polymer(adiprin) composites which have been fabricated by the same technique, show no enhancement of the voltage pyroelectric figure of merit as compared to PZT. In this composite (PZT/adiprin), the polymer used is relatively soft which means that the clamping effect on PZT phase is smaller. Thus, the observed pyroelectric response was thought to be essentially due to the primary part while the composite secondary contribution is negligible [82].

The pyroelectric responses in 1-3 connectivity PZT/polymer composites in which PZT rods are embedded in various polymer matrices (polystyrene, polymethyl methacrylate, nylon 11, polybutylene terephthalate, Hytrel copolymers) have been studied by Galgoci et al [84]. They conclude that at low temperatures, composite secondary pyroelectricity (such as clamping effect) can greatly affect the observed pyroelectricity, while at elevated temperatures, the PZT phase contributes a primary influence of the pyroelectricity. The highest value of the voltage pyroelectric figure of merit, p/ε' (p measured by the direct method) obtained in the composite (PZT/Hytrel copolymers), is only about 1.25 times at 293 K and 2.1 times at 343 K as compared to PZT, which are rather less interesting for pyroelectric materials.

More work is obviously required to produce polymer-ferroelectric composites with a better pyroelectric figure of merit.

6.3. Measurement Technique and Evaluation of Pyroelectric Activity

A variety of techniques may be used for the measurement of the pyroelectric coefficient by measurement of the voltage, charge or current developed during a temperature change of the sample material. These techniques may be classified as : (1) the direct method [85], which is the most accurate method, (11) the dynamic method [86] and (111) the charge integration method [87].

Most of the pyroelectric measurements presented in this thesis were performed using the direct method. Some limited results of pyroelectric response obtained by the dynamic method are also included.

In any measurement, it is necessary to keep the sample under short-circuited condition (zero electric field) so that any conduction current will be essentially eliminated. Under this condition, the pyroelectric coefficient at constant stress is given by Eq.(6.6). However, generally it is not a change in (Q/A) which is measured but rather a change in Q ; thus reported value of pyroelectric coefficients are in error as far as the strict definitions are concerned. From Eq.(6.6), neglecting the change in electroded area, pyroelectric coefficient can be written as :

$$p = (1/A)\left(\partial Q/\partial T\right)_{E=0,X} \qquad (6.24)$$

It has to be noted that unlike inorganic materials, polymers have large thermal expansion coefficient resulting in a significant change of electroded area due to a change of sample temperature.

6.3.1. The direct method

Byer and Roundy [85] developed a direct technique to measure the pyroelectric coefficient which is more straight forward than the dynamic method [86] or the charge integration method [87]. Under a short-circuited condition of a suitably poled sample, a pyroelectric current I produced by a polarization change with temperature may be obtained from Eq.(6.24), such that :

$$p(T) = (1/A)\ I\ /\ (dT/dt) \qquad (6.25)$$

where dT/dt is the rate of temperature change. Therefore if dT/dt is held constant over a wide temperature range, a measurement of the current I (as measured with an appropriate low impedance ammeter) gives a direct plot of pyroelectric coefficient p(T) over that temperature range. The error in dT/dt is the principle factor limiting the accuracy of this method.

The first heating run will normally produces a large depolarization current which will be subsequently reduced on

the following run. The true pyroelectric current (reversible) is established after several successive thermal cycles.

In the present work, the electroded sample film is placed between two contact electrodes in the vacuum system as previously described in chapter 4. Heating is achieved by means of dc supplied heaters and Eurotherm temperature controller (see chapter 4). The poled sample is initially cooled to about 273 K by feeding liquid N_2 into the cold finger of the measurement chamber (see Fig.4.15). Then, by adjusting the dc voltage setting to the heaters and with appropriate Eurotherm setting, it is possible to obtain a linear heating rate (1 degree/minute) in the temperature range from room temperature to 373 K or a bit higher. After the temperature has reached the highest point, the heating is stopped and the sample cooled back to $\sim$273 K using liquid N_2. Heating was then recommenced and this cycle is repeated until little or no change exists between successive current traces. The basic electrical measuring system is as shown in Fig.4.15. With the sample short-circuited, the current is measured by the Keithley 602 electrometer in the fast mode. The fast mode provides the electrometer a lower input impedance and a higher speed of response. The output of the electrometer is then suitably fed to a chart recorder.

6.3.2. The dynamic method

The dynamic method was first described by Chynoweth [86] which involved the measurement of the pyroelectric response of a sample by periodic excitation with modulated incident light.

The absorption of the incident light (white light or laser) would change the polarization of the sample, giving rise to a pyroelectric transient response, whose characteristic is dependent on the intrinsic nature of the material and both electrical and thermal time constants of the system. It is often difficult to determine the absorbed energy with sufficient accuracy for a good determination of the absolute magnitude of pyroelectric coefficient. Consequently, the dynamic method is usually used for the study of the temperature or time variation of polarization and other techniques are used for absolute calibration [1].

A quantitative analysis of the pyroelectric transient response obtained by the dynamic method is given by Simhony and Shaulov [88]. In this analysis, it is assumed that the absorbed radiation causes a spatially uniform small temperature rise ΔT of the sample material. The rise in temperature changes the polarization of the sample, by which the flow of charge will appear in the external circuit connected to the sample (see Fig.6.5). The differential equation describing the process may be equivalently written as:

$$C\,(dV/dt) + (V/R) = I = A\,p\,(dT/dt) \qquad (6.26)$$

where the capacitance C and the resistance R are composed of the sample and amplifier (electrometer) input capacitances and resistances, respectively. V is the pyroelectric voltage developed across the sample and the external load and other symbols are as previously defined. Here, it is assumed that the temperature is well away from the Curie point so that p, as well as the relative permittivity (ε') and the specific heat (c_p) of the material can be considered constant for small ΔT.

For a step radiation, $F(t) = 0$ if $t<0$ and $F(t) = F_o$ if $t>0$ with the boundary condition $V(0) = 0$, Simhony and Shaulov [88] obtained the voltage response as :

$$V(t) = \xi F_o[(1/\tau_E)-(1/\tau_T)]^{-1} [\exp(-t/\tau_T)-\exp(-t/\tau_E)] ,$$

$$\tau_E \neq \tau_T \qquad (6.27)$$

where $\tau_E = RC$: electrical time constant of the system

$\tau_T = C_T/G_T$: thermal time constant of the system

C_T : thermal capacity (= mass x specific heat) of the sample material, $= \rho ALc_p$

G_T : thermal conductance of the coupling between the sample and its ambient (radiative, convective and conductive)

F_o : radiation power absorbed per unit area of the sample at $t>0$

$$\xi = p\, A^2/(C\, C_T)$$

For a dc current I(t) measured across the sample, Eq.(6.27) can also be written as : (note : $X_C >> R$) ,

$$V(t) = I(t)\, R_a = F_o\, p\, A/\,(\rho C\, c_p\, L)$$

$$x\, [(1/\tau_E)-(1/\tau_T)]^{-1}[\exp(-t/\tau_T)-\exp(-t/\tau_E)] \qquad (6.28)$$

Assuming $R_a << R_s$, then $R \simeq R_a$ and letting $\tau_E/\,\tau_T = \theta$, Eq.(6.28) reduces to :

$$I(t) = F_o\, A\, p(T)\, /\, (\rho c_p\, L)$$

$$x\, [1/(1-\theta)][\exp(-t/\tau_T) - \exp(-t/\tau_E)] \qquad (6.29)$$

Eq.(6.29) represents the difference between two exponentials having the same initial value, one decaying with the thermal time constant τ_T and the other decaying with the electrical time constant τ_E (see Fig.6.6). The peak value of the current I_p and the time t_p for the pyroelectric current to reach this value may be obtained by differentiating Eq.(6.29) and equating to zero (for maximum value), which yields :

$$I_p = [F_o\, A\, p(T)/(\rho c_p\, L)]\;\; \theta^{\,\theta/(1-\theta)} \qquad (6.30)$$

and $$t_p = \tau_E \ln \theta/(\theta - 1) \qquad (6.31)$$

These expressions allow the analysis of the pyroelectric response to a step input of radiation. Rewriting Eq.(6.30) as :

$$I_p = K\, p(T) \qquad (6.32)$$

with $$K = [F_o\, A/(\rho c_p L)]\ \theta^{\theta/(1-\theta)}\ , \qquad (6.33)$$

it is possible to evaluate the value of K by measuring p(T) from the direct method and I_p from the dynamic method under the same condition of experiment. This value could be considered as a constant for the same sample material having the same electrode geometry with the incident radiation power and the electrical, the thermal time constants of the system remain unchanged.

In the present work, the radiation power is maintained constant from a well focused white light of tungsten filament which falls on the sample from a suitable distance through a quartz window. The pyroelectric current response on receiving the radiation is measured by the Keithley 602 electrometer in the fast mode , which then suitably fed to a chart recorder to record the trace of current as a function of time.

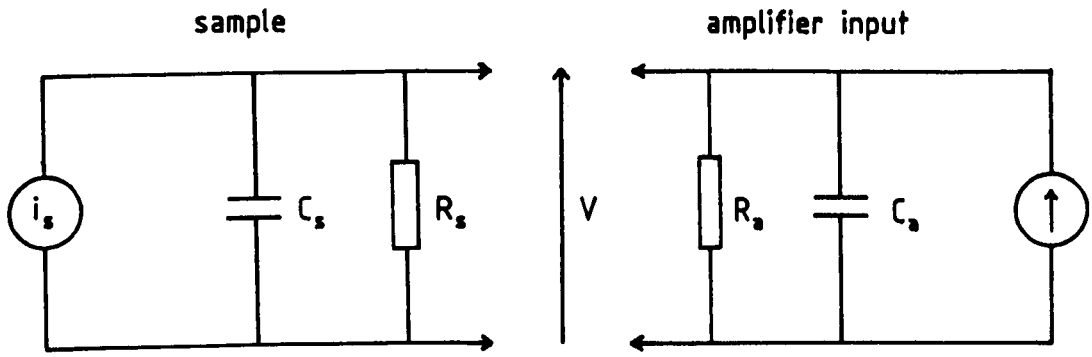

$$\tau_E = RC$$

$$= (R_s \,//\, R_a)(C_s + C_a)$$

Fig. 6.5. Equivalent circuit of sample and electrometer input.

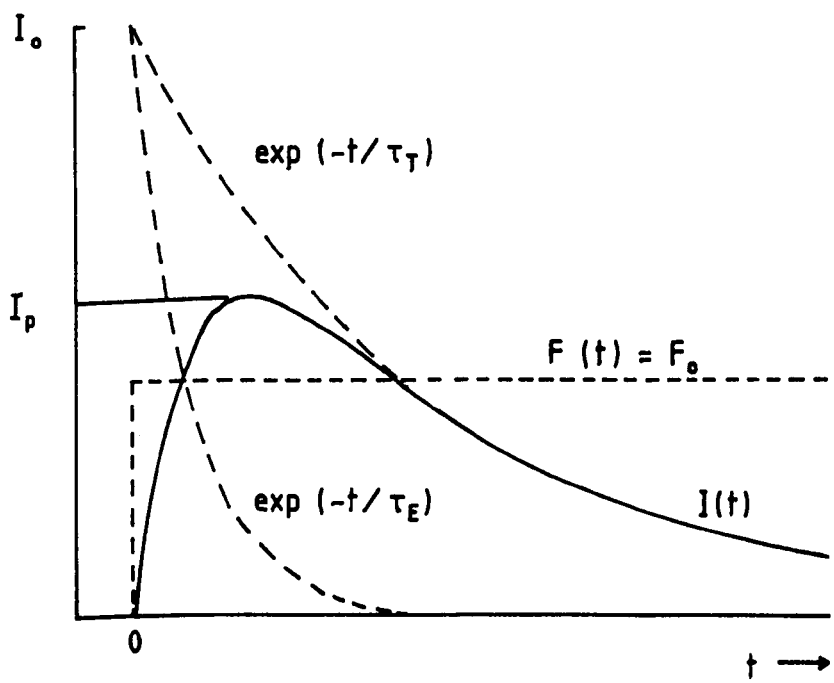

Fig. 6.6. Schematic plot of dynamic pyroelectric current response separated into thermal and electrical components.

6.4. Experimental Results and Discussion

6.4.1. Pyroelectric properties in single phase polymer and ceramic

In the direct method of determining the pyroelectic coefficient, sample is first subjected to the poling process before it is heated at linear rate in a short-circuited condition. The depolarization or the thermally stimulated discharge current (TSDC), produced upon heating, would achieve a reproducible value after several heating runs. Fig.6.7 shows a typical TSDC runs in Form II PVDF film of thickness 130 μm, obtained from Kureha Chemical Company, Japan. The first run shows a high current which subsequently reduced in the following run, as some of space charges, particularly in shallow traps, have been released during the first heating. The third subsequent heating shows no appreciable current reduction, thus establishing a reversible pyroelectric current.

Mizutani et al[90] observed a similar TSDC characteristic in Form II PVDF, in which the observed peaks in the first run of TSDC have been attributed to interfacial polarizations formed by trapped carriers in the surface region of the crystals. It is not the purpose of the present work to study the TSDC behaviour but rather to evaluate the pyroelectric effect.

The pyroelectric coefficient (p) obtained for the above

PVDF film at two poling fields (E_p) may be observed from Fig.6.8, which indicate that the high poling field is needed to achieve high pyroelectric activity in the material. The above observation is in agreement with other workers [35,44,45,89]. The variation of p with temperature was found to be similar to that obtained by Chung et al[91] and Yasuoka and Hirayama [92].

The magnitude and behaviour of the first TSDC run obtained for PVDF(Solef 1008) and VDF-TrFE(Solef 11010) were found to be comparable to that for Kureha PVDF film under the same poling parameters (see Figs.6.7 and 6.9). However, the pyroelectric currents (reversible TSDC) from these films are very much different, particularly at low temperatures (near to room temperature). The low pyroelectric currents obtained in the polymer film prepared in the present work (Solef PVDF and VDF-TrFE) may be related to the low content of the polar crystal form of the materials (see section 6.2.2).

Good reproducibility in the TSDC measurement of VDF-TrFE may be seen in Fig.6.10. It may be noted from this result that the pyroelectric activity may be retained at higher value if the upper temperature limit of the TSDC run was kept below the poling temperature (T_p). The pyroelectric coefficient obtained at two poling fields in PVDF and VDF-TrFE films may be observed from Fig.6.11. At high poling field (E_p= 1.2×10^7 Vm^{-1}) the value of p for VDF-TrFE is about one order of magnitude higher than that of PVDF, at room temperature. The difference in magnitude of p in these materials was observed to be subsequently smaller at higher temperatures. The

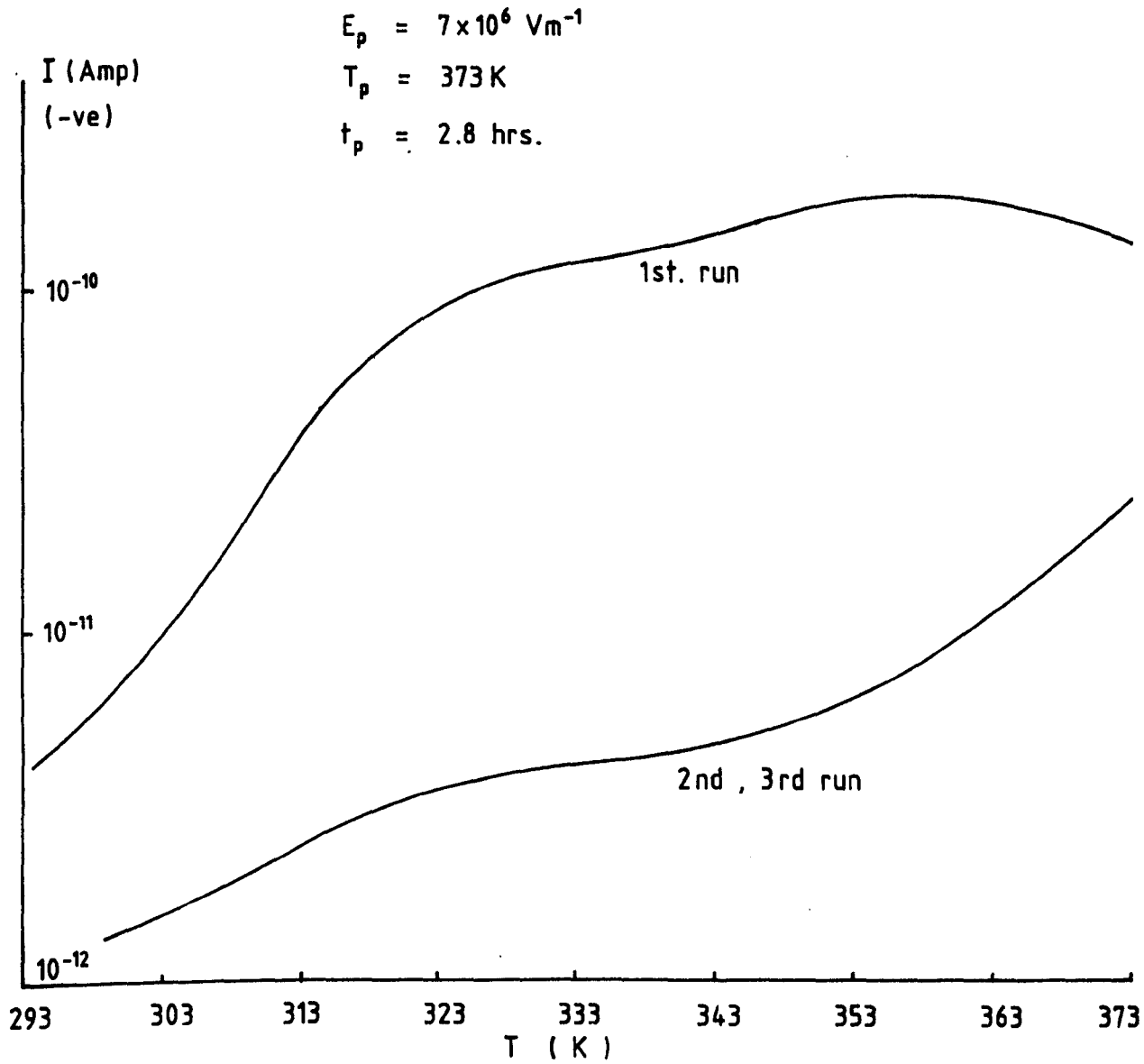

Fig. 6.7. TSDC runs in Kureha PVDF film (Form II).

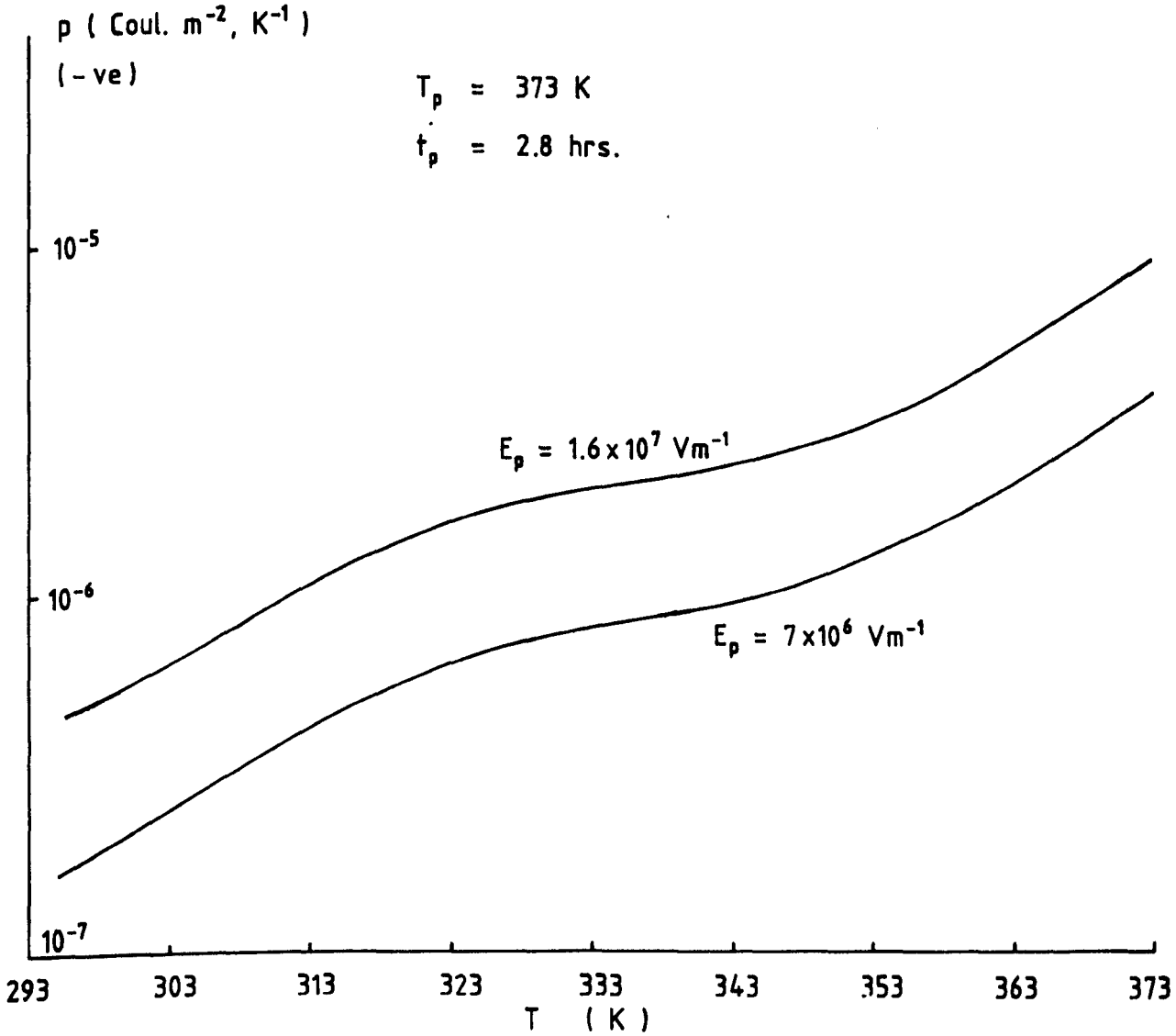

Fig. 6.8. Pyroelectric coefficient in Kureha PVDF film (Form II).

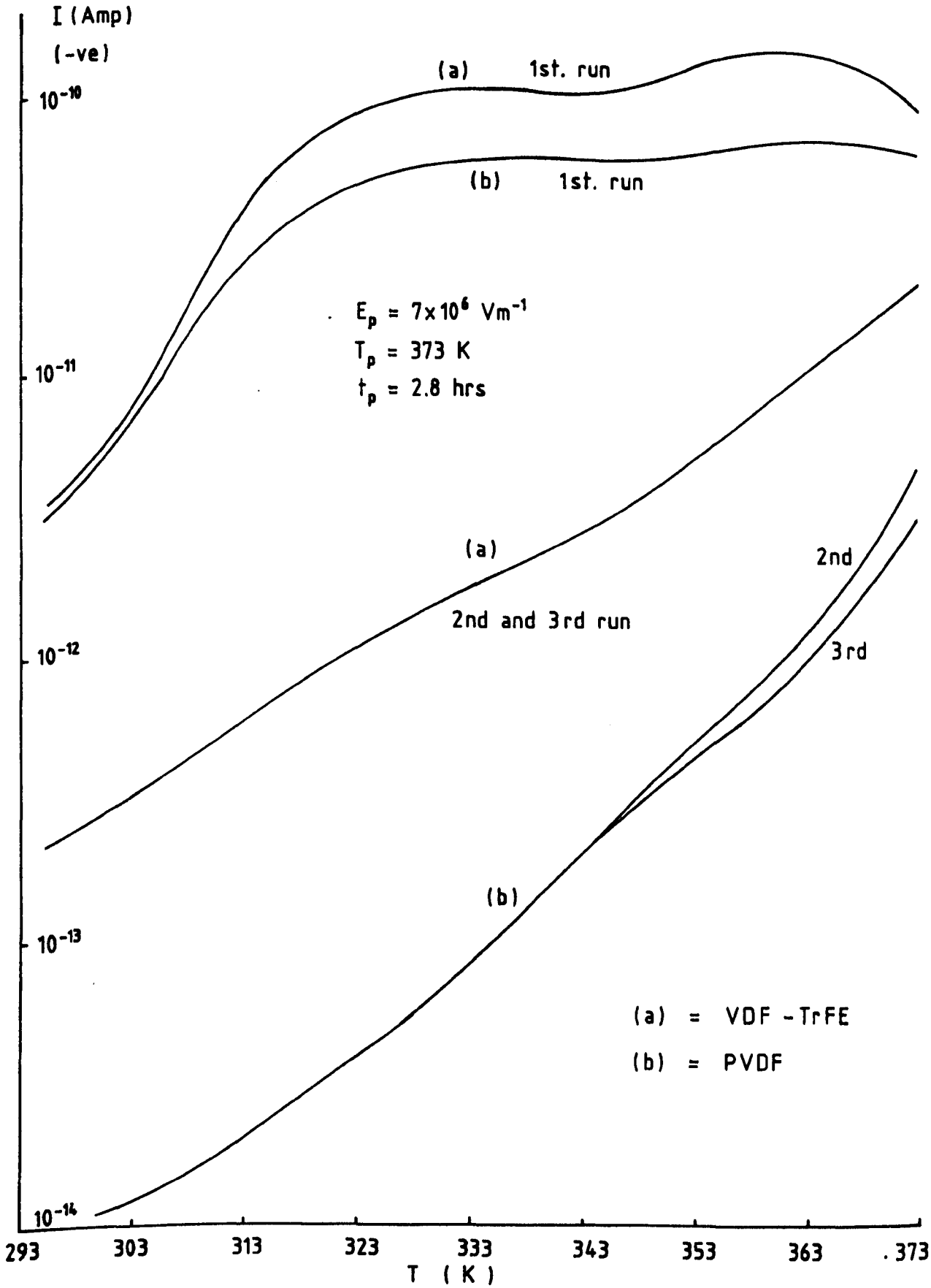

Fig. 6.9. TSDC runs in hot-pressed PVDF (Solef 1008) and VDF-TrFE (Solef 11010).

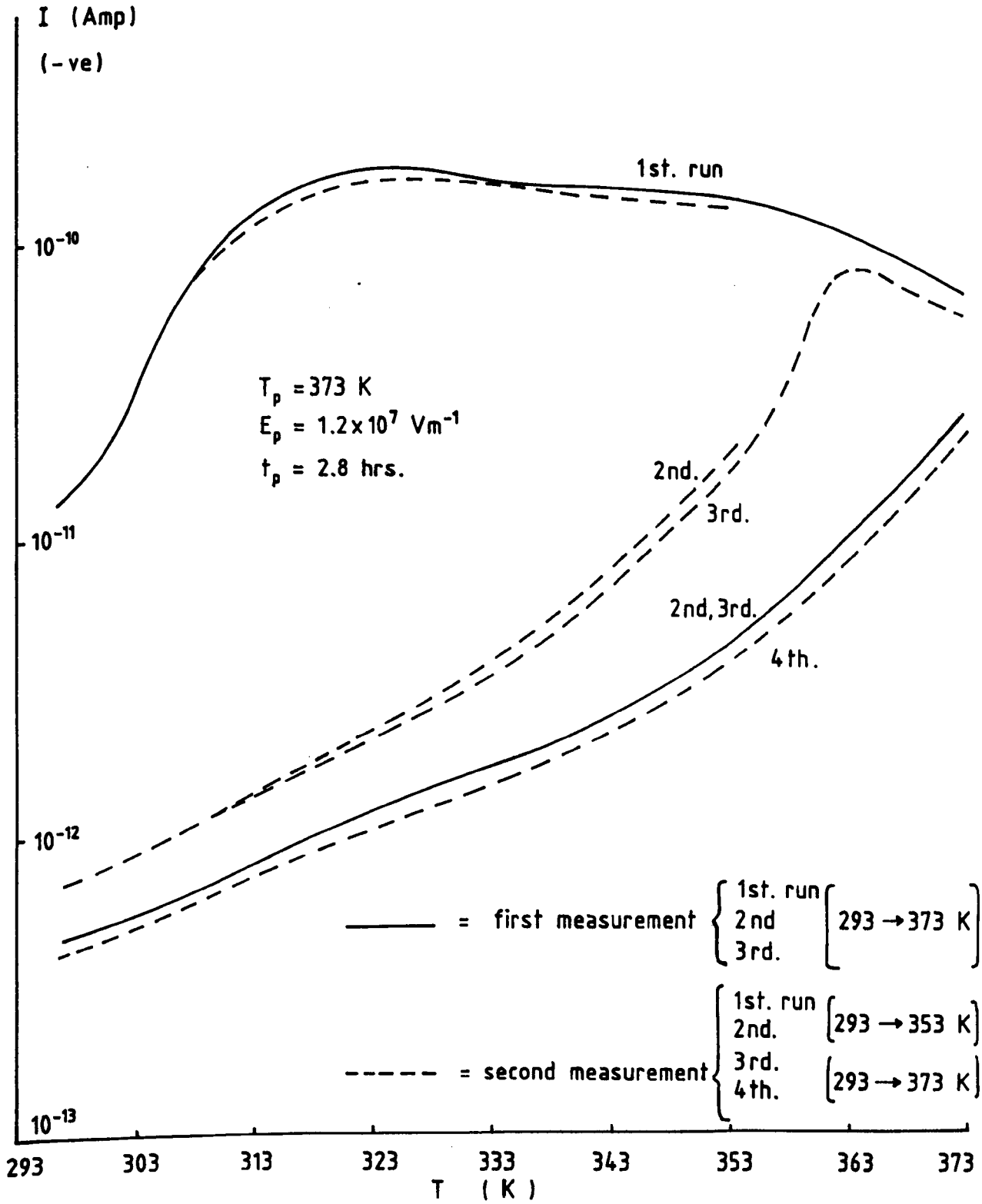

Fig. 6.10. Reproducibility of TSDC runs in VDF-TrFE.

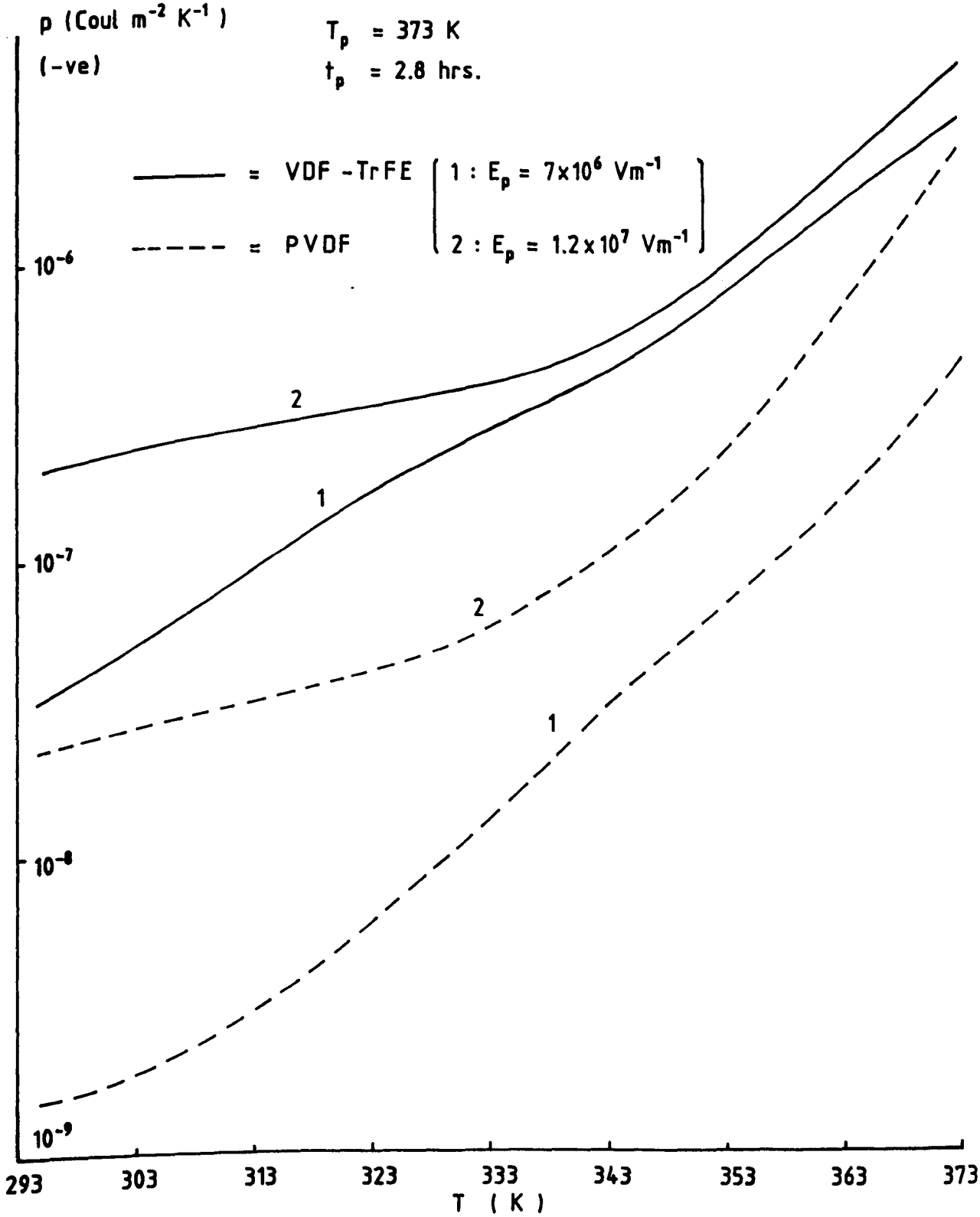

Fig. 6.11. Pyroelectric coefficient in PVDF (Solef 1008) and VDF-TrFE (Solef 11010).

difference in the value of p may again be related to the morphological differences between PVDF and VDF-TrFE. The contribution from the charge injection and trapping in deep localised states towards pyroelectricity may not be ruled out [35,37,59]. In this case, VDF-TrFE may provide more effective trapping than that of PVDF, and hence an enhanced pyroelectric activity.

Typical TSDC runs in PZT5 ceramic may be observed as in Fig.6.12. The large current during the first TSDC run may partly be associated with an irreversible disorientation by 90° switching of domains which presumably were oriented by an equivalent switching during poling [70]. In addition previously localised charges in the bulk of the material may be delocalised during TSDC run, in agreement with previous workers [93,94]. The pyroelectric coefficient as derived from reversible TSDC of this PZT5 sample is given in Fig.6.13 (dashed curve). The magnitude of p at room temperature was found to be $3x10^{-4}$ $C.m^{-2}.K^{-1}$, which is comparable to the values for PZT obtained by other workers [72,73]. The pyroelectric coefficient as a function of temperature for PZT5 sample (sample #2) , obtained from a different batch is also shown in Fig.6.13. It may be observed that although these samples were poled under the same poling parameters (note: the breakdown strength for these samples are found to be $\sim 3x10^{6}$ Vm^{-1} at 373K), the magnitude of p shows a slight difference. This difference may be due to minor changes in impurities and manufacturing process of these samples.

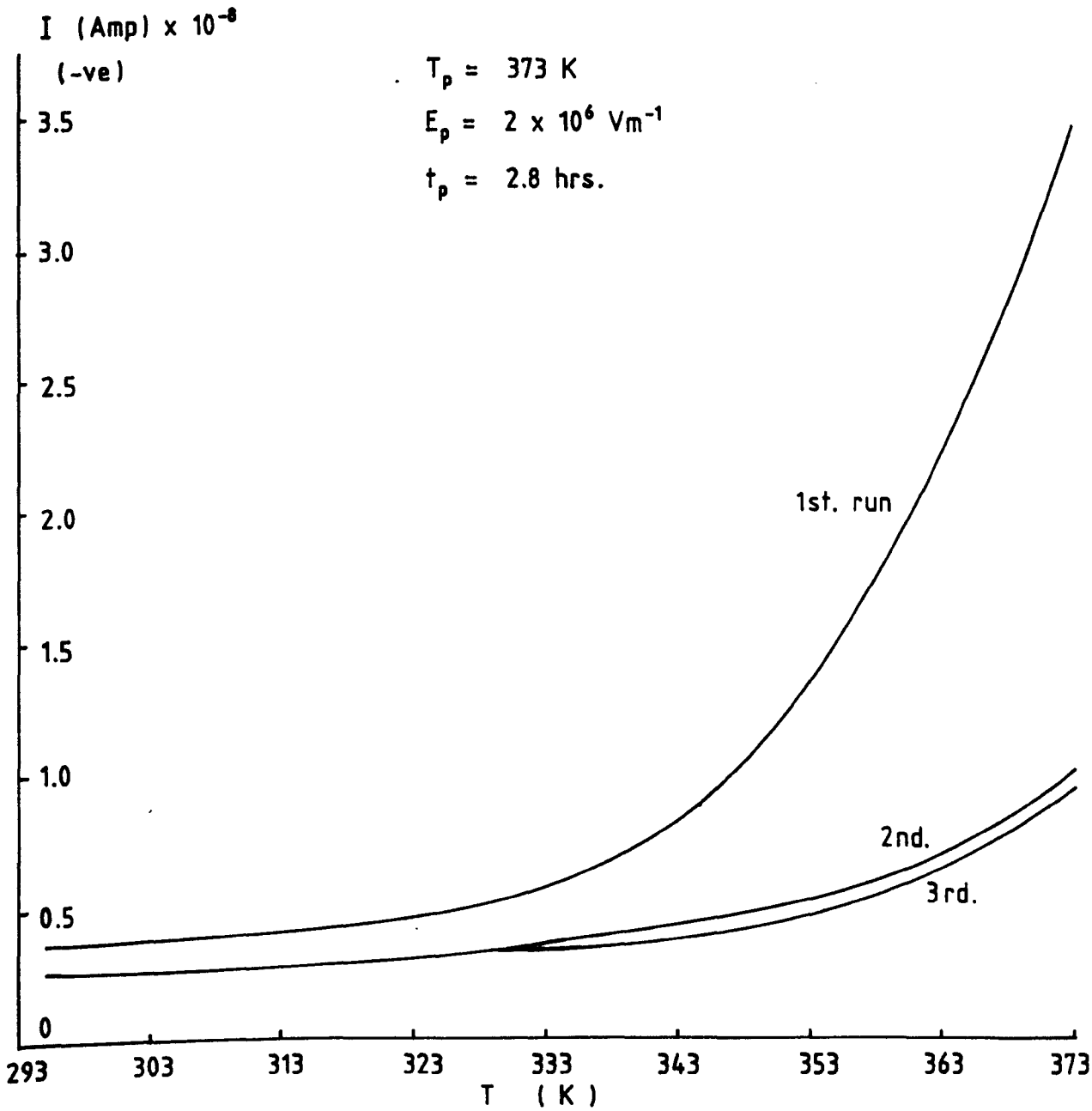

Fig. 6.12. TSDC runs in ferroelectric ceramic PZT 5.

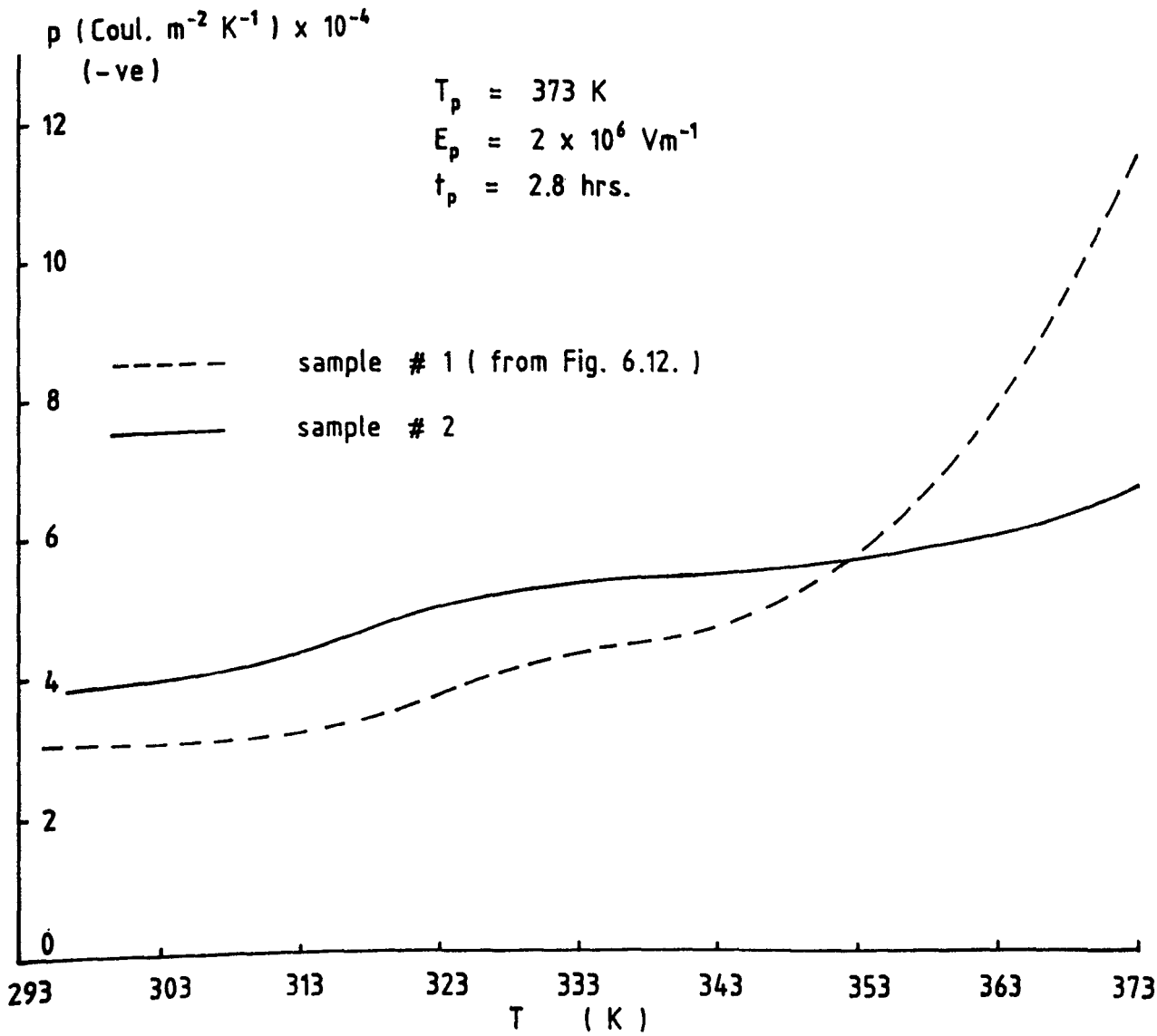

Fig. 6.13, Pyroelectric coefficient in ferroelectric ceramic PZT 5.

6.4.2. Pyroelectric properties in PIEZEL and PZT5/VDF-TrFE composites

Typical TSDC runs in PIEZEL are shown in Fig.6.14. The currents in this composite were observed to lie in between that of polymers and PZT5 ceramic. From the reversible TSDC, the pyroelectric coefficient as a function of temperature was obtained and is shown in Fig.6.15. The values of p obtained from different specimens of PIEZEL was observed to be comparable in magnitude (see Fig.6.15), which may suggest a good uniformity of the PIEZEL composite. The pyroelectric peak current (I_p) obtained from the dynamic method (see section 6.3.2) at different temperatures after 3 cycles of TSDC, is also shown in Fig.6.15. The values of I_p may be observed to increase with an increase of temperature but at a different rate as compared to that of the pyroelectric coefficient obtained by the direct method. Such a difference means that the proportionality between p (direct method) and I_p (dynamic method), i.e. K (Eq.(6.33)), varies with the temperature of measurement. Assuming that the radiation power absorbed by the sample remain the same, then the variation of K with temperature may be due to the thermal properties of the system and further work may be needed to clarify this behaviour (see also the discussion in section 7.3). It may be observed that the behaviour and magnitude of the pyroelectric activity in PIEZEL (Fig.6.14) is comparable to that of PZT5/VDF-TrFE (50/50 Vol.%) composite (Fig.6.16).

Fig.6.16 shows the TSDC behaviour before and after

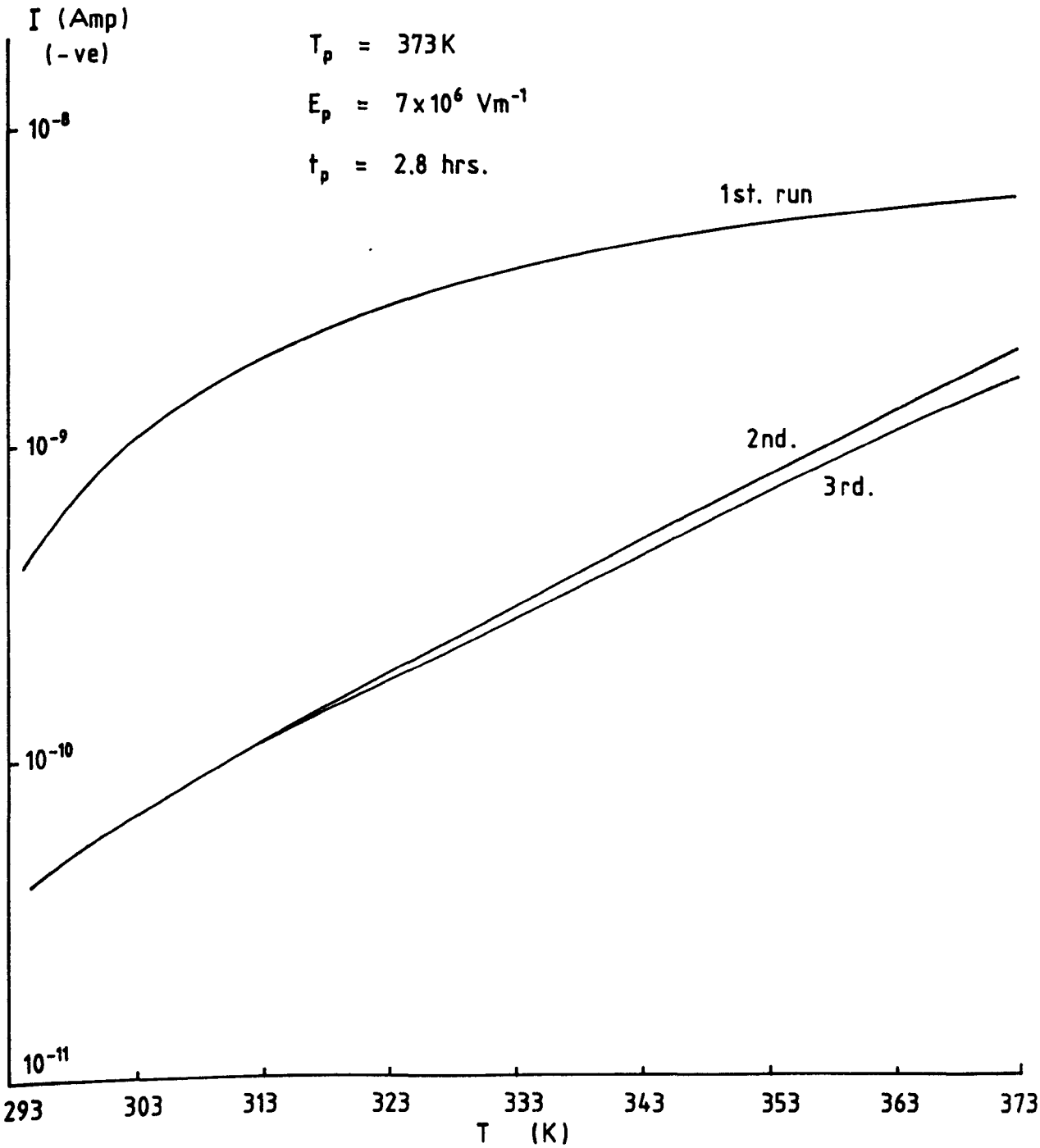

Fig. 6.14. Typical TSDC runs in PIEZEL.

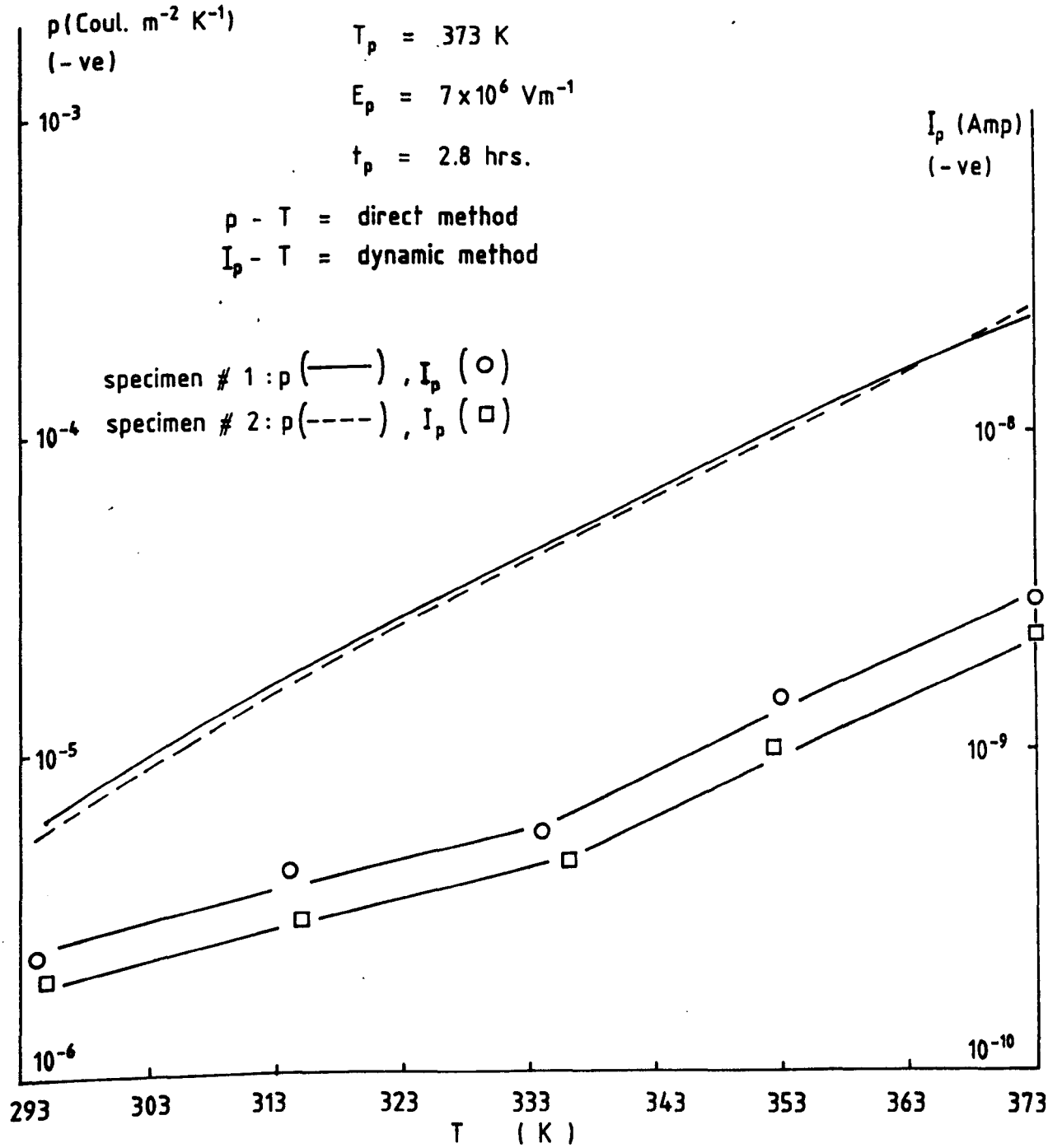

Fig. 6.15. Pyroelectric coefficient and pyroelectric peak current behaviour in PIEZEL.

poling treatment of PZT5/VDF-TrFE (50/50 Vol.%) composite. It may be observed that the TSDC before poling treatment, changes polarity twice, which may possibly arise from delocalisation of charges of opposite polarity with different activation energies. Obviously, the observed TSDC characteristic may depend on the thermal and mechanical history of the sample.

After poling treatment (poling parameters as shown in Fig.6.16), the sample becomes polarized, giving a high current during the first TSDC run. From the shape of the curve, it may be observed that there exists a peak at slightly above 373K. Similar observation had been made by Shakhtakhtinskii et al[95] for PZT/polyethylene composite, in which no peak had been observed below the poling temperature of 373K. The likely appearance of the broad TSDC peak may be due to the presence of a range of activation energies for the trapping sites of charge carriers. Indeed, previous results on the conduction process in PIEZEL composite (see chapter 4) show that the charge carrier trapping process may occur at various levels of the trap distribution. Some of these trapped charges may be released, leading to a substantial reduction of the TSDC level in the following run.

The pyroelectric coefficient (p) obtained from PZT5/VDF-TrFE composite (poling parameters as in Fig.6.16 and cooled under the field to room temperature) is shown in Fig.6.17, from which it may be observed that the value of p increases with an increase of temperature from 8×10^{-6} $C.m^{-2}.K^{-1}$ (at 293K) to 7×10^{-4} $C.m^{-2}.K^{-1}$ (at 373K). These values are indeed very much higher ($\sim$250 times) than those of single phase

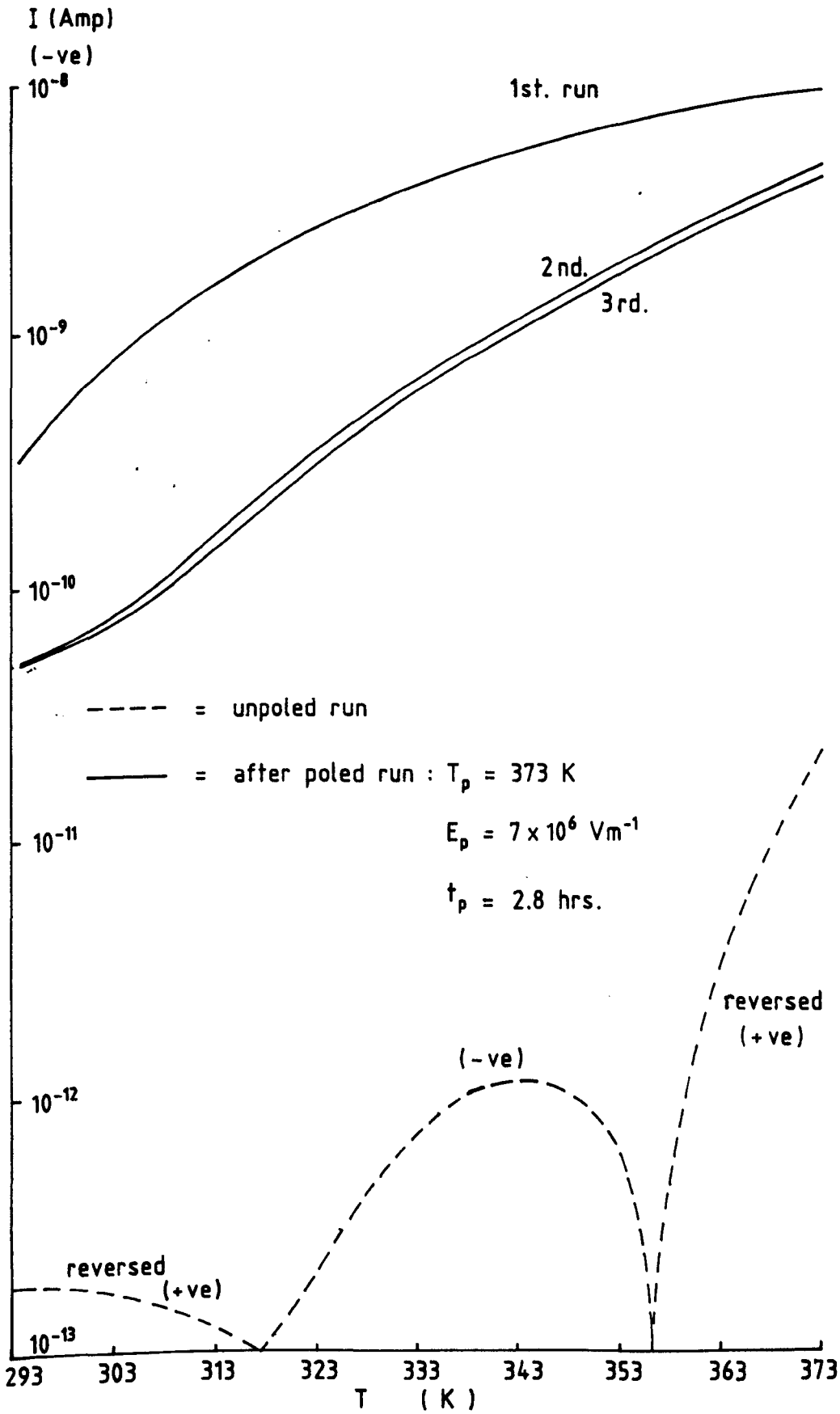

Fig. 6.16. Typical TSDC runs in PZT5/VDF-TrFE with (50/50 Vol.%).

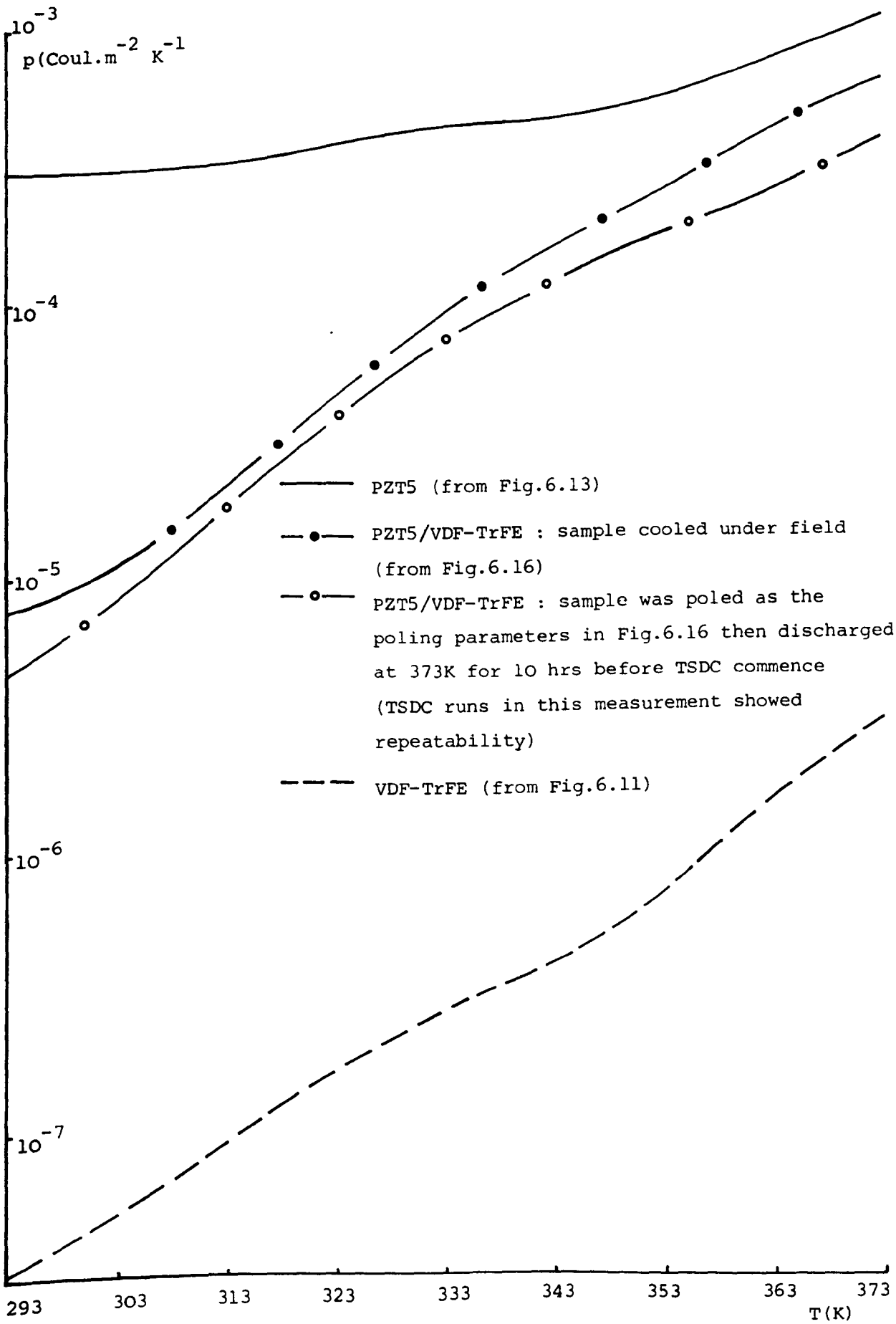

Fig.6.17. Pyroelectric coefficient behaviour in PZT5/VDF-TrFE(50/50 Vol.%), PZT5 and VDF-TrFE .

polymer, poled under the same poling parameters (p-T curves for single phase VDF-TrFE and PZT5 as obtained in Figs.6.11 and 6.13 are included in Fig.6.17 for comparison). As will be seen later, although the value of p for the composite are lower than those of the single phase PZT5, the voltage pyroelectric figure of merit (p/ε') of the former is better over certain range of temperatures. It may also be observed from Fig.6.17 that on maintaining the poling field during the cooling of the sample ($\sim$1 hr), the magnitude of the pyroelectric coefficient was enhanced by 20-65%. Das-Gupta and Duffy [96] observed the enhancement factor of 65% in the two procedure of poling for biaxially stretched PVDF film and noted that the relative difference in the magnitudes of the pyroelectric coefficients in the two cases was progressively less pronounced with the increase in the poling temperature from 333 to 353K.

The effect of upper temperature limit on the pyroelectric currents in PZT5/VDF-TrFE composite is shown in Fig.6.18. Upon heating above the poling temperature, the pyroelectric current was found to be significantly reduced, as expected.

Figs.6.19 and 6.20 show the behaviour of the TSDC (first run) and TSDC (reversible) in PZT5/VDF-TrFE composites for various ceramic volume compositions. It may be observed that in both cases, the currents increase with the increase of ceramic volume fractions and also that the induced polarization is higher for the higher content of ceramic volume fraction in the composite. The increase of the

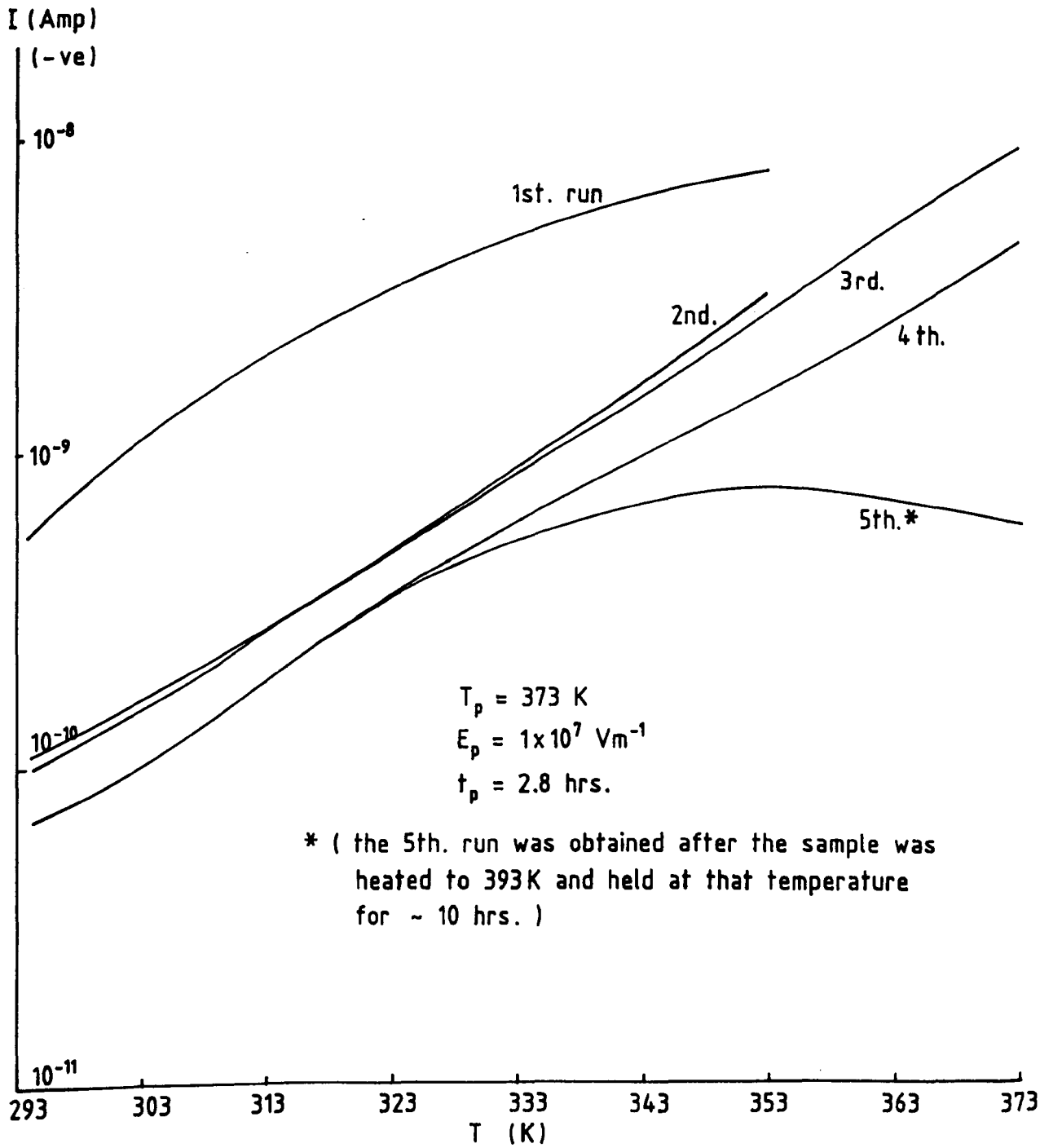

Fig. 6.18. Effect of upper temperature limit on TSDC runs in PZT5/VDF-TrFE (50/50 Vol.%).

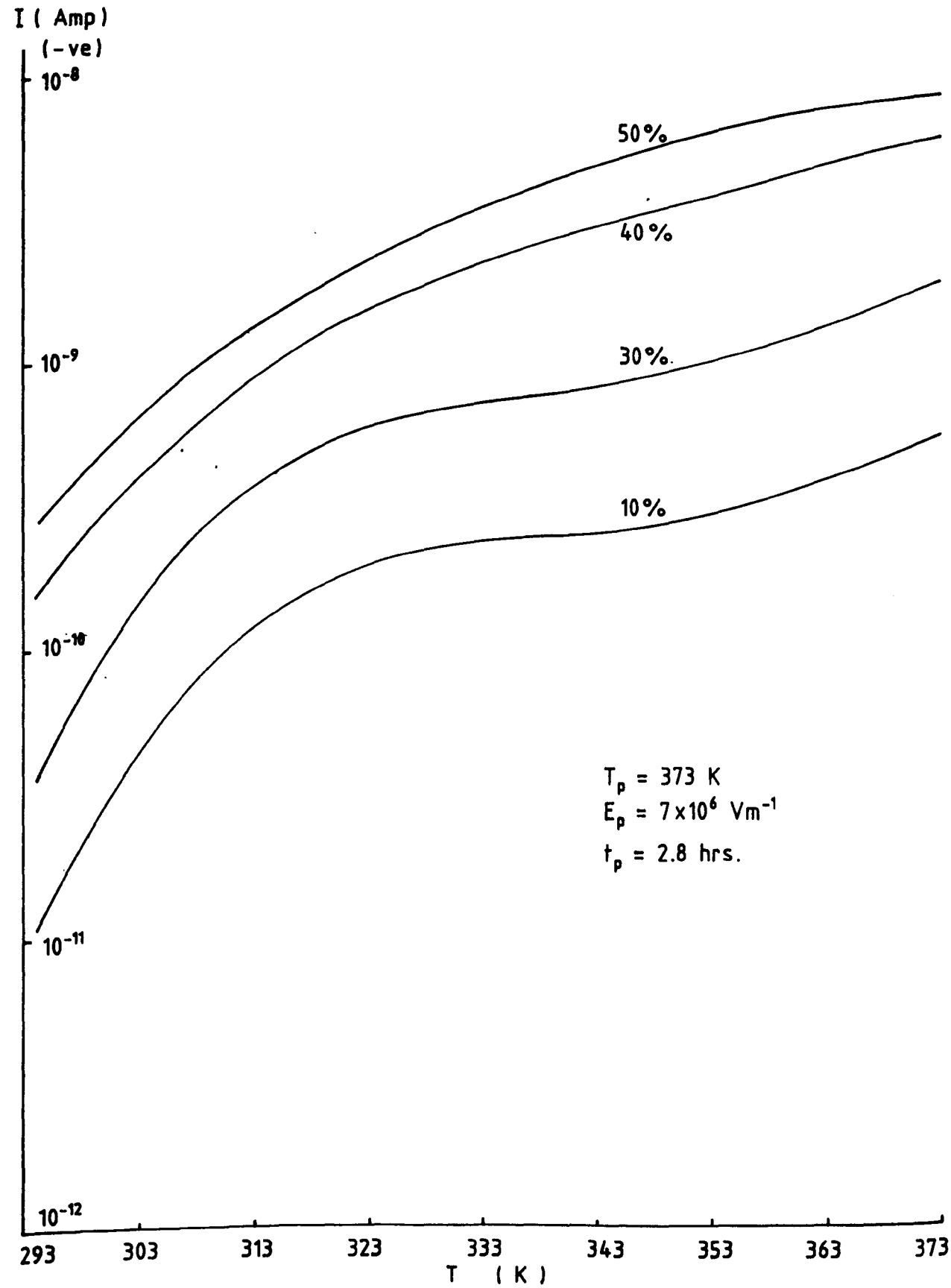

Fig. 6.19. TSDC (first run) behaviour in PZT5/VDF-TrFE for various ceramic volume compositions.

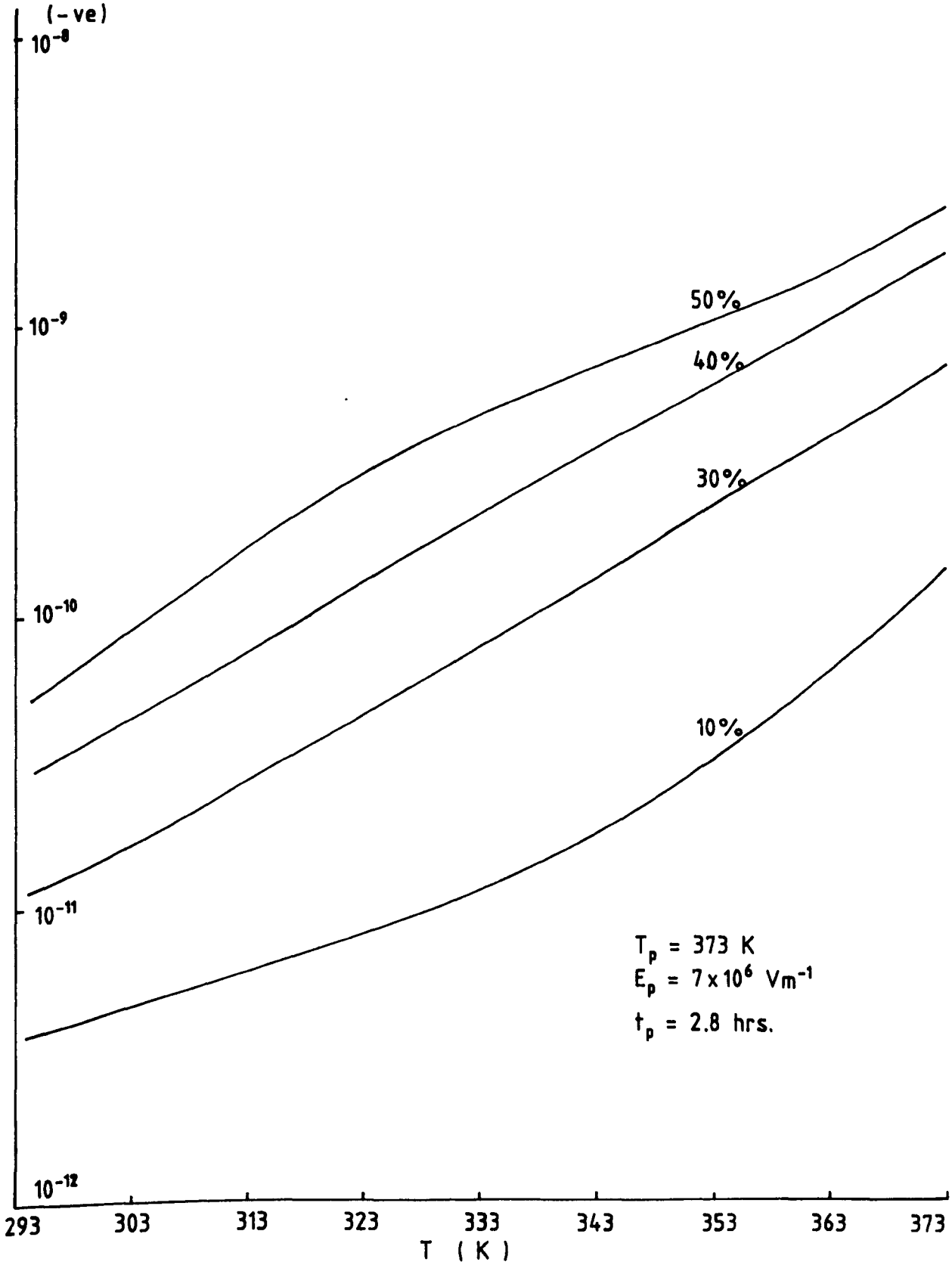

Fig. 6.20. TSDC (reversible) behaviour in PZT5/VDF-TrFE for various ceramic volume compositions.

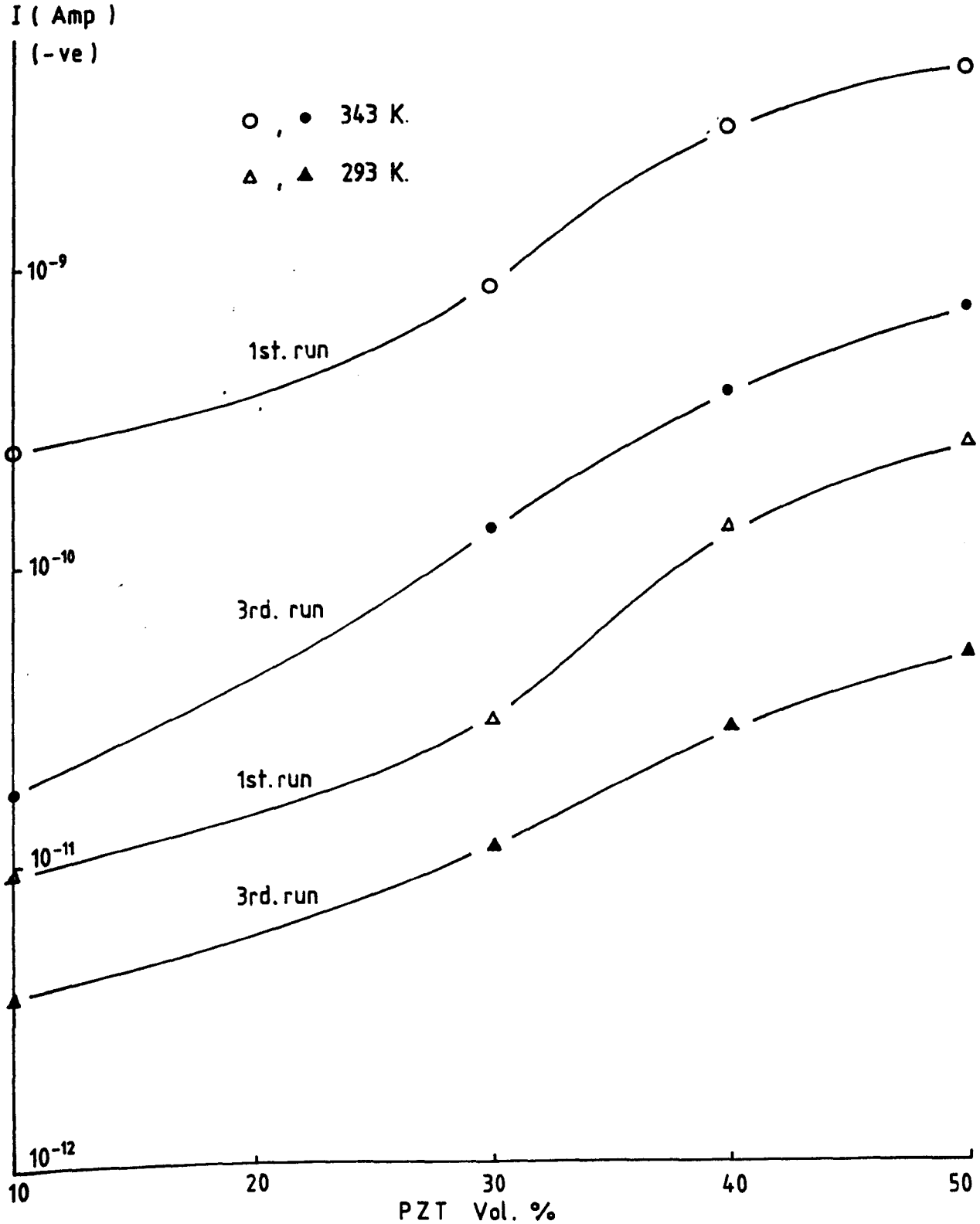

Fig. 6.21. TSDC spectra for various ceramic volume compositions at 293 K and 343 K in PZT5/VDF-TrFE composites.

magnitude of the TSDC with the increase of ceramic volume fraction in the composite may be further observed as in Fig.6.21, at 293K and 343K. Although the currents were observed to increase with ceramic volume fraction, the difference between the current values (first run and third run) is different for different ceramic concentration and for different temperature (e.g. at 293K and 343K). Such difference may be partly explained as follows. From the electrical conduction result (chapter 4), the conductivity of the composite has been suggested to be of ionic origin. The conductivity (σ^-) due to ionic carriers may be expressed thus[97] :

$$\sigma^- \propto \exp\left[-\Delta W/(2\varepsilon' kT)\right] \qquad (6.34)$$

where the activation energy ΔU is given by $\Delta U = \Delta W/2\varepsilon'$ and ΔW is the energy required to separate the ions in a dielectric medium of unit dielectric permittivty. Eq.(6.34) implies that the conductivity increases with an increase in the permittivity ε'. Thus, a higher conductivity would arise for the composite with high ceramic content. In addition, the trapped charge carriers may be located at sites of different energy levels for different composition of the composites. Another point should be noted that an increase in conductivity does not necessarily provide an increase in the reversible pyroelectric current.

The pyroelectric coefficients (obtained from the third TSDC run of Fig.6.21) for various contents of ceramic in

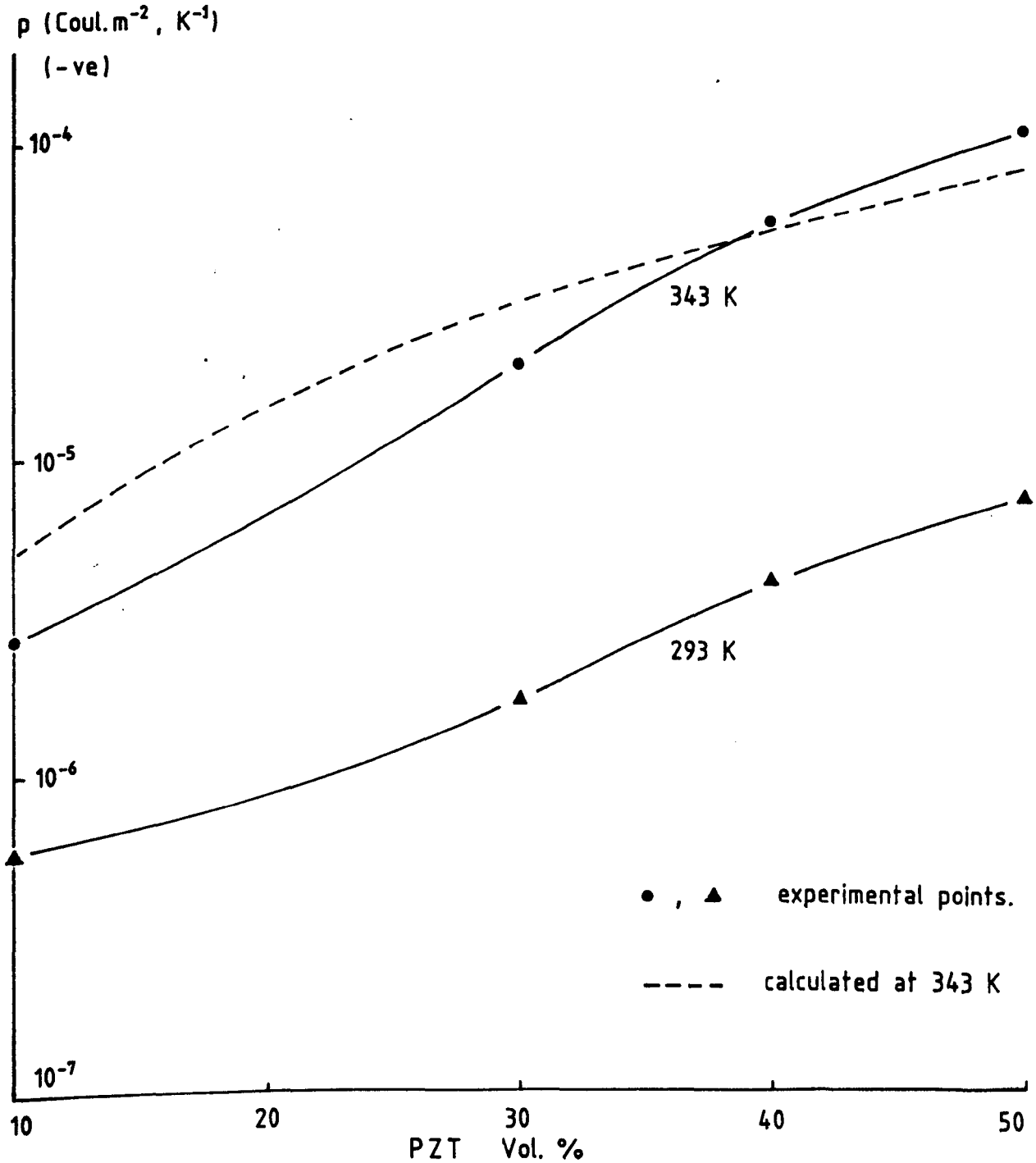

Fig. 6.22. Pyroelectric coefficient as a function of ceramic volume compositions at 293 K and 343 K in PZT5/VDF-TrFE composites.

PZT5/VDF-TrFE composite are shown in Fig.6.22 at temperature 293K and 343K. Again, the pyroelectric coefficient(p) increases as the ceramic content in the composite increases. It may be observed that the values of p for the composite with 50% Vol. of ceramic are ~40 times lower (at 293K) and ~4 times lower (at 343K) than those of PZT5 (Fig.6.13) at the corresponding temperature.

Assuming that the pyroelectric coefficient for the composite is dependent on that of the dispersoid (ceramic) and the permittivity of the polymer, the composite pyroelectric coefficient (p_t) may be expressed as [9,81] :

$$p_t = v_f \alpha G\, p_d \tag{6.35}$$

where v_f is the dispersoid volume fraction, α the poling ratio which is defined as the ratio of the polarization (at the particular poling field) to the saturation polarization of the composite and p_d the pyroelectric coefficient of the dispersoid. The local field coefficient G is approximately given by :

$$G = \frac{s\,\{\varepsilon_2/\varepsilon_1 - 1 + s + (s-1)(\varepsilon_2/\varepsilon_1 - 1)\, v_f\}}{(\varepsilon_2/\varepsilon_1 - 1 + s)^2 + (\varepsilon_2/\varepsilon_1 - 1)\,\{(s-1)^2 - \varepsilon_2/\varepsilon_1\}\, v_f} \tag{6.36}$$

where s, ε_1 , and ε_2 have been previously defined in Eq.(5.16). Using the value of s = 8 and experimentally determined values of $\varepsilon_1 = 8.7$, $\varepsilon_2 = 1200$, $p_d = 5\times10^{-4}$

$C.m^{-2}.K^{-1}$, the calculated values of the pyroelectric coefficients for various composition of the PZT5/VDF-TrFE composites is shown in Fig.6.22 at T=343K (assuming α =0.7 [9]). It should be noted that the value of α =0.7 is only approximate and the determination of its actual value may require further experimenatl work. Yamazaki and Kitayama [81] used the X-ray diffraction technique to determine the value of α from the peak intensity of the polarized and unpolarized sample.

It may be observed that the calculated values of p (Fig.6.22) appear to be comparable to that of experimental values for composites with high content of PZT phase. For low PZT content, the observed values of the pyroelectric coeficients were less than the calculated values. This deviation may be caused by the uncertainties in the value of α. Similar deviation had also been observed by Yamada et al[9] for the calculated and observed values of piezoelectric coefficients in PZT/PVDF composites. Such deviation was attributed to the uncertainties in the value of α, in which for the same poling field, the poling ratio in the low ceramic content would be less than that for the high ceramic content composite.

The dependence of pyroelectric coefficient on poling time (t_p), poling field (E_p) and poling temperature (T_p) for PZT5/VDF-TrFE (50/50 Vol.%) composite may be observed from Figs.6.23-6.25. Generally, these results showed that by increasing the poling parameters (t_p, E_p, T_p), the pyroelectric coefficient increases, although its increase with

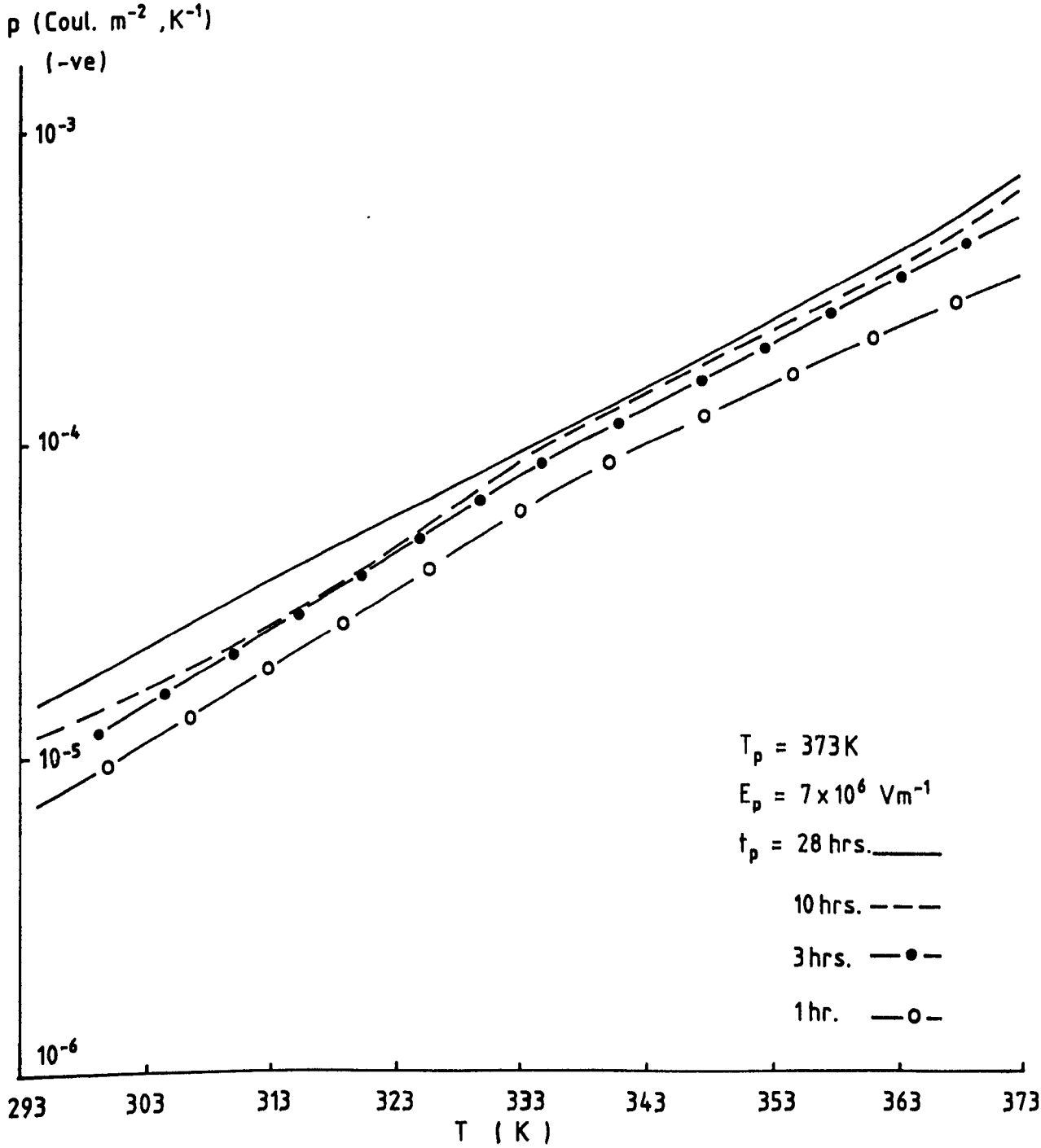

Fig. 6.23. The dependence of pyroelectric coefficient on poling time in PZT5/VDF-TrFE (50/50 Vol.%).

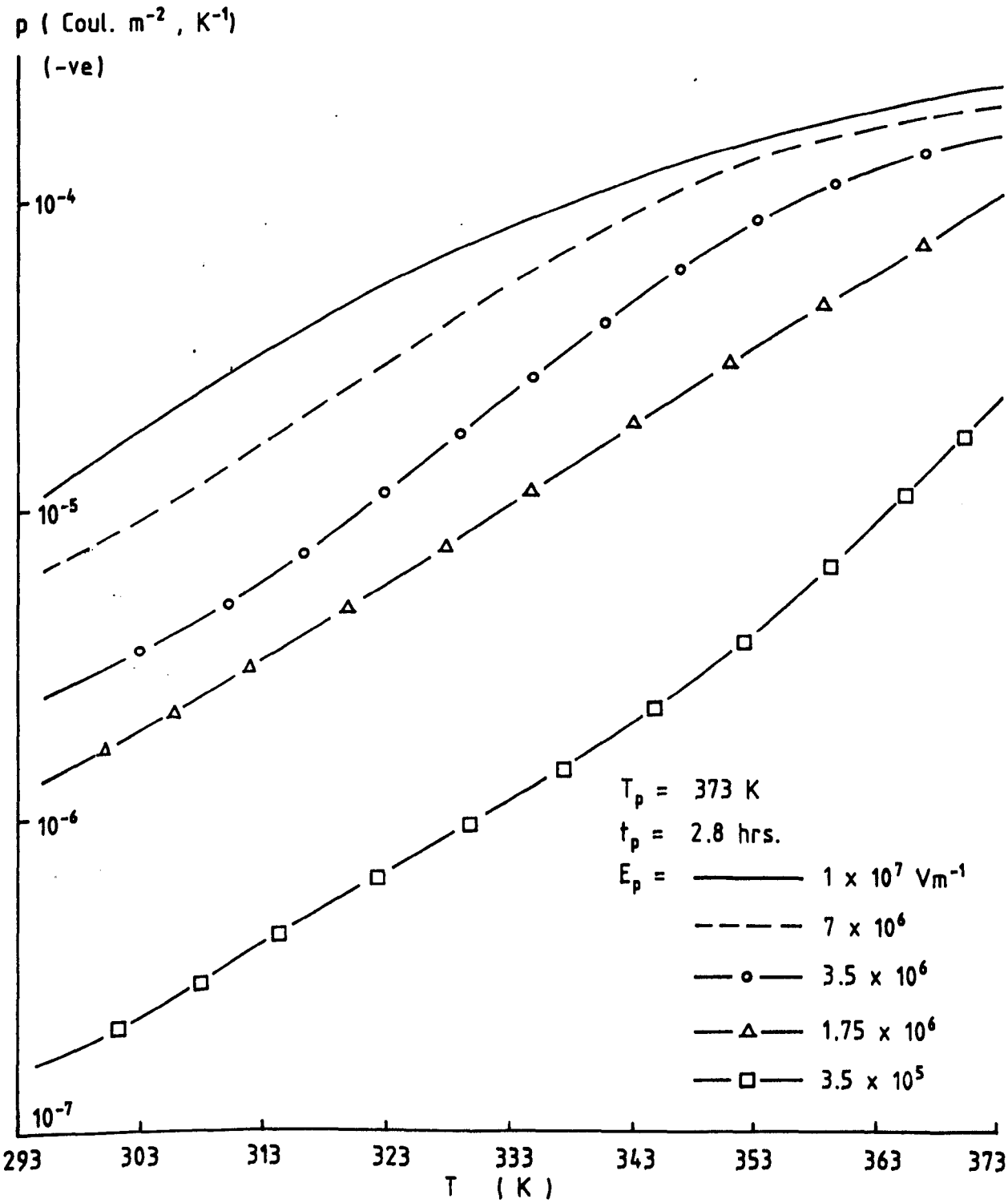

Fig. 6.24. The dependence of pyroelectric coefficient on poling field in PZT5/VDF-TrFE (50/50 Vol.%).

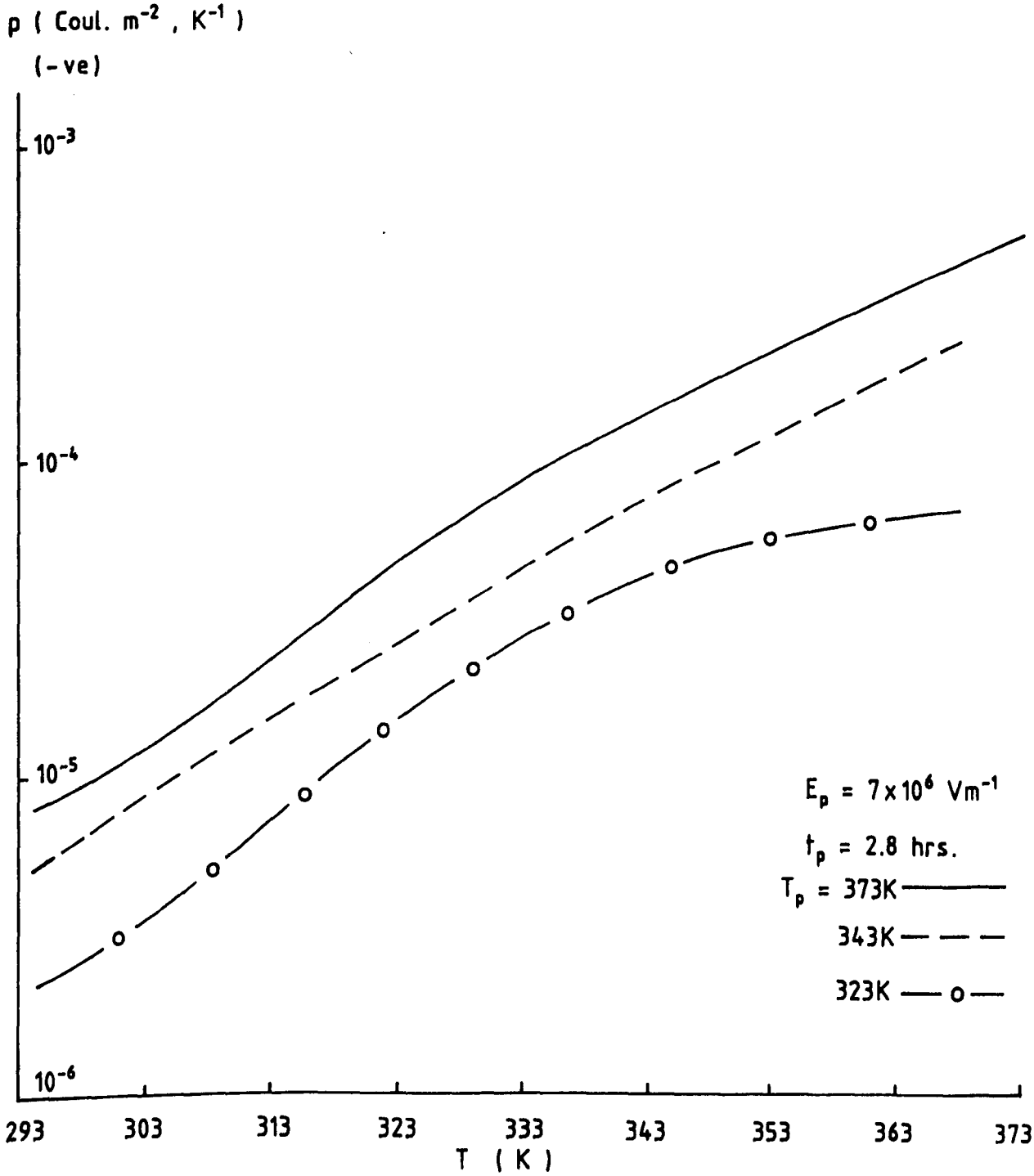

Fig. 6.25. The dependence of pyroelectric coefficient on poling temperature in PZT5/VDF-TrFE (50/50 Vol.%).

temperatures are at different rates. This is particularly noticeable for the pyroelectric coefficients obtained at different poling fields (Fig.6.24). It may be observed that below $\sim$323K, the rate of increase of p with temperature is about the same for all the poling fields in the present work (E_p :(0.35-10)x10^6 Vm^{-1}). However, above $\sim$323K, the rate of increase of p with temperature is found to be lower at higher poling fields. It may be possible that at high temperature and high poling field, there is an almost saturation of polarization thus providing very little change in the value of p with temperature. On the other hand, at low poling field, the induced polarization becomes significantly enhanced with the increase of temperature but not yet reaching a saturation level, thus providing a more pronounced change of p with temperature.

The high poling temperature (T_p) is desirable to obtain the high pyroelectric coefficient of the composite (see Fig.6.25), particularly if the material is to be used at high temperatures. Fig.6.26 shows the dependence of pyroelectric coefficients on poling parameters, measured at 343K. It should be noted that each curve in the figure was obtained with a different specimen of the composite. Obviously, an efficient poling can be achieved at high poling temperature and high poling field as long as it does not reach a limit of breakdown strength (E_B) of the sample (at ambient temperature : E_B $\sim$2.1x10^7 Vm^{-1}). It may also be observed that by extending the poling time (t_p) beyond 3 hours would not give very much improvement in the value of p (i.e. the saturation value of p

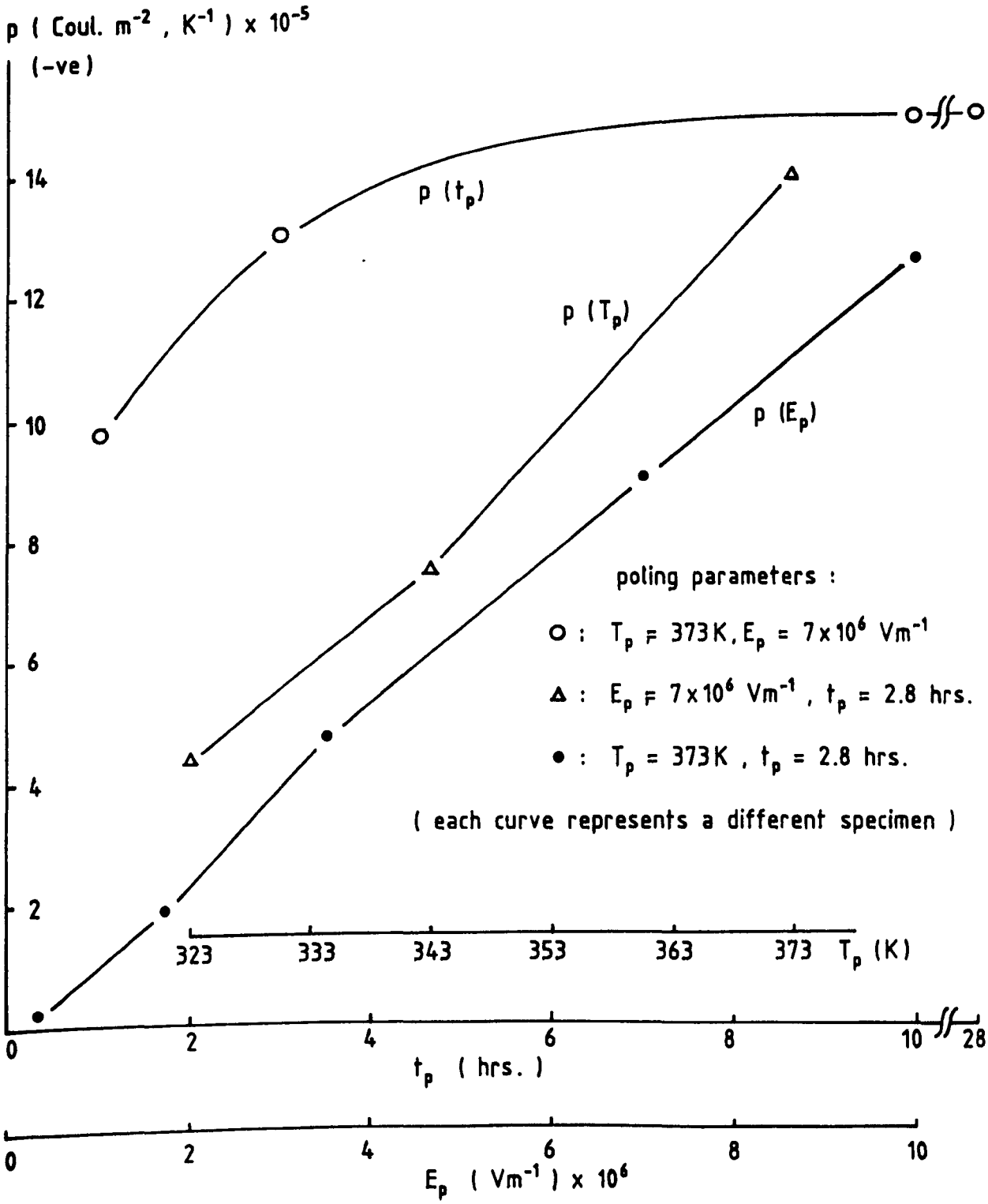

Fig. 6.26. The dependence of pyroelectric coefficient on poling parameters at 343 K in PZT5/VDF-TrFE (50/50 Vol.%).

is only 15% higher than that obtained for 3 hours poling time).

It appears that the highest pyroelectric coefficient at 343K, obtained with the poling parameters of T_p = 373K, E_p = $7x10^6$ Vm^{-1} and t_p = 2.8 hours, is $p=1.4x10^{-4}$ $C.m^{-2}.K^{-1}$. Although this value is lower than that of PZT5 ($p=5x10^{-4}$ $C.m^{-2}.K^{-1}$ at 343K), the voltage pyroelectric figure of merit, p/ε' (as defined in chapter 1) for this composite is about 4 times higher than that of PZT5 (taking measured values of ε'(PZT5/VDF-TrFE)=85, ε'(PZT5)=1200 at 343K). At room temperature, the value of p/ε' for the composite is about a factor of 2.6 less than that of PZT5; however, the values of p/ε' for the composite improves with increasing temperature of the measurement, which eventually becomes better than that of the single phase ceramic at high temperatures. The voltage pyroelectric figure of merit (at 343K) for PIEZEL is about a factor of 2.7 less than that of PZT5/VDF-TrFE composite for the same poling condition.

Fig.6.27 shows the pyroelectric peak current (I_p) obtained by the dynamic method as a function of poling fields at 293K, 333K and 373K in PZT5/VDF-TrFE composite. These data were obtained after completing 3 cycles of heating the poled sample to temperature 373K. It may be observed that the data show an approximately linear relationship between I_p and the poling field at the temperatures and within the range of fields of the measurements, which is consistent with the result obtained for the direct method (Fig.6.26). Result of Fig.6.27 also shows that efficient poling can be achieved at

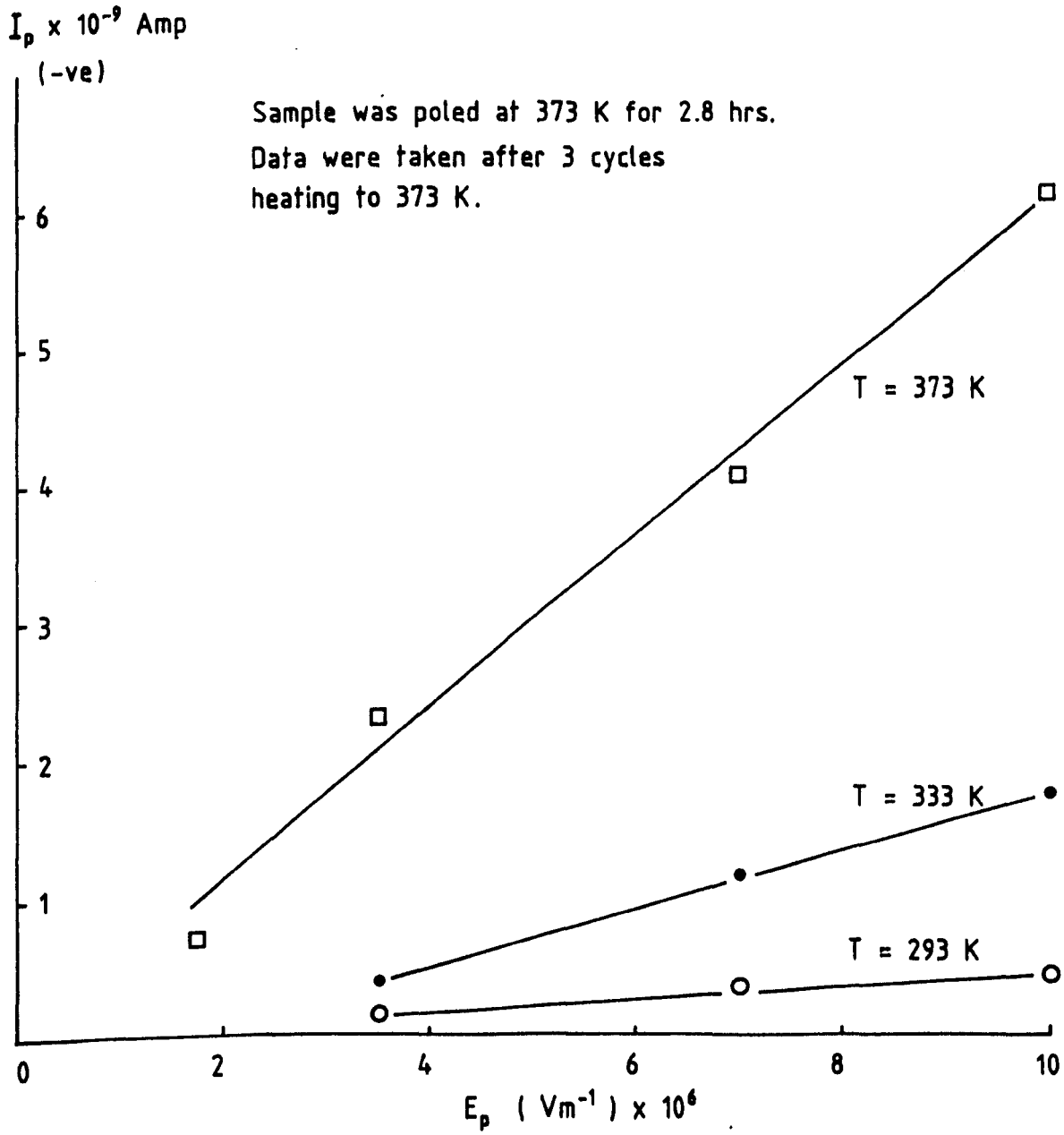

Fig. 6.27. Peak current against poling field in PZT5/VDF-TrFE (50/50 Vol.%).

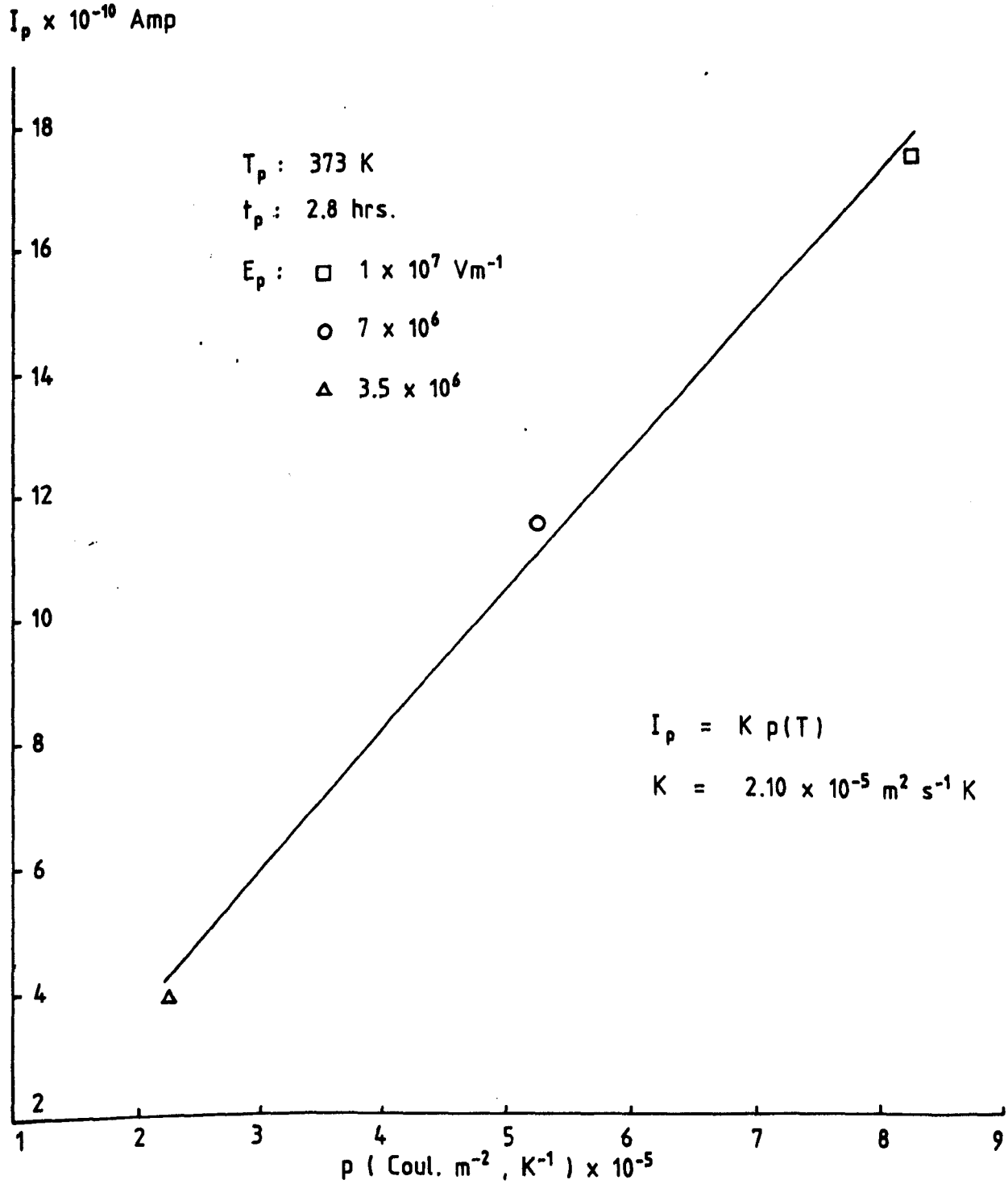

Fig. 6.28. Peak current against pyroelectric coefficient at 333 K in PZT5/VDF-TrFE (50/50 Vol.%).

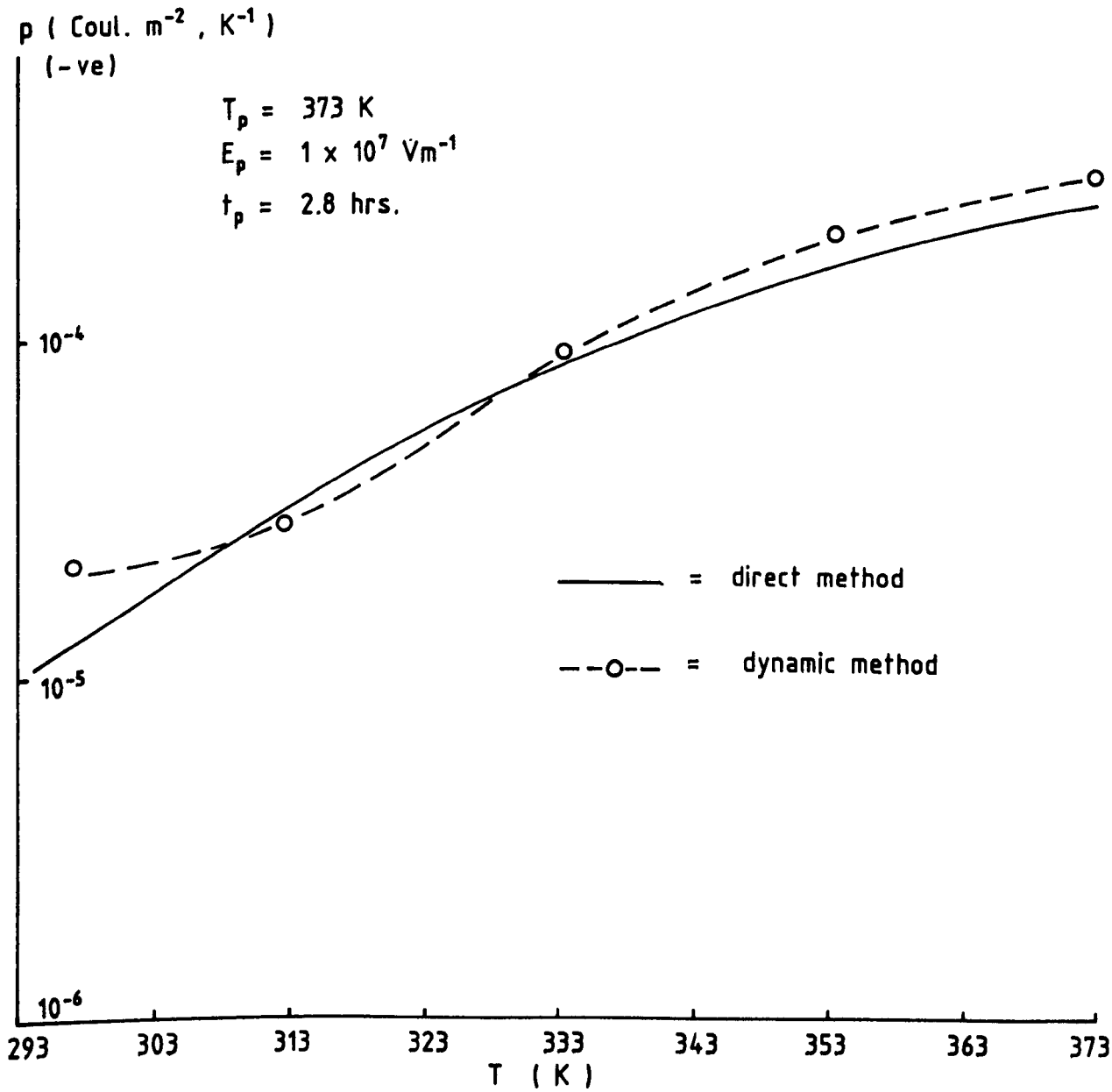

Fig. 6.29. Pyroelectric coeffieient in PZT5/VDF-TrFE (50/50 Vol.%) from the direct method and the dynamic method .

high temperatures and fields. Further measurements on PZT5/VDF-TrFE composite established a linear relationship between I_p and p at 333K (see Fig.6.28), which was obtained by poling the sample at three different fields in the range (3.5-10.0)x10^6 Vm^{-1} and the value of p (from direct method) and I_p (from dynamic method) were appropriately determined; the constant of proportionality K (from Eq.(6.32)) was found to be 2.1x10^{-5} $m^2.s^{-1}.K$. Using the value of K as obtained at T=333K (Fig.6.28), the pyroelectric coefficients calculated from the values of I_p of the dynamic method at various temperatures are shown as in Fig.6.29, together with the value of p from the direct method of the same sample. It may be observed that the values of p obtained from the dynamic and the direct methods are about similar magnitude for temperatures above ~313K. Reason for the discrepancy in the values of p from the two methods below ~313K is likely due to the variation in the values of K with temperature (see chapter 7 for further discussion).

6.4.3. Pyroelectric properties in PZT5/PVDF, PZT4/PVDF, $BaTiO_3$/PVDF and PZT4/PP composites.

The behaviour of the TSDC (first run) of PZT5/PVDF (50/50 Vol.%), PZT4/PVDF(50/50 Vol.%), $BaTiO_3$/PVDF (40/60 Vol.%) and PZT4/PP(50/50 Vol.%) composites are shown in Fig.6.30, which were obtained after the samples have been poled at the same poling parameters of T_p=373K, E_p=7x10^6 Vm^{-1}

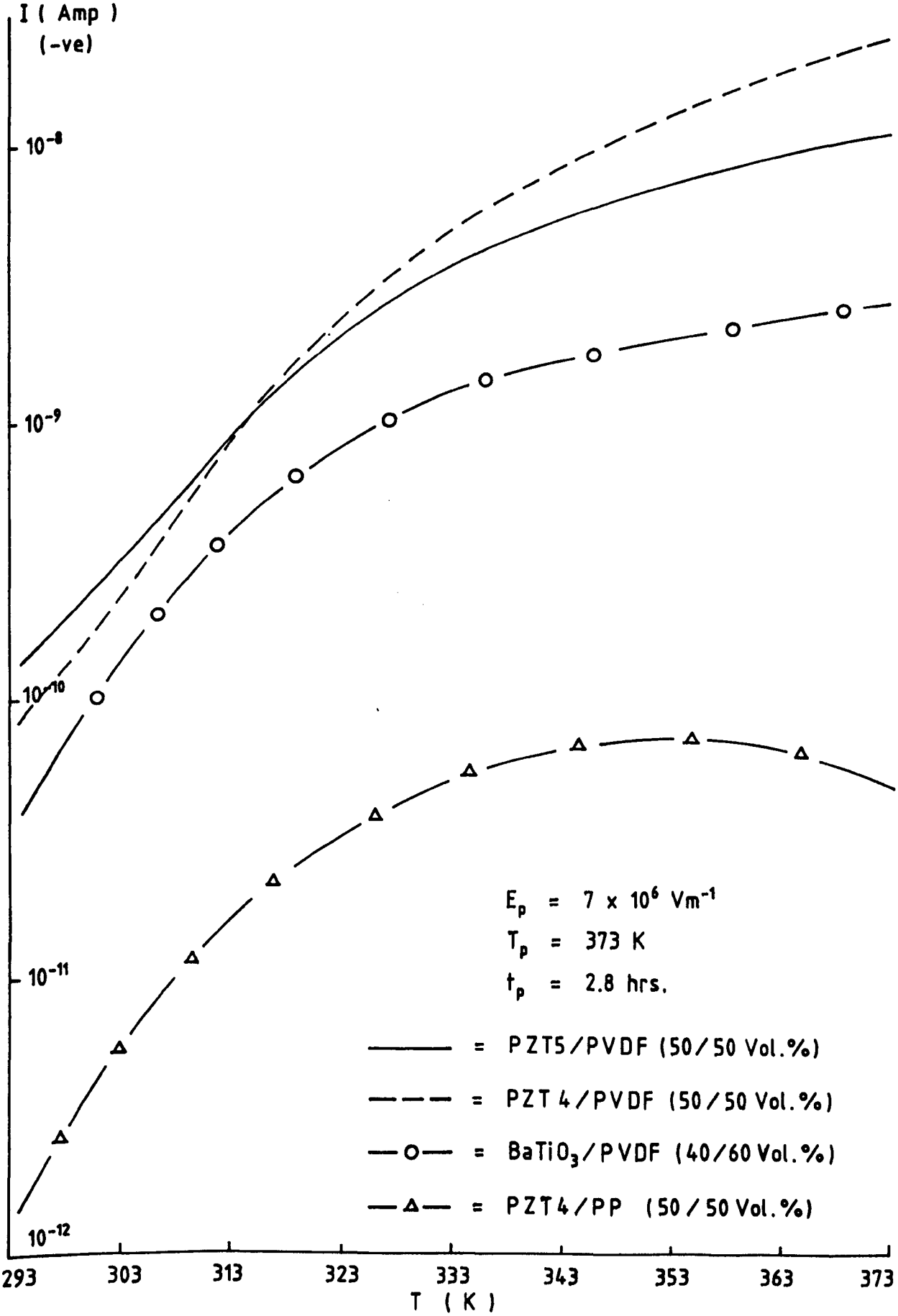

Fig. 6.30. TSDC (1st. run) in PZT5/PVDF, PZT4/PVDF, $BaTiO_3$/PVDF and PZT4/PP composites.

and t_p=2.8 hrs. It may be observed that the magnitude of the currents for PZT5/PVDF and PZT4/PVDF composites are comparable to that of PZT5/VDF-TrFE composite, and the increase of current with temperatures in these composites are almost similar. The TSDC (first run) in $BaTiO_3$/PVDF composite also shows similar behaviour as that for PZT/PVDF(or VDF-TrFE) composites but with the reduced magnitude. Such a reduction in magnitude may be expected as the $BaTiO_3$/PVDF composite has a relatively lower permittivity (see chapter 5). The magnitude of current for PZT4/PP composite shows much lower value as the permittivity in this composite is significantly lower than the other composites. In addition, the broad peak observed at ~353K in the TSDC of PZT4/PP composite may originate from a release of space charges from localised states at the ceramic-polymer interface region.

The pyroelectric coefficient obtained for PZT4/PP composite is shown in Fig.6.31, from which it may be observed that the polarity of the pyroelectric coefficient reverses at ~345K. It may also be observed that the magnitude of the negative values of the pyroelectric coefficient decreases from cycle to cycle until it reaches a reproducible value after the 5th run. Such a decrease of pyroelectric currents may be related to the space charges, which have been subsequently removed following heating process. A reversal of polarity of the pyroelectric response has also been observed with PZT/spurrs polymer (prepared by replamineform technique)[82]. These authors have attributed the observed positive polarity of the pyroelectric coefficient as due to

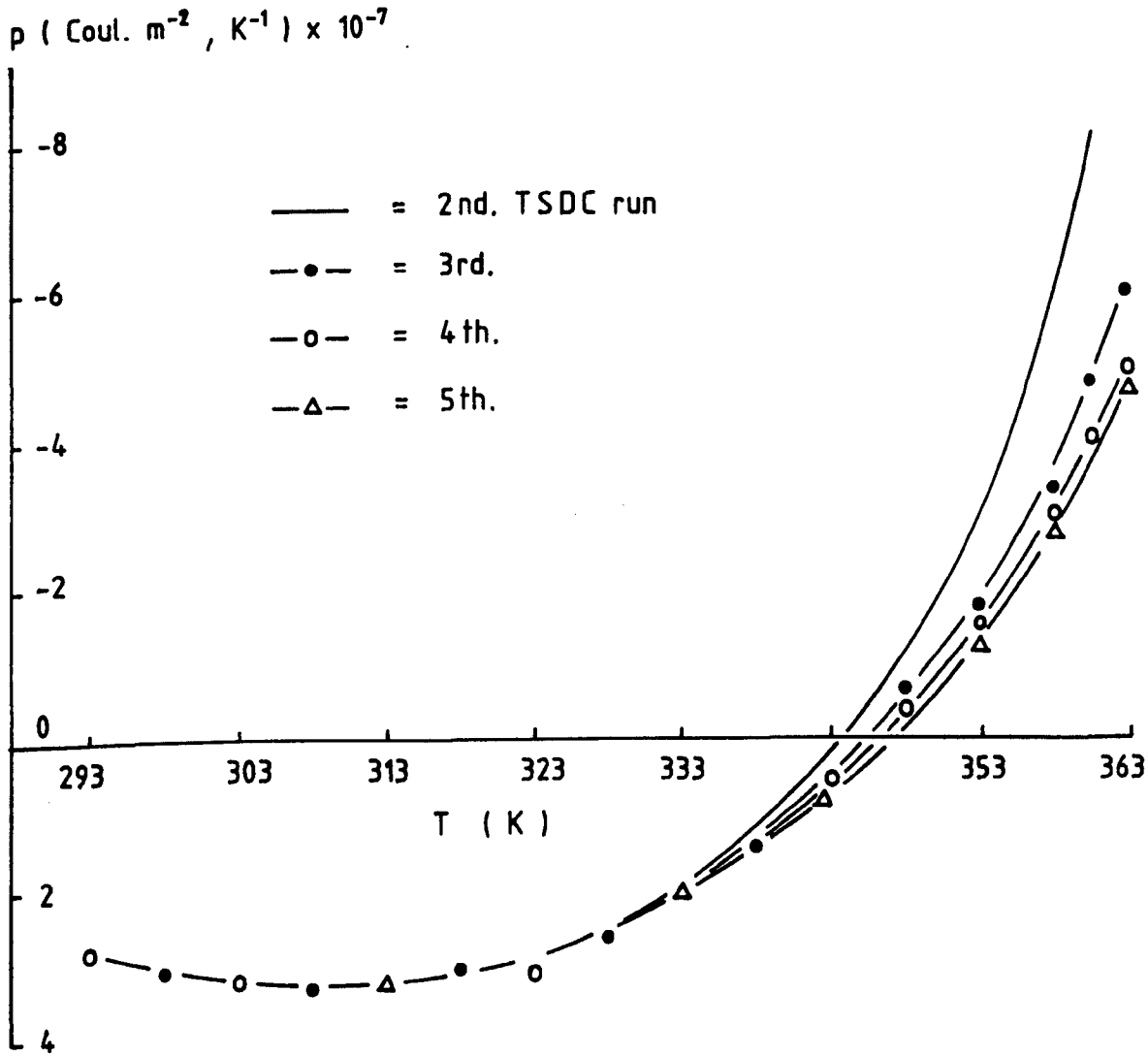

Fig. 6.31. Pyroelectric coefficient in PZT 4 / PP.

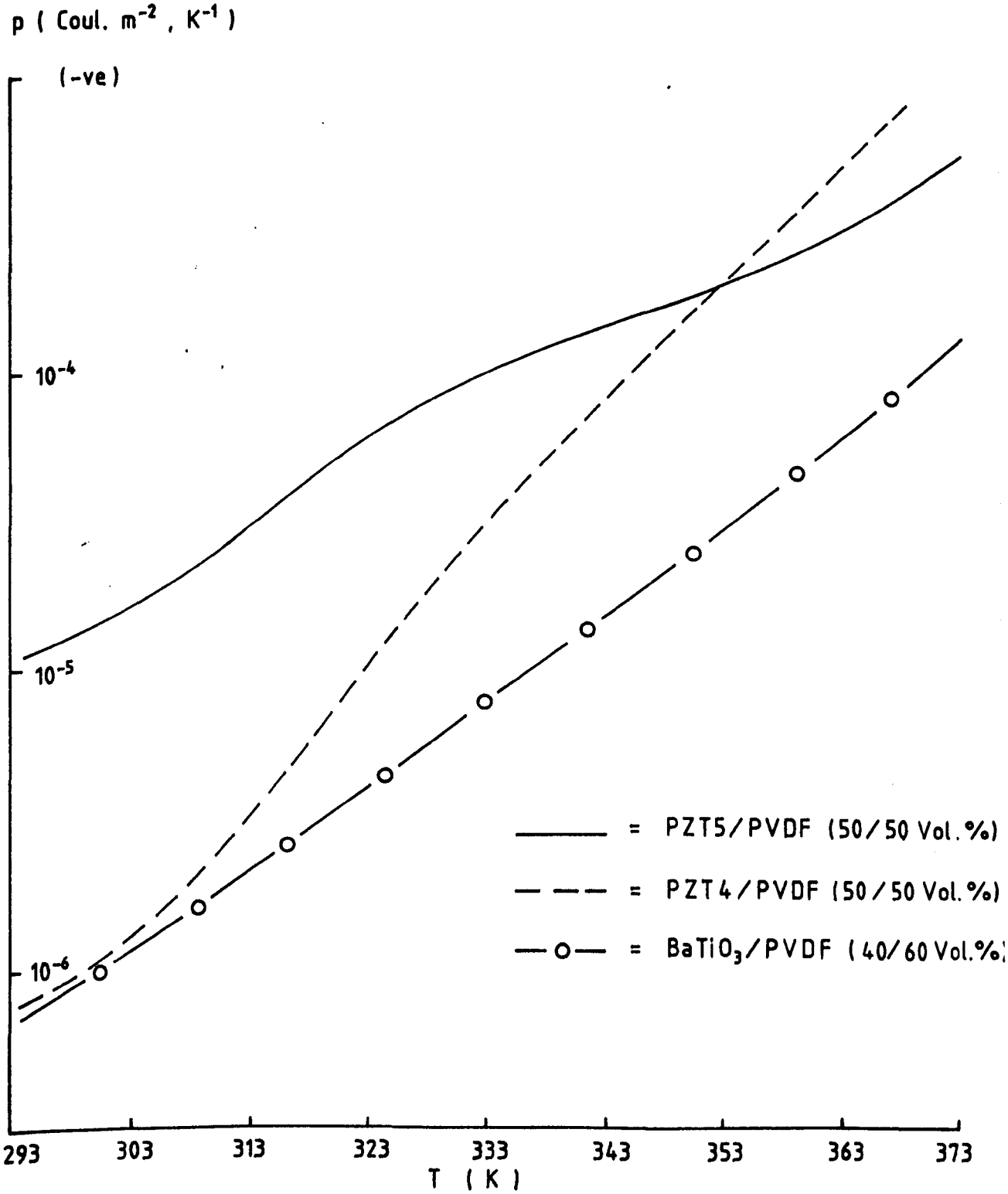

Fig. 6.32. Pyroelectric coefficient in PZT5 / PVDF , PZT4 / PVDF and $BaTiO_3$ / PVDF composites.

the contribution from secondary composite effect arising from thermal expansion mismatch between the polymer and PZT [82]. The present result may also be due to a contribution from such secondary composite effect, although further experimental work (such as by varying the stiffness of the polymer [82]) remain to be performed. At sufficiently high temperatures, the secondary composite effect is very small (since the polymer softens and hence reducing the clamping effect) and thus giving the usual negative polarity of the pyroelectric coefficient (due to polarization change with temperature). The value of p in this composite is extremely low which may possibly mean that the applied field was not sufficient to polarize the PZT particles located in the amorphous phase of the polymer.

The pyroelectric coefficient obtained for PZT5/PVDF composite (Fig.6.32, poling parameters as in Fig.6.30) shows a comparable magnitude and similar behaviour as that for PZT5/VDF-TrFE composite. The pyroelectric coefficient for PZT4/PVDF, however, is about one order of magnitude less than that of PZT5/PVDF (or VDF-TrFE) composite at room temperature. As the temperature increases, the difference in magnitudes in the p-values of the two composites (PZT5/PVDF and PZT4/PVDF, Fig.6.32) tend to reduce and at higher temperatures, the p-values for PZT4/PVDF is greater than that of PZT5/PVDF. It may be noted that PZT5 ceramic is easier to polarize as compared to PZT4 [Unilator Technical Ceramics, U.K.]. As a result PZT5/PVDF composite provides a higher pyroelectric coefficient in comparison with PZT4/PVDF composite. At high

temperatures, the contribution from 90° domain alignment of PZT4 material becomes significant and thus giving high pyroelectric activity for PZT4/PVDF composite. The pyroelectric activity in $BaTiO_3$/PVDF composite appears to be low as compared to PZT/PVDF composites of the present work and is of less interest as pyroelectric material.

CHAPTER 7

GENERAL DISCUSSION AND CONCLUSION

Details of discussion related to the experimental results obtained from each characterization method employed in the present work can be found in the preceding chapters. This chapter highlights a general discussion of the results together with the conclusion of the present achievement. Suggestions for further work are also included.

7.1. Electrical Conduction

In order to have pyroelectric properties, ceramic/polymer composites must be polarized through poling process (i.e. application of electric field at elevated temperature over extended period of time). During the course of this process, several possible polarization mechanisms (such as those given in sections 3.3 and 4.1-4.2) would occur, depending on the intrinsic properties of the materials and the

external conditions imposed on the materials. In the present work, the current associated with the polarization process of ceramic/polymer composites is measured at various electric fields and temperatures. The analysis is performed to determine mechanism responsible for the observed current characteristics.

It is obvious from the results obtained in chapter 4, that the current which flows during the poling (charging) process can be considered to arise from time-dependent process (transient component) and steady-state conduction component. The magnitudes of these current components are greater at high temperatures and electric fields. From measurements on PIEZEL composite, it can be seen that the conduction component is relatively small at low temperatures and low fields, however, its magnitude becomes significant under high temperatures and high fields. Such increase of conduction component apparently masked the behaviour of the transient component. Nevertheless, it was pointed out (see discussion in section 4.5.1) that under the condition where the conduction component is relatively small, the behaviour of the transient current component can be suggested to be due to dipolar and charge carrier hopping. Further, the analysis of the charging currents dependence on electric field and temperature indicates that the charging process involves charge carrier trapping at various energy levels of the trap distribution or it can also be explained in terms of dipolar orientation having a continuous spectrum of relaxation times.

Support for the involvement of charge carrier trapping

in the polarization process may be evident in view of the semicrystalline nature of the polymer (see chapter 2 for the polymer structure). It appears that the traps may be associated with structural defects in the amorphous and at the crystalline-amorphous regions. Such traps are localised states and at different energy levels (trap depth). The presence of ceramic particles in the amorphous region of polymer would obviously generates more localised states in the composite system. The charges will be residing in these traps until they received enough thermal energy to be activated again. The charges which have been released from trap would tend to be trapped again. It is suggested that this charge carrier movement occurs by hopping from one localised state to another. Obviously, there is a tendency for deep localised states to hold charges for long period of time in the absence of large thermal energy. These charges would eventually cause polarization of the nearby regions by means of interfacial polarization (see section 4.2.3 for the theoretical treatment of interfacial polarization).

Accumulated evidences from discharging current data indicate that the discharging process involves trap delocalization of charges followed by subsequent retrapping. It also appears that the process is likely involved relatively shallow localised sites, whereby the charge carriers move by discontinuous hops between the sites. Discharging currents have also been observed to show relaxation behaviour. As has been stated in the discussion of chapter 4, such relaxation can be attributed to the charges at the localised sites which

were accumulated during the charging process. This characteristic is not observable in the charging current behaviour due to the presence of appreciably large conduction current component.

Although the charging and discharging currents of ceramic/polymer composites prepared in the present work were measured at limited electric fields and temperatures (due to shortage of time), the results obtained do contribute to the present understanding of the overall properties of the composite materials. The increase in the magnitude of charging and discharging currents with the increase of ceramic content in the composite is very obvious (see Fig.4.50). This would naturally suggest that the high volume fraction of ceramic is desirable for a large polarization charge in the composite. It should be noted however that the large charging current would not necessarily correspond to the large polarization charge in the material, notably if the magnitude of the conduction current component is very large. This point would become clear if we refer to composite materials which yield Figs.4.56 and 4.58, where large charging currents were produced at high charging field. As will be seen later in the discussion on the pyroelectric activity (see section 7.3), these materials however, appear to have relatively smaller pyroelectric activity as compared to composite materials which produce Figs.4.47 and 4.57, where relatively lower charging currents have been detected at the same charging field of 7×10^6 Vm^{-1}.

Ideally, to have useful pyroelectrics, materials have to show suitable polar properties (high polarization) and

extremely low electrical conductivity. Unfortunately, both of these features are not found in the same material. The use of binding matrix with relatively low electrical conductivity (such as PP) tends to reduce the electrical conductivity of the composite (see Fig.4.59). However, this composite appears to be less interesting due to its low pyroelectric activity. Reason for poor performance of pyroelectricity in this composite will be apparent in a latter discussion (see section 7.3).

It was pointed out in the discussion of chapter 4 that with the exceptions of anomalous charging currents in some composites, the observed transient currents in composites generally show similar behaviour. In particular, the discharging current transients $I_d(t)$ in composites were observed to obey the empirical formula of Eq.(4.101). An estimate of the amount of charge carriers (Q_{disch}) that involve in the discharging current of composites for the same specified pre-applied field, temperature and within measured times of 5 sec to 1000 sec were tabulated in Table 4.2. It should be noted that since the discharging process within this time duration involves charge carriers at relatively shallow localised states (as suggested earlier), the amount of charges calculated would only constitute part of the polarization charge in the materials. In order to compare the actual polarization charges in these materials, an interesting piece of work would be to measure the total polarization charge by performing thermally stimulated discharge current (TSDC) measurement over an appropriate temperature range, which is

the subject of further investigation. The calculated charges in Table 4.2 however do show interesting implications if we compare with the level of pyroelectric activity achieveable in these materials under the same poling conditions. It is obvious that composites which produce small Q_{disch}, for example PZT4/PP and $BaTiO_3$/PVDF composites, show relatively low pyroelectric activity. Composites of PZT5/PVDF and PZT5/VDF-TrFE have comparable values of Q_{disch} and thus subsequently show the same level of pyroelectric activity. PZT4/PVDF composite appears to have a little higher Q_{disch} in comparison with PZT5/PVDF and PZT5/VDF-TrFE composites, its pyroelectric activity however is less as compared to the latter two composites (particularly below 353K, see for example Fig.6.32). This could possibly mean that large amount of charges which have been accumulated at the trap sites (particularly at the ceramic/polymer interface) would not necessarily cause large polarization for pyroelectric activity. Other factors such as polarizability and conductivity of the material contribute to the total polarization required for pyroelectricity, which will be further discussed in section 7.3.

Steady-state currents have been observed in PIEZEL composite at room temperature in the time region of 10^5 sec. The appearance of these currents at earlier times ($< 10^5$ sec) has been shown for increasing applied electric fields and temperatures. It has also been shown that the activation energy of the currents are field-dependent. This does not support the space-charge-limited conduction theory, which

assumes that trap energies are unaffected by electric field. Nevertheless, as has been stated in section 4.5.3, this observation warrants the field dependence of currents to be analysed in accordance to Schottky emission, Poole-Frenkel effect or ionic conduction model. It appears from section 4.5.3 that ionic conduction model is most suited to describe the steady-state conduction mechanism in PIEZEL composite.

The present measurement on PZT5/VDF-TrFE (50/50 Vol.%) composite indicates that the steady-state current could be reached at time approaching 10^5 sec (see Fig.4.47). Due to limited time available, only quasi-steady-state current (current at 10^4 sec) were obtained for this composite at limited fields and temperatures. Nevertheless, analysis of these data seems to indicate that ionic conduction model is also appropriate to describe its conduction process. It has been noted that the calculated jump distance (d) from this model appears to increase with the increase of the ceramic content in the composite. This would naturally suggest that the addition of more PZT phase in composite causes an increase of the mean free path of the ionic carriers.

In concluding this section, it is suggested that the process of charging and discharging currents in ceramic/polymer composites involves charge carrier hopping through localised states (trapping sites) distributed throughout the bulk at different energy levels whereas the steady-state conduction may originate from an ionic hopping mechanism. The increase of ceramic volume fraction would result in increase of the ionic conductivity of the composite.

7.2. Dielectric Properties

Dielectric properties of PIEZEL composite have been measured in the frequency range of 10Hz to 100kHz at temperatures $\sim$273-373K. It was shown that two relaxation peaks appear in loss characteristics, i.e. at low temperature ($\sim$270K, 1kHz) and high temperature ($\sim$348K, 1kHz)(see Fig.5.28). As was pointed out in section 5.4.2, these peaks occur at similar temperature and frequency as that for VDF-TrFE(55/45) copolymer. It was also shown that there was no relaxation peak in the dielectric loss characteristic of PZT5, measured in the range of temperature and frequency of the present work (see Figs.5.24 and 5.25). Further, the occurence of dielectric loss peak in PZT at these temperatures and frequencies has not been reported in literatures. Thus, it is suggested that the dielectric loss process in PIEZEL composite is dominated by the copolymer phase. The low-temperature loss peak is attributed to the micro-Brownian motion of molecular chain segments in the amorphous region while the high-temperature peak is associated with the molecular dipole motion in the crystalline phase of the copolymer. By transforming the time-dependent discharging current into its equivalent frequency-domain, another loss peak has been observed in PIEZEL at temperatures 333-363K in the frequency range of 10^{-5}-10^{-3} Hz (see Fig.4.35). This loss peak has been suggested to be due to accumulated charges at localised states (trapping sites) in the bulk of the material. Moreover, since the loss peak appear to occur at the same temperature as the

loss peak due to dipolar motion in the crystalline phase, it is suggested that the accumulated charges are likely to reside at the crystalline-amorphous interface.

The frequency and temperature dependence of the dielectric loss process in composites prepared in the present work (i.e. PZT5/VDF-TrFE, PZT5/PVDF, PZT4/PVDF, $BaTiO_3$/PVDF) were observed to be similar to the measured properties of the polymers (for example, compare Figs.5.21, 5.32, 5.38). In particular, the location of the dielectric loss peaks are similar in both of those composites and single phase polymers. However, it is obvious that the magnitude of dielectric loss increases as the fraction of ceramic phase increases (see Fig.5.32). It is believed that interfacial charges may be responsible for the observed increase in the magnitude of dielectric loss.

The dielectric permittivity of PVDF and VDF-TrFE used in the present work were observed to be comparable in magnitudes at 370K and 1kHz (see Fig.5.21). Below 370K, however, the permittivities of VDF-TrFE are a bit higher than that of PVDF (for example at 343K, the permittivity of VDF-TrFE is about 20% higher than that of PVDF). Accordingly, it is expected that composites which were prepared from these polymers with the same type of ferroelectric ceramic and having the same volume fraction, would exhibit similar proportion in magnitudes of dielectric permittivities. However, this is not the case if we compare the values of dielectric permittivities obtained for PZT5/PVDF and PZT5/VDF-TrFE composites having the same volume fraction of ceramic phase (see Figs.5.32 and

5.38). From these figures, it is obvious that the dielectric permittivity of PZT5/PVDF composite is higher than that of PZT5/VDF-TrFE (e.g. it is about 11% higher at 343K). Reason for this observation is likely related to the actual volume fraction present in these composite samples. The fabrication method of composites was quite crude in a way that the particles of the inclusions were manually dispersed into the melted polymer matrix on the roller. By this way, composite films are bound to be nonuniform in which the particles concentration is different from one region to another. In view of this, the volume fractions of the component phases would tend to differ from one region to another, unless an alternative method is employed to control the uniformity of the particles distribution. Nevertheless, it is obvious from the present result that the increase of ceramic volume fraction results in the increase of the permittivity of the composites (see Fig.5.34), but this by no means represents the actual 'volume-permittivity' curve in view of the above observation.

Since it is useful to know the permittivity of the composite in terms of the permittivities and volume fractions of their components, an attempt has been made to fit the theoretical 'volume-permittivity' relation to the experimental data. Theoretical model which assumes spherical shape of the included particles (Eq.5.15) was considered and the calculated permittivities from this model were compared with observed data (see Fig.5.34). The model was found to give lower values of permittivities as compared to observed data (e.g. the

difference of permittivities is about 20% for composite with 30% volume fraction of ceramic). Further, the deviation between theoretical value and experimental data was significantly large for composite with 50% volume fraction of ceramic, i.e. observed value was about 2.5 times higher than the calculated one. Although the difference of 20% in permittivities (in case of composite with 30% volume fraction of ceramic) can be accounted for the uncertainty in volume fraction, the large deviation between the observed and the calculated permittivities for composite with 50% volume fraction of ceramic would suggest that the present experimental result can not be appropriately described by the theoretical model of Eq.(5.15).

The model which assumes the ellipsoidal shape of the included particles (Eq.5.16) was also considered to calculate the theoretical permittivity of the composite (see result in Fig.5.34). It is obvious that by assuming certain values of parameter s (s=7.5-8.5) and allowing for about ±10% in the uncertainty of the volume fraction, the calculated permittivities could reasonably fit the experimental data for PZT5/VDF-TrFE composite.

From section 5.4.4, it was shown that the calculated permittivities (with parameter s=8) are lower than the observed permittivities of PZT4/PVDF, PZT5/PVDF and $BaTiO_3$/PVDF composites. However, if we take 15% uncertainty in volume fraction into account, the calculated and observed values of permittivities are in agreement. It should also be noted that the parameter s was obtained through the process of

fitting the calculated values to the experimental data. It is possible in this context, as has been pointed out in section 5.4.4 , that the parameter s varies with the composition and the composites. However, for composites containing the same types of ceramic particles (e.g. PZT5/VDF-TrFE and PZT5/PVDF composites), it is unlikely that the shape of the particles are different from one composite to another, which means that the parameter s should remain invariant. As for composites with different types of ceramic particles (e.g. PZT4/PVDF and $BaTiO_3$/PVDF composites), further work remain to be done, such as by varying the ceramic volume fraction in order to determine the appropriate value of parameter s from the best fit curve of 'volume-permittivity' to experimental data. It is also useful in future work to examine the shape of the particles and its distribution in the composites so that the information obtained could be related to parameter s.

It emerges that general agreement between the calculated and measured permittivities of PZT5/VDF-TrFE composite is obvious using the model (Eq.5.16) which assumes an ellipsoidal shape of the ceramic particles. The same model could also account for the observed data of PZT4/PVDF, PZT5/PVDF and $BaTiO_3$/PVDF composites if there exist deviation of 15% in volume fractions and the value of parameter s is similar to that obtained for PZT5/VDF-TrFE composite. Agreement between the calculated and measured permittivity of PZT4/PP composite is also evident from result in section 5.4.4 if deviation of about 5% in volume fraction is introduced. This latter composite has lower permittivity as compared to the other

composites (for the same volume fractions of ceramic and polymer) in the present work, essentially due to the low permittivity of the polymer phase.

It may be useful to consider an alternative model for calculating the permittivity of composite, however in view of the uncertainty in the actual volume fractions encounter in the present work, the main priority of the future work would be to improve the fabrication technique of composite and thus ensuring the uniformity of the composite film.

7.3. Pyroelectric Properties

The pyroelectric activity in ceramic/polymer composites has been measured by the direct method, in which the reversible pyroelectric current was obtained after several heating runs of the polarized sample. The observed pyroelectricity appears to depend on the components of the composite and shows an increase in magnitude with increasing temperature.

The importance of cooling the sample under the electric field at the end of the poling process, is evident by the result obtained on PZT5/VDF-TrFE composite (see Fig.6.17), where 20-65% enhancement in the pyroelectric activity is achieved. It is believed that such procedure would stabilize the polarization charge in the material.

Attempt has been made to fabricate PZT5/VDF-TrFE composite with higher volume fraction of ceramic phase (i.e. > 50 Vol.%), however, the composite was very brittle and

difficult to be peeled off from the roller machine. Thus, by the present fabrication method, the maximum volume fraction of ceramic would be limited to~50%. From the result in section 6.4.2, it was shown that with the increase of ceramic volume fraction, the pyroelectric activity of the composite was observed to increase. By assuming that the pyroelectric coefficient of the composite is dependent on that of the dispersoid (ceramic) and the permittivity of the polymer, the pyroelectric coefficients have been calculated for composites with various ceramic volume fraction, using Eq.(6.35) and compared with the measured pyroelectric coefficient (see Fig.6.22). The calculated values appear to be in good agreement with the measured data for composites with high volume fraction of ceramic. For composite with low volume fraction of ceramic, the observed values of the pyroelectric coefficients were less than the calculated values. It is suggested that such discrepancy is caused by the uncertainties in the value of poling ratio used in the calculation, in which for the same poling parameters, the poling ratio in composite with low volume fraction of ceramic would be less than that for composite with high volume fraction of ceramic. Further work is obviously needed to evaluate the actual value of poling ratio (e.g. from measurement of X-ray intensity peak of unpoled and poled sample, as noted in section 6.4.2). Moreover, the uncertainty in the actual volume fraction (as discussed in section 7.2) should first be resolved before the comparison between the calculated and measured pyroelectric activity could be fully examined.

A limited measurement of pyroelectric activity by the dynamic method has been performed. It is accomplished by measuring the pyroelectric peak current (I_p) when a step input of radiation was shone onto the sample electrode after the completion of the third TSDC run of the pre-poled sample. As was noted in section 6.3.2, it is difficult to measure the absolute magnitude of pyroelectric coefficient by this method. Thus, attempt has been made to correlate the measured I_p from the dynamic method with the observed pyroelectric coefficient from the direct method. It was shown that a linear relationship exist between these measured quantities at 333K (see Fig.6.28), which yields the proportionality constant (K) as in Eqs.(6.32) and (6.33). Using this value of K and measured I_p, the pyroelectric coefficients were calculated from Eq.(6.32). Good agreement in the values of pyroelectric coefficient from direct and dynamic method are clearly visible at temperatures in the range 313-373K (see Fig.6.29). Near room temperature, however, the agreement between the two methods is less satisfactory. Such discrepancy is likely due to the variation in the values of K with temperature. Further work similar to that which produced Fig.6.28 need to be carried out to determine the value of K at those temperatures of interest, so that the more appropriate comparison between the two methods could be made. Indeed, the result in Fig.6.15 apparently showed that the value of K varies with the temperature of measurement, and this has been suggested to be related to the thermal properties inherence in the measurement system.

It was shown that the magnitude of pyroelectric coefficient increases with an increase of the magnitude of the poling parameters (electric field, temperature and time; see Figs.6.23-6.26). The main conclusion from these results was that an efficient poling can be achieved at high poling temperature and high poling field as long as it does not reach a limit of breakdown strength of the sample. For PZT5/VDF-TrFE and PZT5/PVDF composites with equal volume fraction of ceramic and polymer, the breakdown strength (E_B) was found to be about 1.3×10^7 Vm^{-1} at temperature 373K. Composites of $BaTiO_3$/PVDF (40/60 Vol.%) and PZT4/PVDF(50/50 Vol%) exhibit about similar magnitude of E_B as that of the former two composites while PZT4/PP shows $E_B \sim 1 \times 10^7$ Vm^{-1} at the same temperature of 373K. Obviously, the magnitude of E_B is increased for composite with reduced volume fraction of ceramic. Also, E_B will be lower at higher temperatures. Taking these factors into consideration, the poling temperature of 373K and E_p of 7×10^6 Vm^{-1} were used in poling all the samples for comparing their pyroelectric activity. It is possible to carry out poling at higher temperature, however, it was found that samples started to deform (wrinkle) under such condition. It was also found that poling for longer period of time (beyond 3 hours), would not give very much improvement in the value of pyroelectric coefficient for PZT5/VDF-TrFE composite (see Fig.6.26). Result in Fig.6.26 would also lead to the conclusion that the present composite films are not uniform in the sense that samples which were obtained from the same composite film showed quite different magnitudes in

pyroelectric coefficient under the same poling parameters (e.g. for $p(T_p)$ and $p(E_p)$ curves, obtained from different samples of the same batch of composite film, showed the difference in magnitude of p by a factor of 1.6 under the T_p=373K, E_p=7 x 10^6 Vm^{-1}, t_p=2.8 hrs). This would again point to the need of the proper fabrication method of the composite so that the uniformity in properties could be realized, as has been mentioned in preceding sections.

The relative difference in the magnitudes of pyroelectric activity for the composites in the present work are clearly visible (see Fig.6.15, 6.17, 6.31, 6.32). Composites of PZT5/VDF-TrFE and PZT5/PVDF posses a comparable pyroelectric activity and higher than those of the other composites investigated in the present work. These relative differences in pyroelectric activity can be attributed to factors such as pyroelectricity of the ferroelectric ceramic, the conductivity and permittivity of the component phases of composite. The large difference of dielectric permittivities between ceramic and polymer means that the applied field is, at least initially, greatly reduced in the ceramic phase. However, the field in the ceramic phase is gradually increased with time due to the accumulation of charges (trapped charges) at the interface (particularly at the ceramic/polymer interface ; see section 7.1). Thus, the polarization of the ceramic particles is developing with time, which is governed by the interfacial polarization process. From a simplified model of section 4.2.3 , the field in the ceramic phase (E_2) after a period longer than the sample relaxation time, is

given by :

$$E_2 = (\sigma_1 / \sigma_2) E_1 \qquad \text{(from Eq.4.36)}$$

from which it can be inferred that E_2 is controlled by σ_1 / σ_2, i.e. the ratio of the electrical conductivity of the polymer to that of the ceramic. This implied that the high conductivity of the polymer and the low conductivity of the ceramic is necessary to produce high electric field in the ceramic phase. For this reason, PZT4/PP composite showed very low pyroelectric activity since the low conductivity of polymer phase would not give enough E_2 to polarize the ceramic particles located in the amorphous phase of polymer. It is also obvious that composite employing PZT4 and $BaTiO_3$ showed relatively high conductivity as compared to composites containing PZT5 (with PVDF or VDF-TrFE as binding matrix), at high field and temperature (see Figs.4.47, 4.56, 4.57, 4.58). This would naturally suggest that the relatively high conductivity of the composites (PZT4/PVDF, $BaTiO_3$/PVDF) is likely attributed to the ceramic phase of PZT4 and $BaTiO_3$, which resulted in lower E_2 and hence lower pyroelectric activity of the composites. Furthermore, relative to PZT5, higher field strength is required to produce high polarization charge in PZT4 ceramics [Unilator Technical Ceramics, U.K.].

It appears from the above discussion that the high pyroelectric activity of the ceramic/polymer composites is essentially due to the ceramic phase. The high dielectric permittivity (or high conductivity) of the polymer phase is

required to maintain a continuous and large dielectric displacement flux in the composite medium. The temperature dependence of the pyroelectric coefficient in composites indicates that the behaviour is quite complex, which could possibly arise from various coupling effects between ceramic and polymer properties such as polarization properties, thermal expansion, elastic stiffness and internal stresses (developed during composite fabrication process). Indeed, to study these effects in detail requires further research. Nevertheless, the present results do indicate the merit properties of pyroelectric composite if suitable properties of ceramic and polymer were selected. As has been mentioned, the pyroelectric avtivity in PZT5/VDF-TrFE and PZT5/PVDF composite is comparable and higher than those of the other composites in the present work. However, with inherent lower losses (at most of the temperatures and frequencies measured in the present work ; see chapter 5), PZT5/VDF-TrFE composite would be a better choice as pyroelectric material. Although in this particular composite (PZT5/VDF-TrFE), the pyroelectric figure of merit for voltage responsivity (p/ε') is lower than that of PZT5 ceramic (i.e. about a factor of 2.6 times lower) at room temperature, at higher temperatures the value of p/ε' for the composite is getting better with respect to the ceramic (see section 6.4.2). At temperature 343K for example, the value of p/ε' for the composite is about 4 times higher than that of the ceramic (see also Table 7.1). This figure is also found to be about a factor of 2 improvement over the result obtained by Bhalla et al[[82] of chapter 6] and Galgoci et al[[84] of

chapter 6] on their PZT/polymer composites. Factors such as phase interconnection of the composite, the actual volume fraction and the properties of the component phases and the poling parameters contributes to the difference in the above mentioned result, which could only be fully quantified when the measurement were performed in a single programme of investigation.

Table 7.1 summarised several parameter values for the composites investigated in the present work. It should be noted that the values shown are representative (measured from selected specimen of the composites) and thus variations in the magnitudes are to be expected for different specimens of the same composite, as was pointed out in preceding sections. Nevertheless, relative characteristic of the composites are clearly demonstrated here.

Table 7.1. Summary of Results

Material	σ ($\Omega^{-1}m^{-1}$) (363K)	ε' (343K) 1 kHz	ε'' (343K) 1 kHz	p ($C.m^{-2}.K^{-1}$) (343K)	p/ε'
PZT5	$3x10^{-9}$	1200	1.3	$5x10^{-4}$	$4.2x10^{-7}$
PIEZEL	$3x10^{-11}$	106	3.8	$6.5x10^{-5}$	$6.1x10^{-7}$
PZT5/VDF-TrFE (50/50 Vol.%)	$4.6x10^{-11}$	85	5	$1.4x10^{-4}$	$1.65x10^{-6}$
PZT5/PVDF (50/50 Vol.%)	$3.6x10^{-11}$	95	8.6	$1.4x10^{-4}$	$1.5x10^{-6}$
PZT4/PVDF (50/50 Vol.%)	$2x10^{-10}$	94	7.4	$8x10^{-5}$	$8.5x10^{-7}$
$BaTiO_3$/PVDF (40/60 Vol.%)	$7.8x10^{-10}$	71	6	$1.5x10^{-5}$	$2.1x10^{-7}$
PZT4/PP (50/50 Vol.%)	$5x10^{-13}$	16.2	0.04	$7x10^{-8}$	$4.3x10^{-9}$

7.4. Suggestions for Further Work

There are areas where further research could be pursued to improve the experimental technique, to enhance the present pyroelectric composite properties and also to gain a better understanding of the material properties, which could include the following.

(1) In view of the uncertainty in the actual volume fraction of the ceramic and polymer in composites prepared in the present work (as was pointed out in section 7.2), the main priority for the future work would be to find ways to produce homogenous composite whereby ceramic particles are uniformly distributed in the polymer matrix. An automated system could be designed to disperse ceramic particles in the polymer matrix, thus replacing the less accurate manually controlled system as used in the present work.

(2) The present system of measuring electrical conductivity and pyroelectric current could be improved by the use of an automated data collection fascility through a dedicated computer system. This would also fascilitate data analysis for a quick test on sample materials.

(3) Ceramic particles used in the present work are of variable sizes (see section 4.3.1). It is worth experimenting with larger and uniform size of ceramic particles. The composite containing this ceramic type would be easier to be poled as compared to the one having smaller ceramic particle since the interface area between ceramic particles (in the case of

larger particles) would be reduced for the same volume of composite and this give rise to a more continuous electric flux path in the composite.

(4) As has already been stated, in order to have an instantaneous high electric field in the ceramic phase (for ease of poling process) of the composite, the high conductivity of the polymer matrix is required (see section 7.3). By adding a conductive phase (such as carbon) into the composite, it is expected that the conductivity of the polymer matrix could be increased and thus making the poling easier. This three-phase composite has been experimented in the present work by adding fine-grained silicon powder (not exceeding 3% in volume fraction) into PZT4/PVDF composite. It was found that the samples of this type were not giving any improvement in the measured pyro-coefficient and the dielectric loss was higher than that of the samples without conductive phase. Unfortunately, further experimental test could not be continued due to limited time available and the work along this line has to be abandoned. It may be stated however, that care has to be taken in fabricating this type of samples since the dielectric loss would increase dramatically for an excessive amount of conductive phase and this would become difficult to apply the large electric field required for poling. Furthermore, extreme care has to be exercised to ensure that the conductive phase is well dispersed in the polymer matrix.

(5) It has been mentioned that the present fabrication technique of ceramic-polymer composite could only produce

sample which has limited amount (around 50 Vol.%) of ceramic phase (see section 7.3). Since composite with ceramic phase in excess of 50 Vol.% is required to obtain better pyroelectric properties (see section 6.4.2) , the alternative fabrication process should be deviced to allow higher loading of the ceramic phase.

(6) Factors contributing to the pyroelectric properties of the composites have been discussed in section 7.3. While variable parameters of the component phases for high pyroelectric activity of the composite have been identified, the behaviour of the composites pyroelectric properties with temperature requires further investigation for the subject to be fully understood (see section 7.3). Nevertheless, it emerges from section 7.3 that future pyroelectric composite materials should combine high pyroelectric activity of ceramic (e.g. $PbTiO_3$ and its modified compounds such as those mentioned in section 6.2.3) with polymers of high permittivity (e.g. copolymers of VDF-TrFE (52-48 mole %)).

(7) Published work on single phase PVDF film (see section 6.2.2) showed that pyroelectric activity in this polymer could be enhanced by stretching the film while it is being poled. This technique could be adopted in the fabrication process of the present ceramic/polymer composites to produce favourable orientation of crystallites and hence greater persistent polarization in the samples.

(8) It would be useful for the future work to incorporate X-ray studies of the composite samples. Data from such studies could be used to asses the efficiency of poling , i.e. by

examining the change in the diffraction peak intensity as a function of poling parameters (as noted in section 6.4.2). This technique could also be used to study the effect of ceramic particle size on the state of polarization produced in the composite.

(9) The other processing variable which has not been considered in the present work is thermal annealing, the process by which a sample material is maintained at a known temperature and for a specific length of time. Following such treatment, microstructural properties of the material could be studied by scanning electron microscope (SEM) and X-ray diffraction technique, which could then be correlated with the data on conduction, dielectric and pyroelectric properties of the materials.

(10) Present work employed a conventional technique in poling all the samples for investigation. A useful piece of future work would be to experiment with alternative poling techniques such as corona poling. This letter technique has been successfully used in poling large areas of commercial PVDF films, and so it would be worthwhile to apply to the present composite films and compare the result with that of the conventional technique.

Finally, the present result on the conduction, dielectric and pyroelectric properties of ceramic-polymer composites is certainly provide an essential and useful information to an ever growing field. All the above suggestions may still not complete enough in an effort to obtain the diverse specification of good performance

pyroelectric materials. However, these suggestions would surely pave the way for an active research in this field and thus could further contribute to the present knowledge of the subject, or may even open up a new direction of the field with much to be disclosed.

REFERENCES

CHAPTER 1

1. S.B.Lang, Source Book on Pyroelectricity, Gordon and Breach, New York(1971)
2. M.E.Lines and A.M.Glass, Principles and Applications of Ferroelectric and Related Materials, Oxford University Press, Oxford(1979)
3. L.E.Garn and E.J.Sharp, IEEE Trans.Parts Hybrids Package, 10, 208(1974)
4. D.Berlincourt and H.H.A.Krueger, J.Appl.Phys., 30, 1804(1959)
5. W.J.Merz, Phys.Rev., 91, 513(1953)
6. C.B.Sawyer and C.H.Tower, Phys.Rev., 35, 269(1930)
7. B.Jaffe, W.R.Cook and H.Jaffe, Piezoelectric Ceramics, Academic Press, London(1971)
8. P.D.Southgate, Appl.Phys.Lett., 28, 250(1976)
9. D.K.Das-Gupta and K.Doughty, J.Appl.Phys., 49, 4601(1978)
10. M.G.Broadhurst and G.T.Davis, Topics in Applied Physics : Electrets, Edit. G.M.Sessler, Vol.33, 285-319, Springer Verlag, Berlin(1979)
11. J.B.Lando and W.W.Doll, J.Macromol.Sci.-Phys., B2, 205(1968)

12. J.C.Hicks, T.E.Jones and J.C.Logan, J.Appl.Phys., 49, 6092(1978)

13. K.J.Humphrey, G.M.Garner, N.M.Shorrocks and R.W.Whatmore, Ferroelectrics, Proc.6th Int.Symp.Appl.Ferroelectrics, 543(1986)

14. D.P.Skinner, R.E.Newnham and L.E.Cross, Mat.Res.Bull., 13, 599(1978)

15. J.Runt and E.C:Galgoci, Mat.Res.Bull., 19, 253(1984)

16. R.E.Newnham, D.P.Skinner, K.A.Klicker, A.S.Bhalla, B.Hardiman and T.R.Gururaja, Ferroelectrics, 27, 49(1980)

17. W.B.Harrison and S.T.Liu, Ferroelectrics, 27, 125(1980)

18. H.Yamazaki and T.Kitayama, Ferroelectrics, 33, 147(1981)

CHAPTER 2

1. M.E.Lines and A.M.Glass, Principles and Aplication of Ferroelectrics and Related Materials, Oxford University Press, Oxford(1979)
2. M.DiDomenico Jr and S.H.Wemple, J.Appl.Phys., 40(2), 720(1969)
3. H.Kawai, Jap.J.Appl.Phys., 8, 975(1969)
4. T.Furukawa, J.Aiba and E.Fukada, J.Appl.Phys., 50, 3615(1979)
5. E.Fukada and T.Furukawa, Ultrasonics, 19, 31(1981)
6. G.M.Sessler, J.Acoust.Soc.Am., 70, 1596(1981)
7. A.J.Lovinger, Science, 220, 1115(1983)
8. H.R.Gallantree, IEE Proc., 130, 219(1983)
9. P.A.Howie and H.R.Gallantree, Proc. Ultrason.Symp. IEEE, 566(1983)
10. J.C.McGrath, L.Holt, D.M.Jones and I.M.Ward, Ferroelectrics, 50, 13(1983)
11. L.Eyraud and P.Eyraud, Adv.Ceram.Mater., 1(3), 223(1986)
12. H.Thurnauer and J.Deaderick, U.S.Patent 2, 429, 588, 1947, file 1941
13. B.Jaffe, W.R.Cook and H.Jaffe, Piezoelectric Ceramics, Academic Press, London(1971)
14. J.M.Herbert, Ferroelectric Transducers and Sensors, Gordon and Breach, Science Publishers Inc., London(1982)
15. R.Pepinsky, Y.Okaya and F.Unterleitner, Acta Cryst., 13, 1071(1960)

16. W.Heywang and H.Thomann, Ann. Rev. Mater.Sci., 14, 27(1984)

17. H.J.Hagemann, J.Phys.C :Solid State Phys., 11, 3333(1978)

18. W.Heywang, Z.Angew.Phys., 19(5), 473(1965)

19. G.Arlt, D.Hennings and G.de With, J.Appl.Phys., 58(4), 1619(1985)

20. A.S.Shaikh, R.W.Vest and G.M.Vest, IEEE Symp. on Appl.of Ferroelectric, 126(1986)

21. R.Gerson, J.Appl.Phys., 31, 188(1960)

22. H.Ouchi, M.Nishida and S.Hayakawa, J.Am.Ceram.Soc., 49, 577(1966)

23. Y.Tanaka, T.Ikeda and H.Toyoda, Rev.Elec.Commun.Lab., 13, 744(1965)

24. C.Hall, Polymer Materials, Macmillan Pub.Ltd., Hampshire and London(1981)

25. A.R.Blythe, Electrical Properties of Polymers, Cambridge University Press, Cambridge(1979)

26. A.Keller, Phil. Mag., 2, 1171(1957)

27. P.H.Geil, Polymer Single Crystals, John Wiley and Sons, New York(1963)

28. J.D.Hoffman, G.T.Davis and J.I.Lauritzen Jr., Treatise on Solid State Chemistry, ed. N.B.Hannay, 3, 497-614, Plenum Press, New York(1976)

29. K.Sasaguri, R.Yamada and R.S.Stein, J.Appl.Phys., 35, 3188(1964)

30. H.R.Allcock and F.W.Lampe, Contemporary Polymer Chemistry, Prentice-Hall, Englewood Cliffs, NJ(1981)

31. A.J.Lovinger, Developments in Crystalline Polymers-1, ed. D.C.Basset, 195, Applied Science Publishers, London(1982)

32. W.M.Prest Jr. and D.J.Luca, J.Appl.Phys., 46, 4136(1975)

33. W.W.Doll and J.B.Lando, J.Macromol. Sci.-Phys., B4, 309(1970)

34. K.Tashiro, H.Tadokoro and M.Kobayashi, Ferroelectrics, 32, 167(1981)

35. J.B.Lando, H.G.Olf and A.Peterlin, J.Polym.Sci.A-1, 4, 941(1966)

36. G.T.Davis, J.E.Mckinney, M.G.Broadhurst and S.C.Roth, J.Appl.Phys., 49, 4998(1978)

37. D.K.Das-Gupta and K.Doughty, Appl.Phys.Lett., 31, 585(1977)

38. M.Bachmann, W.L.Gordon, S.Weinhold and J.B.Lando, J.Appl.Phys., 51, 5095(1980)

39. D.K.Das-Gupta and K.Doughty, J.Phys.D, 11, 2415(1978)

40. D.K.Das-Gupta, K.Doughty and D.B.Shier, J.Electrostat., 7, 267(1979)

41. S.L.Hsu, F.J.Lu, D.A.Waldman and M.Muthukumar, Macromolecules, 18, 2583(1985)

42. M.Kobayashi, K.Tashiro and H.Tadokoro, Macromolecules, 8, 159(1975)

43. Y.Takahashi and H.Tadokoro, Macromolecules, 13, 1317(1980)

44. A.J.Lovinger, Macromolecules, 14, 322(1981)

45. A.J.Lovinger, Macromolecules, 15, 40(1982)

46. S.Osaki and Y.Ishida, J.Polym.Sci.Polym.Phys.Ed., 13, 1071(1975)

47. A.Odajima and A.Yoshida, Oyobuturi, 48, 249(1979)

48. H.Kakutani, J.Polym.Sci.A-2, 8, 1177(1970)

49. H.Sasabe, S.Saito, M.Asahina and H.Kakutani, J.Polym.Sci.Polym.Phys.Ed., 7, 1405(1969)

50. S.Yano, J.Polym.Sci., 8, 1057(1970)

51. M.G.Broadhurst and G.T.Davis, Topics in Applied Physics: Electrets, Edit. G.M.Sessler, Vol.33, 285-319, Springer Verlag, Berlin(1979)

52. L.Pauling, The Nature of the Chemical Bond, Cornell Univ. Press, New York(1948)

53. M.G.Broadhurst, G.T.Davis, J.E.McKinney and R.E.Collins, J.Appl.Phys., 49(10), 4992(1978)

54. R.Al-Jishi and P.L.Taylor, J.Appl.Phys., 57(3), 902(1985)

55. R.G.Kepler and R.A.Anderson, CRC Crit.Rev.Mater.Sci., 9, 399(1980)

56. R.G.Kepler and R.A.Anderson, J.Appl.Phys., 49, 4918(1978)

57. J.E.McKinney, G.T.Davis and M.G.Broadhurst, J.Appl.Phys., 51, 1676(1980)

58. R.G.Kepler and R.A.Anderson, J.Appl.Phys., 49, 1232(1978)

59. N.Takahashi and A.Odajima, Ferroelectrics, 32, 49(1981)

60. D.Naegele and D.Y.Yoon, Appl.Phys.Lett., 33, 132(1978)

61. T.Takahashi, M.Date and E.Fukada, Appl.Phys.Lett., 37, 791(1980)

62. T.Furukawa, M.Date and E.Fukada, J.Appl.Phys., 51, 1135(1980)

63. M.Tamura, S.Hagiwara, S.Matsumoto and N.Ono, J.Appl.Phys., 48, 513(1977)

64. E.Fukada, Proc. of 2nd Meeting on Ferro.Mater. and Their Appl., I-1(1979)

65. P.Buchman, Ferroelectrics, 5, 39(1973)

66. M.Tamura, K.Ogasawara, N.Ono and S.Hagiwara, J.Appl.Phys., 45, 3768(1974)

67. R.G.Kepler, Org.Coatings Plast.Chem., 38, 278(1978)

68. A.G.Kolbeck, Polym.Eng.Sci.,22, 444(1982)

69. D.DeRossi, A.S.Reggi, M.G.Broadhurst, S.C.Roth and G.T.Davis, J.Appl.Phys., 53, 6520(1982)

70. A.J.Bur, J.D.Barnes and K.J.Wahlstrand, J.Appl.Phys., 59, 2345(1986)

71. D.H.Reneker and J.Mazur, Polymer, 26, 821(1985)

72. K.Nakagawa and Y.Ishida, J.Polym.Sci. A-2, 11, 1503(1973)

73. G.Pfister and M.A.Abkowitz, J.Appl.Phys., 45, 1001(1974)

74. S.Tasaka, M.Yoshikawa and S.Miyata, Polym. Prepr., Japan, 28, 1778(1979)

75. R.Hayakawa, J.Kusuhara, K.Hattori and Y.Wada, Rep.Prog.Polym.Phys. Japan, 16, 477(1973)

76. P.T.A.Klaase and J.van Turnhout, IEE Conf.Pub.No.177, 411(1979)

77. N.Murayama and H.Hashizume, J.Polym.Sci.Polym.Phys.Ed., 14, 989(1976)

78. K.Ogasawara, K.Shiratori and M.Tamura, Rep.Prog.Polym. Phys. Japan, 19, 313(1976)

79. Y.Wada, Electronic Properties of Polymers, Edit.J.Mort and G.Pfister, 109-160, John Wiley and Sons, New York(1982)

80. T.Yagi and M.Tatemoto, Polym.J., 11, 429(1979)

81. J.B.Lando and W.W.Doll, J.Macromol.Sci.-Phys., B2, 205(1968)

82. T.Yagi, M.Tatemoto and J.Sako, Polym.J., 12, 209(1980)

83. T.Furukawa, G.E.Johnson, H.E.Bair, Y.Tajitsu, A.Chiba and E.Fukada, Ferroelectrics, 32, 61(1981)

84. T.Yamada and T.Kitayama, J.Appl.Phys., 52, 6859(1981)

85. Y.Higashihata, J.Sako and T.Yagi, Ferroelectrics, 32, 85(1981)

86. A.J.Lovinger, G.T.Davis, T.Furukawa and M.G.Broadhurst, Macromolecules, 15, 323(1982)

87. Y.Tajitsu, A.Chiba, T.Furukawa, M.Date and E.Fukada, Appl.Phys.Lett., 36, 286(1980)

88. A.J.Lovinger, T.Furukawa, G.T.Davis and M.G.Broadhurst, Polymer, 24, 1225(1983)

89. A.J.Lovinger, T.Furukawa, G.T.Davis and M.G.Broadhurst, Ferroelectrics, 50, 227(1983)

90. T.Furukawa, Proc.6th Int.Symp. on Electrets, Oxford, England, Edit. D.K.Das-Gupta and A.W.Pattullo, 182(1988)

91. T.Furukawa, J.X.Wen, K.Suzuki, Y.Takashina and M.Date, J.Appl.Phys., 56, 829(1984)

92. J.X.Wen, Jap.J.Appl.Phys., 23, 1434(1984)

CHAPTER 3

1. E.Fatuzzo and W.J.Merz, Ferroelectricity, North-Holland Publishing Company, Amsterdam (1967)
2. J.C.Burfoot, Ferroelectrics - An Introduction to the Physical Principles, D.Van Nostrand Company Ltd., London(1967)
3. T.Mitsui, I.Tatsuzaki and E.Nakamura, An Introduction to the Physics of Ferroelectrics, Gordon and Breach Science Publishers, London(1976)
4. M.E.Lines and A.M.Glass, Principles and Applications of Ferroelectrics and Related Materials, Oxford University Press, Oxford(1979)
5. J.C.Burfoot and G.W.Taylor, Polar Dielectrics and Their Applications, The Macmillan Press Ltd., London(1979)
6. W.J.Merz, Phys.Rev., 95, 690(1954)
7. H.L.Stadler, J.Appl.Phys., 29, 1485(1958)
8. V.M.Fridkin, A.A.Grekov, N.A.Kosonogov and T.R.Volk, Ferroelectrics, 4, 169(1972)
9. J.Janta, Ferroelectrics, 2, 299(1971)
10. G.W.Taylor, Aust.J.Physics, 15, 549(1962)
11. G.W.Taylor, J.Appl.Phys., 37, 593(1966)
12. R.C.Miller, Phys.Rev., 111, 736(1958)
13. R.C.Miller and G.Weinreich, Phys.Rev., 117, 1460(1960)
14. M.Hayashi, J.Phys.Soc.Japan, 33, 739(1972)
15. M.Hayashi, J.Phys.Soc.Japan, 33, 616(1972)
16. H.Barkhausen, Phys.Szk., 20, 401(1919)

17. A.G.Chynoweth, Phys.Rev., 110, 1316(1958)

18. V.M.Rudyak, A.Y.Kudzin and T.V.Panchenko, Sov.Phys.Solid St., 14, 2112(1973)

19. J.C.Slater, Phys.Rev., 78, 748(1950)

20. J.C.Anderson, Dielectrics, Chapman and Hall, London(1964)

21. A.R.Blythe, Electrical Properties of Polymers, Cambridge University Press, Cambridge(1979)

22. A.K.Jonscher, Dielectric Relaxation in Solids, Chelsea Dielectric Press, London(1983)

23. R.Coelho, Physics of Dielectrics for the Engineer, Elsevier Scientific Publishing Company, Netherlands(1979)

24. M.Davies, Some Electrical and Optical Aspects of Molecular Behaviour, Pergamon, Oxford(1965)

25. P.Hedvig, Dielectric Spectroscopy of Polymers, Adam Hilger Ltd., Bristol, U.K.(1977)

CHAPTER 4

1. D.K.Das-Gupta and K.Joyner, J.Phys.D:Appl. Phys., 9, 829-840(1976)
2. J.R.Hanscomb and Y.Kaahwa, J.Phys.D:Appl. Phys., 11, 725-734(1978)
3. E.Sacher, J.Phys.D:Appl. Phys., 5, L17(1972)
4. D.M.Taylor and T.J.Lewis, J.Phys.D:Appl. Phys., 4, 1346(1971)
5. D.K.Das-Gupta, K.Doughty and R.S.Brockley, J.Phys.D:Appl. Phys., 13, 2101-14(1980)
6. T.Kaura and R.Nath, J.Appl.Phys., 54(10), 5887-5892(1983)
7. M.E.Lines and A.M.Glass, Principles and Applications of Ferroelectrics and Related Materials, Oxford Univ. Pres, Oxford (1979)
8. H.J.Hagemann, J.Phys.C:Solid State Phys., 11, 3333(1979)
9. K.H.Hardtl and D.Hennings, J.Amer.Ceram.Soc., 55, 230(1972)
10. W.Heywang and H.Thomann, Ann.Rev.Mater.Sci., 14, 27(1984)
11. J.C.Anderson, Dielectrics, Chapman and Hall, London(1964)
12. G.M.Sessler(Edit.), Topics in Applied Physics : Electrets (Vol.33), Springer Verlag, Berlin(1979)
13. J.G.Simmons, Dc Conduction in Thin Films, Mills and Boon Ltd., London(1971)
14. A.F.Joffe, The Physics of Crystals, McGraw-Hill, New York (1928)
15. G.Jaffe, Ann. Physik, 16, 217(1933)
16. J.R.Macdonald, Phys. Rev., 92, 4(1953)

17. J.R.Macdonald, J.Chem.Phys., 54, 2026(1971)

18. J.R.Macdonald, J.Appl.Phys., 34, 538(1963)

19. E.H.Snow, A.S.Grove, B.E.Deal and C.T.Sah, J.Appl.Phys., 36, 1664(1965)

20. P.Debye, Polar Molecules, Chemical Catalog Company, N.Y(1929)

21. J.Vanderschueren and A.Linkens, J.Appl.Phys., 49(7), 4195(1978)

22. K.S.Cole and R.H.Cole, J.Chem.Phys., 10, 98(1942)

23. K.S.Cole and R.H.Cole, J.Chem.Phys.,9,341(1941)

24. H.Frohlich, Theory of Dielectrics, 2nd Ed., Oxford(1960)

25. F.Bueche, Physical Properties of Polymers, Interscience, New York(1962)

26. M.L.Williams, R.F.Landel and J.D.Ferry, J. Amer. Chem. Soc.,77,3701(1955)

27. R.M.Fuoss, J.Amer.Chem.Soc., 63, 378(1941)

28. H.J.Wintle, J.Non-Cryst. Solids, 15, 471(1974)

29. B.V.Hamon, Proc.Inst. Electr. Engrs., 99, 151(1952)

30. J.C.Maxwell, Electricity and Magnetism, Oxford University Press(1892)

31. K.W.Wagner, Arch. Elektrotechn., 2, 371(1914)

32. R.H.Partridge, J.Polym.Sci..A3, 2817(1965)

33. I.Boustead, Proc.Roy.Soc.(Lond.), A318, 459(1970)

34. P.Wilcox, Can.J.Phys., 50, 912(1972)

35. H.J.Wintle, J.Appl.Phys., 44(6), 2514(1973)

36. S.R.Pollack and C.E.Morris, J.Appl.Phys., 35, 1503(1964)

37. L.Esaki and P.J.Stiles, Phys. Rev. Letts., 16, 1108(1966)

38. C.Cherki, R.Coelho and R.Nannoni, Phys.Stat.Sol.A, 2, 785(1970)

39. K.C.Kao and W.Hwang, Electrical Transport in Solids, Perg.Press, Oxford(1981)

40. B.R.Gossick, Potential Barriers in Semiconductors, Acad. Press, New York(1964)

41. E.M.Conwell, Phys. Rev., 103, 51(1956)

42. N.F.Mott, Can. J. Phys., 34, 1356(1956)

43. T.Kasuya and S.Kiode, J.Phys.Soc.Japan, 13, 1287(1958)

44. A.Miller and E.Abrahams, Phys.Rev., 120, 745(1960)

45. M.Pollak and T.H.Geballe, Phys.Rev., 122(6), 1742(1961)

46. A.K.Jonscher, Electrets, Edit: M.M.Perlman, The Electrochem Soc., N.Y.(1973)

47. R.M.Hill, Phil.Mag., 23, 181, 59(1971)

48. R.H.Cole, Progress in Dielectrics, Eds. J.B.Birks and J.Hart, 3, Heywood, London(1961)

49. A.K.Jonscher, J.Non-Cryst. Solids, 8(10), 293(1972)

50. A.K.Jonscher, Nature, 253, 717(1975)

51. A.K.Jonscher and F.Taiedy, J.Phys.C: Solid State Phys., 8, L107(1975)

52. A.K.Jonscher, Thin Solid Films, 36, 1(1976)

53. A.K.Jonscher, J.of Mater.Sci., 16, 2037(1981)

54. L.A.Dissado and R.M.Hill, Nature, 279, 685(1979)

55. A.K.Jonscher, L.A.Dissado and R.M.Hill, Phys.Stat.Sol.(B), 102, 351(1980)

56. J.R.Yeargan and H.L.Taylor, J.Appl.Phys., 39(12), 5600(1968)

57. M.Ieda, G.Sawa and S.Kato, J.Appl.Phys., 42(10), 3737(1971)

58. V.Adamec and J.H.Calderwood, J.Phys.D: Appl.Phys., 8, 551(1975)

59. D.V.Geppert, J.Appl.Phys., 33, 2993(1962)

60. J.L.Hartke, J.Appl.Phys., 39, 4871(1968)

61. N.F.Mott and R.W.Gurney, Electronic Processes in Ionic Crystals, Oxford Univ. Press, New York(1948)

62. A.Rose, Phys.Rev., 97, 1538(1955)

63. M.A.Lampert and P.Mark, Current Injection in Solids, Acad. Press, New York(1970)

64. P.Mark and W.Helfrich, J.Appl.Phys., 33(1), 205(1962)

65. J.J.O'Dwyer, The Theory of Electrical Conduction and Breakdown in Solid Dielectrics, Oxford Univ.Press, London(1973)

66. B.Jaffe, W.R.Cook and H.Jaffe, Piezoelectric Ceramics, Acad.Press, London(1971)

67. C.Hall, Polymer Materials, Macmillan Pub.Ltd., Hampshire and London(1981)

68. A.R.Blythe, Electrical Properties of Polymers, Cambridge Univ.Press, Cambridge(1979)

69. Technical Information on PIEZEL, Daikin Industries Ltd. Japan(1985)

70. Y.Higashihata, T.Yagi and J.Sako, Ferroelectrics, 68, 63(1986)

71. J.Runt and E.C.Galgoci, Mat.Res.Bull., 19, 253(1984)

72. D.P.Skinner, R.E.Newnham and L.E.Cross, Mat.Res.Bull., 13, 599(1978)

73. J.Mendiola and B.Jimenez, Ferroelectrics, 53, 159(1984)

74. J.R.Hanscomb and E.P.George, J.Phys.D :Appl.Phys., 14, 2285(1981)

75. T.Mizutani, M.Ieda and I.B.Jordan, Jap.J.Appl.Phys., 18, 65(1979)

76. L.Badian, S.M.Gubanski and T.J.Lewis, J.Phys.D: Appl.Phys., 10, 2513(1977)

77. H.J.Wintle, IEEE Trans. on Electr.Insul., 21, 747(1986)

78. D.K.Davies, J.Phys.D: Appl.Phys., 5, 162(1972)

79. V.Adamec and J.H.Calderwood, IEEE Trans.Electr.Insul., 21, 389(1986)

80. M.Takahashi, Jap.J.Appl.Phys., 9, 1236(1970)

81. D.K.Das-Gupta and K.Joyner, J.Phys.D: Appl.Phys., 9, 2041(1976)

82. S.Isoda, H.Miyaji and K.Asai, Jap.J.Appl.Phys., 12, 1799(1973)

83. M.Kosaki, K.Sugiyama and M.Ieda, J.Appl.Phys., 42, 3388(1971)

84. R.A.Foss and W.Danhauser, J.Appl.Polym.Sci., 7, 1015(1963)

85. M.Tavakoli and J.Hirsch, J.Phys.D: Appl.Phys., 21, 454(1988)

86. K.Ikezaki, T.Kaneko and T.Sakakibara, Jap.J.Appl.Phys., 20, 609(1981)

CHAPTER 5

1. A.R.Blythe, Electrical Properties of Polymers, Cambridge University Press, Cambridge(1979)
2. P.Debye, Polar Molecules, Chemical Catalog Co., N.Y.(1929)
3. R.H.Cole and K.S.Cole, J.Chem.Phys., 9, 341(1941)
4. R.M.Fuoss and J.G.Kirkwood, J.Amer.Chem.Soc., 63, 385(1941)
5. D.W.Davidson and R.H.Cole, J.Chem.Phys., 18, 1417(1950)
6. N.E.Hill, W.E.Vaughan, A.H.Price and M.Davies, Dielectric Properties and Molecular Behaviour, Van Nostrand Reinhold Comp. Ltd, London(1969)
7. V.V.Daniel, Dielectric Relaxation, Academic Press, London(1967)
8. P.Hedvig, Dielectric Spectroscopy of Polymers, Hilger, Bristol(1977)
9. R.M.Fuoss, J.Amer.Chem.Soc., 63, 378(1941)
10. M.Matsui, R.Matsui and Y.Wada, Polym.J., 2, 134(1971)
11. R.J.Young, Introduction to Polymers, Chapman and Hall, London(1981)
12. H.Sasabe, S.Saito, M.Asahina and H.Kakutani, J.Polym.Sci. A-2, 7, 1405(1969)
13. S.Yano, J.Polym.Sci.A-2, 8, 1057(1970)
14. K.Nakagawa and Y.Ishida, J.Polym.Sci.Polym.Phys.Ed., 11, 1503(1973)
15. A.Peterlin and J.Elwell, J.Mater.Sci., 2, 1(1967)
16. S.Osaki, S.Uemura and Y.Ishida, J.Polym.Sci.A-2, 9, 585(1971)

17. D.K.Das-Gupta and K.Doughty, Ferroelectrics, 28, 307(1980)

18. D.K.Das-Gupta, K.Doughty and R.S.Brockley, J.Phys.D: Appl.Phys., 13, 2101(1980)

19. V.Adamec, Kolloid Z.Z.Polymere, 249, 1085(1971)

20. D.K.Das-Gupta and K.Joyner, J.Phys.D: Appl.Phys., 9, 829(1970)

21. R.S.Brockley, Ph.D. Thesis, University of Wales (1979)

22. B.Jaffe, W.R.Cook and H.Jaffe, Piezoelectric Ceramics, Academic Press, London(1971)

23. O.Kersten and G. Schmidt, Ferroelectrics, 67, 191(1986)

24. L.A.Dissado and R.M.Hill, Nature, 279, 685(1979)

25. R.M.Hill and A.K.Jonscher, Contemp. Phys., 24, 75(1983)

26. R.Gerson, J.M.Peterson and D.R.Rote, J.Appl.Phys., 34(11), 3242(1963)

27. R.Gerson, J.Appl.Phys., 31(9), 1615(1960)

28. H.J.Hagemann, J.Phys.C: Solid State Phys., 11, 3333(1978)

29. K.H.Hardtl, Ceramics International, 8(4), 121(1982)

30. H.J.Hagemann and H.Ihrig, Phys.Rev.B, 20, 2973(1979)

31. K.H.Hardtl and D.Hennings, J.Amer.Ceram.Soc., 55, 230(1972)

32. K.Carl and K.H.Hardtl, Ferroelectrics, 17, 473(1978)

33. A.S.Shaikh, R.W.Vest and G.M.Vest, IEEE Symp. on Appl. of Ferroelectric, 126(1986)

34. W.R.Tinga, W.A.G.Voss and D.F.Blossey, J.Appl.Phys., 44, 3897(1973)

35. T.Yamada, T.Ueda and T.Kitayama, J.Appl.Phys., 53(6), 4328(1982)

36. W.F.Brown, Jr., J.Chem.Phys., 23, 1514(1955)

37. H.Banno and S.Saito, Jap.J.Appl.Phys., 22, 67(1983)

38. T.Furukawa, K.Fujino and E.Fukada, Jap.J.Appl.Phys., 15(11), 2119(1976)

39. K.W.Wagner, Arch.Elektrotech., 2, 371(1914)

40. H.Kakutani, J.Polym.Sci.Pt.A2, 8, 1177(1970)

41. T.Furukawa and G.E.Johnson, J.Appl.Phys., 52, 940(1981)

42. Y.Higashihata, J.Sako and T.Yagi, Ferroelectrics, 32, 85(1981)

43. S.Yano, K.Tadano and K.Aoki, J.Polym.Sci.Polym.Phys.Edit., 12, 1875(1974)

44. M.Ohuchi, A.Chiba, M.Date and T.Furukawa, Jap.J.Appl.Phys., 22, 1267(1983)

45. N.Koizumi, J.Hagino and Y.Murata, Ferroelectrics, 32, 141(1981)

46. Y.Higashihata, T.Yagi and J.Sako, Ferroelectrics, 68, 63(1986)

47. G.M.Sessler, Topics in Applied Physics : Electrets, Edit. G.M.Sessler, vol.33, 1-12 (1979)

48. C.Muralidhar and P.K.C.Pillai, IEEE Trans.Elec.Ins., 21, 501(1986)

49. R.N.Work, R.D.McCammon and R.G.Saba, J.Chem.Phys., 41, 2950(1964)

50. K.A.Buckingham and W.Reddish, Proc.IRE, 114, 1810(1967)

51. E.W.Anderson and D.W.McCall, J.Poly.Sci., 31, 241(1958)

CHAPTER 6

1. M.E.Lines and A.M.Glass, Principles and Applications of Ferroelectric and Related Materials, Oxford University Press, Oxford(1979)
2. G.Gerliczy and R.Bertz, Sensors and Actuators, 12, 207(1987)
3. R.W.Whatmore, Rep. Prog. Phys., 49, 1335(1986)
4. R.E.Newnham, A.Safari, J.Giniewicz and B.H.Fox, Ferroelectrics, 60, 15(1984)
5. R.E.Newnham, A.Safari, G.Sa-Gong and J.Giniewicz, IEEE Ultrasonic Symposium, 501(1984)
6. T.Furukawa, K.Fujino and E.Fukada, Jap.J.Appl.Phys., 15(11), 2119(1976)
7. T.Furukawa and E.Fukada, Jap.J.Appl.Phys., 16(3), 453(1977)
8. T.Furukawa, K.Ishida and E.Fukada, J.Appl.Phys., 50(7), 4904(1979)
9. T.Yamada, T.Ueda and T.Kitayama, J.Appl.Phys., 53(6), 4328(1982)
10. Y.Higashihata, T.Yagi and J.Sako, Ferroelectrics, 68, 63(1986)
11. J.R.Giniewicz, R.E.Newnham, A.Safari and D.Moffatt, Ferroelectrics, 73, 405(1987)
12. F.I.Mopsik and M.G.Broadhurst, J.Appl.Phys., 46, 4204(1975)

13. M.G.Broadhurst and G.T.Davies, Topics in Applied Physics : Electrets, Edit. G.M.Sessler, Vol.33, 285-319, Springer Verlag, Berlin(1979)

14. K.Iohara, K.Imada and M.Takayanagi, Polym.J., 3, 357(1972)

15. T.Furukawa, Y.Uematsu, K.Asakawa and Y.Wada, J.Appl.Polym.Sci., 12, 2675(1968)

16. Y.Wada and R.Hayakawa, Jap.J.Appl.Phys., 15, 2041(1976)

17. Y.Wada, Electronic Properties of Polymers, Edit. J.Mort and G.Pfister,109-160, John Wiley and Sons, New York(1982)

18. R.E.Salomon, H.Lee, C.S.Bak and M.M.Labes, J.Appl.Phys., 47, 4206(1976)

19. J.Cohen and S.Edelman, J.Appl.Phys., 42, 3072(1971)

20. W.Reddish, J.Polym.Sci.Part C, 14, 123(1966)

21. M.H.Litt, C.Hsu and P.Basu, J.Appl.Phys., 48, 2208(1977)

22. J.J.Crosnier, F.Micheron, G.Dreyfus and J.Lewiner, J.Appl.Phys., 47, 4798(1976)

23. A.J.Curtis, J.Chem.Phys., 36, 3500(1962)

24. R.N.Work, R.D.McCammon and R.G.Saba, J.Chem.Phys., 41, 2950(1964)

25. D.K.Das-Gupta and K.Joyner, J.Phys.D :Appl.Phys., 9, 2041(1976)

26. J.Cohen, S.Edelman and C.F.Vezzetti, Electrets, Edit. M.M.Perlman, 505, The Electrochem. Soc., New York(1973)

27. R.J.Phelan, R.J.Mahler and A.R.Cook, Appl.Phys.Lett., 19, 337(1971)

28. R.J.Phelan, R.L.Peterson, C.A.Hamilton and G.W.Day, Ferroelectrics, 7, 375(1974)

29. A.G.Chynoweth, J.Appl.Phys., 27, 78(1956)

30. A.W.Stephens, A.W.Levine, J.Fech, T.J.Zrebiec, A.V.Cafiero and A.M.Garofalo, Thin Solid Films, 24, 361(1974)

31. M.Sirajuddin and P.Jayarama Reddy, Thin Solid Films, 124, 149(1985)

32. J.G.Bergman, J.H.McFee and G.R.Crane, Appl.Phys.Lett., 18, 203(1971)

33. A.M.Glass, J.H.McFee and J.G.Bergman, J.Appl.Phys., 42, 5219(1971)

34. J.H.McFee, J.G.Bergman and G.R.Crane, Ferroelectrics, 3, 305(1972)

35. G.Pfister, M.Abkowitz and R.G.Crystal, J.Appl.Phys., 44, 2064(1973)

36. H.Burkard and G.Pfister, J.Appl.Phys., 45, 3360(1974)

37. N.Murayama and H.Hashizume, J.Polym.Sci. :Polym.Phys.Ed., 14, 989(1976)

38. R.G.Kepler and R.A.Anderson, J.Appl.Phys., 49, 4490(1978)

39. R.G.Kepler and R.A.Anderson, J.Appl.Phys., 49, 4918(1978)

40. R.G.Kepler, R.A.Anderson and R.R.Lagasse, Ferroelectrics, 57, 151(1984)

41. J.M.Schultz, J.S.Lin, R.W.Hendricks, R.R.Lagasse and R.G.Kepler, J.Appl.Phys., 51, 5508(1980)

42. E.L.Nix, J.Nanayakkara, G.R.Davies and I.M.Ward, J.Polym.Sci. :Part B : Polym.Phys., 26, 127(1988)

43. M.G.Broadhurst, G.T.Davis, J.E.McKinney and R.E.Collins, J.Appl.Phys., 49, 4992(1978)

44. J.E.McKinney, G.T.Davis and M.G.Broadhurst, J.Apl.Phys., 51, 1676(1980)

45. N.Inoue, T.Takada, T.Sakai and K.Nakamura, Jap.J.Appl.Phys., 21, 706(1982)

46. K.Takahashi, H.Lee, R.E.Salomon and M.M.Labes, J.Appl.Phys., 48, 4694(1977)

47. M.Tamura, S.Hagiwara, S.Matsumoto and N.Ono, J.Appl.Phys., 48, 513(1977)

48. D.Naegele and D.Y.Yoon, Appl.Phys.Lett., 33, 132(1978)

49. T.Furukawa, M.Date and E.Fukada, J.Appl.Phys., 51, 1135(1980)

50. R.G.Kepler, E.J.Graeber and P.M.Beeson, Bull.Am.Phys.Soc.Ser.11, 20, 350(1975)

51. R.G.Kepler and R.A.Anderson, J.Appl.Phys., 49, 1232(1978)

52. D.K.Das-Gupta and K.Doughty, Appl.Phys.Lett.,31, 585(1977)

53. D.K.Das-Gupta and K.Doughty, J.Appl.Phys., 49, 4601(1978)

54. D.K.Das-Gupta and K.Doughty, IEEE Trans.Ind.Appl., 14, 448(1978)

55. D.K.Das-Gupta and K.Doughty, J.Phys.D :Appl.Phys., 11, 2415(1978)

56. D.K.Das-Gupta and K.Doughty, J.Phys.D :Appl.Phys., 13, 95(1980)

57. T.T.Wang, J.Appl.Phys., 50, 6091(1979)

58. T.T.Wang and J.E.West, J.Appl.Phys., 53, 6552(1982)

59. H.Sussner and K.Dransfeld, J.Polym.Sci.Polym.Phys.Ed., 16, 529(1978)

60. H.Yamazaki, J.Ohwaki, T.Yamada and T.Kitayama, Appl.Phys.Lett., 39, 772(1981)

61. T.Yamada, J.Appl.Phys., 53, 6335(1982)

62. T.Furukawa, J.X.Wen, K.Suzuki, Y.Takashina and M.Date, J.Appl.Phys., 56, 829(1984)

63. A.I.Baise, H.Lee, B.Oh, R.E.Salomon and M.N.Labes, Appl.Phys.Lett., 26, 428(1975)

64. J.C.Hicks, T.E.Jones and J.C.Logan, J.Appl.Phys., 49, 6092(1978)

65. S.Tasaka and S.Miyata, J.Appl.Phys., 57, 906(1985)

66. K.J.Humphrey, G.M.Garner and R.W.Whatmore, Ferroelectrics, 76, 383(1987)

67. K.J.Humphrey, G.M.Garner, N.M.Shorrocks and R.W.Whatmore, Proc.6th Int.Symp.Appl.Ferroelectrics, 543(1986)

68. T.A.Perls, T.J.Diesel and W.I.Dobrov, J.Appl.Phys., 29, 1297(1958)

69. B.Jaffe, W.R.Cook and H.Jaffe, Piezoelectric Ceramics, Academic Press, London(1971)

70. W.R.Cook, D.A.Berlincourt and F.J.Scholz, J.Appl.Phys., 34, 1392(1963)

71. G.H.Haertling and C.E.Land, J.Amer.Ceram.Soc., 54, 1(1971)

72. S.T.Liu, J.D.Heaps and O.N.Tufte, Ferroelectrics, 3, 281(1972)

73. H.P.Beerman, Infrared Physics, 15, 225(1975)

74. R.W.Whatmore and A.J.Bell, Ferroelectrics, 35, 155(1981)

75. R.W.Whatmore and F.W.Ainger, Proc.SPIE, 395, 261(1983)

76. J.G.Bergman, G.R.Crane and E.H.Turner, J.Solid State Chem., 21, 127(1977)

77. H.Takeuchi, S.Jyomura, Y.Ito and K.Nagatsuma, Ferroelectrics, 51, 71(1983)

78. K.Yokoyama, Y.Yamashita, H.Izumi, H.Okuma and N.Ichinose, Proc.2nd Meeting on Ferroelectric Materials and Their Applications, 227(1979)

79. N.Ichinose, Y.Hirao, M.Nakamoto and Y.Yamashita, Jap.J.Appl.Phys., 24, 178(1985)

80. W.B.Harrison and S.T.Liu, Ferroelectrics, 27, 125(1980)

81. H.Yamazaki and T.Kitayama, Ferroelectrics, 33, 147(1981)

82. A.S.Bhalla, R.E.Newnham, L.E.Cross, W.A.Schulze, J.P.Dougherty and W.A.Smith, Ferroelectrics, 33, 139(1981)

83. D.P.Skinner, R.E.Newnham and L.E.Cross, Mat.Res.Bull., 13, 599(1978)

84. E.C.Galgoci, D.G.Schreffler, B.P.Devlin and J.Runt, Ferroelectrics, 68, 109(1986)

85. R.L.Byer and C.B.Roundy, Ferroelectrics, 3, 333(1972)

86. A.G.Chynoweth, J.Appl.Phys., 27, 78(1956)

87. A.M.Glass, J.Appl.Phys., 40, 4699(1969)

88. M.Simhony and A.Shaulov, J.Appl.Phys., 42, 3741(1971)

89. D.K.Das-Gupta and K.Doughty, J.Appl.Phys., 51, 1733(1980)

90. T.Mizutani, T.Yamada and M.Ieda, J.Phys.D: Appl.Phys., 14, 1139(1981)

91. K.T.Chung, B.A.Newman, J.I.Scheinbeim and K.D.Pae, J.Appl.Phys., 53, 6557(1982)

92. Y.Yasuoka and H.Hirayama, Jap.J.Appl.Phys., 21, 962(1982)

93. C.Alemany, B.Jimenez, J.Mendiola and E.Maurer, J.Mater.Sci., 19, 2555(1984)

94. L.Jingde, L.Deming and H.Di, Ferroelectrics, 70, 7(1986)

95. M.G.Shakhtakhtinskii, B.A.Guseinov, M.A.Kurbanov, Y.N.Gazaryan and A.O.Guliev, Sov.Phys.Solid State, 25, 2145(1983)

96. D.K.Das-Gupta and J.S.Duffy, J.Appl.Phys., 50, 561(1979)

97. A.R.Blythe, Electrical Properties of Polymers, Cambridge University Press, Cambridge(1979)

PUBLICATIONS

Publications associated with the present work are as follows :

1. D.K.Das-Gupta and M.J.Abdullah, "Electro-Active Characterization of Polymer-Ceramic Composite", British Ceramic Proceedings, Ed. R.W.Davidge, No.38, pp.231-243, The Inst.of Ceramics, U.K.(1986)
2. M.J.Abdullah and D.K.Das-Gupta, "Dielectric and Pyroelectric Properties of Polymer-Ceramic Composites", Ferroelectrics, Vol.76, pp.393-401(1987)
3. D.K.Das-Gupta and M.J.Abdullah, "Dielectric and Pyroelectric Properties of Polymer/Ceramic Composites", J.Mater.Sci.Lett., Vol.7, pp.167-170(1988)
4. D.K.Das-Gupta and M.J.Abdullah, "Pyroelectric and Dielectric Properties of Polymer-Ceramic Composites", Mat.Res.Soc.Symp.Proc., Vol.120, pp.205-210, Materials Research Society U.S.A.(1988)
5. D.K.Das-Gupta and M.J.Abdullah, "Electroactive Properties of Polymer-Ceramic Composites", Ferroelectrics, Vol.87, pp.213-228(1988)
6. M.J.Abdullah and D.K.Das-Gupta, "Electrical Properties of Ceramic/Polymer Composites", IEEE Trans.Elec.Ins., Vol.25(3), pp. 605-610(1990)